ADVANCES IN
QUANTUM CHEMISTRY

EDITOR-IN-CHIEF

PER-OLOV LÖWDIN

PROFESSOR EMERITUS

DEPARTMENT OF QUANTUM CHEMISTRY
UPPSALA UNIVERSITY
UPPSALA, SWEDEN

AND

QUANTUM THEORY PROJECT
UNIVERSITY OF FLORIDA
GAINESVILLE, FLORIDA

EDITORS

JOHN R. SABIN
MICHAEL C. ZERNER

QUANTUM THEORY PROJECT
UNIVERSITY OF FLORIDA
GAINESVILLE, FLORIDA

ERKKI BRÄNDAS

DEPARTMENT OF QUANTUM CHEMISTRY
UPPSALA UNIVERSITY
UPPSALA, SWEDEN

VOLUME 34

ACADEMIC PRESS

San Diego London Boston New York Sydney Tokyo Toronto

This book is printed on acid-free paper. ♾

Academic Press
a division of Harcourt Brace & Company
525 B Street, Suite 1900, San Diego, California 92101-4495, USA
http://www.apnet.com

Academic Press
24-28 Oval Road, London NW1 7DX, UK
http://www.hbuk.co.uk/ap/

International Standard Book Number: 0-12-034834-9

PRINTED IN THE UNITED STATES OF AMERICA
99 00 01 02 03 04 QW 9 8 7 6 5 4 3 2 1

Contributors

Numbers in parentheses indicate the pages on which the authors' contributions begin.

Rodney J. Bartlett (271, 295), Quantum Theory Project, University of Florida, Gainesville, Florida 32611-8435

David E. Bernholdt (271), Northeast Parallel Architectures Center, Syracuse University, Syracuse, New York 13244-4100

David Craig (1), The Faculties, Australian National University, Canberra, ACT 0200, Australia

D. E. Ellis (51), Department of Chemistry and Materials Research Center, Northwestern University, Evanston, Illinois 60208

Diana Guenzburger (51), Centro Brasileiro de Pesquisas Físicas–CBPF, Rua Dr. Xavier Sigaud, 150, 22290-180 Rio de Janeiro-RJ, Brazil

Piotr Piecuch (295), Department of Chemistry, Michigan State University, East Lansing, Michigan 48824-1322

Henry F. Schaefer III (143), Center for Computational Quantum Chemistry, University of Georgia, Athens, Georgia 30602

C. David Sherrill (143), Department of Chemistry, University of California, Berkeley, California 94720-1460

Preface

In investigating the highly different phenomena in nature, scientists have always tried to find some fundamental principles that can explain the variety from a basic unity. Today they have shown not only that all the various kinds of matter are built up from a rather limited number of atoms, but also that these atoms are composed of a few basic elements of building blocks. It seems possible to understand the innermost structure of matter and its behavior in terms of a few elementary particles—electrons, protons, neutrons, photons, etc.—and their interactions. Since these particles obey not the laws of classical physics but the rules of modern quantum theory of wave mechanics established in 1925, there has developed a new field of "quantum science" which deals with the explanation of nature on this ground.

Quantum chemistry deals particularly with the electronic structure of atoms, molecules, and crystalline matter and describes it in terms of electronic wave patterns. It uses physical and chemical insight, sophisticated mathematics, and high-speed computers to solve the wave equations and achieve its results. Its goals are great, and today the new field can boast of both its conceptual framework and its numerical accomplishments. It provides a unification of the natural sciences that was previously inconceivable, and the modern development of cellular biology shows that the life sciences are now, in turn, using the same basis. "Quantum biology" is a new field that describes the life processes and the functioning of the cell on a molecular and submolecular level.

Quantum chemistry is hence a rapidly developing field that falls between the historically established areas of mathematics, physics, chemistry, and biology. As a result there is a wide diversity of backgrounds among those interested in quantum chemistry. Because the results of the research are reported in periodicals of many different types, it has become increasingly difficult for both the expert and the nonexpert to follow the rapid development in this new borderline area.

The purpose of this serial publication is to present a survey of the current development of quantum chemistry as it is seen by a number of internationally leading research workers in various countries. The authors have been invited to

give their personal points of view of the subject freely and without severe space limitations. No attempts have been made to avoid overlap—on the contrary, it seems desirable to have certain important research areas reviewed from different points of view.

Although most of Volume 34 is dedicated to modern methods in quantum chemistry, the volume begins with a rather wonderful and personalized historical review of our field by David Craig, who presents many problems still unsolved after so many years of effort. Here, Dr. Craig shows not only his grasp of what theory should do, but also his mastery of experimental physical chemistry. The chapter by Don Ellis and Diana Guenzburger brings us up to date on the discrete variational model approach to density functional theory, a model now being used more and more in treating large systems of current experimental interest.

The last three chapters deal with highly correlated *ab initio* electronic structure methods. The chapter by David Sherrill and Henry "Fritz" Schaefer summarizes recent developments in the configuration interaction model and develops it further in terms of expansions over determinants, rather than configuration state functions. This chapter is an excellent review for anyone interested in details of the configuration interaction model. The last two chapters cover the coupled-cluster model for electron correlation. The first, by David Bernholdt and Rod Bartlett, examines the coupled-cluster singles and doubles model, including third-order triple excitations and its accuracy in studying problems in photoelectron spectra. The last chapter in this volume, by Piotr Piecuch and Rod Bartlett, further develops the equations of motion method, introducing simplifying approximations so that it is easier to apply to problems in calculating the properties of molecular electronically excited states.

The editors enjoyed putting this volume together, and we hope our readers enjoy reading through it, as did we.

THE EDITORS

A JOURNEY WITH GOOD COMPANIONS.

Fifty years of Quantum Chemistry.

By David Craig
The Faculties, Australian National University,
Canberra, ACT. 0200 Australia.

1. INTRODUCTION

The problems for quantum chemists in the mid-forties were how to improve the methods of describing the electronic structure of molecules, valence theory, properties of the low excited states of small molecules, particularly aromatic hydrocarbons, and the theory of reactions. It seemed that the physics needed was by then all to hand. Quantum mechanics had been applied by Heitler, London, Slater and Pauling, and by Hund, Mulliken and Hückel and others to the electronic structure of molecules, and there was a good basis in statistical mechanics. Although quantum electrodynamics had not yet been developed in a form convenient for treating the interaction of radiation with slow moving electrons in molecules, there were semi-classical methods that were adequate in many cases.

There had also been experimental advances calling for theoretical explanations. For example in 1944 Michael Kasha with GN Lewis [200] discovered that the emitting state in the long-lived phosphorescence of simple aromatics was an excited triplet state. There was at that time no theory of the energies and other properties of these states. It was a good time to be starting in these fields of enquiry.

Time travel over five decades takes us back to electro-mechanical calculators, to poorly developed ways of solving the Schrödinger equation, and to the faith that a few precise molecular electronic structures, like the hydrogen molecule ion and the hydrogen molecule, would illuminate molecular electronic structure as a whole. To undertake a new calculation meant feeding numbers into a noisy mechanical contrivance with whirring innards and a carriage that jumped up and down and went end-to-end. When it stopped you wrote down numbers, and later fed the beast again.

Some, like William Moffitt, did not see computation as the business of theoreticians: he took the view that 'If I can't get the numbers on the back of an envelope I do without numbers'. Along this line there were many who put their effort into the theoretical basis of broad features, like aromatic character, and the spatial distribution of valence bonds, and the valence state, which were above the noise level of electronic structure calculations possible at the time.

To those who began work in quantum chemistry in England after the war the scene was sparse. Sir John Lennard-Jones had returned to the Theoretical Chemistry

ADVANCES IN QUANTUM CHEMISTRY, VOLUME 34

0065-3276/99 $30.00

Department at Cambridge, and there were small theoretical groups in Manchester, Liverpool, and other places. It was true that activity in the US had continued more strongly in the war years, diminished but still lively, as a scan of the Journal of Chemical Physics for the war years will confirm. Robert Mulliken was publishing, also Linus Pauling, Bright Wilson and other luminaries. But if, like me, you had a Fellowship tenable in Britain and were attracted to work with CK Ingold at University College London, that in itself settled a course of action.

At that time (1946) there was no indication that Charles Coulson, then at Dundee, would be appointed to a professorship at King's College London, but this welcome event added to the lively atmosphere. He held weekly group seminars that became known as 'coffee parties'. They were stimulating occasions. Coulson was aware that his mathematical background did not fit him tidily into established categories in physics or chemistry, but he was still surprised to have a letter addressed to him at the 'Department of Theatrical Physics' at King's College!

In fundamental science the choice of research topics is influenced by what is going on in the laboratory, by chance events at conferences, by the skills and interests of collaborators, and by one's own view of what are the outstanding problems. However without good colleagues, good students and postdocs, and visitors from other labs, nothing much can be done. The following accounts of my group's research over the five decades 1946-1996, limited by space, centre on the work itself with only brief mention of a small number of the good companions I have been linked to during my lifetime. Others I have listed at the end. What I have written is intended to serve as a testimonial to collaborations that were intellectually and imaginatively rewarding as well as fruitful scientifically.

The research enterprises took place in three locations. After leaving Sydney in 1946 I was in University College London as research fellow and then lecturer. From 1952-56 I was again in Sydney as professor of physical chemistry. Ingold then invited me back to London to a new chair of theoretical chemistry in 1956, and there I expected to remain. However in the mid-sixties the Australian National University decided to establish a Research School of Chemistry. It was a response to the need to attract back to Australia some of the large cohort of young 'scientific emigrants' who had left for the UK and the US. The proposal had firm government support and generous financial backing. AJ Birch, then at the University of Manchester, and I were invited to oversee the design of new laboratories and their equipment to the highest standard, and to become foundation professors. We accepted and began work in 1967. Sir Ronald Nyholm had been invited to join the founding group, but in the event did not accept. I continued in the Research School until retirement at the end of 1984, then moved as emeritus professor to the Department of Chemistry in The Faculties of the ANU. I worked for two or three months of each year 1967-1987 as Visiting Professor at University College.

2. THE Π-ELECTRON STATES OF CONJUGATED MOLECULES

2.1 Configuration Interaction

At University College Ingold had completed his remarkable work on the benzene spectrum at 260 nm [201], drawing for its interpretation on Alfred Sklar's valence-bond calculation suggesting the assignment to an upper state $^1B_{2u}$ [202]. The Herzberg-Teller [203] theory of vibronic intensity stealing was central, the theory having been elaborated in a review of Teller's with Hertha Sponer [204]. Sklar's 1937 paper was followed in 1938 by a molecular orbital calculation of Maria Goeppert-Mayer and Sklar (GMS) [205] on the benzene energy levels.

Before that time molecular orbital calculations had been made with empirical parameters found by fitting a calculated energy interval to experiment in one molecule, usually benzene, and applying it to others. In the GMS paper the required quantities were integrals over molecular orbitals calculated in a basis of Slater orbitals and without empirical quantities. As with all other calculations only the π-electrons were included, the σ-electrons being supposed simply to hold the atoms in a framework. The agreement with experimental intervals in the benzene spectrum was not good, but the paper was a landmark in method.

I read this work in Sydney in about 1945, and with my colleague Allan Maccoll (later Professor of Chemistry at University College London) worked to see how it might be extended to anthracene. Maccoll was the first to teach quantum mechanics in the Sydney Chemistry Department, and had research going in quantum chemistry as well as in his primary field of gas kinetics. He helped me to get started; we have been lifelong friends.

Maccoll was then reviewing evidence on molecular transitions in the visible and ultraviolet regions [206]. Our broad hope in extending the GMS method was to resolve differences in the predictions of the valence-bond and simple (spin-free) molecular orbital theory on the spectroscopic properties of naphthalene and higher aromatics.

According to VB theory the lowest spectroscopic jump was polarized along the longer in-plane molecular axis; MO theory indicated the shorter. Anthracene was chosen as the test case because there were some preliminary experimental results. Even in anthracene the evidence was indirect: RN Jones [207] used the spectral influence of substituents in anthracene to infer short-axis polarization for the first singlet-singlet transition.

This project to extend the GMS method to anthracene proved to be too hard for the times. The starting point was to get the basis molecular orbitals. In benzene they are fully determined by the hexagonal symmetry, but in anthracene have to be found by calculation. For the full computation many integrals were needed including the repulsion integrals (2.1) that now seem easy,

$$\frac{1}{4\pi\varepsilon_0}\int\int a(1)b(2)\frac{e^2}{r_{12}}c(1)d(2)dr_1dr_2 \qquad (2.1)$$

In (2.1) *a*, *b*, *c*, and *d*, not necessarily different, are $2p\pi$ atomic orbitals at carbon centres. and the *r*'s are electron coordinates and separations in an obvious notation. The range of integrals in GMS was limited to two atomic centres. The limitation

was not serious, because the two-centre terms included the largest.

In reworking the 1938 calculations of GMS I was struck by the fact that the basis of single electron configurations, namely ways of assigning electrons to orbitals, which had been highly important in the empirical molecular orbital method in giving physical insight, was not enough in the non-empirical method.

The mixing of different configurations had long been a feature of describing the electronic structure of atoms, but not up to this time, of molecules. It had been assumed that placing the π-electrons in the molecular orbitals of lowest energy would give the state of lowest energy. However in the GMS method the matrix elements of electron repulsion between different configurations of the same overall symmetry, including spin, could be large. Their effect in second order was in some cases more than the diagonal corrections. This was the motive for my work, and that of my group, on configurational interaction (CI) in the MO method [21].

The main drive toward CI had been to show that the differences between results based on empirical MO and VB methods could be removed when basis sets were expanded, account taken of spin, and all configurations included in both methods. This was obvious in a formal sense. Its importance was in establishing which of the earlier conclusions was correct, and in interpreting spectra. We were also to be able to show how CI brought calculations of the oscillator strength in a benzene transition closer to experiment through strong cancellations among terms from different configurational wave functions [28].

The importance of configuration interaction in the MO method was more clearly defined in a later calculation jointly with Robert Parr and my close friend and colleague Ian Ross [25]. Bob Parr was then at the Carnegie Institute of Technology in Pittsburgh. We had not met, and did not meet for ten or more years. However after an exchange of letters we decided on a trans-Atlantic collaboration. Ian Ross (later Professor of Chemistry in the Australian National University, and then Deputy vice-Chancellor) had been my first student in Sydney, and had joined me in London in 1949. Our interests in science and early encounters on the squash court set our paths in parallel. In this paper [25] we estimated the three- and four-centre integrals and recalculated the energy levels, giving improved agreement with experiment. We introduced the term *ab initio.* It began to be used generally, and has continued to the present. The estimates of integrals were rather crude, built from overlap integrals calculated for Slater orbitals.

In this procedure the repulsion between electrons in a Slater orbital was too big, no allowance being made for the relaxation of the orbital in the atomic configuration. However the over-estimate could be allowed for. When the one-centre repulsion was estimated empirically, and combined with non-empirical values for the others, the role of CI was less, but the mixture not altogether satisfying. Later new fully empirical schemes were introduced, notably by Pariser and Parr [208]. Inclusion of CI remains a standard part of molecular electronic calculations.

2.2 Conjugated non-Aromatic Molecules

The status of cyclobutadiene as a putative member of the aromatic series was now able to be studied by a method free of the gross approximations of the empirical VB and MO methods. It was already known that cyclooctatetraene, the next in the series of 4n electron systems, was not aromatic, that it behaved as a poly-olefin, but the situation was confused by the fact that there was non-planarity forced by the σ–framework. Wheland [209] had shown that in cyclobutadiene the empirical descriptions by MO and VB methods were in conflict in a unusual way. The VB picture was that cyclobutadiene was stabilized by resonance, with a (Pauling) resonance energy equal to the VB parameter α. The MO method gave zero.

I noted in a paper in 1950 [23] that the situation was complicated by the fact that the ground state did not belong to the totally symmetrical representation of the point group D_{4h}, but to the B_{2g} representation, out of line with known aromatics. The situation in a planar model of C_8H_8 was the same. This property of the ground state had already been found in the theory of the (then) unknown molecules pentalene and heptalene [16]. In the simple MO method the lowest state of cyclobutadiene is degenerate, with three equi-energetic ways of assigning electrons to orbitals. With CI the degeneracy is split, giving a triad of which the singlet B_{2g} was lowest, as in VB. However it was clear in this calculation that the empirical VB theory grossly exaggerated the resonance stabilization [23]. The non-empirical CI calculation did not give significant stability to the square structure, and collapse to a rectangle, with two long and two short bonds agrees with experiment.

It had become clear that 'Hückel's rule' that only π-electron systems with 2n+2 carbons were aromatic could be generalized to bi- and poly-cyclic systems. The corresponding generalization of the cyclobutadiene case to pentalene and heptalene and more complex molecules was made through the application of what became known as "Craig's Rules" [26]. They dealt adequately with many systems, but were eventually shown to lack full generality. π-systems which had alternating double and single bonds, but were not aromatics, were at first known as pseudo-aromatic, but later anti-aromatic. They included the examples, already mentioned, of pentalene and heptalene. Neither shows aromatic properties.

2.3 Conjugated Cyclic Inorganic Molecules. The Phosphazenes

In 1958 I gave a course of lectures on aromatic character in Coulson's Theoretical Summer School in Oxford. After one of them I met Norman Paddock (later Professor on Chemistry in the University of British Columbia), then working in the research department of Albright and Wilson. The company's commercial interests included the cyclic phosphonitrilic halides (phosphazenes) that Paddock was characterizing. They have ring systems with alternate nitrogen and phosphorus atoms. The substituents on the pentavalent phosphorus atoms may be chlorines or fluorines or other atoms or groups.

He had noticed that cyclic molecules of all numbers of ring atoms, not only the Hückel magic numbers 4n+2, n being an integer, seemed more stable than experience with the nearest noncyclic analogues would have suggested. Since every

alternate atom in the rings belonged to the second row of the Periodic Table we speculated that dπ-orbitals could be involved in the π-electron system. The same could be true also of rings with alternating nitrogen and sulphur atoms, or nitrogen and silicon. Examples of both types of compounds were known.

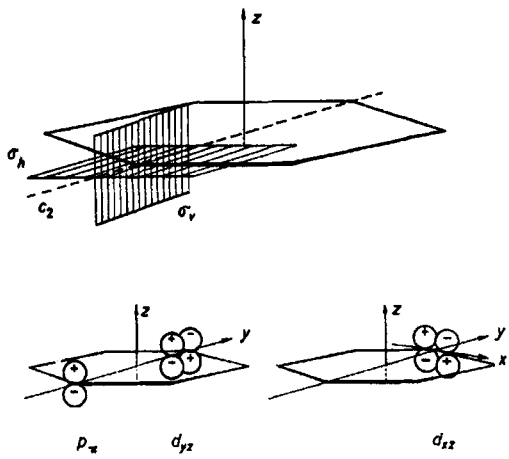

Fig. 1. π-orbitals in a plane hexagonal ring system.
Reproduced from reference [56].

We worked on the theory overnight, thought that it made sense, and published in Nature [49] as the first of many joint papers. The essential point was that of the two dπ orbitals on a ring atom the tangentially directed dπ orbital overlapped its neighbour pπ orbitals (Fig. 1) with opposite signs on the two sides. The radially-directed orbital had the same signs. In symmetry terms the latter behaved in the same way as a pπ orbital, the former did not. By taking account of this difference we could show that Hückel-type alternation with the number of ring atoms did not apply.

The theoretical studies, along with growing experimental activity in these 'inorganic rubbers' and related compounds stimulated interest in commercial uses and even defence applications. My colleague KAR Mitchell (later Professor of Chemistry in the University of British Columbia) and I produced a long review [89a] of these polymeric A-B-A systems. Work in the USSR gave a high-temperature stable methoxy-phosphazene lubricant which we understood was used for a time in jet engines, but was replaced by newly developed hydrocarbon lubricants. There were also small scale uses in pharmaceutical products. Later there were more substantial industrial applications.

3. MOLECULAR CRYSTALS

3.1 Experimental tests of directions of transition moment

The early speculations about transition moment directions in the lower aromatics needed to be tested experimentally. The traditional vapour phase measurements of band lineshapes were not accessible with the spectroscopic resolving power we then had, but came later (sec 4.2). Most absorption systems of aromatics in the UV were in any case diffuse and structureless. The method that could be used was to get the polarization of the light absorbed by the crystal composed of the target molecules. The positions and orientations of the molecules in the laboratory frame were known from X-ray crystal structure analysis. The interpretation of results raised non-trivial theoretical problems of its own. The experiments will be described first.

Our first use of crystal polarization was in hexamethylbenzene. It had all molecular planes parallel to one another and perpendicular to the main faces of a sublimed crystal. It was known that the lowest absorption system was polarized in the molecular plane, conforming with its assignment to a π–π transition. However in the next system of benzene at 200 nm, corresponding to the hexamethylbenzene system at 230 nm, the vapour phase spectrum had been assigned to a Rydberg transition polarized perpendicular to the molecular plane [210].

So far as we knew polarization measurement had not been made at wavelengths close to the quartz limit of 200 nm, and problems of making polarized light at these wavelengths had to be overcome. Quartz Wollaston prisms for polarizing ultraviolet light were not yet made. At this point Lawrence Lyons (later Professor of Chemistry at the University of Queensland) joined the group from the spectroscopy laboratories in the University of Sydney. He first made a multiple reflection polarizer from sheets of a UV-transparent plastic set at the critical angle, following a design with sheets of glass used in the visible. The result was promising but not good enough. We reckoned we needed instead a strongly birefringent crystal transparent at short wavelengths. We eventually turned to geologists' collections of mineral specimens and were given a selection of calcite rhombs, one of which was sufficiently free of impurities to transmit UV light. The emergent light came in two cleanly polarized beams well separated on the photographic plate. Lyons showed conclusively that the transition was in-plane polarized [30].

PC Hobbins and I had in 1950 begun to work on the polarized ultraviolet absorption spectrum of anthracene. We had by that time the use of a quartz Wollaston prism, designed by Dr HG Poole and made by Adam Hilger. It was an important advance, because measurements could be made, one polarized beam at a time, down to a short wavelength limit of about 190 nm. The anthracene solution spectrum shows two absorptions, near 380 nm and near 250 nm. Both are affected by intermolecular forces in the crystal, but could be unravelled to show that the second, very intense, absorption was polarized along the long in-plane molecular axis, in agreement with MO theory.

Other aspects of the experimental task with equipment of the day were not simple. To work at the lowest available temperature was essential. Liquid nitrogen at 130K was not too difficult, but not so the next step down to liquid hydrogen. This was at

the time being made in the laboratories in Oxford in Prof FE Simon's Department. He agreed to supply us. We found a Dewar flask, and Peter Hobbins from time to time brought back supplies of liquid gas on the train. The dangers, barely comprehended, were severe. The main one was that oxygen from the air would condense out on the hydrogen. An explosion in the Oxford laboratory from this cause put an end to our experiments, but we had already done a good deal.

At liquid hydrogen temperature, 20K, the crystal spectrum of anthracene was well resolved. It showed a *b*-crystal axis absorption stronger than *a*-axis. Referred to the molecular framework this meant that the transition was polarized along the shorter molecular axis, again in agreement with the molecular orbital theory (spin-free, single configuration) [41-43]. The only previous work on polarized absorption in anthracene crystals [211] was at higher temperatures with low resolution; it had also shown *b*-absorption greater than *a* but interpretation in terms of molecular directions had not been possible at the time.

3.2 Excitons in Molecular Crystals

This was the start of a line of theoretical and experimental research that lasted in my group over several years. Davydov [212] had shown that in crystals each transition of a free molecule splits into transitions to sub-levels equal in number to molecules in the unit cell. There were new selection rules for the polarization properties in the crystal. The splitting between sublevels in leading order was proportional to the square of the transition moment. In strong transitions this was a dipole moment. In weak transitions, as we later showed, even the octupole moment could appear.

The essential theory is to exploit the translational symmetry of the crystal lattice, and to construct exciton-type wave functions from modulated molecular wave function products of the form,

$$\phi_i^r(\mathbf{k}) = N^{-1/2}\sum_p e^{i\mathbf{k}.\mathbf{r}}\phi_{ip}^r$$
$$\phi_{ip}^r = \varphi_{11}.\ .\ .\ .\ .\varphi_{ip}^r.\ .\ .\ .\ .\varphi_{hN} \qquad (3.1)$$

in which the molecular wave function φ_{ip}^r is for the r-th excited electronic state and the suffices specify the lattice site, in the p-th cell (of N) and the i-th translationally equivalent set (of h). $\mathbf{k}$ is the wave vector for the transformation properties under translations. Spectroscopic transitions at wavelengths large compared with a lattice spacing, as here, go with zero change in the wave vector. The ground state belongs to $\mathbf{k}$=0; transitions go to $\mathbf{k}$=0 in (3.1), ie to an upper state given as a simple (unmodulated) sum of the products in the second line of (3.1). The molecular wave functions are assumed known, and experimental intervals and transition moments used in getting their properties in the crystal.

Anthracene has two molecules in the unit cell, and according to the Davydov theory in dipole approximation, the splitting between the two components, corresponding to

the two values of i in (3.1), is proportional to $\mathbf{M}^2$, where $\mathbf{M}$ is the molecular transition dipole moment. The result depends on the summation of dipole-dipole coupling over all molecules l and m of the entire crystal, each of the form,

$$V_{lm} = \frac{e^2}{4\pi\varepsilon_0 R_{lm}^3}\mathbf{M}^2 \tag{3.2}$$

The sums are shape-dependent (sec. 5.1) but were able to be used for spectral interpretations except in a few special cases.

The theory here sketched had be modified for transitions that were weaker than those to which it had at first been applied. When we used it in the weak system of anthracene at 380 nm [42,43] the intensities of absorption along the crystal axes did not fit either molecular absorption direction. It was not difficult to show that where there was another molecular transition (2 - 0) close in energy to the weak transition (1 - 0), especially if strong, the two were coupled by crystal forces. The coupling energy, analogous to (3.2), is (3.3),

$$V_{lm}^{1,2} = \frac{e^2}{4\pi\varepsilon_0 R_{lm}^2}\mathbf{M}^{(1)}.\mathbf{M}^{(2)} \tag{3.3}$$

Solution of the secular problem for energies of the coupled molecular states enabled the first two states of anthracene to be assigned to short-axis polarized for the first transition and long axis for the second [42]. The agreement with experiment for energies and polarization ratios in the long progression of totally symmetrical vibrations were still not good, but were improved over time. The successive improvements to the theory are described in Stuart Walmsley's and my 1968 book [102a]. The Craig-Davydov theory was successfully applied to many molecular crystal spectra.

3.3 Mixed Molecular Crystals

The applications were extended to mixed molecular crystals such as tetracene contained as a dilute impurity in anthracene. Choudhury and Ganguly [213] had measured the absorption spectrum of tetracene at 480 nm and interpreted it with the assumption, later confirmed by crystal packing calculations, that the molecules are held in the anthracene lattice in almost the same position and orientation as the molecules they replace. They made the remarkable discovery that the intensity ratio for absorption along the *b* and *a* crystal axes was not 7.7:1 expected on the oriented gas model, but around 2:1. We later refined the measurements [84] to give values close to 3:1.

The effect that is dominant in pure crystals, the Davydov splitting, is missing in mixed crystals. There are no first order effects of the crystal field. Second order coupling terms like (3.3), where the superscripts refer to the lowest transitions in the host and guest molecules, cause intensity transfers. In the *b* direction the tetracene intensity is increased by a factor of 3 by transfer from the anthracene 250 nm and 380 nm systems; in the *a* direction there is little change.

By this time Thuraiappah Thirunamachandran had come to me as a PhD student, with study leave from his staff position in the University of Ceylon. He showed [74] that the experimental results in this and some other cases were very well accounted for by the transfer of intensity from strong to weaker transitions under the dipole-dipole coupling (3.3). It had become clear that the oriented-gas model was not a satisfactory approximation.

Thiru went back to Sri Lanka but later returned to a tenured post in the University College Department of Chemistry (he is now Reader in Chemistry). I have enjoyed an enduring and fruitful partnership with this highly talented colleague, as well as friendship, over the years and to the present. I owe much to his precise and meticulous science.

3.4 The Crystal Spectra of Very Weak Molecular Transitions

In the application of the exciton theory to transitions that are forbidden or extremely weak in the vapour another result was found that has proved useful in the interpretation of numerous crystal spectra. In these transitions, in the crystal, the intensity appears partly in the vibrationless pure electronic transition, and in part in vibrationally induced transitions as will be described for the benzene 260 nm system (sec 4.1). Other examples are in naphthalene and phenanthrene and in some nitrogen heterocyclic molecules.

The 320 nm electronic spectrum of naphthalene was the first for which the theory was developed in detail [67]. In the vapour spectrum there are two interpenetrating band systems. One system with oscillator strength f=0.0002 is very weakly electronically allowed and long-axis polarized. The other stronger (f=0.002) system is short axis polarized, and is induced by vibrational perturbation. In the crystal the effect of the crystal field on these systems is different. We had shown experimentally [66] that the origin transition on the one hand and the vibrationally induced transition on the other, were differently affected by crystal interactions. The origin band is split by 151 cm^{-1} and the vibrational by less than 1 cm^{-1}.

Now in the pure electronically allowed system the intensity is so small that transitions caused by higher multipole interactions must be allowed for in addition to the very small transition dipole. In the naphthalene spectrum the next interaction term depends upon the the transition octupole moment. Thus the multipolar expansion of the intermolecular potential energy (3.4) cannot be cut off at the dipole term, as implied in (3.2) and (3.3)

$$\mathbf{V}_{mn} = \frac{1}{4\pi\varepsilon_0}\left(-\sum_{df}\frac{Z_f e^2}{r_{df}} - \sum_{ge}\frac{Z_g e^2}{r_{ge}} + \sum_{cd}\frac{e^2}{r_{cd}} + \sum_{fg}\frac{Z_f Z_g}{r_{fg}} \right) \qquad (3.4)$$

but must be continued to quadrupole and octupole and perhaps higher terms. In (3.4) the electrostatic potential between molecules *m* and *n* is a sum over electron-nuclear, electron-electron, and nuclear-nuclear terms, the *Z*'s standing for nuclear charges. For naphthalene the octupole moment is the next in the expansion of (3.4) that is symmetry-allowed. Its value cannot be estimated from the spectroscopic

properties in the vapour or solution, but upper limits can be assigned from models, or found by calculation. The large splitting of 151 cm^{-1} can be accounted for with realistic values for the moment components. It could be confirmed also that the assignment of the 320 nm transition to long-axis polarized was the only assignment compatible with the observed splitting, so adding further support to conclusions from the rotational contours in the vapour spectrum [63]. This is a straightforward extension of the usual theory.

However the vibrationally induced transitions are a different case. We must now specify in the crystal wave functions (3.1) the molecular vibrational wave functions $\sigma^{r(i)}$ for a molecule in the i-th vibrational quantum level and the r-th electronic state. If the transition is allowed, leading to the zero wave-vector state (3.1), the σ are totally symmetrical, and the transition moments get multiplied by Franck-Condon factors (3.5),

$$\left\langle \sigma^{0(i)} \middle| \sigma^{r(j)} \right\rangle \tag{3.5}$$

for the ground and r-th electronic states, with i and j the vibrational quantum numbers. The case is different for excitation of non-totally symmetrical vibrations. For a one-quantum state of a nontotally symmetrical motion the state function is the product $\phi^r\sigma^{r(1)}$. Under Herzberg-Teller mixing the perturbed wave function is,

$$c_1\phi^r\sigma^{r(1)} + c_2\phi^s\sigma^{s(0)} \tag{3.6}$$

c_1 and c_2 are coefficients, the first near unity and the second typically one or two orders of magnitude less. Calculation of the crystal splitting in the vibrationally induced transitions follows from incorporation of expression (3.6) in the wave functions (3.1), and evaluation of the matrix elements of the interaction potential (3.4). There are three typical terms in the matrix elements for molecules k and l in $\mathbf{V}_{lk}$,

$$\begin{aligned} &c_1^2\left\langle \phi_l^r\sigma_l^{r(1)}\phi_l\sigma_l^{0(0)} \middle| \mathbf{V}_{lk} \middle| \phi_k^r\sigma_k^{r(1)}\phi_k\sigma_k^{0(0)} \right\rangle \\ &+2c_1c_2\left\langle \phi_l^r\sigma_l^{r(1)}\phi_l\sigma_l^{0(0)} \middle| \mathbf{V}_{lk} \middle| \phi_k^s\sigma_k^{s(0)}\phi_k\sigma_k^{0(0)} \right\rangle \\ &+c_2^2\left\langle \phi_l^s\sigma_l^{s(0)}\phi_l\sigma_l^{0(0)} \middle| \mathbf{V}_{lk} \middle| \phi_k^s\sigma_k^{s(0)}\phi_k\sigma_k^{0(0)} \right\rangle \end{aligned} \tag{3.7}$$

The first two terms vanish on account of the orthogonality properties of either nuclear or electronic wavefunctions. The surviving third term, proportional to the square of the very small coefficient of the second term in (3.6), gives a splitting about proportional to the mixed-in dipole intensity, with no contribution by the higher multipoles. This allows many puzzling features of the crystal spectra of such transitions to be explained. In physical terms the small resonance effects reflect the low rate of intermolecular exchange of vibrational, as opposed to electronic, motion.

3.5 Calculation of Aromatic Crystal Packing

The packing of molecules in their crystals, and the dynamics of their motions, are essential to the work described in this section. Also they are a source of information on intermolecular forces. Kitaigorodskii [214] had discussed packing as an expression of interatomic forces. Mason [215] pointed to the importance of hydrogen contacts through the observation that the number of H-H van der Waals intermolecular contacts was closely the same in fourteen of the simplest aromatic hydrocarbons. We undertook a more general study of the crystals of benzene and naphthalene, taking into account electrostatic interactions of the permanent moments, dispersive coupling and H-H, C-H and C-C repulsive forces due to electron overlap [88].

The number and range of variables that could be included in the energy minimization was limited by computer capacity at the time. The space group and distances between molecular centres were kept fixed. The molecules were rotated about the three body axes and the energies computed. The molecular quadrupole moments were not known, but upper limits could be set. Dispersive interactions were estimated for transition moments on single-level and many-level assumptions. The findings were that the coupling of permanent moments was too small to affect either the lattice energy or its variation with angle. They did not influence the packing. Dispersion accounted for the entire attractive energy, but varied too slowly with angle to fix the molecular packing. The H-H repulsions on the other hand show deep minima in plots of energy against rotation angle in all three displacements at positions very close to the known structures. We concluded that H-H repulsions are structure-determining. C-H and C-C repulsions contribute to the repulsion energy and therefore to the net cohesive binding, but not to the packing angles.

Technical advances in computing and use of quaternions for the Euler angle variables enabled less constrained approaches and allowed vacancies and impurities to be studied in their effect on structures. Distances between molecules were varied, giving good agreement with experiment [150].

In naphthalene we were able to show that a vacancy allowed neighbours to relax and recover some of the energy lost by removal of a molecule, in agreement with an earlier finding on vacancies in rare-gas crystals. The impetus for this work was its relevance for the spectroscopy of crystals containing impurities (sec. 3.3), and questions of how impurities fit into perfect lattices and lattices with vacancies and dislocations. We therefore looked at how a larger foreign molecule, anthracene or tetracene, would fit into host naphthalene or anthracene respectively, when the local cage structure was allowed to relax in position and orientation. The cage opened up to accommodate the impurity, but held it nearly parallel with the alignment of the molecule it had replaced. The lattice energy after allowing for relaxation was 20-30 kJ mol^{-1} greater than the pure host. This was not a surprise and agreed with our own and others' experiments.

However the result for a smaller molecule replacing a larger did cause surprise. When a vacancy was created in anthracene, and a naphthalene molecule placed on the vacated lattice site it was unstable, moving to one of two positions in which its

two rings registered with the centre and end rings of the adjacent cage. Its orientation in the lattice was nearly the same as the replaced host [150]. The lattice energy loss was high, 55 kJ mol^{-1}; the barrier between sites 2 kJ mol^{-1}. Other systems gave similar results, but not benzene in naphthalene, in which the guest prefers to occupy the vacant lattice site centrally. Extension of these methods was made to calculate the packing energies for structures different from those found in crystals grown under normal conditions. Anthracene grows with the $P2_1/a$ structure in the familiar herringbone packing. Structures $P2_1/c$ with face-to-face packing are possible and their energies were calculated. They might lead more readily to dimerization reactions (sec. 3.6). Philip Reynolds (now in the Research School of Chemistry, Australian National University) explored several such alternative packings [140]. The key result is that short chains of misoriented molecules in crystals grown at room temperature might be present in about 1% of crystal, providing loci for photochemical reactions.

3.6 Related Experiments on Photochemical Change in Crystals

In the period 1952-1972 of the development of the theory just described there was activity in the experimental chemistry and photochemistry of the organic solid state, mostly in crystals. Topochemistry [216] was accepted as the mechanism to account for the structure of dimers formed in crystals, in which the dimer was preformed by the arrangement of monomers in the perfect lattice, or in some cases, as in 9-cyanoanthracene, by local disordering [98]. Also it was known that the photodimerization of anthracene at room temperature began at emergent surface dislocations. The need was for study of the connections between disordered lattice packing and the course of photochemical change, including migration to traps of some part of the energy from photon absorption.

Spectroscopic methods seemed best. Many took part, including Aldo Brillante (now Professor of Chemistry, University of Bologna), and Albert Mau (now in the Commonwealth Scientific and Industrial Research Organisation, Australia). It was known that after the initial event of photon absorption leading to exciton formation, some excitons could be trapped in molecules or regions of lower excitation energy. Within the radiative lifetime, before emission or other loss processes, the energy was localized. It could cause photochemical change or be emitted with the frequency characteristic of the trap. Molecules displaced near a vacancy or disorder (X-traps) could be to a degree characterized by their orientation. Some disappeared as photochemistry went on, and could be regenerated by heating, with reversal of the chemistry , suggesting that they were photochemically the active molecules [144].

Among the most interesting outcomes of these studies were the results of Jamjan Rajikan [132] (now professor of chemistry in the University of Science, Malaysia) on the laser-induced spectra at liquid helium temperature of anthracene deliberately doped with 2-hydroxyanthracene. This is a persistent impurity in crystalline anthracene, and signs of it could be seen in almost all the published spectra. Spectra at low temperature showed two distinct traps characteristic of the impurities themselves, each accompanied by satellites thought to be X-traps [217].

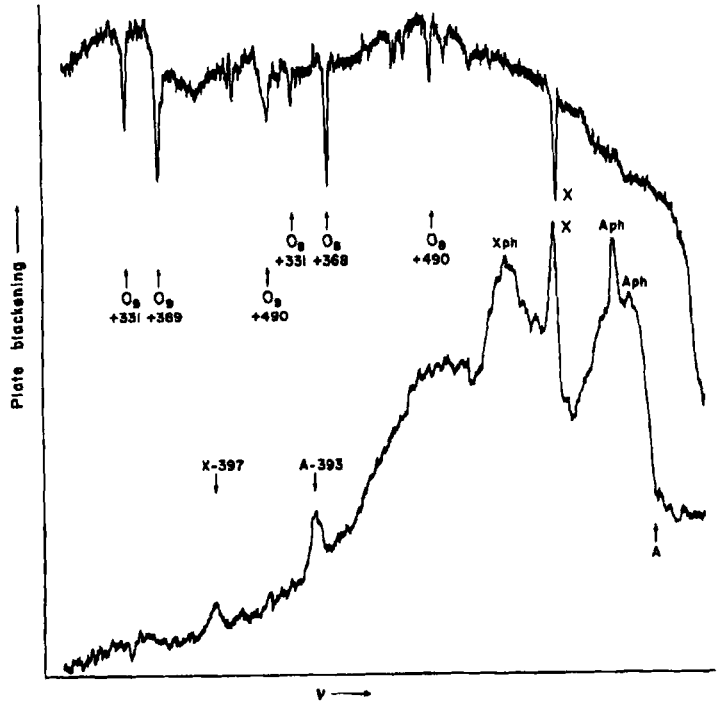

Fig. 2. Absorption (upper) and fluorescence spectra (lower) of anthracene single crystal doped with 2-hydroxyanthracene at about 6K. The X-trap frequencies in absorption and emission are nearly coincident. The X-trap emission is displaced from the X origin by 397 cm^{-1}, showing the emission to be that of a host molecule. O_8 and O_9 belong to the two sites of 2-hydroxyanthracene guests. Reprinted from Chemical Physics Letters, 31, by Brillante, Craig, Mau and Rajikan, 'Optical Absorption by X-traps in Anthracene' pp. 215-219 (1975), with the kind permission of Elsevier Science - NL, Sara Burgerhartsstraat 25, 1055 KV Amsterdam, The Netherlands.

When absorption measurements were made, also at liquid helium temperatures, we showed that for one suspected X-trap the absorption and emission frequencies were coincident within 2 cm^{-1} and that its vibrational intervals corresponded to those of anthracene itself, so confirming the X-trap character. The second X-trap was not found. Moreover we showed [132] that under irradiation the 2-hydroxyanthracene located at one of the trapping sites was destroyed, presumably by joining an anthracene molecule to form a chemically bonded pair, analogous to dianthracene, of which the optical properties were different. Chemical analysis supported the 'mixed pair' interpretation.

When after formation of photoproduct at one of the two sites the crystal was heated and cooled the photoreaction was reversed. We were able to conclude with the help of the packing calculations of sec. 3.2 and other experimental results that those impurity molecules that reacted could not be those that replaced anthracenes in the regular lattice, but must be at dislocations or regions of abnormal packing, where the host and guest were in face-to-face positions. The reaction is thus belongs to the class of the photodimerizations of anthracene, and 9-cyanoanthracene, not of dimers formed topochemically in the normal lattice.

3.7 Advances in Computation

The entire theoretical program of finding the energy levels in the crystal from the properties of free molecules, and that of rationalizing their packing in the crystal, depended on getting the sums over the lattice of the intermolecular energy terms (3.2) and (3.3). It was already an old technical problem that had arisen before in finding the energy of an array of permanent electric dipoles, or more generally multipoles, on a lattice. The methods were either direct summation of (3.2) or (3.3) term by term, or that of Ewald [218] and Kornfeld [219]. In the latter method transforms were found that were rapidly convergent over the direct and reciprocal lattices and added to give the result. Where the sum is over dipoles, for the zero values of the wave vector **k** in (3.1), the result depends on the shape of the volume over which the sum is taken.

The first computations of this type were done taking only molecules within a sphere of radius 2 nm round the target molecule [33]. Computers were not then available. Instead all calculations were done using electro-mechanical calculators. A PhD student could expect to give a third or more of his time to it. The balance between working on theory and routine computation was biased towards the latter.

Working out dipole lattice sums, for any wave vector **k**, became a simpler matter soon after, with computers of the IBM 650 generation, in about 1956-7. Stuart Walmsley (now Reader in Chemistry, University College London) came as my first PhD student after I returned to University College from the University of Sydney in 1956. He had a magic touch with the early computers, and made the first dipole-dipole lattice summations on simple aromatic crystals [220]. Dipole-octupole and octupole-octupole interaction sums were first calculated by Thirunamachandran [221] using the Ferranti Mercury Computer and later extended to quadrupole couplings. These sums are not shape dependent, but were of formidable difficulty at the time.

The coming of computers made a quite extraordinary difference to what was possible. When Ian Ross worked on configuration interaction in the MO theory (loc. cit.) he was already experienced and accurate with electro-mechanical calculating machines, and it is not likely that his time of a full day to extract the lowest eigenvalue of a 9 by 9 CI matrix could have been much bettered. Comparing computational speeds between the early 1950s and the mid 1990s one finds an improvement by a factor of 10^{12} or more.

By 1964 lattice sums were available fairly easily, and the theory of crystal spectra could be worked over critically. Three troublesome features had been in the

background: the representation of transition moments by point moments, the convergence of the multipole series and the coupling of static moments in one molecule to transition moments in others. They could now be dealt with [83]. We showed the degree of sensitivity of results to all three, and suggested how they might be dealt with especially where the dipole-dipole terms were not dominant.

4. INTENSITY BORROWING AND VIBRONIC INTERACTIONS

4.1. In the Benzene 260 nm system

Ingold's analysis of the benzene 260 nm spectrum opened new theoretical pathways, in particular the search to find the nature of the vibrational perturbations that made the electronically forbidden spectrum weakly allowed and to extract information from the intensity distribution along the vibrational progression .

Although the symmetry selection rules allowed any vibration of species E_{2g} of the covering $\mathbf{D}_{6h}$ group to induce intensity in the E_{1u}-A_{1g} transition Ingold had confirmed that one only of the four motions of that symmetry (606 cm^{-1} in the ground state) was effective. The second predominantly skeletal carbon motion at 1596 cm^{-1} barely appeared.

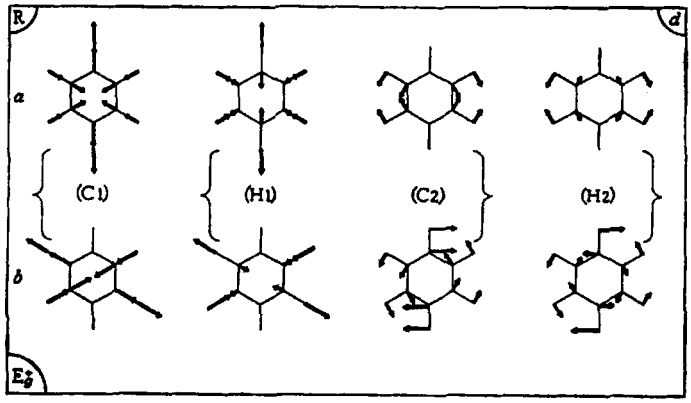

Figure 3. E_{2g} vibration forms of benzene. Reproduced, with permission, from reference [201].

The vibration forms are shown in the figure. Under the molecular force system the actual atomic motions at 606 cm^{-1} closely conform with C1, and at 1596 cm^{-1} with C2. The degenerate components are respectively radial and tangential, only the radial motions being effective. Taking account of the changed potential field of the displaced hexagon one could write for the perturbed B_{2u} upper state [22],

$$\psi'(B_{2u}) = c_1\psi(B_{2u}) + c_2\psi(E_{1u}) \qquad (4.1)$$

with $$\frac{c_2}{c_1} = \frac{\langle \psi(B_{2u}) | V(E_{2g}) | \psi(E_{1u}) \rangle}{\varepsilon(E_{1u}) - \varepsilon(B_{2u})} \qquad (4.2)$$

The ε are electronic energy levels. V is the perturbation caused by the carbon atom displacement in the mode considered. (4.2) is to be averaged over the vibrational motion. The strength of the perturbation was related to the atomic displacements by supposing that while the hexagonal structure of the electron distribution was largely maintained the displaced carbons carried with them in their motion a small effective positive charge. The perturbing potential field was due to electric dipoles of moment equal to this charge multiplied by the displacement.

The 606 cm^{-1} vibration was found to be over 100 times more effective in intensity stealing, in agreement with experiment. Radial displacements destroy the hexagonal symmetry much more effectively than tangential. The second problem, namely the analysis of the distribution of intensity of the 260 nm benzene system along the progression of 992 cm^{-1} is simpler in not needing empirical parameters. The purpose of the analysis is to estimate the change in size of the benzene ring on electronic excitation. Ingold had confirmed that the regular hexagonal structure was maintained; the intensity distribution depended on the overlaps between the ground and excited state vibrations in the totally symmetric vibration mode. Account had to be taken of the frequency change between ground and excited electronic states, and of the associated difference in normal coordinates. In this simple case it was estimated [24] that the ring expanded by 0.0037 nm on excitation, an estimate which was accepted until high resolution spectroscopy enabled analysis of band contours by Callomon, Dunn and Mills giving a value of 0.0038 nm [222].

4.2. The Naphthalene 320 nm System

In the naphthalene spectrum at 320 nm the interpretation hinged on analysis of vibrational interactions in a more complex way. The spectrum is weak, only about ten times stronger than the benzene system in sec. 4.1 already proved to be forbidden electronically. Its assignment to a transition allowed very weakly and intensified by vibrational interaction, appeared likely. McClure [223] had measured the spectrum of naphthalene contained as a dilute impurity in durene. The orientation of the impurity molecules was deduced as that which would cause least disruption to the host lattice.

The directional properties of the naphthalene absorption system pointed to interpenetrating allowed and vibrationally induced bands, the former long-axis and the latter short-axis polarized. There did, however, remain a difficulty. Given the different polarizations the separation between the true and false origin(s) must be the frequency of a nontotally symmetrical vibration. The observed hot band separation however was close to a ground state Raman-active 512 cm^{-1} vibration, known with certainty to be totally symmetrical.

This was the background to a new analysis [60,63,64] of the vapour spectrum of

naphthalene, which was to be coupled to the first calculation for a large molecule of rotational contours. In Sydney, during my period there in 1952-56 Max Redies began the study with a Hilger Large Quartz spectrograph. Elevated temperatures were needed to get enough naphthalene vapour pressure. At times we heated the entire laboratory to 35C, before devising heated cells. The photographic plates at the very limit of their resolution showed that the bands were of two distinct types, single- and double-headed.

In 1956 at University College I was joined by Michael Hollas (later Reader in Chemistry, University of Reading, UK). We were able to use the 20 ft Ebert spectrograph developed by GW King [224]. Ian Ross had placed over the spectroscopy lab door Dante's warning "Abandon hope all ye who enter here". Undeterred, Hollas did enter and found that at the greatly improved resolution the band contours were distinctly different in the origin band and its totally symmetrical progression members on the one hand and in the vibrationally induced false origins and their progressions on the other.

The problem was to connect the contours with the polarization properties of the transitions. Samuel Wait Jr (later Dean of Science at Rensselaer Polytechnic Institute) had joined me from RPI. He set out to compute band contours for the heaviest molecule for which such a calculation had been made. The work was at first done on an IBM 650 by the method of iteration on the continued fraction for levels of the asymmetric rotor, and later on the IBM 704 by matrix diagonalization.

Assumptions had to be made, some of them rather sweeping, on the size and shape of naphthalene in its first electronically excited state. Calculations were made on many different assumptions. The results pointed rather clearly to long-axis polarization for the true origin progression and short-axis for the false origins. The problem of the assignment of the vibration inducing the false origin transitions still remained. It turned out that the critical interval of 506 cm^{-1} was not that of a totally symmetrical vibration as had for a long time been supposed but belonged to a hitherto unknown b_{2g} vibration. The polarization properties of the band system were then understood.

4.3. Totally symmetric vibronic perturbations

Where the molecular covering symmetry is lower than for benzene and naphthalene, for example in the angular three-ring aromatic phenanthrene, there is a new case. Many of the molecular motions are now symmetric under the small number of covering operations. There is then the feature that a given motion may both perturb the electronic structure in a way to bring about mixing between different electronic states, giving intensity stealing, and at the same time form progressions. McClure [225] had found from the crystal spectrum that the first transition in phenanthrene was polarized in-plane along the shorter axis.

R. D. Gordon (later Professor of Chemistry at Queens's University, Ontario) had at this time joined me as an NRC Research Fellow. He measured the first absorption system at 340 nm in the vapour, pure crystal and in mixed crystals in a variety of hosts, for phenanthrene-h_{10} and -d_{10}. Even at high resolution the vapour spectrum yielded little, but at 4 K in the pure crystal there was a splitting of the origin

transition akin to that in naphthalene. Separated from it by 671 cm^{-1} there was a transition with the same polarization property, but showing no splitting, exactly as expected if a totally symmetric vibration were causing intensity stealing from a strong electronic transition of the same symmetry assignment as the 340 nm system. The phenanthrene 340 nm system had also been studied by Hochstrasser and Small [226]. Gerald Small (later Professor of Chemistry, Iowa State University) joined my group when we made the move to the Australian National University in Canberra in 1967. We worked on the theory of totally symmetric vibronic perturbations and showed that the spectrum can be interpreted in detail on this basis [109]. In electronically forbidden systems the transition moment in vibrationally induced transitions is the same in absorption and fluorescence, apart from the effect of the change in the denominator in (4.2). The departure from mirror symmetry is small. The progressions in totally symmetrical vibrations are more or less the same in upward and downward transitions.

4.4 The Adiabatic Approximation

The Born-Oppenheimer Principle in the adiabatic approximation is one among many approximations that are made in molecular theory. The question of how precise is the approximation is not often asked and is difficult to answer. It is often brushed aside. One way to proceed is to compare exact solutions of the full molecular Hamiltonian with solutions found in the adiabatic approximation. It should be possible to test whether the latter solutions approach the former as non-adiabatic corrections are added. It is necessary to work with a Hamiltonian and associated Schrodinger equation that is capable of exact solution.

The problem has not been resolved analytically. Thirunamachandran and I showed that in special cases answers can be given. If we suppose that *both* electronic and vibrational motions are represented as simple harmonic vibrations, and the coupling between them given a sufficiently simple form, then the full Hamiltonian can be solved exactly to find energies and eigenfunctions. These exact solutions can be compared with those found in the adiabatic approximation with non-adiabatic corrections.

By way of example let us take oscillators coupled with a bilinear perturbation, with Hamiltonian,

$$H = \frac{p_x^2}{2m} + \frac{p_y^2}{2M} + \frac{1}{2}m\omega^2 x^2 + \frac{1}{2}M\Omega^2 y^2 + cxy \qquad (4.3)$$

in which x and y are electronic and nuclear coordinates, m and M the masses, and ω and Ω the frequencies. The x-oscillator represents the electronic motion and the y-oscillator the nuclear. Solutions of the Schrodinger equation have to be compared with those in the adiabatic approximation; in that case we first find solutions for an electronic Hamiltonian H_e given by (4.3) without the nuclear kinetic energy. These solutions are for fixed values of the nuclear coordinate y, entering as a parameter. Proceeding in the familiar way the dependence of electronic energy on y defines the potential energy for nuclear motions.

It is well known that (4.3) can be solved exactly, but to make the comparison it is better to solve (4.3) in a perturbation expansion, and take the adiabatic result with non-adiabatic correction. We find agreement at least to terms quadratic in the coupling constant c [186]. It is further possible to show that the adiabatic approximation goes to an asymptotic limit that is not precisely equal to the exact solution, but very close to it even in pathological conditions.

5 MOLECULAR QUANTUM ELECTRODYNAMICS

5.1 Dispersion coupling and chiral interactions

Dirac's 1929 comment [227] 'The underlying physical laws necessary for the mathematical theory for a large part of physics and the whole of chemistry are thus completely known, and the difficulty is only that the exact application of these laws leads to equations much too difficult to be soluble' has become a part of the Delphic wisdom of our subject. To this confident statement Richard Feynman [228] added in 1985 a codicil 'But there was still the problem of the interaction of light and matter', and ' ... the theory behind chemistry is quantum electrodynamics'. He goes on to say that he is writing of non-covariant quantum electrodynamics, for the interaction of the radiation field with the slow-moving particles in atoms and molecules.

I had been made receptive to these ideas a long time before coming across molecular quantum electrodynamics. During the second world war I had the extraordinary good fortune to be posted for a time as ADC to Lieut-General Sir Iven Mackay, a citizen-soldier who served with distinction in the Middle East and New Guinea. He had read physics in Cambridge after the 1914-18 war and before joining the Physics Department in the University of Sydney. We had opportunities to talk physics. He gave me his 1919 copy of the celebrated biography of James Clerk Maxwell [229] and enabled me to meet Julius Adams Stratton, who was on a scientific mission, and whose book [230] remains for me a model of clarity in technical writing. Maxwell's tortured mechanical model of the displacement current was hard to see through. Stratton's vector presentation made it seem easy.

I first learned of the possibilities of quantum electrodynamics in chemical physics from reading a paper by William Simpson [231] on retardation in the interaction of transition dipole moments. He showed that over the entire range of separation distances R the interaction potential of transition dipoles parallel to the intermolcular join is,

$$V^{long}(k,R) = -\frac{1}{2\pi\varepsilon_0 R^3}(\cos kR + kR\sin kR) \qquad (5.1)$$

where k is the transition wavenumber. Now in our work on the excited states of molecular crystals there were problems in the shape dependence of the dipole lattice sums (sec. 3.2), arising from taking the interactions to very large distances, at least.

At University College I had as a colleague EA Power (later Professor of Mathematics, University College London) whose work in quantum electrodynamics

was already well known and later published in an excellent source book [232]. I talked with him on the influence of retardation in this and other intermolecular cases of which the only one then known to us was the Casimir-Polder dispersion calculation [233]. This was the start of a collaboration involving Power, Thirunamachandran, and myself in various combinations. We got out many new results, some of which will be described. Thiru and I later published a book on what we termed Molecular Quantum Electrodynamics [164a].

The importance of retardation has become increasingly recognized in radiation-molecule and molecule-molecule interactions. The combination of quantum mechanics for the electronic structure of molecular systems, and quantum electrodynamics for the interaction of radiation with these systems, and for coupling between them, with retardation automatically allowed for, is among the best theories we have. It is essential at distances beyond a reduced wavelength, and also to get the correct transition between the short range (electrostatic) results and the long range (electromagnetic) ones. Moreover for calculation of the rates of the many so-called 'spontaneous' processes of which the first to be recognized was radiative emission from excited atoms and molecules QED is also essential. Feynman (op. cit.) noted that QED could be used with confidence since "At the present time ... there is no *significant difference* between experiment and theory".

The central feature of QED is that there is a closed system of particles and fields that act on each other, the particles associated with the radiation field being photons. The states of the entire system can be dealt with, and its properties, including rates of transitions in which the number of particles changes, calculated as accurately as desired. Typically in applications to molecules (MQED) the Hamiltonian is written in the form (5.2) with the interaction between molecule and fields separated out as a small term to be treated as a perturbation,

$$H = H_{mol} + H_{rad} + H_{\text{int}} \tag{5.2}$$

The first two terms are the molecular Hamiltonian and the radiation field Hamiltonian. The molecular Schrodinger equation for the first term in (5.2) is assumed solved, with known eigenvalues and eigenfunctions. Solutions for the second term in (3.4) *in vacuo* are taken in second-quantized form. H_{int} can be taken in minimal-coupling form (5.3) allowing for the variation of the radiation field over the extent of the molecule,

$$H_{\text{int}} = \frac{e}{m}\boldsymbol{p}.\boldsymbol{a}(\boldsymbol{q}) \tag{5.3}$$

where $\boldsymbol{p}$ is a sum over particle momenta and $\boldsymbol{a}(\boldsymbol{q})$ the vector potential of the radiation field at position $\boldsymbol{q}$. In dipole approximation, molecule dimensions being assumed small compared with radiation wavelength, an alternative but equivalent form of interaction is (5.4),

$$H_{\text{int}} = -\varepsilon_0^{-1}\boldsymbol{\mu}.\boldsymbol{d}^{\perp} \tag{5.4}$$

μ the transition dipole moment coupled to the transverse displacement field. The matrix elements of (5.3) or (5.4) are enumerated with the help of time-ordered diagrams. An example is given in Fig 4. The first application of molecular QED was Casimir and Polder's calculation of the influence of retardation on the London-van der Waals forces [233]. They showed that at long range the interaction energy is (5.5) in terms of the isotropic static polarizabilities α and has distance dependence R^{-7}. This was not simply an extra term added to the usual R^{-6} dispersion energy, but the new term cancelled and replaced it progressively as the range increased,

$$V(R) = -\frac{23}{4\pi}\hbar c\frac{\alpha(1)\alpha(2)}{R^7} \tag{5.5}$$

Important technical improvements to the methods of non-covariant QED were made by Power and Zienau [234] They showed that the Coulomb-gauge Hamiltonian (5.6) obtained by canonical transformation of the minimal coupling Hamiltonian (5.7) written for the two molecules k and l and their coupling to the radiation field,

$$\mathbf{H} = H_k + H_l + H_{rad} - \varepsilon_0\mu(k).\mathbf{d}^{\perp}(R_k) - \varepsilon_o\mu(l).\mathbf{d}^{\perp}(R_l) - \mathbf{m}(k).\mathbf{b}(R_k) - \mathbf{m}(l).\mathbf{b}(R_l) \tag{5.6}$$

$$\mathbf{H} = H_k + H_l + \mathbf{V}_{kl} + \frac{e}{m}\sum_i \mathbf{p}_i.\mathbf{A}_i(R_k) + \frac{e}{m}\sum_i \mathbf{p}_i.\mathbf{A}_i(R_l) + \frac{e^2}{2m}\mathbf{A}_i^2(R_k) + \frac{e^2}{2m}\mathbf{A}_i^2(R_l) + H_{rad} \tag{5.7}$$

(5.7)

is valid under the conditions of molecule-molecule and molecule-radiation coupling, so generalizing earlier work [235], and opening the way for simpler calculations of chemical systems. In (5.6) and (5.7) $\mathbf{m}$(k) is the magnetic dipole operator, $\mathbf{b}(R_k)$ the magnetic field strength at the molecular position and V_{kl} the electrostatic interaction between the molecules. The Casimir-Polder result (5.5) was recovered in simpler ways, including by application in second order of the perturbation, [113],

$$\mathbf{V} = -\frac{1}{2}\alpha(1)\mathbf{d}^2(1) - \frac{1}{2}\alpha(2)\mathbf{d}^2(2) \tag{5.8}$$

quadratic in the displacement vector at the positions of the molecules. It was also generalized to anisotropic polarizabilities.

The methods were straightforward to use for chiral molecules generally, as discussed in sec 6, [116], and for particular applications such as circular dichroism induced by a chiral neighbour [138].

5.2 The resonance interaction and excitation exchange

The resonance coupling between a pair of identical atoms or molecules, one in an excited state, is of profound importance in chemical physics. It was first given in the form (5.9) by McLone and Power [236], and is a generalization of (5.1),

$$V_{ij}(k,R) = \frac{1}{4\pi\varepsilon_0 R^3}\left[\ \beta_{ij}(\cos kR + kR\sin kR) - \alpha_{ij}k^2R^2\cos kR\ \right] \quad (5.9)$$

where β_{ij} is the dyadic (5.10) and α_{ij} the transverse coupling dyadic (5.11),

$$\beta_{ij} = \delta_{ij} - 3\hat{R}_i\hat{R}_j \quad (5.10)$$

$$\alpha_{ij} = \delta_{ij} - \hat{R}_i\hat{R}_j \quad (5.11)$$

and k the wave number for the transition. As we would expect, the result (5.9) is the same as the classical expression for the coupling of a source antenna to a receiver antenna tuned to the same frequency, found by solving Maxwell's equations.

Resonance transfer is the process in which incident radiant energy absorbed by one molecule is transferred through the potential (5.9) to an identical partner. At distances of less than a reduced wavelength ($\lambda/2\pi$) the coupling is electrostatic; at long distances it is electromagnetic in an emission-absorption event, as in a gas, or in most practical cases, in solution. The microscopic starting point is the problem of pairwise transfer at any distance, as modified by other molecules present. Solution of this problem should lead to a theory of the absorption spectrum of molecules in solution in full detail, band structure and absorption coefficient.

The parent problem is to find the effect on resonance coupling of a third body [176]. At short distances photon exchange between excited and unexcited molecules is very fast, and we have to think of A and B in a stationary state <A*B+AB*> , where the star denotes an excited molecular state. The direct matrix element for the A-B coupling in the near-zone is,

$$M_{fi}^{direct} = \frac{1}{4\pi\varepsilon_0|S|^3}\mu_j^{0n}(A)\ \mu_j^{n0}(B)\left(\delta_{ij} - 3\hat{S}_i\hat{S}_j\right) \quad (5.12)$$

and for indirect coupling through a third molecule C,

$$M_{fi}^{indir} = \frac{1}{\left(4\pi\varepsilon_0\right)^2 R^3R'^3}\mu_i^{0n}(A)\mu_j^{n0}(B)\alpha_{kl}(C;k)\left(\delta_{il} - 3\hat{R}_i\hat{R}_l\right)\left(\delta_{jk} - 3\hat{R}'_j\hat{R}'_k\right) \quad (5.13)$$

$\boldsymbol{R}$ and $\boldsymbol{R}'$ are the positions of A and B relative to C, and $\boldsymbol{S} = \boldsymbol{R}_B - \boldsymbol{R}_A$. For AB separation of 4 nm, and C midway between the ratio direct/indirect can be as much as 20:1. In a physical situation summation is required over all C, which will determine how significant the indirect mechanism is.

Similarly the parent problem for fluorescence of phosphorescence emission in dilute gases or solution is the influence of coupling to foreign molecules on spontaneous emission [189]. The emission rate for an isolated molecule A is given by the Einstein A coefficient,

$$A = \frac{\omega^3 \mu^3}{3\varepsilon_0 \pi \hbar c^3} \tag{5.14}$$

where ω and μ are the frequency and transition dipole moment. In the presence of another molecule B, not resonant with A, the emission rate is modified. The time-ordered diagrams to give the matrix elements are shown in Fig 4.

The top diagram is for spontaneous emission, in which B is passive, leading to the Einstein rate in (5.14). In the third order the lower six diagrams apply, with three interaction vertices. The influence of molecule B in this order introduces dependence on the molecular separation $\boldsymbol{R}$.

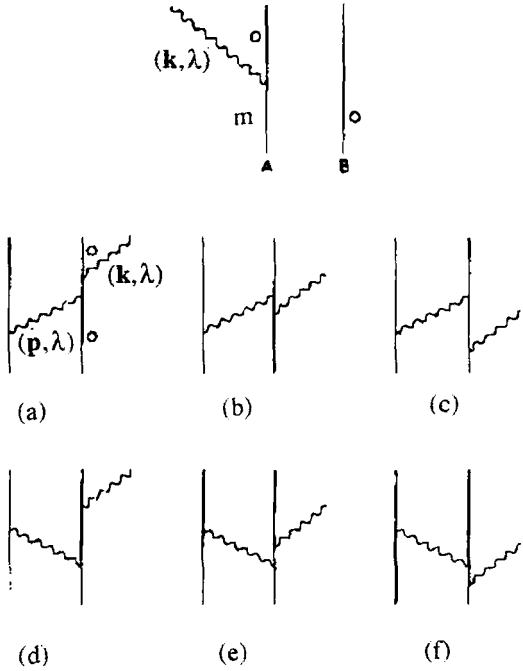

Fig. 4. First-order (top) and third-order (lower six) time ordered diagrams for spontaneous emission by molecule A in the presence of B. Reproduced from reference [189], by permission of Messrs Taylor and Francis.

The leading contribution to the emission rate is through the cross term for the first and third order matrix element,

$$\Gamma_{1-3} = \frac{\omega_{m0}^3}{12\pi^2\varepsilon_0^2\hbar c^3 R^3}\left|\mu_{m0}(A)\right|^2 \alpha^B(\omega_{m0}) \times\left(kR\sin 2kR + 2\cos 2kR - \frac{5\sin 2kR}{kR} - \frac{6\cos 2kR}{k^2R^2} + \frac{3\sin 2kR}{k^4R^4}\right) \tag{5.15}$$

Expression (5.15) has a remarkable property. To find its behaviour at short distances (near zone) we expand and go to the small kR limit. There is no kR-independent term; the leading term is in k^2R^2, giving for the short-range result, with k given its value on the energy shell k^{m0},

$$\Gamma_{1-3}^{\lim} = \frac{11\omega_{m0}^5}{90\pi^2\varepsilon_0^2\hbar c^5 R}\left|\mu_{m0}(A)\right|^2 \alpha_B(\omega_{m0}) \tag{5.16}$$

There is thus no static limit. At all distances the cross-term correction is purely radiative. Its value is of order 10^{-6} times the A-coefficient at 0.5 nm separation distance.

6. INTERACTIONS BETWEEN CHIRAL SYSTEMS.

6.1 Chiral Discrimination.

Professor DP Mellor was my master's degree supervisor. He had been a co-worker of Linus Pauling at Cal Tech working on magnetochemistry. He also studied metal chelates, some of which were chiral. We were discussing in about 1953 our colleague FP Dwyer's new results on chiral discrimination, published in 1956 [237]. He challenged me to find a way to describe the external field of a chiral system, that would allow the calculation of the 'discrimination energy'; in the simplest case this is the energy difference between a dextro-laevo and a dextro-dextro pairwise coupling energy. My collaborators and I worked on and around this problem for several years. Some time later it gave me pleasure to write with Mellor a review of the full range of discriminating interactions [139].

Many of the clearest examples of chiral discrimination then known depend on properties of crystals, such as the difference of melting point between (+) tartaric acid (170C) and racemic acid (204C) [238]. Differences in packing energies, determined by short-range, or contact, interactions are responsible. The influence of longer-range forces was suggested by differences in redox potentials in systems of enantiomeric complex cations in the presence of a second species of chiral ion [237]. Another case, not involving a solid-liquid interface, is the effect on the rate of racemization of an initially optically pure compound of the presence of a second chiral species. The stimulus was to deal theoretically with the entire range of external fields of chiral systems.

In the days of Mellor's challenge the electrostatic field seemed likely as the mechanism by which chiral information is conveyed. It would be contained in the multipole expansion of expression (3.4). PE Schipper (later in the Department of Theoretical Chemistry, University of Sydney) and I looked at this expansion [131] to select multipole components that were chiral, that is to say components that lacked symmetry to improper rotations. The multipole components (6.1) transform under the operations of inversion (i), reflection (σ_h,σ_v), and rotation (iC_p) as spherical harmonics according to (6.2),

$$Q(nl) = \sum_j e_j r_j^n P_n^l\left(\cos\theta_j\right)\exp\left(il\phi_j\right) \tag{6.1}$$

$$\begin{aligned} iQ(nl) &= (-1)^n Q(nl) \\ \sigma_h Q(nl) &= (-1)^{l+n} Q(nl) \\ \sigma_v Q(nl) &= Q(n,-l) \\ iC_p Q(nl) &= \exp(2\pi il/p) Q(nl) \end{aligned} \tag{6.2}$$

e_i and r_i are respectively the charge and position of the i-th particle and the P_n^l associated Legendre polynomials. The relations (6.2) can be used to show that every multipole component is symmetric to at least one improper rotation. It follows that a combination of two moments is the least requirement for chirality, one of even order and one of odd. The simplest that includes a dipole is a combination with a quadrupole moment, but with the dipole axis not coincident with a quadrupole axis. We called this source a skewed dipole-quadrupole.

The quadrupole contribution to intermolecular energy drops as the inverse fifth power of the distance and the chiral property of the field is lost as the quadrupole component of the field dies away. It is in any case of interest only at short distances, influencing the packing in crystal formation, or in contacts between ionic or molecular species in solutions. At separations long enough to allow free molecular rotation all electrostatic interactions vanish. To make a more comprehensive study of interactions capable of conveying chiral information including those that persist when the sources are freely rotating we need to begin with the complete Hamiltonian (5.7) for a pair of molecules, including the radiation field (see also sec. 5).

There are some technical reasons for preferring the multipolar form for the interaction terms (see, for example, [164a] written as,

$$\mathbf{H} = H_k + H_l + H_{rad} - \varepsilon_0 \mu(k).\mathbf{d}^{\perp}(R_k) - \varepsilon_o \mu(l).\mathbf{d}^{\perp}(R_l) - \mathbf{m}(k).\mathbf{b}(R_k) - \mathbf{m}(l).\mathbf{b}(R_l) \tag{6.3}$$

in which the entire coupling between molecules is mediated by the radiation field. The μ and $\boldsymbol{m}$ operators apply to electric and magnetic dipole moments.

Mavroyannis and Stephen [239] were the first to show that between freely rotating molecules there is a discrimination energy from terms in the total dispersion energy arising from virtual magnetic dipole transitions. A general theory, with this as a

special case was given by us later [117]. Discrimination depends on the rotatory strength $R^{t0}{}_{ij}$ tensor for a molecular transition *t-0*,

$$R_{ij}^{t0} = \mathrm{Im}\ \mu_i^{0t} m_j^{t0} \tag{6.4}$$

Replacement of the molecule by its optical enantiomer changes the sign of (6.5) so that in the term in the dispersion energy (6.6) that depends on electric-magnetic coupling changes sign when one molecule is replaced,

$$\Delta E_{E-M} = \frac{1}{8\pi^2 \varepsilon_0^2 c^2 R^6} \beta_{ik} \beta_{jl} \sum_{r,s} \frac{R_{ij}^{r0} R_{kl}^{s0}}{E_{r0} + E_{s0}} \tag{6.5}$$

R is the separation distance and

$$\beta_{ij} = \delta_{ij} - 3\hat{R}_i \hat{R}_j \tag{6.6}$$

is the dyadic for full dipolar coupling, with Kronecker delta and components of the unit vector along the intermolecular join. The discrimination energy is smaller by three orders of magnitude or less than the usual (electric-electric) dispersion energy at the same separation. For freely rotating molecules the energy becomes,

$$\Delta E_{\mathrm{E-M}} = \frac{\hbar^3 c}{3\pi^3 \varepsilon_0^2 R^9} \sum_r \frac{R^{r0}}{E_{r0}^2} \sum_s \frac{R^{s0}}{E_{s0}^2} \tag{6.7}$$

Other averages were also worked out. At very long separation distances we are used to the idea that the usual dispersion energy going as the inverse sixth power of distance is *replaced* by the Casimir-Polder inverse seventh power coupling entirely due to the radiative terms in the interaction. Likewise it was shown [117] that the electric-magnetic term (6.8) is replaced at very long range by (6.8),

$$\Delta E_{\mathrm{E-M}} = \frac{\hbar^3 c}{3\pi^3 \varepsilon_0^2 R^9} \sum_r \frac{R^{r0}}{E_{r0}^2} \sum_s \frac{R^{s0}}{E_{s0}^2} \tag{6.8}$$

The resonance coupling (sec. 5.2) between identical molecules, one in an excited state, has a discriminating component, in the case that the molecules are optically active. The source of this term is emission or absorption by one molecule through the magnetic dipole transition dipole moment, with absorption or emission by the electric dipole of the other. This is a purely radiative discriminating interaction with no short-range static limit, and is very small. We estimated a magnitude of up to 0.1 cm^{-1}. Its value is given in (6.9) for limiting short distances,

$$\varepsilon_{E-M} = \varepsilon_{ijk} \hat{R}_k \frac{1}{\lambda R^2} \left\{ \langle n^a | \mu_i | 0 \rangle + \langle n^b | \mu_i | 0 \rangle + \langle 0 | i m_j | n^b \rangle + \langle 0 | i m_j | n^a \rangle \right\} \tag{6.9}$$

where ε_{ijk} is the alternating tensor and the reduced wavelength appears in the denominator.

6.2 Promotion of chiral effects by Jahn-Teller Coupling

Molecules belonging to the symmetry groups $\mathbf{D}_{2d}$ and $\mathbf{S}_4$ are achiral. There is the interesting possibility that after excitation to degenerate upper states they may be unstable and collapse into structures that are chiral. The instability is Jahn-Teller in nature, the ground state symmetry being too high to support electronic degeneracy in molecules with certain vibrational degrees of freedom. It was explored in about 1974 [137] by Peter Stiles (now Assoc. Prof of Chemistry at Macquarie University). Examples in simple molecules are allene and spiro[4,4]nonatetraene. In allene the line of the three carbons is the rotary-reflection axis of the $\mathbf{D}_{2d}$ group. After electronic excitation to the degenerate upper state allene is unstable to torsion about this axis, and collapses to one of two new equilibrium positions of equal energies of the chiral group $\mathbf{D}_2$.

The Hamiltonian for the molecules including the Jahn-Teller instability is,

$$H = H^{el} + \sum_{i=1.2}\left[-\frac{\hbar^2}{2m_i}\frac{\partial^2}{\partial q_i^2} + \frac{1}{2}k_i q_i^2 + L_i q_i + \ldots\right] \qquad (6.10)$$

where H^{el} is the Hamiltonian for the undisplaced structure. The masses and displacements in the square brackets apply to displacements in the i-th vibrational mode, k_i and L_i are respectively the harmonic force constant and the linear (Jahn-Teller) vibronic coupling coefficient.

We had the help of the Bologna theoretical group with whom I had a long association. Palmieri, Zauli, Styles and I calculated that in spirononatetraene the magnitude of the Jahn-Teller instability is a torsional displacement of 2.5° and a well depth 110 cm^{-1} [149]. One would expect that the molecule would acquire chirality by induction when dissolved in one enantiomer of a chiral substance, in which one torsionally displaced form would be stabilized below the other. Efforts have been made to verify this. The spectra are complex and have not yet been analyzed in enough detail.

7. d-ORBITALS IN VALENCE BINDING

The studies described in sec. 2.3 on of dπ orbitals in conjugated systems went along with another line of enquiry, on the question of the tendency of second row elements to display their higher covalencies, five in the case of phosphorus, six in sulphur, towards the more electronegative first row elements. Pauling had proposed the use of d-orbitals in bonds in his classic 1931 paper [240].

The work of Maccoll, Nyholm, Orgel, Sutton and myself [38,39] had its starting point in the calculation of overlap integrals for atoms in which d-orbital bonding seemed important, as in SF_6, where an atomic configuration in sulfur of sp^3d^2 was indicated. The view that the strength of a covalent bond could be given a rough measure in terms of the overlap integral between the bonded orbitals had been proposed by Maccoll [241]. He had shown that in bonds to carbon the bond

dissociation energy was correlated with the overlap integral in the sequence of hybrids $sp>sp^2>sp^3$.

Now if the 3d Slater orbitals were assigned exponents according to Slater's rules the overlaps for σ-type bonds were found to be far too small to contribute to binding, according to the accepted views of the time. The small exponents were an expression of the high degree of screening of the nuclear charge by other electrons, so that the d-electrons felt only a small effective charge, and were diffuse. For π-bonds d-orbital participation was more favourable, as in the phosphazenes (sec. 2.3).

For σ-bonding the physical picture was developed [36,45,47,71,72] that the diffuse orbitals were contracted by the presence of adjacent electronegative atoms like F or O. These ligand atoms acted in first approximation as positive charges, the size of the charge being related to the electronegativity. One had the concept of 'orbital contraction' added to covalent bonding through overlap. Although it was difficult to make convincing estimates of the charges to be taken to be equivalent to the outer electron electronegativities the theory gave a physical picture that was much used at the time.

8. **Conclusion.**

In a journey beginning now travellers in quantum chemistry could look forward to a new range of problems. There are new ways of solving them, Computational Chemistry being the leading example; it is a subject in its own right, going forward magisterially with advances in computer power, realizing calculations that fifty years ago were dismissed as wildly out of reach, such as plotting decomposition pathways, and predicting structures of stable and metastable species.

Many of the new tasks would be at the boundary with materials science. There are some that are obviously applications-oriented, like the electronic theory of high temperature superconduction in the layered copper-oxide perovskites, and other aspects of nanotechnology. There are also fundamental valence problems, such as accounting for the structures and properties of quasicrystals. Why is the association of transition metals and aluminium apparently of central importance? How do we deal with the valence properties of systems where the free energy of formation or phase transition is dominated by the entropy term?

However thinking of what is apparent now is a poor guide. How are we going to be *surprised?* Where is the 'undiscovered land'? That is where the excitement will come from, in the new that could not have been foreseen, even in the most ingenious extrapolation, from the old.

It is also possible to be surprised in retrospect. In the days when requests for reprints measured the interest in a published paper Charles Coulson told me that he was many a time perplexed to find that papers he had tossed off in an afternoon proved to be so popular that he quickly exhausted his reprint supply. Others with results that had been hard to get and that he thought important seemed to pass by unnoticed and wither on the vine. It is a common experience. Paper [49] with

Norman Paddock on $p\pi$-$d\pi$ delocalization in ring systems caused something of a stir. There was a nice element of surprise. It was written in a few hours. Papers [103, 116] with Thirunamachandran, on a new approach to the definition and evaluation of the valence state, were built on novel solutions to old problems and were quite difficult. They were barely noticed. We could account for it only on the ground that sophisticated approximations of that class were being replaced by computations.

While we have seen a great forward movement in the technical side of quantum chemistry, indeed in science as a whole, it would be hard to establish a claim that research in basic science enjoys more outside esteem, or is better supported, than 50 years ago. Attitudes have changed little from the time of Benjamin Franklin's famous 'What is the use of a new born baby' to the question 'what is the use of your new discovery?'. In the words of Benedetto Croce, speaking of liberty, basic science leads 'a dangerous and fighting life', in which each generation of scientists has to find its own new way to keep a place in the sun.

More good companions. The list of research enterprises is far from complete. In a longer one I would have been able to mention Don Akon, David Bishop, Bob Bray, John Christie, Tom Claxton, Michael Collins, Peter Dacre, Graham Doggett, Gad Fischer, Graham Chandler, Margaret Clarke, Len Dissado, Ian Elsum, Ray Lindsay, Robert Maclagan, Eric Magnusson, Chris Mallett, Bruce Markey, Peter Petelenz, Michael Philpott, John Ogilvie, David Santry, Piero Sarti-Fantoni, Bat-Sheva Sommer, Jai Singh, and John Walsh.

It has been a good journey.

Acknowledgments. I have been greatly helped by Prof Ian Ross, Dr T Thirumamachandran, Prof Allan Maccoll, and by family members, Andrew, Hugh, Mary Louise and Douglas Craig, and, above all, by my wife Veronica.

References.

1. Magnetic Studies of Coordination Compounds: Factors Affecting the Nature of Bonds Between Nickel and Certain Non-Metallic Atoms.
D.P. Mellor and D.P. Craig.
J. Roy. Soc. N.S.W., 74, 475-494 (1940).

2. Magnetic Studies of Coordination Compounds: Square Coordinated Cobalt Compounds.
D.P. Mellor and D.P. Craig.
J. Roy. Soc. N.S.W., 74, 495-501 (1940).

3. Magnetic Studies of Coordination Compounds: Binuclear Copper Derivatives of Diphenyl-Methylarsine.
D.P. Mellor and D.P. Craig.
J. Roy. Soc. N.S.W., 75, 27-30 (1941).

4. The Magnetic Behaviour of Potassium Cyanonickelite.
D.P. Mellor and D.P. Craig.
J. Roy. Soc. N.S.W., 76, 281-282 (1942).

5. A Note on the Nitrosyl Group in Metal Complexes.
D.P. Mellor and D.P. Craig.
J. Roy. Soc. N.S.W., 78, 25-27 (1944).

6. Some Difficulties in the Lewis and Calvin Theory of Light Absorption.
D.P. Craig.
J. Roy. Soc. N.S.W., 79, 160-163 (1945).

7. Absorption Spectra of Acridines: Aminoacridines.
D.P. Craig and L.N. Short.
J. Chem. Soc., 419-422 (1945).

8. A Note on the Magnetic Behaviour of Verdohaemochromogen.
D.P. Mellor and D.P. Craig.
J. Roy. Soc. N.S.W., 78, 258-259 (1946).

9. Absorption Spectra of Acridines: Steric Interference with Ionization.
D.P. Craig.
J. Chem. Soc., 534-537 (1946).

10. Electronic Structure of Fulvene.
C.A. Coulson, D.P. Craig and A. Maccoll.
Proc. Phys. Soc., 61, 22-30 (1947).

10a. P-Quinodimethane and its Diradical.
C.A. Coulson, D.P. Craig, A. Maccoll and Mme. A. Pullman.
Disc. Far. Soc., No. 2 36-38 (1947).

11. Energy Levels of Naphthalene.
D.P. Craig.
Proceedings of the International Congress of Pure and Applied Chemistry.
London, 11, 411-418 (1947).

12. The Non-Benzenoid Aromatic Hydrocarbon Pentalene.
D.P. Craig and A. Maccoll.
Nature, 161, 481 (1948).

13. On Some Problems in the Study of Excited Molecular States of Aromatics.
D.P. Craig.
Comptes Rendus, 227, 126-128 (1948).

14. Energy Levels of Aromatic Hydrocarbons.
D.P. Craig.
J. Chem. Phys., 17, 1358 (1949).

15. The Low Excited States of Simple Aromatic Hydrocarbons.
D.P. Craig.
Disc. Far. Soc., 9, 5-14 (1950).

16. The Non-Benzenoid Aromatic Hydrocarbon Pentalene. A Theoretical Discussion.
D.P. Craig and A. Maccoll.
J. Chem. Soc., 964-971 (1949).

17. On the Assignment of the Triplet-Singlet Emission of Benzene.
D.P. Craig.
J. Chem. Phys., 18, 236-237 (1950).

18. Polar Structures in the Theory of Conjugated Molecules. I. Identification of the Ethylene π-Electron States.
D.P. Craig.
Proc. Roy. Soc., A200, 272-283 (1950).

19. Polar Structures in the Theory of Conjugated Molecules. II. Symmetry Properties and Matrix Elements for Polar Structures.
D.P. Craig.
Proc. Roy. Soc., A200, 390-401 (1950).

20. Polar Structures in the Theory of Conjugated Molecules. III. The Energy Levels of Benzene.
D.P. Craig.
Proc. Roy. Soc., A200, 401-409 (1950).

21. Configurational Interaction in Molecular Orbital Theory. A Higher Approximation in the Non-Empirical Method.
D.P. Craig.
Proc. Roy. Soc., A200, 474-486 (1950).

22. The Role of E_{2g} Vibrations in the 2600A Band System of Benzene.
D.P. Craig.
J. Chem. Soc., 59-62 (1950).

23. Electronic Levels in Simple Conjugated Systems. I. Configuration Interaction in Cyclobutadiene.
D.P. Craig.
Proc. Roy. Soc., A202, 499-506 (1950).

24. The Franck-Condon Principle and the Size of the Excited Benzene Molecule.
D.P. Craig.
J. Chem. Soc., 2146-2151 (1950).

25. Molecular Orbital Calculations of Benzene, Configuration Interaction included.
R.G. Parr, D.P. Craig and I.G. Ross.
J. Chem. Phys., 18, 1561-1563 (1950).

26. On Cyclobutadiene and Some Other pseudo-Aromatic Compounds.
D.P. Craig.
J. Chem. Soc., 3175-3182 (1951).

27. Electronic Levels in Simple Conjugated Systems. III. The Significance of Configurational Interaction.
C.A. Coulson, D.P. Craig and J. Jacobs.
Proc. Roy. Soc., A206, 297-308 (1951).

28. The Intensity of the A_{1g}-E_{1u} Transition in Benzene.
C.W.L. Bevan and D.P. Craig.
Trans. Far. Soc., 47, 564-569 (1951).

29. On the Assignment of the Naphthalene Bands at 3200-2900A.
D.P. Craig and L.E. Lyons.
J. Chem Phys., 20, 1499-1500 (1952).

30. Polarization of the Second Ultraviolet System in Hexamethylbenzene.
D.P. Craig and L.E. Lyons.
Nature, 169, 1102 (1952).

31. Aromatic and Pseudo-Aromatic Hydrocarbons.
D.P. Craig.
J. de Chim. Phys., 49, 143-146 (1952).

32. The Electronic Spectra of the Simple Aromatic Hydrocarbons.
D.P. Craig.
Revs. Pure and Appl. Chem., 3, 207-240 (1953).

33. Polarized Ultraviolet Absorption of Anthracene.
D.P. Craig and P.C. Hobbins.
Nature, 171, 566 (1953).

34. Some Aspects of the Ultraviolet Spectroscopy of Simple Aromatic Molecules.
D.P.Craig.
Boll. Sci. della Fac. Chim. Ind. Bologna, 11, 1-5 (1953).

35. Non-equivalent Zinc Bonds in Chalcophanite.
D.P. Craig and A.D. Wadsley.
J. Chem. Phys., 22, 346-347 (1954).

36. Orbital Contraction in the Theory of Metal Complexes.
D.P. Craig.
Revs. Pure and Appl. Chem., 4, 4-14 (1954).

37. Assignment of the Intense Acene Absorption Systems.
D.P. Craig, P.C. Hobbins and J.R. Walsh.
J. Chem. Phys., 22, 1616-1617 (1954).

38. Chemical Bonds Involving d-Orbitals. Part I.
D.P. Craig, A. Maccoll, R.S. Nyholm, L.E. Orgel and L.E. Sutton.
J. Chem. Soc., 332-353 (1954).

39. Chemical Bonds Involving d-Orbitals. Part II.
D.P. Craig, A. Maccoll, R.S. Nyholm, L.E. Orgel and L.E. Sutton.
J. Chem. Soc., 354-357 (1954).

40. The Triplet-Triplet Absorption Spectra of Some Aromatic Hydrocarbons and Related Substances.
D.P. Craig and I.G. Ross.
J. Chem. Soc., 1589-1606 (1954).

41. The Polarized Spectrum of Anthracene. Part I. The Assignment of the Intense Short Wave-Length System.
D.P. Craig and P.C. Hobbins.
J. Chem. Soc., 539-548 (1955).

42. The Polarized Spectrum of Anthracene. Part II. Weak Transitions and Second-Order Crystal Field Perturbations.
D.P. Craig.
J. Chem. Soc., 2302-2308 (1955).

43. The Polarized Spectrum of Anthracene. Part III. The System at 3800A.
D.P. Craig and P.C. Hobbins.
J. Chem. Soc., 2309-2319 (1955).

44. The Kinetics of Isotope Exchange Reactions.
C.A. Bunton, D.P. Craig and E.A. Halevi.
Trans. Far. Soc., 51, 196-204 (1955).

45. d-Orbital Contraction in Chemical Bonding.
D.P. Craig and E.A. Magnusson.
J. Chem. Soc., 4895-4909 (1956).

46. Intermolecular Effects in Napthalene Crystal Spectra.
D.P. Craig and J.R. Walsh.
J. Chem. Phys., 24, 471-472 (1956).

47. Atomic Orbital Modification in Molecule Formation.
D.P. Craig and E.A. Magnusson.
J. Chem. Phys., 25, 383-384 (1956).

48. Exciton Shape Dependence and Davydov Splitting in Aromatic Crystals.
D.P. Craig and J.R. Walsh.
J. Chem. Phys., 25, 588-589 (1956).

Book. Theoretical Chemistry, Looking Before and After.
48a. D.P. Craig
H.K. Lewis (London) 1957.
See also Chem. and Ind. 3 - 7 (1958).

49. A Novel Type of Aromaticity.
D.P. Craig and N.L. Paddock.
Nature, 181, 1052-1053 (1958).

49a. The Place of Chemistry. VIII. In Australia.
D.P. Craig and R.S. Nyholm
Proc. Chem. Soc., 135, May 1958.

50. Calculations of the Crystal Spectra of Benzene and Naphthalene.
D.P. Craig and J.R. Walsh.
J. Chem. Soc., 1613-1623 (1958).

51. Orbital Modification in Metal Complexes.
D.P. Craig and E.A. Magnusson.
Disc. Far. Soc., 26, 116-122 (1958).

52. Orbital Size and Bond Type in Sulphur Compounds.
D.P. Craig.
Chem. Soc. Spec. Publ., 12, 343-360 (1958).

53. Upper Limit to the Intensity of the 3400A Singlet-Triplet Absorption in Benzene.
D.P. Craig, J.M. Hollas and G.W. King.
J. Chem. Phys., 29, 974 (1958).

54. Modified Atomic Orbitals in Molecular Wave Functions.
D.P. Craig.
Calcul des Fonctions d'onde Moleculaire, Editions du Centre National de la Recherche Scientifique, Paris, 63-72 (1958).

55. Quantum Organic Chemistry.
D.P. Craig.
Chem. Soc. Ann. Rep., 55, 168-178 (1958).

56. Aromatic Character.
D.P. Craig.
Proceedings of the Kekulé Symposium. Butterworths, London, 20-34 (1958).

57. Aromaticity.
D.P. Craig.
Non-Benzenoid Aromatic Compounds. Ed. Ginsburg. Interscience, New York, 1-42 (1959).

58. Delocalization in pπ-dπ Bonds.
D.P. Craig.
J. Chem. Soc., 997-1001 (1959).

59. The Crystal Spectrum of Vibrationally Induced Transitions: the Naphthalene 3200A System at 40K.
D.P. Craig, L.E. Lyons, S.H. Walmsley and J.R. Walsh.
Proc. Chem. Soc., 389-390 (1959).

60. The Vapour Absorption Spectrum of Naphthalene at 3200A.
D.P. Craig, J.M. Hollas, M.F. Redies and S.C. Wait.
Proc. Chem. Soc., 361-362 (1959).

61. The Calculation of Basis Atomic Orbitals for Molecular Wave Functions.
D.P. Craig and C. Zauli.
Gazz. Chim. Ital., 90, 1700-1711 (1960).

61a. Aromatic Character and the Inorganic Aromatics.
D.P. Craig.
Suomen Kemistilehti A33, 142 (1960).

62. Delocalization and Magnetic Properties of the Phosphonitrilic Halides.
D.P. Craig, M.L. Heffernan, R. Mason and N.L. Paddock.
J. Chem. Soc., 1376-1382 (1961).

63. Analysis of the Naphthalene Vapour Absorption Bands at 3200A. I. Naphthalene h-8.
D.P. Craig, J.M. Hollas, M.F. Redies and S.C. Wait.
Phil. Trans. Roy. Soc., A253, 543-568 (1961).

64. Analysis of the Napthalene Vapour Absorption Bands at 3200A. II. Naphthalene d-8.
D.P. Craig and J.M. Hollas.
Phil. Trans. Roy. Soc., A253, 569-581 (1961).

65. Weak Transitions in Molecular Crystals.
D.P. Craig and S.H. Walmsley.
Electrical Conductivity in Organic Solids. Eds. Kallman and Silver. Interscience, New York, 163-181 (1961).

66. The Crystal Spectra of Very Weak Transitions. I. Measurements of the Naphthalene 3200A System at 40K.
D.P. Craig, L.E. Lyons and J.R. Walsh.
Mol. Phys., 4, 97-112 (1961).

67. The Crystal Spectra of Very Weak Transitions. II. Theoretical.
D.P. Craig and S.H. Walmsley.
Mol. Phys., 4, 113-124 (1961).

68. Crystal Splitting of the Anthracene 3800A System.
T.A. Claxton, D.P. Craig and T. Thirunamachandran.
J. Chem. Phys., 35, 1525-1526 (1961).

69. Intermolecular Interactions in Mixed Crystals.
D.P. Craig and T. Thirunamachandran.
Proc. Chem. Soc., 253 (1961).

Book. Compound, Homopolar, and other entries.
69a. D.P. Craig
Encyclopaedic Dictionary of Physics, Pergamon, Oxford.

70. The Ultraviolet Spectra of Molecular Crystals.
D.P. Craig.
Advances in Molecular Spectroscopy. Ed. Mangini, Pergamon Press, Oxford, London, 16-28 (1962).

71. d-Orbitals in Compounds of Second-Row Elements. I. SF_4.
D.P. Craig and C. Zauli.
J. Chem. Phys., 37, 601-608 (1962).

72. d-Orbitals in Compounds of Second-Row Elements. II. Comparison of H, C, F, and Cl as Ligands.
D.P. Craig and C. Zauli.
J. Chem. Phys., 37, 609-615 (1962).

73. Electron Distribution in Cyclic $p\pi$-$d\pi$ Systems.
D.P. Craig and N.L. Paddock.
J. Chem. Soc., 4118-4133 (1962).

74. The electronic Spectra of Mixed Crystals.
D.P. Craig and T. Thirunamachandran.
Proc. Roy. Soc., A271, 207-217 (1963).

75. Some Recent Developments in the Exciton Theory.
D.P. Craig and T. Thirunamachandran.
Boll. Sci. della Fac. Chim. Ind. Bologna, XXI, 15-22 (1963).

76. Theoretical Basis of the "Rare-Gas Rule".
D.P. Craig and G. Doggett.
J. Chem. Soc., 4189-4198 (1963).

77. The Inductive Effect in the Anilinium Ion.
D.M. Bishop and D.P. Craig.
Mol. Phys., 6, 139-151 (1963).

78. Visible and Ultraviolet Absorption by Molecular Crystals.
D.P. Craig and S.H. Walmsley.
Physics and Chemistry of the organic solid state. Eds. Fox, Labes and Weissberger, Interscience, New York, 585-655 (1963).

79. The Nature of the Metal-Ligand Bond.
D.P. Craig and R.S. Nyholm.
Chelating Agents and Metal Chelates, Eds. Dwyer and Mellor. Academic Press, Ch. 2, p. 51-93 (1964).

80. Note on the Absorption and Fluorescence of Crystalline Naphthalene.
D.P. Craig and H.C. Wolf.
J. Chem. Phys., 40, 2057-2059 (1964).

81. Triplet-Triplet Polarisation Measurements in Mixed Crystals.
D.P. Craig and G. Fischer.
Proc. Chem. Soc., 176 (1964).

82. The Orbital Penetration Term in Aromatic Substitutuent Effects.
D.P. Craig and G. Doggett.
Mol. Phys., 8, 485-495 (1964).

83. On Multipole Interaction Methods in Exciton Theory.
D.P. Craig and T. Thirunamachandran.
Proc. Phys. Soc., 84, 781-793 (1964).

84. Polarization Ratios in Tetracene-Anthracene Mixed Crystals.
C.D. Akon and D.P. Craig.
J. Chem. Phys., 41, 4000-4001 (1964).

85. Absorption, Excitation, and Transfer Processes in Molecular Solids.
D.P. Craig.
Physical Processes in Radiation Biology, Eds. Augenstein, Mason and Rosenberg. Academic Press, 1-10, 1964, (Proceedings of the Michigan Conference, 1963).

86. Model Calculations in the Theory of Mixed-Crystal Spectra.
D.P. Craig.
Advances in Chemical Physics, Ed. Daudel. Interscience, VIII, 27-46 (1964).

87. The Changing Concept of Aromatic Character.
D.P. Craig.
Education in Chemistry, 136-143 (1964).

88. Molecular Packing in Crystals of the Aromatic Hydrocarbons.
D.P. Craig, R. Mason, P. Pauling and D.P. Santry.
Proc. Roy. Soc., A286, 98-116 (1965).

89. "Island" and Cyclic Delocalistion in pπ-dπ Systems.
D.P. Craig and K.A.R. Mitchell.
J. Chem. Soc., 4082-4090 (1965).

89a. Polymeric A-B-A systems of First- and Second-row Elements,
D.P. Craig and K.A.R. Mitchell.
Explosives Research and Development Establishment, Report 1/EMR/67, (1967)).

90. The Crystal Spectra of Phenanthrene and Phenanthrene-d_{10} Near 3400A.
D.P. Craig and R.D. Gordon.
Proc. Roy. Soc., A288, 69-97 (1965).

91. d-Orbital Sizes in Sulfur.
D.P. Craig and T. Thirunamachandran.
J. Chem. Phys., 43, 4183 (1965).

92. Intermolecular Forces in Crystals of the Aromatic Hydrocarbons.
D.P. Craig, P.A. Dobosh, R. Mason and D.P. Santry.
Disc. Far. Soc., 40, 110-116 (1965).

93. The Electronic State of Mixed Molecular Crystals. I.
Theory for Shallow Traps.
D.P. Craig and M.R. Philpott.
Proc. Roy. Soc., A290, 583-601 (1965).

94. The Electronic States of Mixed Molecular Crystals. II.
Application of the Theory to the Mixed Crystals of Naphthalene and Deuteronaphthalene.
D.P. Craig and M.R. Philpott.
Proc. Roy. Soc., A290, 602-612 (1966).

95. The Closed Shell in Molecules.
D.P. Craig.
Studies on Chemical Structure and Reactivity, Methuen and Co. Ltd., Ch. 1.1-10 (1966).

96. Polarization Ratio of Anthracene Fluorescence.
C.D. Akon and D.P. Craig.
Trans. Farad. Soc., 62, 1673-1677 (1966).

97. The Electronic States of Mixed Molecular Crystals. III. The General Trapping Problem.
D.P. Craig and M.R. Philpott.
Proc. Roy. Soc., A293, 213-234 (1966).

98. Photochemical Dimerisation in Crystalline Anthracenes.
D.P. Craig and P. Sarti-Fantoni.
Chem. Comm., 742-743 (1966).

99. d-Orbitals in the Excited Sulfur Atom.
D.P. Craig and T. Thirunamachandran.
J. Chem. Phys., 45, 3353-3364 (1966).

100. Ultraviolet Polarization Ratios in Anthracene-Tetracene Mixed Crystals.
C.D. Akon and D.P. Craig.
Trans. Far. Soc., 63, 56-60 (1967).

101. Triplet-Triplet Spectra of Aromatic Molecules in Mixed Crystals.
D.P. Craig and G. Fischer.
Trans. Far. Soc., 63, 530-539 (1967).

102. Electronic States of Mixed Crystals.
D.P. Craig.
Journal de physique, 28, (Suppl. 5-6) p. C3-129 (1967).

Book. Excitons in Molecular Crystals - Theory and Applications.
102a. D.P. Craig and S.H. Walmsley.
W.A. Benjamin Inc., 1968, New York and Amsterdam.

103. The Resonance Valence State.
D.P. Craig and T. Thirunamachandran.
Proc. Roy. Soc., A303, 233-257 (1968).

104. Radiation Damping of Exciton States.
D.P. Craig and L.A. Dissado.
J. Chem. Phys., 48, 516-517 (1968).

105. New Themes in Theoretical Chemistry.
D.P. Craig.
Aust. J. Sci., 30, 427-432 (1968).

106. Exciton Damping.
D.P. Craig and L.A. Dissado.
Excitons, Magnons and Phonons in Molecular Crystals.,
Cambridge University Press, (International Meeting on Excitons and Phonons, Beirut), 203-211 (1968).

107. Retarded Interactions in Mixed Crystal Spectra.
D.P. Craig and P.D. Dacre.
Proc. Roy. Soc., A310, 297-312 (1969).

108. Long Range Cut-Off in the Retarded Two-Molecule Interaction.
D.P. Craig and L.A. Dissado.
Proc. Roy. Soc., A310, 313-318 (1969).

109. Totally Symmetric Vibronic Perturbations and the Phenanthrene 3400A Spectrum.
D.P. Craig and G.J. Small.
J. Chem Phys., 50, 3827-3834 (1969).

110. Progress Report: Theoretical Chemistry.
D.P. Craig.
Education in Chemistry, Vol. 6 No. 1, 5-8 (Published by R.I.C.) (1969).

111. The Asymptotic Casimir-Polder Potential for Anisotropic Molecules.
D.P. Craig and E.A. Power.
Chem. Phys. Letters. 3, 195-196 (1969).

112. The Electronically Excited States of NSF at 4000A and 5300A.
D.P. Craig and G. Fischer.
Chem. Phys. Letters, 4, 227-228 (1969).

113. The Asymptotic Casimir-Polder Potential from Second-Order Perturbation Theory and its Generalization for Anisotropic Polarizabilities.
D.P. Craig and E.A. Power.
Int. J. Quantum Chem., 3, 903-911 (1969).

114. d-Orbitals in Excited Configurations of Chlorine.
D.P. Craig and R.G.A.R. Maclagan.
J. Chem. Soc., A. 1431-1439 (1970).

115. The Interaction of Optically Active Molecules.
D.P. Craig, E.A. Power and T. Thirunamachandran.
Chem. Phys. Letters, 6, 211-214 (1970).

116. Ionic Terms in Valence States.
D.P. Craig and T. Thirunamachandran.
Proc. Roy. Soc., A317, 341-357 (1970).

117. The Interaction of Optically Active Molecules.
D.P. Craig, E.A. Power and T. Thirunamachandran.
Proc. Roy. Soc., A322, 165-179 (1971).

*Book. Aromaticita.
117a. D.P. Craig.
Encyclopedia Della Chimica. Ed. Uses, Florence, 27-31 (1971).

*Book. The Concept of Aromatic Character.
117b. D.P. Craig.
Introduction a l'histoire des sciences. Ed. Hachette, 2, p.168-173 (1971).

*Book. Chemical Binding and Delocalization in Phosphonitrilic Derivatives.
117c. D.P. Craig and N.L. Paddock.
Nonbenzenoid Aromatics,Vol 2 Ed. James P. Snyder. Acamemic Press, New York - London, . 273-357 (1971).

*Book . Aromatic Character and the Benzene Nucleus.
117d. G. Chandler and D.P. Craig.
Rodd's Chemistry of Carbon Compounds, Ed. S. Coffey, Elsevier Publishing Co., p. 5-44 (1971).

118. Absorption and Fluorescence by Thin Molecular Crystals. I. Theory.
D.P. Craig and L.A. Dissado.
Proc. Roy. Soc. A325, 1-21 (1971).

119. The Influence of Final-State Spectrum in Radiationless Transitions. Part I.
J.R. Christie and D.P. Craig.
Int. J. Mol. Phys., 23, 345-351 (1972).

120. The Influence of Final-State Spectrum in Radiationless Transitions. Part II. Application to Benzene.
J.R. Christie and D.P. Craig.
Int. J. Mol. Phys., 23, 353-363 (1972).

121. Acenaphthylene in Acenaphthene: Identification of Two Impurity Sites.
R.G. Bray and D.P. Craig.
Chem. Phys. Letters, 13, 577-578 (1972).

*Book. Electronic Energy Levels of Molecular Solids.
121a. D.P. Craig.
Orbital Theories of Molecules and Solids, Ed. N.H. March, Clarendon Press, Oxford, p. 344-375 (1974).

*Book. Ronald Sydney Nyholm 1917-1971.
121b. D.P. Craig.
Biog.Memoirs of Fellows of the Royal Society, 18, p. 445-475 (1972).

122. Absorption and Fluorescence by Thin Molecular Crystals. II. Application to Anthracene.
D.P. Craig and L.A. Dissado.
Proc. Roy. Soc. Lond. A332, 419-437 (1973).

123. The Neutral Exciton Model for Triplet Factor-Group Splittings in Aromatic Crystals.
D.P. Craig and Bat-Sheva Sommer.
Chem. Phys. Letters, 22, 239-242 (1973).

124. The $2 \times \nu_3$ Transition in Crystal SiF_4.
D.P. Craig and V. Schettino.
Chem. Phys. Letters, 23, 315-317 (1973).

125. Optical Activity and Energy Discrimination (H.G. Smith Memorial Lecture 1972).
D.P. Craig.
Proc. RACI 41, 1-5 (1974).

126. The Research School of Chemistry, Australian National University.
D.P. Craig.
Proc. Roy. Aust. Chem. Inst. 41, 29-33 (1974).

127. Permanent Moment Contributions to Chiral Discrimination.
D.P. Craig and P.E. Schipper.
Chem. Phys. Letters, 25, 476-479 (1974).

128. Induced Circular Dichroism: A Theoretical Description.
D.P. Craig, E.A. Power and T. Thirunamachandran.
Chem. Phys. Letters, 27, 149-153 (1974).

129. Substitutional and Surface Fluorescence in Pentacene-Anthracene Crystals.
A. Brillante and D.P. Craig.
Chem. Phys. Letters, 29, 17-20 (1974).

130. Impurity Induced Phosphorescence in Anthracene Crystal.
A. Brillante, D.P. Craig, A.W.-H. Mau and J. Rajikan.
Chem. Phys. Letters, 30, 5-10 (1975).

131. Electrostatic Terms in the Interaction of Chiral Molecules.
D.P. Craig and P.E. Schipper.
Proc. Roy. Soc. Lond. A342, 19-37 (1975).

132. Optical Absorption by X-Traps in Anthracene.
A. Brillante, D.P. Craig, A.W.-H. Mau and J. Rajikan.
Chem. Phys. Letters, 31, 215-219 (1975).

133. A Pairwise Additivity Scheme for Conformational Energies of Substituted Ethanes.
D.P. Craig, L. Radom and P.J. Stiles.
Proc. Roy. Soc. Lond. A343, 1-10 (1975).

134. Intramolecular Chiral Discrimination Between *meso* and *d,l* Isomers.
D.P. Craig, L. Radom and P.J. Stiles.
Proc. Roy. Soc. Lond. A343, 11-16 (1975).

135. Host and Guest Emission in Pentacene-Anthracene Mixed Crystals.
A. Brillante and D.P. Craig.
J. Chem. Soc., Faraday Transactions II, 71, 1457-1472 (1975).

136. Dispersion and Resonance Terms in Exciton-Phonon Coupling: Absorption Band Profiles in Molecular Crystals.
D.P. Craig and L.A. Dissado.
Chemical Physics, 14, 89-110 (1976).

137. Circular Dichroism of D_{2d} Molecules in Chiral Environments Promoted by Jahn-Teller Coupling.
D.P. Craig and P.J. Stiles.
Chem. Phys. Letters, 41, 225-227 (1976).

138. The Dynamic Terms in Induced Circular Dichroism.
D.P. Craig, E.A. Power and T. Thirunamachandran.
Proc. Roy. Soc. A348, 19-38 (1976).

139. Discriminating Interactions Between Chiral Molecules.
D.P. Craig and D.P. Mellor.
Topics in Current Chemistry, 63, 1-48, Springer-Verlag, Berlin, 1976.

140. Calculated Molecular Orientational Disorder in Anthracene Crystals.
D.P. Craig, J.F. Ogilvie and P.A. Reynolds.
J. Chem. Soc., Faraday Transactions II, 72, 1603-1612 (1976).

141. Exciton Trapping and Self-Trapping in Molecular Crystals.
D.P. Craig, L.A. Dissado and S.H. Walmsley.
Chem. Phys. Letters, 46, 191-196 (1977).

142. The Hamiltonian for Exciton-Phonon Coupling in Molecular Crystals.
D.P. Craig and L.A. Dissado.
Chem. Phys. Letters, 44, 419-424 (1976).

143. Site Selective Photochemical Change in Anthracene Crystals Doped with 2-Hydroxyanthracene.
D.P. Craig and J. Rajikan.
Chem. Phys. Letters, 47, 20-22 (1977).

144. Emission Centres in Anthracene Single Crystals. Effects of Irradiation.
D.P. Craig and J. Rajikan.
J. Chem. Soc., Faraday Transactions II, 74, 292-303 (1978).

145. Multiply Charged Aromatic Cations: The Heptalenium Dication.
D.P. Craig, L. Radom and Henry F. Schaefer III.
Aust. J. Chem., 31, 261-266 (1978).

146. A Theory of Vibrational Circular Dichroism in Terms of Vibronic Interactions.
D.P. Craig and T. Thirunamachandran.
Mol. Phys., 35, 825-840 (1978).

147. Strong and Weak Exciton-Phonon Coupling in Molecular Crystals.
M.D. Clarke, D.P. Craig and L.A. Dissado.
Mol. Cryst. Liq. Cryst., 44, 309-322 (1978).

148. Exciton-Phonon Coupling in Molecular Crystals: Absorption Band Profiles in the First Singlet System of Anthracene.
D.P. Craig and L.A. Dissado.
Proc. Roy. Soc. A363, 153-173 (1978).

149. Electronic Circular Dichroism of Twisted [4.4]- Spirononatetraene.
D.P. Craig, P.J. Stiles, P. Palmieri and C. Zauli.
J. Chem. Soc., Faraday Transactions II, 75, 97-104 (1979).

*Book. Chiral Discrimination.

149a. D.P. Craig.
NATO Advanced Study Institute Series, Ed. Stephen F. Mason.
D. Reidel Publishing Company, p. 293-318 (1979).

150. Structural Disturbance and Lattice Relaxation in Molecular Crystal Packing Calculations.
D.P. Craig, B.R. Markey and A.O. Griewank.
Chem. Phys. Letters, 62, 223-229 (1979).

151. Exciton-Phonon Coupling in Molecular Crystal Trapping Processes.
D.P. Craig, L.A. Dissado and S.H. Walmsley.
Chemical Physics, 46, 87-105 (1980).

*Book. Interactions Between Chiral Molecules: Discriminating Interactions.

151a. D.P. Craig.
Horizons of Quantum Chemistry, ed. K. Fukui and B. Pullman, D. Reidel Publishing Company, p. 123-143 (1980).

152. Masking of Trap Effects on Exciton Bands by Exciton-Phonon Coupling.
D.P. Craig and J. Singh.
Chem. Phys. Letters, 71, 409-414 (1980).

153. A Simple Model of Photoinduced Lattice Instability.
M.A. Collins and D.P. Craig.
Chemical Physics, 54, 305-321 (1981).

154. Elementary Derivation of Long-Range Moments of Two Coupled Centrosymmetric Systems.
D.P. Craig and T. Thirunamachandran.
Chem. Phys. Letters, 80, 14-17 (1981).

155. Stereochemical Constraints and Lattice Relaxation in Crystal Photochemistry.
D.P. Craig and B.R. Markey.
Mol. Cryst. Liq. Cryst., 58, 77-94 (1980).

156. An Improved Approximate Diagonalization for Exciton-Phonon Coupling in Molecular Crystals.
D.P. Craig and J. Singh.
Chem. Phys. Letters, 82, 405-409 (1981).

157. Dynamic Instabilities in Excited Molecular Crystals. Packing Calculations in Anthracenic Systems.
D.P. Craig and C.P. Mallett.
Chemical Physics, 65, 129-142 (1982).

158. Dispersive and Other Second-Order Terms in Exciton-Phonon Coupling.
D.P. Craig.
Chem. Phys. Letters, 88, 362-368 (1982).

159. Craig, D.P., Maccoll, A., Nyholm, R.S., Orgel, L.E. and Sutton, L.E. Citation Classic. Current Contents, 28, 20 (1982).

160. Molecular Crystals and Light: Chemical Reactions in Cages (The Liversidge Research Lecture 1982).
D.P. Craig.
Journal and Proceedings, Royal Society of New South Wales, 115, 61-67 (1982).

161. Chiral Discrimination in the Liquid State: A Hard-Core Model for the Role of Repulsive Forces.
D.P. Craig and I.R. Elsum.
Chemical Physics, 73, 349-362 (1982).

162. Radiation-Molecule Interactions in Chemical Physics.
D.P. Craig and T. Thirunamachandran.
Advances in Quantum Chemistry, 16, 97-160 (1982).

163. A Model of Localization, Soliton Propagation, and Self-Trapping in an Electronically Excited Atomic Lattice.
D.P. Craig and M.A. Collins.
Chemical Physics, 75, 191-214 (1983).

164. The Effect of Molecular Excitation on Crystal Packing. 9-cyano- and 9,10-dimethylanthracene as Excited Guest/Host and Host/Guest Pairs.
K. Norris, P. Gray, D.P. Craig, C.P. Mallett and B.R. Markey.
Chemical Physics, 79, 9-20 (1983).

Book 164a. MOLECULAR QUANTUM ELECTRODYNAMICS. An Introduction to Radiation-Molecule Interactions.
D.P. Craig and T. Thirunamachandran.
Academic Press, London, 1984.

165. An Interpretation of Anthracene-TCNB Photocurrent Spectra.
D.P. Craig and P. Petelenz.
Chem. Phys. Letters, 105, 17-21 (1984).

166. Mixed-Crystal Packing Calculations. 9-Methoxyanthracene in Host 9-Cyanoanthracene.
D.P. Craig, R.N. Lindsay and C.P. Mallett.
Chemical Physics, 89, 187-197 (1984).

167. The Adiabatic Approximation in the Ground-State Manifold.
D.P. Craig and T. Thirunamachandran.
Can. J. Chem., 63, 1773-1779 (1985).

168. Radiation-Molecule and Molecule-Molecule Interactions. A Unified Viewpoint from Quantum Electrodynamics.
D.P. Craig and T. Thirunamachandran.
Accounts of Chem. Res. 19, 10 - 16 (1986).

169. Change in chiroptical properties caused by intermolecular coupling.
D.P. Craig and T. Thirunamachandran.
Proc. Roy. Soc. Lond. A 410, 337 - 351 (1987).

170. Chiral-achiral Molecular Coupling: The Effect on the Chiral Partner.
D.P. Craig and T. Thirunamachandran.
Int. J. Quant. Chem. 31, 417 (1987).

171. Crystal Constraints and Photochemical H-transfer in the Acridine-Fluorene Mixed Crystal.
D.P. Craig, R.N. Lindsay, J.F. Ogilvie and D. Stehlik.
Chem. Phys. 114, No 2, 259 - 265 (1987).

172. Science: The Private and the Public Faces.
D.P. Craig.
Journal and Proceedings, Royal Society of NSW, 20, 3 - 8 (1987).

173. The Permanent Moment Contribution to Two-photon Absorption.
D.P. Craig and T. Thirunamachandran.
Chem. Phys. Letters. 148, No 1, 97 - 100 (1988).

174. On the Adiabatic Approximation in Vibronic Problems.
D.P. Craig and T. Thirunamachandran.
J. Mol. Struct. 189, 43 - 54 (1988).

175. Essay Review: Shaping Science and Industry, by C.B. Schedvin.
D.P. Craig.
Annals of Science. 46, 423-425 (1988)

176. Third-Body Mediation of Resonance Coupling between Identical Molecules
D.P. Craig and T. Thirunamachandran.
Chem. Physics. 135, 37-48 (1989)

177. Intermolecular Forces from the Viewpoint of Quantum Electrodynamics
D.P. Craig.
J. Jortner and B. Pullman (eds.), Perspectives in Quantum Chemistry 9-39 (1989).
Kluwer Academic Publishers.

178. Partnerships in `Improving Natural Knowledge': Chemical Science. Bologna-Australia.
D.P. Craig
Atti del Convegno Bologna-Nationes. L'Australia.
Giovanna Capone (Ed)
University of Bologna, Longo, Editore, Ravenna (1989).

179. Molecular Quantum Electrodynamics in Chemical Physics
D.L. Andrews, D.P. Craig, T.Thirunamachandran.
International Reviews in Physical Chemistry, 1989, Vol. 8, No. 4, 339-383
Taylor & Francis Ltd (1989).

180. The Long March to the Clever Country .
D.P. Craig.
Current Affairs Bulletin, Volume 68, Number 2, July 1991.

181. An Analysis of Models for Resonant Transfer of Excitation using Quantum Electrodynamics.
D. P. Craig and T. Thirunamachandran.
Chemical Physics, 167 No 3, 229-240 (1992).

182. Light, Crystal Forces, and Photochemistry.
D. P. Craig.
Chemistry in Australia, Vol 59, No. 12, December 1992.

183. Australian Science in the Global Scene.
D. P. Craig.
Proceedings of the 1992 Invitation Symposium - Australian Academy of Technological Sciences and Engineering, 13 October 1992.

184. Science and Technology Policy Research.
D. P. Craig.
New Perspectives on Global Science and Technology Policy
The Proceedings of NISTEP the Third International Conference on Science and Technology Policy Research, 9-11 March 1992, Tokyo, Japan

185. Australian Science and Technology. Running Fast to Stay Still?
D. P. Craig.
TGH Jones Memorial Lecture, Department of Chemistry, University of Queensland,October 1993

186. Model Calculations testing the Adiabatic Born-Oppenheimer Approximation and its non-Adiabatic Corrections.
D. P. Craig and T. Thirunamachandran
Theoretica Chimica Acta, 89, 123-136 (1994).

187. The Usefulness of Science.
D. P. Craig.
Australian Science, 16, 2 (1995).

188. EXCON '94: Inaugural Address.
D. P. Craig.
Pure and Applied Chem. 67, 375-376 (1995).

189. The Influence of Intermolecular Coupling on Spontaneous Emission.
D. P. Craig and T. Thirunamachandran.
Molecular Physics, 88, 631 (1996).

200. G. N. Lewis and M. Kasha, J. Amer. Chem. Soc., 66, 2100 (1944).

201. C. R. Bailey, C. K. Ingold, H. G. Poole and C. L. Wilson, J Chem Soc p222 (1946).

202. A. L. Sklar, J. Chem. Phys., 5, 669 (1937).

203. G. Herzberg and E. Teller, Z. Physikal. Chem., B21, 410 (1933).

204. H. Sponer and E. Teller, Rev Mod Phys , 13, 75 (1941).

205. M. Goeppert-Mayer and A. L. Sklar, J Chem Phys, 6, 645 (1948).

206. A. Maccoll, Quart. Revs, 1, 16 (1947).

207. R. N. Jones, Paper read at the A C S Symposium, December 1946.

208. R. Pariser and R. G. Parr, J. Chem. Phys., 21, 466 (1953).

209. G. W. Wheland, Proc. Roy. Soc. Lond., A164, 397 (1938).

210. V. J. Hammond, W. C. Price, J. P. Teegan and A. D. Walsh, Disc. Faraday Soc., 9, 53 (1940).

211. I. W. Obreimov and A. Prikhotjko, Phys. Z. Sowjetunion, 9, 34 (1936).

212. A. S. Davydov, Zhur. Exp. Teor. Phys., 18, 210 (1948).

213. N. K. Choudhury and S C Ganguly, Proc. Roy. Soc. Lond., A259, 410 (1960)..

214. A.I.Kitaigorodskii, Tetrahedron, 14, 230 (1961).

215. R. Mason, Molecular Physics, 4, 413 (1961).

216. M. D. Cohen and G. M. J. Schmidt, J. Chem. Soc. p1996 (1964).

217. L. E. Lyons and L. J. Warren, Australian J. Chem. 25, 1427 (1972).

218. P. P. Ewald, Ann. Phys., 64, 253 (1921)

219. H. Kornfeld, Zeit. fur Physik., 22, 27 (1924).

220. S. H. Walmsley, Thesis, University of London, 1959.

221. T. Thirunamachandran, Thesis, University of London, 1961.

222. J. H. Callomon, T. M. Dunn and I. M. Mills, Phil. Trans. Roy. Soc. Lond., A259, 499 (1966).

223. D. S. McClure, J. Chem. Phys. 22, 1668 (1954).

224. G. W. King, J. Sci. Instr., 22, 1668 (1958).

225. D. S. McClure, J. Chem. Phys., 25, 481, (1956).

226. R. M. Hochstrasser and G. J. Small, J. Chem, Phys., 35, 2270 (1966).

227. P. A. M. Dirac, Proc. Roy. Soc. London, A 123, 714 (1929).

228. R. P.Feynman, *QED, The Strange Theory of Light and Matter,* Princeton University Press, 1985, p8.

229. L. Campbell and W. Garnett,*The Life of James Clerk Maxwell,* McMillan and Co, London 1888.

230. J. A Stratton, *Electromagnetic Theory* , McGraw Hill, 1941.

231. W.T.Simpson, Radiation Research, 20, 87 (1963).

232. E. A. Power, *Introductory Quantum Electrodynamics.* Longmans, London, 1964.

233. H. B. G. Casimir and B. G. Polder, Phys. Rev. , 73, 360 (1948).

234. E. A. Power and S. Zienau, Phil. Trans. Roy. Soc. Lond. A 251, 54 (1959).

235. M. Goeppert-Mayer, Phys. Lpz. Ann., 9, 273 (1931).

236. R. R. McLone and E. A. Power , Mathematika, 11, 91 (1964).

237. D. S. Barnes, J. R. Backhouse, F. P. Dwyer, and E. C. Gyarfas, Proc. Roy. Soc, NSW,, **80**, 151 (1956).

238. *Handbook of Chemistry and Physics*, 55th Ed, 1974, Chemical Rubber Publishing Co., Cleveland Ohio.

239. C. Mavroyannis and M. J . Stephen, Mol. Physics. , 5, 620 (1962).

240. L. Pauling, J. Amer. Chem. Soc., 53, 1378 (1931).

241. A. Maccoll, Trans. Faraday Soc., 46, 369 (1950).

The Discrete Variational Method in Density Functional Theory and its Applications to Large Molecules and Solid-State Systems

*D.E. Ellis and Diana Guenzburger**

Department of Chemistry and Materials Research Center
Northwestern University, Evanston IL 60208, U.S.A.

*Centro Brasileiro de Pesquisas Físicas - CBPF
Rua Dr. Xavier Sigaud, 150
22290-180 - Rio de Janeiro-RJ, Brasil

ABSTRACT

The Discrete Variational method for molecules and clusters (DVM), in the framework of Density Functional theory, is described in detail. The numerical grids utilized, basis functions and potential are discussed, as well as spin-polarization for magnetic systems, total energy and dynamics. The relativistic version of the DV method is also described. Applications to large molecules range from porphyrins, a transition metal complex of thiophene, the circular molecule "ferric wheel" containing ten Fe atoms and other transition metal complexes investigated by fragments. Examples of relativistic calculations are given for 5d-metal complexes. Calculations for solids, represented by embedded clusters as large as 65-75 atoms, include transition metals, perovskites, silicates and rare-earth borocarbides. Properties investigated and analysed are structural, optical, hyperfine, magnetic and superconducting. The electronic structure and chemical bonds are also studied by Mulliken populations and charges, bond order, density of states and spin density maps; results are related to experimentally observed characteristics.

Key-words: Density functional; Electronic structure; Molecules; Solids.

ADVANCES IN QUANTUM CHEMISTRY, VOLUME 34

0065-3276/99 $30.00

Contents

1 Introduction

For many decades, first principles computational Quantum Chemistry methods were primarily based on Hartree-Fock (HF) theory and HF augmented by various levels of perturbation theory. These methods have served well as tools to study in full detail the spectroscopic and structural properties of small molecules, with perhaps as many as ten light atoms [1],[2]. Much insight has been gained on the relationships between ground state properties, single-electron orbitals and chemical reactions. While the energy-minimization principle defining the HF wavefunction limits the accurracy of excited state descriptions, nevertheless, much useful information has been obtained about excitation properties and spectra. With perturbative treatment of electron correlation, the systems successfully studied have been extended to "average"-sized molecules (10-50 atoms) containing first-row elements such as C, N or O, or smaller molecules containing a transition element of the first period. The development of effective core potentials, in which inner-shell electrons are "frozen" and do not participate in variational relaxation, has permitted the extension of HF methodology to transition metal particles and heavy atom systems [3],[4]. Nevertheless, the computational load rises rapidly with some power (N^3 or N^4 for HF, N^5 or greater for correlation corrections) of the number of basis functions N, with the exchange interaction being the main bottleneck.

Full-scale treatments of correlation effects, found to be necessary to repair some of the known deficiencies of the HF model wavefunction, generally are done by Configuration Interaction theory [1],[5]. With highly developed computer codes it has been found possible to include more than $10^5 - 10^6$ determinants, either explicitly or implicitly in the wavefunction expansion. Unfortunately, procedures for selecting the most important terms in the CI expansion have proved to be a source of difficulty, despite successes of Coupled Cluster methods and related schemes [6],[7].

However, during the last decades we have witnessed a great evolution and development in the synthesis of new and complex molecules. Large molecules with exotic geometries, polynuclear transition-metal complexes, transition-metal planar molecules stacked to form one-dimensional metals, are but a few examples of the challenging structures that can now be prepared. Moreover, the extraordinary advances in material sciences, frequently motivated by technological developments, have increased the relevance of solid-state materials to chemists, with problems such as heterogeneous catalysis, adhesion and other surface phenomena, synthesis of new complex crystals, impurities and defects in solids, etc.

To meet these new challenges, during the last decade Quantum Chemists have turned

more and more frequently to first-principles methods based upon Density Functional (DF) theory [8],[9],[10]. Its simplest implementation, the Local Density approximation (LDA) already provides a surprisingly accurate approximation to the many-body interelectronic potential and a relatively fast means to obtain the electronic structure and properties of molecules and solids [11],[12]. More sophisticated approaches, which employ gradients of the electron density in approximating the electronic exchange and correlation have been shown capable of delivering "chemical accuracy" (2 – 5 kcal/mole) in atomic binding energies and precision in bond lengths and angles approaching that of experiment [8]-[12].

Since the LDA has been used in the huge majority of published work, we will largely focus on it in the following. We want to emphasize however, that the newer methodologies such as GGA (Generalized Gradient Approximation [13]) provide useful, but relatively small corrections to an essentialy correct picture of electronic structures. One can of course find examples (e.g., the magnetic ground state of bcc iron), where LDA is qualitatively incorrect and so-called nonlocal corrections are essential.

LDA methods have been employed to investigate solids in two types of approaches. If the solid has translational symmetry, as in a pure crystal, Bloch's theorem applies, which states that the one-electron wave function ϕ_n at point $(\vec{r}+\vec{R})$, where $\vec{R}$ is a Bravais lattice vector, is equal to the wave function at point $\vec{r}$ times a phase factor:

$$\phi_n(\vec{r}+\vec{R}) = e^{i\vec{k}.\vec{R}}\phi_n(\vec{r}) \tag{1}$$

Based on this property, LDA band-structure methods were generated [14], in which the electronic energy levels are obtained in the reciprocal $\vec{k}$ space. Since the early 60's, there have been developed a large number of band structure methods, differing among themselves mainly in the way the crystal potential is treated, and in the choice of expansion bases. Frequently they may be recognized in the literature by their initials: APW, LMTO, FLAPW, KKR, etc.

However, if translational symmetry is missing, band-structure calculations are not possible, or else become highly artificial in nature. This includes a number of interesting and important cases such as impurities in solids (substitutional or interstitial), vacancies, local geometry distortions, atoms or molecules on surfaces, disordered materials, etc. For these cases, DF methods in real space may be applied, if one considers a group of atoms (cluster) to represent the solid. In fact, the same methodology as designed for molecules may be applied, with one important difference: an adequate embedding scheme has to be devised, to insert the cluster in its proper environment in the solid.

The Discrete Variational (DV) Method [15],[16] is an all-numerical self-consistent

method based on DF theory, in which the one-electron wave-functions of the molecule or the cluster are expanded on a basis of numerical atomic orbitals (NAO), obtained from DF calculations for atoms or ions. These features make the DVM less computer-time consuming than the Gaussian-basis DF counterparts, and thus suitable to treat large molecules and sizable clusters representing solid-state systems. Heavy atoms may also be included, such as transition-metals, lanthanides and actinides. A relativistic version with four-component one-electron functions is also available [17],[18]. For treating clusters, embedding schemes are built in, which include short-range effects of the first neighbors, as well as long-range Coulomb potentials, in the case of charged atoms.

Although most DVM applications so far have been made within the Local Density approximation, non-local corrections to exchange and correlation [13],[19] have been implemented for calculation of dissociation energies and structural properties.

In this review we shall attempt to describe the main features of the DV method in its current form, and give examples of both molecular and cluster calculations, and of the many different properties that may be investigated.

2 The Discrete Variational Method for Molecules and Clusters

2.1 General Formulation of the Method

The purpose of the DV method is to solve self-consistently the set of Kohn-Sham equations [8], [9], [20] (in Hartree atomic units):

$$h_{KS}\phi_i(\vec{r}) \equiv \left[-\nabla^2/2 - \sum_q \frac{Z_q}{|\vec{r}-\vec{R}_q|} + \int \frac{\rho(\vec{r}')}{|\vec{r}-\vec{r}'|}d^3r' + V_{xc}\right]\phi_i(\vec{r}) = e_i\phi_i(\vec{r}) \qquad (2)$$

with

$$\rho(\vec{r}) = \sum_i n_i|\phi_i(\vec{r})|^2 \qquad (3)$$

where $\phi_i(\vec{r})$ are the one-particle functions for the molecule or the cluster with occupation n_i, and $\rho(\vec{r})$ is the n-representable density. The first term in Eq. (2) is the kinetic energy, the second term is the Coulomb potential of the nuclei V_n, the third term the electronic Coulomb potential V_e and V_{xc} is the exchange and correlation potential. In the DV scheme, the one-electron functions are expanded on a basis of numerical atomic orbitals (NAO), obtained themselves by LDA calculations [14], [21]-[25]

$$\phi_i(\vec{r}) = \sum_\ell \chi_\ell(\vec{r})c_{\ell i} \qquad (4)$$

An error functional Δ_{ij} is defined, related to approximate solutions of Eqs. (2), which is minimized with respect to variations of the coefficients c_{ij} of Eq. (4), on a discrete set of points $\vec{r}_k$ with weight $\omega(\vec{r}_k)$ in three-dimensional space:

$$\Delta_{ij} = \langle\phi_i|h_{KS}-\varepsilon|\phi_j\rangle = \sum_k \omega(\vec{r}_k)\phi_i^*(\vec{r}_k)(h_{KS}-\varepsilon)\phi_j(\vec{r}_k) \qquad (5)$$

Substituting (4) in (5), we obtain:

$$\Delta_{ij} = \sum_k \sum_\ell \sum_m \omega(\vec{r}_k)\left[c_{\ell i}^*\chi_\ell^*(\vec{r}_k)(h_{KS}-\varepsilon)\chi_m(\vec{r}_k)c_{mj}\right] \qquad (6)$$

To minimize the functional Δ_{ij} with respect to variations of the eigenfunctions ϕ_i, it is required that

$$\frac{\partial\Delta_{ij}}{\partial c_{\ell i}} = 0 \qquad (7)$$

for all i, j and ℓ. This procedure results in the secular equations in matrix form, formally identical to those of the analytical Rayleigh-Ritz variational method:

$$([H]-[E][S])[C] = 0 \qquad (8)$$

By solving Eqs. (8) self-consistently, the eigenvalues and eigenvectors of the Kohn-Sham operator in Eq. (2) are obtained. In fact, calculating $[C]$ for a given initial h_{KS} leads to a new $\rho(\vec{r})$ through Eqs. (3) and (4), and thus to a new operator, since the potential is a functional of ρ. The matrix elements of the energy matrix $[H]$ and the overlap matrix $[S]$ are summations over the set of the points $\vec{r}_k$:

$$H_{\ell m} = \sum_k \omega(\vec{r}_k)\chi_\ell^*(\vec{r}_k)h_{KS}(\vec{r}_k)\chi_m(\vec{r}_k)$$
$$S_{\ell m} = \sum_k \omega(\vec{r}_k)\chi_\ell^*(\vec{r}_k)\chi_m(\vec{r}_k) \tag{9}$$

More generally, after the self-consistent ρ is obtained, for any operator $\hat{O}$ the expectation value is defined as:

$$\langle \hat{O} \rangle = \sum_k \omega(\vec{r}_k) \sum_i n_i \phi_i^*(\vec{r}_k)\hat{O}\phi_i(\vec{r}_k) \tag{10}$$

2.2 The Three-Dimensional Point Grid

The scheme of sampling, with weights $\omega(\vec{r}_k)$, is quite flexible, allowing concentration of computational effort in regions of greatest interest. It also allows the users to choose the level of precision of results, permitting rapid surveys of general features, as well as precise calculation of sensitive quantities. Three types of sampling schemes have been implemented, which can be used separately or in combination: pseudorandom, product rules, and partitioning rules.

2.2.1 Pseudorandom Scheme

The basic grid of points in three dimensions is generated with the Diophantine method [26]-[28], which is pseudo-random in the sense that the same "random" point distribution is obtained for the same set of initial parameters. This grid is generally adequate for the region between the atoms, where the valence functions dominate and no large variations in the density occur.

In the Diophantine method as originally formulated [26], [27], the integral I of a periodic function of n variables with period L is estimated by the summation:

$$I = \int F(\vec{r})dx_1 \cdots dx_n \cong \frac{1}{N}\sum_{m=1}^{N} F(\vec{r}_m) \tag{11}$$

This summation converges to I as N^{-K}, $K \geq 1$.

The points $\vec{r}_m$ are given by [26]

$$\vec{r}_m = mL\vec{\alpha} \tag{12}$$

where $\vec{\alpha} = (\alpha_1 \alpha_2 \cdots \alpha_m)$ is a vector with components given by linearly independent irrational numbers.

This method may be adapted for a molecule or crystal, by choosing spherical coordinates centered at each nuclei as integration variables [28]. These may be mapped to periodic variables in the interval [0,1]

$$\begin{aligned} 0 \leq r < \infty &\longrightarrow 0 \leq \xi < 1 \\ 0 \leq \theta < \pi &\longrightarrow 0 \leq \nu < 1 \\ 0 \leq \phi < 2\pi &\longrightarrow 0 \leq \mu < 1 \end{aligned}$$

by the transformations:

$$\begin{aligned} \xi(r) &= \int_0^r r^2 D(r) dr \\ \theta &= arc\ cos(1 - 2\nu) \\ \phi &= 2\pi\mu \end{aligned} \tag{13}$$

where $D(\vec{r})$ is the Wronskian of the transformation

$$I = \int_0^\infty \int_0^\pi \int_0^{2\pi} \frac{F(\vec{r})}{D(r)} D(r) r^2 sin\theta dr d\theta d\phi = \int_0^1 \int_0^1 \int_0^1 G(\xi, \nu, \mu) d\xi d\nu d\mu \ . \tag{14}$$

We may thus write from Eq. (11):

$$I \cong \frac{1}{N} \sum_{k=1}^{N} G(\xi_k, \nu_k, \mu_k) = \sum_{k=1}^{N} \frac{F(\vec{r}_k)}{N D(\vec{r}_k)} \equiv \sum_{k=1}^{N} \omega(\vec{r}_k) F(\vec{r}_k) \tag{15}$$

It is convenient to define the distribution function $D(r)$ in such a way as to assure a much higher density of points near the nuclei, where the core functions oscillate strongly. This is achieved by defining $D(\vec{r})$ as a summation of Fermi functions centered at the nuclei q:

$$D(\vec{r}) = \sum_q t_q \, d_q(r_q) \tag{16}$$

with

$$d_q(r_q) = \frac{A_q}{4\pi r_q^2 [1 + e^{\alpha_q (r_q - R_0^q)}]}$$

where t_q is the fraction of points assigned to nucleus q and A_q a normalization constant such that

$$\int d_q(r) d^3\vec{r} = 1$$

Parameters α_q and R_o^q are usually chosen as equal to one and to half the interatomic distance, respectively.

In Fig. (1) is shown the mapping of variable r into ξ through the Fermi function; the point distribution is more dense near the nucleus:

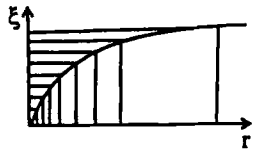

Fig. 1

Finally, the points generated around each nucleus as described above are referred to a common cartesian coordinate system.

If N points are distributed in space according to the distribution function $D(\vec{r})$, then on the average the density of points around a point $\vec{r}$ will be $ND(\vec{r})$. Thus the volume per point around $\vec{r}$ will be

$$\omega(\vec{r}) = 1/(N \times D(\vec{r})) \tag{17}$$

which is the definition of the weight in Eqs. (5), (6), (9) and (10).

2.2.2 Product Rules

The classical product rules of numerical integration [29] are capable of integrating limited regions around an atom to high precision. They are typically of the form of a Gauss-Legendre polynomial rule in (θ, ϕ), multiplied by a radial rule adapted for the asymptotic exponential decay of integrand with distance from the nucleus:

$$w(\vec{r}_k) = u(\theta_i, \phi_i)\nu(r_j) \tag{18}$$

The angular mesh implemented consists of 6, 12, 24, 32, 50, or 74 points, capable of integrating successively higher order polynomials, or a uniform-area mesh of N^2 points. The radial integration is a modified Simpson's rule in the variable ℓnr, with outer radius r_{max}, number of points, and logarithmic step selected as input.

The scheme is recommended for atomic volumes in which better precision is needed in the core region; e.g. for total energy, hyperfine interactions, and core-level spectroscopy.

2.2.3 Partitioning Rules

The Fermi distributions of the pseudorandom scheme form a set of overlapping atom-centered functions whose density $D(\vec{r})$ provides a sampling scheme with expectation values $\langle O \rangle$ which converge to their integrals. A generalization of this approach can be derived from the long-used *partitioning* methods of X-ray and neutron crystallography. Let

$$D(\vec{r}) = \sum_q t_q d_q(r_q) = 1 \tag{19}$$

where $t_q > 0$ are weights and $d_q(r)$ are selected functions centered on atoms, bonds, points of symmetry, etc. Then the expectation value of $F(\vec{r})$ is given as

$$\langle F \rangle = \langle DF \rangle = \sum_q t_q \langle d_q F \rangle = \sum_q t_q F_q \tag{20}$$

so that each component F_q can be treated independently.

The partitioning functions have been chosen variously as Gaussians, atomic-like densities (proatoms, [30]), and inverse powers of r; the latter is implemented in the DV program. One advantage of this approach, as emphasized by Becke [31], is that classical product rules can be applied to the overlapping multicenter density, to obtain integrals of high precision.

2.3 Basis Sets

2.3.1 Generation of NAOs

As described in Section 2.1, the one-electron functions are expanded on a numerical atomic basis (NAO) (LCAO approximation).

To obtain the basis functions, numerical Local Density calculations are performed for free atoms or ions, employing the same type of exchange-correlation potential as in the molecular (or cluster) calculation (this, of course, is not a necessary condition, but is usually done for the sake of coherence). The atomic self-consistent calculations seek to

solve the Kohn-Sham equations on a numerical grid in one-dimension, for an atom with spherical density, such that the atomic orbitals are of the form:

$$\chi_{n\ell} = R_{n\ell}(r)\mathcal{Y}_\ell^m(\theta\phi) \tag{21}$$

where $R_{n\ell}(r)$ are radial functions and $\mathcal{Y}_\ell^m(\theta\phi)$ are real spherical harmonics, which are linear combinations of the usual spherical harmonics Y_ℓ^m.

The grid in the "r" coordinate has a maximum of 300 points, which are distributed according to a logarithmic scale, such that their density is higher near the nucleus.

The LDA radial Schrödinger equation is solved by matching the outward numerical finite-difference solution to an inward-going solution (which vanishes at infinity) of the same energy, near the classical turning point. Continuity of $P_{nl}(r) = rR_{n\ell}(r)$ and its derivative determines the eigenvalue ε_{nl}. The second order differential equation is actually solved as a pair of simultaneous first-order equations, so that the nonrelativistic and relativistic (Dirac equation) procedures appear similar.

One very significant feature of the DV method is thus the flexibility gained by creating the basis functions specifically for a given molecular or cluster calculation, as opposed to methods where "standard" Gaussian basis are employed. This allows one to utilize basis sets of good quality with a considerably smaller number of functions, thus making possible calculations for large systems. There are several ways in which the basis functions may be adapted to some molecule or cluster. One way is to perform a Mulliken population analysis [32], [33] for the atoms in the molecule or cluster, after a first set of iterations is performed. For these preliminary iterations, the basis set is constituted of atomic functions obtained for the free atoms in their ground-state configuration (or free ions, in the case of ionic compounds). The result of the Mulliken analysis after this first self-consistency procedure will give new (fractional) occupation numbers for the atomic orbitals. These occupations, more representative of the situation in the compound, are in turn used to generate new basis functions by atomic self-consistent calculations. Fractional occupation of orbitals is a concept compatible with Density Functional theory. The following schematic representation summarizes this procedure:

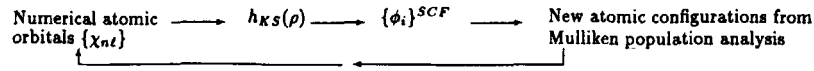

The NAO basis usually contains all the occupied orbitals of the atom, plus some unoccupied level(s) very close in energy. For example, transition metals will include all occupied levels up to nd, $(n+1)s$ and also the virtual level $(n+1)p$. Some additional features make it possible to further improve the basis. If the atom has a negative charge, or if additional virtual orbitals of higher energy are to be included as very diffuse functions, the atomic SCF calculation may be performed in the presence of a "potential well". This well may also be employed when it is desirable to contract the valence atomic basis functions, as is often the case with solids. The well is best described by the following diagram:

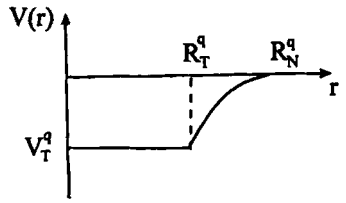

Fig. 2

$$V_A^q = \begin{cases} V^q(r) + V_T^q, & r \le R_T^q \\ V^q(r) + V_T^q \cdot \dfrac{(R_N^q - r)^2 \times (r - \frac{3R_T^q - R_N^q}{2})}{(R_N^q - R_T^q)^3/2}, & R_T^q < r < R_N^q \\ V^q(r), & r \ge R_N^q \end{cases} \tag{22}$$

where V_A^q is the modified atomic potential generating the NAO, $V^q(r)$ is the unmodified atomic potential of atom "q", V_T^q is the depth of the well and R_T^q, R_N^q are truncation distances. The parameters V_T^q, R_T^q and R_N^q depend on the size of the atom and the degree of contraction desired, and their values are dictated by the bonding characteristics of the system.

Sometimes it is inconvenient to use NAOs derived from a specific atomic configuration; e.g., as defined by Mulliken SCF cluster or molecular populations. A marginally better set can be obtained directly from the SCF cluster or molecular *potential*, spherically averaged about each atom site, with an additional well like that of Eq. (22). This NAO basis provides perhaps the most compact and efficient expansion set.

2.3.2 Symmetry Orbitals

For both molecules and clusters, point summetry, if present, is an asset to be exploited. As is known from group theory, the Hamiltonian matrix in the secular equations (Eq. 8) will be separated in smaller blocks which may be diagonalized independently, if the basis used is constituted by functions which transform according to the irreducible representations of the point group of the molecule or cluster. Accordingly, these are obtained previously, utilizing a very general code that can deal with both single and double groups, the latter for relativistic calculations [34], [35]. The non-relativistic symmetrized basis functions are thus of the form:

$$\chi^{\eta}(\vec{r}) = \sum_{q,m} b^{\eta}_{qm} R_{n\ell}(r_q) \mathcal{Y}^m_\ell(\theta_q \phi_q) \tag{23}$$

where $\eta = (k, \lambda)$ specify the point group irreducible representation and its matrix column, for which the linear combination Eq. (23) forms a basis. Therefore, the linear expansion in Eq. (4) is substituted by:

$$\phi^{\eta}_i(\vec{r}) = \sum_{\ell} \chi^{\eta}_\ell(\vec{r}) c^{\eta}_{\ell i} \tag{24}$$

and all matrix elements are calculated with the symmetrized basis.

In general, clusters which represent a solid, with or without impurities or defects, may present considerable symmetry if the center of coordinates is placed at a conveniently chosen atom or interstitial site. In the case of one impurity, it is usually advantageous if possible to place it at the center to obtain a point group of higher order. Inorganic molecules and transition-metal complexes also usually have symmetry groups of high order. In the case of large organic molecules, organometallics or biological molecules, symmetry is usually low or nonexistent; this of course will increase the computational time and impose limitations on the size of the basis. On the other hand, of course, organic molecules or organic ligands are usually constituted of small atoms, such as C, N, O, etc. Thus the maximum size of the system that can be treated will depend on a balance among several factors such as number and size of the atoms and symmetry group.

2.3.3 Orthogonalization and Frozen Core

The core orbitals of atoms are those which, by definition, are negligibly modified by the molecular or solid environment. Such orbitals can be excluded from the variational space with a significant improvement in computational time and space. This is accomplished by explicitly orthogonalizing the molecular or cluster valence functions against the core

basis functions in the first iteration. In this respect the DV scheme differs from many others, which use parametrized Effective Core Potentials [36] to achieve similar results.

The choice of which orbitals may be "frozen"; i.e., placed in the core, and which should remain in the variational space depends upon properties and precision required. For example, in first-period transition metals it is important to include the 3s, 3p "shallow core" in the variational space when sensitive properties such as the Electric Field Gradient are required. In the process of basis optimization described above, the core orbitals also evolve to become adapted to their environment.

Once the basis functions are obtained, the points of the radial grid around each nucleus where the radial functions $R_{n\ell}(r)$ are defined are interpolated, such that the values of the basis functions are obtained in the three-dimensional grid where the molecular or cluster calculation will be performed.

2.4 Magnetic Systems

In the presence of unpaired electrons, the molecule or solid becomes magnetic. Since the total number of electrons with $s_z = +1/2$ is different from those with $s_z = -1/2$, the exchange interaction, which exists only among electrons with the same spin, will be different for the two sets of electrons, and so will be the exchange-correlation potential V_{xc}. If the density for spin up electrons is allowed to be different from spin down, by allowing the orbitals in Eq. (4) to be different for each spin σ:

$$\phi_i^\sigma(\vec{r}) = \sum_\ell \chi_\ell(\vec{r}) c_{\ell i}^\sigma \tag{25}$$

then the exchange-correlation potential V_{xc} in the Kohn-Sham equations (Eq. 2), which is different for each spin, will indeed generate $\rho_\uparrow(\vec{r}) \neq \rho_\downarrow(\vec{r})$ after self-consistency. This is the basis for the spin-polarized method, through which a spin-density $[\rho_\uparrow(\vec{r}) - \rho_\downarrow(\vec{r})]$ is generated in the three-dimensional grid, being related to magnetic properties such as magnetic moments and hyperfine fields.

In the spin-orbitals of Eq. (25), the spin-dependence appears only in the coefficients $c_{\ell i}^\sigma$, the basis being the same for both spins. Attempts to use spin-polarized functions in the basis are hindered by the resulting linear-dependence problems. A consequence of this is that the polarization of the localized core orbitals is deficient, due to lack of flexibility. For properties in which spin-polarization of the core is important, the latter must be treated in a different manner. We will return to this subject in a later stage.

2.5 Charges, Configurations and Magnetic Moments

2.5.1 Population Analysis

The expansion in the NAO basis allows the analysis of the charge distribution among the atoms according to the Mulliken populations concept [32], which is based on the LCAO coefficients. In the usual Mulliken scheme, the off-diagonal elements of the charge matrix (overlap populations) are divided equally between the corresponding two diagonal elements, i.e., $q_i = \sum_j Q_{ij}$ where q_i's are the atomic occupation numbers and the Q_{ij}'s are the elements of the charge matrix. In the scheme usually adopted with the DVM [33] the off-diagonal charges are divided in proportion to the diagonal elements, i.e., $q_i = \sum_j [2Q_{ii}/(Q_{ii} + Q_{jj})]Q_{ij}$. This scheme is more satisfactory because it minimizes the negative populations that frequently occur for atomic orbitals that take part in molecular orbitals of antibonding character, for example, the $4s$ and $4p$ orbitals of first-row transition elements.

When the system is magnetic and a spin-polarized calcula on is performed, the Mulliken-type populations may be used to define magnetic moments:

$$\mu^q = P^q_\uparrow - P^q_\downarrow \tag{26}$$

where μ^q is the total magnetic moment on atom q (in Bohr magnetons), defined as the difference between the spin up and spin down populations P^q_σ.

Mulliken-type populations are a useful tool when it comes to analysing the charge and spin distribution in a molecule or solid. However, one must bear in mind that there is rigorously no such thing as an "atom" in a molecule or in a crystal, and thus such analysis must be viewed somewhat critically. Especially when atomic orbitals are very diffuse, their Mulliken-type populations may not be very realistic. On the other hand, the Mulliken analysis has the advantage that individual atomic orbital occupations may be obtained.

2.5.2 Volume-resolved Analysis

An alternative manner of analysing charge and spin distributions is to divide space in volumes pertaining to each atom and integrating the charge or spin density inside this volume. In the DVM scheme, of course, the integrations are substituted by the summations:

$$C^q = Z - \sum_{k \in WS} \omega(\vec{r}_k)\rho(\vec{r}_k) \tag{27}$$

$$\mu^q = \sum_{k \in WS} \omega(\vec{r}_k)[\rho_\uparrow(\vec{r}_k) - \rho_\downarrow(\vec{r}_k)]$$

where Z is the atomic number, C^q the charge on atom "q", μ_q its spin moment and WS the Wigner-Seitz volume. This last is defined for each atom as the volume enclosed by the planes intersecting at mid-distance the lines joining the atom to its neighbors. Alternatively, spheres with radii proportional to the atomic or ionic radii may be used.

The volume charge and spin-density partitioning, in some instances, may be more realistic than the Mulliken. The simple sampling procedure of Eq. (27) has the disadvantage that only *total* charges or spin moments are extracted. Also, WS or any particular volume partitioning (see Sec. 2.2.3) is as arbitrary as Mulliken analysis, so that convenience and internal consistency provide the best rationale for choosing one method over another. We note that ℓm-projected components of the densities can be extracted by defining the weights in Eq. (27) as $\omega_{k\ell}^{qm}(\vec{r}_k) \cong \omega(\vec{r}_k)\mathcal{Y}_\ell^m(\hat{r}_q)$ where $\hat{r}_q$ are angular coordinates of sample point $\vec{r}_k$, measured with respect to the center of interest, at $\vec{t}_q$. To be more precise, $\omega(\vec{r}_k)$ should form an integration rule, or the projection polynomials $\mathcal{Y}_\ell^m$ should be orthogonalized on the sample mesh $\{\vec{r}_k\}$.

2.6 The Potential

2.6.1 Coulomb Interaction

In calculating matrix elements of the Kohn-Sham Hamiltonian of Eq. (2), the greatest problem is posed by the electronic Coulomb repulsion. To render this term tractable, it is convenient to cast the electron density $\rho(\vec{r})$ in a model form, so as to calculate the potential by one-dimensional integrations. This is accomplished by approximating ρ by a multicenter overlapping multipolar expansion ρ_M [37]:

$$\rho_M = \sum_j d_j \sum_q{}' \sum_m C_{\ell q}^{\beta m} R_N(r_q) \mathcal{Y}_\ell^m(\theta_q \phi_q) \equiv \sum_j d_j \rho_j(\vec{r}) \tag{28}$$

Here $j \equiv (I, \ell, \beta, N)$ denotes a symmetry-equivalent set of atoms I (or any group of atoms for which the model density will be the same), a particular partial wave character (ℓ, β) and a particular radial degree of freedom N. The q summation runs over symmetry-equivalent (or selected group) sites, $\mathcal{Y}_\ell^m$ are the real spherical harmonics and $\vec{r}_q = \vec{r} - \vec{t}_q$ is the local coordinate relative to site $\vec{t}_q$. The coefficients $C_{\ell q}^{\beta m}$ are chosen to be those of the totally symmetrical representation of the point group of the molecule or cluster, to reflect the known symmetry of the density, and d_j are coefficients to be determined variationally.

The radial expansion functions are constituted of two groups: in the first group R_N are the spherical atomic densities obtained from the radial functions $R_{n\ell}$ of the basis, and in the second group R_N are radial functions localized in the range $r_N < r_q < r_{N+1}$, chosen to be piecewise parabolic. In general, only a small number of the latter functions are necessary for each (ℓ, β) partner in the fully symmetric representation to converge the potential.

In many applications, the real density has indeed an approximately spherical distribution around each atom; this is the case, for example, of metals and alloys with compact structures. For such systems the first group of R_N functions is already sufficient to represent ρ within a reasonable approximation. For these cases we have simply:

$$\rho_j(\vec{r}) = \sum_q{}' |R_{n\ell}(r_q)|^2 Y_0^0(\theta_q \phi_q) \tag{29}$$

since combinations of functions of this kind pertaining to the totally symmetric representation will have coefficients equal to unity.

The d_j coefficients are obtained by a least-squares fit to the charge density in the three-dimensional grid:

$$\sum_k w_k [\rho(\vec{r}_k) - \sum_j d_j \rho_j(\vec{r}_k)]^2 \equiv \langle (\rho - \sum_j d_j \rho_j)^2 \rangle = \delta \tag{30}$$

where δ is minimized subject to the constraint that ρ_M integrates to the total number of electrons N_e. This condition is incorporated as a Lagrange multiplier and δ is minimized with respect to the coefficients d_j:

$$\left\{ \frac{\partial}{\partial d_i} \left[\langle (\rho - \sum_j d_j \rho_j)^2 \rangle + \lambda \sum_j d_j \int \rho_j dv \right] = 0 \right\} \tag{31}$$

The integral sign denotes numerical integration in one dimension (r), which is performed with precision $< 10^{-8}$. Eqs. (31) give the set of equations:

$$\left\{ \sum_j d_j \langle \rho_j \rho_i \rangle - 2 \langle \rho \rho_i \rangle + \lambda \int \rho_i dv = 0 \right\} \tag{32}$$

which are solved simultaneously with:

$$\sum_j d_j \int \rho_j dv = N_e \, .$$

Making use of the well-known expansion [38]:

$$\frac{1}{|\vec{r} - \vec{r}'|} = \sum_{\ell=0}^{\infty} \frac{r_<^\ell}{r_>^{\ell+1}} P_\ell(cos\alpha) \tag{33}$$

where $P_\ell(cos\alpha)$ are the Legendre polynomials and $cos\alpha = (\vec{r}.\vec{r}')/rr'$, and of the addition theorem for spherical harmonics, we arrive at the expression for the Coulomb potential $V_C = V_e + V_n$ (electronic and nuclear):

$$V_C(\vec{r}) = \sum_j d_j \sum_q{}' \sum_{m=-\ell}^{+\ell} C_{\ell q}^{\beta m} V_{N\ell m}(\vec{r}_q) - \sum_q \frac{Z_q}{r_q} \tag{34}$$

where:

$$V_{N\ell m}(\vec{r}_q) = \frac{4\pi}{2\ell+1} \mathcal{Y}_\ell^m(\theta_q \phi_q) \left[\int_0^{r_q} R_N(r_q') \frac{r_q'^{\ell+2}}{r_q^{\ell+1}} dr_q' + \int_{r_q}^{\infty} R_N(r_q') \frac{r_q^\ell}{r_q'^{\ell-1}} dr_q' \right] \tag{35}$$

In the case where only the first group of (spherical) functions is considered, we have:

$$V_C(\vec{r}) = \sum_j d_j \sum_q{}' 2\sqrt{\pi} \left[\int_0^{r_q} |R_{n\ell}(r_q')|^2 \frac{r_q'^2}{r_q} dr_q' + \int_{r_q}^{\infty} |R_{n\ell}(r_q')|^2 r_q' dr_q' \right] - \sum_q \frac{Z_q}{r_q} \tag{36}$$

In the case of a spin-polarized calculation, a similar fit is performed for the spin density $\rho_s = \rho_\uparrow - \rho_\downarrow$.

2.6.2 Exchange and Correlation

The exchange-correlation potential in Eq. (2) is a functional of the electron density and may be cast in the general form:

$$V_{xc}^\sigma = K \rho_\sigma^{1/3} [1 + f_\sigma(\rho_\uparrow, \rho_\downarrow)] \tag{37}$$

In spin-polarized calculations for magnetic systems, V_{xc}^σ will be different for each spin σ. One of the earliest approximations, known as $X\alpha$, included only the first term in Eq. (37) with an empirical parameter X_α [39]:

$$V_{xc}^\sigma = -3X_\alpha (3\rho_\sigma/4\pi)^{1/3} \tag{38}$$

The Kohn-Sham-Gaspar potential derived from density-functional theory has a similar expression for V_{xc}^σ with $X_\alpha = 2/3$, and only took into account exchange [20],[40]. To include correlation, several forms were proposed for f_σ, with parameters obtained from fits to RPA calculations or more accurate Monte Carlo simulations [41] and different spin interpolations. The current version of the DVM code contains altogether nine choices of V_{xc}^σ, the preferred form being the Vosko, Wilk and Nusair [42] parametrization of the Ceperley and Alder Monte Carlo simulations [43].

To give an idea of orders of magnitude, in a typical cluster calculation the Coulomb energy $\langle \rho V_C \rangle$ is of the order of $\geq 10^5$ Hartrees, while the exchange-correlation energy $\langle \rho_\sigma V_{xc}^\sigma \rangle$ is one order of magnitude smaller. The correlation corrections associated with f_σ are one order of magnitude further reduced.

2.6.3 External Potential (Embedding)

In the case of clusters representing a solid, to the cluster density (and model density) are added the densities of several shells of neighboring external atoms at the crystal sites:

$$\rho = \rho_{\text{cluster}} + \rho_{\text{host}} \tag{39}$$

with

$$\rho_{\text{cluster}} = \sum_{i,\sigma} n_{i\sigma} |\phi_{i\sigma}|^2$$

and

$$\rho_{\text{host}} = \sum_{q}{}' \rho_q(r_q) \ .$$

This constitutes a critical portion of the embedding scheme, leading to what may be called Potential Embedding. The prime in the summation denotes exclusion of the cluster atoms. The external densities are obtained by LDA atomic calculations. To avoid the spurious migration of the cluster electrons towards the external atoms, the attractive potential of the latter is truncated at a certain value, to simulate the Pauli exclusion principle. Typical truncation is at -0.2 hartrees relative to the Fermi energy E_F, with a range of $2.2 - 2.5$ a.u. from each atomic nucleus.

As is done with the basis, the embedding may be improved by generating external atomic densities for atoms with the configurations that they have in the cluster, as obtained by the Mulliken population analysis:

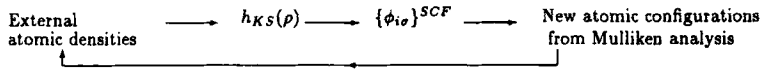

For the case of ionic solids, the method of Ewald summations [44] is employed to take into account the long-range Coulomb potential of the crystal (Madelung potential).

2.7 Total Energy and Structural Properties

Once the self-consistent electron density is obtained for the molecule or cluster, it may be used to calculate the total energy and derived properties, such as dissociation energies,

equilibrium interatomic distances, vibration frequencies, etc. Generalizing for a spin-polarized calculation, the expression given by local density theory for the total energy E_t is [8], [9], [20]:

$$E_t = \sum_{k,\sigma} e_{k,\sigma} n_{k,\sigma} + \sum_{\sigma} \int \rho_\sigma \left(-\frac{1}{2} V_e - V_{xc,\sigma} + \varepsilon_{xc} \right) d^3r + \frac{1}{2} {\sum_{pq}}' \frac{Z_p Z_q}{r_{pq}} \tag{40}$$

where $e_{k,\sigma}$ are the Kohn-Sham eigenvalues of Eq. (2), $V_{xc,\sigma}$ is the exchange-correlation potential also known as chemical potential, ρ_σ the model charge density for spin σ as defined in Section 2.6 and V_e the electronic Coulomb potential. The prime in the summation is to leave out self-interaction among the nuclei, and ε_{xc} is the exchange-correlation energy density:

$$E_{xc}[\rho] = \int \rho \varepsilon_{xc}(\rho) d^3r \tag{41}$$

It has been demonstrated [45] that when the density employed in Eq. (40) is the model density ρ_M, as described in section 2.6, the total energy is stationary with respect to variations in ρ_M. In the DV numerical sampling procedure, a scheme is devised to control numerical error, derived mainly from the core region of the atoms, where the wave functions oscillate strongly [45]-[48]. The total energy associated with a volume Ω with nuclei at positions $\{\vec{R}_q\}$ is defined as the expectation value (sum over integration mesh) of the energy density $\varepsilon(\vec{r}, \{\vec{R}_q\})$ over the volume. In order to cancel numerical errors, the computation of E_Ω is made via point-by-point subtraction of a reference system of *noninteracting* (NI) atoms located at the atomic nuclei of a molecule, or at the cluster and embedding atomic nuclei in the case of a solid:

$$E_\Omega = \langle \varepsilon(\vec{r}, \{\vec{R}_q\}) - \varepsilon^{NI}(\vec{r}, \{\vec{R}_q\}) \rangle_\Omega + E_\Omega^{NI} \tag{42}$$

where $\langle\ \rangle$ denote summation in the numerical grid.

The energy density may be defined conveniently as:

$$\varepsilon(\vec{r}, \{\vec{R}_q\}) = \sum_{\sigma} \left[\rho_{e,\sigma}(\vec{r}) - \frac{1}{2} \left[\rho_\sigma(\vec{r}) + {\sum_{q}}' Z_q \delta(\vec{r} - \vec{R}_q) \right] V_C(\vec{r}) + \rho_\sigma(\vec{r}) \left[\varepsilon_{xc}(\vec{r}) - V_{xc,\sigma}(\vec{r}) \right] \right] \tag{43}$$

where the single-particle energy is:

$$\rho_{e,\sigma}(\vec{r}) = \sum_{i} n_{i\sigma} e_{i\sigma} |\phi_{i\sigma}(\vec{r})|^2 \tag{44}$$

and is partitioned into atom-localized contributions in a manner similar to Eq. (28). This step introduces no error, since the partitioning is constructed so as to leave the total

(integral) single-particle energy invariant. The sum and δ function in Eq. (43) restrict the nuclear contribution to sites within the integration volume. The prime in the summation leaves out self-interaction of the nuclei. The least-squares determined model density is employed, consistent with the SCF procedure.

In practice, the densities of the non-interacting atoms is obtained from the functions in the NAO basis, to assure maximum error cancellation. When calculating dissociation energies (in molecules) or cohesive energies (in solids), the energy difference between the free atoms and the atoms in the basis, E(free atoms)–E(NI), must be taken into account.

As mentioned in the Introduction, non-local corrections to the LDA total energy of Eq. (40) have been implemented. It has been found that *gradient*-corrected exchange and correlation energies make significant improvements in bond energies and bond lengths. Very little additional improvement is found upon inclusion in the SCF procedure. The simple formula suggested by Becke [19] for exchange correction,

$$\Delta E_x = -\beta \sum_\sigma \int p_\sigma^{4/3} \frac{x_\sigma^2}{(1 + 6\beta x_\sigma sinh^{-1} x_\sigma)} d^3r \tag{45}$$

with $x_\sigma = |\nabla \rho_\sigma| / \rho_\sigma^{4/3}$ and $\beta = 0.0042$ a.u., has found wide use, and was followed here. The gradient formula developed by Perdew [13] for correlation correction,

$$\Delta E_c = \int d^{-1} e^{-\Phi} C \frac{|\nabla \rho|^2}{\rho^{4/3}} d^3r \tag{46}$$

was chosen, with C, Φ and d being given functions of ρ and ρ_σ. The sum

$$\Delta E_{xc} = \Delta E_x + \Delta E_c \tag{47}$$

may be added to Eqs. (40) and (41) for improved accuracy. Of course, it is the (smaller) difference between molecule and free atoms ΔE_{xc}(molecule) - ΔE_{xc}(free atoms) which enters into structural properties.

2.8 Relativistic DVM

In the preceeding sections we have discussed the DV scheme as it has been applied in nonrelativistic DF theory; here we extend the discussion to solutions of the relativistic Dirac equation,

$$(c\boldsymbol{\alpha} \cdot \vec{p} + mc^2 \boldsymbol{\beta} + V(\vec{r}) - \varepsilon_i) \Psi_i(\vec{r}, \xi) = 0 \tag{48}$$

Here $\boldsymbol{\alpha}$ and $\boldsymbol{\beta}$ are 4×4 matrix operators composed from the Pauli spin matrices, $c = 137.037$ is the speed of light in a.u. and $V(\vec{r})$ is an approximation to the potential seen

by an electron with (space, spin) coordinates $(\vec{r}, \xi)$. The one-electron wavefunction Ψ_i are 4-vectors composed of the so-called large and small components of mixed spin, as described in standard texts [49]. The development of suitable potentials V has an extensive literature both in the context of Dirac-Fock theory [50] and Density Functional theory [51]. The principal unresolved problem is that the Coulomb potential as normally written is not Lorentz invariant, and partial solutions such as the Breit interaction and their DF counterparts [52] have not been established as leading to significant improvements in predicted properties. In general it seems that corrections to the commonly used nonrelativistic DF potentials are important essentially for core orbitals, and for the wavefunction structure close to the nucleus [53]. In the following we will assume that the potential V is constructed by the same procedure as in the nonrelativistic case, however, making use of the relativistic density, again defined as in Eq. (3). This methodology has been found to yield quantitatively useful results, in band structure [54], molecules and clusters [17], [55]. The primary differences between nonrelativistic (NR) and relativistic (R) potentials are readily seen in atomic calculations [56]:

1. In the *direct* effects, the s and $p_{1/2}$ shells contract and gain binding energy, due to the kinetic energy operator.

2. The *spin-orbit* interaction partially lifts the degeneracy of the (n, l) shells, leading to states characterized by (n, l, j) with total angular momentum $\mathbf{j}$.

3. In the *indirect* effects, the d and f shells react to the increased nuclear screening and expand, altering the ground state configuration significantly for the heavy metals.

These features carry over into molecules and solids, but are generally more subtle due to the mixing between AOs of different character on different sites.

Since we are interested in magnetic interactions and frequently encounter open-shell systems, an analog of the convenient nonrelativistic spin-polarized scheme is needed. Fortunately, the well-known two-fold Kramer's degeneracy of relativistic wavefunctions, related to time-reversal symmetry, provides a simple solution. We have thus introduced the so-called *moment-polarized* scheme in which functions Ψ_i and $\tau\Psi_i$, where τ is the time-reversal operator, are analogous to the up- and down-spin nonrelativistic spin-orbitals [53, 57]. In atoms, these functions consist of $+m_j$, $-m_j$ components of the (n, l, j) shells and in the absence of a magnetic field are easily shown to be degenerate. External magnetic fields or internal (exchange) fields lift the degeneracy in exactly the same fashion as for up- and down-spin states, and in fact the orbitals are identical for $\ell = 0$ (s-states).

As in the spin-polarized NR case, the convenience of having only two potentials to represent magnetic interactions is obtained at a price. This price includes some contamination of the SCF solutions with a mixture of multiplets, which can sometimes be resolved by projection techniques, including for example, the Slater Sum Rule of atomic theory. The ease of calculation of an R potential which treats exchange in open-shell heavy atom systems reasonably well, without introducing artificial (and incorrect) spin-polarization is a considerable advantage.

Symmetry is also easily exploited in the relativistic case, making use of the double groups and projection operator techniques [58]. A general numerical procedure has been incorporated in the DV codes to generate 4-component NAO symmetry orbitals for all relativistic point groups [34], [35]. The resulting SCF equations and procedures are identical to those of the nonrelativistic case, except that in general matrix elements and wavefunctions are complex numbers. Standard techniques for finding eigenvalues and eigenvectors of Hermitean matrices are used to solve Eq. (8) [59]. As a practical matter, we observe that SCF solutions of the Dirac equation take about twice as much computer time as for the nonrelativistic problem, in a typical application.

2.9 DVM as a Subroutine for Dynamics

In many materials problems, for example at surfaces or interfaces, the chemical composition and nuclear coordinates are not fully known. Indeed, any information which can be obtained by theory on these basic structural properties will be useful, in conjunction with experiment. Spatially Resolved Electron Energy Loss Spectroscopy (SREELS), X-ray near-edge absorption (XANES) and emission, Mössbauer spectra, etc. provide site-specific probes which can be combined with theory to help resolve structures.

In principle, DF calculations can not only provide total energies versus geometry, but also atomic forces [60]. The DF equivalent of the Hellman-Feynman theorem, augmented by contributions due to incomplete basis sets, does indeed provide a viable scheme for molecules and systems with relatively high symmetry [61]. Various methodologies, including gradient-based steepest descent, variable metric, [62] and pseudo-dynamical simulated annealing [63] provide strategies for locating the equilibrium geometry. However, in complex systems; e.g., a metal particle of tens or hundreds of atoms, a stacked-molecular polymer or a grain boundary in a ceramic, there are simply too many degrees of freedom to be attacked in a single quantum calculation. More importantly, there are typically an enormous number of local minima and even physically important transient and metastable

states which play a role in the observed spectra and thermodynamic properties.

We have chosen to break the problem into two parts:

1. Use parametrized interatomic potentials to sample the geometry, using classical Molecular Dynamics (MD) or Monte Carlo/Generalized Simulated Annealing (MC/GSA).

2. Take snapshots of the electronic structure at selected geometries and/or time intervals, with DF methods

3. Use the electronic structures calculated to refine the interatomic potentials

4. Project physical properties from a characteristic set of states, and form thermal and/or spatial averages for comparison with experiment.

The MD and MC classical methods are well described in the literature [64] for defects, interfaces and grain boundaries, an embedding scheme is used to focus computational effort on the region of interest [65], [66]. The MD scheme is most useful to extract thermodynamic averages, vibrational data, and to observe evolution of the model system from a selected initial state. On the other hand, the MC/GSA schemes give the option to sample the *entire* parameter space (with sufficient patience) and map out the multiple basins of the potential surface. Of course the results are totally dependent upon the input potentials; thus it is critical to be able to verify and improve their parametrization. In simple molecules and bulk systems this can be done by direct reference to experimental bond lengths, bond angles, cohesives energies, sublimation energies, etc. For example, the GROMOS data base [67] provides a very useful parametrization of a large number of molecular interactions (Hook's law, van der Waals, bilinear angular terms, Coulomb), which can be easily updated. For metals, two body potentials of the van der Waals type and many-body interactions such as the Embedded Atom Method [68] (EAM) and its extensions have found much use and are readily executed. For ionic solids, particularly the oxides, a considerable literature exists, ranging from two-body potentials of the Buckingham type to shell-model potentials which include some aspects of electronic polarization and embedding [69].

In complex systems, particularly with defects and interfaces, experimental data are almost never availabe in sufficient detail to determine the interatomic potentials. Thus theory has an indespensible role in verifying and improving the potential data. We have therefore constructed a hybrid MD/MC-DV procedure which implements classical and quantum aspects just described into a coupled sequence of steps [70]. Without exagger-

ation, we may call this a "Theorist's Scanning Microscope", as it surveys spatial and temporal characteristics of a system much as an experimental scanning microscope does.

2.10 Summary of the Computer Code

As described in the earlier sections, the DV method is entirely numerical, and thus all variables are defined in the three-dimensional grid. The fundamental characteristic of the architecture of the DVM system of codes is that procedures are executed in the memory for a block of grid points at a time. The blocks of points are created and stored in temporary disk space, from where they are recalled. All variables are calculated and stored in disk for the same blocks. In the current version, blocks of 600 points are used. For the larger calculations, typically $1.0 - 1.5$Gb of temporary disk space must be reserved for this purpose.

A short summary of a SCF calculation is as follows:

1. The program reads in data for the atoms in the cluster, such as Z values and nuclear coordinates, and other parameters.

   A symmetry program determines the point group and generates the coefficients of the symmetry functions for the irreducible representations. This program is entirely general, and works also with the double groups related to the relativistic calculations.

2. The basis functions are generated by local density atomic calculations.

3. The crystal atoms (in the case of solids) are generated at the exterior sites to produce the embedding.

4. The three-dimensional points grid is generated by the Diophantine procedure and/or more accurate schemes. Basis functions, densities, etc., are obtained on the grid points.

5. An initial model charge density ρ_M is constructed by superposing the atomic densities of the basis atoms.

6. The matrix elements are obtained for the matrices in Eq. (8), which are solved by diagonalizing $[H]$. The set of eigenvectors obtained determines a density ρ according to Eq. (3).

7. A new ρ_M is obtained by least-squares fitting the ρ obtained to the expansion in Eq. (28), carried to the desired degree of accuracy.

8. A new model Coulomb potential is obtained according to Eq. (36). Steps (6)-(8) are repeated until the desired degree of self-consistency is reached.

9. When self-consistency is achieved, the related eigenvalues and ρ are stored in a permanent disk file, for further use in calculations of total energy and several other properties.

Finally, it is interesting to emphasize some advantageous features of the DV method:

a) Any operator may be added to the Kohn-Sham hamiltonian, in a simple and straightforward manner, as for example $\vec{E}_0.\vec{r}$ where $\vec{E}_0$ is an external electric field (Stark effect) and $s_z H_0$ (Zeeman effect) where H_0 is an external magnetic field.

b) The usual and most convenient basis sets employed are numerical; however, one may use analytical basis functions such as Slater or Gaussian if desired, simply by tabulating their values in the grid points.

c) A preliminary evaluation of a given physical or chemical system may be done with little computational effort, using few points in the numerical integration grid and less accurate model density.

d) Practically, we observe that the numerical DV scheme scales computationally with the number of basis functions N as N^2, whereas DF methods with Gaussian basis sets scale as N^3, Hartree-Fock as N^4 and GVB or many-body perturbation at the MP2 level as N^5 or higher.

e) In the solution of the secular equations, considerable point-by-point cancellation of numerical errors is achieved.

f) The numerical LDA atomic calculations generate conveniently compact and environment-adapted basis with a small number of functions.

3 Molecules

3.1 Porphyrinic Molecules and Solids

The porphyrins and their derivatives, such as the tetraazaporphines, continue to exhibit a rich chemistry due to varied possibilities of metal and ligand substitution. They appear in an enourmous variety of settings, from industrially important dyes, to biological and

water-soluble catalysts, to molecular metals, to model one-dimensional magnetic systems. Gross features of the electronic structure are dominated by the "core", consisting of a divalent metal like Mg or Cu (or H_2) in square planar coordination to C or N ligands. Properties are "tuned" by choice of core elements, and by substitution of peripheral ligands at the outer carbon "fence", see Fig. 3.

From the point of view of transport and low-lying optical excitations, a principal point of interest is the competition between ring-based p_π orbitals and metal-centered orbitals, particularly transition metal 3d orbitals. The balance between, and admixture of, these two components can be modified and thus leads to a varied electrical conductivity and magnetic coupling among elements in the stacked metal conductors based on the monomer porphyrinic building blocks. The partially oxidized metal phthalocyanines, like Cu(Pc)I and $Cu_{1-x}Ni_x$(Pc)I provide a fascinating class of materials with a complex temperature dependence of conductivity and magnetic susceptibility. As more highly purified materials have become available, their intrinsic properties are becoming apparent, and permit systematic properties design based upon doping and substitution strategies [71].

These molecules show strong characteristic electronic absorption in the visible region (Q-band, ca. 680 nm) and UV (Soret or B-band, a broad band with peak $\sim$ 330 nm), with band-splitting and shifts linked to overall symmetry and composition of the macrocycles. Synthesis of molecules with peripherally fused-benzo rings (PC) and dithiolene groups (PZ) permits a detailed analysis of the role of peripheral ligands. A single Q-band peak is observed for 4PZ and 4PC high symmetry (D_{4h}) macrocycles. Ligand substitution leads to the splitting of the Q-band into two peaks in the lower symmetry 2PC/2 PZ cis, 3 PC/1 PZ, 1 PC/3 PZ (C_{2v}) and 2 PC/2 PZ trans (D_{2h}) configurations. Intensities and band splittings and shifts calculated in the DV framework have been compared in detail with qualitative molecular orbital models and experiment in the visible and UV [72].

The partial density of states (PDOS) provides a convenient analysis of wavefunction composition versus energy, making use of the Mulliken population analysis of individual orbitals. Here PDOS is defined as

$$D^q_{n\ell}(E) = \sum_p P^q_{n\ell,p} L(E - e_p, \delta) \tag{49}$$

where $P^q_{n\ell,p}$ is the population of atomic orbital $(n\ell)$ on site q in energy level p, and $L(E - e_p, \delta)$ is a line-shape function with width δ. We typically use a Lorentzian, with $\delta \sim 0.1$ eV for this purpose. A typical PDOS, for the high symmetry 4PZ Ni tetraazaporphyrazine (TAP) case, is shown in Fig. 4.

Here are shown the total DOS and important Ni, C, N and S ligand contributions; an extensive mixing of orbital character in the valence bands is evident. The pinning of the Ni 3d band around the Fermi energy E_F is characteristic of an open shell atom. Unlike the magnetic (S=1/2) copper analogs, the Ni-based compounds are experimentally diamagnetic, as confirmed by the calculations. The mixed $Cu_{1-x}Ni_x$ stacked compounds provide an interesting example of magnetically diluted one-dimensional interactions, whose properties are still being investigated.

Dipole-allowed optical transitions are described in the one-electron DF model in the usual way, with absorption intensity given by

$$I(e) = \sum_{i,f} L(e - e_{if}, \delta) n_i (1 - n_f) f(e_{if}) \tag{50}$$

with $e_{if} = e_f - e_i$, and oscillator strengths f,

$$f(e_{if}, \hat{e}) = \frac{2m}{\hbar^2} e_{if} \left| \langle \phi_f | \vec{r} \cdot \hat{e} | \phi_i \rangle \right|^2 \tag{51}$$

Theoretical and experimental absorption bands of 4PZ Ni (TAP) are given in Fig. 5. The theoretical bands were calculated using the *ground state* wavefunctions; the low-lying Q-band is seen to be in excellent agreement with experiment. The B-band region which marks the onset of strong UV absorption, typically associated with charge-transfer transitions, is fairly well represented. The W-band, centered at $\sim$ 2.5 eV in experiment and attributed to S-based transitions, is considerably blue shifted in the calculations. This may be due in part to substitution by hydrogens in the calculations for terminal groups far away from the porphyrazine ring (-$(CH_2CH_2O)_3H$ in star-porphyrazine and -$(CH_2)_7CH_3$ in the phthalocyanine macrocycle) which are attached to the outer oxygen atoms. In order to test effects of H termination, calculations were also performed using methyl groups as terminators in several cases. No significant differences in *occupied region* electronic structure were found; however, perturbation of the excited state region could occur. Some aspects of electronic relaxation effects on optical transitions were explored, by use of the Transition State (TS) scheme [39]. This approach gives a reasonably good account of excitation energies, when the nuclear framework does not shift significantly between ground and excited states. TS calculations on the Q-band showed shifts of a few tenths eV from one compound to the other, but made no significant overall improvement in the comparison of experiment and theory. TS studies were not made on the higher energy W- and B-band regions; here the effects of electronic rearrangement in the excited state are expected to be greater, and merit further study.

Finally, we touch upon recent work on intermolecular interactions in stacked chain systems, concentrating on Cu(Pc)I. In undoped Cu(Pc), the monomers stack in a slipped herringbone pattern; in the partially oxidized Cu(Pc)I the stacking is vertical. In the latter case, the interplanar spacing is observed as $\Delta Z = 3.19\mathring{A}$ with a staggered configuration: each molecule is rotated $\Delta\theta = 42^0$ about the stacking axis with respect to its neighbor below. These values are typical for a wide range of compounds.

MD/MC simulations on dimers and tetramers, using only van der Waals interactions from a standard molecular data base reproduce these features surprisingly well, with predicted values of $\Delta Z = 3.20\mathring{A}$ and $\Delta\theta = 45^0$. DF calculations made on the dimer produce very similar results, with the advantage that the angle and distance dependent energy $E_{bind}(z,\theta)$ provides a basis for refinement of the semiempirical potential parameters [70]. An interesting interpretation of the mechanisms of electronic repulsion which favor the staggered ground state configuration was given by Rosa and Baerends [73]. The antiferromagnetic (AF) alignment of Cu moments in the dimer was found to be the ground state, in agreement with the observed AF properties of the solid. This represents a short-range order of the one-dimensional chains; the observed bulk ordering at 4K is believed to be due to three-dimensional interactions among the chains.

3.2 $[Cp\ (CO)_2\ Fe\ (\eta^1\text{-}T)]^+$

A subject of technological interest is the bond between thiophene and a transition metal M. This is due to the hydrodesulfurization of petroleum, which is performed in the presence of a transition metal catalyst [74]

$$C_xH_yS + nH_2 \stackrel{cat}{\rightarrow} \text{hydrocarbons} + H_2S$$

Thiophene is the compound present in petroleum from which it is most difficult to remove the sulphur, due to this atom begin part of an aromatic ring.

One of the modes of coordination of thiophene to catalyst surfaces most frequently suggested is the S or η^1, in which the bond is formed directly between the sulphur and a transition metal atom. In examples of the S-bonding mode which have been well-characterized by X-ray diffraction, a pyramidal geometry has been found [75], which is also present in the absorption of thiophene on metallic surfaces such as copper [76].

To investigate the bond between thiophene and M in the S (or η^1) mode, DV calculations were performed for the complex ion $[Cp\ (CO)_2Fe\ (\eta^1\text{-}T)]^+$ (Cp=cyclopentadienyl, T=thiophene) [77]. Due to the strong covalency between the Fe and the ligands, the electron configuration is a low-spin closed-shell, so that no spin-polarization is present.

Total energy calculations were performed for several values of the angle θ between the plane of the thiophene and the Fe-S bond (see Fig. 6), to determine the equilibrium value. Two minima were revealed, one at 120^0 (deeper) and the other at $\sim 210^0$ (see Fig. 7). An analysis of the changes in the orbitals brought about by the angular variation reveals that the mechanism leading to $\theta < 180^0$ is the reduction of the antibonding interaction between the occupied Fe d_π orbitals and the S π canonical lone pair in free thiophene. This mechanism is consistent with the idea of $sp^2 \rightarrow sp^3$ rehybridization of the S atom in thiophene, which explains the pyramidal geometry.

3.3 The Molecular "Ferric Wheel"

Systems of nanoscale or mesoscopic dimensions containing a finite number of magnetic transition-metal atoms display a number of interesting or unusual properties and have been the subject of many recent investigations [78], [79]. Properties observed include superparamagnetism [80] and quantum tunnelling [81]. Important technological applications may also be envisaged, such as magnetic refrigeration and data storage [82].

Large polynuclear organometallic molecules are among such systems, that are in the borderline of isolated and collective magnetic behavior [83], [84]. These are usually formed by a core of transition metal atoms bridged by O or S, encapsulated within a crown of organic ligands. Thus magnetic collective effects are due entirely to interactions within the molecule.

One example of such systems is the circular molecule $[Fe(OMe)_2(O_2CCH_2Cl)]_{10}$ denominated "ferric wheel" [84], of which the ground state is antiferromagnetic (S=0). A transition-metal molecule of this size constitutes a challenge for DF calculations.

Electronic structure SCF spin-polarized calculations were performed with the DV method for the cluster $[Fe(OC)_2(O_2CC)]_{10}$ formed by stripping the "ferric wheel" molecule of its peripheral H and Cl atoms (see Fig. 8) [85]. Mössbauer spectroscopy measurements have been reported [84]; calculations of the hyperfine parameters were performed and compared to experiment. The magnetic moment obtained on the Fe was $4.3\mu_B$ and the charge +2.3 [85].

The isomer shift is defined as [86]:

$$\delta = 2/3e^2\pi Z S'(Z)\Delta < r^2 > [\rho_A(0) - \rho_S(0)] \equiv \alpha\Delta\rho(0) \qquad (52)$$

where $\Delta < r^2 >$ is the variation of the mean square radius of the nucleus between excited and ground states of the Mössbauer transition, S'(Z) is a correction for relativistic effects,

and the term is brackets is the difference between the electron density at the nucleus in the absorber A and source S (in other words, between a given compound and a standard system). As defined, δ is linear against $\rho(0)$ for a series of compounds or ionic states of Fe. In a non-relativistic approximation, only orbitals containing s-states of Fe contribute to $\rho(0)$.

The quadrupole splitting ΔEQ of the excited state of the 14.4 KeV transition of ^{57}Fe is given by [86]:

$$\Delta EQ = 1/2\ eV_{zz}Q\left(1+\frac{\eta^2}{3}\right)^{1/2} \tag{53}$$

where Q is the quadrupole moment of the nucleus in the excited state (I=3/2), V_{zz} the electric field gradient and η the asymmetry parameter.

The electric field gradient is produced by the non-spherical charge distribution of the nuclei and electrons around the probe nucleus. It is a traceless tensor whose components are defined as

$$V_{ij} = \frac{\partial^2 V}{\partial x_i \partial x_j}\ (x_i, x_j = x, y, z) \tag{54}$$

where V is the eletrostatic potential. Each one of the six independent components of the symmetric tensor was calculated with the expression (in atomic units) [87]-[90]:

$$V_{ij} = -\int \rho(\vec{r})(3x_i x_j - \delta_{ij}r^2)/r^5 dv + \sum_q Z_q^e(3x_{qi}x_{qj} - \delta_{ij}r_q^2)/r_q^5 \tag{55}$$

The first term in Eq. (55) is the electronic contribution, obtained with the molecular $\rho(\vec{r})$, and the second term the contribution of the surrounding nuclei shielded by the core electrons, with effective charge Z_q^e. After diagonalization, the electric field gradient is defined by the convention:

$$|V_{zz}| > |V_{yy}| \geq |V_{xx}| \tag{56}$$

with the asymmetry parameter η given by:

$$\eta = \frac{V_{xx} - V_{yy}}{V_{zz}} \tag{57}$$

The Contact (or Fermi) component H_c of the magnetic hyperfine field at the Fe nucleus may be expected to be by far the largest in the present compound. H_c is proportional to the spin density at the Fe nucleus

$$H_c = (8\pi/3)g_e\mu_B[\rho_\uparrow(0) - \rho_\downarrow(0)] \times \frac{1}{2} \tag{58}$$

In Table I are given calculated and experimental values of δ and ΔEQ. The sign of the latter was not determined experimentally. The magnetic hyperfine field was not measured,

since at 4.2K no magnetic splitting of the Mössbauer lines was observed [84]. In calculating the spin-density at the Fe nucleus, only the valence contribution is obtained from the molecular calculation. The core contribution is obtained from a separate calculation for a free Fe ion with the configuration as found for the molecule. This is due to the lack of flexibility of the core basis, which inhibits spin-polarization.

3.4 Molecular Fragments

In this section we wish to show how analysis of molecular fragments, using the embedding scheme described previously, relates to properties of the complete system. In particular we focus on the convergence of the electronic charge distribution around the active center of a penta-coordinate Ru complex, whose catalytic activity is of great interest. Selective catalysts for oxidation of organic compounds generally involve the formation and stabilization of metal-oxo intermediates. Chelating ligands containing amide donors have received considerable attention [92], notably including porphyrins and macrocyclic amides which impose a rigid planar array of four donor atoms [93]. The recent discovery of a Ru^{V} oxidation catalyst, and analysis of the related Ru^{VI}-oxo complex has shown the possibility of utilizing a more flexible coordination geometry and properties of the d^3 metal configuration [94]. These novel electron-rich systems with flexible ligands have important implications for oxidation catalyst design and may give insight into performance of the hypothetical d^3 perferryl species.

Semiempirical molecular orbital (MO) analyses have been made to rationalize and predict the relative stability of penta-coordinate transition metal complexes [95]. Symmetry arguments and Hückel-type MO calculations on model compounds were used to discuss σ- and π-bonding interactions of D_{3h} trigonal bipyramidal (TBP) and C_{4v} square pyramidal (SP) geometries for d^n metal configurations. Discussions specific to d^2 oxo complexes have focussed upon the interrelation between planar and distorted ligand structures and amido-N σ- and π-donor capacity [96]. Properties of the newly discovered paramagnetic mono-oxo ruthenium complex $Pr_4N[Ru^{V}(O)PHAB]$ and the diamagnetic complex $[Ru^{VI}(O)PHAB]$, where H_4PHAB is *bis* 1,2-(2,2-diphenyl-2- hydroxyethanamido) benzene, have been similarly interpreted in terms of MO calculations on $[RuOH_4]$ complexes of TBP and SP symmetry [94]. Both complexes facilitate C-H bond activation and oxygen atom transfer reactions, and in addition the Ru^{V} complex catalyzes the air oxidation of triphenylphosphine.

In order to obtain a more quantitative understanding of metal-ligand interactions

and the relationships between electronic structure, coordination geometry, and reactivity of the Ru penta-coordinate environment, DV calculations were undertaken on several related complexes [97], including $[RuOH_4]^q$, $[RuOCl_4]^q$ and $[Ru(O)PHAB]^q$ with q=0, -1. Anyone who has done quantum chemical molecular calculations will recognize that the terms "Ru^V, Ru^{VI}" with nominal configurations $4d^3 5s^0 5p^0$ and $4d^2 5s^0 5p^0$ represent an oversimplification of the electronic structure, which may be nevertheless very useful for qualitative discussions. The enormous Coulomb forces implied by ionic charges of +5 and +6 would immediately be screened by electron density from the ligands; it is this effect which we wish to discuss here. We choose the most extreme case, of $[Ru^{VI}(O)PHAB]^O$ for analysis, with atomic coordinates of the first coordination shell given in Table II, and analyze 6,20, and 36 atom fragments centered on Ru, along with the entire molecule. The Ru Mulliken populations and net charges on Ru and the three oxygen and two nitrogen ligands are presented in Table III. The present data are derived from *neutral* fragments, which represent an unbiased starting point; clearly the atomic charges found on the larger clusters provide information which can be used to refine the model for smaller clusters.

The fragment results, along with the entire molecule, give a consistent picture; the charge state of "Ru^{VI}" is actually something like Ru^{+2} $d^{5.7}s^{0.1}p^{0.2}$. In addition to the two d-electrons invoked in bonding interactions in semiempirical models, with low-lying empty d-states supposedly responsible for catalytic activity, we find an additional ~ 3.7 d-electrons involved in metal-ligand bonding. It is important to note that the screening mechanism which we expected is found to be short range; i.e., it derives from additional localized d-occupancy through covalent charge sharing with the ligands, and not with diffuse metal s, p charge. A typical MO near the top of the valence band is found to be a strong covalent mixture of Ru-d and ligand-p character. Analysis of corresponding "Ru^V" fragments and complexes leads to the identical conclusion, with an additional twist: the net d-populations hardly change in the two chemically distinct Ru^V and Ru^{VI} environments. This implies that understanding of the strong differences in stability and catalytic activity observed in the two species will rest more upon interpretation of modifications of the ligand p-electron structure, which is so intimately mixed with the rather stable metal d configuration.

3.5 Relativistic Effects in Molecules with 5d-metals

3.5.1 $[Ir(CN)_5]^{3-}$

The ligand CN forms bonds with transition-metal atoms that are very covalent in nature, resulting in strong electronic delocalization. Added to this, the presence of a relativistic atom induces complex and interesting effects. The low-spin complex ion $[Ir(CN)_5]^{3-}$, in which Ir is in the unusual formal oxidation state +2, has been obtained by irradiation of the hexacoordinated diamagnetic Ir(+3) complex with electrons or X-rays in solid alkali halide matrices [98]. $[Ir(CN)_5]^{3-}$ has a square-pyramidal structure (see Fig. 9) and one unpaired electron in the HOMO.

The electronic structure of $[Ir(CN)_5]^{3-}$ has been obtained with the DV method in both the non-relativistic and relativistic frameworks, to assess the relativistic effects in the chemical bonds [99]. The basis functions used for Ir were $4f_{5/2}$, $4f_{7/2}$, $5s_{1/2}$, $5p_{1/2}$, $5p_{3/2}$, $5d_{3/2}$, $5d_{5/2}$, $6s_{1/2}$, $6p_{1/2}$ and $6p_{3/2}$. All other orbitals were kept in the core. For C and N all orbitals were included in the variational space.

In Table IV are given the populations and atomic charges derived from the calculations. It is seen that the main difference in the Ir populations is in the 6s orbital, which acquires 0.14 electrons in the relativistic calculation (from 0.09 to 0.23). This is due to the stabilization of the MO's containing 6s, an effect discussed in Section 2.8, and which is also seen in the energy levels. On the other hand, 5d-containing MO's are destabilized by relativistic effects and thus the 5d population slightly decreased. The overall charge on Ir is slightly less positive in the relativistic calculation. The charges on C and N, as expected, hardly change at all.

In Table IV are also compared the bond orders for the nonrelativistic and relativistic calculations. There is a significant increase of the Ir-C bond order due to relativistic effects: therefore the latter contribute to stabilize the molecule. On the other hand, as expected, the C-N bond order is not affected.

3.5.2 Metal-cluster Halogen Complexes

As discussed in section 2.8, relativistic effects on the valence electronic structure of atoms are dominated by spin-orbit splitting of (nl) states into (nlj) subshells, and stabilization of s- and p-states relative to d- and f-states. Here we examine consequences of relativistic interactions for cubo-octahedral metal-cluster complexes of the type $[M_6X_8X_6]$ where M=Mo, Nb, W and X=halogen, which have a well defined solution chemistry, and are building blocks for many interesting crystal structures.

Relativistic effects will be largest in the tungsten complexes, and it is useful to begin with the W_6 fragment, where the nominal $W^0 5d^4 6s^2 6p^0$ configuration is expected to produce a typical metallic s-d band straddling the Fermi energy. As shown in Fig. 10, this is the result for both nonrelativistic (NR) and relativistic (R) calculations, using interatomic distances [100] taken from the chloride complex $[W_6Cl_8Cl_6]^{2-}$. Note that the nominal valence of tungsten is +2 in this complex; i.e., with configuration d^4s^0.

As we see from the figure and the populations of Table V, our expectations are fulfilled; the bare cluster reveals a normal s-d band with populations shifted from d-> s,p in the R case.

An extensive study has recently been made of $[W_6X_8X_6]^{2-}$ clusters, comparing DF theory, Hückel MO results, an experimental luminescence and absorption bands [101]. Here we focus mainly on the NR vs R consequences. The Mulliken populations and net atomic charges of the $[W_6X_8^iX_6^a]^{2-}$ clusters obtained from NR and R DV calculations are presented in Table VI. The symmetry type of the frontier orbitals and the gap between the HOMO and LUMO are summarized in Table VII; experimental absorption edge and emission maxima are also included. The atomic orbital compositions of the HOMO and LUMO from the two calculations differ primarily in their W 5d content, in the order NR> R as expected.

The presence of a bonding-antibonding (B-AB) gap or valence band-conduction band gap (VB-CB) of $\sim$ 2.7eV is a dominant feature of the NR results. The NR and R levels correlate to each other as follows: $a_1 \longrightarrow \gamma_6$, $a_2 \longrightarrow \gamma_7$, $e \longrightarrow \gamma_8$, $t_1 \longrightarrow \gamma_6 + \gamma_7$, $t_2 \longrightarrow \gamma_7 + \gamma_8$ (for both gerade (g) and ungerade (u) representations), where γ_6, γ_7 and γ_8 are the (2-,2-, and 4-fold) irreducible representations of the double-group O_h^*. Correlations between the NR and R energy levels of the chloride are shown in Fig. 11; we see that R splitting and energy level shifts act to considerably reduce the band gap.

While the formal charges on the metal and halide atoms are +2 and −1, respectively, one would expect smaller values if covalent bonding is present within the clusters. The NR calculations produce charges which suggest a high degree of covalent bonding within the cluster, especially within the W_6X_8 core, and are similar to those calculated for the analogous molybdenum clusters [102]. It can be seen that as one goes through the halide series, the charges on the metal become significantly smaller, 1.07>0.50>0.75 for Cl, Br, and I respectively, indicating increasing covalent bonding. Absolute values of Mulliken charges of course depend upon the basis set; however, trends and shifts have great interpretative value. The net charges are consistent with experimental chemical data; i.e.. the stronger covalent bonds within the cluster core (as compared with the W-

X^a bonds) predicted by the DV calculations is seen in the substitution chemistry of the cluster. The outer ligands are fairly labile and can be replaced under mild conditions, but the inner halides are much more tightly bound and only can be replaced under harsh conditions. The NR results (Table VI) give Mulliken populations for the three clusters showing a smooth trend of increasing W 5d, 6s, 6p occupancy in the halide series; there are significant contributions from the tungsten 6s and 6p orbitals. There is a small but significant halide d-orbital contribution, 0.07-0.09e in the NR case; the largest values are found on the inner Cl, indicating there a direct Cl-d participation in bonding. Table VI also reveals the considerable effects of relativity on the charge distribution; while the general trends of the NR case are preserved, the magnitude of ionic charge transfer is accentuated. The R populations show the expected shifts in orbital occupation compared with the NR results; some electron density has moved from the W 5d, X^i and X^a p orbitals into the W 6s and 6p and (to a lesser extent) X d orbitals. The net W $5d_{(3/2,5/2)}$ occupancy of $3.40 < 3.80 < 3.94$ for X=Cl, Br, and I respectively is thus considerably less than in the NR model, and also less than the formal W^{2+} d^4 value. An increase in the W $6s_{1/2}$ $6p_{(1/2,3/2)}$ occupancy across the series is noted. Both X^i and X^a d orbitals have gained significant electron density; apparently the more diffuse R orbitals are useful for bonding to the cluster core. The net R halide d-occupancy decreases from 0.51 to 0.11 for X^i and from 0.20 to 0.11 for X^a across the series. The greater contribution of the X^i d orbitals for the smaller halides apparently offers greater stabilization through directional covalent bonding.

The emission spectra of the $[W_6X_8^iX_6^a]^{2-}$ clusters are dominated by bands in the red and infrared [103]. It has been suggested that the emission maximum corresponds to the transition from the LUMO to the HOMO; Hückel MO calculations support this interpretation [102]. However, the extremely long emissive lifetimes (2.2, 16 and 26 μs for Cl, Br and I, respectively), similar to those displayed by the related molybdenum clusters, may be assumed to be the result of a *spin-* and symmetry-forbidden transition. The trend in emission energies seen in the series from chloride to iodide, with band maxima at 1.83 (Cl), 1.85 (Br) and 2.05 (I) eV, suggests that there is some halide character in the HOMO and/or LUMO, consistent with our calculations. This blue shift with increasing ligand size is, however, contrary to that expected (and calculated by DF) for the unoccupied MOs; thus the emissive state may represent a triplet, with energy significantly shifted with respect to the LUMO. Experiments with ligand substitution show that the shift in emissive energy varies more with the inner halides than the outer ligands, indicating that the inner halides give the primary ligand contribution to the frontier orbitals. Since the

absorption bands are strongly blue-shifted with respect to experimental emission bands, we suppose (along with other authors) that excitations into the AB peak rapidly decay by a nonradiative process into a long-lived low lying triplet. Our previous study on the Mo_6-based analogs suggests that geometric distortion accompanies this process [102]. The present results indicate, and the observed temperature dependence of the emission bands suggests, that most likely geometric relaxation and excited-state multiplet structures must be taken into account in order to predict emission quantitatively.

First-principles DF one-electron ground state energy levels are not expected to show quantitative agreement with either experimental absorption or emission data. Often semi-quantitative comparisons can be made and trends can be discerned. In the present case, the NR HOMO-LUMO gap is too large in the cloride and bromide, while the iodide value coresponds quite well with the emission peak, probably by accident. The trend in gap energy is a red shift, expected due to the ligand-p atomic level systematics, 2.70>2.05>1.95 eV, the opposite of that observed in the emission data. The NR LUMO-HOMO transition is symmetry-forbidden in the chloride and bromide cases, but is symmetry-allowed in the iodide case. It can be seen from Table VII that the chloride an bromide clusters share the same HOMO, while the LUMO is the same for the bromide and iodide clusters. The HOMOs are fully occupied for all three clusters, giving as ground state a totally symmetric ^1A_g singlet.

Since there are many closely-spaced energy levels in the vicinity of E_F, it is clear that electronic absorption and emission bands involve more than a single discrete molecular orbital pair. A typical NR PDOS diagram of the chloride cluster, given in Fig. 12, shows the B-AB band gap centered around the Fermi energy E_F (set to zero), while in the R model (Fig. 12) E_F falls in the midst of a densely spaced set of levels near the top of the occupied valence band. The metal contribution is similar in all three clusters, with a partially-filled d-band consistent with the net 5d population close to 4.7-4.8. Interactions between the metals and the inner halides to produce the cluster core have resulted in a lowering of the X^i s and p orbitals relative to those of the outer ligands, reflecting the higher stability of the core. The W-X^i overlap can be seen at ca. -5 eV, while the W-X^a overlap is at higher energy (-1 to -2 eV). It is seen that the HOMO region is dominated by the X^a p orbitals, and the LUMO region contains primarily W 5d and X^a p character. The DV results thus support the interpretation that the absorption maxima for the $[M_6X_8^iX_6^a]^{2-}$ clusters are due to ligand-to-metal charge transfer transitions.

The DV results are therefore in qualitative agreement with experimental assignments. The most prominent feature in the region $E>E_F$ is the antibonding metallic peak, located

at 3.5, 3.0 and 3.1 eV above the corresponding bonding peak for X=Cl, Br, and I respectively. The agreement with experimental absorption is semiquantitative; e.g., the VB-CB gap of 2.70 eV for the chloride can be compared with the band onset at 490 nm (2.53 eV) in polymethyl methacrylate (PMMC) films, which exhibit well defined absorption features at 400, 350, 310 and 280 nm (3.10, 3.54, 4.00, and 4.42 eV) at low temperature.

The broadening of both valence and conduction band due to spin-orbit splitting of levels, and the net upward shift and broadening of the W 5d component of the VB are largely responsible for the differences seen in comparing NR and R DOS in Fig. 12.

In looking at the frontier orbitals, the first observation to be made is the dramatic closing of the VB-CB gap in the R model. It can be seen from Fig. 11 that a number of VB levels in the NR case are raised in energy, and a number of CB levels are lowered when relativistic effects are considered. This is expected, in view of the atomic/ionic spin-orbit splittings of 0.73 and 1.31 eV for W 5d and 6p levels, respectively, and 0.51 eV for the Br 4p level. In addition, detailed level counting shows some mixing among the original NR VB and CB orbitals. Lifting of j-degeneracy has the striking effect here of pushing the HOMO down into the midst of the valence band, closing the HOMO-LUMO gap. In that sense the DOS diagram for the R case resembles that of a metal.

The implications of this result for spectroscopic predictions are considerable. The composition and symmetry of the HOMOs and LUMOs have changed considerably from the NR case, and we see that the HOMO-LUMO transition is now essentially irrelevant with respect to the IR emission spectra. In the simplified one-electron picture, we predict absorption in the extreme IR up to 0.7 eV for Cl-, 1.0 eV for Br-, and 0.2 eV for the I-ligand clusters. Dipole allowed one-electron transitions in the IR emission region are predicted to have a threshold at $\sim$ 2.8 eV for Cl-, $\sim$2.7 eV for Br-, and $\sim$ 1.1. eV for I-ligand clusters. From the DOS diagrams, we can predict intense absorption into the antibonding peak located 4.1, 3.7 and 3.0 eV above E_F for X=Cl, Br and I respectively.

4 Solids

4.1 Magnetism and Superconductivity in Borocarbides

The recently synthesized rare-earth quaternary borocarbides such as RM_2B_2C (R=rare earth, M=transition metal) have stimulated much interest because of interactions between their magnetic and superconducting (SC) properties. For example, superconductivity coexists with magnestism over a limited temperature range in the Dy, Ho, Er, and Tm

nickel compounds [104]. The layered crystal structure can be described schematically as (RC)-$(MB)_2$-(RC)- with square four-fold coordinated R-C sheets alternating with metal boride slabs with prominent MB_4 interlinked tetrahedral units. The M atoms form a plane with interatomic distances characteristic of a metal; e.g., R(Ni-Ni)=2.45 $\AA$ in YNi_2B_2C is slightly shorter than in the pure metal (2.50$\AA$). The nature of chemical bonding in this structure and its consequences on transport properties is not immediately apparent: despite its great structural anisotropy, band structure calculations suggest [105] rather isotropic electronic densities of states. Torque magnetometry measurements of YNi_2B_2C show high isotropy [106], while superconducting critical fields of the rare earth compounds show some angular dependence [107].

Magnetic moments on the nominally trivalent R ions provide the driving force for polarization of the conduction electrons and resulting effects on superconductivity. R-moments within a given plane are found by neutron diffraction to align ferromagnetically, with the net moment lying in, or close to, the (a-b) RC plane. Below the antiferromagnetic (AF) ordering temperature, ranging from 1.5K (Tm) to 20K (Gd) in RNi_2B_2C the net moments in alternating RC planes align opposed to each other. Over a limited temperature interval, more complex incommensurate spiral c-axis AF structures are observed [108]. The existence of regions of coexistence between AF and SC states, and the detailed mechanisms by which the magnetic coupling lowers the superconducting transition temperature T_c, suppressing SC entirely for the light rare-earth compounds, pose severe challenges for theory.

We have utilized the embedded cluster DV scheme to study the electronic structure of the $Y(Ni_{1-x}M_x)B_2C$ superconductors (M=Fe, Co, and Ru), with 71 atom variational clusters centered on the substitutional site [109] as shown in Fig. 13. Bonding within the RC plane is found to be highly ionic, while B-C and Ni-B bonding structures are analyzed as typically covalent. In addition, the strong overlap between atoms in the transition metal plane has typical metallic character. Thus the entire spectrum of chemical bonding including ionic, covalent, and metallic structures is found within this peculiar crystal structure. The Ni-B slab is found to be electron-rich, as the result of charge transfer from the RC planes.

DOS analysis shows that both Ni and B character dominate the region around E_F, as also predicted by band structures. Doping by Co, Fe, or Ru causes a broadening (lattice disorder) and weakening (dilution effect) of the Ni-dominated peak which correlates reasonably well with the experimentally observed depression of T_c. A simple rigid-band+dilution model works adequately for low doping levels, but is inadequate for

> 20% impurities. The integrated transition metal PDOS or net metal d-population was found to correlate strongly with T_c, as an alternative to the frequently used $D(E_F)$ peak height. A small, but significant Y 4d, 5sp DOS component reveals hybridizaton of R valence states with C, and through the B-C bonds, interaction with the M-conduction electrons which turns out to be crucial for understanding the magnetic interactions.

Variation of electronic structure with rare earth, in the series $R(Ni_{0.99}Fe_{0.01})_2B_2C$ with R=Y, Gd, Tb, Dy, Ho, and Er was studied both by theory and by Mössbauer spectroscopy [110]. Quadrupole Splittings ΔEQ and Isomer Shifts δ were obtained for substitutional ^{57}Fe; the experimental δ measuring the local electron density showed very little variation with R, while the ΔEQ displayed a systematic shift. Low temperature measurements on the Tb compound revealed a combined quadrupole and magnetic interaction on the Fe nucleus, from which the sign, $V_{zz} < 0$, was additionally determined. The calculations are in excellent agreement with $|\Delta EQ|$ of experiment, see Fig. 14, and predict $V_{zz} < 0$ in all cases. The trend of ΔEQ vs R is traced to a lattice "pressure" effect; namely, compression within the (a-b) metal plane driven by reduction of R-ionic radii with increasing atomic number. Both the positive valence (mostly d-electron) and negative core/nuclear contributions to ΔEQ increase in magnitude with (a-b) compression; the more rapid variation of the valence term leads to the observed overall decrease in the magnitude of ΔEQ.

Self-consistent spin densities and their related magnetization and exchange fields were studied in the RNi_2B_2C compounds with R=Pr, Nd, Sm, Gd, Ho, and Tm [111]. One of the main puzzles, the coexistence of SC and AF order for the *heavy* rare earth compounds, and the total absence of SC in the light-R compounds, can now be more or less quantitatively explained. Most simply, we can think of the interaction between the R 4f-moment and the (mostly Ni) conduction electrons which participate in SC pairs as a multi-link process:

1. The R 4f polarizes and is hybridized with the R 5d.
2. The 5d mixes strongly with the C 2p, polarizing it.
3. Strong C-B covalency passes the polarization wave into the Ni-B slab.
4. Paramagnetic Ni (or transition metal substituent) picks up and amplifies the polarization.
5. Induced polarization weakens the SC pairs, mostly by exchange interaction.

The most important physical parameter across the rare earth series which affects this process is the strength of the 4f-5d interaction, which depends strongly on the mean distance between shells in the ion: $<r_{5d}>-<r_{4f}>$. Across the R series, both radii decrease; however, the *difference* increases almost linearly with Z, rapidly weakening the f-d interaction. Guo and Temerman have previously suggested strong f-d hybridization as the main factor in suppressing SC in $PrBa_2Cu_3O_{7-x}$, in contrast to all other isostructural $RBa_2Cu_3O_{7-x}$ compounds [112]. We find, as they did, that the f-d interaction is not simply dipolar; i.e., polarization at a distance, but strongly involves f-d hybridization as permitted by the crystalline and ligand fields. As an example, Fig. 15 shows spin-density contours on the (011) plane containing Nd, Ni, B, and C in two models: with the Nd 4f in the variational space, and in the frozen core with hybridization suppressed. Large qualitative changes and quantitative reduction in the spin density ρ_s are evident when hybridization is suppressed.

The multi-link spin transfer and polarization process is best seen in a bond-line diagram (Fig. 16). Here a zig-zag path is followed, starting at one rare earth, and following the chain R-C-B-Ni-B-C-R to the oppositely polarized R ion on an adjacent RC plane. As can be easily seen, the lighter ions Pr and Nd with smaller $<r_{5d}>-<r_{4f}>$ strongly polarize the lattice, including the distant Ni. On the other hand the heavy, weakly coupled, Ho and Tm induce much less polarization even though Ho has a considerably larger spin magnetic moment than Pr.

4.2 γ-Fe and γ-Fe/Al Particles in Copper

Pure bulk iron in the fcc crystal structure (γ-Fe) only exists at very high temperatures (between 1183 and 1667K). However, γ-Fe may be stabilized at low temperatures as small coherent precipitates in copper or copper-alloy matrices or as thin epitaxial films on a Cu or Cu-based alloy substrate [113], [114]. Recently the interest in γ-Fe has been revived due to the existence of multiple magnetic states revealed by band-structure calculations [115], which is believed to be related to INVAR phenomena in γ-Fe-based alloys [116].

A 62-atoms embedded cluster in cubic geometry was considered to represent γ-Fe (see Fig. 17), and spin-polarized SCF calculations were performed for both the ferromagnetic (FM) and antiferromagnetic (AFM) states, at several lattice constants. For the AFM, a layered arrangement of up and down spins (illustrated in Fig. 17) was considered.

Measurements of the magnitude of the magnetic Hyperfine Field by Mössbauer spectroscopy revealed small values at small interatomic distances and much larger values at

larger distances (Fig. 18) [114]. This was ascribed to a large difference in the magnetic moment between AFM γ-Fe, more stable at small lattice constants, and FM γ-Fe, more stable at large lattice constants [115]. It is the spin-polarization induced by the Fe spin magnetic moment (mainly 3d) in the s shells that originates the hyperfine field. However, the calculations of the magnetic moments for the two states AFM and FM (Fig. 19) [117] did not show such a large difference that would justify the large experimental gap in Fig. 18. The results of calculations of the hyperfine field according to Eq. (58) of section (3.3), displayed in Fig. 20, reveal that the large difference observed experimentally in the magnitude of the hyperfine fields of AFM and FM γ-Fe originates mainly from different signs of the valence electron contribution, which is positive for AFM and negative for FM, and not from large differences in the Fe magnetic moment in the the two states. This result shows clearly that the common practice of considering the hyperfine field as proportional to the magnetic moment may be very misleading.

Since many experimental studies of γ-Fe were performed for γ-Fe particles in a Cu matrix (or Cu alloy, including Cu-Al) [113], [114], it is important to probe the electronic structure of the particle-matrix systems. Embedded-cluster methods are ideally taylored to treat small particles of a metal in a host matrix, a system that would require a very large supercell in band-structure calculations. DV calculations were performed for the 14-atom Fe particle in copper shown in Fig. 21 [118]. Spin-density contour maps were obtained to assess the polarization of the Cu matrix by the coherent magnetic γ-Fe particle. Examples are given in Figs. 22 and 23 for a Fe particle in Cu and γ-Fe in Cu with two substitutional Al. If the matrix is a Cu-Al alloy, this element is known to penetrate the Fe particle [114].

It is seen from the figures that the Cu 3d electrons present a small polarization parallel to the Fe 3d, and the (4s,4p) electrons polarize antiparallel. This is also veryfied by analyzing the Mulliken populations. The polarization of the (3s,3p) electrons of Al is always antiparallel to that of the neighbors. The presence of Al substituting for Fe was found to disrupt the AFM spin arrangement: for the AFM γ-Fe particle in copper, the presence of two Al atoms resulted in non-convergence of the SCF potential, indicative of the instability of that state. In pure AFM γ-Fe the two Al impurities caused a tendency to local ferromagnetic arrangement of the host atoms. Al substitution in FM γ-Fe causes a reduction in the 3d moment of the Fe neighbors; this same result has been reported for bcc Fe with Al impurities [119].

4.3 Annite, A Silicate Mineral

Silicates make up a large part of the earth's crust, and their physico-chemical properties have obvious importance in geochemistry and minerology. Typically structurally complex, they have been mostly studied by very approximate theories with limited predictive power, including small clusters [120]. More recently, band structure studies have begun to reveal some of the secrets of the simpler silicates [121]. In this section we briefly discuss some recent DV cluster studies on *annite*, a layered iron-bearing silicate which belongs to a class of both natural minerals and synthetic materials of interest as absorbers, carriers, and catalysts [122].

Annite has a mica-like layer structure with the monoclinic space group C2/m and two molecules per unit cell. It has the so-called 2:1 structure with a symmetric arrangement of two tetrahedral layers attached to opposite faces of a single octahedral sheet (T-O-T-K-T-O-T) [123]. The molecular formula for ideal *annite* may be written as KFe_3 $(AlSi_3)$ O_{10} $(OH)_2$ where three-fourths of the tetrahedral sites are occupied by tetravalent silicon and one-quarter by trivalent aluminum ions. Fe-atoms, nominally in the bivalent state, are octahedrally surrounded by six fourfold coordinated oxygens of two types, termed O_{TO} and O_H. Each anion is shared by three octahedra; however, each O_{TO} is also the apex of a tetrahedron whereas O_H, which is bonded to one H atom forming the OH^- group, is unshared. The hydroxyls are arranged around Fe in different positions, giving rise to *cis* and *trans* Fe^{2+} sites respectively in the ratio 2:1 along the octahedral layer. There are two other types of O, which are twofold coordinated to tetrahedral cations (Al or Si). In the present calculations they are considered to be equivalent and defined as type O_{TT}. Finally, the mobile K cations occupy the interlayer sites and ensure the electrical neutrality of the structure.

The existence of extensive Mössbauer studies of ^{57}Fe in this material provides a motivation for detailed study, since theory and experiment can be closely compared [124]. One important result of the Mössbauer work is the observation of some Fe^{3+} on the octahedral sites, presumably to relieve stress due to misfit between ionic radius of Fe^{2+} and packing requirements of the structure. Since the hyperfine fields are known to be sensitive probes of the local environment, a comparison of results with different cluster sizes and boundary conditions will give a clear indication of convergence and reliability of the model, which can be applied more generally to silicates.

Several different sites and cluster sizes were used to generate a self-consistent model of the crystal. All clusters were embedded in the potential field of the infinite ideal

layered structure, with Coulomb interactions fully summed by the Ewald procedure. Two iron-centered clusters were considered to describe the O-sites: $FeO_4(OH)_2$ and $Fe(Si_4O_{14})(OH)_2$, the smaller cluster includes the first coordination shell of Fe in the variational space, and the second includes the next "shell", of silicate tetrahedra. The T-site environment was represented by variational clusters AlO_4, SiO_4 and $Al(SiFe)_3O_4$ and $Si(SiFe)_3O_4$ centered on Al and Si respectively. General features of the self-consistent atomic configurations and net charges can be seen in Table VIII; for a detailed analysis the reader is referred to Ref. [122]. The charge distributions show that the ionic character of the bonding is ordered as Al-O>Fe-O>Si-O, with self-consistent cation charge equal to +2.91, +1.90 and +3.33 for Al, Fe and Si-centered large clusters respectively. This result is consistent with the nominal electronegativities of the cation and anion. The inequivalence of three types of oxygens (O_H, O_{TO}, O_{TT}) is well described by the largest clusters, where the bonding capacity is fulfilled for O_{TO} and O_{TT}. In this case, it is observed that the charge on O tends to converge when the cluster size increases; we find the charge on O_{TT}=-1.39, -1.48 when O_{TT} is respectively bonded to Al and Si. Such a result is compatible with experiment, in which O_{TT} of two types are determined according to the occupation of the cation tetahedral site: either Al or Si. The charge on the fourfold coordinated O_{TO} converges to -1.63; it interesting to observe that this charge does not depend on the cations in $Al(SiFe)_3O_4$ and $Si(SiFe)_3O_4$ clusters. The oxygen type O_H is twofold coordinated in both Fe-centered clusters. It is reasonable to assume the configuration $2s^{1.95}2p^{5.84}$ due to the largest cluster as the most probable; however, it is worth mentioning that O_H can occupy trans and cis positions in the octahedral layer and in the present calculations the cis position is completely neglected.

With the Coulomb potentials of the crystal now determined, we may consider its magnetic properties, starting with a description of the spin-polarized valence band region. The higher-energy valence bands straddling the Fermi level are primarily of Fe 3d character, with a large exchange splitting of ~2.7 eV between spin up and spin down components. The majority spin band is fully occupied, as expected. The twofold substructure is comparable to the splitting of electronic energy levels of a high-spin d^6 ion embedded in a distorted octahedral crystal-field. Distortion of the octahedron lifts degeneracy of e_g and t_{2g} orbitals; in the relevant C_{2h} group there are no degenerate orbitals. However, the 3d states are clearly split into two distributions which are remnants of the cubic character with an energy separation between them, corresponding to the $10D_q$ parameter of ligand field theory, of ~0.6 eV. The five spin up (↑) electrons in the filled subband are ordered in energy values as $3d_{z^2} < 3d_{x^2-y^2} < 3d_{xy} < 3d_{yz} < 3d_{xz}$. This result is compatible with

the neighboring anions geometry; for example the lobes of the $3d_{xz}$ function point toward the O_H ligands. The minority spin distribution encloses the last occupied $20a_g \downarrow$ orbital with 95% Fe $3d_{z^2}$ character. The nearby conduction-band unoccupied levels are predominantly Fe $3d\downarrow$ and Si 3s3p, with Al excited states falling to higher energy. This picture is consistent with general features of magnetic transition metal oxides; details of level composition will be revealed upon consideration of the hyperfine fields, and in particular, the Mössbauer quadrupolar splitting and the magnetic dipolar field.

The calculated spin magnetic moment on Fe is $+3.96\mu_B$, almost entirely due to the 3d-moment; this value is very close to the maximal spin of $+4\mu_B$ and compatible with the Fe^{2+} configuration. This value is in good agreement with that adopted to model the natural single-crystal *annite* in order to explain the experimental saturation magnetization derived from high-spin SQUID magnetometry [125]. The oxygen atoms gain a spin polarization moment; it is larger for the six oxygen nearest neighbors as expected: $+0.014$ and $+0.008\mu_B$ for O_H and O_{TO} respectively. Details of the contact spin density, electric field gradient (EFG), asymmetry parameter (defined in Section 3.3), and magnetic dipolar field (MDF) are given in Table IX. The components of the magnetic dipolar field tensor are given by:

$$M_{ij} = \mu_B \int \rho_s(\vec{r})(3x_i x_j - \delta_{ij} r^2)/r^5 dv \tag{59}$$

where μ_B is the Bohr magneton and ρ_s is the spin density $[\rho_\uparrow(\vec{r}) - \rho_\downarrow(\vec{r})]$. We find that the anisotropic EFG and MDF, which depend very sensitively upon the angular character and weight of occupied Fe 3d orbitals, differ greatly from the minimal cluster model, to the cluster with two coordination shells of neighbors. This is consistent with experience with other supposedly ionic systems, and gives some measure of the influence of covalent interactions in silicates along with other simpler oxides. The data from the larger cluster can be fit very well to the experimental Mössbauer spectra, and indicate that the EFG principal axis and the internal magnetic field H_F are parallel. This prediction can be checked in principal by making measurements at low temperature in an external magnetic field. On the strength of these results, we believe we have obtained an adequate model for the *annite* system and have established a good basis for further studies on these fascinating materials.

4.4 An Electroceramic Grain Boundary

Electroceramics include a wide variety of technically important materials with nonlinear electrical properties, including devices such as varistors, thermistors, boundary layer

capacitors, and ferroelectric memories. Their behavior is largely governed by electrically active grain boudaries (GB), whose dielectric permittivity, capacitance, and resistive behavior are closely linked with microscopic geometry, chemical environment, and electronic structure. Tailoring of GB to specific needs by controlling processing conditions and incorporation of impurities forms a large part of the art of producing useful materials.

$SrTiO_3$ is one such functional electroceramic, much studied because of its relatively simple perovskite structure and its GB capacitative behavior, obtained upon aliovalent doping. Studies of GB structure by high resolution spatially resolved electron microscopy and energy loss spectroscopy have revealed enough of the local geometry, on a 3-5$\AA$ length scale, to make detailed modelling feasible [126]. Atomistic modelling has been done, using a lattice statics approach to find low energy configurations compatible with experimental data. Not only are the resulting structures complex, with different stoichiometry than the ideal bulk, but they are numerous. For example, for the well characterized 36.8^0 symmetric tilt $\sum = 5$ GB a total of fourteen low energy structures were found compatible with experiment [127]. One of these, shown in Fig. 24, was selected for detailed electronic structure studies on the basis of chemical intuition and "feel"; details are given in the literature [128], here we touch briefly on differences in Ti environment in the GB versus the bulk, and on the effects of transition metal substituents at the Ti site.

In the ideal cubic perovskite structure, Ti^{4+} is surrounded by six O^{2-} in the first coordination shell, followed by eight Sr^{2+}. DV calculations on clusters with up to ~ 50 atoms reveal a self-consistent atomic configuration of $Ti^{+2.88}\ 3d^{0.99}4s^{0.02}4p^{0.08}$ showing the considerable effects of Ti 3d - O 2p covalency. Examination of geometry around titanium in the GB core shows that most often, the local oxygen coordination is reduced from six to five; in addition, the average Ti-O bond length is significantly reduced. Self-consistent calculations show that the response of Ti at the GB core is partial reduction, with a typical configuration of $Ti^{+2.68}3d^{1.17}4s^{0.03}4p^{0.12}$ representing an accumulation of electronic charge at the GB core, relative to bulk. The strontium coordination is also reduced (from 12 to $\sim$9) in the GB, and its response is similar. In bulk, its configuration is found to be highly ionic: $Sr^{+1.93}4d^{0.04}5s^{0.01}5p^{0.03}$, while in a typical GB environment we find $Sr^{+1.66}4d^{0.31}5s^{0.03}5p^{0.03}$, reflecting accumulation of some covalent character due to reduced Sr-O bond lengths. Again, the net result is accumulation of electronic charge at the GB core, helping to build up the Schottky barrier responsible for capacitive behavior.

Deliberate doping of strontium titanate by transition metal acceptors, including Mn, Fe, and Ni which concentrate at the grain boudaries, is known to enhance the GB capacitative effect and is an essential component for commercial materials. Calculations

on transition metal-doped $SrTiO_3$ were made, substituting for Ti both in bulk crystal and at the GB. A typical result for Mn shows an ideal crystal ionic configuration of $Mn^{+2.08}3d^{4.84}4s^{0.02}4p^{0.04}$; thus Mn is indeed divalent, but accepts only ~0.80e instead of the nominal 2e expected from formal valency, due to the lesser charge initially on Ti. Attempts to stabilize Mn^{3+}, which is experimentally observed at lower concentration, always led to the divalent self-consistent state. This suggests that the trivalent ion is associated with oxygen vacancies, known to exist in significant numbers, and to contribute to space charge and conduction processes. Similar calculations of Mn substitution at the GB core yield a typical configuration $Mn^{+1.84}3d^{4.96}4s^{0.07}4p^{0.11}$, showing again partial reduction with respect to the bulk state. The most significant feature here is that Mn accepts $\sim 0.84e$ at the GB core, slightly greater than in bulk, again contributing to formation of the Schottky barrier. Doping by electron donors which may concentrate in the bulk, is expected to compensate the bulk acceptors, leaving the desired space charge region around the GB.

Further studies are underway, using the MD/MC methodology described in section 2.9, to refine the local geometry in view of first-principles determination of ionic charges different from nominal values, and taking into account differing ionic radii of substituents. We see that very simple ideas arising from calculated electronic charge distribution are already useful in helping to construct viable models of electroceramic grain boundaries. More detailed theoretical analyses, relating to the X-ray near-edge abosorption and high resolution electron energy loss data, can be expected to contribute further to understanding local geometry and atomic configuration of substituents.

Acknowledgments

Part of the calculations reported were performed at the Cray Y-MP of the Supercomputing Center of the Universidade Federal do Rio Grande do Sul. Work supported in part by CNPq (Brasil) and by the MRSEC program of the National Science Foundation (DMR-9632472) at the Materials Research Center of Northwestern University, and through NSF Grant No. INT-9600016.

Table I - ^{57}Fe hyperfine parameters of $[Fe(OMe)_2(O_2CCH_2Cl)]_{10}$. Values of the isomer shift δ relative to Fe metal. Value of α from ref. [87].

Isomer Shift		
$\rho(0)(a_0^{-3})$ (3s+valence)	$\delta(mm/s)$ (calculated)	$\delta(mm/s)$ (experimental)[a]
145.43	0.48	0.52

Electric field gradient					
V_{xx} (a_0^{-3})	V_{yy} (a_0^{-3})	V_{zz} (a_0^{-3})	η	$\Delta EQ(mm/s)$ (calculated)[b]	$\lvert\Delta EQ\rvert(mm/s)$ (experiment)[a]
0.439	-0.311	-0.128	0.416	+0.73	0.62

Magnetic hyperfine field		
	$\Delta\rho(0)$ (a_0^{-3})	H_c (kG)
1s-3s	-0.906	-474
valence	+0.077	+40
Total	-0.829	-434

a) From reference [84].

b) Q (^{57}Fe) = 0.16b (from ref. [91]).

Table II – Cartesian coordinates ($\AA$) of nearest neighbor ligands to Ru^{VI} in [Ru(O)PHAB]

atom	x	y	z
O1	−1.296	−1.018	0.426
O2	0.565	1.276	1.285
O3	−0.953	1.393	−1.086
N1	0.768	−0.496	−1.672
N2	1.579	−0.981	0.676

Table III - Net Mulliken populations for Ru and ligand atomic charges in [Ru(O)PHAB] for 6 (embedded), 20 and 36 (naked) atom fragments, and the entire (66 atom) complex. Net charge = 0 for each fragment.

	6 atoms	20 atoms	36 atoms	entire
Ru 4d	5.63	5.78	5.74	5.74
5s	0.06	0.11	0.10	0.06
5p	0.13	0.23	0.25	0.15
net	2.19	1.87	1.90	2.04
O1				
net	-0.44	-0.44	-0.43	-0.53
O2				
net	-0.52	-0.44	-0.45	-0.63
O3				
net	-0.46	-0.52	-0.56	-0.42
N1				
net	-0.38	-0.39	-0.44	-0.63
N2				
net	-0.40	-0.39	-0.53	-0.44

Table IV – Mulliken populations , charges and bond orders from non-relativistic and relativistic calculations for $[Ir(CN)_5]^{3-}$. Ax and eq stand for axial and equatorial ligands, respectively.

Populations and Charges						
	Nonrelativistic			Relativistic		
Ir	5s	1.94	Ir	$5s_{1/2}$	1.96	
Populations	5p	5.91	Populations	$5p_{1/2}$	1.98	
	5d	7.43		$5p_{3/2}$	3.94	5p 5.92
	6s	0.09		$5d_{3/2}$	3.17	
	6p	0.45		$5d_{5/2}$	4.21	5d 7.38
				$6s_{1/2}$	0.23	
Charges	Ir	+1.18		$6p_{1/2}$	0.19	
	C_{ax}	+0.07		$6p_{3/2}$	0.32	6p 0.51
	N_{ax}	-0.85				
	C_{eq}	+0.02				
	N_{eq}	-0.87	Charges	Ir	+1.01	
				C_{ax}	+0.08	
				N_{ax}	-0.84	
				C_{eq}	+0.05	
				N_{eq}	-0.86	

Bond orders		
	Nonrelativistic	Relativistic
Ir–C_{ax}	0.30	0.48
Ir –C_{eq} (each)	0.31	0.48
C_{ax}–N_{ax}	1.36	1.36
C_{eq}–N_{eq} (each)	1.31	1.31

Table V - Self-consistent Mulliken populations in NR and R models of a W_6 cluster.

Orbital		Nonrelativistic	Relativistic
5d	3/2	4.94	2.07
	5/2		2.22
6s		0.54	0.72
6p	1/2	0.55	0.30
	3/2		0.73

Table VI - Mulliken atomic orbital populations and net charges for $[W_6X^i_8X^a_6]^{2-}$ complexes from DV calculations. NR is nonrelativistic model; R is relativistic. Angular momentum subshells j=1/2, 3/2, 5/2 and an extended ligand basis set of valence ns, np, nd and (n+1)s optimized functions are indicated.

Orbital			Chloride		Bromide		Iodide	
			NR	R	NR	R	NR	R
W	5d	3/2	4.66	1.65	4.77	1.87	4.82	1.94
		5/2		1.76		1.93		2.00
	6s	1/2	0.02	0.62	0.08	0.87	0.14	0.87
	6p	1/2	0.28	0.17	0.25	0.24	0.33	0.26
		3/2		-0.06		0.02		0.09
		charge	1.07	2.10	0.94	1.21	0.75	0.96
X^i	s	1/2	1.97	2.03	1.97	2.03	1.96	2.02
	p	1/2	5.48	1.81	5.42	1.82	5.32	1.85
		3/2		3.60		3.52		3.42
	d	3/2	0.08	0.22	0.07	0.05	0.09	0.04
		5/2		0.29		0.08		0.07
	s*	1/2		0.22		0.21		0.15
		charge	-0.55	-1.16	-0.48	-0.70	-0.38	-0.55
X^a	s	1/2	1.98	2.03	1.99	2.01	1.97	2.00
	p	1/2	5.68	1.88	5.64	1.87	5.59	1.92
		3/2		3.68		3.56		3.48
	d	3/2	0.02	0.08	0.01	0.04	0.02	0.05
		5/2		0.12		0.06		0.06
	s*	1/2	0.01	0.09	0.01	0.08		0.06
		charge	-0.68	-0.87	-0.70	-0.61	-0.55	-0.56

Table VII - Comparison of symmetry type and gap (eV) between valence and conduction bands for $[W_6X_8^iX_6^a]^{2-}$ clusters, together with experimental emission and absorption bands.

Species	Method	HOMO	LUMO	VB-CB Gap
Chloride				
	NR[a]	t_{2u}	e_u	2.7
	R[b]	γ_{8u}	$\gamma_{8u}, \gamma_{8u}^e$	2.8
	absorption[c]			2.5
	emission[d]			1.83
Bromide				
	NR	t_{2u}	t_{2u}	2.1
	R	γ_{8g}	γ_{7u}	2.7
	emission			1.85
Iodide				
	NR	t_{1g}	t_{2u}	2.0
	R	γ_{8g}	γ_{7u}	1.1
	emission			2.05

a) Gap=HOMO-LUMO energy.

b) HOMO and LUMO lie within VB, gap=VB peak to CB peak, see text.

c) Absorption edge of $(Bu_4N)_2Mo_6Cl_{14}$ in PMMC.

d) Emission band maximum.

e) Degenerate levels.

Table VIII - Mulliken populations and net atomic charges in cluster models of *annite*. Si_p and Fe_p indicate atoms in groups at periphery of cluster.

		$[RO_4(OH)_2]$	$[R(Si_4O_{14})(OH)_2]$		$[RO_4]$	$[R(SiFe)_3O_4]$	$[RO_4]$	$[R(SiFe)_3O_4]$
		R=Fe			R=Al		R=Si	
Cluster charge		-8.0	-12.0		-5.0	+13.0	-4.0	+14.0
	3d	6.00	5.98	3s	0.04	0.01	0.21	0.22
R	4s	0.13	0.06	3p	0.12	0.08	0.43	0.45
	4p	0.10	0.06		+2.84	+2.91	+3.36	+3.33
		+1.77	+1.90					
O_H	2s	1.94	1.95					
	2p	5.70	5.84					
		-1.64	-1.79					
O_{TO}	2s	2.00	1.95		1.98	1.95	1.96	1.90
	2p	5.93	5.81		5.88	5.69	5.87	5.72
		-1.93	-1.76		-1.86	-1.64	-1.83	-1.62
O_{TT}	2s		1.96		2.00	1.97	1.97	1.94
	2p		5.83		5.98	5.42	5.87	5.54
			-1.79		-1.98	-1.39	-1.84	-1.48
H	1s	0.38	0.22					
		+0.62	+0.78					
Si_p	3s		0.20			0.51		0.48
	3p		0.50			0.18		0.13
			+3.30			+3.31		+3.39
Fe_p	3d					5.44		5.49
	4s					0.49		0.26
	4p					0.08		0.05
						+1.99		+2.20

Table IX - Charge density $\rho_c(0)$ at the nucleus and Isomer Shift δ, Electric Field Gradient tensor, contact spin density $\rho_s(0)$, Magnetic Dipolar Field tensor, and net magnetic field H_F at iron site in *annite*. Results are given for clusters containing only first, and first plus second coordination shells about iron. Principal values and directions of principal axes (in parentheses) are given for EFG and dipolar field. The ^{57}Fe nuclear quadrupole moment is taken as 0.16 barn [91].

			$FeO_4(OH)_2$	$Fe(Si_4O_{14})(OH)_2$
$\rho_c(0)^a$				
3s	shallow core		140.53	140.02
	valence		1.66	1.90
			142.19	141.92
4s	valence		0.50	0.41
	TOTAL		142.69	142.33
δ(mm/s)^b			+1.15	+1.23
			EFG tensor(a_0^{-3})	
		V_{xx}	+1.10	-0.01
			(1.0,0.0,0.0)	(0.0,1.0,0.0)
		V_{yy}	+1.74	-2.35
			(0.0,1.0,0.0)	(0.0,0.0,1.0)
		V_{zz}	-2.84	+2.36
			(0.0,0.0,1.0)	(1.0,0.0,0.0)
η			0.23	0.99
ΔEQ(mm/s)			-4.59	+3.81
$\rho_s(0)^a$				
	core		-1.59	-1.60
	shallow core		+0.77	+0.77
	valence		+0.04	+0.14
	TOTAL		-0.78	-0.69
H_D tensor (a_o^{-3})		M_{xx}	+1.15	-0.13
			(1.0,0.0,0.0)	(0.0,1.0,0.0)
		M_{yy}	+1.75	-2.37
			(0.0,1.0,0.0)	(0.0,0.0,1.0)
		M_{zz}	-2.89	+2.48
			(0.0,0.0,1.0)	(1.0,0.0,0.0)
H_c(kOe)			-411	-362
H_D(kOe)			-181	+151
H_F(kOe)			-592	-211

[a]In units of a_0^{-3}. [b]Related to α iron.

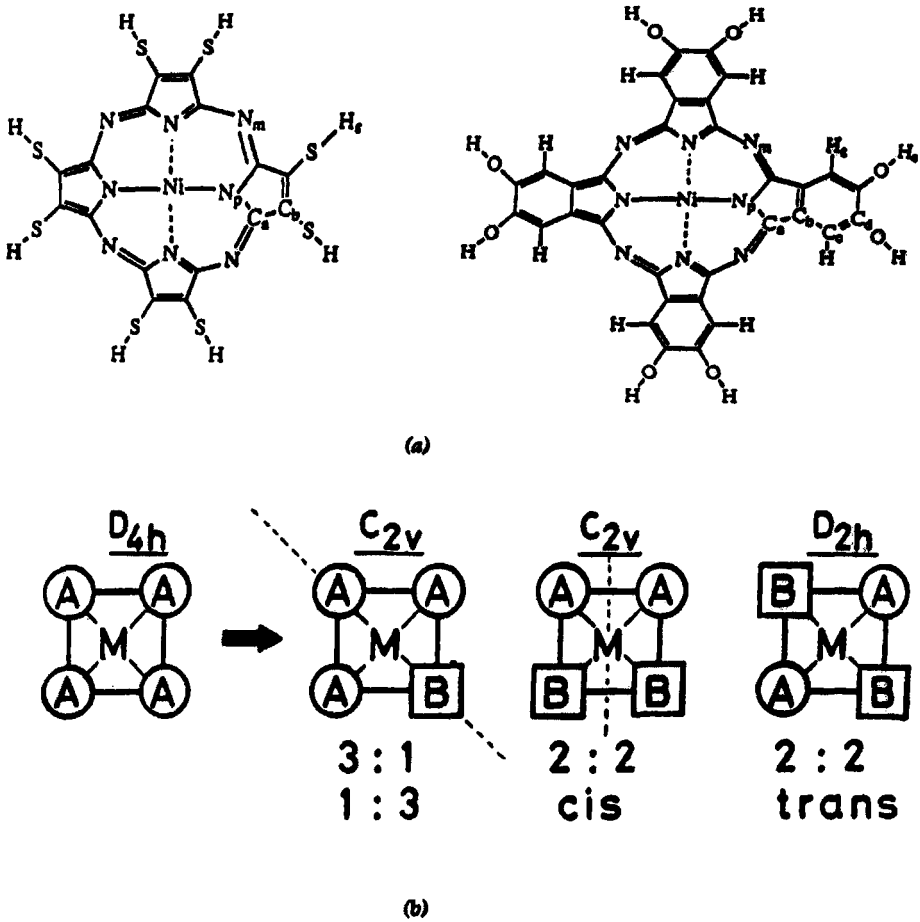

Fig. 3 – Some typical porphyrinic molecules: a) Ni star-porphyrazine, with four fused thiolene groups (4PZ), b) basic porphyrazine structure with peripherally fused-benzo rings (PC) and c) dithiolene groups (PZ).

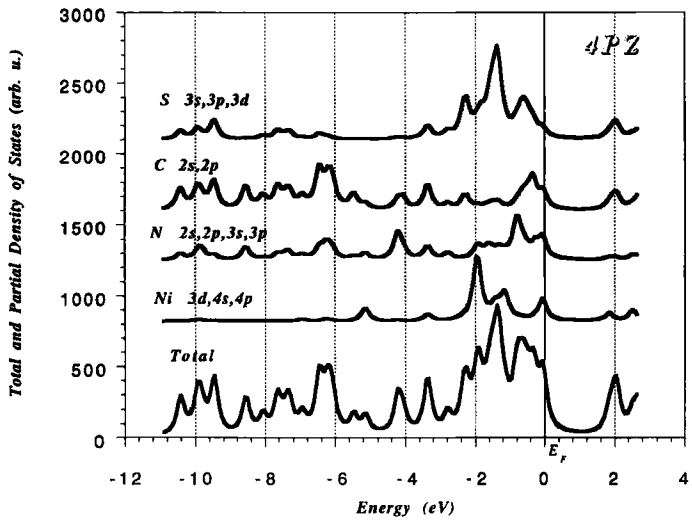

Fig. 4 - PDOS of 4PZ nickel porphyrazine

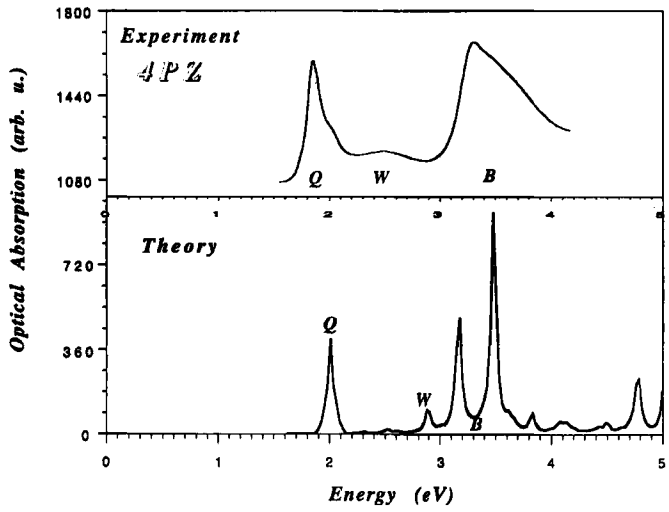

Fig. 5 – Theoretical and experimental absorption bands of 4PZ Ni(TAP).

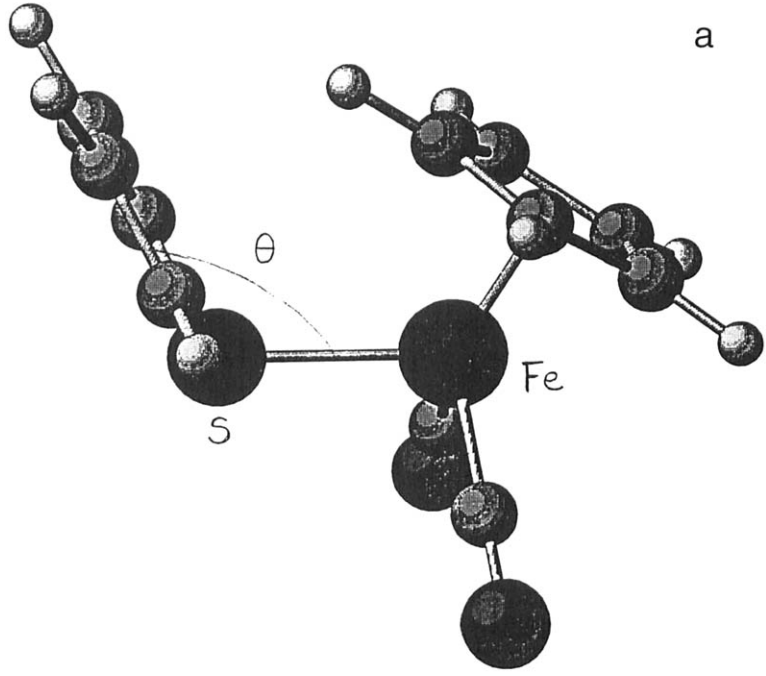

Fig. 6 – Views of $[Cp(CO)_2Fe(\eta^1\text{-}T)]^+$. a) $\theta = 120^0$, b) $\theta = 180^0$.

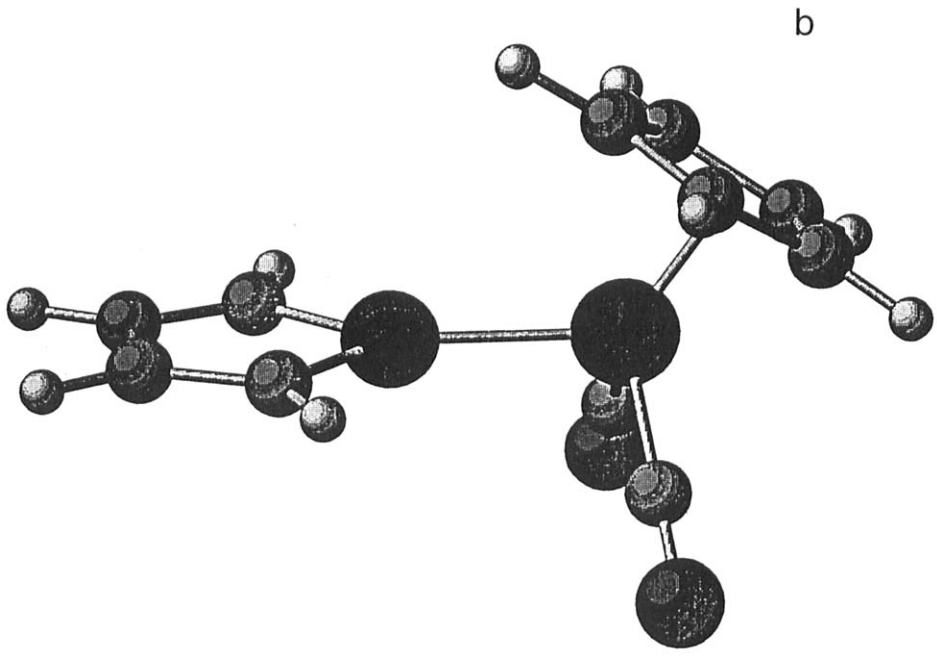
b

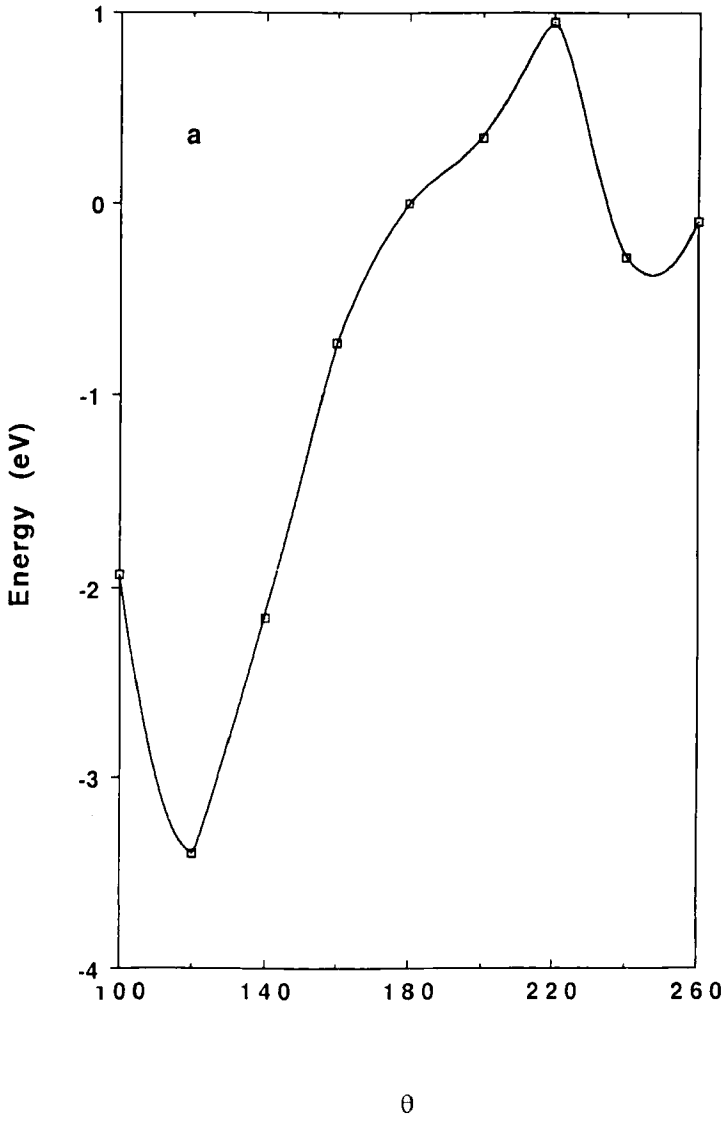

Fig. 7 - Variation of the calculated total energy of $[Cp(CO)_2Fe(\eta^1\text{-}T)]^+$ as a function of θ. a) Without 3d orbitals in the S basis, b) with 3d orbitals on the S. The reference energy is for the coplanar geometry ($\theta = 180^0$).

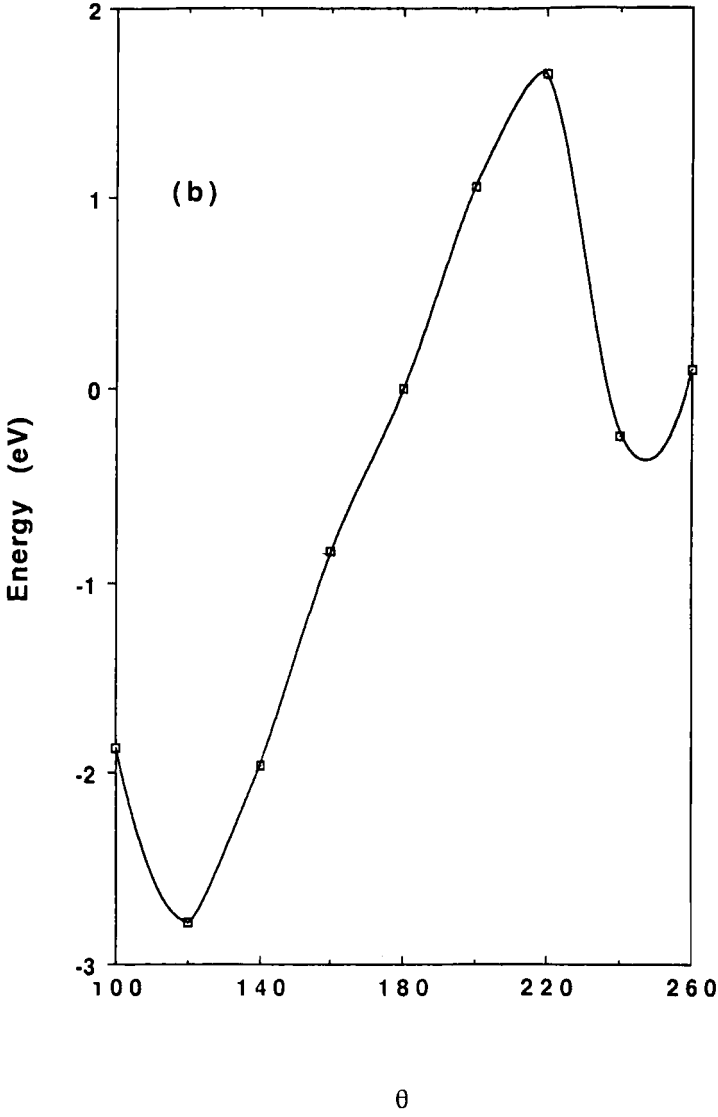
(b)
Energy (eV)
2
1
0
-1
-2
-3
100
140
180
220
260
θ

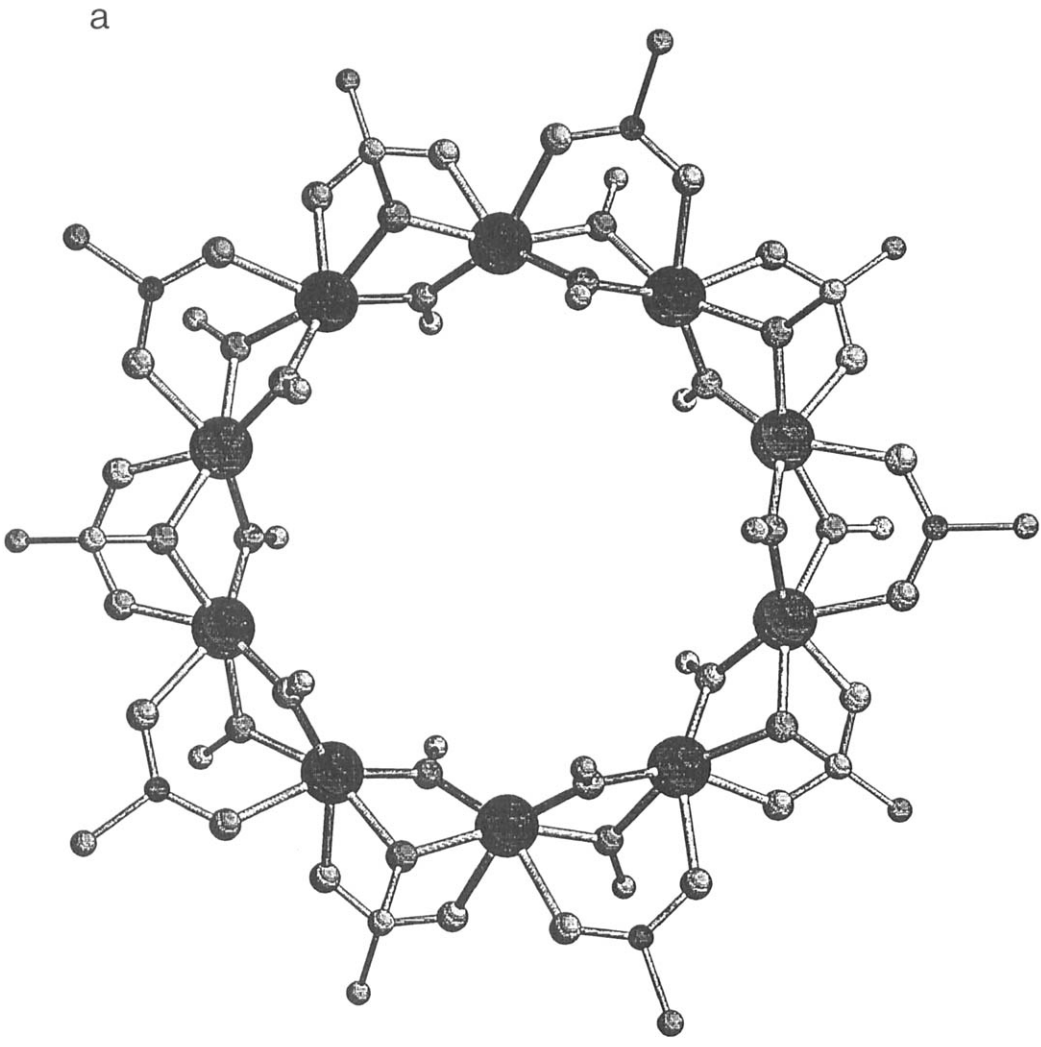

Fig. 8 – Views of the cluster $[Fe(OC)_2(O_2CC)]_{10}$, representing the molecule "ferric wheel". a) Top view (z=0 plane), b) Side view.

b

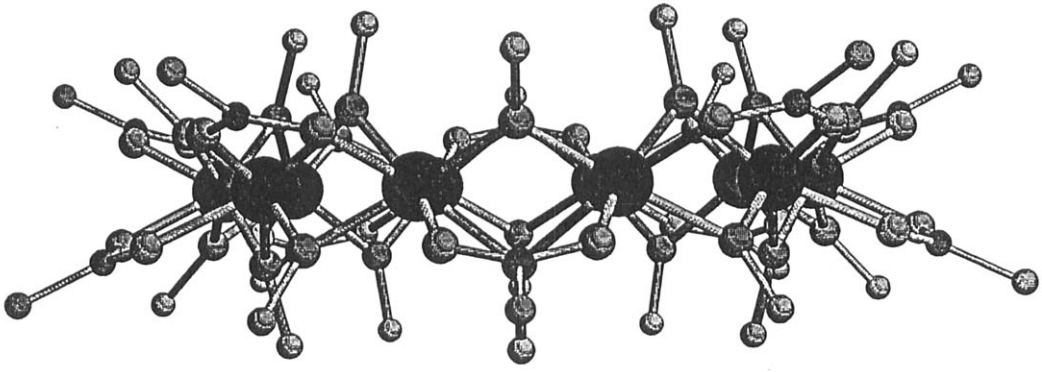

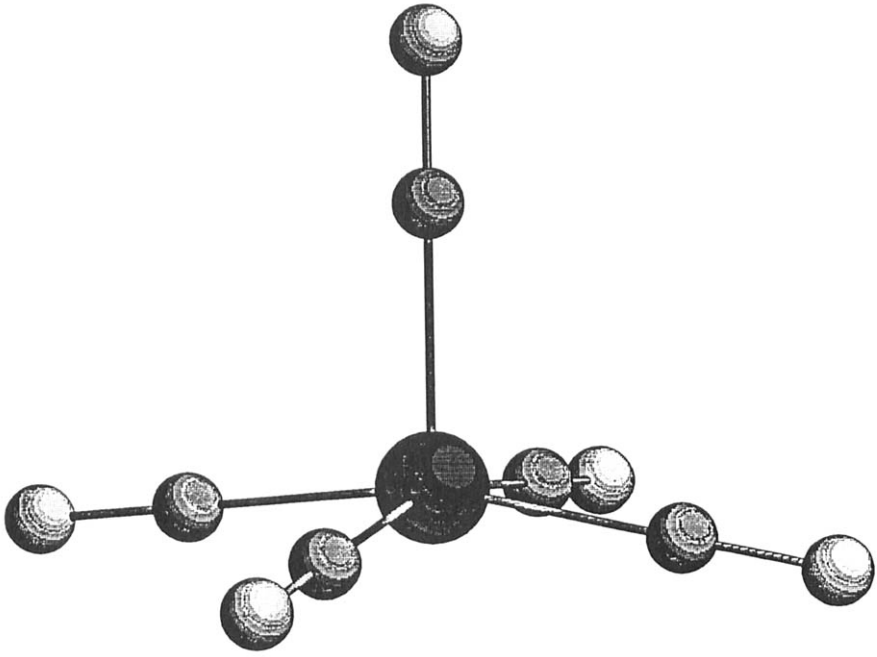

Fig. 9 - The square-pyramidal complex $[Ir(CN)_5]^{3-}$. Ir is at the center; neighbour atoms are C.

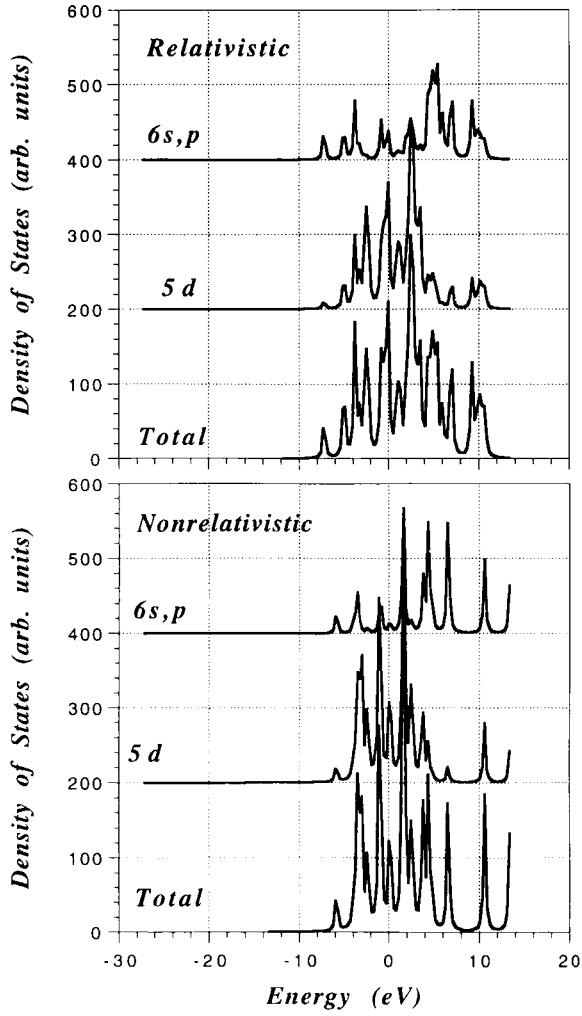

Fig. 10 - Partial and total densities of states of neutral W_6 clusters.

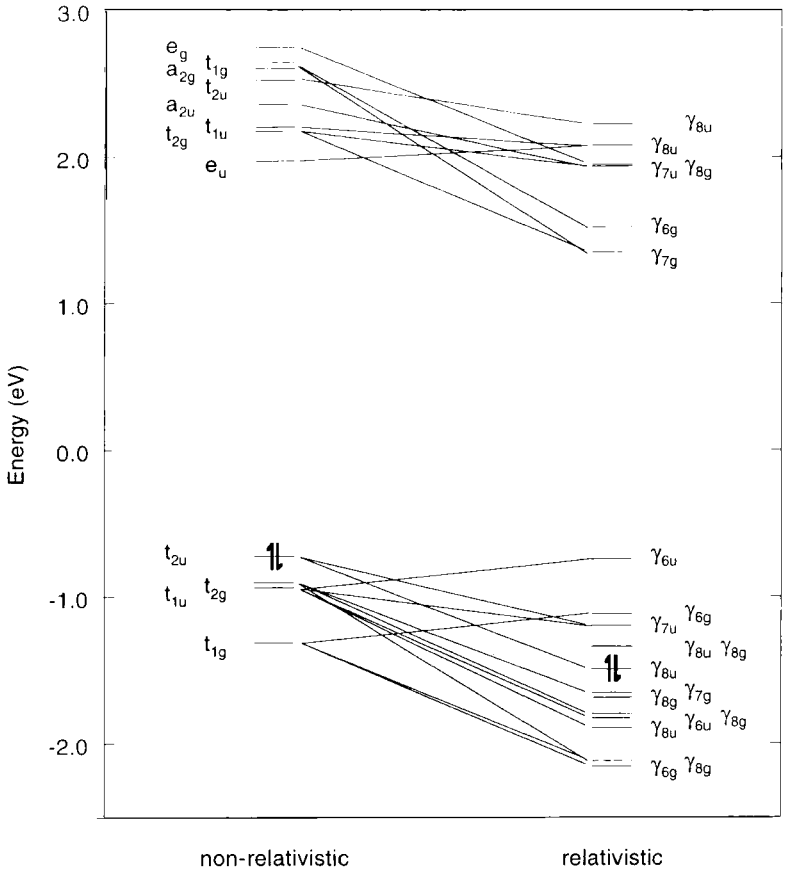

Fig. 11 - Nonrelativistic and relativistic energy levels of $[W_6Cl_8^iCl_6^a]^{2-}$.

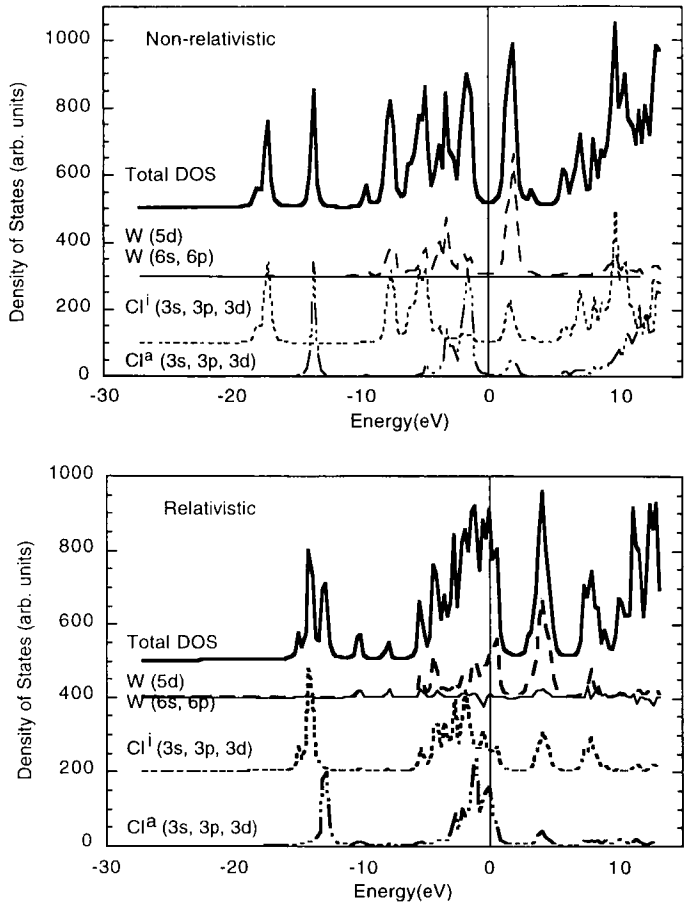

Fig. 12 - Partial and total densities of states of $[W_6Cl_8^iCl_6^a]^{2-}$ in the nonrelativistic (top) and relativistic (bottom) models.

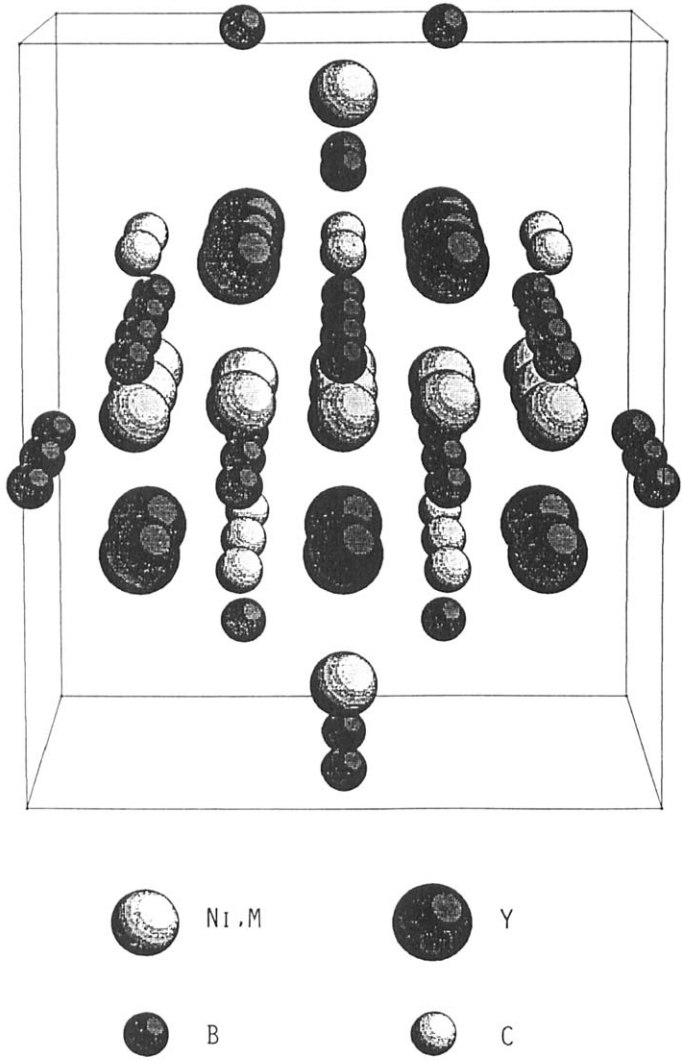

Fig. 13 - $R_{12}M_{15}B_{32}C_{12}$ transition-metal centered cluster representing RM_2B_2C compounds.

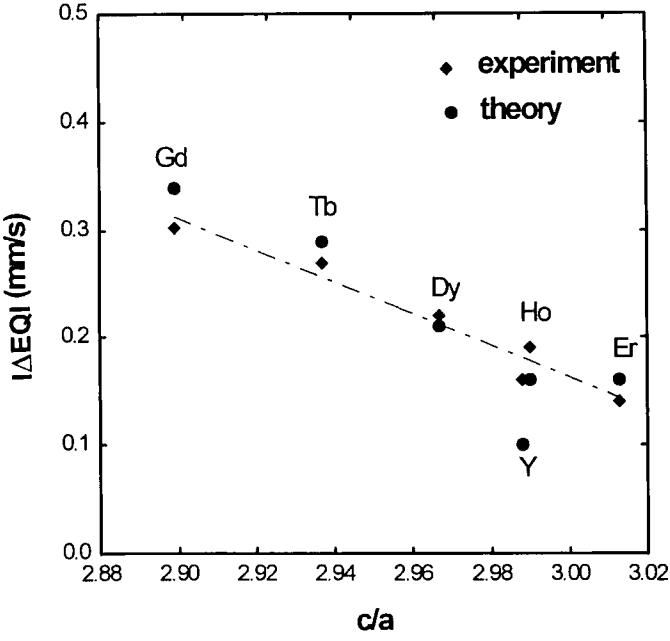

Fig. 14 - Experimental and calculated absolute values of ^{57}Fe quadrupolar splitting in $R(Ni_{0.99}Fe_{0.01})_2B_2C$ versus ratio of lattice parameters c/a.

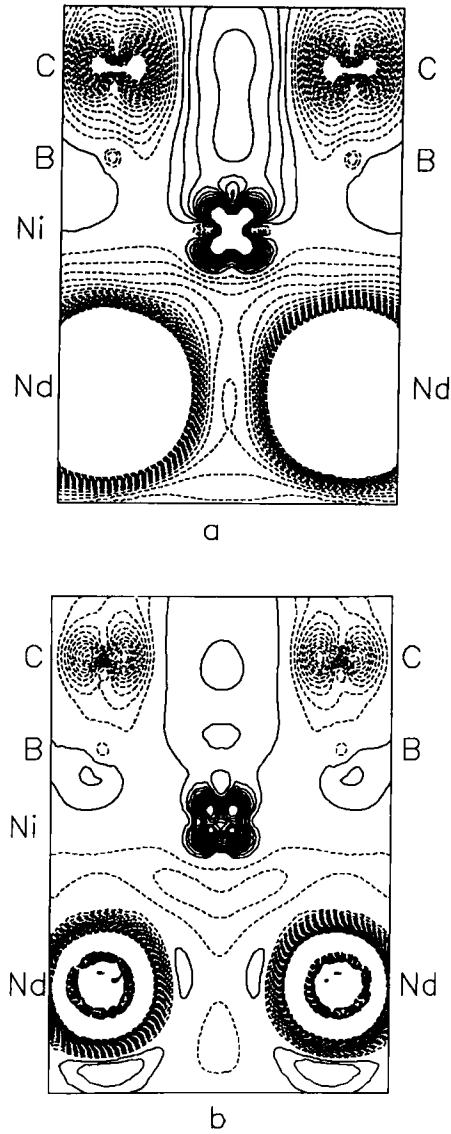

Fig. 15 - Spin-density $[\rho_\uparrow(\vec{r}) - \rho_\downarrow(\vec{r})]$ contours on the (011) plane of $NdNi_2B_2C$. a) Nd 4f in variational space, b) Nd 4f placed in frozen core. Contour levels are from -0.002 to +0.002 e/au^3 with intervals of 0.0001. Full lines are positive values.

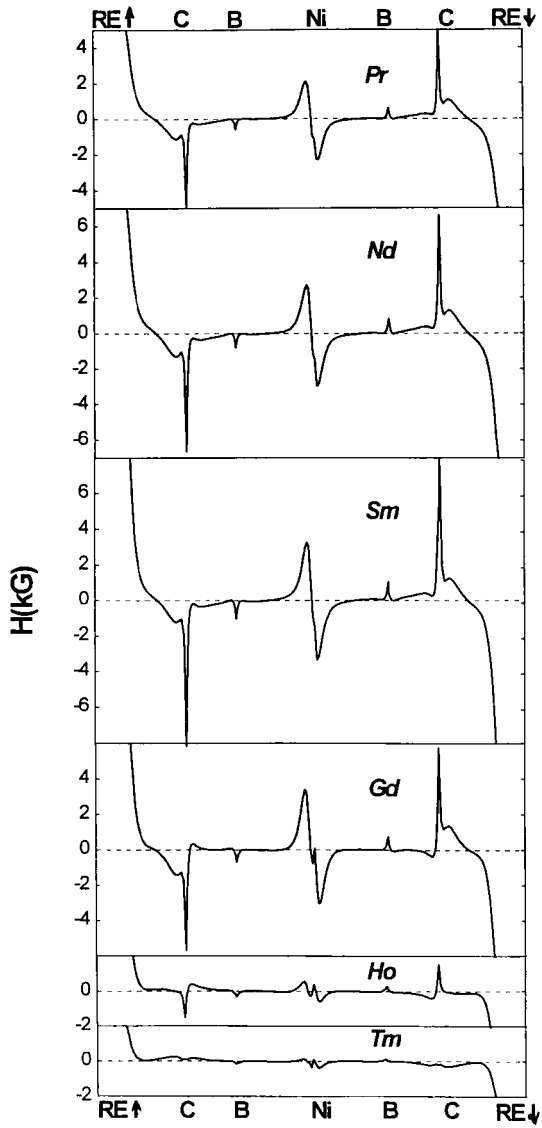

Fig. 16 - Bond-line plots of the polarization field H for antiferromagnetic RNi_2B_2C, beginning at one rare-earth and passing from atom to atom along bond lines, terminating at a R in the next plane (distance c/2) above or below. $H=(8\pi/3)\mu_B[\rho_\uparrow(\vec{r}) - \rho_\downarrow(\vec{r})]$.

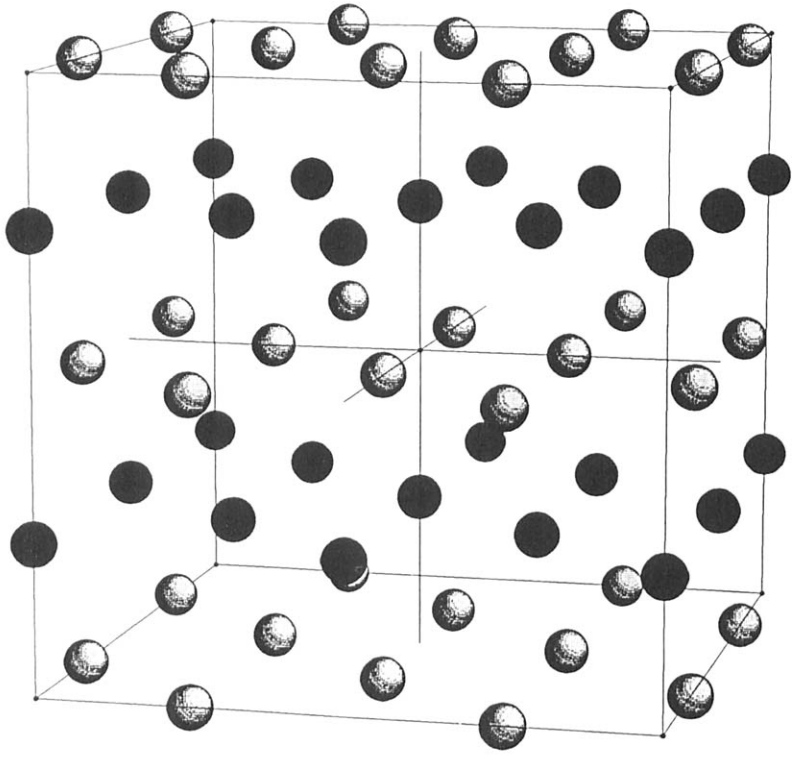

Fig. 17 - 62-atoms cluster representing fcc Fe. Light and dark spheres represent alternating layers of spins in the AFM configuration.

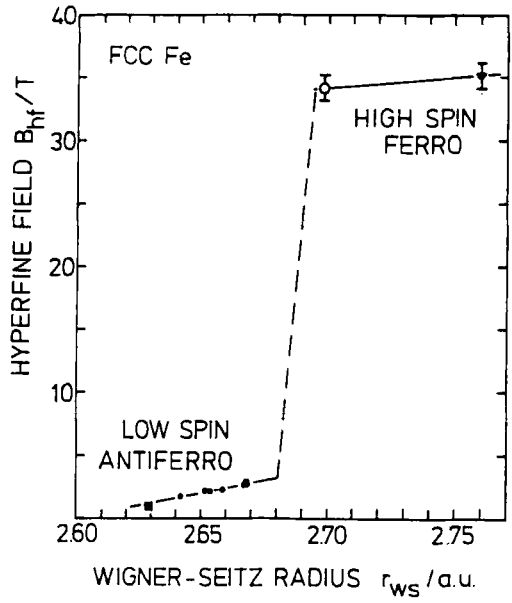

Fig. 18 – Experimental values of the magnitude of the hyperfine field of fcc Fe at several lattice constants

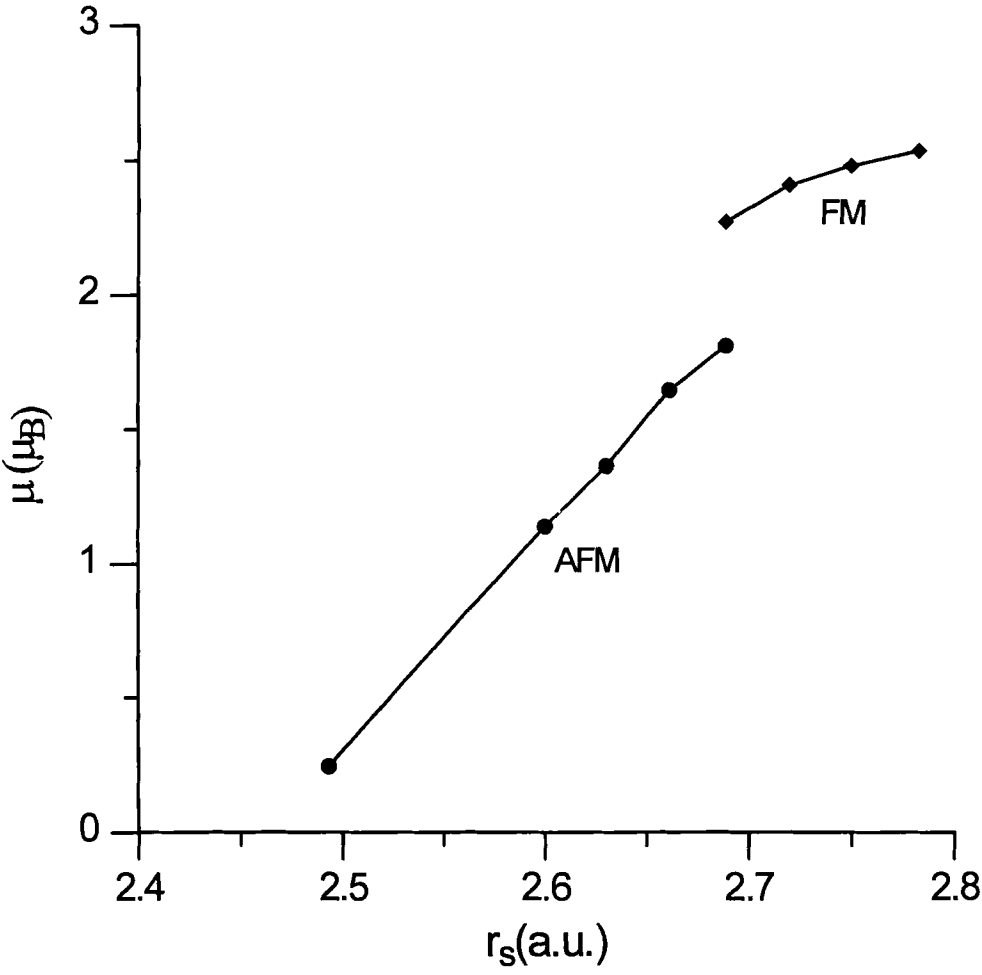

Fig. 19 – Calculated spin magnetic moments μ plotted against the Wigner-Seitz radius r_s of γ-Fe (from ref. [117]).

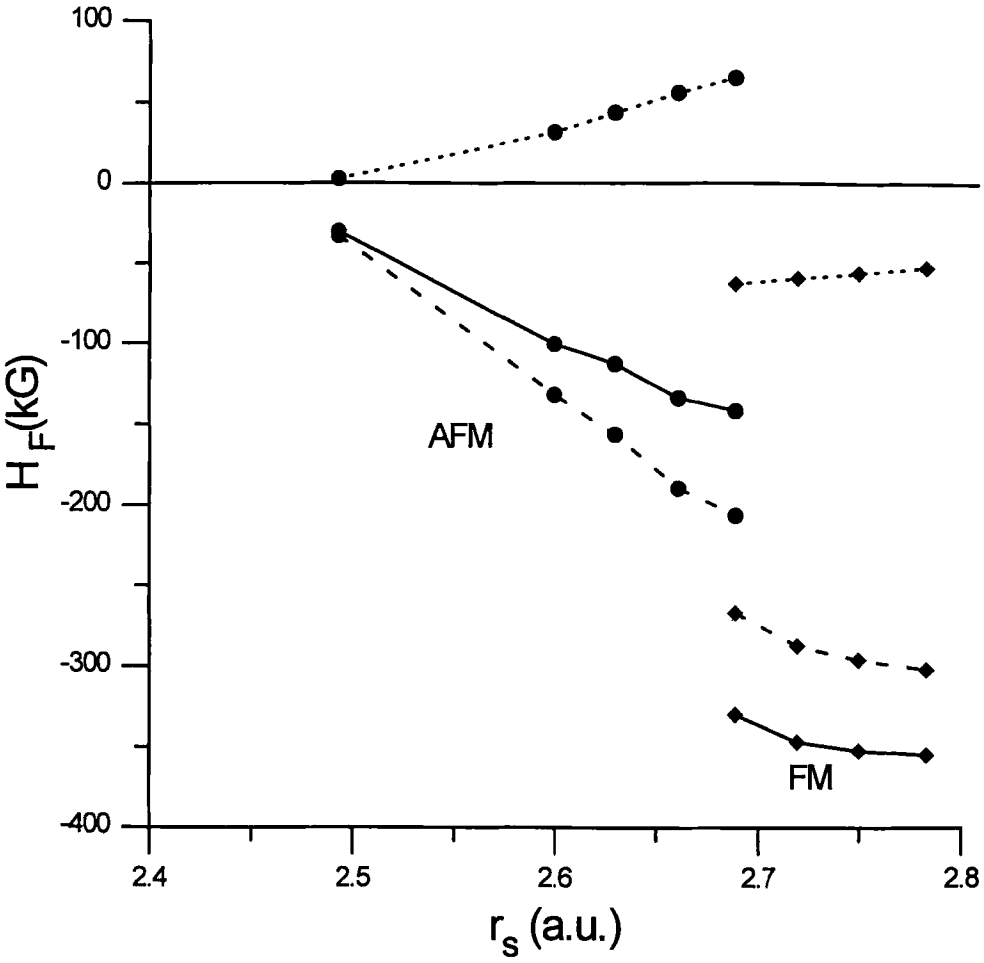

Fig. 20 - Total hyperfine field H_F and components plotted against the Wigner-Seitz radius r_s of γ-Fe (from ref. [117]). Valence electrons contribution, ·····; core electrons contribution, — — — —, total, _____

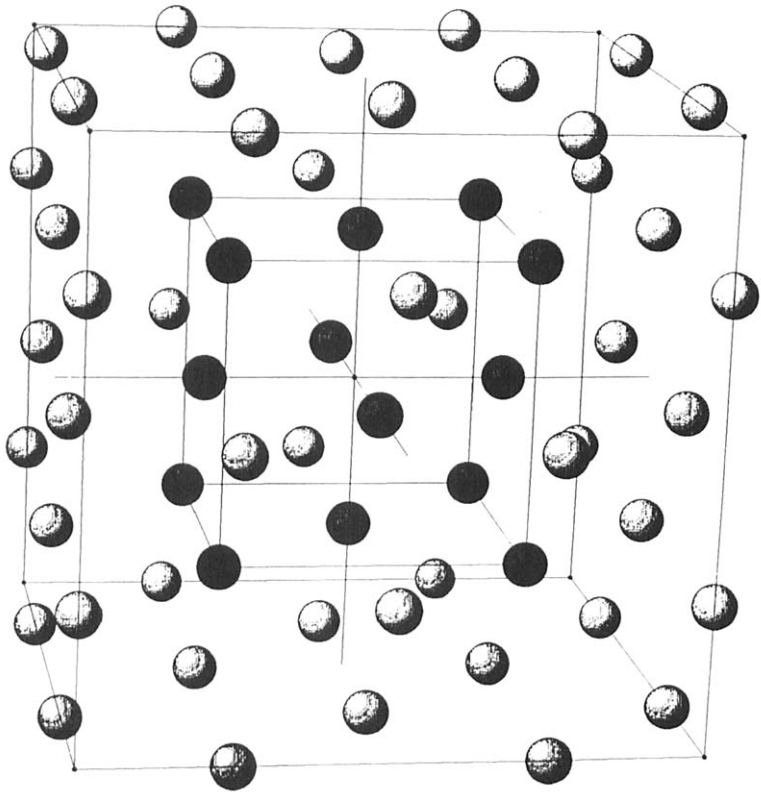

Fig. 21 - Cluster representing a cubic particle of Fe with 14 atoms in the fcc structure, surrounded by Cu atoms. Darker spheres represent Fe.

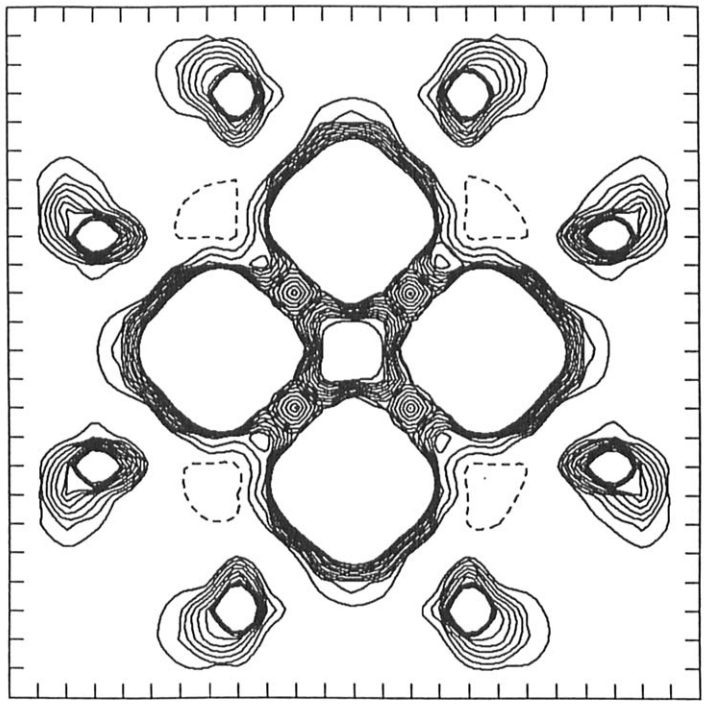

Fig. 22 - Spin density contours for FM γ-Fe particle surrounded by copper, in the (x,z) plane. From -0.01 to +0.01 e/a.u.^{3} with intervals of 0.001 e/a.u.^{3}. Full lines are positive values.

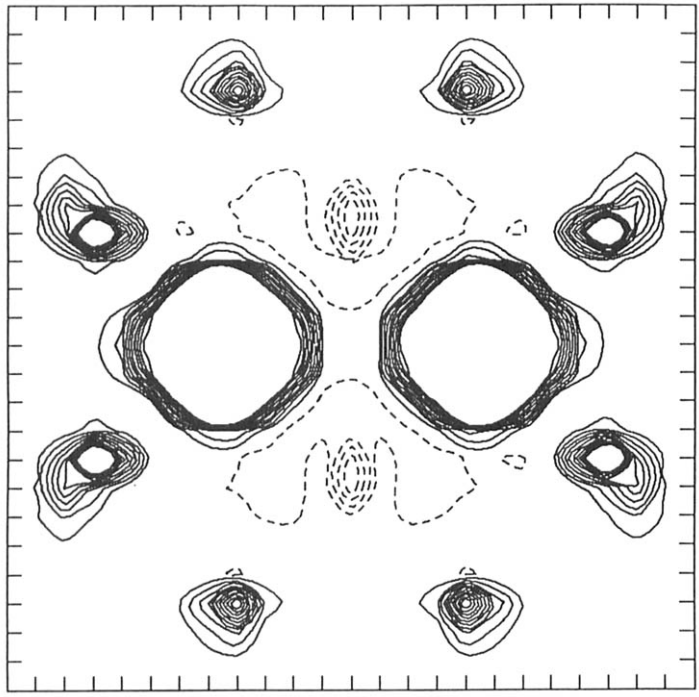

Fig. 23 - Spin density contours for FM γ-Fe particle surrounded by Cu in the (x,z) plane with two Al on the z axis substituting for Fe. Contour specifications as in Fig. 22.

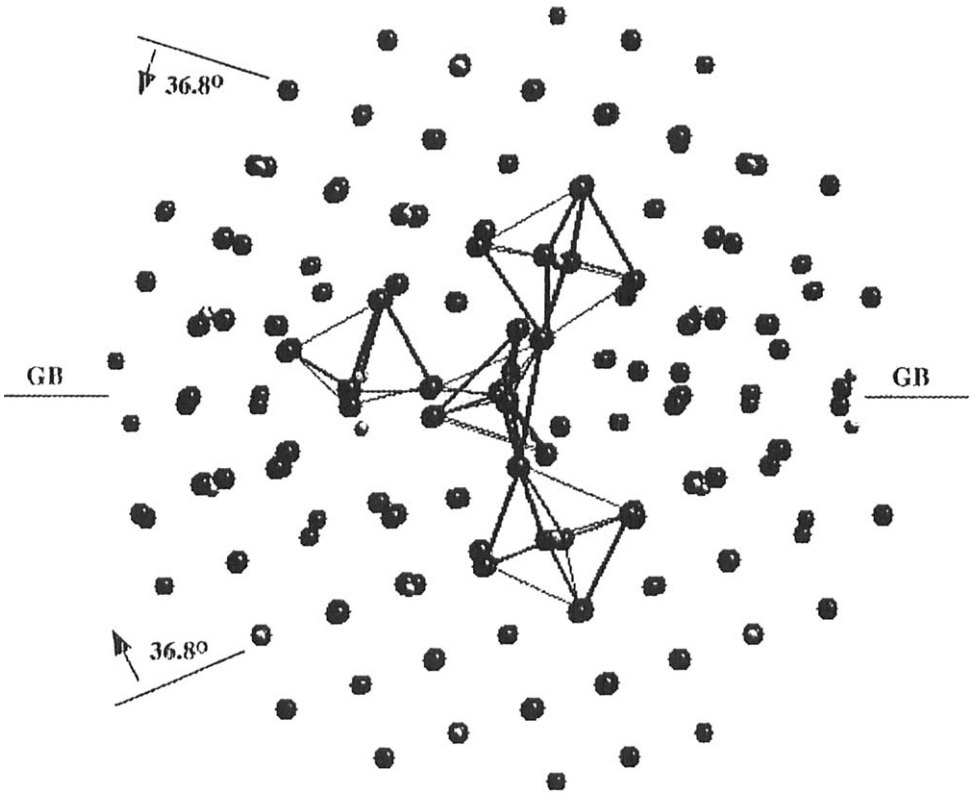

Fig. 24 – Schematic of 36.8^0 symmetric tilt $\sum = 5$ grain boundary in $SrTiO_3$, showing a Ti-centered variational cluster at the GB core. Small spheres: Ti, medium spheres: Sr, and large spheres: O.

REFERENCES

[1] T.H. Dunning, Jr. and P.J. Hay, in "Methods of Electronic Structure Theory", Ch. 1, ed. H.F. Schaefer III, (Plenum Press, New York, 1977).

[2] W.J. Hehre, L. Random, P. Schleyer and J.A. Pople, "Ab Initio Molecular Orbital Theory", (John Wiley & Sons, New York, 1986).

[3] S. Huzinaga, M. Klobukowski and Y. Sakai, J. Phys. Chem. **88**, 4880 (1984).

[4] P.J. Hay and W.R. Wadt, J. Chem. Phys. **82**, 270, 284, 299 (1985).

[5] For example: I. Shim and K.A. Gingerich, in "Physics and Chemistry of Small Clusters", P. Jena, B.K. Rao and S.N. Khanna, editors, (Plenum, New York, 1987) p. 523.

[6] J. Cized, J. Chem. Phys. **45**, 4256 (1966).

[7] R.J. Bartlett, J. Phys. Chem. **93**, 1697 (1989).

[8] R.G. Parr and W. Yang, "Density Functional Theory of Atoms and Molecules", Oxford University Press, New York (1989).

[9] E.S. Kryachko and E. Ludena, "Density Functional Theory of Many-Electron Systems", Kluwer Academic, Dordrecht (1990).

[10] J. Callaway and N.H. March, in "Solid State Physics", ed. H. Ehrenreich and D. Turnbull, Academic, New York (1984).

[11] "Density Functional Methods in Chemistry", J.K. Labanowski and J.W. Andzelm, editors, (Springer-Verlag, Berlin, 1991).

[12] "Density Functional Theory of Molecules, Clusters, and Solids", D.E. Ellis, editor, (Kluwer Academic, Dordrecht, 1995).

[13] J.P. Perdew, Phys. Rev. **B33**, 8822 (1986); ibid **B34**, 7406 (1986).

[14] See, for example: J. Callaway, "Energy Band Theory", "Pure and Applied Physics" monograph no. 16, Academic Press, New York (1964).

[15] D.E. Ellis and G.S. Painter, Phys. Rev. B2, 2887 (1970).

[16] D.E. Ellis and J. Guo, in "Electronic Density Functional Theory of Molecules, Clusters and Solids", ed. D.E. Ellis, Kluwer, Dordrecht (1995) p. 263.

[17] A. Rosen and D.E. Ellis, J. Chem. Phys. **62**, 3039 (1975).

[18] D.E. Ellis, in "Actinides in Perspective", edited by N.M. Edelstein (Pergammon, New York, 1992) p. 123.

[19] A.D. Becke, Phys. Rev. A**38**, 3098 (1988).

[20] P. Hohenberg and W. Kohn, Phys. Rev. **136**, B847 (1964); W. Kohn and L.J. Sham, Phys. Rev. **137**, A1697 (1965); W. Kohn and L.J. Sham, Phys. Rev. **140**, A1133 (1965).

[21] G.S. Painter and D.E. Ellis in "Computational Methods in Band Theory", Plenum, N. York (1971), pg. 271 and 277.

[22] G.S. Painter and D.E. Ellis, Phys. Rev. B **1**, 4747 (1970).

[23] D.E. Ellis and F.W. Averill, J. Chem. Phys. **60**, 2856 (1974).

[24] E.J. Baerends, D.E. Ellis and P. Ros, Chem. Phys. **2**, 41 (1973).

[25] A. Rósen, D.E. Ellis, H. Adachi and F.W. Averill, J. Chem. Phys. **65**, 3629 (1976).

[26] C.B. Haselgrove, Math. Comp. **15**, 323 (1961).

[27] H. Conroy, J. Chem. Phys. **47**, 5307 (1967).

[28] D.E. Ellis, Int. J. Quant. Chem. **2S**, 35 (1968).

[29] A.H. Stroud, "Approximate calculation of multiple integrals", Prentice Hall, Englewood Cliffs, NJ (1971).

[30] F.L. Hirshfeld, Theor. Chim. Acta **44**, 129 (1977).

[31] A. Becke, J. Chem. Phys. **88**, 2547 (1988).

[32] R.S. Mulliken, J. Chem. Phys. **23**, 1833 (1955); ibid, 1841 (1955).

[33] C. Umrigar and D.E. Ellis, Phys. Rev. B **21**, 852 (1980).

[34] T.D. Bouman and G.L. Goodman, J. Chem. Phys. **56**, 2478 (1972).

[35] D.E. Ellis and G.L. Goodman, Int. J. Quant. Chem. **25**, 185 (1984).

[36] P.J. Hay and W.R. Wadt, J. Chem. Phys. **82**, 229 (1985); M. Boring and J.H. Wood, J. Chem. Phys. **71**, 32 (1979); **71**, 392 (1979).

[37] B. Delley and D.E. Ellis, J. Chem. Phys. **76**, 1949 (1982).

[38] J.D. Jackson, "Classical Electrodynamics", Wiley, N. York (1975).

[39] J.C. Slater, "The self-consistent field for molecules and solids", vol. 4, McGraw-Hill, New-York (1974).

[40] R. Gaspar, Acta Phys. Acad. Sci. Hung. **3**, 263 (1954).

[41] J.M. MacLaren, D.P. Clougherty, M.E. McHenry and M.M. Donovan, Computer Physics Communications **66**, 383 (1991), and references therein.

[42] S.H. Vosko, L. Wilk and M. Nusair, Can. J. Phys. **58**, 1200 (1980).

[43] D.M. Ceperley and B.J. Alder, Phys. Rev. Lett. **45**, 566 (1980); D. Ceperley, Phys. Rev. B **18**, 3126 (1978).

[44] C. Kittel, "Introduction to Solid State Physics", 7th. edition, J. Wiley, New York (1996), appendix B.

[45] B. Delley, D.E. Ellis, A.J. Freeman, E.J. Baerends and D. Post, Physical Review B **27**, 2132 (1983).

[46] P.K. Kowash and D.E. Ellis, Phys. Rev. B **39**, 1908 (1989).

[47] D. Guenzburger and D.E. Ellis, Phys. Rev. Letters **67**, 3832 (1991).

[48] D. Guenzburger and D.E. Ellis, Phys. Rev. B **45**, 285 (1992).

[49] H.A. Bethe and R.W. Jackson, "Intermediate Quantum Mechanis", McGraw-Hill, New York (1968);
M.E. Rose, "Relativistic Effects in Atoms, Molecules, and Solids", Plenum, New York (1983).

[50] I.P. Grant, Proc. Roy. Soc. London, Ser A **262**, 555 (1961);
R.D. Cowan and D.C. Griffin, J. Opt. Soc. Am. **66**, 1010 (1976);
J.-P. Desclaux and P. Pyykkö, Chem. Phys. Lett. **29**, 534 (1974);

P.J. Hay, W.R. Wadt, L.R. Kahn, and F.W. Bobrowicz, J. Chem. Phys. **69**, 984 (1978).

[51] T. Ziegler, J.G. Snijders and E.J. Baerends, J. Chem. Phys. **74**, 1271 (1981).

[52] B.X. Xu, A.K. Rajagopal, and M.V. Ramana, J. Phys. C, **17**, 1339 (1984); M. Vijayakumar, N. Vaidehi, and M.S. Gopinathan, Phys. Rev. **A40**, 6834 (1989).

[53] D.E. Ellis, J. Phys. B **10**, 1 (1977) and references therein.

[54] D.D. Koelling and A.H. MacDonald, in "Relativistic Effects in Atoms, Molecules, and Solids", G.L. Malli, ed., Plenum, New York (1983), p. 227.

[55] S.R. Nogueira and D. Guenzburger, Int. J. Quant. Chem. **57**, 471 (1996). D.E. Ellis, in "Actinides in Perspective", N.M. Edelstein, ed., Pergamon, New York (1982), p. 123; C.Y. Yang, J. Chem. Phys. **68**, 2626 (1978).

[56] D.A. Liberman, J.T. Waber, and D.T. Cromer, Phys. Rev. **A27**, 137 (1965); P. Pyykkö and J.-P. Desclaux, Acct. Chem. Res. **12**, 276 (1979); M. Pepper and B.E. Bursten, Chem. Rev. **91**, 719 (1991).

[57] D.E. Ellis, Int. J. Quantum Chem. Symp. **11**, 201 (1977); D.E. Ellis, in "Handbook on the Physics and Chemistry of the Actinides", A.J. Freeman and G.H. Lander, eds., North-Holland, Amsterdam (1985), p. 1.

[58] M. Tinkham, "Group Theory and Quantum Mechanics", McGraw-Hill, New York (1964).

[59] H. Wilkinson, "The Algebraic Eigenvalue Problem", Clarendon Press, Oxford (1965).

[60] A. Berces and T. Ziegler, Topics in Curr. Chem. **182**, 41 (1996).

[61] G.A. Benesh and D. Gebreselasie, Phys. Rev. **B54**, 5940 (1996).

[62] P.E. Gill, W. Murray, and M.H. Wright, "Practical Optimization", Academic, London (1981).

[63] R. Carr and M. Parinello, Phys. Rev. Lett. **55**, 247 (1985); R. Car and M. Parinello, in "Simple Molecular Systems at Very High Density", A. Polian, P. Loubeyre and N. Boccara, eds., Plenum, New York (1989); P.J. Kelley and R. Car, Phys. Rev. **B45**, 6543 (1992).

[64] S. Kirkpatrick, C.D. Gelat, and M.P. Vecchi, Science **220**, 671 (1983);
S. Kirkpatrick, J. Stat. Phys. **34**, 975 (1984);
E.P.G. Arêas, P.G. Pascutti, S. Schreier, K.C. Mundim, and P.M. Bisch, J. Phys. Chem. **99**, 14882 (1995);
F. Yonezawa, ed., "Molecular Dynamics Simulations", Springer-Verlag, Berlin, (1992).

[65] J.F. Lutsko, D. Wolf, S. Yip, S.P. Philpott, and T. Nguyen, Phys. Rev. **B38**, 2887 (1988).

[66] R.W. Grimes, C.R.A. Catlow, and A.L. Shluger, eds., "Quantum Mechanical Calculations in Solid State Studies", World Scientific, Singapore (1992).

[67] GROMOS: Gröningen Molecular Simulation Data Base, developed at Gröningen University.

[68] M.S. Daw and M.I. Baskes, Phys. Rev.. **B29**, 6443 (1984);
S.M.. Foiles, M.I. Baskes, and M.S. Daw, Phys. Rev. **B33**, 7983 (1986).

[69] C.R.A. Catlow, I.D. Faux and M.J. Norgett, J. Phys. C **9**, 419 (1976).

[70] L. Guo, D.E. Ellis, K.C. Mundim and B.M. Hoffman, submitted.

[71] J.R. Ferraro, Coord. Chem. Rev. **43**, 205 (1982);
J. Martinsen, R.I. Green, S.M. Palmer and B.M. Hoffman, J. Am.. Chem. Soc. **105**, 677 (1983);
L.J. Pace, J. Martinsen, A. Ulman, B.M. Hoffman and J.A. Ibers, J. Am. Chem. Soc. **105**, 2612 (1983);
T.P. Newcomb, M.R. Godfrey, B.M. Hoffman and J.A. Ibers, Inorg. Chem. **29**, 223 (1990);
M.Y. Ogawa, S.M. Palmer, K. Liou, G. Quiron, J.A. Thompson, M. Poirier and B.M. Hoffman, Phys. Rev. B **39**, 682 (1989); M.Y. Ogawa, J. Martinsen, S.M. Palmer, J.L. Stanton, J. Tanaka, R.L. Greene, B.M. Hoffman and J.A. Ibers J. Am. Chem. Soc. **109**, 1115 (1987).

[72] L. Guo, D.E. Ellis, B.M. Hoffman and Y. Ishikawa, Inorg. Chem. **35**, 5304 (1996).

[73] A. Rosa and E.J. Baerends, Inorg. Chem. **31**, 4717 (1992); **32**, 5637 (1993); **33**, 584 (1994).

[74] B.C. Wiegand and C.M. Friend, Chem. Revs. **92**, 491 (1992).

[75] R.A. Sánchez-Delgado, J. Mol. Catal. **86**, 287 (1994), and references therein.

[76] B.A. Sexton, Surf. Sci. **163**, 99 (1985).

[77] L. Rincón, J. Terra, D. Guenzburger and R.A. Sánchez-Delgado, Organometallics **14**, 1292 (1995).

[78] D.D. Awschalom and D.P. DiVincenzo, Physics Today **48**, 43 (1995).

[79] D.D. Awschalom, D.P. DiVincenzo and J.F. Smyth, Science **258**, 414 (1992).

[80] G.C. Papaefthymiou, Phys. Rev. B **46**, 10366 (1992).

[81] D.D. Awschalom, J.F. Smyth, G. Grinstein, D.P. DiVincenzo and D. Loss, Phys. Rev. Letters **68**, 3092 (1992).

[82] R.D. Michael, R.D. Schull, L.J. Swartzendruber, L.H. Bennett and R.E. Watson, J. Mag. Mag. Mat. **111**, 29 (1992); R. Sessoli, D. Gatteschi, A. Caneschi and M.A. Novak, Nature **365**, 141 (1993).

[83] D. Gatteschi, E. Sessoli, W. Plass, A. Müller, E. Krickemeyer, J. Meyer, S. Sölter and P. Adler, Inorg. Chem. **35**, 1926 (1996).

[84] K.L. Taft, C.D. Delfs, G.C. Papaefthymiou, S. Foner, D. Gatteschi and S.J. Lippard, J. Am. Chem. Soc. **116**, 823 (1994).

[85] Z. Zeng, Y. Duan and D. Guenzburger, Phys. Rev. B, in press.

[86] N.N. Greenwood and R.C. Gibb, "Mössbauer Spectroscopy", Chapman and Hall, London (1971).

[87] J. Terra and D. Guenzburger, J. Phys. Chem. **99**, 4935 (1995).

[88] D. Guenzburger and D.E. Ellis, Phys. Rev. B **22**, 4203 (1980).

[89] J. Terra and D. Guenzburger, Phys. Rev. B **44**, 8584 (1991).

[90] D. Guenzburger and D.E. Ellis, Phys. Rev. B **36**, 6971 (1987).

[91] P. Dufek, P. Blaha and K. Schwarz, Phys. Rev. Letters **75**, 3545 (1995).

[92] R.H. Holm, Chem. Rev. **87**, 1401 (1987).

[93] S. Alexander, J.L. Séris, and B. Meunier, Science **268**, 1163 (1995); R.A. Sheldon, and J.A. Kochi, *Metal-Catalyzed Oxidation of Organic Compounds*, Academic Press, New York (1981).

[94] N.L.P. Fackler, S.S. Zhang, and T.V. O'Halloran, J. Am. Chem. Soc. **118**, 481 (1996).

[95] A.R. Rossi and R. Hoffmann, Inorg. Chem. **14**, 365 (1975).

[96] F.K. Winkler and J.D. Dunitz, J. Mol. Biol. **59**, 169 (1971); F.C. Anson, T.J. Collins, S.L. Gipson, J.T. Keech, T.E. Kraft and G.T. Peake, J. Am. Chem. Soc. **108**, 6593 (1986).

[97] D.E. Ellis, N.F.L. Fackler, and T.V. O'Halloran, submitted.

[98] N.V. Vugman, R.P.A. Muniz and J. Danon, J. Chem. Phys. **57**, 1297 (1972).

[99] S.R. Nogueira and D. Guenzburger, Int. J. Quant. Chem. **57**, 471 (1996).

[100] T.C. Zietlow, W.P. Schaefer, B. Sadeghi, N. Hua, and H.B. Gray, Inorg. Chem. **25**, 2195 (1986).

[101] R. Bain, D.E. Ellis, L.M. Robinson, and D.F. Shriver, submitted.

[102] L.M. Robinson, R. Bain, D.F. Shriver and D.E. Ellis, Inorg. Chem. **34**, 5588 (1995).

[103] T.C. Zietlow, M.D. Hopkins and H.B. Gray, J. Solid State Chem. **57**, 112 (1985); T.C. Zietlow, D.G. Nocera and H.B. Gray, Inorg. Chem. **25**, 1351 (1986).

[104] B.K. Cho, P.C. Canfield, L.L. Miller, D.C. Johnston, W.P. Beyermann, and A. Yatskar, Phys. Rev. **B52**, 3684 (1995) and references therein.

[105] W.E. Pickett and D.J. Singh, Phys. Rev. Letters **72**, 3702 (1994); L.F. Mattheiss, Phys. Rev. **B49**, 13279 (1994).

[106] E. Johnston-Halperin, J. Fiedler, D.E. Farrel, M. Xu, K. Cho, P.C. Canfield, D.K. Finnemore, and D.C. Johnston, Phys. Rev. **B51**, 12852 (1995).

[107] B.K. Cho, M. Xu, P.C. Canfield, L.L. Miller, and D.C. Johnston, Phys. Rev. **B52**, 3676 (1995).

[108] A.I. Goldman, C. Stassis, P.C. Canfield, J. Zarestky, P. Dervenagas, B.K. Cho, D.C. Johnston and B. Sterlieb, Phys. Rev. **B50**, 9668 (1994);
Z. Zarestky, C. Stassis, A.I. Goldman, P.C. Canfield, P. Dervenagas, B.K. Cho, and D.C. Johnston, Phys. Rev. **B51**, 678 (1995).

[109] Z. Zeng, D.E. Ellis, D. Guenzburger, and E.M. Baggio-Saitovitch, Phys. Rev. **B53**, 6613 (1996).

[110] Z. Zeng, D.R. Sanchez, D. Guenzburger, D.E. Ellis, E.M. Baggio-Saitovitch, and H. Micklitz, Phys. Rev. **B55**, xxxx (1997).

[111] Z. Zeng, D. Guenzburger, D.E. Ellis and E.M. Baggio-Saitovitch, Physica C **271**, 23 (1996); Z. Zeng, D.E. Ellis, D. Guenzburger and E.M. Baggio-Saitovitch, Phys. Rev. B **54**, 13020 (1996).

[112] G.Y. Guo and W.M. Temerman, Phys. Rev. **B41**, 6372 (1990).

[113] T. Ezawa, W.A.A. Macedo, U. Glos, W. Keune, K.P. Schletz and U. Kirchbaum, Physica B **161**, 281 (1989), and references therein.

[114] W. Keune, T. Ezawa, W.A.A. Macedo, U. Glos and K.P. Schletz, Physica B **161**, 269 (1989), and references therein.

[115] J. Kübler, Phys. Lett. **81A**, 81 (1981); C.S. Wang, B.M. Klein and H. Krakauer, Phys. Rev. Lett. **54**, 1852 (1985).

[116] E.F. Wassermann, Phys. Scr. **T25**, 209 (1989).

[117] D. Guenzburger and D.E. Ellis, Phys. Rev. B **51**, 12519 (1995).

[118] D. Guenzburger and D.E. Ellis, Phys. Rev. B **52**, 13390 (1995).

[119] H. Chacham, E. Galvão da Silva, D. Guenzburger and D.E. Ellis, Phys. Rev. B **35**, 1602 (1987).

[120] J.A. Tossel and G.V. Gibbs, Phys. Chem. Mineral **2**, 21 (1977).
G.V. Gibbs, Am. Mineral. **67**, 421 (1982);
J. Sauer, J. Chem. Rev. **89**, 199 (1989);
A.C. Lasaga, Rev. Mineral. **23**, 17 (1990);
B.J. Teppen, D.M. Miller, S.Q. Newton and L. Schäfer, J. Phys. Chem. **98**, 12545 (1994);

H.V. Brand, L.A. Curtiss and L.E. Iton, J. Phys. Chem. **96**, 7725 (1992);
D.H. Sherman, Phys. Chem. Minerals **14**, 355 (1987); **14**, 364 (1987); Ame. Mineral. **75**, 256 (1990).

[121] R. Dovesi, C. Pisani, C. Roetti and B. Silvi, J. Chem. Phys. **86**, 6967 (1987);
A.C. Hess and V.R. Saunders, J. Phys. Chem. **96**, 4367 (1992); J.C. White and A.C. Hess, J. Phys. Chem. **97**, 6398 (1993); **97**, 8703 (1993);
Yong-nian Xu and W.Y. Ching, Phys. Rev. **B44**, 11048 (1991).

[122] J. Terra and D.E. Ellis, Proc. Latin Amer. Conf. Mössbauer Effect, 1996, to be published.

[123] R.W.G. Wyckoff, *Crystal Structures*, Wiley, New York, (1968) vol. 4.

[124] G.J. Redhamer, A. Beran, E. Dachs and G. Amthauer, Phys. Chem. Minerals **20**, 382 (1993).
D.G. Rancourt, I.A.D. Christie, M. Royer, H. Kodama, J.-L. Robert, A.E. Lalonde and E. Murad, Am. Mineral **79**, 51 (1994);
D.G. Rancourt, Phys. Chem. Minerals **21**, 250 (1994);
D.G. Rancourt, J.Y. Ping and R.G. Berman, Phys. Chem. Minerals **21**, 258 (1994);
G.J. Redhamer, E. Dachs and G. Amthauer, Phys. Chem. Minerals **22**, 282 (1995);
D.G. Rancourt, J.Y. Ping, B. Boukili and J.-L. Robert, Phys. Chem. Minerals (in press).

[125] D.G. Rancourt, I.A.D. Christie, G. Lamarche, I.S. Swainson and S. Flandrois, J. Mag. Magnetic Mat. **138**, 31 (1994).

[126] V. Ravikumar and V.P. Dravid, Ultramicros **52**, 557 (1993);
M.M. McGibbon, N.D. Browning, M.F. Chisholm, A.J. McGibbon, S.J. Pennycook, V. Ravikumar and V.P. Dravid, Science **266**, 102 (1994);
H. Gu, M. Ceh, S. Stemmer, H. Mullejans and M. Ruhle, Ultramicros. **59**, 215 (1995).

[127] V. Ravikumar, D. Wolf, and V.P. Dravid, submitted.

[128] R.P. Rodrigues, Ph.D thesis, Northwestern University, 1997;
R.P. Rodrigues, H.J. Chang, D.E. Ellis and V.P. Dravid, submitted.

The Configuration Interaction Method: Advances in Highly Correlated Approaches

C. David Sherrill† and Henry F. Schaefer III

Center for Computational Quantum Chemistry
University of Georgia
Athens, Georgia 30602

Abstract

Highly correlated configuration interaction (CI) wavefunctions going beyond the simple singles and doubles (CISD) model space can provide very reliable potential energy surfaces, describe electronic excited states, and yield benchmark energies and molecular properties for use in calibrating more approximate methods. Unfortunately, such wavefunctions are also notoriously difficult to evaluate due to their extreme computational demands. The dimension of a full CI procedure, which represents the exact solution of the electronic Schrödinger equation for a fixed one-particle basis set, grows factorially with the number of electrons and basis functions. For very large configuration spaces, the number of CI coupling coefficients becomes prohibitively large to store on disk; these coefficients must be evaluated as needed in a so-called direct CI procedure. Work done by several groups since 1980 has focused on using Slater determinants rather than spin ($\hat{S}^2$) eigenfunctions because coupling coefficients are easier to compute with the former. We review the fundamentals of the configuration interaction method and discuss various determinant-based CI algorithms. Additionally, we consider some applications of highly correlated CI methods.

†Present address: Department of Chemistry, University of California, Berkeley, CA 94720-1460

ADVANCES IN QUANTUM CHEMISTRY, VOLUME 34

0065-3276/99 $30.00

Contents

1 Introduction

Most chemists picture the electronic structure of atoms or molecules by invoking orbitals. The orbital concept has its basis in Hartree-Fock theory, which determines the best wavefunction $|\Psi\rangle$ under the approximation that each electron experiences only the *average* field of the other electrons. This is also called the "one-electron," or "independent particle" model. While the Hartree-Fock method gives very useful results in many situations, it is not always quantitatively or even qualitatively correct. When this approximation fails, it becomes necessary to include the effects of electron correlation: one must model the *instantaneous* electron-electron repulsions present in the molecular Hamiltonian.

The most broadly applicable method for describing electron correlation is configuration interaction (CI), which expresses the wavefunction as a linear combination of $\hat{S}_z$ eigenfunctions (Slater determinants) or $\hat{S}_z$ and $\hat{S}^2$ eigenfunctions (configuration state functions, or CSFs) describing the distribution of N electrons. If all possible N-electron functions are included in the CI procedure (subject to spatial and spin symmetry restrictions), then the Schrödinger equation is solved exactly within the space spanned by the one-particle basis functions. Hence, in its most general form, CI applies to difficult cases such as excited states, open-shell systems, and systems far from their equilibrium geometries. However, the dimension of this "full CI" procedure grows factorially with molecular size, so it is necessary to select only the most important N-electron functions.

A common approach is to restrict the CI space to the Hartree-Fock self-consistent-field (SCF) configuration and those configurations related to it by single and double substitutions of orbitals, in a procedure denoted CISD. In cases where the SCF method yields a good approximate wavefunction, CISD with double-ζ plus polarization (DZP) single-particle basis sets typically predicts equilibrium bond lengths of small molecules within 0.4% of experiment and harmonic vibrational frequencies within 4%.[1] Unfortunately, CISD (and most other standard CI methods short of full CI) are not size extensive, meaning that their performance degrades with increasing molecular size. Size extensive alternatives include many-body perturbation theory (MBPT) and coupled-cluster (CC) methods. The coupled-cluster singles and doubles (CCSD) method outperforms CISD with only a moderately increased computational effort (the cost of both methods scales as the sixth power of the system size) because CCSD accounts for some triple and quadruple substitutions from the SCF configuration by approximating them as products of single and double substitutions. When employed with a triple-ζ plus double polarization basis set (TZ2P), the CCSD generally predicts bond lengths within 0.2% of experiment and harmonic vibrational frequencies within 2%.[2]

More accurate results can be obtained by using larger one-particle basis sets and employing the CCSD(T) method, which accounts for the effects of irreducible (or connected) triple substitutions in a single non-iterative step scaling as n^7.[3-5] Furthermore, recent equation-of-motion (EOM) or linear-response coupled-cluster theories for singly-excited electronic states[6,7] also outperform CISD in the prediction of excitation energies because CISD is biased towards the state described by the reference wavefunction.

Even the coupled-cluster methods eventually break down in cases where the SCF wavefunction is not a qualitatively correct description of the system. This can occur during bond-breaking reactions, for example, or for transition metals.[8,9] Hence, it is necessary to make the zeroth-order wavefunction multiconfigurational. Although multireference coupled-cluster theories are very difficult to formulate, multireference CI methods have been used for many years.[10,11] These methods typically include single and double substitutions from a set of "reference" configurations required to describe nondynamical electron correlation. Unfortunately, reference selection is not trivial, since the list of important references depends on the molecule and its geometry. This tends to make MR-CI methods unsuitable as a "model chemistry,"[12] since the quality of the wavefunction is not uniform across different molecules. One MR-CI wavefunction which is largely free from these difficulties is second-order CI (SOCI),[13] which is a multi-reference CISD in which the references are chosen as all possible distributions of electrons within a given "active space" (unfortunately, the acronym SOCI is also sometimes used to mean spin-orbit CI). The SOCI wavefunction requires much less computational effort than a full CI, yet it produces potential energy surfaces which nearly parallel the full CI surfaces.[14-17] If the active space is large enough, one can expect the SOCI method to provide equally good results for any small molecule at any geometry, making it a suitable model chemistry (SOCI is still not rigorously size extensive, so it may be necessary to apply size extensivity corrections for systems with eight electrons or more[15]). Unfortunately, the SOCI method is too computationally expensive to be generally applicable.

Hence there is a need to make SOCI more computationally efficient so that it can be used for larger chemical systems, and to develop related methods which scale better with the system size. Although the CI space can be reduced by individual selection of references or N-electron functions, for the reasons stated above it is beneficial to select the CI space in an *a priori* manner, once a minimal set of parameters, such as the active space, has been specified. For example, we have advocated a method we call CISD[TQ],[16-18] which is a SOCI in which higher-than-quadruple substitutions have been excluded. For systems dominated by a single reference, CISD[TQ] performs nearly as well as SOCI.[16,17]

Although extremely costly to determine, full CI results are invaluable in the calibration of such multireference CI methods, or indeed of essentially any *ab initio* electronic structure method, including many-body perturbation theory (MBPT)[19–23] and coupled-cluster approaches.[4,6,7,17,19,22,24–37] A few full CI benchmarks[17,38,39] have been carried out using the loop-driven graphical unitary group (LD-GUGA) CI approach,[40–43] which uses a spin eigenfunction, or CSF, basis. However, a majority of the full CI calculations to date have employed Slater determinants, even though this typically makes the CI vector 2-4 times longer. In 1980, Handy demonstrated that the benefits of Slater determinants can outweigh their disadvantages, primarily because the evaluation of the required matrix elements becomes so much simpler.[44] In his 1980 article, Handy introduced the alpha and beta string notation which has commonly been used in the development of new CI algorithms. After an important reformulation of the direct CI method by Siegbahn,[45] Knowles and Handy introduced a vectorized full CI algorithm that enabled a whole series of full CI benchmark studies by Bauschlicher, Langhoff, Taylor, and others.[15] In 1988, Olsen and co-workers showed how to improve the Knowles-Handy algorithm by reducing the operation count while still maintaining vectorization in the innermost loops.[46] Another important advance was the extension to certain types of truncated CI spaces in which determinants are chosen according to how many electrons they place in each of three orbital subspaces. This restricted active space (RAS) CI procedure is capable of evaluating SOCI and CISD[TQ] wavefunctions. Subsequently, other full CI algorithms involving basically the same amount of computational effort as Olsen's algorithm have been presented by Harrison and Zarrabian[47] and by Bendazzoli and Evangelisti.[48–50]

In this article, we provide an updated look at the configuration interaction method in general, and at highly correlated CI methods in particular. Special emphasis is given to methods which select the CI space in an *a priori* manner. After reviewing the basic theory of the CI method and the typical approximations employed, we discuss features common to all implementations: transformation of the one- and two-electron integrals from the atomic orbital to the molecular orbital basis, and iterative diagonalization methods. Next, we survey several determinant-based algorithms for full and RAS CI wavefunctions. We describe some technical issues in considerable detail and describe our experience with our own determinant-based CI program. Finally, we discuss some of the applications of highly correlated CI methods. Although crucial to the efficient determination of optimized geometries and vibrational frequencies, analytic gradients of CI wavefunctions are not discussed in this article; we refer the reader to the recent article by Shepard[51] and the monograph by Yamaguchi *et al.*[52] Furthermore, additional considerations may arise when designing a CI program to be used along with orbital optimization in the mul-

ticonfigurational (MC) or complete-active-space (CAS) SCF methods; these issues are discussed elsewhere.[9,53-56]

2 The Configuration Interaction Method

This section presents the essential elements of the configuration interaction method and is meant to be accessible to those who are not experts in CI. The classic review by Shavitt covers the theoretical fundamentals and various formulations given prior to 1977.[57] More recent reviews have been presented by Siegbahn,[58] Karwowski,[59] and Duch.[60]

2.1 Fundamentals

Configuration interaction is conceptually the simplest method for solving the time-independent electronic Schrödinger equation $\hat{H}|\Psi\rangle = E|\Psi\rangle$ under the Born-Oppenheimer approximation. The electronic wavefunction $|\Psi\rangle$ is approximated by a linear expansion of N-electron basis functions (where N is the number of electrons in the system), i.e.,

$$|\Psi\rangle = \sum_I c_I |\Phi_I\rangle. \tag{1}$$

The linear expansion coefficients c_I are the *CI coefficients*. Substituting this linear expansion into the electronic Schrödinger equation, one obtains[61] a matrix form more suitable for computation:

$$\mathbf{Hc} = E\mathbf{Sc}, \tag{2}$$

where the Hamiltonian operator $\hat{H}$ has been replaced by a matrix $\mathbf{H}$ and the CI wavefunction $|\Psi\rangle$ has been replaced by a column vector of coefficients $\mathbf{c}$. In principle, this "matrix mechanics" formulation is equivalent to the original electronic Schrödinger equation;[62] hence it is said that CI constitutes an "exact theory." In practice, however, the matrix equations are not exact because the expansion in equation (1) must be truncated to a finite number of terms. The matrix elements of the Hamiltonian are given by $H_{IJ} = \langle\Phi_I|\hat{H}|\Phi_J\rangle$ and $\mathbf{S}$ is the overlap matrix with elements $S_{IJ} = \langle\Phi_I|\Phi_J\rangle$. If orthonormal functions $|\Phi_I\rangle$ are used for the expansion, then of course $\mathbf{S}$ becomes the unit matrix and the equation becomes an eigenvalue equation. Since $\mathbf{H}$ is a Hermitian matrix, the number of orthogonal eigenvectors is equal to the dimension of the matrix. The lowest-energy solution represents the electronic ground state, and higher-energy solutions represent excited electronic states.

It is generally helpful to build into the expansion functions $\{|\Phi_I\rangle\}$ the symmetry properties of the system. According to the antisymmetry principle,

a wavefunction describing a system of electrons (more generally, fermions) must be antisymmetric with respect to the interchange of spatial and spin coordinates for any pair of electrons. This requirement is very commonly satisfied by making the expansion functions Slater determinants. A Slater determinant in which the one-electron functions $\phi_i, \phi_j, \ldots, \phi_k$ are occupied may be written

$$\Phi = \frac{1}{\sqrt{N!}} \begin{vmatrix} \phi_i(\mathbf{x}_1) & \phi_j(\mathbf{x}_1) & \ldots & \phi_k(\mathbf{x}_1) \\ \phi_i(\mathbf{x}_2) & \phi_j(\mathbf{x}_2) & \ldots & \phi_k(\mathbf{x}_2) \\ \vdots & \vdots & & \vdots \\ \phi_i(\mathbf{x}_N) & \phi_j(\mathbf{x}_N) & \ldots & \phi_k(\mathbf{x}_N) \end{vmatrix} \tag{3}$$

and abbreviated as $|\phi_i \phi_j \ldots \phi_k\rangle$ or simply as $|ij \ldots k\rangle$. Note that this determinant is uniquely specified (up to a phase factor) by the list of occupied orbitals. It is easy to see that such a determinant satisfies the antisymmetry principle, since the interchange of coordinates for a pair of electrons translates to the swapping of rows of the determinant, which introduces a sign change. We may also write the above determinant as

$$\Phi = \frac{1}{\sqrt{N!}} \sum_P (-1)^p \hat{P} \phi_i(\mathbf{x}_1) \phi_i(\mathbf{x}_2) \cdots \phi_k(\mathbf{x}_N), \tag{4}$$

where $\hat{P}$ is a permutation of electron coordinates with sign $(-1)^p$. In this context it can be useful to define the *antisymmetrizer* as

$$\mathcal{A} = \frac{1}{\sqrt{N!}} \sum_P (-1)^p \hat{P}. \tag{5}$$

This operator produces a Slater determinant when applied to a simple product of spin orbitals. The antisymmetrizer is Hermitian, it commutes with $\hat{H}$, and its square is proportional to itself, i.e., $\mathcal{A}^2 = \sqrt{N!}\mathcal{A}$.

An electronic wavefunction can be described exactly by equation (1) if the expansion includes all possible Slater determinants formed from a complete set of one-electron functions $\{\phi\}$.[63] Such a procedure has been called *complete CI*.[40] Since a truly complete set of orbitals will typically be infinite, a complete CI is technically impossible to perform. However, if the one-electron basis set is truncated, then only a finite (albeit large) number of Slater determinants can be formed. Using all of these determinants in the expansion constitutes a *full CI* procedure, and the resulting eigenfunctions and eigenvalues are exact within the space spanned by the one-electron basis set. Although full CI results are extremely costly to compute, they are essential for benchmarking more approximate methods.

It is straightforward to show that if the exact wavefunction $|\Psi\rangle$ is an eigenfunction of some Hermitian operator $\hat{A}$, then expansion functions $|\Phi_I\rangle$ which are eigenfunctions of $\hat{A}$ with different eigenvalues do not contribute to the CI wavefunction and can be neglected in the expansion (1). If the Slater determinants are formed from spin-orbitals which are eigenfunctions of $\hat{s}_z$ and spatial symmetry operators, then the Slater determinants themselves will also be eigenfunctions of these spatial symmetry operators and of $\hat{S}_z$. However, a Slater determinant is not generally an eigenfunction of $\hat{S}^2$. Hence, a common alternative to Slater determinants are *configuration state functions* (CSFs), which are simply linear combinations of Slater determinants chosen to be eigenfunctions of $\hat{S}^2$. The benefit of using CSFs over determinants is that fewer N-electron functions are needed to describe the same state. The drawback is that matrix elements of the Hamiltonian are easier to compute using determinants. Of course, there are other possible choices for the N-electron basis functions. For instance, one can incorporate functions of two electrons (geminals),[64–67] as is done in the Hylleraas treatment of the helium atom.[68,69] Nevertheless, N-electron functions built from single-particle functions remain the most common.

Unfortunately, even with an incomplete one-electron basis, a full CI is computationally intractable for any but the smallest systems, due to the vast number of N-electron basis functions required (the size of the CI space is discussed in section 2.4.1). The CI space must be reduced, hopefully in such a way that the approximate CI wavefunction and energy are as close as possible to the exact values. By far the most common approximation is to begin with the Hartree-Fock procedure, which determines the best single-configuration approximation to the wavefunction that can be formed from a given basis set of one-electron orbitals (usually atom centered and hence called atomic orbitals, or AOs). This yields a set of molecular orbitals (MOs) which are linear combinations of the AOs:

$$\phi_i(\mathbf{x}_1) = \sum_{\mu} C_{\mu}^{i} \chi_{\mu}(\mathbf{x}_1), \tag{6}$$

where $\chi_\mu(\mathbf{x}_1)$ denotes an atomic orbital and C_μ^i is an *SCF coefficient.* The CI space can then be expanded according to substitution or "excitation" level relative to the SCF "reference" determinant, i.e.,

$$|\Psi\rangle = c_0|\Phi_0\rangle + \sum_{ia} c_i^a|\Phi_i^a\rangle + \sum_{a<b,i<j} c_{ij}^{ab}|\Phi_{ij}^{ab}\rangle + \sum_{a<b<c,i<j<k} c_{ijk}^{abc}|\Phi_{ijk}^{abc}\rangle + \ldots \tag{7}$$

where $|\Phi_i^a\rangle$ means the Slater determinant formed by replacing spin-orbital i in $|\Phi_0\rangle$ with spin orbital a, etc. The widely-employed CI singles and doubles (CISD) wavefunction includes only those N-electron basis functions which represent single or double substitutions relative to the reference state. Since the

Hamiltonian operator includes only one- and two-electron terms, only singly and doubly substituted configurations can interact directly with the reference, and they typically account for about 95% of the basis set correlation energy of small molecules at their equilibrium geometries,[38] where $|\Phi_0\rangle$ provides a good zeroth-order description. Truncation of the CI space according to excitation class is discussed more fully in section 2.4.1.

2.2 The Variational Theorem

One attractive feature of configuration interaction is that the computed lowest energy eigenvalue is always an upper bound to the exact ground state energy. This follows from the fact that the CI energy is given by the expectation value formula, or Rayleigh quotient,

$$E = \frac{\langle \Phi | \hat{H} | \Phi \rangle}{\langle \Phi | \Phi \rangle}. \tag{8}$$

The variational theorem may be proven by expressing the approximate wavefunction $|\Phi\rangle$ as a linear combination of the exact eigenvectors $|\Psi_i\rangle$; one easily obtains

$$E - \mathcal{E}_0 = \sum_i c_i^* c_i (\mathcal{E}_i - \mathcal{E}_0), \tag{9}$$

where $\mathcal{E}_i$ is the ith *exact* energy eigenvalue, i.e., $\hat{H}|\Psi_i\rangle = \mathcal{E}_i|\Psi_i\rangle$. Since the right-hand side of eq. (9) is necessarily non-negative, $E \geq \mathcal{E}_0$. Likewise, we can also insert an expansion over the exact eigenvectors *for a given one-electron space* to prove that the CI energy must be an upper bound to the full CI energy in the same one-electron basis set. Equation (9) demonstrates that the approximate wavefunction approaches the exact one ($c_0 \approx 1$) as the energy E is minimized (see section 2.2.1). Minimizing E is equivalent to minimizing the right-hand side of eq. (9); that is, the sum of squares of the absolute values of the coefficients of excited states is minimized with weight factors $(\mathcal{E}_i - \mathcal{E}_0)$. This means that other properties do not generally converge as quickly with CI space expansion as the energy. In fact, the error in the energy is quadratic in the wavefunction error. This can be shown by writing the energy as

$$E = \frac{\langle \Psi - \Delta\Psi | \hat{H} | \Psi - \Delta\Psi \rangle}{\langle \Psi - \Delta\Psi | \Psi - \Delta\Psi \rangle}, \tag{10}$$

with $|\Psi\rangle$ the exact wavefunction and the error $|\Delta\Psi\rangle$ chosen orthogonal to $|\Psi\rangle$. From this expression it is simple to demonstrate that all terms linear in $|\Delta\Psi\rangle$ are vanishing and that only quadratic terms remain.

It is easy to extend proofs of the variational theorem to the case of states which are the lowest roots of a given spatial and spin symmetry.[70] Since the

self-consistent-field (SCF) and multiconfigurational SCF (MCSCF) wavefunctions can be written as a linear expansion (1) containing one or a few Slater determinants, with an energy given by eq. (8), they also obey the variational theorem. Furthermore, just as the lowest CI eigenvalue is an upper bound to the exact ground-state energy, more generally any CI eigenvalue E_i is an upper bound to the corresponding exact excited state energy $\mathcal{E}_i$.[71] Additionally, as other N-electron basis functions are added to the CI space, the eigenvalues obey the MacDonald-Hylleraas-Undheim relations[71,72]

$$E_{i-1}^{(m)} \leq E_i^{(m+1)} \leq E_i^{(m)} \tag{11}$$

where m is the number of N-electron basis functions.

2.2.1 The Method of Linear Variations

Since the variational theorem proves that the energy of a CI wavefunction is always an upper bound to the exact energy, one might start simply from the linear expansion (1) and attempt to minimize the energy by varying the CI coefficients subject to the constraint that they remain normalized. It is easy to show[63] that this method of linear variations, or the Ritz method,[73] yields the matrix equation

$$\mathbf{Hc} = E\mathbf{Sc}. \tag{12}$$

That is, the method of linear variations is identical to the matrix formulation of the Schrödinger equation. Another way of viewing this result is that only solutions to eq. (12) are energetically stable with respect to variations in the linear expansion coefficients.

2.2.2 The Correlation Energy

Since the CI energy is always an upper bound to the exact energy, approximate CI methods can be judged according to what fraction of the correlation energy they recover. The correlation energy is defined as the difference between the energy in the Hartree-Fock limit (E_{HF}) and the exact nonrelativistic energy of a system ($\mathcal{E}_0$)

$$E_{\text{corr}} = \mathcal{E}_0 - E_{HF}. \tag{13}$$

This energy will always be negative because the Hartree-Fock energy is an upper bound to the exact energy. The exact nonrelativistic energy $\mathcal{E}_0$ could be calculated, in principle, via a full CI in a complete one-electron basis. If we have an incomplete one-electron basis set, then we can only compute the *basis set correlation energy*, which is the correlation energy for a given one-electron basis. Frequently the term correlation energy implies basis set correlation

energy. The correlation energy is the energy recovered by fully allowing the electrons to avoid each other; the Hartree-Fock method, rather than using the true instantaneous Coulomb repulsion between pairs of electrons, instead only allows each electron to experience an average potential due to all the other electrons. However, this description of *dynamical correlation* is not complete. When a molecule is pulled apart, the electrons should not need to avoid each other as much, so the magnitude of the correlation energy should decrease. In fact, the opposite is true, as shown by the basis set correlation energies given in Table 1 for H_2O at five different geometries.

Table 1: Correlation Energy in H_2O with a cc-pVDZ Basis as Both O–H Bonds are Stretched Simultaneously.

Geometry	E_{corr} (hartree)[a]
R_e	-0.217 821
$1.5 \cdot R_e$	-0.269 961
$2.0 \cdot R_e$	-0.363 954
$2.5 \cdot R_e$	-0.476 747
$3.0 \cdot R_e$	-0.567 554

[a]Data from Olsen *et al.*, ref 22.
All ten electrons are correlated.

The magnitude of the correlation energy increases as the O–H bonds are stretched beyond their equilibrium length because equation (13) also includes a more subtle effect called the *nondynamical* or *static* correlation energy. This part of the correlation energy reflects the inadequacy of a single reference in describing a given molecular state, and is due to nearly degenerate states or rearrangement of electrons within partially filled shells. Shavitt[57] has pointed out this deficiency in the correlation energy definition and has suggested that multiconfigurational Hartree-Fock may prove a more useful baseline than single-configuration Hartree-Fock in equation (13).

2.3 Matrix Elements in Terms of One- and Two-electron Integrals

2.3.1 Slater's Rules

The matrix elements $H_{IJ} = \langle \Phi_I | \hat{H} | \Phi_J \rangle$ can be expressed in terms of one- and two-electron integrals. If we employ Slater determinants, the matrix elements

may be evaluated using Slater's rules (also called the Slater-Condon rules)[74–76] if a common set of one-electron orbitals are used for all determinants and if these orbitals are orthonormal. If nonorthogonal orbitals are employed (e.g., atomic orbitals) then the more complicated Löwdin rules[77] apply.

Slater's rules are expressed here in terms of spin-orbitals, which are functions of the spatial and spin coordinates of a single electron. The one-electron integrals are written as

$$[i|\hat{h}|j] = \int \phi_i^*(\mathbf{x}_1)\hat{h}(\mathbf{x}_1)\phi_j(\mathbf{x}_1)d\mathbf{x}_1 \tag{14}$$

and the two-electron integrals, in Mulliken notation, are written as

$$[ij|kl] = \int \phi_i^*(\mathbf{x}_1)\phi_j(\mathbf{x}_1)\frac{1}{\mathbf{r}_{12}}\phi_k(\mathbf{x}_2)^*\phi_l(\mathbf{x}_2)d\mathbf{x}_1 d\mathbf{x}_2. \tag{15}$$

Before Slater's rules can be used, the two Slater determinants must be rearranged so that they have the maximum possible number of columns in common (recalling that each column swap causes a sign change). After the determinants are in maximum coincidence, we see how many spin orbitals they differ by and employ the following rules:

1. Identical Determinants:

$$\langle\Phi_1|\hat{H}|\Phi_1\rangle = \sum_m^N [i|\hat{h}|i] + \sum_{i>j}^N \{[ii|jj] - [ij|ji]\}\,. \tag{16}$$

2. Determinants that Differ by One Spin Orbital:

$$\begin{aligned} |\Phi_1\rangle &= |\cdots i\cdots\rangle \\ |\Phi_2\rangle &= |\cdots j\cdots\rangle \\ \langle\Phi_1|\hat{H}|\Phi_2\rangle &= [i|\hat{h}|j] + \sum_k^N \{[ij|kk] - [ik|kj]\}\,. \end{aligned} \tag{17}$$

3. Determinants that Differ by Two Spin Orbitals:

$$\begin{aligned} |\Phi_1\rangle &= |\cdots ij\cdots\rangle \\ |\Phi_2\rangle &= |\cdots kl\cdots\rangle \\ \langle\Phi_1|\hat{H}|\Phi_2\rangle &= [ik|jl] - [il|jk]. \end{aligned} \tag{18}$$

Some of the terms above may vanish after integrating over spin coordinates, and a pair of determinants differing by more than two spin orbitals have a matrix element of zero. A derivation of these rules can be found in the introductory text by Szabo and Ostlund.[63] The rules for evaluating Hamiltonian matrix elements in a CSF basis are more complicated and are generally derived[40,42,78] using second quantization, which we consider next.

2.3.2 Second Quantization

We are free to write the matrix elements in the more general form

$$H_{IJ} = \sum_{pq}^{n} \gamma_{pq}^{IJ} (p|\hat{h}|q) + \frac{1}{2} \sum_{pqrs}^{n} \Gamma_{pqrs}^{IJ} (pq|rs), \tag{19}$$

where the use of parentheses rather than square brackets denotes a switch to spatial orbital notation rather than spin orbital notation. Also note the factor of $1/2$ in the two-electron term. The constants γ_{pq}^{IJ} and Γ_{pqrs}^{IJ} are called the one- and two-electron coupling coefficients, respectively. The CI energy in terms of these coupling coefficients is

$$E = \sum_{IJ}^{CI} c_I \left[\sum_{pq}^{n} \gamma_{pq}^{IJ} (p|\hat{h}|q) + \frac{1}{2} \sum_{pqrs}^{n} \Gamma_{pqrs}^{IJ} (pq|rs) \right] c_J, \tag{20}$$

where we assume that the CI coefficients are real. The one- and two-electron reduced density matrices are defined as

$$\gamma_{pq} = \sum_{IJ}^{CI} c_I c_J \gamma_{pq}^{IJ}, \tag{21}$$

$$\Gamma_{pqrs} = \sum_{IJ}^{CI} c_I c_J \Gamma_{pqrs}^{IJ}, \tag{22}$$

and using these definitions the energy may be written more compactly as

$$E = \sum_{pq}^{n} \gamma_{pq} (p|\hat{h}|q) + \frac{1}{2} \sum_{pqrs}^{n} \Gamma_{pqrs} (pq|rs). \tag{23}$$

Some authors absorb the factor of $1/2$ into the definition of the two-electron coupling coefficient and reduced density matrix.

These coupling coefficients are generally derived using second quantization,[63,79] in which the Hamiltonian is written (for a given one-particle basis set) as

$$\hat{H} = \sum_{pq}^{2n} a_p^\dagger a_q [p|\hat{h}|q] + \frac{1}{2} \sum_{pqrs}^{2n} a_p^\dagger a_r^\dagger a_s a_q [pq|rs], \tag{24}$$

where $a_p^\dagger$ and a_p are the creation and annihilation operators, respectively, for an electron in spin orbital p. Note that the second-quantized form of the Hamiltonian is independent of the number of electrons. If the spatial parts of α and β spin orbitals are identical, it is easy to re-write the second-quantized Hamiltonian in terms of the following shift operators, which Paldus has shown[40] to be generators of the unitary group:

$$\hat{E}_{ij} = a_{i\alpha}^\dagger a_{j\alpha} + a_{i\beta}^\dagger a_{j\beta}. \tag{25}$$

Due to the anticommutation relations of creation and annihilation operators,

$$\hat{E}_{ij}^{\dagger} = \hat{E}_{ji} \tag{26}$$

$$[\hat{E}_{ij}, \hat{E}_{kl}] = \hat{E}_{il}\delta_{jk} - \hat{E}_{kj}\delta_{il}. \tag{27}$$

The resulting Hamiltonian in terms of these operators is

$$\hat{H} = \sum_{pq}^{n} h_{pq}\hat{E}_{pq} + \frac{1}{2}\sum_{pqrs}^{n}(pq|rs)\left(\hat{E}_{pq}\hat{E}_{rs} - \delta_{qr}\hat{E}_{ps}\right), \tag{28}$$

where we have used the more compact notation $h_{pq} = (p|\hat{h}|q)$. It is clear that the one- and two-electron coupling coefficients can be written as

$$\gamma_{pq}^{IJ} = \langle\Phi_I|\hat{E}_{pq}|\Phi_J\rangle, \tag{29}$$

$$\Gamma_{pqrs}^{IJ} = \langle\Phi_I|\hat{E}_{pq}\hat{E}_{rs} - \delta_{qr}\hat{E}_{ps}|\Phi_J\rangle. \tag{30}$$

Furthermore, using equations (26) and (27), one can deduce the following:

$$\gamma_{pq}^{IJ} = (\gamma_{qp}^{JI})^* \tag{31}$$

$$\Gamma_{pqrs}^{IJ} = \Gamma_{rspq}^{IJ} = (\Gamma_{srqp}^{JI})^* = (\Gamma_{qpsr}^{JI})^*. \tag{32}$$

2.4 Reducing the Size of the CI Space

This section discusses strategies for reducing the number of N-electron basis functions in the CI space (given that, in the general case, it is impossible to include all of them). We have already discussed how N-electron functions with the wrong symmetry properties (e.g., point-group symmetry, or spin symmetry) can be dismissed immediately.

2.4.1 Truncating by Excitation Level

As noted in equation (7), the CI expansion is typically truncated according to excitation level; in the vast majority of CI studies, the expansion is truncated (for computational tractability) at doubly-substituted configurations. Since the Hamiltonian contains only two-body terms, only singles and doubles can interact directly with the reference; this is a direct result of Slater's rules (cf. section 2.3.1). Furthermore, the matrix elements of singly substituted determinants (or CSFs) with the reference are zero when canonical SCF orbitals are used, according to Brillouin's theorem. Hence, one expects double excitations to make the largest contributions to the CI wavefunction after the reference

state. Indeed, this is what is observed. Even though singles, triples, etc., do not interact directly with the reference, they can still become part of the CI wavefunction (i.e., have non-zero coefficients) because they mix with the doubles, directly or indirectly. Although singles are much less important to the energy than doubles, they are generally included in CI treatments because of their relatively small number and because of their greater importance in describing one-electron properties.

After singles and doubles, the most important determinants are triples and quadruples, because only these can interact directly with the doubles. The importance of a determinant to the final CI wavefunction is expected to fall off with increasing substitution or excitation level relative to the reference, assuming that the reference is a reasonable zeroth-order description of the desired electronic state. Table 2 demonstrates the importance of various excitation classes in obtaining CI energies. Singles and doubles account for 95% of the correlation energy at the equilibrium geometries of the molecules listed. Quadruple excitations are more important than triples, at least as far as the energy is concerned. At stretched geometries, the CISD and CISDT methods become markedly poorer, yet the CISDTQ method still recovers a very high (and nearly constant) fraction of the correlation energy, suggesting that CISDTQ should give reliable results for energy differences across potential energy surfaces for small molecules so long as no more than two bonds are broken at once (simultaneously breaking three bonds would require up to sextuple substitutions).

Table 3 demonstrates that the number of N-electron basis functions increases dramatically with increasing excitation level. A DZP basis should be considered the minimum adequate basis for a meaningful benchmark study.[15,81] While it is generally possible to perform CISD calculations on small molecules with a good one-electron basis, the CISDTQ method is limited to molecules containing very few heavy atoms, due to the extreme number of N-electron functions required. Full CI calculations are of course even more difficult to perform, so that despite their importance as benchmarks, few full CI energies using large one-electron basis sets have been obtained.

The size of the full CI space in CSFs can be calculated (including spin symmetry but ignoring spatial symmetry) by Weyl's dimension formula.[82] If N is the number of electrons, n is the number of orbitals, and S is the total spin, then the dimension of the CI space in CSFs is given by

$$D_{nNS} = \frac{2S+1}{n+1} \begin{pmatrix} n+1 \\ N/2-S \end{pmatrix} \begin{pmatrix} n+1 \\ N/2+S+1 \end{pmatrix}. \tag{33}$$

The dimension of the full CI space in determinants (again, ignoring spatial

Table 2: Percentage of correlation energy recovered by various CI excitation levels for some small molecules.

	Percent Corr. Energy[a]		
Molecule	CISD	CISDT	CISDTQ
BH	94.91	n/a	99.97
HF	95.41	96.49	99.86
H_7^+	96.36	96.87	99.96
$H_2O(R_e)$	94.48	95.85	99.85
$H_2O(1.5\ R_e)$	89.36	92.05	99.48
$H_2O(2.0\ R_e)$	80.21	84.59	98.40
NH_3	94.44	95.43	99.84

[a]Results are for a DZP basis and are taken from refs 38 (BH, HF), 17 (H_7^+), 22 (H_2O), and 80 (NH_3). H_2O results correlate all ten electrons and employ the cc-pVDZ basis.

Table 3: Number of CSFs required for small molecules at several levels of CI.

	CSFs required[a]			
Molecule	CISD	CISDT	CISDTQ	FCI
BH	568	n/a	28 698	132 686
HF	552	6 712	48 963	944 348
H_7^+	1 271	24 468	248 149	2 923 933
H_2O	1 311	27 026	332 491	94 165 610
NH_3	2 443	52 595	619 235	48 642 057

[a]Results are for a DZP basis and are taken from refs 38 (BH, HF), 17 (H_7^+), 22 (H_2O), and 80 (NH_3). H_2O results correlate all ten electrons and employ the cc-pVDZ basis.

Table 4: Dimension of Full CI in Determinants (CSFs in parentheses)

	Number of electrons			
Orbitals	6	8	10	12
10	14.4×10^3	44.1×10^3	63.5×10^3	44.1×10^3
	(4.95×10^3)	(13.9×10^3)	(19.4×10^3)	(13.9×10^3)
20	1.30×10^6	23.5×10^6	240×10^6	1.50×10^9
	(379×10^3)	(5.80×10^6)	(52.6×10^6)	(300×10^6)
30	16.5×10^6	751×10^6	20.3×10^9	353×10^9
	(4.56×10^6)	(172×10^6)	(4.04×10^9)	(62.5×10^9)

symmetry) is computed simply by

$$D_{nN_\alpha N_\beta} = \begin{pmatrix} n \\ N_\alpha \end{pmatrix} \begin{pmatrix} n \\ N_\beta \end{pmatrix}, \tag{34}$$

or, in a form closer to equation (33),

$$D_{nNS} = \begin{pmatrix} n \\ N/2+S \end{pmatrix} \begin{pmatrix} n \\ N/2-S \end{pmatrix}. \tag{35}$$

Table 4 shows the dimension of the full CI space (neglecting spatial symmetry) in determinants and in CSFs for closed-shell systems. Current full CI algorithms are typically limited to several million determinants. Although there have been reports of larger calculations (including more than a billion determinants[83,84]), the computational expense is currently too great for routine calculations of this size.

2.4.2 Multireference Configuration Interaction

A full CI wavefunction is invariant to orbital rotations and even to the choice of the reference function. By contrast, the simple CISD method is quite sensitive to the choice of reference and orbitals. This explains the poor performance of CISD when the bonds are stretched in H_2O (cf. Table 2): the SCF wavefunction becomes an inadequate reference at stretched geometries, and CISD is unable to overcome this inadequacy. Such difficulties can occur even at equilibrium geometries if multiple low-lying electronic states are present. For

example, the zeroth-order wavefunction for a singlet diradical often requires two electron configurations: one doubly occupies the MO formed from in-phase radical orbitals, while the other doubly occupies the out-of-phase MO. Another example is the $\tilde{c}$ state of CH_2, which also requires a two-configuration treatment: the two configurations correspond to the two choices for the lone pair of electrons, either in the molecular plane or perpendicular to it.[85,86] More than two configurations can be critical for transition metals or when multiple bonds are broken.

If a CISD procedure includes all the important N-electron functions from the zeroth-order wavefunction (the "references") and also the single and double substitutions for *each* of these references, then the resulting method is referred to as multireference (MR) CISD. The MR-CISD wavefunction may be written

$$|\Phi_{MRCI}\rangle = \sum_R c(R)|\Phi(R)\rangle + \sum_R \sum_{ix} c_i^x(R)|\Phi_i^x(R)\rangle + \sum_R \sum_{ijxy} c_{ij}^{xy}(R)|\Phi_{ij}^{xy}(R)\rangle, \tag{36}$$

where R denotes a reference function, and i, j (x, y) run over orbitals which are occupied (unoccupied) for a given R. Clearly, a determinant or CSF which is generated as a single or double substitution from one reference state might also be generated as a single or double from a different reference; only unique N-electron functions are included in the MR-CISD procedure. If a sufficient number of references are included, then a MR-CISD can provide results nearly as good as the full CI[14,15,87] at a dramatically reduced computational expense. In the MR-CI method, the set of orbitals which are occupied in any of the references constitutes the *internal space*, and all other orbitals are in the *external space*. Sometimes a further distinction is made among the internal space orbitals: those whose occupancy is constant for all references are called *inactive* (even though their electrons may be excited in the final wavefunction), and the rest are called *active*. In the direct CI method[88] (see section 4), it is more convenient to rewrite (36) in an equivalent form which emphasizes the number of external orbitals:

$$|\Phi_{MRCI}\rangle = \sum_I c_I|\Phi_I\rangle + \sum_S \sum_a c_S^a|\Phi_S^a\rangle + \sum_P \sum_{ab} c_P^{ab}|\Phi_P^{ab}\rangle, \tag{37}$$

where a and b are external orbitals, and I, S, and P denote internal states (including spin coupling) with N, $N-1$, and $N-2$ electrons, respectively.

One very straightforward, *a priori* selection scheme is to make references of all those N-electron functions which can be obtained by distributing electrons in all possible ways in a subset of the most important orbitals (the "active space"). This results in the second-order CI (SOCI),[13] which is known[16,17,89] to provide high-quality potential energy surfaces nearly parallel to those from a full CI. Unfortunately, this prescription typically produces too many references

and the final CI space is too large to be computationally tractable. One strategy which has received relatively little attention[17,46,90] is to approximate a SOCI by restricting the references according to their excitation level. It is often reasonable to assume that the most important references are single and double substitutions from a dominant single reference.[16,17,91] Making this restriction leads to a MR-CISD which includes those triples and quadruples which have no more than two electrons outside the active space. This wavefunction has been designated CISD[TQ] to emphasize the variational treatment of limited triples and quadruples, and it has been shown to closely match SOCI when a single reference configuration dominates.[16,17] Although the CISD[TQ] expansion is much smaller than SOCI, it remains intractable for systems with more than two or three heavy atoms. Further strategies to reduce the cost of a CISD[TQ] are discussed later.

A much more common procedure for reference selection is to accept references whose estimated importance is greater than some given threshold; this can involve perturbative estimates of a function's energetic contribution or its coefficient in some preliminary wavefunction. These approaches are more successful at obtaining the best wavefunction at the lowest expense, but they sacrifice the simplicity of the excitation class selection and can become more difficult to implement and to use. One complication is that potential energy surfaces determined using such methods may not be smooth; to alleviate this, one may need to determine the important references at each geometry and use the union of these sets at every point.

Discarding some of the single and double excitations is another way to reduce the CI space. As with reference selection, the most common approaches involve estimates of a function's energetic contribution or coefficient. The CIPSI method of Malrieu and co-workers selects determinants based on perturbation theory estimates of their coefficients in the first-order wavefunction.[92,93] Alternatively, Buenker and Peyerimhoff[10] select spatial orbital configurations on the basis of each configuration's energetic contribution to a small CI consisting only of the references and the CSFs formed from that configuration. Obviously this involves solving a very large number of small CI problems. Alternatively, one can estimate the importance of all configurations simultaneously via a procedure such as Gershgorn and Shavitt's B_k method.[94,95] Shavitt's 1977 review article[57] surveys these and related alternatives.

Finally, Siegbahn has suggested two procedures for reducing the number of variational parameters in a MR-CISD wavefunction. The first method, *externally contracted* MR-CISD,[88] expresses eq. (37) as

$$|\Phi_{EC-MRCI}\rangle = \sum_I c_I|\Phi_I\rangle + \sum_S c_S \sum_a \tilde{c}_S^a|\Phi_S^a\rangle + \sum_P c_P \sum_{ab} \tilde{c}_P^{ab}|\Phi_P^{ab}\rangle$$

$$= \sum_I c_I|\Phi_I\rangle + \sum_S c_S|\Phi_S\rangle + \sum_P c_P|\Phi_P\rangle, \tag{38}$$

where the external contraction coefficients $\tilde{c}_S^a$ and $\tilde{c}_P^{ab}$ are determined perturbatively and the coefficients c_I, c_S, and c_P are determined variationally; hence, this is a type of variational perturbation theory.[96-98] Note that the total number of variational coefficients is now drastically reduced compared to eq. (37). Siegbahn states[58] that the error in the correlation energy due to external contraction is roughly 1-3%.

An alternative contraction scheme which has received more attention is *internally contracted* multireference CISD (usually denoted simply CMRCI), which was first discussed by Meyer[99] and Siegbahn.[100] This method applies the single and double excitation operators to a single multiconfigurational reference wavefunction *as a whole*, including the reference coefficients. Thus, if the reference wavefunction is

$$|\Phi_0\rangle = \sum_R c_R|\Phi_R\rangle, \tag{39}$$

then there are at least three other classes of expansion functions—singly external, semi-internal, and doubly-external:[58]

$$|\Phi_i^a\rangle = \hat{E}_{ai}|\Phi_0\rangle = \sum_S d_S|\Phi_S^a\rangle \tag{40}$$

$$|\Phi_{ij}^{ak}\rangle = \hat{E}_{ai}\hat{E}_{kj}|\Phi_0\rangle = \sum_S d_S|\Phi_S^a\rangle \tag{41}$$

$$|\Phi_{ijp}^{ab}\rangle = (\hat{E}_{ai}\hat{E}_{bj} + p\hat{E}_{aj}\hat{E}_{bi})|\Phi_0\rangle = \sum_P d_P|\Phi_P^{ab}\rangle, \tag{42}$$

where p is +1 (-1) for singlet (triplet) coupling of a and b. The coefficients d are not variational parameters, but fixed linear combinations of the reference coefficients c_R. The final wavefunction is then

$$|\Phi_{IC-MRCI}\rangle = c_0|\Phi_0\rangle + \sum_{ia} c_i^a|\Phi_i^a\rangle + \sum_{ijka} c_{ij}^{ak}|\Phi_{ij}^{ak}\rangle + \sum_{ijpab} c_{ijp}^{ab}|\Phi_{ijp}^{ab}\rangle. \tag{43}$$

Once again, the contraction has dramatically reduced the number of variational parameters. One difficulty with the internally contracted multireference CI method is that the relevant coupling coefficients become considerably more difficult to calculate. Werner and Knowles[101] alleviate this problem by leaving internal and singly-external configurations uncontracted, i.e.,

$$|\Phi_{IC-MRCI}\rangle = \sum_I c_I|\Phi_I\rangle + \sum_{Sa} c_S^a|\Phi_S^a\rangle + \sum_{ijpab} c_{ijp}^{ab}|\Phi_{ijp}^{ab}\rangle. \tag{44}$$

The remaining coupling coefficients still require elements of the third and fourth order reduced density matrices, which can now be evaluated each time

they are required due to advances by Werner and Knowles.[54,102] The contraction error in the internally contracted MR-CISD method is generally only 0.1-0.2%.[58]

2.4.3 Other CI Selection Schemes

In 1988, Olsen and co-workers[46] presented the restricted active space (RAS) CI, which specifies the CI space in an *a priori* manner reminiscent of the second-order CI (SOCI) and its derivatives. Olsen partitions the orbitals into three subspaces, labeled RAS I, RAS II, and RAS III. Typically, RAS I contains occupied and possibly very important virtual orbitals, RAS II contains the most important virtuals, and RAS III contains the less important virtuals. The CI space includes all determinants with a minimum of p electrons in RAS I and a maximum of q electrons in RAS III. There is no restriction on RAS II, which is akin to the complete active space. Using this simple procedure, it is possible to formulate any CI space truncated according to excitation level (e.g., CISD, CISDT, etc.) as well as excitation class selected MR-CI spaces, such as SOCI and CISD[TQ]. The RAS CI method is discussed more fully in section 4.8.

There are of course many other possible ways to select the CI space. For example, it is possible to generalize the RAS scheme to allow for more flexible CI spaces; work along these lines is presented later. In contrast, it is also possible to make the CI selection process essentially random. A recent paper by Greer discusses the unusual strategy of selecting CSFs using a Monte Carlo algorithm.[103]

2.4.4 The First-Order Interacting Space

Another way of limiting the size of the CI space is to include only those N-electron functions which contribute to the first-order wavefunction in Rayleigh-Schrödinger perturbation theory. This is the motivation behind the *interacting space* classification: the zeroth-order interacting space consists of the set of references, and the first order interacting space includes all those N-electron functions which have a nonzero Hamiltonian matrix element with some member of the zeroth-order interacting space.[104–106] Similarly, it is possible to define n-th order interacting spaces as those functions having nonzero Hamiltonian matrix elements with some member of the $(n-1)$th order interacting space.[106] Various methods for obtaining the first-order interacting space have been presented by Bunge,[104] Schaefer and co-workers,[43,105] and McLean and Liu.[106]

The first-order interacting space restriction is generally used to reduce the number of double substitutions included in single- or multi-reference CISD

wavefunctions. Although single substitutions from a Hartree-Fock reference determinant may be noninteracting due to Brillouin's theorem, they are often included nevertheless because of their strong interaction with the doubles and their importance in describing one-electron properties. For closed shell systems, the first-order interacting space criterion is inconsequential because Slater's rules dictate that all double substitutions are interacting. However, for open-shell systems there can be CSFs whose *spatial* orbital configuration differs from the reference by two electrons but which are noninteracting because of their spin coupling. In a basis of Slater determinants, one can enforce the first-order interacting space restriction simply by ensuring that all determinants differ from the reference by at most two *spin orbitals*. Aside from being more compact, wavefunctions limited to the first-order interacting space can exhibit certain orbital invariance properties.[107]

2.4.5 Computational Scaling

Depending on the relative sizes of the number of electrons, the number of orbitals, and the excitation level, one can derive several different simple estimates of the computational cost of a configuration interaction procedure. Obviously that cost relates to the number of N-electron functions in the linear expansion of the wavefunction, and the size of the CI space for various methods has already been discussed in section 2.4.1.

For present purposes, it is sufficient to work with spin orbitals. Typically, the dimension of the CI space is dominated by determinants with the highest excitation level, m. Thus

$$N_{det} \sim \left(\begin{array}{c} N \\ m \end{array} \right) \left(\begin{array}{c} n_v \\ m \end{array} \right) \sim \frac{1}{(m!)^2} N^m n_v^m, \tag{45}$$

with n_v spin orbitals unoccupied in the reference. Most CI procedures solve only for the lowest or lowest few eigenvectors, via an iterative procedure (cf. section 3.2). In such situations, the scaling is much less than the $\mathcal{O}(N_{det}^3)$ typical of standard matrix diagonalization methods. The most expensive step in iterative procedures such as the Davidson method[108] is the construction of the so-called σ vectors,

$$\sigma_i = \mathbf{H}\mathbf{b}_i, \tag{46}$$

where $\mathbf{b}_i$ belongs to a set of trial vectors which is expanded each iteration until convergence is reached. If the Hamiltonian matrix $\mathbf{H}$ were formed directly, this procedure would require $\mathcal{O}(N_{det}^2)$ operations. This is never actually done because the storage requirements would be too great, and such an approach ignores the fact that the Hamiltonian contains only two-body terms, so that the majority of the matrix elements are zero.

Each element of a trial vector $\mathbf{b}_i$ need only be multiplied by the nonzero elements of $\mathbf{H}$. The Hamiltonian will connect a maximally excited determinant with other maximally excited determinants and with other determinants having excitation level $m \geq m' \geq m-2$. The number of interacting determinants is roughly

$$\begin{pmatrix} m \\ 2 \end{pmatrix} \begin{pmatrix} n_v + m \\ 2 \end{pmatrix} + \begin{pmatrix} m \\ 2 \end{pmatrix} \begin{pmatrix} N-m \\ 2 \end{pmatrix} + m^2 n_v (N-m), \tag{47}$$

which we further approximate as

$$\frac{1}{4} m^2 (n_v + m)^2 + \frac{1}{4} m^2 (N-m)^2 + m^2 n_v (N-m). \tag{48}$$

Each element in $\mathbf{b}_i$ must be multiplied by the relevant nonzero matrix elements, leading to an overall operation count on the order of

$$\mathcal{O}(N^m n_v^m \left\{ m^2 n_v^2 + m^2 N^2 + m^2 N n_v \right\}). \tag{49}$$

Except for full CI, we typically expect $N, n_v >> m$. Furthermore, we almost always have $n_v > N$, so that the leading term becomes

$$\mathcal{O}(N^m n_v^{2+m}). \tag{50}$$

Thus the number of operations for a CISD procedure has a sixth power dependence on the total number of orbitals, while CISDTQ scales as the tenth power. For a given system, the number of occupied orbitals is fixed, and the cost of increasing the basis set size scales as $\mathcal{O}(n_v^{2+m})$; for CISD and CISDTQ, this scaling becomes $\mathcal{O}(n_v^4)$ and $\mathcal{O}(n_v^6)$, respectively.

The scaling of a multireference CI procedure can be estimated by multiplying the single-reference scaling by the number of references. The scaling of the CISD[TQ] method, for example, is roughly $\mathcal{O}(N^4 n_v^4)$, since the number of references is roughly N^2 if the active space is small relative to the external orbital space. For very high levels of excitation, including full CI, the number of interacting matrix elements for a given determinant becomes approximately $N^2 n^2$, so that the computational cost becomes roughly

$$\mathcal{O}^{FCI}(N_{det} N^2 n^2), \tag{51}$$

where we have replaced the term $N^m n_v^m$ with the actual number of determinants, N_{det}. For comparison, for n spatial orbitals the determinant full CI algorithm of Knowles and Handy[109] scales as $\mathcal{O}(N_{det} n^4)$, while the algorithm of Olsen *et al.*[46] and similar approaches scale as $\mathcal{O}(N_{det} N^2 (n - N/2)^2)$ for a closed-shell system. Although the exponents appearing in (51) are smaller than those in (50), it is important to remember that N_{det} contains a factorial dependence on N and n (see section 2.4.1); hence, a full CI procedure is extremely demanding computationally.

2.4.6 Size Extensivity Corrections

If we truncate the CI (either in the one-electron or N-electron space), we no longer have an exact theory. Of course either of these truncations will introduce an error in the wavefunction, which will cause errors in the energy and all other properties. One particularly unwelcome result of truncating the N-electron basis is that CI energies are no longer size extensive or size consistent.

These two terms—size extensive and size consistent—are used somewhat loosely in the literature. Of the two, size extensivity is the most well-defined. A method is said to be size extensive if the energy calculated thereby scales linearly with the number of particles N; the word "extensive" is used in the same sense as in thermodynamics. A method is called size consistent if it gives an energy $E_A + E_B$ for two well separated subsystems A and B. While the definition of size extensivity applies at any geometry, the concept of size consistency applies only in the limiting case of infinite separation. In addition, size consistency *usually* also implies correct dissociation into fragments; this is the source of much of the confusion arising from this term. Thus restricted Hartree-Fock (RHF) is size extensive, but it is not necessarily size consistent, since it cannot properly describe dissociation into open-shell fragments. It can be shown that many-body perturbation theory (MBPT) and coupled-cluster (CC) methods are size extensive, but they will be size consistent only if they are based on reference wavefunction which dissociates properly.

As previously stated, truncated CI's are neither size extensive nor size consistent. A simple (and often used) example makes this clear. Consider two noninteracting hydrogen molecules. If the CISD method is used, then the energy of the two molecules at large separation will not be the same as the sum of their energies when calculated separately. For this to be the case, one would have to include *quadruple* excitations in the supermolecule calculation, since local double excitations could happen simultaneously on A and B.

Clearly the fraction of the correlation energy recovered by a truncated CI will diminish as the size of the system increases, making it a progressively less accurate method. There have been many attempts to correct the CI energy to make it size extensive. The most widely-used (and simplest) of these methods is referred to as the Davidson correction,[110,111] which is

$$\Delta E_{DC} = (1 - c_0^2)(E_{CISD} - E_{SCF}). \tag{52}$$

This correction approximately accounts for the effects of "unlinked quadruple" excitations (i.e. simultaneous pairs of double excitations), and there are many similar expressions in use. For instance, the "renormalized" Davidson correction[112] is

$$\Delta E_{RDC} = \frac{1 - c_0^2}{c_0^2}(E_{CISD} - E_{SCF}). \tag{53}$$

Note that, when $c_0^2 \approx 1$, the two versions are nearly equivalent. A number of other variations exist,[113,114] some of which force the correction to vanish for two-electron systems.

A multireference version of Davidson's correction is given by[115]

$$\Delta E_{MR-DC} = \left(1 - \sum_{i \in \text{Ref}} |c_i|^2\right)(E_{MRCI} - E_{MR}), \tag{54}$$

where E_{MRCI} is the multireference CI energy and E_{MR} is the energy obtained from a CI in the space spanned by the references. We have simply replaced the CISD correlation energy in eq. (52) with the analogous multireference correlation energy, and we have replaced c_0^2 with the analogous sum of squares of all the reference coefficients. If the sum of the squares of reference coefficients is not near unity, better results may be obtained by using the renormalized version of this equation:

$$\Delta E_{MR-RDC} = \frac{1 - \sum_{i \in \text{Ref}} |c_i|^2}{\sum_{i \in \text{Ref}} |c_i|^2}(E_{MRCI} - E_{MR}). \tag{55}$$

It should be noted, however, that for a fixed system size, increasing the number of references decreases size extensivity errors. Indeed, for very highly correlated MR-CI wavefunctions, applying corrections such as (54) and (55) can sometimes lead to less reliable results.

There are a number of other *a posteriori* size extensivity corrections, most of which are computationally trivial once the wavefunction has been obtained. Duch[114] compares several of the more common corrections. Of course it is also possible to allow coupling between the wavefunction and the size extensivity correction. This leads to such methods as the coupled electron pair approximation (CEPA),[116] and the coupled pair functional (CPF) approaches.[117] This is also the motivation behind the quadratic configuration interaction method of Pople, Head-Gordon, and Raghavachari.[118] These authors determine the correlation energy and CI coefficients for quadratic CI with singles and doubles (QCISD) by the following set of projection equations, in spin-orbital notation:

$$\langle \Phi_0 | \hat{H} | \hat{C}_2 \Phi_0 \rangle = E_{corr} \tag{56}$$

$$\langle \Phi_i^a | \hat{H} - E_{scf} | (\hat{C}_1 + \hat{C}_2 + \hat{C}_1 \hat{C}_2) \Phi_0 \rangle = c_i^a E_{corr} \tag{57}$$

$$\langle \Phi_{ij}^{ab} | \hat{H} - E_{scf} | (1 + \hat{C}_1 + \hat{C}_2 + \frac{1}{2}\hat{C}_2^2) \Phi_0 \rangle = c_{ij}^{ab} E_{corr}, \tag{58}$$

where intermediate normalization ($\langle \Phi_0 | \Phi \rangle = 1$) has been employed, the Brillouin condition has been assumed ($\langle \Phi_i^a | \hat{H} | \Phi_0 \rangle = 0$), and $\hat{C}_1$ and $\hat{C}_2$ are the

standard single and double substitution operators,

$$\hat{C}_1 = \sum_{ia} c_i^a a_a^\dagger a_i \tag{59}$$

$$\hat{C}_2 = \frac{1}{4} \sum_{ijab} c_{ij}^{ab} a_a^\dagger a_b^\dagger a_j a_i. \tag{60}$$

The QCISD projection equations differ from the equivalent CISD equations only in the addition of the quadratic terms $\hat{C}_1\hat{C}_2$ and $\frac{1}{2}\hat{C}_2^2$, which lead to size-extensive energies. Alternatively, the QCISD equations may be considered an approximation to CCSD in which certain terms have been neglected. Pople and co-workers show how to extend this approach to include triples fully (QCISDT) or perturbatively [QCISD(T)].[118]

A multireference method building approximate size extensivity into the wavefunction is the Averaged Coupled Pair Functional (ACPF) method of Gdanitz and Ahlrichs,[119] which introduces an electron number dependence into the denominator of the MR-CISD energy functional. A similar method has been presented by Szalay and Bartlett under the name multireference averaged quadratic coupled-cluster (MR-AQCC).[120,121] Also noteworthy is the work of Malrieu and co-workers, who have presented a state-specific self-consistent dressing of the MR-CISD Hamiltonian matrix which gives size extensive results.[122–124]

2.4.7 The Frozen Core Approximation

It is quite common in correlated methods (including many-body perturbation theory, coupled-cluster, etc., as well as configuration interaction) to invoke the frozen core approximation, whereby the lowest-lying molecular orbitals, occupied by the inner-shell electrons, are constrained to remain doubly-occupied in all configurations. The frozen core for atoms lithium to neon typically consists of the 1s atomic orbital, while that for atoms sodium to argon consists of the atomic orbitals 1s, 2s, $2p_x$, $2p_y$ and $2p_z$. The frozen molecular orbitals are those made primarily from these inner-shell atomic orbitals.

A justification for this approximation is that the inner-shell electrons of an atom are less sensitive to their environment than the valence electrons. Thus the error introduced by freezing the core orbitals is nearly constant for molecules containing the same types of atoms. In fact, it is often preferable to employ the frozen core approximation as a general rule because most of the basis sets commonly used in *ab initio* quantum chemistry do not provide sufficient flexibility in the core region to accurately describe the correlation of the core electrons. Recently, Woon and Dunning have attempted to alleviate this problem by publishing correlation consistent core-valence basis sets.[125]

Not only does the frozen core approximation reduce the number of configurations, but it also reduces the computational effort required to evaluate matrix elements between the configurations which remain. Assuming that all frozen core orbitals are doubly occupied and orthogonal to all other molecular orbitals, it can be shown[126] that

$$\langle \Phi_I | \hat{H} | \Phi_J \rangle = \langle \bar{\Phi}_I | \hat{H}_0 | \bar{\Phi}_J \rangle, \tag{61}$$

where $\bar{\Phi}_I$ and $\bar{\Phi}_J$ are identical to Φ_I and Φ_J, respectively, except that the core orbitals have been deleted from $\bar{\Phi}_I$ and $\bar{\Phi}_J$, and $\hat{H}$ has been replaced by $\hat{H}_0$ defined by

$$\hat{H}_0 = E_c + \sum_{i=1}^{N-N_c} \hat{h}_c(i) + \sum_{i>j}^{N-N_c} \frac{1}{r_{ij}}, \tag{62}$$

where N is the number of electrons and N_c is the number of core electrons. E_c is the so-called "frozen-core energy," which is the expectation value of the determinant formed from only the N_c core electrons doubly occupying the $n_c = N_c/2$ core orbitals

$$E_c = 2\sum_{i}^{n_c} h_{ii} + \sum_{ij}^{n_c} \{2(ii|jj) - (ij|ji)\}. \tag{63}$$

Finally, $\hat{h}_c(i)$ is the one-electron Hamiltonian operator for electron i in the average field produced by the N_c core electrons,

$$\hat{h}_c(i) = \hat{h}(i) + \sum_{j=1}^{n_c} \left\{ 2\hat{J}_j(i) - \hat{K}_j(i) \right\}, \tag{64}$$

with $\hat{J}_j(i)$ and $\hat{K}_j(i)$ representing the standard Coulomb and exchange operators, respectively. Note that, although we have written the frozen core energy E_c and frozen core operator $\hat{h}_c$ in terms of molecular orbitals, it is not necessary to explicitly transform the one- and two-electron integrals involving core orbitals. Assuming real orbitals, we can define a frozen core density matrix[127] in atomic (or symmetry adapted) orbitals as

$$P^c_{\rho\sigma} = \sum_{i}^{n_c} C^i_\rho C^i_\sigma, \tag{65}$$

where C^i_ρ is the contribution of atomic orbital ρ to molecular orbital i. Now the frozen core operator in atomic orbitals becomes

$$h^c_{\mu\nu} = h_{\mu\nu} + 2\sum_{\rho\sigma}(\rho\sigma|\mu\nu)P^c_{\rho\sigma} - \sum_{\rho\sigma}(\rho\mu|\nu\sigma)P^c_{\rho\sigma}, \tag{66}$$

and the frozen core operator in molecular orbitals h^c_{ij} can be obtained simply by transforming $h^c_{\mu\nu}$. Similarly the frozen core energy can be evaluated as

$$\begin{aligned} E_c &= \sum_{\mu\nu} P^c_{\mu\nu} \left(h_{\mu\nu} + h^c_{\mu\nu} \right) \\ &= Tr(P^c h) + Tr(P^c h^c). \end{aligned} \tag{67}$$

An analogous approximation is the *deleted virtual* approximation, whereby a few of the highest-lying virtual (unoccupied) molecular orbitals are constrained to remain unoccupied in all configurations. Since these orbitals can never be occupied, they can be removed from the CI procedure entirely. The rationalization for this procedure is that it is unlikely that electrons will choose to partially populate high-energy orbitals in their attempt to avoid other electrons. However, this conclusion is generally true only for very high-lying virtual orbitals (such as those formed by antisymmetric combinations of core orbitals for a given atom). For all other virtual orbitals, such simplistic reasoning is insufficient. Indeed, Davidson points out that those high energy SCF virtual orbitals which result from the antisymmetric combination of the two basis functions describing each valence atomic orbital in a double-ζ basis set (such as the 3p-like orbital formed from the minus combination of the larger and smaller 2p atomic orbitals on oxygen) often make the largest contribution to the correlation energy in Møller-Plesset (MPn) wavefunctions.[128]

2.5 Choice of Orbitals

The results of any configuration interaction procedure depend on the choice of the atomic orbital (AO) basis. However, for a fixed AO basis, certain choices of molecular orbitals give equivalent CI wavefunctions. CI wavefunctions which are based on a single closed-shell reference and are truncated at a given excitation level are invariant to nonsingular linear transformations which mix doubly occupied orbitals with each other or unoccupied orbitals with each other. The invariance properties of CI wavefunctions based on open-shell references are more complicated, and the energy is generally not invariant to the rotation of open-shell orbitals unless certain extra references are added or the spin couplings are restricted to the first-order interacting space.[107] A full CI is invariant to all nonsingular linear transformations among the orbitals, even those that mix occupied and unoccupied orbitals; hence, the choice of the "reference" is irrelevant for a full CI procedure.

Some of the more elaborate CI spaces also exhibit invariance properties. Shavitt has defined the *full class CI* as one which partitions the orbitals into an arbitrary number of orthogonal subsets and includes all or none of the

N-electron functions which have a given partitioning of electrons among the subspaces.[57] The RAS CI wavefunctions are of this type, as are the RAS formulations of SOCI and CISD[TQ]. Such CI wavefunctions are invariant to separate, nonsingular linear transformations within any of the orbital subspaces. This property is relevant to the formulation of analytic gradients.[129]

For bond breaking processes, the restricted Hartree-Fock approximation will not yield a good reference. This can be remedied by employing a generalized valence bond (GVB)[130] reference or an unrestricted Hartree-Fock reference. However, the latter entails spin contamination in the CI wavefunction by states of higher spin multiplicity. Another alternative is to use a multiconfigurational (MC)[53] or complete-active-space (CAS) SCF[55,131] reference, which can be constructed to behave properly at all locations on the potential energy surface.

For multireference CI's such as SOCI and CISD[TQ], or any RAS CI which uses the RAS II orbital subspace, it is important that the orbitals of the active space be good correlating orbitals (i.e., they should be localized in the same region of space as the occupied orbitals). This is equally important for selected CI procedures, in that the number of configurations needed to achieve a given accuracy will be reduced. This localization criterion is not generally satisfied by canonical SCF virtual orbitals, whose construction is not physically motivated because they are based on an N-electron potential rather than an $(N-1)$ electron potential. One possible solution is to determine the virtual orbitals using a different (and more suitable) effective Hamiltonian than that used for the occupied orbitals, and to orthogonalize the resulting orbitals against the occupied orbitals. This is the procedure in the improved virtual orbital (IVO) method of Hunt and Goddard.[132] IVO's look like excited state orbitals and are more contracted than canonical SCF orbitals. Nevertheless, they remain somewhat too diffuse for making the CI expansion as small as possible. A related and improved method is the modified virtual orbital (MVO) approach of Bauschlicher,[133] who obtains virtual orbitals by diagonalizing the virtual subspace of a Fock matrix constructed for the core electrons only (eq. 64). Another possibility for obtaining compact virtual orbitals is Davidson's K-orbital approach.[134]

More commonly, good correlating orbitals are obtained with the MCSCF[53] or CASSCF[55] methods. Yet another possibility are the natural orbitals from a CISD wavefunction. Natural orbitals (NOs)[77,135] are defined as the eigenfunctions of the one-particle density matrix; the eigenvalues are called the occupation numbers of the NOs. One drawback of NOs is that the Hamiltonian is no longer diagonally-dominant,[136] and this can decrease the efficiency of iterative diagonalization methods (section 3.2).

Grev and Schaefer have shown for a number of small molecules that the

SOCI method performs just as well when based on CISD NOs as when based on CASSCF orbitals.[16] Furthermore, they demonstrated that this is not merely due to the highly accurate treatment of correlation in the SOCI method, because a SOCI wavefunction based on canonical SCF orbitals performs notably worse. One advantage of CISD natural orbitals is that they can be easier to compute than CASSCF orbitals. Another is that their importance to the CI wavefunction falls off very rapidly with occupation number. This means that one can delete several of the most weakly-occupied NOs from the MR-CISD procedure with little loss in the correlation energy recovered; such considerations do not necessarily hold for high-lying MCSCF or CASSCF orbitals. Additionally, Parisel and Ellinger have investigated the use of CI natural orbitals in variation-perturbation methods which employ a CI wavefunction as the zeroth-order solution in a subsequent second-order perturbation treatment,[137] and Blomberg and Liu have considered the use of CI natural orbitals in SOCI transition moment calculations.[138] Balasubramanian uses SOCI natural orbitals in his relativistic CI procedure.[139]

Finally, it has long been recognized that spatially localized orbitals should allow an efficient truncation of the CI space (see, for example, the PCILO method of Malrieu and co-workers[140,141]). SCF orbitals can be localized according to the Boys procedure[142] or various other methods. In most cases, the savings realized should outweigh any extra effort due to the loss of point-group symmetry. In the 1980s, Saebø and Pulay developed various localized correlation methods (including CISD) which can achieve computational savings in two distinct ways: first, the pair correlation energy for distant pairs can be neglected (or estimated), and second, the set of virtual orbitals used as correlating orbitals can be restricted to the atomic orbitals in the vicinity of the orbital to be correlated (with components of occupied orbitals projected out).[143,144] Since standard CISD scales as the sixth power of the system size, some type of localized correlation treatment is inevitable as quantum chemists seek to apply correlated methods to large molecules.

2.6 Excited Electronic States

Here we will briefly discuss configuration interaction descriptions of excited electronic states. As previously mentioned, excited states are described by higher-energy eigenvectors of the Hamiltonian. However, since one can apply spin and spatial symmetry restrictions to the N-electron basis functions, solving for excited states which are energetically the lowest of a given symmetry species proceeds just as for the ground state. In this way, one can use orbitals which are optimal for each state.

Much more challenging is the case when several states of the same symme-

try species are required. Here, all but the lowest state are described by higher roots of the CI secular equations. Better zeroth-order descriptions are obtained if molecular orbitals are optimized separately for each state. However, this means that the resulting CI wavefunctions are interacting and nonorthogonal (complicating, for example, the evaluation of transition moments). The states can be made noninteracting and orthogonal by carrying out a non-orthogonal CI procedure,[77,145–148] which requires the matrix **S** of overlaps between N-electron functions and a more complex procedure for evaluating matrix elements of the Hamiltonian (the Slater-Condon rules no longer apply because they assume a single set of orthonormal orbitals). Using orbitals optimized separately for each excited state should allow one to use smaller CI expansions to achieve a given level of accuracy.[145,149]

However, optimizing excited state orbitals can be difficult because variational optimization always finds the lowest solution of a given symmetry species; this problem is generally called "variational collapse".[150] One solution is to first obtain the SCF ground state solution, and then obtain the first excited state solution by requiring it to remain orthogonal to the ground state;[151] this process could in principle be repeated for higher-lying excited states. Another solution is to optimize the orbitals by following a higher root of the MCSCF secular equations. An early application of this idea was presented by Bauschlicher and Yarkony,[85] who optimized orbitals for the $2\ ^1A_1$ state of methylene by following the second root in a two-configuration SCF procedure. A correlated treatment of this state was obtained by solving for the second root of a two-reference CISD. This same procedure, in conjunction with more highly correlated CI methods, was recently used to re-examine the $2\ ^1A_1$ state of methylene.[86] In 1987, Allen and Schaefer presented analytic gradients for this type of TCSCF-CI procedure and used them to study the $2\ ^1A_1$ state of formaldehyde and ketene.[150,152]

Unfortunately, the MCSCF optimization generally worsens the description of the ground state while it improves the description of the excited state. Frequently it happens that the energetic ordering of the two states will become swapped, in a process called "root flipping," and further optimization will yield orbitals describing the ground state.[53] One way around these difficulties is to use a single set of orbitals for all the states of a given symmetry. The improved virtual orbitals (IVO) and modified virtual orbital (MVO) methods described in the preceding section may be useful in this respect. A more typical approach is to modify the MCSCF method to yield a set of compromise orbitals; these can be obtained by the "state-averaged" procedure, which optimizes an averaged MCSCF energy obtained from averaged one- and two-electron reduced density matrices.[54] A related possibility is to use averaged natural orbitals (NOs).[153] Finally, one might simply use ground state orbitals

in conjunction with a CI method including a sufficiently complete treatment of electron correlation that the choice of orbitals becomes less important.

The most commonly used CI procedure, CISD based on the ground state configuration and using SCF orbitals, yields excitation energies which are substantially too large. One reason for this is that the ground state is correlated by all singles and double substitutions, whereas singly excited states are correlated only by singles and those doubles that involve replacement of the singly excited electron. Hence, the correlation treatment is imbalanced in favor of the ground state. This has been considered in more detail by Head-Gordon and Lee, who have analyzed the performance of CISD for excited states in the context of perturbation theory for electronic excitation energies; they find that CISD is not even correct through second order.[154] Another problem is that the SCF orbitals themselves bias results towards the ground state.

Alternatively, one might specifically design modified CI methods for excited states; the symmetry-adapted cluster (SAC) CI approach of Nakatsuji is such a method,[32,155,156] although it also contains elements from coupled-cluster theory.[6] Another alternative is the CASPT2 method of Andersson, Malmqvist, Roos, and co-workers,[157-159] which is a second-order perturbation theory based on a CASSCF reference function. Rather than employ more complex CI approaches, Pople, Head-Gordon, and others have advocated the use of configuration interaction with only singles (CIS) as a qualitative excited state theory and as a starting point for more advanced treatments.[154,160] Clearly CIS offers no improvement for the ground state (Brillouin's theorem), but higher roots represent excited states with an accuracy in the excitation energies of around 1 eV (23 kcal mol^{-1}). CIS has the unusual property of being both size extensive and variational; no other truncated CI method is size extensive. Its low computational cost and size extensivity make CIS applicable to large systems. Head-Gordon and co-workers have introduced a perturbative doubles correction for CIS which they denote CIS(D);[161] this method tends to improve excitation energies, but it does not necessarily improve geometries or other properties.[162]

The performance of simple CIS for open-shell systems such as radicals is not as good as for closed-shell systems, regardless of whether an unrestricted Hartree-Fock (UHF) or restricted open-shell Hartree-Fock (ROHF) reference is used.[163] Maurice and Head-Gordon find improved results for these systems by using a spin-pure CI wavefunction, denoted XCIS, which adds to the singles those doubly substituted determinants in which the excited electron has its spin flipped and one of the open-shell electrons is also spin flipped to conserve S_z.[164] It is interesting to note that these limited double substitutions are actually single substitutions from the point of view of spatial orbital configurations; this problem of the non-transferability of the substitution level (or

"excitation level") definition between determinants and CSFs has occasionally been mentioned in the literature.[35,165] Size extensivity is maintained in the XCIS method by uncoupling the SCF solution from the excited states. More flexible approaches which still scale favorably with system size would provide a useful alternative to the more expensive EOM-CCSD[6] and CASPT2[159] methods and are eagerly anticipated.

3 Common Features of Implementations

This section briefly discusses two elements common to all configuration interaction programs: transformation of integrals, and iterative subspace diagonalization of the Hamiltonian.

3.1 Integral Transformation

As discussed in section 2.3, the Hamiltonian matrix elements are generally written in terms of one- and two-electron integrals in the molecular orbital (MO) basis. However, these integrals are originally calculated in the atomic orbital (AO) basis, or perhaps the symmetry-adapted orbital (SO) basis. Therefore it is necessary to transform the AO or SO integrals into the MO basis, according to

$$h_{ij} = \sum_{\mu\nu} C_\mu^i C_\nu^j h_{\mu\nu}, \tag{68}$$

$$(ij|kl) = \sum_{\mu\nu\rho\sigma} C_\mu^i C_\nu^j C_\rho^k C_\sigma^l (\mu\nu|\rho\sigma), \tag{69}$$

where C_μ^i is the coefficient for the contribution of atomic orbital μ to molecular orbital i, and real orbitals have been assumed. Although the coefficients C_μ^i are generally the SCF coefficients, they might instead be the coefficients of the CI natural orbitals in the atomic orbital basis, etc.

3.1.1 One-electron Integrals

The transformation of the one-electron integrals is computationally inexpensive and easily accomplished: without point group symmetry, this transformation can be performed as two half-transformations, each of which requires a multiplication of the one-electron integral matrix by the SCF coefficient matrix, for a total of $2n^3$ multiplications. Spatial symmetry reduces this cost because the one-electron integral and SCF coefficient matrices are block diagonal according to irreducible representation (irrep), and the transformation can be carried out an irrep at a time (cf. Figure 1). Note that it would also be

Figure 1: Transformation of one-electron integrals.

Loop over irreps Γ
$h^{\Gamma}_{\mu j} = \sum_{\nu} C^{\Gamma}_{\nu j} h^{\Gamma}_{\mu\nu}$ (matrix mult)
$h^{\Gamma}_{ij} = \sum_{\mu} C^{\Gamma}_{\mu i} h^{\Gamma}_{\mu j}$ (matrix mult)
end loop over Γ

possible to utilize the permutational symmetry $h_{ij} = h_{ji}$, but this would typically reduce efficiency because the transformation could no longer be written in terms of matrix multiplications, which are very fast on vector supercomputers (e.g., CRAY C90) or pipelined workstations (e.g., IBM RS/6000).[166] Note that if orbitals are frozen in the correlated procedure (cf. section 2.4.7), $h_{\mu\nu}$ is replaced by the frozen core operator $h^{c}_{\mu\nu}$ (eq. 66).

3.1.2 Two-electron Integrals

Transforming the two-electron integrals is considerably more time-consuming. Equation (69) implies that this transformation is an n^4 process for each of n^4 integrals $(ij|kl)$ (or n^8 overall), but of course it can be carried out as four separate quarter-transformations analogous to the two half-transformations required for the one-electron integrals; this strategy requires $4n^5$ multiplications if symmetry is neglected and it constitutes a fairly demanding computational procedure if n is larger than 100 or so. Fortunately, the full transformation is not necessary for the simple CIS method because only MO integrals with two internal and two external indices are relevant. Matrix elements for most other CI wavefunctions are expressed in terms of the full set of MO integrals, but by performing some compensating work, one can avoid the full transformation for CISD,[167,168] internally-contracted MR-CISD,[101,168] and even uncontracted MR-CISD.[169] For the latter, however, Saunders and van Lenthe argue that the extra steps required to avoid the full transformation may cost more than the transformation itself unless the AO integral list exhibits considerable sparsity.[127] In the general case, the full set of integrals is required. Therefore, various methods for employing spatial and permutational symmetry have been proposed to reduce the operation count. In this context, the "permutational symmetry" refers to the eight-fold redundancy in the two-electron integrals for real orbitals.

Wilson[170] provides a very clear and helpful survey of four-index transformation methods published before 1987. More recent work has focused attention on the sparsity of quantities in the AO basis. For example, Häser, Almlöf, and Feyereisen have presented an integral-direct transformation algorithm which

Figure 2: Pre-sorting the two-electron AO integrals in TRANSQT.

Form frozen core density matrix, eq. (65)
Initialize Yoshimine structure for sorting AO two-el ints
Read two-el ints from disk; form frozen core operator, eq. (66)
    and write integrals to Yoshimine buffers
Complete Yoshimine sort, ensuring $p \geq q$, $r \geq s$, but not $pq \geq rs$
Free Yoshimine pre-sort structure
Evaluate frozen core energy, eq. (67)

employs integral pre-screening techniques and can even exploit non-abelian point-group symmetry.[171] However, our attention here is focused on integral transformation routines for highly correlated CI wavefunctions, which typically means that one can consider only small molecules for which there is less benefit in exploiting sparsity in the AO basis. Of the conventional approaches discussed by Wilson, one of the most promising is the Saunders-van Lenthe algorithm,[127] which has an operation count of $\sim 25n^5/24$ (the operation count is somewhat less if the number of transformed orbitals is less than the number of AO's). Saunders and van Lenthe present an explicit algorithm for the case of no spatial symmetry.[127] However, in our experience it is not entirely straightforward to symmetry adapt their algorithm and simultaneously maintain a high degree of vectorization. On the other hand, we find it straightforward to symmetry adapt a simpler series of quarter transformations in which some of the permutational symmetry of the integrals is ignored. This simpler code remains efficient because it calls optimized matrix multiplication subroutines. This new program, TRANSQT, developed by Daniel Crawford, Justin Fermann, and the present authors, runs faster than previous transformation programs produced by this group which take more advantage of permutational symmetries.

The algorithm consists of three major parts: a pre-sort of the two-electron SO integrals, the first half-transform, and the second half-transform (Figures 2–4). To keep track of spatial symmetry, the loops over orbitals are broken up into loops over irreps of the point group and over orbitals within those irreps. The atomic orbitals are numbered consecutively within each irrep, which allows the use of relative indices (denoted by capital letters in the figures) for numbering orbitals with a fixed irrep. Molecular orbitals are also numbered this way until they are written out at the end of the transformation, when they are renumbered according to whatever order is used by subsequent programs. As seen in the figures, all multiplications which give zero by symmetry are

avoided. The use of matrix multiplications means that the algorithm takes only partial advantage of permutational symmetry. The pre-sorted integrals P use the permutational symmetries $(pq|rs) = (qp|rs) = (pq|sr) = (qp|sr)$, but they do not allow the swapping of the first pair of indices with the last pair [e.g., $(pq|rs) = (rs|pq)$]. These same permutational symmetries are employed during multiplication except that if $rsym = ssym$, then the symmetry $(pq|rs) = (pq|sr)$ is not utilized. Similar considerations apply to the second half-transform: the half-transformed integrals J are stored similarly to P, with $(pq|kl) = (pq|lk) = (qp|kl) = (qp|lk)$.

The TRANSQT algorithm employs canonical indices[57] for pairs of orbitals, such as $pq =$`ioff`$[p] + q$. These indices are useful for computing the address of an element in a symmetric matrix which is stored by writing only the lower triangle to a linear array. The array `ioff`$[p]$ contains the address of the first element in row p, and it is assumed that $p \geq q$. If orbital numbering starts from zero, then `ioff`$[0] = 0$ and `ioff`$[p] = p +$ `ioff`$[p$-1]. The memory requirements are for two matrices (A and B) with dimension equal to the number of atomic orbitals, a matrix of SCF coefficients for each irrep, two blocks which hold all two-electron integrals $(pq|rs)$ with a fixed pair of first indices pq, and various buffers associated with Yoshimine sorting. This sorting method, first described by Yoshimine[172] in 1969, is needed to sort the integrals so that they can be read sequentially in the required order. The pre-sort is necessary because the first half-transform requires all $(pq|rs)$ for a given pq, but the integrals are not stored this way in the disk file produced by our integrals program, where they posses the full eight-fold permutational symmetry. For instance, the first half-transform will require integrals such as (11|43), but this integral is only stored as (43|11) on disk. The pre-sort adds the redundant integrals $(kl|ij) = (ij|kl)$ and places them all in the correct order for reading. The second Yoshimine sort involves the half-transformed integrals: these integrals are formed in the order $(pq|kl)$, where pq is fixed. In the second half-transform, however, the program needs to read all $(kl|pq)$ for a *fixed* kl.* Since the integrals were not written in this order, they must be sorted so they can be read this way.

3.2 Iterative Techniques for Solving Hc = *E*c

Standard numerical methods exist for diagonalizing real symmetric matrices such as the Hamiltonian **H**.† However, such methods usually require the stor-

*The convention used here is to write the fixed orbital pair first in the two-electron integral. However, one must exercise caution because the half-transformed integrals do not possess the symmetry $(pq|kl) = (kl|pq)$ since a distinction must be drawn between the AO and MO pairs.

†Once again, real orbitals have been assumed, along with a nonrelativistic Hamiltonian.

Figure 3: First half-transform in TRANSQT.

```
Initialize tmp matrices A and B and buffers Pblock and Jblock
Loop psym over irreps
    Loop p over orbitals in irrep psym
        Loop qsym over irreps w/ qsym ≤ psym
            Loop q over orbitals in irrep qsym w/ q ≤ p
                pq = ioff[p] + q
                Read (pq|rs) for all rs given pq into Pblock
                Loop rsym over irreps
                    Compute ssym from psym, qsym, rsym
                    Loop r over orbitals in irrep rsym (relative idx R)
                        Loop s over orbs in ssym w/ s ≤ r (rel idx S)
                            rs = ioff[r] + s
                            A[R][S] = Pblock[rs]
                            if rsym = ssym, A[S][R] = Pblock[rs]
                        end loop over s
                    end loop over r
                    matrix multiply:
                    loop rel idx R over orbs in rsym
                        loop rel idx L over active orbs in ssym
                            loop rel idx S over orbs in ssym
                                B[R][L] = B[R][L] + A[R][S] * C^ssym[S][L]
                    end loops over S, L, R
                    matrix multiply:
                    loop rel idx K over active orbs in rsym
                        loop rel idx L over active orbs in ssym
                            loop rel idx R over orbs in rsym
                                A[K][L] = A[K][L] + (C^rsym)^T[K][R] * B[R][L]
                    end loops over R, L, K
                    loop k over active orbitals in rsym (rel idx K)
                        loop l over active orbs in ssym (rel idx L), l ≤ k
                            kl = ioff[k] + l
                            Jblock[kl] = A[K][L]
                    end loops over l, k
                    Write Jblock to Yoshimine buffers
                end loop over rsym
            end loop over q
        end loop over qsym
    end loop over p
end loop over psym
flush, close I/O files
free Pblock
Yoshimine sort half-transformed integrals J, free Yoshimine struct
```

Figure 4: Second half-transform in TRANSQT.

Loop $ksym$ over irreps
  Loop k over active orbitals in irrep $ksym$
    Loop $lsym$ over irreps w/ $lsym \leq ksym$
      Loop l over active orbitals in irrep $lsym$ w/ $l \leq k$
      $kl = ioff[k] + l$
      zero $Jblock$
      Read all $(kl|pq)$ for given kl into $Jblock$
      Loop $psym$ over irreps
      Compute $qsym$ from $ksym$, $lsym$, and $psym$
      if $(qsym > psym)$ next $psym$
        Loop $qsym$ over irreps, with $qsym \leq psym$
          Loop p over orbs in $psym$ (rel idx P)
            Loop q over orbs in $qsym$ (rel idx Q)
              $pq = ioff[p] + q$ if $p \geq q$, else $ioff[q] + p$
              $A[P][Q] = Jblock[pq]$
            end loop over q
          end loop over p
            matrix multiply:
            Loop rel idx P over orbs in $psym$
              Loop rel idx J over active orbs in $qsym$
                Loop rel idx Q over orbs in $qsym$
                  $B[P][J] = B[P][J] + A[P][Q] * C^{qsym}[Q][J]$
            End loops over Q, J, P
            matrix multiply:
            Loop rel idx I over active orbs in $psym$
              Loop rel idx J over active orbs in $qsym$
                Loop rel idx P over orbs in $psym$
                  $A[I][J] = A[I][J] + (C^{psym})^T[I][P] * B[P][J]$
            end loops over P, J, I
            Write matrix A to buffer
          End loop over $qsym$
        End loop over $psym$
      End loop over l
    End loop over $lsym$
  End loop over k
End loop over $ksym$
free $Jblock$
flush and close I/O buffers

age of **H** in core memory (if eigenvectors are also computed, then one actually needs memory to store *two* matrices of this size). If the CI includes a mere 10,000 determinants (certainly a small CI space), storing the full matrix **H** would require 800 megabytes. As of 1997, this represents a large amount of core memory (although disk storage would not be a problem). It is little consolation that the symmetry of **H** could be used to cut this requirement approximately in half. Another very important difficulty is the time required to diagonalize matrices this size or larger. Most diagonalization routines scale as $O(n^3)$, which is certainly problematic for $n \geq 10^4$. Only for smaller matrices do the standard methods become practical.

In typical applications, only the ground electronic state or perhaps a few of the low lying excited states are of interest. Hence methods which obtain only the lowest few roots of the CI matrix are greatly preferred over methods which compute the entire spectrum. Furthermore, storage requirements are greatly reduced if **H** is not stored at all; *direct CI* methods, discussed in section 4, form products $\mathbf{Hc} = \sigma$ directly from the MO integrals.

Most techniques for solving large eigenvalue problems fall under the category of *subspace iteration* methods, which iteratively solve the eigenvalue problem in a linear vector subspace spanned by only a few vectors. Malmqvist[173] provides a concise review of the subspace iteration methods most commonly found in quantum chemistry. Here we will outline some of these methods and note recent advances.

3.2.1 Davidson's Method

Davidson's method for the iterative solution of the lowest few eigenvalues and eigenvectors of large real, symmetric matrices[108] is undoubtedly the most widely used technique for solving the CI secular equations. In this method, one applies standard diagonalization methods to a small Hamiltonian matrix formed in a subspace $\{\mathbf{b}_i\}$ of L orthonormal expansion vectors, where L increases from iteration to iteration but is typically very much smaller than the dimension of **H** (the subspace generally includes less than a dozen vectors per root). At each iteration, the Davidson algorithm estimates a correction vector for each root currently under consideration and adds it to the set $\{\mathbf{b}_i\}$ after Schmidt orthogonalization.

Davidson used perturbation theory to argue[108] that the best correction vector δ to the current iteration's guess vector **c** satisfies

$$(\mathbf{H} - \lambda\mathbf{I})\delta = -(\mathbf{H} - \lambda\mathbf{I})\mathbf{c}. \tag{70}$$

In the Davidson method, one approximates λ by the current iteration's eigenvalue, and **H** is assumed to be diagonally dominant so that δ can be approxi-

mated by

$$\delta = -(\mathbf{H}_d - \lambda\mathbf{I})^{-1}(\mathbf{H} - \lambda\mathbf{I})\mathbf{c}, \tag{71}$$

where $\mathbf{H}_d$ is the diagonal of $\mathbf{H}$ and the denominator is referred to as the *preconditioner.*

Liu showed how to extend Davidson's method to solve for several roots simultaneously,[174] leading to what is called the Simultaneous Expansion Method, the Davidson-Liu method, or the block Davidson method. The detailed Davidson-Liu algorithm, adapted from ref. 174, is presented in Figure 5.

At each iteration, the current approximations to the eigenvalues of $\mathbf{H}$ are given by the eigenvalues of the small matrix $\mathbf{G}$, which is the Hamiltonian in the subspace spanned by the expansion vectors $\{\mathbf{b}_i\}$, with matrix elements $G_{ij} = (\mathbf{b}_i, \mathbf{H}\mathbf{b}_j)$. Likewise, the current approximate eigenvectors are linear combinations of the subspace vectors with coefficients given by the eigenvectors α of $\mathbf{G}$:

$$\mathbf{c}^k = \sum_{i=1}^{L} \alpha_i^k \mathbf{b}_i. \tag{76}$$

The convergence of the k-th root can be checked by the sum of squares of the last m components of α^k in step 2 or by the norm of the residue vector $\mathbf{r}$ in step 3.

Unless very tight convergence criteria are specified, it is possible for the Davidson-Liu method to converge on the wrong eigenvector if the initial guess vectors are poor. Although this will not happen for the ground state unless a completely inappropriate guess is provided, it occasionally happens when several roots are sought. Davidson and co-workers recommend initial loose convergence of more roots than are actually needed, and then tighter convergence on the desired roots.[175] Possible choices for the initial vectors include unit vectors (chosen according to the diagonal elements of $\mathbf{H}$ with the largest magnitudes) or eigenvectors of some small block of $\mathbf{H}$.

Equations (73) and (75) show that after a matrix-vector product $\sigma_i = \mathbf{H}\mathbf{c}_i$ is computed it is needed again in subsequent iterations. Since the construction of the vectors $\{\sigma_i\}$ is the most time consuming step in the iterative diagonalization of $\mathbf{H}$, they are stored on disk along with the expansion vectors $\{\mathbf{b}_i\}$. The original Davidson method converges one root at a time and requires storage for two (segments of) vectors at once in core memory. If more core memory is available, then the Davidson-Liu method can reduce computational and I/O requirements. For example, one pass through the subspace expansion vectors is sufficient to construct several correction vectors δ simultaneously. Likewise, a single construction of the matrix elements of $\mathbf{H}$, several σ vectors can be formed simultaneously.

Note that the preconditioner in eq. (74) requires the diagonal elements of

Figure 5: The Davidson-Liu Iterative Method for the Lowest Few Eigenvectors and Eigenvalues of Real, Symmetric Matrices (Ref. 174)

1. Select a set of L orthonormal guess vectors, at least one for each root desired, and place in the set $\{\mathbf{b}_i\}$.

2. Use a standard diagonalization method to solve the $L \times L$ eigenvalue problem
$$\mathbf{G}\alpha^k = \lambda^k \alpha^k, k = 1, 2, \ldots, M \tag{72}$$
where
$$G_{ij} = (\mathbf{b}_i, \mathbf{H}\mathbf{b}_j) = (\mathbf{b}_i, \sigma_j), 1 \leq i, j \leq L \tag{73}$$
and M is the number of roots of interest.

3. Form the correction vectors $\{\delta^k\}, k = 1, 2, \ldots, M$, defined as
$$\delta_I^k = (\lambda^k - H_{II})^{-1} r_I^k, I = 1, 2, \ldots, N \tag{74}$$
where
$$\mathbf{r}^k = \sum_{i=1}^{L} \alpha_i^k (\mathbf{H} - \lambda^k)\mathbf{b}_i \tag{75}$$
and N is the number of determinants or CSFs.

4. Normalize $\{\delta^k\}$.

5. Schmidt orthonormalize δ^1 against the set $\{\mathbf{b}_i\}$ and append the result to $\{\mathbf{b}_i\}$. Repeat this process for each of the other $M-1$ correction vectors, neglecting those whose Schmidt orthonormalized norm is less than some threshold $T \sim 10^{-3}$. This results in the addition of m new $\mathbf{b}$ vectors, with $1 \leq m \leq M$.

6. Increase L by m and return to step 2.

the Hamiltonian. These can be precomputed and stored on disk, or they can be computed on-the-fly. Alternatively, they can be approximated in some cases using orbital energies. In a determinantal basis, Davidson's preconditioner can actually cause the CI vector to break spin symmetry. Indeed, Knowles and Handy noted this difficulty in their pioneering 1984 paper on determinant based configuration interaction.[109] They found that this problem can be avoided if the diagonal elements of the Hamiltonian H_{II} are replaced by an average $\tilde{H}_{II}$ over all determinants which have the same spatial orbital configuration as determinant I but differ in the distribution of spins.

If several roots are sought, or convergence takes many iterations, then the number of vectors stored on disk can become large, leading to I/O delays during the construction of $\mathbf{G}$ or $\mathbf{r}$. Furthermore, disk storage can become a problem if the vectors themselves are very large. One solution is to apply compression algorithms to the subspace vectors and σ vectors.[176,177] Additionally, the Davidson-Liu method can be restarted with only M expansion vectors by using the current approximation to each eigenvector, eq. (76), as the new starting guess vectors. Clearly this procedure hinders the rate of convergence because information is lost after the vector subspace is collapsed: subsequent diagonalizations have less variational freedom because of the reduced dimension of the subspace. However, in 1990 van Lenthe and Pulay presented the remarkable conclusion[178] that when only a single root is sought, collapsing the subspace does not substantially degrade the rate of convergence if the subspace is collapsed down to two vectors instead of just one. This procedure, which may be justified by the theory of conjugate gradients, was later generalized to multiple roots by Murray, Racine, and Davidson.[175] The collapsed vector subspace contains the current guess vector for each root, as before, and also the guess vectors from the previous iteration (after they have been Schmidt orthogonalized against the other vectors in the collapsed subspace).

Other work has focused on improving the correction vector. As noted by Olsen,[83] Saad,[179] Sleijpen and van der Vorst,[180] and others,[181,182] Davidson's equation (70) seems to imply that the optimal update vector δ is just the negative of the current guess CI vector $\mathbf{c}$. Clearly, this would not allow for the expansion of the vector subspace. Sleijpen *et al.*[180] have pointed out that Davidson assumed that δ is orthogonal to $\mathbf{c}$ in deriving eq. (70). However, Davidson's method only enforces this orthogonality after δ has already been determined. Hence, a more effective preconditioner may result from explicitly enforcing this orthogonality while δ is being constructed, and several authors have recently proposed such preconditioners.[83,181,182]

Another improvement suggested by these authors and others[54,56,173] is to lift the assumption of strict diagonal dominance of the Hamiltonian in the preconditioner. One selects a subspace of the most important N-electron functions

in the CI space and, for the purposes of the preconditioner, approximates the Hamiltonian as

$$\mathbf{H} \approx \begin{bmatrix} \mathbf{H}' & 0 \\ 0 & \mathbf{\Lambda}'' \end{bmatrix}, \tag{77}$$

where primes denote the small selected subspace and double primes denote the complement subspace. Although relatively few (up to several hundred) determinants might be included in the selected space, it is important to take complete sets of determinants which are capable of forming spin eigenfunctions so that the spin symmetry of the CI vector can be maintained during the iterative procedure. Note that the Hamiltonian is assumed diagonal in the complement subspace and coupling is ignored. This leads to two equations for the correction vector:

$$(\delta^k)' = -(\mathbf{H}' - \lambda^k \mathbf{I}')^{-1} (\mathbf{r}^k)' \tag{78}$$

$$(\delta^k)'' = -(\mathbf{\Lambda}'' - \lambda^k \mathbf{I}'')^{-1} (\mathbf{r}^k)''. \tag{79}$$

The second equation of course becomes

$$(\delta_I^k)'' = \frac{(r_I^k)''}{\lambda_k - H_{II}}, \tag{80}$$

and is analogous to eq. (74). The first equation can be written in terms of the eigenvalues μ^l and eigenvectors $\mathbf{u}^l$ of the small matrix $\mathbf{H}'$:

$$(\delta_I^k)' = \sum_l \frac{u_I^l (\mathbf{u}^l \cdot (\mathbf{r}^k)')}{\lambda^k - \mu^l} \tag{81}$$

3.2.2 Olsen's Method

Realizing the difficulties of storing several $\mathbf{b}$ and σ vectors for very large CI spaces, Olsen proposed that each correction vector be added directly to the current CI vector, and that the resulting (renormalized) vector be used as the next iteration's guess vector. Of course for this scheme to work well, the correction vector must be as good as possible. Olsen therefore introduced an improved method for generating the correction vector, using some of the ideas just discussed above. If the current (normalized) CI vector is denoted $\mathbf{c}$, then its energy is

$$E = (\mathbf{c}, \mathbf{Hc}). \tag{82}$$

The Hamiltonian is then divided into two terms,

$$\mathbf{H} = \mathbf{H}^{(0)} + \mathbf{H}^{(1)}, \tag{83}$$

and the CI eigenvalue equation can be written

$$(\mathbf{H}^{(0)} + \mathbf{H}^{(1)})(\mathbf{c} + \delta\mathbf{c}) = (E + \delta E)(\mathbf{c} + \delta\mathbf{c}), \tag{84}$$

where $\delta\mathbf{c}$ and δE are the corrections to the current CI vector and energy. If $\delta\mathbf{c}$ is required to be orthogonal to $\mathbf{c}$ then (neglecting quadratic terms)

$$\delta\mathbf{c} = -(\mathbf{H}^{(0)} - E)^{-1}\left[(\mathbf{H} - E)\mathbf{c} - \mathbf{c}\delta E\right], \tag{85}$$

where

$$\delta E = \frac{(\mathbf{c}, (\mathbf{H}^{(0)} - E)^{-1}(\mathbf{H} - E)\mathbf{c})}{(\mathbf{c}, (\mathbf{H}^{(0)} - E)^{-1}\mathbf{c})} \tag{86}$$

The correction vector $\delta\mathbf{c}$ is superior to that used in the standard Davidson method since it remains rigorously orthogonal to $\mathbf{c}$ and therefore retains the ability to introduce new character into the CI vector even near convergence.[83] This correction vector was also derived by Bofill and Anglada from other considerations.[181] In 1990, Olsen, Jørgensen, and Simons used this method to perform three iterations of the first one-billion determinant CI calculation.[83] The zeroth-order part of the Hamiltonian $\mathbf{H}^{(0)}$ was defined as a 400×400 block of determinants formed from the lowest diagonal elements of $\mathbf{H}$, and as the diagonal of $\mathbf{H}$ outside this block. This procedure requires the storage of four vectors on disk (three if the diagonal elements of $\mathbf{H}$ are computed as needed).

Although the Olsen method can be very helpful when disk space is limited, its convergence characteristics are not always very good. Indeed, as first pointed out by Mitrushenkov,[183] the Olsen method does not guarantee that the energy decreases every iteration. However, it is of course possible to use Olsen's preconditioner in conjunction with iterative methods which keep more than one CI vector and σ vector. Mitrushenkov[183] advocates diagonalizing the Hamiltonian in the space of the current and previous CI vectors:

$$H_{ii} = (\mathbf{c}^{(i)}, \sigma^{(i)}) \tag{87}$$

$$H_{i,i-1} = H_{i-1,i} = (\sigma^{(i)}, \mathbf{c}^{(i-1)}). \tag{88}$$

Explicitly, the nonorthogonal pseudo-eigenvalue equation is

$$\begin{pmatrix} H_{i-1,i-1} & H_{i-1,i} \\ H_{i,i-1} & H_{i,i} \end{pmatrix} \begin{pmatrix} \alpha_{i-1} \\ \alpha_i \end{pmatrix} = E_i \begin{pmatrix} 1 & s \\ s & 1 \end{pmatrix} \begin{pmatrix} \alpha_{i-1} \\ \alpha_i \end{pmatrix}, \tag{89}$$

where s is the overlap between the current and previous CI vectors, $(\mathbf{c}^{(i)}, \mathbf{c}^{(i-1)})$. At each iteration, the current CI vector is recomputed as $\mathbf{c}^{(i)} = \alpha_{i-1}\mathbf{c}^{(i-1)} + \alpha_i\mathbf{c}^{(i)}$, and $\sigma^{(i)} = \alpha_{i-1}\sigma^{(i-1)} + \alpha_i\sigma^{(i)}$. H_{ii} is set to E_i in eq. (89), and then the new vector $\mathbf{c}^{(i+1)}$ is computed using Olsen's method. This process is repeated until convergence is reached. In our experience Mitrushenkov's method

improves convergence substantially in the first few iterations compared to the single-vector version of Olsen's method. Unfortunately, as CI vector approaches convergence, eq. (89) becomes ill-conditioned because $H_{i-1,i}$ approaches H_{ii} and s approaches unity. This difficulty can be avoided by reverting to the single-vector Olsen method near convergence.

4 Determinant-Based Algorithms for Highly Correlated CI

This section describes several determinant-based CI algorithms. The alpha and beta string formalism of Handy[44] is introduced, and the equations for $\sigma = \mathbf{Hc}$ within this formalism are derived for the full CI and RAS CI cases.[46] Practical considerations for implementation are also discussed.

4.1 Slater Determinants, CSFs, and Direct CI

Slater determinants are eigenfunctions of $\hat{S}_z$; therefore, the CI space includes only those determinants with a given value of M_s unless a spin-dependent Hamiltonian is used.[184] However, Slater determinants are not eigenfunctions of $\hat{S}^2$ as are configuration state functions (CSFs), and dimension of the CI space in Slater determinants is typically about 2-4 times larger than in CSFs (for more about CSFs, see the books by Pauncz[185,186]). Thus it would seem that CSFs are preferable to Slater determinants for use as CI expansion functions. However, determinants offer certain advantages in the context of "direct CI" methods that can outweigh the disadvantage of a larger CI space.

In computational quantum chemistry the term "direct" has come to mean that certain quantities, which are too large to hold in core memory, are computed on-the-fly instead of being stored on disk and read as needed. A *direct SCF* implies that the two-electron integrals are computed on-the-fly. For a *direct CI*,[88] the integrals are still held on disk, but the Hamiltonian matrix itself is not explicitly constructed or stored. Instead, the vector $\sigma = \mathbf{H}c$, which is required in iterative subspace methods for diagonalizing the Hamiltonian (cf. section 3.2), is computed directly from the one- and two-electron integrals and the CI vector; the construction of σ is the time-consuming step in the direct CI method. The coefficients for multiplying the CI vector by the integrals have already been introduced (cf. section 2.3.2) as the one- and two-electron coupling coefficients; these may be written to disk in a file traditionally called the "formula tape." Unfortunately, this procedure is still unsuitable for a direct CI, since the coupling coefficients will require as much storage space as the Hamiltonian matrix itself, leading to long I/O delays. Hence, in a direct

CI, the coupling coefficients should be calculated as needed (or they should be built into the program). A next step would be to eliminate storage of the CI vector itself; efforts along these lines have been described as *superdirect CI*.[187,188] Alternatively, Carter and co-workers have considered pseudospectral approaches which eliminate the need to construct two-electron integrals as separate intermediates.[189–192]

The direct CI method was first introduced in 1972 by Roos for the case of CISD from a closed-shell reference function.[193] However, generalization to more complex CI spaces, such as MR-CISD, proved exceedingly difficult due to the large number of special cases. The next breakthrough did not occur until Shavitt[41,42] cast the work of Paldus on the unitary group approach (UGA)[40,78] into a graphical formalism which represents CSFs in the Gelfand-Tsetlin canonical basis as walks on a directed graph. Not only did this graphical representation make the UGA more accessible to chemists, but it also provided a convenient formalism for carrying out computations. Any pair of walks (CSFs) forms a loop, and matrix elements are evaluated based on the shapes of these loops, with only certain loop types giving nonzero matrix elements.[41,42] For example, one-electron coupling coefficients are expressed as

$$\gamma_{ij}^{IJ} = \prod_{k=i}^{j} W(T_k, b_k), \tag{90}$$

where T_k identifies the shape of the loop formed by walks I and J at level k on the Shavitt graph, and b_k is the "b-value" of the vertex on walk J at level k (see ref. 42 for more details). The coupling coefficient vanishes unless walks I and J coincide everywhere below level $i-1$ and above level j on the graph (assuming $i < j$). This graphical unitary group approach (GUGA) was developed with a philosophy similar to that of the direct CI. The idea was to use each coupling coefficient, specified by a loop on the Shavitt graph, for a whole series of Hamiltonian matrix elements differing in their common upper and lower walks. The first multireference CI method based on the ideas of Paldus and Shavitt was developed by Brooks and Schaefer.[43] Particularly notable was their computation on the $^1B_{1u}$ state of ethylene involving all single and double excitations relative to three open-shell singlet reference configurations.[43] However, a detailed analysis of the "loop-driven" GUGA CI program of Brooks and Schaefer indicates that, in practice, few loops contribute to very many matrix elements, and it remains more efficient to write the coupling coefficients to the formula tape rather than to recompute them as needed.

Nevertheless, the graphical approach afforded new insight into the structure of the Hamiltonian. In particular, for CI spaces which allow only one or two electrons in the external space, the graphical representation of the external space becomes very regular, and the external portion of a loop can only have

a few possible shapes.[194] Siegbahn made the crucial observation that the one- and two-electron coupling coefficients can be factored into contributions from the internal orbitals and from the external orbitals,

$$\gamma_{ij}^{IJ} = {}^{int}\gamma_{ij}^{IJ} \times {}^{ext}\gamma_{ij}^{IJ} \tag{91}$$

$$\Gamma_{ijkl}^{IJ} = {}^{int}\Gamma_{ijkl}^{IJ} \times {}^{ext}\Gamma_{ijkl}^{IJ}, \tag{92}$$

and that the calculation can be "direct" in the external space when the external factors are very simple.

In 1979, Siegbahn showed[195] that for the case of single replacements from a reference wavefunction which is a full CI in the active space (i.e., first-order CI[13]), the external factors for the coupling coefficients are all simply +1; hence, only the internal space coupling coefficients must be precomputed and stored on the formula tape. This results in a substantial savings because the number of internal coupling coefficients will be much smaller than the total number of coupling coefficients. In 1980, Siegbahn extended these ideas to the general case of all single and double substitutions for an arbitrary set of references (i.e., MR-CISD).[194] Once again, the external coupling coefficient factors are simple (± 1, $\pm\sqrt{2}$, and 2) and can be dealt with in a direct fashion. The shape-driven GUGA program of Saxe, Fox, Schaefer, and Handy[91] is based in part on Siegbahn's approach, as is the program of Saunders and van Lenthe[127] and the COLUMBUS program of Shavitt, Lischka, Shepard, and co-workers.[196–198]

Unfortunately, these simplifications are not directly applicable[91] when more than two electrons are allowed into the external space (e.g., CISDT, CISDTQ, and full CI). Furthermore, even for MR-CISD wavefunctions, large active spaces can lead to a large number of internal coupling coefficients, which can become difficult to deal with.[197] The next advance was once again due to Siegbahn, who suggested a factorization of the two-electron coupling coefficients by inserting the resolution of the identity:

$$\Gamma_{ijkl}^{IJ} = \sum_K \gamma_{ij}^{IK}\gamma_{kl}^{KJ} - \gamma_{il}^{IJ}\delta_{jk}. \tag{93}$$

Although the resolution of the identity requires an infinite sum in principle, in this case only a finite number of states $|\Phi_K\rangle$ are relevant. For fixed i, j, k, l, I, and J, the product term will vanish unless $|\Phi_K\rangle$ is obtained from $|\Phi_J\rangle$ by a single substitution from orbital l to orbital k and from $|\Phi_I\rangle$ by a single substitution from orbital i to orbital j. For configuration state functions, this completely specifies the orbital configuration of $|\Phi_K\rangle$, and only a few spin couplings must be summed over. This approach led Knowles and Handy[109] to present a vectorized full CI algorithm based on Slater determinants rather than CSFs. For Slater determinants, the one-electron coupling coefficients

appearing in (93) and elsewhere are very easy to calculate on-the-fly, allowing a fully direct CI procedure. For Slater determinants $|I\rangle$ and $|J\rangle$, $\gamma_{ij}^{IJ} = \langle I|\hat{E}_{ij}|J\rangle$ is 0 unless determinant $|J\rangle$ becomes determinant $|I\rangle$ (within a sign) when an alpha or beta electron is moved from orbital j to orbital i, in which case γ_{ij}^{IJ} becomes ± 1. For the special case $i = j, I = J$, γ_{ii}^{II} counts the number of electrons in orbital i for determinant I, yielding 0, 1, or 2.

Because of this simplicity and the ability to carry out computations in a fully direct fashion, many of the full and restricted CI algorithms developed over the last ten years have employed Slater determinants, and in this section we will focus our attention on these determinant-based methods. However, we should note that further progress has also been made in CSF-based approaches. Much of the recent work in direct CI methods has been based on the symmetric group approach (SGA)[199–203] rather than the related unitary group approach (UGA).[40–42,78] Given the factorization (93), the problem of formulating a fully direct CI procedure can be turned into the problem of determining the one-electron coupling coefficients on-the-fly in the desired order. Knowles and Werner presented a way of doing this in 1988.[102] They use the identity

$$\hat{E}_{ij} = \hat{E}_{ia}\hat{E}_{aj}, \tag{94}$$

which holds for any orbital ϕ_a which is always unoccupied. This hypothetical orbital, referred to as a "ghost" orbital, does not actually appear in any of the integrals. The one-electron coupling coefficient becomes

$$\gamma_{ij}^{IJ} = \sum_{K_s} \langle I|\hat{E}_{ia}|K_s\rangle\langle K_s|\hat{E}_{aj}|J\rangle, \tag{95}$$

where the sum is over all spin couplings of the uniquely-specified orbital configuration K. By fixing one of the two orbital indices, it becomes feasible to store the intermediates needed to evaluate the one-electron coupling coefficients efficiently in the desired order. This ghost-orbital technique was used by Werner and Knowles in their implementation of internally-contracted multireference CI.[101] That method requires third- and fourth-order reduced density matrices, which can be evaluated by approaches analogous to (93). Another possibility along the lines of Siegbahn's internal/external factorization has been suggested by Malmqvist, Rendell, and Roos in their implementation of the RAS SCF method.[56] They modify the GUGA method to split all walks into upper and lower portions and calculate coupling coefficients as products of upper and lower factors. Although the upper factors are not necessarily very simple for a RAS case, the storage requirements are substantially reduced in this approach.

Finally, we note that many other important advances have been made in CSF-based approaches, even outside the context of direct CI. Much of this effort in recent years has focused on extending the unitary and symmetric group

approaches to the spin-dependent Hamiltonians needed to account for relativistic effects.[204-210] Examples of other work include specialized unitary group approaches for MRCI wavefunctions based on CAS references[211] and application of the unitary group approach to CI calculations on atoms using Hylleraas coordinates[65] and to spin-adapted open-shell coupled-cluster theory.[212] However, we now turn our attention to determinant-based formulations of direct CI.

4.2 Alpha and Beta Strings

A 1980 paper by Handy[44] represented a major advance in determinant-based CI, even though the paper was more concerned with how integrals and CI coefficients are stored than with the computational advantages of determinants over CSFs. Handy realized that if determinants are used as N-electron basis functions, and particularly if these determinants are expressed as "alpha strings" and "beta strings," then the vector σ can be evaluated very efficiently.

Although Handy was the first to use alpha and beta strings, we will employ the subsequent notation of Olsen *et al.*[46] An alpha string is defined as an ordered product of creation operators for spin orbitals with alpha spin. If I_α contains a list $\{i, j, \ldots k\}$ of the N_α occupied spin orbitals with alpha spin in determinant $|I\rangle$, then the alpha string $\alpha(I_\alpha)$ is $a^\dagger_{i\alpha} a^\dagger_{j\alpha} \ldots a^\dagger_{k\alpha}$. A beta string is defined similarly. Thus a Slater determinant $|I\rangle$ in terms of alpha and beta strings is

$$|I\rangle = |\alpha(I_\alpha)\beta(I_\beta)\rangle = \alpha(I_\alpha)\beta(I_\beta)|\rangle. \tag{96}$$

For example, consider the Slater determinant $|I\rangle = |\phi_{1\alpha}\phi_{2\alpha}\phi_{3\alpha}\phi_{1\beta}\phi_{2\beta}\phi_{4\beta}\rangle$. Then the alpha string $\alpha(I_\alpha)$ is given by

$$\alpha(I_\alpha) = a^\dagger_{1\alpha} a^\dagger_{2\alpha} a^\dagger_{3\alpha}, \tag{97}$$

and the beta string is given by

$$\beta(I_\beta) = a^\dagger_{1\beta} a^\dagger_{2\beta} a^\dagger_{4\beta}. \tag{98}$$

Note that the order of the creation operators matters; if we swap the order of two creation operators within the alpha string (or within the beta string), then we introduce a sign change due to the anticommutation relation of creation operators. Also, applying the alpha string to the vacuum first, rather than the beta string, may introduce a minus sign, depending on the number of alpha and beta electrons. Typically, the beta string will be placed to the right of the alpha string in equations like (96). Further, within each string, orbitals are listed in strictly increasing order.

Since a determinant is now specified by an ordered pair of indices representing its alpha and beta components, the Ith element of the CI vector becomes $c(I_\alpha, I_\beta)$. Note that this vector can also be considered as a matrix with coordinates I_α and I_β. Both vector and matrix addressing schemes are computationally useful. The σ vector,

$$\sigma_I = \sum_J H_{IJ} c_J, \tag{99}$$

can be written in the new notation as

$$\sigma(I_\alpha, I_\beta) = \sum_{J_\alpha, J_\beta} \langle \beta(J_\beta)\alpha(J_\alpha)|\hat{H}|\alpha(I_\alpha)\beta(I_\beta)\rangle c(J_\alpha, J_\beta), \tag{100}$$

where we have used $H_{IJ} = H_{JI}^*$ and assumed that $\mathbf{H}$ is a real matrix to obtain the form most commonly seen in the literature when this notation is used. Handy realized the following advantages to alpha and beta strings:

1. Direct CI methods often require an index vector which points to a list of all allowed excitations from a given N-electron basis function. Using alpha and beta strings, the index vector need not be the length of the CI vector—its size is dictated by the number of alpha or beta strings, which (for a full CI) is approximately the square root of the number of determinants. This results from the fact that in determinant-based CI, electrons in alpha spin-orbitals can be excited only to other alpha spin-orbitals, and electrons in beta spin-orbitals can be excited only to other beta spin-orbitals (because of the restriction to a single value of M_s).

2. To form $\sigma(I_\alpha, I_\beta)$ in equation (100), all functions $|\alpha(J_\alpha)\beta(J_\beta)\rangle$ which have non-zero matrix elements with $|\alpha(I_\alpha)\beta(I_\beta)\rangle$ are generated, one at a time, with the appropriate integral being looked up and multiplied by the appropriate CI coefficient. No time is wasted considering determinants which are noninteracting, and the coefficients of the integrals are easy to evaluate.

3. Efficiency is increased by realizing that all integrals which enter the expression $\langle \alpha(I_\alpha)\beta(I_\beta)|\hat{H}|\alpha(J_\alpha)\beta(I_\beta)\rangle$ (equation 100), where $\alpha(J_\alpha)$ differs from $\alpha(I_\alpha)$ by two orbitals, are independent of $\beta(I_\beta)$.

This approach allowed several benchmark full CI computations, including the first CI procedure (1981) to include more than one million determinants.[38,213]

4.3 The Vectorized Full CI Algorithm of Knowles and Handy

In 1984, Knowles and Handy introduced a new direct CI algorithm for full CI wavefunctions.[109,214] As Siegbahn had pointed out,[45] the efficiency of direct CI algorithms is increased if, for a given $|K\rangle$, all one-electron coupling coefficients γ_{kl}^{KJ} are available together. Examination of Siegbahn's expression for σ elucidates this observation:[45]

$$\sigma_I = \sum_J H_{IJ} c_J \tag{101}$$

$$= \sum_{ij} \sum_J \gamma_{ij}^{IJ} h_{ij} c_J + \frac{1}{2} \sum_{ijkl} (ij|kl) \sum_J \Gamma_{ijkl}^{IJ} c_J \tag{102}$$

$$= \sum_{ij} \{h_{ij} - \frac{1}{2} \sum_l (il|lj)\} \sum_J \gamma_{ij}^{IJ} c_J$$

$$+ \frac{1}{2} \sum_{ijkl} (ij|kl) \sum_K \gamma_{ij}^{IK} \sum_J \gamma_{kl}^{KJ} c_J, \tag{103}$$

where the resolution of the identity has been used to turn the two-electron coupling coefficients into products of one-electron coupling coefficients (eq. 93). Notice that part of the two-electron contribution has been folded into the one-electron term. The remaining two-electron term is the time consuming part in the evaluation of σ_I, and it is most efficiently written as

$$\sigma_I^{(2)} = \frac{1}{2} \sum_K \sum_{ij} \gamma_{ij}^{IK} \sum_{kl} (ij|kl) \sum_J \gamma_{kl}^{KJ} c_J. \tag{104}$$

Thus this part of σ_I can be evaluated by the following set of operations:

$$D_{kl}^K = \sum_J \gamma_{kl}^{KJ} c_J \tag{105}$$

$$E_{ij}^K = \sum_{kl} (ij|kl) D_{kl}^K \tag{106}$$

$$\sigma_I^{(2)} = \frac{1}{2} \sum_K \sum_{ij} \gamma_{ij}^{IK} E_{ij}^K. \tag{107}$$

The one-electron coupling coefficients would ordinarily be stored on disk, making the evaluation of the D and σ quantities I/O intensive and thus inefficient. However, Knowles and Handy noted that in a basis of determinants the one-electron coupling coefficients can be evaluated on-the-fly (direct CI) even in the general case. A given determinant $|K\rangle$ can interact with at most two

other determinants $|I\rangle$, and their contributions can be separated by rewriting the shift operator in $\gamma_{ij}^{IK} = \langle I|\hat{E}_{ij}|K\rangle$ as

$$\hat{E}_{ij} = \hat{E}_{ij}^{\alpha} + \hat{E}_{ij}^{\beta}, \tag{108}$$

where $\hat{E}_{ij}^{\alpha}$ replaces an α-spin electron in orbital j with an α-spin electron in orbital i (cf. section 2.3.2). Note that this approach requires a sum over a complete set of intermediate determinants $|K\rangle$ (or at least all determinants which interact with the allowed determinants through $\hat{E}_{ij}$), including those determinants with the wrong spatial symmetry. This means that the Knowles and Handy algorithm would be considerably less efficient for restricted CI.

Given equation (108), it is possible to write the one-electron coupling coefficients in terms of alpha and beta strings:

$$\begin{aligned} \gamma_{ij}^{IJ} &= \langle\alpha(I_\alpha)\beta(I_\beta)|\hat{E}_{ij}^{\alpha}|\alpha(J_\alpha)\beta(J_\beta)\rangle\delta(I_\beta, J_\beta) \\ &+ \langle\alpha(I_\alpha)\beta(I_\beta)|\hat{E}_{ij}^{\beta}|\alpha(J_\alpha)\beta(J_\beta)\rangle\delta(I_\alpha, J_\alpha), \end{aligned} \tag{109}$$

where $|\alpha(I_\alpha)\rangle$ is related to $|\alpha(J_\alpha)\rangle$ by a single excitation (and likewise for $|\beta(I_\beta)\rangle$ and $|\beta(J_\beta)\rangle$). Thus the one-electron coupling coefficients are generated from lists of strings related by single excitations. For each alpha (beta) string, one stores a list of all allowed single replacements to other alpha (beta) strings; for closed-shell systems, the two lists will be identical and only one must be stored. Each list contains the address of the new string, the orbital index ij, and a phase factor, denoted by $\mathrm{sgn}(ij)$, which is ± 1. The sign can be determined as $(-1)^p$, where p is the number of transpositions of creation operators needed to bring an excited string to its canonical form. String addresses were computed by table lookups using a canonical addressing scheme explained in section 4.9.2. One can take advantage of the permutational symmetries $(ij|kl) = (ji|kl) = (ij|lk) = (ji|lk)$ of the two-electron integrals by requiring $i \geq j$, $k \geq l$. This entails replacing γ_{kl}^{KJ} in (105) by $(\gamma_{kl}^{KJ} + \gamma_{lk}^{KJ})$, an analogous change for (107), and a modification of the integrals to avoid double counting when $i = j$ or $k = l$.

The algorithm of Knowles and Handy is described as "vectorized" because each of the three major operations (105)-(107) may be written as an operation performed on an entire vector at once. This is very beneficial for vector supercomputers, which actually perform such operations a vector at a time and give substantial increases in speed. To illustrate, consider Fig. 6, which shows the Knowles-Handy algorithm for the formation of D, eq. (105). Due to memory limitations, operations are performed for a block of strings at a time. In the first half of Fig. 6, the operations in the innermost loop are identical but independent of each other for different K_β. In the second half of the algorithm, the same applies to K_α; hence, this operation can be performed for a

Figure 6: Knowles-Handy Vectorized Formation of D (Refs. 109,214).

loop alpha strings K_α in block
  loop over excitations $|\alpha(J_\alpha)\rangle = \mathrm{sgn}(ij)\hat{E}^\alpha_{ij}|\alpha(K_\alpha)\rangle$
    loop over K_β in block
      $|K\rangle = |\alpha(K_\alpha)\beta(K_\beta)\rangle, |J\rangle = |\alpha(J_\alpha)\beta(K_\beta)\rangle$
      $D(K_\alpha, K_\beta, ij) = D(K_\alpha, K_\beta, ij) + \mathrm{sgn}(ij)c(J_\alpha, K_\beta)$

loop alpha strings K_β in block
  loop over excitations $|\beta(J_\beta)\rangle = \mathrm{sgn}(ij)\hat{E}^\beta_{ij}|\beta(K_\beta)\rangle$
    loop over K_α in block
      $|K\rangle = |\alpha(K_\alpha)\beta(K_\beta)\rangle, |J\rangle = |\alpha(K_\alpha)\beta(J_\beta)\rangle$
      $D(K_\alpha, K_\beta, ij) = D(K_\alpha, K_\beta, ij) + \mathrm{sgn}(ij)c(K_\alpha, J_\beta)$

whole range of K_β (K_α) values simultaneously with a vector processor. These same considerations apply to the analogous eq. (107). The remaining (and most time consuming) step, (106), can be performed as a matrix multiplication when one uses compound indices ij and kl, and of course this is also a vectorized operation.

These concerns about vectorization remain relevant even though quantum chemists now perform a substantial fraction of their computations on workstation machines which lack vector processors. Nevertheless, workstations (and now even personal computers, or PCs) feature *pipelined* processors. Pipelines allow machine instructions to overlap to some extent, giving the processor a limited ability to perform several tasks at once.[166] The superscalar IBM RS/6000 POWER2 workstation processor has two floating point pipelines, each of which can hold up to twelve instructions. If the processor can keep a steady stream of independent instructions coming down the pipeline, then overall performance will be increased substantially. However, if one instruction depends on results from another, then the pipeline can become stalled and performance is degraded. Since vectorizable code implies many similar but independent operations, as a general rule, vectorizable code becomes good pipelined code.

The Knowles-Handy approach was expected to be very efficient on vector supercomputers, and indeed it enabled many important full CI benchmark calculations.[15] Nevertheless, one can see that this algorithm does more work than is strictly necessary. Equation (106) demonstrates that the operation count for the time-consuming step is approximately $\frac{1}{4}\tilde{N}_{det}n^4$, where n is the number of orbitals and $\tilde{N}_{det}$ is the number of interacting intermediate states,

which may be larger than the number of determinants in the full CI space because the intermediate states are not subject to spatial symmetry restrictions. The factor of $\frac{1}{4}$ arises from the permutational symmetries of the integrals. As discussed previously in section 2.4.5, the computational cost of a full CI procedure should actually scale as $\mathcal{O}(N_{det}N^2n^2)$. Thus, the Knowles-Handy algorithm replaces N_{det} with the larger $\tilde{N}_{det}$, and N^2 with the larger n^2. Some of the extra work is due to the fact that the intermediate matrix D can contain a substantial number of zeros. For example, D^K_{kl} will be zero when K has orbital k unoccupied or orbital l doubly occupied (D becomes less sparse under the condition $k \geq l$). Even though matrix multiplications are ideal for vector computers, Olsen and co-workers[46] realized that abandoning the matrix formulation (105)-(107) might still lead to a faster algorithm due to the substantially reduced operation count.

4.4 Olsen's String-Based Full CI Algorithm

In order to avoid the unnecessarily large operation counts in the full CI algorithm of Knowles and Handy, Olsen *et al.* abandoned the explicit use of a complete set of intermediate states and returned to some of Handy's original (1980) ideas[44] concerning string-driven full CI approaches.

4.4.1 Full CI σ Equations

We begin by describing Olsen's expressions for the σ vector. In second quantized-form (cf. section 2.3.2), $\hat{H}$ becomes

$$\hat{H} = \sum_{kl}^{n} h_{kl}\hat{E}_{kl} + \frac{1}{2}\sum_{ijkl}^{n}(ij|kl)\left(\hat{E}_{ij}\hat{E}_{kl} - \delta_{jk}\hat{E}_{il}\right). \tag{110}$$

Inserting this expression into that for σ, eq. (100), yields

$$\begin{aligned}\sigma(I_\alpha, I_\beta) &= \sum_{J_\alpha, J_\beta} \langle\beta(J_\beta)\alpha(J_\alpha)|\sum_{kl}^{n} h_{kl}\hat{E}_{kl} \\ &+ \frac{1}{2}\sum_{ijkl}^{n}(ij|kl)\left(\hat{E}_{ij}\hat{E}_{kl} - \delta_{jk}\hat{E}_{il}\right)|\alpha(I_\alpha)\beta(I_\beta)\rangle c(J_\alpha, J_\beta)\end{aligned} \tag{111}$$

Now expanding the shift operators into their two spin components, $\hat{E}_{kl} = \hat{E}^\alpha_{kl} + \hat{E}^\beta_{kl}$, we write σ as a sum of three terms:[46]

$$\sigma(I_\alpha, I_\beta) = \sigma_1(I_\alpha, I_\beta) + \sigma_2(I_\alpha, I_\beta) + \sigma_3(I_\alpha, I_\beta), \tag{112}$$

where

$$\sigma_1(I_\alpha, I_\beta) = \sum_{J_\beta} \sum_{kl}^{n} \langle \beta(J_\beta)|\hat{E}^\beta_{kl}|\beta(I_\beta)\rangle \left[h_{kl} - \frac{1}{2}\sum_{j}^{n}(kj|jl) \right] c(I_\alpha, J_\beta) + \frac{1}{2}\sum_{J_\beta}\sum_{ijkl}^{n} \langle \beta(J_\beta)|\hat{E}^\beta_{ij}\hat{E}^\beta_{kl}|\beta(I_\beta)\rangle (ij|kl) c(I_\alpha, J_\beta), \quad (113)$$

$$\sigma_2(I_\alpha, I_\beta) = \sum_{J_\alpha} \sum_{kl}^{n} \langle \alpha(J_\alpha)|\hat{E}^\alpha_{kl}|\alpha(I_\alpha)\rangle \left[h_{kl} - \frac{1}{2}\sum_{j}^{n}(kj|jl) \right] c(J_\alpha, I_\beta) + \frac{1}{2}\sum_{J_\alpha}\sum_{ijkl}^{n} \langle \alpha(J_\alpha)|\hat{E}^\alpha_{ij}\hat{E}^\alpha_{kl}|\alpha(I_\alpha)\rangle (ij|kl) c(J_\alpha, I_\beta), \quad (114)$$

$$\sigma_3(I_\alpha, I_\beta) = \sum_{J_\alpha, J_\beta} \sum_{ijkl}^{n} \langle \beta(J_\beta)|\hat{E}^\beta_{ij}|\beta(I_\beta)\rangle \langle \alpha(J_\alpha)|\hat{E}^\alpha_{kl}|\alpha(I_\alpha)\rangle (ij|kl) c(J_\alpha, J_\beta). \quad (115)$$

For efficient implementation, it is convenient to precompute the quantities

$$h'_{kl} = h_{kl} - \frac{1}{2}\sum_{j}^{n}(kj|jl). \quad (116)$$

Note that the first term (σ_1) involves only beta shift operators, the second (σ_2) involves only alpha shift operators, and the third (σ_3) involves both alpha and beta shift operators. These terms are also called the $\beta\beta$, $\alpha\alpha$, and $\alpha\beta$ terms.[48,49] Several determinant-based CI algorithms presented over the last few years[83,183,215,216] have been based on this set of σ equations or the analogous equations for restricted CI (see section 4.8.1).

4.4.2 Simplifications for $M_s = 0$

Certain simplifications arise if the $M_s = 0$ component of an electronic state is used. The first of these is the time-reversal symmetry of the CI vector, which may be expressed as

$$c(I_\alpha, I_\beta) = (-1)^S c(I_\beta, I_\alpha), \quad (117)$$

where S is the spin quantum number. Olsen *et al.* use this fact to show how the σ_2 contribution can be determined entirely from the σ_1 contribution when $M_s = 0$.[46] The remarkably simple result is

$$\sigma_2(I_\alpha, I_\beta) = (-1)^S \sigma_1(I_\beta, I_\alpha). \quad (118)$$

Likewise, it is also possible to show that the $ijkl$-th component of σ_3 satisfies the relation

$$\sigma_3^{ijkl}(I_\alpha, I_\beta) = (-1)^S \sigma_3^{klij}(I_\beta, I_\alpha). \tag{119}$$

This equation may be used to eliminate contributions from $I_\beta > I_\alpha$ or $(kl) > (ij)$, where (ij) and (kl) are compound indices. Olsen argues that the restriction $I_\alpha \geq I_\beta$ is to be preferred where this can be used to eliminate entire blocks of the σ_3 matrix. If all alpha/beta strings with the same irreducible representation are grouped together, then states which are not totally symmetric in their molecular point group will have off-diagonal blocks which can be eliminated using this restriction. On the other hand, when applied to totally symmetric states, this restriction eliminates the upper half of each symmetry block of σ_3. Since this reduces the average vector length in the vectorized algorithm, Olsen recommends using the alternative restriction $(ij) \geq (kl)$ in these cases. This may be accomplished by rewriting σ_3 as

$$\begin{aligned} \sigma_3(I_\alpha, I_\beta) &= \sum_{(ij)\geq(kl)} \sigma_3^{ijkl}(I_\alpha, I_\beta) + \sum_{(ij)<(kl)} (-1)^S \sigma_3^{klij}(I_\beta, I_\alpha) \\ &= \sigma_3'(I_\alpha, I_\beta) + (-1)^S \sigma_3'(I_\beta, I_\alpha), \end{aligned} \tag{120}$$

where

$$\sigma_3'(I_\alpha, I_\beta) = \sum_{(ij)\geq(kl)} \sigma_3^{ijkl}(I_\alpha, I_\beta)(1 + \delta_{(ij),(kl)})^{-1}. \tag{121}$$

Hence the total σ vector can be evaluated as

$$\sigma(I_\alpha, I_\beta) = \sigma_1(I_\alpha, I_\beta) + \sigma_3'(I_\alpha, I_\beta) + (-1)^S \left[\sigma_1(I_\beta, I_\alpha) + \sigma_3'(I_\beta, I_\alpha)\right]. \tag{122}$$

The $M_s = 0$ simplifications therefore reduce computational expense by roughly a factor of two.

One further observation must be made about the loss of spin symmetry in the CI vector in the iterative diagonalization of the Hamiltonian. Even very slight deviations from (117), such as might occur from roundoff errors, become magnified in subsequent iterations and cause the iteration procedure to become numerically unstable because precise adherence to (117) is *assumed* if any of the $M_s = 0$ simplifications just described. If necessary, these difficulties can be avoided by explicitly enforcing the spin symmetry of any new vector in the subspace expansion. In this respect it is important to modify the diagonal elements of the Hamiltonian in the preconditioner for the subspace iteration method, as already discussed in section 3.2.

4.4.3 Algorithms for Computing σ

From (113), one can see that the mathematical operations required to form $\sigma_1(I_\alpha, I_\beta)$ are identical but independent of each other for different I_α. That is,

Figure 7: Olsen's Vectorized Algorithm for σ_1 (Ref. 46).

loop over beta strings I_β
  Zero array F
  Loop over excitations $\hat{E}^\beta_{kl}$ from $|\beta(I_\beta)\rangle$
    $|\beta(K_\beta)\rangle = \mathrm{sgn}(kl)\hat{E}^\beta_{kl}|\beta(I_\beta)\rangle$
    $F(K_\beta) = F(K_\beta) + \mathrm{sgn}(kl)h'_{kl}$
    Loop over excitations $\hat{E}^\beta_{ij}$ from $|\beta(K_\beta)\rangle$
      $|\beta(J_\beta)\rangle = \mathrm{sgn}(ij)\hat{E}^\beta_{ij}|\beta(K_\beta)\rangle$
      $F(J_\beta) = F(J_\beta) + (1/2)\mathrm{sgn}(kl)\mathrm{sgn}(ij)(ij|kl)$
    end loop over $\hat{E}^\beta_{ij}$
  end loop over $\hat{E}^\beta_{kl}$
  loop over beta strings J_β and alpha strings I_α
    $\sigma_1(I_\alpha, I_\beta) = \sigma_1(I_\alpha, I_\beta) + F(J_\beta)c(I_\alpha, J_\beta)$; vect'd
  end loop over I_α, J_β
end loop over I_β

column I_β of σ_1 can be constructed by two multiplications of scalars by columns (J_β) of c. Hence the construction of σ_1 is vectorizable over I_α. The vectorized algorithm for the evaluation of σ_1, adapted from Olsen *et al.*,[46] appears in Figure 7. An analogous algorithm can be used to obtain σ_2. However, one can also obtain σ_2 for $M_s = 0$ cases by (118). These algorithms require the same string replacement lists used by Knowles and Handy[109] (sec. 4.3). Note that the vector F is sparse, and multiplication of F by c should only take place for nonzero values of F.

Unfortunately, the construction of σ_3 (115) is harder to vectorize. A simple, non-vectorized algorithm for σ_3 is presented in Fig. 8. One can see that this does not appear as a simple set of arithmetic operations on vectors. For example, the contributions of the beta strings are not identical for different alpha strings because each alpha string connects to a different set of excited alpha strings with different indices k and l. Olsen *et al.* remedy this by operating a fixed kl at a time;[46] this makes their algorithm vectorizable in the innermost loop. Their algorithm, adapted and expanded from Ref. 46, is presented in Fig. 9. Note that this algorithm also employs scatter/gather (i.e., data rearrangement) operations to ensure that all of the data relevant to the multiplication step $V = Fc'$ are contiguous. This avoids "indirect addressing," which could substantially degrade performance due to long waits for data to be fetched from scattered memory locations.[166] For $M_s = 0$, an improvement to the σ_3 algorithm can be made by utilizing equations discussed in section 4.4.2.

Figure 8: Simple Algorithm for σ_3.

loop over I_α
  loop over $|\alpha(J_\alpha)\rangle = \mathrm{sgn}(kl)\hat{E}^\alpha_{kl}|\alpha(I_\alpha)\rangle$
    loop over I_β
      loop over $|\beta(J_\beta)\rangle = \mathrm{sgn}(ij)\hat{E}^\beta_{ij}|\beta(I_\beta)\rangle$
        $\sigma_3(I_\alpha, I_\beta) = \sigma_3(I_\alpha, I_\beta) + \mathrm{sgn}(ij)\mathrm{sgn}(kl)(ij|kl)c(J_\alpha, J_\beta)$
      end loop over J_β
    end loop over I_β
  end loop over J_α
end loop over I_α

Furthermore, if the integrals possess the full eightfold permutational symmetry, then $\hat{E}^\alpha_{kl}$ can be replaced by $(\hat{E}^\alpha_{kl} + \hat{E}^\alpha_{lk})(1+\delta_{kl})^{-1}$ in order to increase the average vector length in the formation of V. Note once again that F is sparse.

Clearly this algorithm takes less advantage of vector processors than the Knowles-Handy algorithm, since it involves some overhead (setup of the L and R arrays, and the scatter and gather) and uses smaller vector lengths. Nevertheless, one would expect this algorithm to be faster in many cases due to the substantially reduced number of mathematical operations performed. Counting only multiplications, the operation counts for each part of σ are approximately[46]

$$N_1 \approx \frac{1}{4} N_{det} N_\beta^2 (n - N_\beta)^2 \tag{123}$$

$$N_2 \approx \frac{1}{4} N_{det} N_\alpha^2 (n - N_\alpha)^2 \tag{124}$$

$$N_3 \approx N_{det} N_\alpha N_\beta (n - N_\alpha)(n - N_\beta). \tag{125}$$

When $N_\alpha = N_\beta$, the overall operation count is thus approximately

$$N_{op} \approx \frac{3}{2} N_{det} N_\alpha^2 (n - N_\alpha)^2. \tag{126}$$

Recall that this operation count can be cut approximately in half for $M_s = 0$ cases. Knowles and Handy are also able to take advantage of time reversal symmetry for singlet states, by employing the combinations $2^{-1/2}(\alpha(I_\alpha)\beta(I_\beta) + \alpha(I_\beta)\beta(I_\alpha))$. Recalling that the operation count for the Knowles-Handy algorithm is approximately $\frac{1}{4}\tilde{N}_{det} n^4$, we might expect the greatest savings for Olsen's algorithm when n/N is large.

Figure 9: Olsen's Vectorized Algorithm for σ_3 (Ref. 46).

loop over kl
  set up lists $L(I)$, $R(I)$, and $\mathrm{sgn}(I)$, such that
    $|\alpha[L(I)]\rangle = \mathrm{sgn}(I)\hat{E}^{\alpha}_{kl}|\alpha[R(I)]\rangle$
  loop over list entries I and beta strings J_β
    $c'(I, J_\beta) = c(L(I), J_\beta)\mathrm{sgn}(I)$; vect'd gather
  end loop over I and J_β
  loop over I_β
    zero array F
    loop over excitations $\hat{E}^{\beta}_{ij}$ from $|\beta(I_\beta)\rangle$
      $|\beta(J_\beta)\rangle = \mathrm{sgn}(ij)\hat{E}^{\beta}_{ij}|\beta(I_\beta)\rangle$
      $F(J_\beta) = F(J_\beta) + \mathrm{sgn}(ij)(ij|kl)$
    end loop over $\hat{E}^{\beta}_{ij}$
    loop over beta strings J_β and list entries I
      $V(I) = F(J_\beta)c'(I, J_\beta)$; vect'd over I
    end loop over J_β, I
    loop over list entries I
      $\sigma_3(R(I), I_\beta) = \sigma_3(R(I), I_\beta) + V(I)$; vect'd scatter
    end loop over I
  end loop over I_β
end loop over kl

4.5 Zarrabian's Reduced Intermediate Space

Shortly after the publication of the 1988 paper by Olsen *et al.*, Zarrabian, Sarma, and Paldus presented[217] an alternative approach to avoid the unnecessarily large scaling of the Knowles-Handy full CI algorithm. These workers employed an $(N-2)$-electron intermediate space for the two-electron contributions rather than an N–electron intermediate space. Their expressions for σ were originally derived using generators of the group SO(4), but to avoid introducing new notation we will consider the later derivation of Harrison and Zarrabian,[47] which uses only the standard spin-orbital creation and annihilation operators.

We begin by rewriting (24) over spatial orbitals, as

$$\hat{H} = \sum_{ij}^{n} h_{ij} \sum_{\sigma=\alpha,\beta} a_{i\sigma}^{\dagger} a_{j\sigma} + \frac{1}{2} \sum_{ijkl}^{n} (ij|kl) \sum_{\lambda,\sigma=\alpha,\beta} a_{i\sigma}^{\dagger} a_{k\lambda}^{\dagger} a_{l\lambda} a_{j\sigma}. \tag{127}$$

Next, insert the resolution of the identity between the pairs of creation and annihilation operators in the two-electron term. Clearly, the sum must run over $(N-2)$-electron states. The expression for σ becomes

$$\begin{aligned} \sigma_I &= \sum_J H_{IJ} c_J \qquad (128) \\ &= \sum_J \sum_{ij}^{n} h_{ij} \sum_{\sigma=\alpha,\beta} \langle I^{(N)} | a_{i\sigma}^{\dagger} a_{j\sigma} | J^{(N)} \rangle c_J \\ &+ \frac{1}{2} \sum_{JK} \sum_{ijkl}^{n} (ij|kl) \sum_{\lambda,\sigma=\alpha,\beta} \langle I^{(N)} | a_{i\sigma}^{\dagger} a_{k\lambda}^{\dagger} | K^{(N-2)} \rangle \langle K^{(N-2)} | a_{l\lambda} a_{j\sigma} | J^{(N)} \rangle c_J, \end{aligned}$$

where the superscripts (N) and $(N-2)$ denote the number of electrons for each state. The one-electron terms are exactly the same as before. The two-electron contributions to σ, denoted $\sigma^{(2)}$, may be written in terms of separate contributions from each possible spin case:

$$\begin{aligned} \sigma_{\alpha\alpha}^{(2)} &= \sum_{JK} \sum_{i>k,j>l}^{n} [(ij|kl) - (il|jk)] \langle I^{(N)} | a_{i\alpha}^{\dagger} a_{k\alpha}^{\dagger} | K^{(N-2)} \rangle \langle K^{(N-2)} | a_{l\alpha} a_{j\alpha} | J^{(N)} \rangle c_J \\ \sigma_{\beta\beta}^{(2)} &= \sum_{JK} \sum_{i>k,j>l}^{n} [(ij|kl) - (il|jk)] \langle I^{(N)} | a_{i\beta}^{\dagger} a_{k\beta}^{\dagger} | K^{(N-2)} \rangle \langle K^{(N-2)} | a_{l\beta} a_{j\beta} | J^{(N)} \rangle c_J \\ \sigma_{\alpha\beta}^{(2)} &= \sum_{JK} \sum_{ijkl}^{n} (ij|kl) \langle I^{(N)} | a_{i\beta}^{\dagger} a_{k\alpha}^{\dagger} | K^{(N-2)} \rangle \langle K^{(N-2)} | a_{l\alpha} a_{j\beta} | J^{(N)} \rangle c_J, \end{aligned} \tag{129}$$

where the restrictions over the orbital indices in the $\sigma_{\alpha\alpha}^{(2)}$ and $\sigma_{\beta\beta}^{(2)}$ terms is made possible by the permutational symmetry of the integrals and the anticommutation relations of the creation and annihilation operators. Likewise, the two

Figure 10: Harrison and Zarrabian's Vectorized Algorithm for $\sigma^{(2)}_{\alpha\alpha}$ (Ref. 47).

loop over alpha strings I_α
  loop over orbital pairs $i > k$ (creation op.)
    define $(N_\alpha - 2)$-electron string K_α
    $|\alpha(K_\alpha)\rangle = \mathrm{sgn}(ik) a_{k\alpha} a_{i\alpha} |\alpha(I_\alpha)\rangle$
    loop over orbital pairs $j > l$ (annihilation op.)
      define new N_α-electron string J_α
      $|\alpha(J_\alpha)\rangle = \mathrm{sgn}(jl) a^\dagger_{j\alpha} a^\dagger_{l\alpha} |\alpha(K_\alpha)\rangle$
      $V = \mathrm{sgn}(ik)\mathrm{sgn}(jl)[(ij|kl) - (il|kj)]$
      loop over beta strings I_β
        $\sigma^{(2)}_{\alpha\alpha}(I_\beta, I_\alpha) = \sigma^{(2)}_{\alpha\alpha}(I_\beta, I_\alpha) + V * c(I_\beta, J_\alpha)$

mixed contributions $\alpha\beta$ and $\beta\alpha$ have been combined in $\sigma^{(2)}_{\alpha\beta}$, eliminating the coefficient of $\frac{1}{2}$.

The algorithm for constructing $\sigma^{(2)}_{\alpha\alpha}$, adapted from Harrison and Zarrabian,[47] is given in Fig. 10. The algorithm for $\sigma^{(2)}_{\beta\beta}$ is of course analogous. It is easy to show that the number of floating-point multiplications involved in the construction of $\sigma^{(2)}_{\beta\beta}$ and $\sigma^{(2)}_{\alpha\alpha}$ with this algorithm are

$$N_1 = \frac{1}{4} N_{det} N_\beta (N_\beta - 1)(n - N_\beta + 2)(n - N_\beta + 1) \tag{130}$$

$$N_2 = \frac{1}{4} N_{det} N_\alpha (N_\alpha - 1)(n - N_\alpha + 2)(n - N_\alpha + 1), \tag{131}$$

which are basically the same as the approximate operation counts (123)-(124) for Olsen's algorithm.[46] Harrison and Zarrabian point out that this algorithm can be parallelized over the outermost loop. Note that they address the CI vector with the beta string as the row index instead of the alpha string; the earlier paper by Zarrabian *et al.* used the alternative convention. This choice can have some relevance for $\sigma^{(2)}_{\alpha\alpha}$ and $\sigma^{(2)}_{\beta\beta}$ when only one of the terms is explicitly constructed (i.e., when $M_s = 0$). In that case, it is best to access the data in C sequentially (i.e., with "unit stride").[166]

For $\sigma^{(2)}_{\alpha\beta}$, one can use a similar loop structure to that in Fig. 9 or Fig. 10.[217] This yields an operation count[47] of

$$N_3 = N_{det} N_\alpha N_\beta (n - N_\alpha + 1)(n - N_\beta + 1). \tag{132}$$

However, Harrison and Zarrabian suggest that for parallel-vector machines, it is better to revert to a matrix multiplication such as that used by Knowles and Handy.[109] This algorithm is produced in Fig. 11. These loops are run

Figure 11: Harrison and Zarrabian's Vectorized Algorithm for $\sigma^{(2)}_{\alpha\beta}$ (Ref. 47).

precompute info for adding orbs to $(N_\alpha - 1)$-elec. α string
precompute info for adding orbs to $(N_\beta - 1)$-elec. β string
zero D
loop over orbitals l to be added to $(N_\alpha - 1)$-elec. string K_α
  loop over orbitals j to be added to $(N_\beta - 1)$-elec. string K_β
    loop over $(N_\alpha - 1)$-electron strings K_α
      define N_α–electron string J_α
      $|\alpha(J_\alpha)\rangle = \mathrm{sgn}(l) a^\dagger_{l\alpha} |\alpha(K_\alpha)\rangle$
      loop over $(N_\beta - 1)$-electron strings K_β
        define N_β–electron string J_β
        $|\beta(J_\beta)\rangle = \mathrm{sgn}(j) a^\dagger_{j\beta} |\beta(K_\beta)\rangle$
        $D(K_\beta, K_\alpha, jl) = D(K_\beta, K_\alpha, jl) + \mathrm{sgn}(k)\mathrm{sgn}(j) c(J_\beta, J_\alpha)$
      end loop over K_β
    end loop over K_α
  end loop over j
end loop over l

call optimized matrix multiply for $E_{K,ik} = D_{K,jl}\langle jl|ik\rangle$

loop over orbitals k to be added to $(N_\alpha - 1)$-elec. string K_α
  loop over orbitals i to be added to $(N_\beta - 1)$-elec. string K_β
    loop over $(N_\alpha - 1)$-electron strings K_α
      define N_α–electron string I_α
      $|\alpha(I_\alpha)\rangle = \mathrm{sgn}(k) a^\dagger_{k\alpha} |\alpha(K_\alpha)\rangle$
      loop over $(N_\beta - 1)$-electron strings K_β
      $|\alpha(I_\alpha)\rangle = \mathrm{sgn}(k) a^\dagger_{k\alpha} |\alpha(K_\alpha)\rangle$
        define N_β–electron string I_β
        $|\beta(I_\beta)\rangle = \mathrm{sgn}(i) a^\dagger_{i\alpha} |\beta(K_\beta)\rangle$
        $\sigma^{(2)}_{\alpha\beta}(I_\beta, I_\alpha) = \sigma^{(2)}_{\alpha\beta}(I_\beta, I_\alpha) + \mathrm{sgn}(i)\mathrm{sgn}(k) E(K_\beta, K_\alpha, ik)$
      end loop over K_β
    end loop over K_α
  end loop over i
end loop over k

for blocks of several intermediate states K at a time, and additional loops account for spatial symmetry. Note the use of two-electron integrals in Dirac notation rather than Mulliken notation; i.e., $\langle jl|ik\rangle = (ij|kl)$ for real integrals. Furthermore, the integrals are stored without any permutational symmetry. This algorithm has an operation count of

$$N_3 = N_{det}N_\alpha N_\beta n^4/(n - N_\alpha + 1)(n - N_\beta + 1), \tag{133}$$

which can be obtained[47] by using $N_\alpha/(n-N_\alpha+1)$ as the ratio of the number of $(N_\alpha - 1)$-electron strings to the number of N-electron strings (and by ignoring spatial symmetry). Note that this operation count is not too much greater than that of the non-matrix version (132) when $m >> N_\alpha, N_\beta$. In such cases, and given $N_\alpha = N_\beta$, the overall number of multiplications $N_1 + N_2 + N_3$ is about $\frac{3}{2}N_{det}N_\alpha^2 n^2$, compared to $\frac{1}{4}\tilde{N}_{det}n^4$ for the Knowles-Handy algorithm.

Although the work done by this algorithm is basically equivalent to that done in Olsen's algorithm, Zarrabian *et al.* suggest[47,217] that their approach would be better suited for the evaluation of three- and four-electron reduced density matrices, which are important in the context of internally contracted MR-CISD.[101] They also note that it should be possible to adapt their algorithm to restricted CI spaces,[47,217] and some work along these general lines has been presented by Duch.[203]

4.6 The Table-Based Algorithm of Bendazzoli and Evangelisti

Using Handy's alpha and beta string formalism,[44] along with some of the notation of Olsen,[46] Bendazzoli and Evangelisti have presented a full CI algorithm[48,49] which uses tables to represent the excitation operators $\hat{E}_{ij}^{\beta}$ rather than the string replacement lists of Knowles and Handy. The operation count of their method is essentially the same as that of Olsen *et al.*[46] and of Zarrabian *et al.*,[47,217] but the data are organized differently and the authors note that their loop structure is more easily parallelized than that of Olsen *et al.*[46] The algorithm of Bendazzoli and Evangelisti[48] for σ_1 (which they call the $\beta\beta$ term), is presented in Figure 12. When $M_s = 0$, σ_2 can be obtained from (118) just as in Olsen's approach.[46]

The tables $OOVV$ represent the shift operator products $\hat{E}_{il}^{\beta}\hat{E}_{jk}^{\beta}$; for a given set of orbitals (i, j, k, l), $OOVV(i, j, l, k)$ gives a list of all beta strings with orbitals i, j occupied and l, k unoccupied. This is the list of all strings which can be acted on to the left by the shift operator product. Similarly, $OOVV(l, k, i, j)$ gives a list of all strings which can be acted on to the right by this same product. The clever aspect of this approach is that the Ith entry of $OOVV(i, j, l, k)$ (denoted I_1) is the *same* as the string produced by applying $\hat{E}_{il}^{\beta}\hat{E}_{jk}^{\beta}$ to the Ith

Figure 12: Bendazzoli and Evangelisti's Algorithm for σ_1 (Ref. 48).

loop over $i > j, k > l$
  $V = (ik|jl) - (il|jk)$
  loop over $I = 1$, length of list $OOVV(i,j,k,l)$
    $I_1 = I$th entry of list $OOVV(i,j,l,k)$
    $S_1 =$ sign associated with I_1
    $VS = V * S_1$
    $I_2 = I$th entry of list $OOVV(l,k,i,j)$
    loop over $J = 1$, number of alpha strings
      $\sigma(J,I_2) = \sigma(J,I_2) + c(J,I_1) * VS$
    end loop over J
  end loop over I
end loop over i,j,k,l

element of $OOVV(l,k,i,j)$ (denoted I_2). Bendazzoli and Evangelisti have so far limited their attention to full CI; for restricted CI, the size of the lists OV and $OOVV$ will rapidly become large relative to the size of the CI vector (sec. 4.9.4), so that these lists are probably appropriate only for full CI.

The σ_3 algorithm is presented in Figure 13. Note the same scatter/gather structure as in Figures 9 and 22. Like our own version (cf. section 4.9.5), this algorithm eliminates the F array and uses a DAXPY operation[166] in the innermost loop. Compared to the algorithm in Figure 22, our initial attempts to implement this algorithm for σ_3 yielded a program running roughly 50% slower on the IBM RS/6000 POWER2 model 3CT workstation.

More recently, Evangelisti, Bendazzoli, and co-workers have developed a parallel implementation of their algorithm for the Cray T3D, a distributed memory machine.[50,84] The newest out-of-core version of their program allows the CI and σ vectors to be processed one symmetry block at a time. To avoid storage of the diagonal of the Hamiltonian, they approximate it using orbital eigenvalues. Following Olsen[83] (sec. 3.2.2), they minimize storage space by using only one CI vector and one σ vector in their iterative diagonalization method, although the details of their iterative procedure differ somewhat from those of Olsen and co-workers. In 1996, this parallelized version was used on a 64-processor Cray T3D to obtain[84] the full CI wavefunction for Be_2, with all electrons correlated and using a 9s2p1d basis (derived from a 4s2p1d ANO basis by uncontracting the primitive Gaussians corresponding to the five largest coefficients in the first ANO orbital). This represents the first converged CI calculation requiring more than one billion Slater determinants

Figure 13: Bendazzoli and Evangelisti's Algorithm for σ_3 (Ref. 48).

loop over k, l

  loop over $I = 1$, length of list $OV(l, k)$
    $I_2 = I$th entry of $OV(l, k)$
    $S_2 =$ sign associated with I_2
    loop over $J = 1$, number of beta strings
      $c'(I, J) = c(I_2, J) * S_2$
    end loop over J
  end loop over I

  loop over i, j
    $V = (ij|kl)$
    loop over $J = 1$, length of list $OV(i, j)$
      $J_1 = J$th entry of $OV(i, j)$
      $J_2 = J$th entry of $OV(j, i)$
      $S_2 =$ sign associated with J_2
      $VS = V * S_2$
      loop over $I = 1$, length of $OV(l, k)$
        $\sigma'(I, J_2) = \sigma'(I, J_2) + c'(I, J_1) * VS$
      end loop over I
    end loop over J
  end loop over i, j

  loop $I = 1$, length of list $OV(l, k)$
    $I_1 = I$th entry of $OV(l, k)$
    loop $J = 1$, number of beta strings
      $\sigma(I_1, J) = \sigma'(I, J)$
    end loop over J
  end loop over I

end loop over k, l

(an unconverged calculation on the Mg atom involving more than a billion determinants was reported in 1990 by Olsen, Jørgensen, and Simons[83]).

4.7 Approximate Full CI Methods

In 1989, Knowles introduced[81] a modified full CI procedure which exploits the sparsity of the Hamiltonian matrix and affords approximate full CI results at a dramatically reduced computational cost. Employing the Davidson method[108] (cf. section 3.2.1), the correction to the current CI vector is given by

$$\Delta c_I = \frac{r_I}{(E - H_{II})}, \tag{134}$$

where r_I is the residual $\sigma_I - Ec_I$. Knowles estimates the importance of these corrections using the following simple expression inspired by second-order perturbation theory:

$$\Delta E_I = r_I \Delta c_I. \tag{135}$$

If $|\Delta E_I|$ is less than some threshold, Δc_I is neglected. Thus far fewer determinants are actually included in the correction vector, which is stored on disk in a packed format. One problem with this approach is that neglected corrections Δc_I can reappear during the standard Schmidt orthogonalization against previous subspace vectors (cf. section 3.2). Knowles thus avoids the Schmidt orthogonalization step and employs a non-orthogonal space of expansion vectors. This allows for tight control over the size of the expansion space vectors.

A potential difficulty of this approach is that the σ vectors (which must also be stored) are not necessarily sparse. Knowles notes[81] that even when $\mathbf{c}$ is only 1% populated, typically 50% of σ will be nonzero. Nevertheless, in order to obtain variationally correct energies, the full σ vector must be formed in core memory and its dot product taken with all expansion vectors $\mathbf{c}$. However, once this is done, the only further use of σ is in the construction of new subspace vectors; hence, Knowles only writes to disk those elements of σ greater than some threshold. According to (134)-(135), these neglected elements of σ would only contribute to elements of $\Delta\mathbf{c}$ which make very small energy contributions.

Given the Knowles-Handy full CI algorithm of section 4.3, it is clear that the matrix formulation no longer applies with a sparse CI vector $\mathbf{c}$. Instead, the the formation of σ is driven from the list of nonzero elements in $\mathbf{c}$, employing scatter and gather operations to obtain some vectorization in the innermost loops; this approach is therefore similar to the original string-driven approach of Handy[44] or the subsequent algorithm of Olsen *et al.*[46] To avoid core storage problems, the exact σ can be formed one symmetry block at a time (where a symmetry block of σ contains all elements σ_I having the same alpha string

symmetry). Memory requirements can be further reduced, with some loss in efficiency, by processing σ in smaller batches of arbitrary size.[81]

Knowles and Handy demonstrated the power of this approach by estimating the full CI energy of NH_3 in an atomic natural orbital (ANO) basis set of DZP quality.[218] The full CI expansion contains more than 209 million determinants, yet Knowles and Handy were able to obtain an apparently reliable variational energy of -56.4235 hartree using a CI vector with only 665,247 nonzero elements (0.3% of the full CI vector). Employing perturbation theory to estimate the remaining energy error (presumably via equation 135), Knowles and Handy arrived at a final estimate of -56.4236 $\pm$ 0.0001 hartree.[218]

Using perturbation theory to estimate the importance of determinants in configuration interaction is a very old idea (see Ref. 57 for a detailed review). Indeed, it is perturbation theory which provides the justification for truncating the CI space at only singles and doubles from one or several references (i.e., the CISD and MR-CISD methods). The CIPSI method (1973) of Huron, Malrieu, and Rancurel[92] diagonalizes the Hamiltonian in some subspace of selected determinants and uses the resulting eigenvector as the zeroth-order wavefunction in a subsequent perturbation theory treatment. Determinants having a contribution to the first-order wavefunction greater than some threshold η are added to the selected CI space, and this process is repeated until the selection threshold is considered acceptably small or until the selected CI space becomes too large to handle. The effect of unselected determinants is evaluated by second-order perturbation theory. The procedure of Knowles[81,218] is similar to this, but differs in two important respects: first, Knowles selects determinants based on a perturbative estimate of their contribution to the energy rather than to the first-order wavefunction, and second, Knowles applies the selection *during* the Davidson procedure, whereas CIPSI solves the CI problem exactly for each selected CI space. A more recent version of the CIPSI method[93] is somewhat more flexible and introduces a third class of determinants of intermediate importance; interacting determinants with an estimated CI coefficient less than η but greater than a second threshold τ can be treated by higher-order perturbation theory or variationally, while those with contributions less than τ are treated by second-order perturbation theory as before. The CIPSI scheme should yield wavefunctions approaching the full CI limit, and indeed it has been benchmarked against full CI.[93,122,123,215,219] The most recent studies have added a self-consistent dressing of the Hamiltonian matrix to ensure size consistency.[122,123]

Another long-established approach to approximating full CI is to employ successively larger MR-CISD spaces. Since the size of the CI space grows very rapidly as the number of references is increased, Buenker and Peyerimhoff (1974-5)[10,11] suggested retaining only the most important singly and doubly

substituted configurations and treating discarded configurations by Brillouin-Wigner perturbation theory and extrapolation procedures; they call their procedure MRD-CI. Their strategy implies that the most compact wavefuntions are obtained by truncating the singles and doubles space rather than the reference space, and indeed CIPSI studies support this idea.[122,219] Unlike the CIPSI method, Buenker and Peyerimhoff do not use perturbation theory in the configuration selection; rather, orbital configurations are accepted or rejected on the basis of the energy lowering they cause when added to the reference space. A separate small CI procedure is required for each possible spatial orbital configuration. Although this may require somewhat more effort than the perturbational estimates of CIPSI, the energy lowerings can be reused in the extrapolations to zero threshold.[10,11] Alternative approaches to making MR-CISD more computationally tractable are the internal and external contraction schemes discussed in section 2.4.2.

Knowles' 1989 program[81,218] was able to approach the full CI limit more closely than selected CI methods such as MRD-CI and CIPSI because it was efficient enough to treat a much larger number of determinants variationally. Subsequently in 1992, Povill, Rubio, and Illas noted[215] that the principal difficulty with the standard CIPSI program was its need to store the Hamiltonian matrix **H**, allowing it to handle no more than 50,000 determinants variationally. Hence, they presented[215] the direct selected configuration interaction using strings (DISCIUS) algorithm employing the alpha and beta string formalism of Handy;[44] the notation, $(\alpha\alpha, \beta\beta, \alpha\beta)$ spin decomposition, and $M_s = 0$ simplifications of Olsen *et al.*;[46] and the reduced intermediate space of Zarrabian *et al.*[47,217] Special ordering and addressing schemes, which make use of large index arrays, allow for some degree of vectorization despite the lack of a well-defined structure in the CI space.[215] Nevertheless, a more recent (1995) version of this algorithm by Povill and Rubio[220] largely abandons the vectorization of σ_3, noting that the average vector length for selected CI spaces is generally too small for effective vectorization. These authors also found that too much time is spent checking to see if doubly excited strings in the construction of σ_1 or σ_2 belong to the selected space; hence, they consider every pair of allowed strings and determine all single and double excitations connecting them. The DISCIUS algorithm is capable of treating selected CI spaces with more than one million determinants.[220]

A related algorithm, which has also been coupled to the CIPSI approach, was presented by Caballol and Malrieu[221] in 1992. Their approach is also direct and determinant-based, but the strings are written as particle-hole excitations from a single reference state; the program is named SCIEL, for selected CI with excitation labeling. For a determinant with excitation level m, the particle-hole labeling lists m holes and m particles. This is inefficient for full CI,[221] since

it would require the listing of $2N_\alpha$ orbitals for a maximally-excited ($m = N_\alpha$) alpha string, rather than only N_α orbitals in the standard approach. However, for CI spaces dominated by determinants with a relatively low excitation level, this formalism could offer some benefits. Povill *et al.* have commented that the DISCIUS and SCIEL programs seem to have similar efficiencies.[122]

Similar improvements have been made to the MRD-CI program of Buenker and Peyerimhoff,[10,11] which was previously limited to about 50,000 configurations.[222] In 1995, Krebs and Buenker presented[222] a new table-direct CI algorithm for use in the MRD-CI selection scheme which is capable of handling variational spaces including at least several hundred thousand determinants.

Knowles' 1989 sparse CI method has been the subject of additional study in the last few years. In 1994, Mitrushenkov presented a very similar method[183] which differs primarily in that it selects components of the CI vector based on their magnitude (134) and not on their expected energy lowering (135). This choice was motivated by the belief that it would yield more physical CI vectors less likely to give errors for properties other than the total energy.[183] Mitrushenkov described how to adapt Olsen's full CI algorithm to implement his approach, which he has called dynamic CI. Of particular interest is his technique for avoiding core storage of the entire σ vector: he calculates $\sigma(I_\alpha, I_\beta)$ for a fixed I_β (i.e., the algorithm is driven by σ rather than by nonzero elements of **c**). The exact σ values are used to update the Hamiltonian in the small Davidson subspace, and then components larger than a given cutoff are written to disk. Like Knowles, Mitrushenkov uses a nonorthogonal Davidson subspace; however, he uses only two vectors and employs the improved preconditioner of Olsen *et al.*[83] (cf. section 3.2.2). Mitrushenkov reported results for NH_3, H_2O, and Mg test cases,[183] but unfortunately no results were presented for systems where the exact full CI result was known (DZP NH_3 full CI results have subsequently been reported,[50,80] see below).

In 1991, Harrison emphasized the use of second-order perturbation theory to approach the full CI results more rapidly.[223] In Harrison's method, denoted CI+PT, one chooses an initial reference space (perhaps a single determinant), and an initial selection threshold η. A CI is performed in the reference space, yielding eigenvectors for all roots of interest. Unlike most of the other algorithms discussed in this section, Harrison's program employs CSFs rather than determinants; two-electron coupling coefficients are evaluated as products of one-electron coupling coefficients, which in turn are evaluated by the method of Knowles and Werner[102] (see section 4.1). For every configuration I interacting with (but not included in) the reference space, the second-order perturbation theory energy contribution is determined for each of the desired roots k, using

the selected-space eigenvectors $\mathbf{c}^k$ as zeroth-order solutions:

$$\Delta E_I^k = \frac{|\langle I|\hat{H}|\mathbf{c}^k\rangle|^2}{E^k - \langle I|\hat{H}|I\rangle}. \tag{136}$$

The set of all configurations I with $|\Delta E_I^k| > \eta$ is added to the reference space, and the new Hamiltonian is diagonalized; this process is repeated until no new important configurations are found. The reference selection is thus self-consistent, and Harrison notes[223] that typically only two iterations are required. The sum of the estimated energy lowerings (136) provides a perturbative correction for excluded configurations, and the total energy (variational energy plus perturbative correction) is an approximation to the full CI energy. An increasingly accurate sequence of wavefunctions is generated by repeating this whole process for a series of thresholds η with decreasing values. Note, however, that those configurations which do not interact directly with any reference function are completely neglected. Although the individual contributions of such configurations should be very small, there are a large number of them. Harrison finds that the CI+PT method approaches the full CI energy from above, suggesting that the error due to the neglect of noninteracting configurations is greater than the error due to the perturbative estimates of configurations which are interacting but not included in the reference space (the latter correction, being nonvariational, could conceivably lead to energies below the full CI limit). Harrison's approach is similar to the original two-class CIPSI algorithm,[92] but it selects references based on their contributions to the energy rather than to the first-order wavefunction; Harrison notes that for properties other than the energy, this might not be the optimal choice.[223] An advantage of his program was that it could handle larger variational spaces than the versions of the CIPSI and MRD-CI programs available at that time (recent improvements in these programs are described above). Results for H_2O, O, and O^- were compared to full CI and indicate that the perturbation theory energy correction rapidly accelerates convergence to the full CI energy. For example, the full CI energy for H_2O at three different geometries was obtained within 0.1 kcal mol^{-1} with a variational reference space and perturbative interacting space spanning less than 0.23% and 25%, respectively, of the full CI space (these results correspond to a selection threshold of $\eta = 4 \times 10^{-7}$).

The wavefunction operator (WFO) approach of Luzanov, Wulfov, and Krouglov (1992)[224] seems to be the same as Harrison's CI+PT approach, although it is formulated differently and implemented using determinants. This method appears to involve the same amount of work as other determinant-based sparse CI methods,[215,220,221] but it uses rather different intermediate arrays. Explicit algorithms for the WFO method were presented in 1996 by Wulfov,[225] who obtained results for HF dimer in a 4s3p1d/2s1p basis using a

personal computer (PC) equipped with only 16 megabytes (MB) of RAM and 50 MB of disk space. The largest computation, with threshold $\eta = 10^{-7}$, considered 65,751 determinants variationally and treated an unreported number of interacting determinants perturbatively.

Perturbation theory corrections to variational energies have also been considered recently by Mitrushenkov and Dmitriev (1995),[216] who express the second-order energy correction as

$$\begin{aligned} \Delta E &= \sum_{I_\alpha I_\beta} \frac{\sigma_0(I_\alpha, I_\beta)[\sigma_0(I_\alpha, I_\beta) - E_0 c_0(I_\alpha, I_\beta)]}{E_0 - H^D_{sa}(I_\alpha, I_\beta)} \\ &= (\mathbf{c}_0, \hat{H}\Delta\mathbf{c}), \end{aligned} \tag{137}$$

where $\mathbf{c}_0$ is the current CI vector and $\Delta\mathbf{c}_0$ is the correction vector. The term $H^D_{sa}(I_\alpha, I_\beta)$ is the diagonal element of the Hamiltonian for determinant $|I_\alpha I_\beta\rangle$, and the subscript *sa* indicates an average over all determinants with the same spatial orbital configuration (cf. section 3.2.1). This correction is essentially the same used by Harrison[223] and others. Rather than employ this expression exactly as it is, Mitrushenkov and Dmitriev note[216] that for a converged full CI vector $\mathbf{c} = \mathbf{c}_0 + \Delta\mathbf{c}$, the full CI energy can be expressed as:

$$\begin{aligned} E &= \frac{(\mathbf{c}_0, \hat{H}\mathbf{c})}{(\mathbf{c}_0, \mathbf{c})} \\ &= \frac{E_0 + (\mathbf{c}_0, \hat{H}\Delta\mathbf{c})}{1 + (\mathbf{c}_0, \Delta\mathbf{c})}. \end{aligned} \tag{138}$$

Mitrushenkov and Dmitriev designate this the norm-consistent zero threshold full CI estimate. When $\Delta\mathbf{c}$ is orthogonal to $\mathbf{c}$, this is the second-order perturbation theory estimate (137). However, since selection in the dynamic CI occurs during the subspace iteration process, $\Delta\mathbf{c}$ and $\mathbf{c}$ are not orthogonal. Of course the exact σ_0 and $\Delta\mathbf{c}$ must be used in the evaluation of (138); these are evaluated for fixed I_β as described above. Mitrushenkov and Dmitriev demonstrated this zero threshold energy (ZTE) estimate for Ne, NH_3, Mg, and H_2O; for Ne, comparisons with full CI indicate that the ZTE estimates approach the correct energy much faster than the variational energies with respect to decreasing threshold, but the approach is not monotonic and can occur from below. Very recently, Mitrushenkov has extended this approach to perform the dynamic CI+ZTE in the active space and to treat the external space using only second-order perturbation theory.[226]

In order to compare some of these selected CI methods, we present results for DZP NH_3 in Table 5. These results were obtained in point group C_s with the 1a′ core orbital frozen (i.e., constrained to remain doubly occupied). The

Table 5: Selected and Full Configuration Interaction Benchmarks for NH_3 with an ANO DZP Basis Set.[a]

Threshold	N_{CI}	E_{CI}	E_{CI}- E_{FCI}	N_{PT} $\times 10^6$	E_{CI+PT}	E_{CI+PT}- E_{FCI}
Knowles and Handy, Ref. 218:[b]						
2.0×10^{-4}	171 867	-56.4219	0.0021	n/a	-56.4220	0.0020
1.0×10^{-4}	393 666	-56.4229	0.0011	n/a	-56.4230	0.0010
5.0×10^{-5}	450 763	-56.4232	0.0008	n/a	-56.4234	0.0006
4.0×10^{-5}	665 247	-56.4235	0.0005	n/a	-56.4236	0.0004
Harrison, Ref. 223:[c]						
1.0×10^{-4}	786	-56.390631	0.033376	0.61	-56.422854	0.001153
1.3×10^{-5}	1 889	-56.411996	0.012011	1.04	-56.423766	0.000241
1.6×10^{-6}	5 814	-56.417497	0.006510	2.93	-56.423748	0.000259
3.9×10^{-7}	18 921	-56.420203	0.003804	5.92	-56.423719	0.000288
2.0×10^{-7}	32 288	-56.421211	0.002796	7.68	-56.423737	0.000270
Povill *et al.*, Ref. 123:[d]						
6.0×10^{-6}	1.00×10^6	-56.423659	0.000348	2.49	-56.423681	0.000326
0.4×10^{-6}	1.17×10^6	-56.423785	0.000222	6.55	-56.423824	0.000183
0.1×10^{-6}	1.25×10^6	-56.423825	0.000182	15.10	-56.423875	0.000132
Mitrushenkov and Dmitriev, Refs. 183, 216:[b,e]						
1.0×10^{-3}	2 000	-56.4085	0.0155	n/a	-56.42397	0.00004
1.0×10^{-4}	34 000	-56.4195	0.0045	n/a	-56.42392	0.00009
1.0×10^{-5}	590 000	-56.4235	0.0005	n/a	-56.42400	0.00001

[a]Basis set and geometry of Ref. 218. Only valence electrons are correlated. N_{CI} denotes the size of the variational space, and N_{PT} denotes the size of the interacting space treated by second-order perturbation theory. All energies are given in hartree.

[b]Number of nonzero elements in final CI vector.

[c]Dimensions are given in CSFs instead of determinants.

[d]The CIPSI algorithm uses two thresholds, η and τ. η is given, and $\tau = 10^{-10}$.

[e]Mitrushenkov reports the number of nonzero elements in the CI vector as a percentage of the full CI space (209 626 425 determinants); the N_{CI} values given are thus only approximate.

first highly accurate NH_3 benchmark using a basis set this large was that of Knowles and Handy in their 1989 demonstration of their new selected CI method.[218] Hence, most subsequent selected CI benchmarks on this system have used their geometry and atomic natural orbital basis set. An exception is the wavefunction operator (WFO) benchmark,[224] which employed a different basis set; that method is therefore excluded from the table. The exact full CI energy of NH_3 with this basis set was unavailable when these selected CI benchmarks were published, and the Knowles-Handy[218] extrapolated selected CI estimate of -56.4236 hartree has sometimes been used in place of the full CI value. The apparent convergence of this estimate led Knowles and Handy to propose error bars of ± 0.0001 hartree. However, in 1994 Povill *et al.*[123] used the 3-class CIPSI method[93] to select the most important 1.25 million determinants and obtained a variational energy of -56.423825 hartree using the DISCIUS algorithm.[215] This energy is lower than the lowest estimate of Knowles and Handy, including the error bar. This difficulty was cleared up in 1995 by Evangelisti *et al.*,[50] who used the full CI program of Bendazzoli and Evangelisti[48,49] to obtain an energy of -56.424007 hartree (this same value was obtained independently by Olsen[80]). This demonstrates that the energy of Knowles and Handy was not converged as tightly as expected, and that it is easy to underestimate the importance of a large number of neglected determinants.

The data in Table 5 show that the perturbation theory corrected energies are better approximations to the full CI energy than the purely variational results, and that the full CI energy is always approached from above; these conclusions are in general agreement with previous benchmarks for smaller systems.[93,216,223,224] However, we note that the perturbation theory corrections become less effective for large variational spaces, and conversely, the CI+PT energies are slowly convergent (and not monotonic) with the relatively small CI spaces used in Harrison's study[223] (note, however, that Harrison's N_{CI} values are in CSFs rather than determinants, making his variational space look smaller than it actually is). The norm-consistent zero threshold energies of Mitrushenkov and Dmitriev[216] appear particularly effective, although they do not approach the full CI energy monotonically.

Table 5 demonstrates that it is difficult to establish the convergence of the energy for selected CI methods. Another problem which has received relatively little attention is the convergence of properties other than the energy. It would be expected that other properties should not converge as quickly with respect to the size of the CI space as the energy (cf. section 2.2), particularly for selected CI methods which use an energy selection criterion rather than a coefficient criterion. However, a 1992 study by Cave, Xantheas, and Feller[227] used a selected CI method which is similar to the two-class CIPSI[92] method but

uses energy-based selection. These authors came to the remarkable conclusion that most one-electron properties considered in their study (including isotropic hyperfine values and dipole and quadrupole moments) converged even more rapidly than the energy.[227] Additionally, Wulfov[228] has recently considered the convergence of the equilibrium geometries and harmonic vibrational frequencies of several diatomic molecules as a function of the selection threshold value.[224,225] The convergence of these properties could not be firmly established due to the lack of corresponding exact full CI values; however, a recent full CI benchmark study by our group[229] on C_2 and CN^+ finds only very small errors in Wulfov's best CI+PT geometries and frequencies (less than 0.001 Å and 4.0 cm^{-1}, respectively).

4.8 Restricted Active Space CI

Rather than select individual determinants based on computational estimates of their importance, one might instead select entire classes of determinants which are expected *a priori* to be important based on their partitioning of electrons among various orbital subspaces. This is the motivation behind the truncation of the CI space according to "excitation level" (how many electrons are placed in the virtual subspace) and the second-order CI (SOCI),[13] which includes all determinants with at most two electrons in the external subspace. Such CI selection schemes were described in general terms by Shavitt,[57] who defined the *full class CI* as one which partitions the orbitals into an arbitrary number of orthogonal subsets and includes all or none of the N-electron functions which have a given partitioning of electrons among the subspaces. As Shavitt points out, a full-class CI wavefunction is invariant to separate, nonsingular linear transformations within any of the orbital subspaces.

A benefit of such class selection schemes is that the CI space exhibits a regular structure which can be used to advantage in computational implementations. Additionally, it appears to be easier to gauge the general reliability of wavefunctions obtained using class selection schemes as opposed to individual selection. However, class selection methods will invariably include some less important determinants and therefore cannot yield wavefunctions as compact as those from an individual selection method.

A specialization of the full class CI which uses only three orbital subspaces is the Restricted Active Space (RAS) CI approach introduced by Olsen *et al.*[46] in 1988 along with the string-based full CI algorithm already discussed (section 4.4). The three subspaces are labeled I, II, and III, and the CI space is limited by requiring a *minimum of p electrons in RAS I* and a *maximum of q electrons in RAS III* (cf. Figure 14). There are no restrictions on the number of electrons in RAS II, and thus it is analogous to the complete active space

(CAS). There may be an additional frozen core subspace in which each orbital is constrained to remain doubly occupied; these core electrons and orbitals need not be treated explicitly in the RAS procedure (cf. section 2.4.7). The full CI space may be obtained as the maximum limit of the RAS space. The focus of Olsen's paper was on the utility of the RAS method in limiting the size of CI calculations, but thus far its maximum impact has been on the development of determinant-based full CI algorithms.[83,183]

Figure 14: Orbital partitioning and configuration selection in the Restricted Active Space Configuration Interaction method. The CI space includes all determinants in which at least p electrons are in RAS I and at most q electrons are in RAS III.

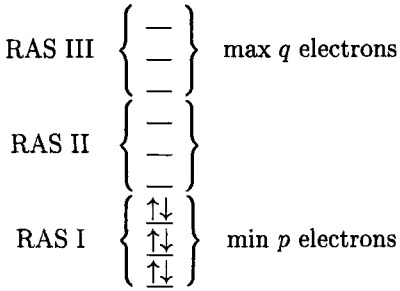

Any CI space truncated according to excitation level may be formulated within the RAS CI framework: the occupied orbitals are placed in RAS I, and the unoccupied orbitals are placed in RAS III, and the RAS II subspace is absent. The maximum number of electrons in RAS III is set equal to the maximum excitation level, and the minimum number of electrons in RAS I is simply the total number of electrons N minus the maximum excitation level. A full CI can be obtained by applying trivial restrictions, such as a minimum of zero electrons in RAS I and a maximum of N electrons in RAS III.

One may also formulate excitation class selected MR-CI spaces within the RAS framework. A SOCI can be obtained by setting RAS I equal to the active space, deleting RAS II, allowing a maximum of two electrons in RAS III, and requiring a minimum of $N-2$ electrons in RAS I. Alternatively, this same CI space may be constructed by placing the virtual orbitals of the active space in RAS II, allowing a maximum of two electrons in RAS III, and requiring zero electrons in RAS I. To obtain the CISD[TQ] wavefunction mentioned in section 2.4.2, one places occupied orbitals in RAS I and virtual active space

Figure 15: Two formulations of the SOCI wavefunction within the RAS CI method.

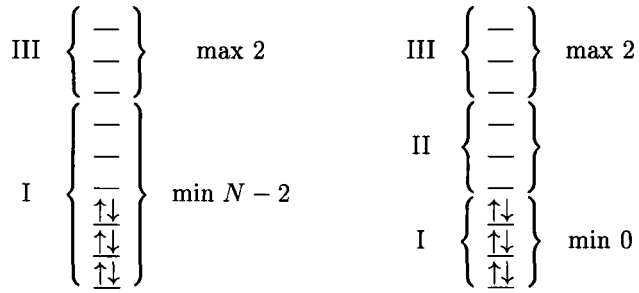

orbitals in RAS II. A maximum of two electrons are allowed in RAS III, and a minimum of $N-4$ electrons are required in RAS I (cf. Figure 16). Some possibilities of extending the RAS selection scheme are discussed in section 4.8.3.

Figure 16: Formulation of the CISD[TQ] wavefunction within the RAS method.

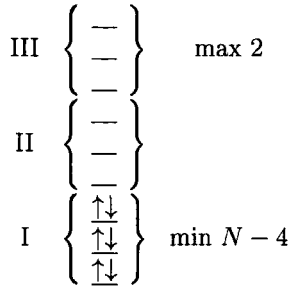

The RAS CI algorithm of Olsen *et al.*[46] relies on Handy's separation of determinants into alpha and beta strings (cf. section 4.2). As in other determinant-based CI methods, the determinants are restricted to those having a given value of M_s. Since the number of electrons N is also fixed, this means that the alpha and beta strings always have constant lengths of N_α and N_β, respectively. For a full CI, one forms all possible alpha and beta strings for a given N_α and N_β,

and the determinants employed are all possible combinations of these alpha and beta strings. In a RAS CI wavefunction, the CI space is restricted in two ways: first, not all alpha and beta strings are allowed, and secondly, not all combinations of alpha and beta strings to form determinants are accepted. This is best understood from an example: consider the case of 6 orbitals, with $N_\alpha = N_\beta = 3$. If orbitals 4, 5, and 6 constitute RAS III, with a maximum of 2 electrons allowed, then clearly alpha strings such as $a^\dagger_{4\alpha}a^\dagger_{5\alpha}a^\dagger_{6\alpha}$ are not allowed. Similarly, even though $a^\dagger_{1\alpha}a^\dagger_{4\alpha}a^\dagger_{5\alpha}$ and $a^\dagger_{1\beta}a^\dagger_{4\beta}a^\dagger_{5\beta}$ are allowed alpha and beta strings, these strings cannot be combined with each other because the resulting determinant would place four electrons in RAS III.

If the CI coefficient vector is viewed as a matrix, $c(I_\alpha, I_\beta)$, then these restrictions, as well as those due to point-group symmetry, can be implemented by allowing only certain blocks of c to be nonzero. If strings with the same irreducible representation are numbered consecutively, then only those blocks of the CI coefficient matrix with the correct overall symmetry (determined as the direct product of the alpha and beta string irreducible representations) are allowed to be nonzero. For the RAS restrictions, it is convenient to assign a particular code to each alpha and beta string which represents the distribution of electrons among the RAS orbital subspaces. This means that the allowed combinations of strings may be determined directly from their respective codes. In Olsen's nomenclature,[46] these codes correspond to different string graphs; string representation and addressing is discussed further in section 4.9. If strings with a given code (or within a given graph) are numbered consecutively, then the allowed combinations of strings become allowed subblocks of the symmetry blocks in the CI coefficient matrix. These are referred to henceforth as the RAS subblocks. For a full CI, one can group all strings belonging to the same irreducible representation in the same graph, so that the RAS subblocks are the same as the symmetry blocks.

4.8.1 RAS CI σ Equations

The products of shift operators in equations (113) and (114) mean that some alpha/beta strings can contribute to the σ vector even if they are not necessary to describe the CI space. Therefore the string lists must include all valid strings and all the singly substituted strings derived from them. For a full CI, all possible strings for a given number of alpha/beta electrons are allowed, so all singly substituted strings are automatically present. For a restricted CI, however, including all singly substituted strings is an inefficient procedure.

Olsen *et al.* showed[46] how to eliminate the contributions from these "out-of-space" strings for the case of a RAS CI wavefunction. Since the equation for σ_3 (115) contains no products of shift operators, only σ_1 and σ_2 can contain

contributions from out-of-space strings. Moreover, since σ_2 is analogous to σ_1 (and can be derived from it for $M_s = 0$ cases), it is sufficient to focus on σ_1. Olsen's approach is to change the sum over i, j, k, l into a restricted sum, $(ij) \geq (kl)$, where (ij) and (kl) are canonical indices defined as

$$(ij) = in + j, \tag{139}$$

if there are n orbitals and the numbering starts from zero. Consider the term

$$\sum_{J_\beta} \sum_{(ij)\geq(kl)} \langle \beta(J_\beta)|\hat{E}^\beta_{ij}\hat{E}^\beta_{kl}|\beta(I_\beta)\rangle (ij|kl)c(I_\alpha, J_\beta). \tag{140}$$

An out-of-space string K_β can only contribute if it is produced by $\hat{E}^\beta_{kl}|\beta(I_\beta)\rangle$, and if $\hat{E}^\beta_{ij}$ transforms it back into an allowed string (J_β). But if the orbitals are numbered consecutively within each RAS space, and if equation (139) is used to define the canonical index (ij), such contributions are impossible. For example, consider the case where a maximum of two electrons are allowed in RAS III. If string I_β already contains two electrons in RAS III, then a single replacement $\hat{E}^\beta_{kl}|\beta(I_\beta)\rangle$ which promotes a third electron to RAS III will yield an out-of-space string. The shift operator $\hat{E}^\beta_{ij}$ could produce an allowed string again if it moves any of the three electrons in RAS III back down into RAS I or RAS II. However, if the summation over orbitals is restricted to $(ij) \geq (kl)$, this is impossible, since $k > i$.

Using the commutation relationship

$$\left[\hat{E}^\beta_{ij}, \hat{E}^\beta_{kl}\right] = \delta_{kj}\hat{E}^\beta_{il} - \delta_{il}\hat{E}^\beta_{kj}, \tag{141}$$

one can rewrite (113) to employ this restriction. The result[46] is:

$$\begin{aligned} \sigma_1(I_\alpha, I_\beta) &= \sum_{J_\beta}\sum_{kl}\langle \beta(J_\beta)|\hat{E}^\beta_{kl}|\beta(I_\beta)\rangle g_{kl}c(I_\alpha, J_\beta) \\ &+ \sum_{J_\beta} \sum_{(ij)\geq(kl)} \langle \beta(J_\beta)|\hat{E}^\beta_{ij}\hat{E}^\beta_{kl}|\beta(I_\beta)\rangle (ij|kl)c(I_\alpha, J_\beta)(1+\delta_{(ij),(kl)})^{-1}, \end{aligned} \tag{142}$$

where g is an asymmetric matrix defined as

$$g_{kl} = \begin{cases} h_{kl} - \sum_{j<k}(kj|jl) - (kk|kl)(1+\delta_{kl})^{-1} & k \geq l \\ h_{kl} - \sum_{j<k}(kj|jl) & k < l. \end{cases} \tag{143}$$

4.8.2 Algorithms for Computing σ

The full CI algorithms must be modified to treat the more general RAS case. Most significantly, the σ_1 and σ_2 equations for RAS CI spaces differ from

the full CI equations: (142) requires that the summation over orbitals obey $(ij) \geq (kl)$ (recall that introducing this restriction into the full CI algorithm is one way to reduce effort when $M_s = 0$). The other required modification is that the innermost loops must sum over allowed combinations of alpha and beta strings only. For instance, the loop over I_α near the end of the σ_1 algorithm in Figure 7 must be split into two loops: one over alpha string graphs, and another over strings within each graph. This allows for the sum over J_β to run over only those beta strings which are allowed to combine with strings from the current alpha string graph. Similar modifications must be made to the σ_2 and σ_3 algorithms.

It is perhaps not entirely obvious what is the most efficient way to adapt Olsen's algorithms to account for point group symmetry and RAS restrictions. Although it is a relatively simple matter to introduce a loop over graphs in the multiplication of F by c or c', it is also necessary to introduce loops over graphs in earlier parts of the algorithm; otherwise, F can contain irrelevant entries. When the CI vector is processed a symmetry block at a time or a RAS subblock at a time, it seems best to place these loops over graphs within the σ_1, σ_2, and σ_3 routines. However, when the CI vector is processed a RAS subblock at a time, these loops over graphs may be placed outside the σ subroutines. Further details are presented in section 4.9.

4.8.3 Beyond RAS: More Flexible *a priori* CI Space Selection

Although many useful CI spaces can be obtained in the RAS CI method, it may nevertheless be beneficial to employ more complex CI spaces. Olsen has begun to investigate CI spaces formed as the union of two RAS spaces,[80] while we have considered the addition of another orbital subspace.[18] As first pointed out by Grev and Schaefer,[16] the most weakly occupied CISD natural orbitals contribute almost exclusively to singly and doubly substituted configurations, rather than to triples, quadruples, etc. This suggests the utility of extending the RAS method to include another orbital subspace, formed from the most weakly occupied natural orbitals. Labeling this new orbital set as "RAS IV" may be somewhat misleading, in the sense that the orbital index restriction $(ij) \geq (kl)$ is no longer sufficient to remove out-of-space contributions from (142): we have alternatively referred to this new orbital set as the "tertiary virtual subspace".[18]

Let us assume that the occupied orbitals are collected in RAS I, and that if an electron occupies RAS IV, the determinant must represent a single or double substitution of the reference determinant. Out-of-space contributions arise if one electron occupies RAS IV and another electron occupies RAS II or RAS III: such strings are allowed, but the promotion of another electron

from RAS I results in a disallowed string $|\beta(K_\beta)\rangle = \hat{E}^\beta_{kl}|\beta(I_\beta)\rangle$. Application of the other shift operator in the σ_1 equation, $\hat{E}^\beta_{ij}$, can result in an allowed string $|\beta(J_\beta)\rangle$ with $(ij) \geq (kl)$ if the electron in RAS IV is moved into one of the lower RAS subspaces, as long as it occupies an orbital $i > k$. Thus it is necessary to include in the string space all allowed strings, plus the disallowed strings which have one electron in RAS IV and two electrons in (RAS II + RAS III). Once these strings are included, the RAS σ equations can be used for σ_1 and σ_2. As in the standard RAS method, no out-of-space strings can contribute to σ_3. By definition, the out-of-space strings are not allowed to combine with other strings to form RAS subblocks of the c or σ matrices. Alternatively, in some cases these out-of-space contributions might be dealt with by employing the $(N-2)$-electron reduced space of Zarrabian *et al.*[47,217] (cf. section 4.5).

4.9 Implementation of Determinant-Based Algorithms

In this section we discuss some of the practical issues relevant to the actual implementation of the determinant-based CI algorithms. We also describe our experience with our own fully direct CI program, DETCI, which is capable of evaluating any CI wavefunction which can be formulated as a RAS CI, subject to memory and disk limitations. This program is based in part on the alpha and beta string formalism of Handy[44] and the algorithms of Olsen *et al.*[46,83] It has been modified to allow more complex CI spaces, as described in sections 4.8.3 and 5.4.

Our program requires at least two memory buffers for CI vectors, where a buffer can be either the length of the entire vector, or a spatial symmetry block, or a RAS subblock. Using the fastest algorithm, the program also requires a smaller memory buffer to hold a portion of the CI coefficients in a given RAS subblock. An additional buffer the size of the largest RAS subblock may also be required for taking transposes of the c subblocks if $M_s = 0$ symmetry is employed (this is determined by the core memory option, and if possible the same buffer is used for transposes and gathered CI coefficients). For diagonalizing the Hamiltonian, we have implemented many of the iterative methods described in section 3.2.

4.9.1 Graphical Representation of Alpha and Beta Strings

As discussed in the previous section, it is necessary to have a method for numbering the alpha and beta strings and a reasonable way of grouping these strings together so that allowed combinations of strings can be determined a group at a time. Olsen *et al.* use a graphical method to compute string addresses, and they group strings together by placing them on the same graph.[46]

We have employed a similar method.

The present approach is based on the work of Duch, who has described[230] the graphical representation of CI spaces in considerable detail. First, we consider the simple two-slope directed graphs ("digraphs") which represent alpha or beta strings without consideration of point group symmetry. Figure 17 presents a digraph representing all strings with five electrons in seven orbitals. Each string is represented by a "walk" on the graph, from the head (at $e = o = 0$) to the tail (at $e = N_{\alpha/\beta}$, $o = n$). Moving straight down from vertex (e, o) to vertex $(e, o+1)$ indicates that orbital $o+1$ is unoccupied in the current string, while moving down diagonally from vertex (e, o) to vertex $(e+1, o+1)$ indicates that orbital $o+1$ is occupied. Each vertex on the graph is assigned a weight $x(e, o)$, and each arc connecting two vertices is assigned an arc weight $Y(e, o)$ for the arc leaving vertex (e, o). Since, in general, two different arcs can leave a given vertex, we write $Y_0(e, o)$ for the arc originating from vertex (e, o) which leaves orbital $o+1$ unoccupied, and $Y_1(e, o)$ for the arc which occupies orbital $o+1$.[‡] The index or address of a string or walk is obtained by adding weights for each arc contained in the walk, i.e.,

$$I_\alpha(L^\alpha) = X(L^\alpha) + \sum_{i=0}^{n} Y_{L_i}(e_i, i), \tag{144}$$

where L_i is the occupation (0 or 1) of the ith arc, and (e_i, i) are the coordinates of the vertices crossed by L^α. The term $X(L^\alpha)$ gives the offset of a given graph, if more than one graph is employed. The relative index for a determinant in a block may be given by $I(L^\alpha, L^\beta) = I_\alpha(L^\alpha)S_\beta + I_\beta(L^\beta)$, where S_β is the number of beta strings in the block.

There are several different methods for assigning the arc weights by which one evaluates the index of a string according to equation (144). Under the *lexical ordering* scheme, the tail (N_α, n) of an alpha string graph is assigned a weight $x = 1$. Other vertex weights are computed according to the recursive formula

$$x(e, o) = x(e+1, o+1) + x(e, o+1). \tag{145}$$

Using lexical ordering, typically all arc weights $Y_0(e, o)$ are set equal to zero, and the arc weights $Y_1(e, o)$ are determined according to

$$Y_1(e, o) = x(e+1, o+1) + x(e+1, o) + \cdots + x(e+1, e+1). \tag{146}$$

Figure 17a features vertex and arc weights computed in this manner. A result of the lexical ordering scheme is that paths with a fixed upper part and an

[‡]This differs somewhat from Duch,[230] who sometimes uses $\bar{Y}(e, o)$ to denote the arc *entering* vertex (e, o) in reverse-lexical addressing.

Figure 17: Alpha string graph for $n_\alpha = 5, n = 7$. Vertex weights are determined according to lexical ordering, and arc weights are given so that the rightmost path has index zero. (a) All unoccupied arc weights $Y_0(e, o)$ are zero. (b) All occupied arc weights $Y_1(e, o)$ are zero.

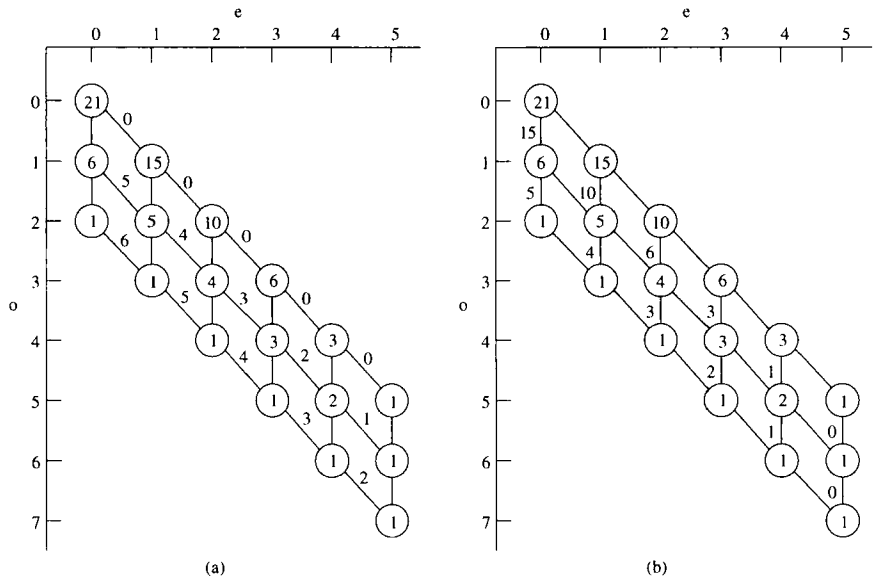

arbitrary lower part have consecutive indices. The particular choice of Y values above is appropriate if the rightmost path is to have an index of zero. The same effects can be achieved using

$$Y_1(e,o) = 0 \tag{147}$$
$$Y_0(e,o) = x(e+1,o+1), \tag{148}$$

as illustrated in Figure 17b. Any walk has the same index in Figures 17a and 17b. For instance, the walk $a^\dagger_{2\alpha}a^\dagger_{3\alpha}a^\dagger_{4\alpha}a^\dagger_{5\alpha}a^\dagger_{7\alpha}$ has an index of 5+4+3+2+2 = 16 (equation 144) from Figure 17a, and an index of $15+1=16$ from Figure 17b.

In the so-called "reverse-lexical" ordering scheme, all upper paths for a fixed lower path have consecutive indices. Vertex weights are now determined as

$$\bar{x}(e,o) = \bar{x}(e,o-1) + \bar{x}(e-1,o-1), \tag{149}$$

where the overbar indicates reversed-lexical ordering. Figure 18a depicts a reversed-lexical graph with all non-occupied orbital arcs set to zero. The occupied orbital arcs are computed as

$$\bar{Y}_1(e,o) = \bar{x}(e+1,o). \tag{150}$$

Figure 18b is the same except that now all occupied arcs have weights of zero. The non-occupied arc weights are

$$\bar{Y}_0(e,o) = \bar{x}(e,o) + \bar{x}(e+1,o+1) + \cdots + \bar{x}(N-1,o+N-e-1). \tag{151}$$

Note that string indices for reverse-lexical ordering are not necessarily the same as indices for lexical ordering. For the string $a^\dagger_{2\alpha}a^\dagger_{3\alpha}a^\dagger_{4\alpha}a^\dagger_{5\alpha}a^\dagger_{7\alpha}$ considered previously, the index is calculated as $1+1+1+1+6=10$ from Figure 18a, or as $5+5=10$ from Figure 18b.

The arc weights given in Figures 17 and 18 cause the rightmost path to have an index $I(R_m)=0$. If we change the arc weights so that the leftmost path has index $I(L_m)=0$, we obtain four more addressing schemes. The two simplest schemes for $I(L_m)=0$ are

$$Y_0(e,o)=0 \quad Y_1(e,o)=x(e,o+1) \tag{152}$$
$$\bar{Y}_1(e,o)=0 \quad \bar{Y}_0(e,o)=\bar{x}(e-1,o) \tag{153}$$

where the overbars indicate that reversed-lexical vertex weights have been used. Alpha strings for 5 electrons in 7 orbitals employing these addressing schemes are depicted in Figure 19.

If we add another coordinate Γ to each vertex, we can extend these simple digraphs to include point group symmetry. However, this procedure is not

Figure 18: Alpha string graph for $n_\alpha = 5, n = 7$. Vertex weights are determined according to reverse-lexical ordering, and arc weights are given so that the rightmost path has index zero. (a) All unoccupied arc weights $Y_0(e, o)$ are zero. (b) Occupied arc weights $Y_1(e, o)$ are set to zero.

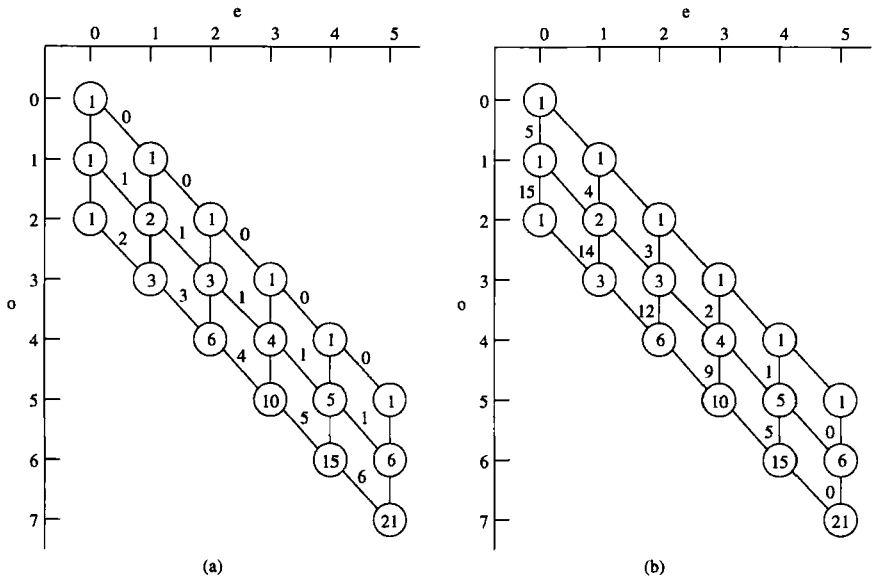

Figure 19: Alpha string graph for $n_\alpha = 5, n = 7$, with arc weights determined so that the leftmost path has index zero. (a) Vertex weights for lexical ordering, and arc weights according to $Y_0(e,o) = 0$, $Y_1(e,o) = x(e,o+1)$. (b) Vertex weights according to reverse-lexical ordering, and arc weights according to $\bar{Y}_1(e,o) = 0$, $\bar{Y}_0(e,o) = \bar{x}(e-1,o)$.

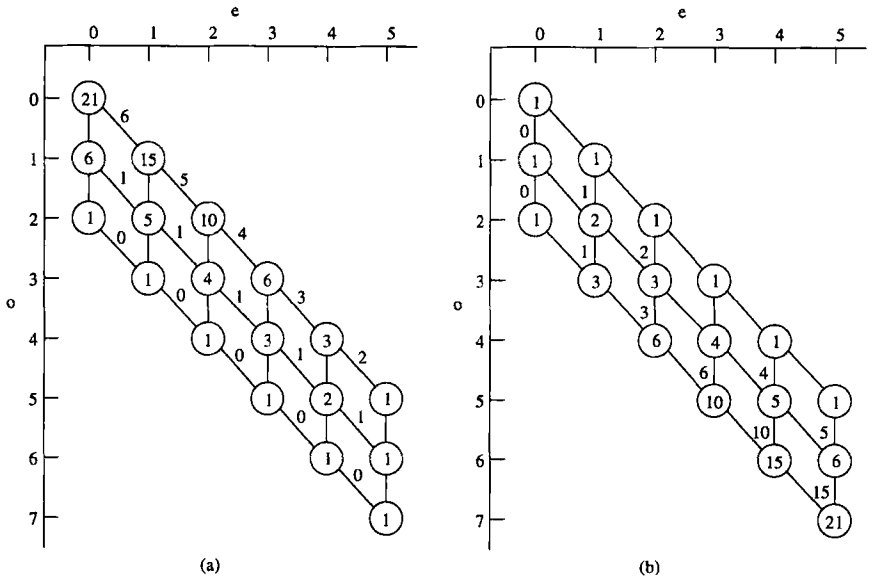

really necessary as long as strings with different irreps are placed on different graphs. These two-slope digraphs are actually simpler versions of the four-slope digraphs first used by Shavitt to compute the addresses of configuration state functions (CSFs) in the graphical unitary group approach.[41] The indexing scheme used by DETCI is the reverse-lexical ordering with all unoccupied arc weights set to zero, as depicted in Figure 18a. Olsen *et al.*[46] use the lexical ordering of Figure 17a.

In order to make the CI coefficient matrix block diagonal according to irreducible representation, it is necessary to number the strings consecutively within each irrep. This is accomplished by grouping strings with the same irrep into the same graph. For RAS CI spaces, it is also useful to number the strings such that only certain subblocks of each symmetry block are nonzero. This is accomplished by forming a different string graph for each different distribution of electrons among the RAS subspaces; for example, all strings with irrep a_1 having four electrons in RAS I and two electrons in RAS III are grouped together, whereas strings with irrep a_1 but five electrons in RAS I and one electron in RAS III are grouped together in a separate graph. In this way, the allowed combinations of strings become allowed combinations of graphs, and each allowed pair of alpha and beta graphs becomes a RAS subblock.

4.9.2 Nongraphical Methods for String Addressing

In their full CI program, Bendazzoli and Evangelisti[48,49] dispense with the graphs entirely and compute string addresses directly from their bit patterns, with one bit for each orbital; set bits (ones) represent occupied orbitals. Strings of N_α ones and $n-N_\alpha$ zeroes are a common representation of the combinations of n objects taken N_α at a time, and there exist standard numerical methods of computing lexical addresses for such bit patterns.[231]

Knowles and Handy present an explicit formula for computing a string's address from a list of its occupied orbitals.[109] They employ an auxiliary array defined according to

$$\begin{aligned} Z(k,l) &= \sum_{m=n-l}^{n-k-1} \left[\binom{m}{N-k-1} - \binom{m-1}{N-k-2} \right] \\ & \quad n-N+k \geq l \geq k; k < N-1 \\ Z(k,l) &= l+1-N \quad n \geq l \geq N; k = N-1 \end{aligned} \tag{154}$$

where k labels electrons, l labels orbitals, n is the number of orbitals, and N is the number of electrons (we have modified the equation so that electron and orbital numbering starts from zero). The address of a string is then computed

according to:

$$I_\alpha = \sum_{i=0}^{N_\alpha - 1} Z(i, \phi_i). \tag{155}$$

Unfortunately, generalizing this formula to assign consecutive indices to strings with the same irrep becomes complicated. Bendazzoli *et al.* note that, since their strings are generated in the desired order, they can write the string's address to intermediate arrays and thus obviate the need to compute string addresses on-the-fly. Such considerations are also true of Olsen's program and of ours. However, storing all strings with their single replacement information can require a very large amount of memory, as discussed in section 4.9.4. In this case, it becomes useful to compute string addresses on-the-fly as rapidly as possible.

If only occupied orbitals are assigned arc weights in the graphical procedure, it is possible to obtain an equation similar to (155), but using the graphical numbering scheme instead of the Knowles-Handy numbering. This is easily seen by comparing equation (155) to equation (144) when only occupied arcs have nonzero weights:

$$I_\alpha(L^\alpha) = X(L^\alpha) + \sum_{i=0}^{N_\alpha - 1} Y(i, \phi_i). \tag{156}$$

This method of evaluation can be very efficient if the matrix Y (with dimension $N_\alpha \times n$) is stored for each of the string graphs. The memory requirement for this approach will generally be manageable, and far preferable to storing the string replacement lists or Bendazzoli and Evangelisti's OV and $OOVV$ lists.[48,49] In the worst case, each excited string would then require N_α matrix lookups and $(N_\alpha - 1)$ additions to determine its address. However, note that a single excitation changes the occupancy of perhaps one and at most two RAS subspaces. It can be seen from eq. (156) that the contribution of unchanged RAS spaces to the string address are *constant* and need only be computed once. Graphically, this means that certain RAS spaces are traversed by the same segment of a walk. Finally, unless fast access to the arc weights is required, it is preferable to keep the arc weights and other graph information in a compact form which stores only allowed vertices.

4.9.3 Example of CI Vector and String Addressing

This section applies the CI vector and string addressing methods just discussed to the specific case of a CISD for H_2O in a minimal basis. Assume that the calculation is performed in C_{2v} symmetry, and that the core orbital has been frozen. The orbitals are then ordered according to Figure 20. Note that the

Figure 20: Orbital ordering for minimum basis CISD H_2O in C_{2v} symmetry.

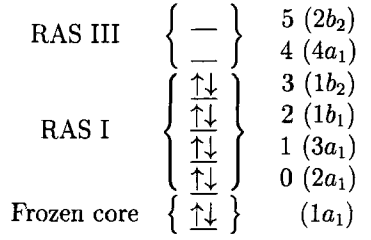

Table 6: Allowed strings for minimum basis CISD H_2O in C_{2v} symmetry.

Graph	Γ	N_{III}	Strings
0	a_1	1	(0 1 3 5)
1	a_1	2	(0 3 4 5), (1 3 4 5)
2	a_2	0	(0 1 2 3)
3	a_2	1	(0 2 3 4), (1 2 3 4), (0 1 2 5)
4	a_2	2	(0 2 4 5), (1 2 4 5)
5	b_1	1	(0 1 2 4), (0 2 3 5), (1 2 3 5)
6	b_1	2	(2 3 4 5)
7	b_2	1	(0 1 3 4)
8	b_2	2	(0 1 4 5)

frozen core orbital is not assigned a number by DETCI because the frozen core electrons are treated implicitly (cf. section 2.4.7).

The distribution of electrons among RAS subspaces can be determined simply from the number of electrons in RAS III, since there are only two RAS subspaces in this particular example. For a given string, there can be 0, 1, or 2 electrons in RAS III, and since there are four irreps in C_{2v}, there can be up to twelve string graphs. For this closed-shell case, the same set of graphs can be used to represent both alpha and beta strings. Table 6 lists all 15 allowed strings. Note that some strings transform as a_2 even though there are no a_2 orbitals; as a general rule for larger cases, strings are almost evenly distributed among irreps. The strings in Table 6 are listed in increasing index order. For the few graphs containing more than one string, it is straightforward to verify using the techniques of section 4.9.1 that the relative addresses within the graph are in the order shown if reverse-lexical ordering is used.

Table 7: Single replacement list for the first string in minimum basis CISD H_2O. J^g is the graph of the target string and J is the target string's relative index.

i	j	J^g	J	Sgn
0	0	0	0	+
1	1	0	0	+
3	3	0	0	+
5	5	0	0	+
4	0	1	1	+
4	1	1	0	−
2	5	2	0	−
2	3	3	2	+
2	0	5	2	−
2	1	5	1	+
4	5	7	0	+
4	3	8	0	+

As discussed later in section 4.9.4, it is necessary to compute lists of all singly excitations from each string. These excitations can be written in the form $|\alpha(J_\alpha)\rangle = \mathrm{sgn}(ij)\hat{E}^\alpha_{ij}|\alpha(I_\alpha)\rangle$, and for each string I_α, the lists need to contain the address of J_α, the sign, and the pair of orbitals ij. The string replacement lists for string 0 are given in Table 7.

Finally, it is helpful to show how this string ordering determines the addressing of the CI vector. There are two restrictions on the pairing of alpha strings with beta strings: first, the direct product of the two string irreps must be the irrep of the electronic state of interest (a_1); second, the total number of electrons in RAS III must be two or less. Due to the arrangement of the graphs, these restrictions can be satisfied for pairs of graphs rather than for pairs of strings. Each allowed pair of graphs becomes a RAS subblock. Table 8 lists the allowed RAS subblocks. An interesting feature of this unusually small CI space is that not all allowed strings contribute to allowed determinants: there are no beta strings which can be combined with alpha strings from graphs 1, 6, or 8 which give allowed determinants.

4.9.4 String Replacement Lists

One of the first steps in implementing Olsen's algorithm is the construction of string lists which hold the information needed to generate all single replace-

Table 8: Allowed RAS subblocks for minimum basis CISD H_2O.

Block	α Graph	β Graph	Dets
0	0	0	1
1	2	2	1
2	2	3	3
3	2	4	2
4	3	2	3
5	3	3	9
6	4	2	2
7	5	5	9
8	7	7	1

ments for each string; for example, $|\beta(J_\beta)\rangle = \mathrm{sgn}(ij)\hat{E}^\beta_{ij}|\beta(I_\beta)\rangle$ in Figure 9. For each excited string, one needs i, j, (or a composite index ij), the string address J_β, and $\mathrm{sgn}(ij)$, which tells whether $\hat{E}^\beta_{ij}$ sends $\beta(I_\beta)$ into plus or minus $\beta(J_\beta)$. The sign is most easily derived using the rules of second quantization, recalling that the phase convention is defined by always listing alpha/beta strings according to increasing orbital number (cf. section 4.2). Note that the equations require the inclusion of operators $\hat{E}_{ii}$, which might not normally be considered "single substitutions."

In the innermost loop of Olsen's σ_3 algorithm, $V(I) = \sum_{J_\beta} F(J_\beta)c'(I, J_\beta)$, the summation should be restricted to only allowed pairs of strings (I, J_β). If loops over graphs are introduced, then one loops over J_α belonging to a given alpha string graph (J^g_α) and J_β belonging to a given beta string graph (J^g_β), where (J^g_α,J^g_β) is an allowed combination of graphs. Now the problem of summing over all substituted strings becomes one of summing over all substituted strings belonging to a given graph. Thus DETCI divides the list of single replacements into multiple lists, one for each target graph. A counter array is used to store how many singly substituted strings there are for each graph. For a large number of graphs (there can be several hundred), this method of storage can be very memory intensive, since the number of pointers for each string is proportional to the number of graphs; however, this method also provides very fast access to the relevant replacement information in the innermost loops.

It is important to point out that the string lists can become very large if there are more than a few thousand strings. For a full CI, the number of strings is approximately equal to the square root of the number of determinants, so quite large full CI spaces can be described using only a small number of strings.

Table 9: Number of strings and determinants for selected CI problems.

CI problem	Fzc	Strings	Dets	Str/Det
cc-pVDZ+ Ne full CI[a]	0	8 568	9 185 280	9.3×10^{-4}
DZ H_2O full CI	0	2 002	1 002 708	2.0×10^{-3}
DZ H_2O full CI	1	715	128 829	5.5×10^{-3}
DZP H_2O CISDTQ	1	10 626	558 823	1.9×10^{-2}
DZP H_2O CISD[TQ][b]	1	4 326	78 895	5.5×10^{-2}
DZP H_2O CISDT	1	5 781	50 187	1.2×10^{-1}
DZP H_2O CISD	1	1 221	2 349	5.2×10^{-1}

[a]Using the basis set of Koch *et al.*[7]

[b]The RAS II space consists of the $2b_2$,$4a_1$,$2b_1$, and $5a_1$ orbitals.

However, it is perhaps not well appreciated that for RAS CI spaces, the number of strings can grow much faster with the number of determinants: this is illustrated in Table 9. Such considerations indicate that any method of storing the string replacement lists whose memory requirements are proportional to the number of strings (with a large coefficient, no less) is unmanageable for large-scale RAS CI procedures.

If the number of determinants remains much larger than the number of strings for a given case, one might consider storing the string lists to disk and loading them as needed. Indeed, such an approach would probably work in conjunction with the σ_3 algorithm. However, this strategy is not amenable to the σ_1 algorithm as implemented by Olsen *et al.*,[46] because one must consider single replacements from *all* graphs which can be reached from the graph containing the strings I_β. It seems preferable to form the string replacement information on-the-fly. A prototype method for doing this exists in DETCI, but it is inefficient: walking down graphs to add up arc weights is rather slow with our current storage scheme for the graphs. However, if the arc weights are stored in a slightly different format, it is possible to compute string addresses much more quickly; indeed, it is possible to compute addresses a RAS space at a time, meaning that arc weight contributions from RAS spaces with fixed orbital occupancies are constant. This strategy was discussed in section 4.9.2 and is currently being implemented in DETCI. Another option is to use an entirely different implementation for restricted CI where storage of string replacement information becomes a problem. Malmqvist *et al.*[56] have implemented RAS CI using a split-graph unitary group approach, and this algorithm may be more efficient for CI spaces which are not close to the full CI.

4.9.5 Algorithms for σ_2 and σ_3 Used by DETCI

Assuming that the string replacement lists are available in-core, the algorithms used by our program for computing σ_2 and σ_3 (simplified somewhat for clarity) are presented in Figures 21 and 22 for the case in which σ is computed a RAS subblock at a time, where the loops over combinations of strings allowed by symmetry and CI space restrictions are placed outside the σ_2 and σ_3 subroutines. The symbol γ in Fig. 22 represents an irreducible representation of the molecular point group. These are the same algorithms used by our program for full CI; if enough memory is available to hold a symmetry block of $\mathbf{c}$ and σ in core, then the RAS subblocks are the same as the symmetry blocks for a full CI. Otherwise, one can use a larger number of string graphs and smaller subblocks. For $M_s = 0$ cases, it is possible to compute only the lower (or upper) triangle of σ, according to (119). Thus only one of each pair of off-diagonal subblocks is determined explicitly. For diagonal blocks, (119) is used to impose the restriction $(ij) \geq (kl)$ in the evaluation of σ_3 (cf. section 4.4.2). In FORTRAN, presumably it is best to eliminate redundant subblocks from the upper triangle, since blocks with only a few rows will typically be found in the upper triangle (assuming that larger indices are assigned to strings with more electrons in RAS III): these blocks do not vectorize well due to short vector lengths. In C, exactly the opposite holds: it is presumably most efficient to eliminate the lower triangle subblocks. However, it is also true that longer vector lengths require more time to set up the lists L, R, and Sgn.

The signs are actually taken care of by very fast bitwise logic operations. σ_2 is computed instead of σ_1 because the preferred direction of vectorization is reversed in c as compared to FORTRAN. In the present context, this means that the step $[\sigma_2(I_\alpha, I_\beta) = \sigma_2(I_\alpha, I_\beta) + F(J_\alpha) * c(J_\alpha, I_\beta)]$ is performed with unit-stride access to σ_2 and c. Note that this is in fact a DAXPY operation, which could be performed by calling the **daxpy** function from the BLAS library. For the IBM RS/6000 POWER2 implementation, calling the BLAS library from the σ_2 or σ_3 routines resulted in no real savings. In fact, this slowed down the σ_3 subroutine, presumably due to the overhead of placing the function call within nested loops.

Note that the σ_2 routine is actually quite close to Olsen's σ_1 routine (swapping alphas for betas, of course), except that the adaptation to point group symmetry and RAS restrictions is now explicit. The σ_3 routine is also similar to Olsen's (with alphas swapped for betas), although the intermediate vector F has been eliminated (see below). Note that this particular version of the σ_3 routine takes advantage of the $(ij) \geq (kl)$ simplification possible for $M_s = 0$ cases; this restriction cannot be used for off-diagonal RAS subblocks if only unique subblocks of σ are computed.

Figure 21: DETCI algorithm for σ_2.

Enter subroutine for block (I_α^g, I_β^g) of σ_2 and block (J_α^g, I_β^g) of c
 loop $I_\alpha = 1$, number of strings in I_α graph I_α^g
  zero $F(J_\beta)$
  loop over alpha string graphs K_α^g
   $Kcnt = cnt(I_\alpha, K_\alpha^g)$
   $Kidx = idx(I_\alpha, K_\alpha^g)$
   $Kij = ij(I_\alpha, K_\alpha^g)$
   loop $K = 1, Kcnt$
    $kl = Kij(K)$
    $K_\alpha = Kidx(K)$
    $S_1 =$ sign associated with K_α
    if $(K_\alpha^g = J_\alpha^g)$
     $F(K_\alpha) = F(K_\alpha) + S_1 * h(kl)$
    $Jcnt = cnt(K_\alpha, J_\alpha^g)$
    $Jidx = idx(K_\alpha, J_\alpha^g)$
    $Jij = ij(K_\alpha, J_\alpha^g)$
    loop $J = 1, Jcnt$
     $J_\alpha = Jidx(J)$
     $S_2 =$ (sign associated with J_α) $* S_1$
     $ij = Jij(J)$
     $F(J_\alpha) = F(J_\alpha) + 0.5 * (ij|kl) * S_2$
    end loop over J
   end loop over K
  end loop over K_α^g
  loop $J_\alpha = 1$, number of alpha strings in J_α^g
   if $(F(J_\alpha) = 0)$ skip to next J_α
   loop $I_\beta = 1$, number of beta strings in I_β graph I_β^g
    $\sigma_2(I_\alpha, I_\beta) = \sigma_2(I_\alpha, I_\beta) + F(J_\alpha) * c(J_\alpha, I_\beta)$
   end loop over I_β
  end loop over J_α
 end loop over I_α

Figure 22: DETCI algorithm for σ_3.

Enter subroutine for block (I_α^g, I_β^g) of σ_3 and block (J_α^g, J_β^g) of c
loop over ij
if $(\gamma(i) \otimes \gamma(j) \otimes \gamma(J_\beta^g) \otimes \gamma(I_\beta^g) \neq 0)$ skip to next ij
$jlen$ = form_list$(I_\beta^g, J_\beta^g, ij, L, R, Sgn)$
if $(jlen = 0)$ skip to next ij
loop $I_\alpha = 1$, number of alpha strings in I_α^g
loop $J = 1, jlen$
$c'(I_\alpha, J) = c(I_\alpha, L(J)) * Sgn(J)$
end loop over J
end loop over I_α

loop $I_\alpha = 1$, number of strings in graph I_α^g
$Jacnt = cnt(I_\alpha, J_\alpha^g)$
$Jaidx = idx(I_\alpha, J_\alpha^g)$
$Jaij = ij(I_\alpha, J_\alpha^g)$
zero V
loop $Ja = 1, Jacnt$ AND $((kl = Jaij(Ja)) <= ij)$
$J_\alpha = Jaidx(Ja)$
S_1 =sign associated with J_α
$VS = 0.5 * \delta_{ij,kl} * (ij|kl) * S_1$
loop $Jb = 1, jlen$
$V(Jb) = V(Jb) + VS * c'(J_\alpha, Jb)$
end loop over Jb
end loop over Ja

loop $Jb = 1, jlen$
$\sigma_3(I_\alpha, R(Jb)) = \sigma_3(I_\alpha, R(Jb)) + V(Jb)$
end loop over Jb
end loop over I_α
end loop over ij

The figures clearly indicate that an efficient algorithm should take advantage of the sparsity of F in both the σ_2 and σ_3 routines. Although it is possible to ignore this sparsity in order to obtain more highly vectorized algorithms, this results in a slower code due to the large number of multiplications by zero. Attempts to formulate the σ_3 algorithm as a standard matrix multiplication resulted in a program which was slower by a factor of at least four (and usually more) on the IBM RS/6000 model 3CT. The reader may wonder whether further reductions in the overall operation count might increase efficiency: after all, formulating the innermost loop as a DAXPY requires a certain amount of overhead work (namely, the gather and scatter operations). Indeed, a very simple algorithm which performs the minimum number of operations has already been presented in Fig. 8. However, there are a number of reasons to think that this algorithm should be less efficient than that in Figure 22 for workstation computers. One reason is that indirect addressing in the innermost loop causes cache misses and thus longer waits for elements of c. Another is that the simple algorithm takes no advantage of the pipelining features of current workstations, discussed in section 4.3. For DZ H_2O full CI (1 million determinants), using the algorithm in Fig. 22 instead of the simple algorithm in Fig. 8 results in a speedup by a factor of five on the IBM 3CT. However, it is also important to point out that the smaller block sizes in a RAS CI (as opposed to a full CI) mean that the payoff for vectorization is less.

A few remaining comments should be made about our σ_3 algorithm in Fig. 22. First, note that the intermediate vector F has been eliminated. Storage to and retrieval from this array requires several extra operations, yet the efficiency of the DAXPY operation is not enhanced by the use of F, since F is sparse (the only work saved is for excitations which map a string into itself). Second, writing the innermost loop of this routine (and also of the σ_1 routine) as a DAXPY is particularly efficient on the RS/6000 architecture, which performs each pair of floating point multiplications and additions in the *same* machine instruction, the floating point multiply-add (FMA).

In order to gauge the efficiency of our new determinant-based CI program, several timing comparisons have been made between DETCI and the standard Schaefer group CI program GUGACI. Table 10 presents averaged CPU and total times for several full CI test cases. Both programs used the standard Davidson method, keeping on disk the c and σ vectors for every iteration; this lead to noticeable I/O delays for some of the larger test cases. Our new program is also capable of using iteration methods which require fewer vectors on disk (cf. section 3.2). Although we do not have access to Olsen's code, he has reported that his program takes about 40s per iteration for the 1 million determinant DZ H_2O full CI calculation,[232] whereas DETCI requires 30s per iteration on the same model workstation (IBM RS/6000 model 590).

Table 10: CPU and total times per iteration to evaluate several benchmark full CI wavefunctions using the IBM RS/6000 model 3CT. Fzc/Fzv denote the number of frozen core/frozen virtual orbitals.

				Time/Iter (seconds)			
				GUGACI		DETCI	
Molecule	Fzc/Fzv	CSFs	Dets	CPU	Tot	CPU	Tot
DZ H_2O	1/0	37 353	128 829	77	79	3	3
DZ H_2O	0/0	256 473	1 002 708	1430	1465	28	33
cc-pVDZ+ Ne[a]	0/0	2 083 968	9 185 280	13788	14007	282	532
DZP C_2	2/2	6 571 116	27 944 940	32489	34831	1329	3160

[a]Using the basis set of Koch *et al.*[7]

5 Applications of Highly Correlated CI

Most studies limit the CI space to single and double substitutions from a single reference (CISD). Occasionally, when one reference does not provide a sufficient zeroth-order wavefunction, the multi-reference CISD method will be employed. The applications of such methods are too numerous to discuss here; their general performance has already been described in section 2. We consider studies which go beyond CISD for one or a few references; such highly correlated wavefunctions are useful when very accurate results are desired or when several electron configurations are needed for a qualitatively correct reference wavefunction (such as when multiple bonds are broken). We will limit our attention to methods which select the CI space in an *a priori* fashion based on the distribution of electrons among various orbital subspaces.

5.1 Full CI

The most highly correlated configuration interaction method is of course full CI, which solves the Schrödinger equation exactly within the space spanned by the single-particle basis set (section 2.1). Unfortunately, as explained in section 2.4.1, the full CI space grows factorially with the number of electrons or single-particle basis functions; currently, full CI is limited to very small molecules (one or two heavy atoms with a few hydrogen atoms) described by a basis set of double-ζ or perhaps triple-ζ quality. Furthermore, errors due to the incompleteness of the single-particle basis set are generally more severe than those introduced by the neglect of triple, quadruple, etc., substitutions in the treatment of electron correlation. Hence full CI is useful primarily as

a benchmark method for evaluating approximate treatments of correlation. Given their extreme computational requirements, it is perhaps surprising how many full CI benchmarks have been reported. Here we will focus primarily on the more noteworthy or more recent benchmarks, and on systems containing more than four electrons.

The early (1980) full CI algorithm of Handy[44] enabled Saxe, Schaefer, and Handy to obtain the exact variational solution for the ground state of H_2O within a modest double-ζ (DZ) basis set; this represented the first CI wavefunction to include more than one million determinants.[213] In 1983, Harrison and Handy used this same algorithm, along with the loop-driven graphical unitary group approach CI (LD-GUGACI) program of Brooks and Schaefer,[43] to report full CI results for H_2O and NH_3 with a DZ basis and for BH and HF in a double-ζ plus polarization (DZP) basis.[38] These two studies, which also gave results for the CISD, CISDT, and CISDTQ methods, clearly demonstrated that triply and quadruply substituted configurations account for nearly all of the error in the CISD correlation energy (cf. Table 2). Moreover, by comparing to Harrison and Handy's results for H_2O, Bartlett, Sekino, and Purvis demonstrated that fourth-order many-body perturbation theory [MBPT(4)] performs poorly when both O–H bonds are stretched,[19] even though it partially accounts for quadruple excitations. This occurs because the restricted Hartree-Fock determinant provides an inadequate zeroth-order wavefunction as the bonds are stretched too far from their equilibrium lengths, and it emphasizes the need for multireference approaches.

The subsequent (1984) vectorized full CI algorithm[109] of Knowles and Handy allowed Bauschlicher, Taylor, Langhoff, and others to carry out a series of important benchmark calculations. In 1986, these authors, along with Partridge, presented full CI results for the Ne atom using a triple-ζ plus double polarization (TZ2P) basis set.[233] Once again, the CISDTQ wavefunction yielded more than 99% of the basis set correlation energy; furthermore, the contribution of quintuple and higher substitutions decreased with increasing basis set size. Subsequent benchmark results using a DZP basis were presented for HF and NH_2;[234] H_2O, F, and F^-;[235] the $^1A_1$–$^3B_1$ separation in CH_2;[236] the barrier height to the reaction F + H_2 → HF + H;[237] the $^1A_1$, $^1B_1$, and $^3B_1$ states of SiH_2;[238] the 2 $^1A_1$ states of CH_2 and SiH_2 and the $^2A_1$ and $^2B_2$ states of CH_2^+;[239] the low-lying states of C_2;[240] N_2, NO, and O_2;[241] the CH_3 radical;[242] and Be_3.[243] Bauschlicher and co-workers have also investigated transition metals. They estimated the ^5D–^5F energy separation for the Fe atom using a 5s4p2d1f basis set,[244] excitation energies and oscillator strengths for the ^{2}D Rydberg series in the Al atom with a 7s6p4d3f ANO basis,[245] the ^3F–^5F separation for the Ti atom, and the $^4\Phi$–$^2\Delta$ separation for TiH in a 5s4p3d1f/2s basis set.[246] Illas, Rubio, Ricart, and Bagus used the

Knowles-Handy program to obtain full CI energies for the first row atoms and their hydrides in 4s3p1d/2s1p basis sets; these benchmarks were used to evaluate the CIPSI method[219] and the performance of ANO basis sets versus more traditional segmented basis sets.[247] Casanovas, Rubio, and Illas have also performed full CI studies on the interaction of H atom with Cu_5 and Ag_5 cluster models to investigate the transferability of the correlation contribution to the chemisorption bond for different pseudopotentials.[248]

Several of these studies considered molecules at three geometries, with equivalent bonds simultaneously stretched to 1.0, 1.5, and 2.0 times their equilibrium lengths; hence, approximate methods could be judged not only by what fraction of the correlation energy they recovered, but also by how well they paralleled the full CI potential energy surface. The MR-CISD method was found to parallel full CI very well, particularly when CASSCF orbitals are used and all configurations present in the CASSCF are used as references. More recently, these authors have used large basis set full CI benchmarks to examine core-core and core-valence correlation effects[249] and to calibrate more approximate MR-CISD approaches for the dissociation energy of BH.[250] Many of these results are summarized in a 1990 review article by Bauschlicher, Langhoff, and Taylor.[15]

Most of the full CI studies just discussed involved CI spaces spanning tens of millions of determinants. More recent full CI algorithms, which follow Olsen *et al.* in sacrificing some degree of vectorization for reduced operation counts,[46,48,49] have allowed for CI spaces including hundreds of millions of determinants. Indeed, Olsen, Jørgensen, and Simons reported a full CI calculation on the Mg atom using a 5s3p2d1f ANO basis and requiring more than one billion determinants; unfortunately, it was not possible to fully converge the wavefunction due to the extreme amount of CPU time required.[83] The first *converged* full CI benchmark requiring more than one billion determinants was reported recently by Evangelisti, Bendazzoli, Ansaloni, Durí, and Rossi, who presented an out-of-core adaptation of their full CI program for distributed-memory parallel computers and used it to obtain the full CI energy of Be_2, with all electrons correlated, in a 4s2p1d ANO basis set partially uncontracted to 9s2p1d.[84]

In 1995, these workers used an in-core version of this algorithm to resolve an uncertainty concerning the full CI energy of NH_3 with an ANO DZP basis set.[50] Knowles and Handy had in 1989 presented an energy of -56.4236 $\pm$ 0.0001 hartree using their approximate full CI method which truncates the σ vector; 665,247 of 209,626,425 determinants were treated variationally, and the convergence limit was estimated perturbatively.[218] This value underestimates the importance of the large number of neglected determinants, as was first demonstrated by Povill, Rubio, Caballol, and Malrieu.[123] The true full CI

energy was shown to be -56.424007 hartree.[50,80] The program of Bendazzoli and Evangelisti[48] has also been applied to DZ H_8 and N_2[49] and to $C_{18}H_{18}$ using a simple Pariser-Parr-Pople (PPP) Hamiltonian.[48]

In 1996, Olsen, Jørgensen, Koch, Balková, and Bartlett presented DZP full CI results for H_2O at three geometries, where all ten electrons were correlated. Although the basis set was not designed to describe core correlation, these results are valuable in that they are fully invariant to orbital rotations, whereas they would not have been if the 1s-like orbital on oxygen were frozen.[22] As shown by Handy and co-workers,[20] it is fairly straightforward (and valuable) to generalize a full CI program to produce many-body perturbation theory (MBPT) energies order by order. Hence, Olsen *et al.* considered MBPT through 15th order and examined the convergence of the series as the two OH bonds are simultaneously stretched, causing the zeroth-order wavefunction to become progressively worse. In another 1996 study, Olsen, Christiansen, Koch, and Jørgensen examined the convergence of MBPT for several small molecules using DZP and larger basis sets. These authors concluded that perturbation theory corrections grow with increasing basis size and that, remarkably, the inclusion of diffuse functions can cause the perturbation series to diverge even for well-behaved molecules such as HF.[23,251] Olsen's algorithm has also been used to provide benchmark full CI excitation energies for CH^+;[252] BH, CH_2, and Ne atom;[7] H_2O, N_2, and C_2;[37] and H_2O^+.[22]

Most full CI studies have focused solely on energies. A few papers, however, have presented full CI results for other molecular properties. In 1987 Bauschlicher and Taylor presented full CI dipole moments and polarizabilities for HF, CH_2, SiH_2, and F^- with a DZP basis.[253] Moreover, Bauschlicher and Langhoff gave full CI equilibrium geometries, dissociation energies, and harmonic vibrational frequencies for CH, NH, and OH using flexible ANO basis sets.[254] The following year, these authors presented full CI and SOCI transition moments for two transitions in CH_2 and selected dipole and quadrupole transitions in BeO,[255] and Bauschlicher presented geometries, frequencies, and the dipole moment for the $^4\Phi$ and $^2\Delta$ states of TiH.[246] Later, Bauschlicher and Taylor also presented full CI transition moments for H_2 and BH in a comparison of the length and velocity representations for the transition moment.[256] Full CI transition moments and polarizabilities for CH^+ have been presented by Olsen and co-workers.[252] Koch and Bauschlicher have presented a method for computing analytically the frequency dependent linear and quadratic response functions for full CI wavefunctions; they have considered Be atom in a 9s9p5d basis set and have reported transition energies and dipole moments for several states, the first polarizability at real and imaginary frequencies, and the static second hyperpolarizability.[257] Bauschlicher *et al.* have determined the full CI isotropic hyperfine coupling constant for the nitrogen atom using

basis sets as large as 8s4p2d.[258] Spin-orbit coupling has been investigated at the full CI level for CH_2 by Vahtras *et al.*[259] and for LiBe by Marino *et al.*[260]

Researchers have even obtained exact full CI equilibrium geometries for a few polyatomic systems with a DZP basis: the linear transition state for the reaction $F + H_2 \rightarrow HF + H$;[237] the systems H_6, H_7^+ and $H_5^+ \cdot He$;[17,261] the $\tilde{X}\ ^2B_1$ and $\tilde{A}\ ^2A_1$ states of NH_2;[262] BH_3;[39,262] H_5^+;[263] and the four lowest-lying states of methylene[262,264] and NH_2^+.[265] For the latter four molecules, full CI dipole moments and harmonic vibrational frequencies have been reported at the full CI equilibrium geometries.[39,263–265] The DZP full CI studies of methylene clearly demonstrate the need to use larger basis sets: predictions for the singlet-triplet energy gap[236,262,264] are at least 2.5 kcal mol^{-1} too large compared to experiment.[264] We have recently completed a considerably more challenging full CI benchmark study of the four lowest states of methylene using the more reliable TZ2P basis set.[266]

In the past few years, full CI benchmarks have been used to calibrate methods for systems featuring weak interactions. Woon has obtained the full CI well-depth, equilibrium separation, and harmonic vibrational frequency for He_2 with basis sets as large as augmented correlation-consistent polarized quadruple-ζ (aug-cc-pVQZ).[267] In a subsequent study, van Mourik and van Lenthe used the full CI program of Harrison and Zarrabian[47] to obtain dimer energies at two separate geometries using large basis sets including h-type polarization functions and bond functions.[36] One interesting conclusion of this study, which could only be determined using highly correlated wavefunctions, was that the usually-reliable CCSD method is unsuitable for obtaining accurate potential energy curves for He_2. Other recent full CI studies have also focused on helium dimer,[268–271] as well as the dimer of two H_2 molecules[268–270] and the He–H_2 system.[268,269] Such benchmarks have been helpful in examining the problem of basis set superposition error.[270]

5.2 Second-Order CI

One important conclusion from the full CI benchmark studies of Bauschlicher, Taylor, Langhoff, and others in the 1980's is that the MR-CISD method based on CASSCF orbitals provides potential energy surfaces which accurately parallel the full CI surfaces.[14,15,234,238–240,242,254] For example, the CASSCF MR-CISD method predicts singlet-triplet energy separations in CH_2 and SiH_2 within 0.01 kcal mol^{-1} and 0.03 kcal mol^{-1}, respectively, of the full CI results.[236,238] The best results are obtained when no threshold is used for reference selection: that is, when all CSFs in the CASSCF wavefunction are used as references. This CAS-ref MR-CISD procedure is intimately related[107] to second-order configuration interaction (SOCI), which distributes electrons in

all possible ways as long as no more than two electrons are allowed in external orbitals at once (of course, spatial symmetry and spin symmetry may also be imposed on the final N-electron basis functions). For closed-shell systems these procedures are identical, but they can differ for open-shell systems. In cases where all occupied orbitals which are correlated in the SOCI are included in the active space, one can guarantee that the SOCI space is generated by using as references all CSFs arising from CASSCF wavefunctions of all possible spatial symmetries.[107] SOCI wavefunctions are invariant to orbital rotations within the active space, whereas this is not necessarily the case for CAS-ref MR-CISD when the references are symmetry-restricted. In cases where there are "inactive" orbitals (occupied orbitals which are correlated in the SOCI but not included in the CASSCF), Bauschlicher has recommended that the SOCI be defined according to the RAS CI scheme, such that one places inactive orbitals in RAS I, active orbitals in RAS II, and external orbitals in RAS III;[15] this maintains the desired orbital invariance properties. This SOCI can alternatively be generated an MR-CISD in which the references are now all CSFs arising from all CASSCF wavefunctions of every spatial and spin symmetry.

The reliability of SOCI, coupled with its essentially *a priori* selection of the CI space, makes it an attractive alternative to full CI. Unfortunately, for reasonable active spaces the dimension of the SOCI grows very rapidly with system size and thus the method is applicable only to small molecules. Nevertheless, for quite a few molecules it is possible to use the SOCI method in conjunction with large one-particle basis sets and hence to obtain wavefunctions very close to the exact nonrelativistic Born-Oppenheimer limit. Below, we will attempt to give the reader a sense of the types of problems to which the SOCI method has been applied. Bauschlicher, Langhoff, and Taylor have already given[15] an excellent review of the related CASSCF MR-CISD method, and we refer the reader to their article for a discussion of additional important studies.

The SOCI method has been applied primarily to diatomics and triatomics. Two of the early applications of SOCI were studies of Be_2 by Blomberg, Siegbahn, and Roos[272] (1980) and by Lengsfield, McLean, Yoshimine, and Liu[89] (1983). With only four active electrons, a SOCI for this system is identical to the CISD[TQ] method discussed in the following section. The Be_2 molecule is challenging to theory because of the near degeneracy of the $1s^2 2s^2$ and $1s^2 2p^2$ configurations in the the Be atom and because the bonding in the dimer is dominated by dispersion forces. The latter study[89] used a 6s4p3d1f Slater basis set to yield a SOCI dissociation energy of $D_e = 1.87$ kcal mol^{-1} (2.04 ± 0.21 kcal mol^{-1}, including estimates of core correlation and basis set errors), in contradiction to previous coupled-cluster studies[273] giving $D_e \leq 0.2$ kcal mol^{-1}; the experimental value[274] is 2.26 ± 0.09 kcal mol^{-1}, signaling a success

of the SOCI method and a failure of coupled-cluster models which neglect connected triple substitutions. A SOCI study of the related Mg_2 molecule using large ANO basis sets was reported[275] in 1990 by Partridge *et al.* Other SOCI studies on the ground states of diatomic molecules include an investigation of the potential energy curves of NeN^{2+} and NeN^{+} by Koch, Liu, and Frenking,[276] and of N_2 and O_2 by Langhoff, Bauschlicher, and Taylor.[277] The latter study used a 5s4p3d2f1g basis and reported equilibrium bond lengths, harmonic vibrational frequencies, and dissociation energies of (1.101 Å, 2343 cm^{-1}, 9.723 eV) for N_2 and (1.209 Å, 1561 cm^{-1}, 5.139 eV) for O_2, in excellent agreement with experimental values of (1.0977 Å, 2358 cm^{-1}, 9.905 eV) and (1.2075 Å, 1580 cm^{-1}, 5.214 eV), respectively. The multi-reference Davidson correction for size extensivity (section 2.4.6) improves the SOCI dissociation energies but worsens the predicted bond lengths and vibrational frequencies. A subsequent study by Almlöf *et al.*[278] considered even larger basis sets (including *i* polarization functions), core-valence correlation, and basis set superposition effects in an investigation of remaining sources of error in the dissociation energy of N_2; their best theoretical estimate was within about 2 kcal mol^{-1}, or 1% of the experimental dissociation energy.

Several studies have used the SOCI method to describe excited electronic states of diatomic molecules. In 1988, Partridge *et al.*[279] reported SOCI potential energy curves for the $A'\ ^5\Sigma_g^+$ and $C''\ ^5\Pi_u$ states of N_2; these results had important implications for theories of the N_2 afterglow and for the first time allowed an assignment of the Hermann infrared system. Also in 1988, Bauschlicher *et al.*[280] reported SOCI spectroscopic constants (r_e, T_e, and ω_e) for several low-lying quartet states of AlC; this study indicated that the SOCI results based on CASSCF orbitals optimized separately for each state were nearly identical to SOCI using a common set of state-averaged CASSCF orbitals. Balasubramanian has used the SOCI method along with relativistic pseudopotentials to study diatomics incorporating elements below the second row of the periodic table. His work has included studies of the low-lying electronic states of InSb;[281] Ga_2, Ga_2^-, and Ga_2^+;[282] GeH and GeH^+;[283] WH;[284] GaH;[285] TlH and InH;[286] and GeCl.[287] Another study by Balasubramanian considers the low-lying states of the transition metal hydrides YH-CdH.[288]

The SOCI method has also been used for a number of triatomics, including the much-studied[264] methylene molecule (CH_2). An early application of the SOCI method to methylene was presented by Saxe, Schaefer, and Handy,[289] who used Handy's 1980 string-based determinant CI program[44] to obtain an estimate of T_e = 10.5 kcal mol^{-1} for the singlet-triplet energy gap using a 8s5p3d/4s1p basis set. More recently, Bauschlicher, Taylor, and Langhoff have used the SOCI method in conjunction with a 5s4p3d2f1g/4s3p2d ANO basis set to predict[290] optimized geometries for the $\tilde{X}\ ^3B_1$ and $\tilde{a}\ ^1A_1$ states of

CH_2 of (1.079 Å, 133.6°) and (1.110 Å, 102.0°), which compare to experimentally derived estimates of (1.0753 Å, 133.93°) and (1.116 Å, 101.8°), respectively. McLean *et al.*[291] used the SOCI method with a 4s3p2d1f/3s2p basis to obtain 37 energy points which were fit with a nonrigid bender Hamiltonian model to yield $\nu_1 = 2985 \pm 20$ cm^{-1} and $\nu_3 = 3205 \pm 20$ cm^{-1} for the fundamental stretching frequencies, compared to experimentally derived values of 2992 and 3213 cm^{-1}. For the singlet-triplet energy splitting (T_e), the 5s4p3d2f1g/4s3p2d ANO SOCI estimate of 9.13 kcal mol^{-1} by Bauschlicher *et al.*[290] and the TZ3P(2f,2d)+2diff SOCI estimate of 9.02 kcal mol^{-1} by Yamaguchi *et al.*[86] compare very favorably with the best nonrelativistic Born-Oppenheimer-corrected experimental estimate of 9.372 kcal mol^{-1}.[264,292-294] Yamaguchi *et al.* also report[86] SOCI excitation energies for the $\tilde{b}\ ^1B_1$ and $\tilde{c}\ ^1A_1$ states which will hopefully guide further experimental efforts.

Among the numerous other studies of polyatomic molecules using the SOCI method, Balasubramanian has reported energies and optimized geometries for low-lying states of SnH_2;[139,295] PbH_2;[139] GaH_2, GaH_2^+, GaH_3, and GaH_3^+;[285] YH_2^+ and ZrH_2^+;[296] AsH_2, AsH_2^+, SbH_2^+, and BiH_2^+;[297] GeH_2;[139,283] HfH_2;[298] TlH_2, TlH_2^+, InH_2, and InH_2^+;[286] and PH_2, PH_2^+, and PH_2^-.[299] Yarkony *et al.* have used SOCI wavefunctions as zeroth-order solutions in first-order perturbation theory treatments of the full Breit-Pauli spin-orbit Hamiltonian; in this fashion, these workers have studied the spin-forbidden decay of systems including $\tilde{X}\ ^2\Pi$ HS^{2+},[300] $\tilde{a}\ ^3\Sigma_1^+$ NO^+,[301] and $\tilde{a}\ ^4\Sigma^-$ CH.[302] SOCI has also been used to assess the quality of the CCSD(T) method for electron affinities,[303] to obtain accurate barrier heights for the termolecular reaction of $3H_2$,[261] and to yield transition moments.[138,255]

Finally, we note that it may be advantageous to use natural orbitals (NOs) rather than the CASSCF orbitals usually employed in SOCI studies. Grev and Schaefer[16] have shown for a number of small molecules (NH_2, CH_3, SiH_2, N_2) that a SOCI procedure based on CISD natural orbitals yields energies which are very close to the CASSCF SOCI energies, even when several bonds are simultaneously stretched to twice their equilibrium length. Blomberg and Liu have also observed similar performance of MCSCF orbitals and SOCI natural orbitals for energies and transition moments of CH and CH^+,[138] although we note that CISD NOs are much less expensive to obtain than SOCI NOs. CISD NOs are also easier to obtain than CASSCF orbitals, and they are better suited to orbital truncation; that is, the energy lost by deleting a few of the most weakly occupied NOs will typically be smaller than that lost by deleting a few of the highest-lying CASSCF orbitals. This allows for an effective reduction in the number of determinants included in a SOCI wavefunction with minimal loss in accuracy. Moreover, the energy lost by deleting these weakly occupied NOs is primarily due to neglected singly and doubly substituted determinants

which occupy these orbitals, and not to neglected triples, quadruples, etc.[16,17] This suggests a strategy of using a smaller NO basis to treat higher-than-double substitutions, and this idea has been implemented in the CISD[TQ] method described in section 5.4.

5.3 Restricted Active Space CI

As already discussed, many commonly encountered CI spaces can be formulated within the RAS CI scheme. However, at the moment our attention is focused on CI calculations using the RAS CI program of Olsen and co-workers.[46] Examples of full CI calculations using Olsen's program have already been discussed above, so here we limit our attention to truncated CI wavefunctions.

The RAS CI method can be very valuable when used in conjunction with the multiconfigurational linear response (MCLR) method, which allows calculation of excitation energies, transition moments, and second-order properties such as polarizability. In 1989, Olsen and co-workers compared MCLR and full CI results for CH^+ and found that for highly accurate results, it is necessary to provide more extensive treatments of electron correlation than the valence CAS. Furthermore, these authors found that the RAS method provides an accurate means of reducing the size of the CI space in these MCLR studies. Jensen *et al.* were able to show that the RAS MCLR calculations which include dynamical correlation give very reliable frequency-dependent polarizabilities for the nitrogen molecule.[304] Sanchez de Merás *et al.* found that the polarizabilities of H_2O and CO_2 obtained using the RAS MCLR method with polarized basis sets were within 5% of experiment.[305] More recently, Sundholm and Olsen have used the RAS approach as part of a finite element multiconfigurational Hartree-Fock method for determining the atomic quadrupole moment of Ca (3d4s; ^1D) and the electron affinity of the ^1S ground state.[306,307]

5.4 CISDTQ and CISD[TQ]

Few studies have employed configuration interaction with all singles, doubles, triples, and quadruples (CISDTQ) because the number of triple and quadruple substitutions grows very rapidly with the number of electrons and basis functions (cf. Table 3). CISDTQ results are most commonly reported in benchmark full CI studies to indicate the fraction of the basis set correlation energy recovered by triples and quadruples.[17,22,39,80,234,241,264] Nevertheless, the CISDTQ method has occasionally been used for benchmarking in cases where the full CI was not technically feasible, because the CISDTQ results are expected to be very close to full CI for small molecules. For systems with eight electrons or less at their equilibrium geometries, the CISDTQ method recovers more

than 99.8% of the correlation energy for a DZP basis set (cf. Table 2). One benchmark study by Lee *et al.* examined the effects of triple and quadruple excitations on equilibrium geometries, harmonic vibrational frequencies, and infrared intensities of several small molecules.[308] A similar study by Scuseria, Hamilton, and Schaefer[309] used CISDTQ equilibrium geometries and harmonic vibrational frequencies to evaluate the performance of the CCSDT method for several diatomic molecules.[4]

Chemical applications of the CISDTQ method include the 1988 study by Scuseria and Schaefer[310] on the barrier height for the $F + H_2 \rightarrow FH + H$ reaction, which is very sensitive to the level of theory employed. By truncating the CI space at quadruples, these authors were able to increase the basis set from 28 functions (in Bauschlicher and Taylor's full CI study[237]) to 47 basis functions and enabled them to consider the effects of correlating the fluorine 2s orbital. Additionally, Tanaka and Nishimoto have used CISDTQ to examine the reaction mechanism for 1,3 hydrogen transfer in excited states of formamide,[311] and Du, Hrovat, and Borden[312] have used CISDTQ as part of a study on singlet-triplet gaps in diradicals.

Multireference CISD methods generally offer a more economical treatment of the dominant effects of triple and quadruple substitutions and allow the use of larger one-particle basis sets. The primary disadvantage of MR-CISD compared to CISDTQ is that the choice of references (and truncation, if any, of the generated singles and doubles space) must be performed carefully so as not to bias the results. An *a priori* selection scheme for MR-CISD which has been investigated in our laboratory is the CISD[TQ] method,[16] which selects as references all single and double substitutions in the active space. This is equivalent to a CISDTQ in which no more than two electrons are allowed into external orbitals, or to a second-order CI (SOCI) in which greater-than-quadruple substitutions have been eliminated. This method was used by Saxe *et al.* in a 1982 study of ethylene using a DZP basis and the shape-driven graphical unitary group approach (SD-GUGA) CI program.[91] The resulting wavefunction (spanning more than 1 million CSFs) was considered a benchmark result. In 1992 study of NH_2, CH_3, SiH_2, C_2, and N_2, Grev and Schaefer[16] found that the CISD[TQ] method provides results which are very close to SOCI when a single reference function dominates. A subsequent study of several other small molecules by Fermann *et al.*[17] reinforced these conclusions. Some results from these studies which indicate the ability of CISD[TQ] to parallel the SOCI and full CI surfaces are presented in Table 11. The CISD[TQ] and SOCI wavefunctions were based on CISD natural orbitals, which perform as well as CASSCF orbitals for SOCI.[16] Although the savings in the number of CSFs for CISD[TQ] compared to SOCI in Table 11 is relatively modest, this savings increases very rapidly with basis set and number of electrons: for

Table 11: Errors in Total Energies (millihartree) Relative to Full CI for Several Molecules Using a DZP Basis.[a]

Method	No. CSFs	E(r_e)	E(1.5 $\cdot r_e$)	E(2.0 $\cdot r_e$)
$^2B_1$ NH_2 (Ref. 16):				
CISD	898	9.003	23.475	69.168
CISD[TQ]	18 396	2.897	2.630	4.957
SOCI	21 687	2.853	2.107	1.703
Full CI	2 435 160	0.000	0.000	0.000
$^2A_2''$ CH_3 (Ref. 16):				
CISD	1 385	8.384	23.216	70.646
CISD[TQ]	51 818	2.156	2.065	4.910
SOCI	76 660	2.090	1.254	0.889
Full CI	9 591 312	0.000	0.000	0.000
$^1A_1$ H_2O (Ref. 17):				
CISD	926	12.851	30.421	75.644
CISDTQ	151 248	0.397	1.547	6.280
CISD[TQ]	32 361	1.630	2.537	6.867
SOCI	76 660	1.276	1.058	1.020
Full CI	6 740 280	0.000	0.000	0.000

[a]CISD[TQ] and SOCI methods employed CISD natural orbitals.

DZP ethylene, a CISD[TQ] description requires over 1 million CSFs, whereas a SOCI requires over 42 million. In addition to these results, Grev and Schaefer[16] also demonstrate that the CISD[TQ] method yields reliable dissociation energies for the difficult N_2 and C_2 molecules.

More recent work has explored the quality of CISD[TQ] equilibrium geometries and harmonic vibrational frequencies. King *et al.*[313] have found that for H_2O with a TZ2P basis, the equilibrium geometry predicted by CISD[TQ] differs from that of CISDTQ by less than 0.0001 Å in the bond length and 0.2° in the bond angle. Furthermore, the CISD[TQ] harmonic vibrational frequencies differ from those of the complete CISDTQ by an average of only 5 cm^{-1}. Such agreement is outstanding, particularly in view of the fact that the CISD[TQ] wavefunction contains 45 times fewer CSFs than CISDTQ. In related work, Hoffman *et al.*[314] have found similar results for H_2S. Another study by Leininger and Schaefer[315] considers the ozone molecule, which is challenging to theory because of the unusual importance of triple and quadruple substitutions. It is not currently feasible to obtain the complete CISDTQ wavefunction with a DZP basis, but the DZP CISD[TQ] equilibrium geometry differs from experiment by only 0.009 Å, and the harmonic vibrational frequencies differ by an average of 2.4%, with the treacherous antisymmetric stretching frequency predicted within 4.5%.

Finally, even though the computational cost of a CISD[TQ] procedure is substantially reduced compared to CISDTQ, the scaling with system size (cf. section 2.4.5) remains unfavorable. Hence, it is necessary to seek further reductions in the CI expansion with a minimal loss in the quality of the wavefunction. One promising strategy was suggested by Grev and Schaefer's 1992 study[16] on the use of CISD natural orbitals (NOs) in the CISD[TQ] and SOCI methods. This work indicated not only that CISD NOs are as effective as CASSCF orbitals at providing good correlating orbitals in the active space, but also that the most weakly occupied NOs contribute almost negligibly to the energy. Furthermore, the errors in the energy caused by deleting weakly occupied orbitals are almost entirely due to the neglect of singles and doubles occupying these orbitals, and not to triples or quadruples. This suggests a more compact CISD[TQ] wavefunction[17] which splits the external orbital space into two sets. If the unoccupied (virtual) orbitals of the active space are labeled the primary virtual subspace, then the external orbitals are divided into secondary and tertiary virtual subspaces, where the tertiary subspace comprises the set of the most weakly occupied NOs. One may then modify the CISD[TQ] method to eliminate those triple and quadruple substitutions which place an electron in one of the most weakly occupied orbitals.[17,18,90] In effect, one uses a larger basis set for the singles and doubles than for the triples and quadruples.

This "split-virtual" CISD[TQ] method has been implemented in our de-

Table 12: Correlation Energy Recovered (Relative to CISDTQ) by the Split-Virtual CISD[TQ] Method for H_2O in a cc-pVTZ Basis Set.[a]

Method/ Secondary Space	NO Cutoff	Number of Dets	%SDTQ Energy
CISD		15 939	93.1
CISDT		938 679	95.8
CISDTQ		28 085 271	100.
CISD[TQ] w/ primary space $2b_2 4a_1 2b_1 5a_1$			
(18 7 9 15)	none	984 789	98.8
(9 4 6 8)	10^{-4}	320 531	98.6
(3 1 1 2)	10^{-3}	41 261	96.5
(0 0 0 0)		16 713	94.7

[a]CISD[TQ] methods employed CISD natural orbitals (NOs). The secondary orbital space selects all virtual orbitals with NO occupation numbers greater than the given cutoff and is identified according to how many orbitals of each irrep of C_{2v} it contains, in the order (a_1, a_2, b_1, b_2). Only valence electrons are correlated.

terminant based CI program (cf. section 4.8.3), and we have presented some preliminary results[18] for the neon atom and for H_2O. Table 12 gives some of our results for H_2O with a cc-pVTZ basis set. We find the NO-based selection scheme to be effective in obtaining the dominant effects of triple and quadruple substitutions while using fewer CSFs, and we believe this promising strategy should be even more effective in the coupled-cluster approach, where the connected triples ($\hat{T}_3$ operator) could be evaluated using a smaller NO space.

Acknowledgments

We thank Dr. Jeppe Olsen, Dr. Wesley Allen, and Matthew Leininger for helpful discussions, and Dr. Daniel Crawford and Dr. Justin Fermann for their work on the two-electron integral transformation algorithm. This work was sponsored by the U.S. National Science Foundation, grant no. CHE-9527468, and by NSF graduate and postdoctoral fellowships (grant no. CHE-9626094) to C.D.S.

References

[1] J. R. Thomas, B. J. DeLeeuw, G. Vacek, and H. F. Schaefer, J. Chem. Phys. **98**, 1336 (1993).

[2] J. R. Thomas, B. J. DeLeeuw, G. Vacek, T. D. Crawford, Y. Yamaguchi, and H. F. Schaefer, J. Chem. Phys. **99**, 403 (1993).

[3] K. Raghavachari, G. W. Trucks, J. A. Pople, and M. Head-Gordon, Chem. Phys. Lett. **157**, 479 (1989).

[4] G. E. Scuseria and T. J. Lee, J. Chem. Phys. **93**, 5851 (1990).

[5] G. E. Scuseria, Chem. Phys. Lett. **94**, 27 (1991).

[6] J. F. Stanton and R. J. Bartlett, J. Chem. Phys. **98**, 7029 (1993).

[7] H. Koch, O. Christiansen, P. Jørgensen, and J. Olsen, Chem. Phys. Lett. **244**, 75 (1995).

[8] B. O. Roos, The multiconfigurational (MC) SCF method, in *Methods in Computational Molecular Physics*, edited by G. H. F. Diercksen and S. Wilson, pages 161–187. D. Reidel, Dordrecht, 1983.

[9] B. O. Roos, The multiconfigurational (MC) self-consistent field (SCF) theory, in *Lecture Notes in Quantum Chemistry: European Summer*

School in Quantum Chemistry, edited by B. O. Roos, volume 58 of *Lecture Notes in Chemistry*, pages 177–254. Springer-Verlag, New York, 1992.

[10] R. J. Buenker and S. D. Peyerimhoff, Theor. Chim. Acta **35**, 33 (1974).

[11] R. J. Buenker and S. D. Peyerimhoff, Theor. Chim. Acta **39**, 217 (1975).

[12] J. A. Pople, in *Energy, Structure and Reactivity: Proceedings of the 1972 Boulder Summer Research Conference on Theoretical Chemistry*, edited by D. W. Smith and W. B. McRae, page 51. Wiley, New York, 1973.

[13] H. F. Schaefer, *Configuration Interaction Wave Functions and the Properties of Atoms and Diatomic Molecules*, PhD thesis, Stanford University, Stanford, CA, 1969.

[14] F. B. Brown, I. Shavitt, and R. Shepard, Chem. Phys. Lett. **105**, 363 (1984).

[15] C. W. Bauschlicher, S. R. Langhoff, and P. R. Taylor, Accurate quantum chemical calculations, in *Advances in Chemical Physics*, edited by I. Prigogine and S. A. Rice, volume 77, pages 103–161. Wiley, New York, 1990.

[16] R. S. Grev and H. F. Schaefer, J. Chem. Phys. **96**, 6850 (1992).

[17] J. T. Fermann, C. D. Sherrill, T. D. Crawford, and H. F. Schaefer, J. Chem. Phys. **100**, 8132 (1994).

[18] C. D. Sherrill and H. F. Schaefer, J. Phys. Chem. **100**, 6069 (1996).

[19] R. J. Bartlett, H. Sekino, and G. D. Purvis, Chem. Phys. Lett. **98**, 66 (1983).

[20] N. C. Handy, P. J. Knowles, and K. Somasundram, Theor. Chim. Acta **68**, 87 (1985).

[21] S. A. Kucharski, J. Noga, and R. J. Bartlett, J. Chem. Phys. **90**, 7282 (1989).

[22] J. Olsen, P. Jørgensen, H. Koch, A. Balková, and R. J. Bartlett, J. Chem. Phys. **104**, 8007 (1996).

[23] J. Olsen, O. Christiansen, H. Koch, and P. Jørgensen, J. Chem. Phys. **105**, 5082 (1996).

[24] G. D. Purvis and R. J. Bartlett, J. Chem. Phys. **76**, 1910 (1982).

[25] W. D. Laidig and R. J. Bartlett, Chem. Phys. Lett. **104**, 424 (1984).

[26] Y. S. Lee, S. A. Kucharski, and R. J. Bartlett, J. Chem. Phys. **81**, 5906 (1984).

[27] Y. S. Lee, S. A. Kucharski, and R. J. Bartlett, J. Chem. Phys. **82**, 5761(E) (1985).

[28] J. Noga and R. J. Bartlett, J. Chem. Phys. **86**, 7041 (1987).

[29] J. Noga and R. J. Bartlett, J. Chem. Phys. **89**, 3401(E) (1988).

[30] J. D. Watts, G. W. Trucks, and R. J. Bartlett, Chem. Phys. Lett. **157**, 359 (1989).

[31] J. D. Watts and R. J. Bartlett, J. Chem. Phys. **93**, 6104 (1990).

[32] H. Nakatsuji and M. Ehara, J. Chem. Phys. **98**, 7179 (1993).

[33] X. Li, P. Piecuch, and J. Paldus, Chem. Phys. Lett. **224**, 267 (1994).

[34] A. Balková and R. J. Bartlett, J. Chem. Phys. **102**, 7116 (1995).

[35] X. Li and J. Paldus, J. Chem. Phys. **102**, 8059 (1995).

[36] T. van Mourik and J. H. van Lenthe, J. Chem. Phys. **102**, 7479 (1995).

[37] O. Christiansen, H. Koch, P. Jørgensen, and J. Olsen, Chem. Phys. Lett. **256**, 185 (1996).

[38] R. J. Harrison and N. C. Handy, Chem. Phys. Lett. **95**, 386 (1983).

[39] J. M. Galbraith, G. Vacek, and H. F. Schaefer, J. Mol. Structure **300**, 281 (1993).

[40] J. Paldus, J. Chem. Phys. **61**, 5321 (1974).

[41] I. Shavitt, Int. J. Quantum Chem. Symp. **11**, 131 (1977).

[42] I. Shavitt, Int. J. Quantum Chem. Symp. **12**, 5 (1978).

[43] B. R. Brooks and H. F. Schaefer, J. Chem. Phys. **70**, 5092 (1979).

[44] N. C. Handy, Chem. Phys. Lett. **74**, 280 (1980).

[45] P. E. M. Siegbahn, Chem. Phys. Lett. **109**, 417 (1984).

[46] J. Olsen, B. O. Roos, P. Jørgensen, and H. J. Aa. Jensen, J. Chem. Phys. **89**, 2185 (1988).

[47] R. J. Harrison and S. Zarrabian, Chem. Phys. Lett. **158**, 393 (1989).

[48] G. L. Bendazzoli and S. Evangelisti, J. Chem. Phys. **98**, 3141 (1993).

[49] G. L. Bendazzoli and S. Evangelisti, Int. J. Quantum Chem. Symp. **27**, 287 (1993).

[50] S. Evangelisti, G. L. Bendazzoli, R. Ansaloni, and E. Rossi, Chem. Phys. Lett. **233**, 353 (1995).

[51] R. Shepard, The analytic gradient method for configuration interaction wave functions, in *Modern Electronic Structure Theory*, edited by D. R. Yarkony, volume 2 of *Advanced Series in Physical Chemistry*, pages 345–458. World Scientific, Singapore, 1995.

[52] Y. Yamaguchi, Y. Osamura, J. D. Goddard, and H. F. Schaefer, *A New Dimension to Quantum Chemistry: Analytic Derivative Methods in Ab initio Molecular Electronic Structure Theory.* Oxford, New York, 1994.

[53] R. Shepard, The multiconfiguration self-consistent field method, in Ab Initio *Methods in Quantum Chemistry–II*, edited by K. P. Lawley, volume 69 of *Advances in Chemical Physics*, pages 63–200. Wiley, New York, 1987.

[54] H.-J. Werner, Matrix-formulated direct multiconfiguration self-consistent field and multiconfiguration reference configuration-interaction methods, in Ab Initio *Methods in Quantum Chemistry–II*, edited by K. P. Lawley, volume 69 of *Advances in Chemical Physics*, pages 1–62. Wiley, New York, 1987.

[55] B. O. Roos, The complete active space self-consistent field method and its applications in electronic structure calculations, in Ab Initio *Methods in Quantum Chemistry–II*, edited by K. P. Lawley, volume 69 of *Advances in Chemical Physics*, pages 399–445. Wiley, New York, 1987.

[56] P.-Å. Malmqvist, A. Rendell, and B. O. Roos, J. Phys. Chem. **94**, 5477 (1990).

[57] I. Shavitt, The method of configuration interaction, in *Methods of Electronic Structure Theory*, edited by H. F. Schaefer, pages 189–275. Plenum Press, New York, 1977.

[58] P. E. M. Siegbahn, The configuration interaction method, in *Lecture Notes in Quantum Chemistry: European Summer School in Quantum Chemistry*, edited by B. O. Roos, volume 58 of *Lecture Notes in Chemistry*, pages 255–293. Springer-Verlag, New York, 1992.

[59] J. Karwowski, The configuration interaction approach to electron correlation, in *Methods in Computational Molecular Physics*, edited by S. Wilson and G. H. F. Diercksen, pages 65–98. Plenum Press, New York, 1992.

[60] W. Duch, J. Mol. Struct. (Theochem) **80**, 27 (1991).

[61] R. McWeeny, *Methods of Molecular Quantum Mechanics*. Academic Press, New York, 2nd edition, 1992.

[62] E. Schrödinger, Ann. d. Phys. **79**, 734 (1926).

[63] A. Szabo and N. S. Ostlund, *Modern Quantum Chemistry: Introduction to Advanced Electronic Structure Theory*. McGraw-Hill, New York, 1989.

[64] W. Klopper, R. Röhse, and W. Kutzelnigg, Chem. Phys. Lett. **178**, 455 (1991).

[65] R. D. Kent and M. Schlesinger, Phys. Rev. A **46**, 6881 (1992).

[66] W. Cencek and J. Rychlewski, J. Chem. Phys. **102**, 2533 (1995).

[67] B. J. Persson and P. R. Taylor, J. Chem. Phys. **105**, 5915 (1996).

[68] E. A. Hylleraas, Z. Phys. **54**, 347 (1929).

[69] E. A. Hylleraas, The Schrödinger two-electron atomic problem, in *Advances in Quantum Chemistry*, edited by P.-O. Löwdin, volume 1, pages 1–33. Academic Press, New York, 1964.

[70] L. Pauling and E. B. Wilson, Jr., *Introduction to Quantum Mechanics with Applications to Chemistry*. McGraw-Hill, New York, 1935.

[71] J. K. L. MacDonald, Phys. Rev. **43**, 830 (1933).

[72] E. A. Hylleraas and B. Undheim, Z. Phys. **65**, 759 (1930).

[73] W. Ritz, J. Reine Angew. Math. **135**, 1 (1909).

[74] J. C. Slater, Phys. Rev. **34**, 1293 (1929).

[75] E. U. Condon, Phys. Rev. **36**, 1121 (1930).

[76] J. C. Slater, Phys. Rev. **38**, 1109 (1931).

[77] P. O. Löwdin, Phys. Rev. **97**, 1474 (1955).

[78] J. Paldus, Int. J. Quantum Chem. Symp. **9**, 165 (1975).

[79] J. Olsen, The method of second quantization, in *Lecture Notes in Quantum Chemistry: European Summer School in Quantum Chemistry*, edited by B. O. Roos, volume 58 of *Lecture Notes in Chemistry*, pages 37–87. Springer-Verlag, New York, 1992.

[80] J. Olsen, unpublished.

[81] P. J. Knowles, Chem. Phys. Lett. **155**, 513 (1989).

[82] H. Weyl, *The Classical Groups, Their Invariants and Representations.* Princeton University Press, Princeton, 1946.

[83] J. Olsen, P. Jørgensen, and J. Simons, Chem. Phys. Lett. **169**, 463 (1990).

[84] S. Evangelisti, G. L. Bendazzoli, R. Ansaloni, F. Durí, and E. Rossi, Chem. Phys. Lett. **252**, 437 (1996).

[85] C. W. Bauschlicher and D. R. Yarkony, J. Chem. Phys. **69**, 3875 (1978).

[86] Y. Yamaguchi, C. D. Sherrill, and H. F. Schaefer, J. Phys. Chem. **100**, 7911 (1996).

[87] P. G. Burton and P. D. Gray, Chem. Phys. Lett. **96**, 453 (1983).

[88] P. E. M. Siegbahn, The direct CI method, in *Methods in Computational Molecular Physics*, edited by G. H. F. Diercksen and S. Wilson, pages 189–207. D. Reidel, Dordrecht, 1983.

[89] B. H. Lengsfield, A. D. McLean, M. Yoshimine, and B. Liu, J. Chem. Phys. **79**, 1891 (1983).

[90] M. M. Steiner, W. Wenzel, K. G. Wilson, and J. W. Wilkins, Chem. Phys. Lett. **231**, 263 (1994).

[91] P. Saxe, D. J. Fox, H. F. Schaefer, and N. C. Handy, J. Chem. Phys. **77**, 5584 (1982).

[92] B. Huron, J. P. Malrieu, and P. Rancurel, J. Chem. Phys. **58**, 5745 (1973).

[93] S. Evangelisti, J. P. Daudey, and J. P. Malrieu, Chem. Phys. **75**, 91 (1983).

[94] Z. Gershgorn and I. Shavitt, Int. J. Quantum Chem. **2**, 751 (1968).

[95] V. Sychrovský and P. Čársky, Mol. Phys. **88**, 1137 (1996).

[96] O. Goscinski and E. Brändas, Chem. Phys. Lett. **2**, 299 (1968).

[97] J. Cullen and M. C. Zerner, Int. J. Quantum Chem. Symp. **9**, 343 (1975).

[98] J. M. Cullen and M. C. Zerner, Int. J. Quantum Chem. **33**, 373 (1988).

[99] W. Meyer, Configuration expansion by means of pseudonatural orbitals, in *Methods of Electronic Structure Theory*, edited by H. F. Schaefer, pages 413–446. Plenum Press, New York, 1977.

[100] P. E. M. Siegbahn, Int. J. Quantum Chem. **18**, 1229 (1980).

[101] H.-J. Werner and P. J. Knowles, J. Chem. Phys. **88**, 5803 (1988).

[102] P. J. Knowles and H.-J. Werner, Chem. Phys. Lett. **145**, 514 (1988).

[103] J. C. Greer, J. Chem. Phys. **103**, 1821 (1995).

[104] A. Bunge, J. Chem. Phys. **53**, 20 (1970).

[105] C. F. Bender and H. F. Schaefer, J. Chem. Phys. **55**, 4798 (1971).

[106] A. D. McLean and B. Liu, J. Chem. Phys. **58**, 1066 (1973).

[107] C. W. Bauschlicher and H. Partridge, Theor. Chim. Acta **85**, 255 (1993).

[108] E. R. Davidson, J. Comp. Phys. **17**, 87 (1975).

[109] P. J. Knowles and N. C. Handy, Chem. Phys. Lett. **111**, 315 (1984).

[110] E. R. Davidson, Configuration interaction description of electron correlation, in *The World of Quantum Chemistry*, edited by R. Daudel and B. Pullman. D. Reidel, Dordrecht, 1974.

[111] S. R. Langhoff and E. R. Davidson, Int. J. Quantum Chem. **8**, 61 (1974).

[112] E. R. Davidson and D. W. Silver, Chem. Phys. Lett. **52**, 403 (1977).

[113] L. Meissner, Chem. Phys. Lett. **146**, 204 (1988).

[114] W. Duch and G. H. F. Diercksen, J. Chem. Phys. **101**, 3018 (1994).

[115] P. J. Bruna, S. D. Peyerimhoff, and R. J. Buenker, Chem. Phys. Lett. **72**, 278 (1980).

[116] W. Kutzelnigg, Pair correlation theories, in *Methods of Electronic Structure Theory*, edited by H. F. Schaefer, pages 129–188. Plenum Press, New York, 1977.

[117] R. Ahlrichs, P. Scharf, and C. Ehrhardt, J. Chem. Phys. **82**, 890 (1985).

[118] J. A. Pople, M. Head-Gordon, and K. Raghavachari, J. Chem. Phys. **87**, 5968 (1987).

[119] R. J. Gdanitz and R. Ahlrichs, Chem. Phys. Lett. **143**, 413 (1988).

[120] P. G. Szalay and R. J. Bartlett, J. Chem. Phys. **103**, 3600 (1995).

[121] L. Füsti-Molnár and P. G. Szalay, J. Phys. Chem. **100**, 6288 (1996).

[122] A. Povill, R. Caballol, J. Rubio, and J. P. Malrieu, Chem. Phys. Lett. **209**, 126 (1993).

[123] A. Povill, J. Rubio, R. Caballol, and J. P. Malrieu, Chem. Phys. Lett. **218**, 283 (1994).

[124] J. P. Malrieu, J. P. Daudey, and R. Caballol, J. Chem. Phys. **101**, 8908 (1994).

[125] D. E. Woon and T. H. Dunning, J. Chem. Phys. **103**, 4572 (1995).

[126] R. P. Hosteny, T. H. Dunning, R. R. Gilman, A. Pipano, and I. Shavitt, J. Chem. Phys. **62**, 4764 (1975).

[127] V. R. Saunders and J. H. van Lenthe, Mol. Phys. **48**, 923 (1983).

[128] E. R. Davidson, Perspectives on *ab initio* calculations, in *Reviews in Computational Chemistry*, edited by K. B. Lipkowitz and D. B. Boyd. VCH Publishers, New York, 1990.

[129] M. Page, P. Saxe, G. F. Adams, and B. H. Lengsfield, J. Chem. Phys. **81**, 434 (1984).

[130] F. W. Bobrowicz and W. A. Goddard, The self-consistent field equations for generalized valence bond and open-shell Hartree-Fock wave functions, in *Methods of Electronic Structure Theory*, edited by H. F. Schaefer, pages 79–127. Plenum Press, New York, 1977.

[131] B. O. Roos, P. R. Taylor, and P. E. M. Siegbahn, Chem. Phys. **48**, 157 (1980).

[132] W. J. Hunt and W. A. Goddard, Chem. Phys. Lett. **3**, 414 (1969).

[133] C. W. Bauschlicher, J. Chem. Phys. **72**, 880 (1980).

[134] D. Feller and E. R. Davidson, J. Chem. Phys. **74**, 3977 (1981).

[135] E. R. Davidson, *Reduced Density Matrices in Quantum Chemistry.* Academic Press, New York, 1976.

[136] I. Shavitt, B. J. Rosenberg, and S. Palalikit, Int. J. Quantum Chem. Symp. **10**, 33 (1976).

[137] O. Parisel and Y. Ellinger, Chem. Phys. **189**, 1 (1994).

[138] M. R. A. Blomberg and B. Liu, J. Chem. Phys. **89**, 6870 (1988).

[139] K. Balasubramanian, J. Chem. Phys. **89**, 5731 (1988).

[140] S. Diner, J. P. Malrieu, P. Claverie, and F. Jordan, Chem. Phys. Lett. **2**, 319 (1968).

[141] J. P. Malrieu, The pcilo method, in *Semiempirical Methods of Electronic Structure Calculation*, edited by G. A. Segal, volume 7 of *Modern Theoretical Chemistry*, pages 69–103. Plenum Press, New York, 1977.

[142] S. F. Boys, Localized orbitals and localized adjustment functions, in *Quantum Theory of Atoms, Molecules, and the Solid State*, edited by P.-O. Löwdin, pages 253–262. Academic Press, New York, 1966.

[143] S. Saebø and P. Pulay, Chem. Phys. Lett. **113**, 13 (1985).

[144] S. Saebø and P. Pulay, J. Chem. Phys. **88**, 1884 (1988).

[145] I. D. Petsalakis, G. Theodorakopoulos, C. A. Nicolaides, and R. Buenker, J. Chem. Phys. **81**, 3161 (1984).

[146] P.-Å. Malmqvist, Int. J. Quantum Chem. **30**, 479 (1986).

[147] R. Broer and W. C. Nieuwpoort, Theor. Chim. Acta **73**, 405 (1988).

[148] P.-Å. Malmqvist and B. O. Roos, Chem. Phys. Lett. **155**, 189 (1989).

[149] R. J. Buenker and S. D. Peyerimhoff, J. Chem. Phys. **53**, 1368 (1970).

[150] W. D. Allen and H. F. Schaefer, J. Chem. Phys. **87**, 7076 (1987).

[151] G. Fitzgerald and H. F. Schaefer, J. Chem. Phys. **83**, 1162 (1985).

[152] T. J. Lee, W. D. Allen, and H. F. Schaefer, J. Chem. Phys. **87**, 7062 (1987).

[153] S. A. Houlden and I. G. Csizmadia, Theor. Chim. Acta **30**, 209 (1973).

[154] M. Head-Gordon and T. J. Lee, Single reference coupled cluster and perturbation theories of electronic excitation energies, in *Modern Ideas in Coupled Cluster Theory*, edited by R. J. Bartlett. World Scientific, Singapore, 1997.

[155] H. Nakatsuji, Chem. Phys. Lett. **67**, 329 (1979).

[156] H. Nakatsuji, Chem. Phys. Lett. **67**, 334 (1979).

[157] K. Andersson, P.-Å. Malmqvist, B. O. Roos, A. J. Sadlej, and K. Wolinski, J. Chem. Phys. **96**, 5483 (1990).

[158] K. Andersson, P.-Å. Malmqvist, and B. O. Roos, J. Chem. Phys. **96**, 1218 (1992).

[159] K. Andersson and B. O. Roos, Multiconfigurational second-order perturbation theory, in *Modern Electronic Structure Theory*, edited by D. R. Yarkony, volume 2 of *Advanced Series in Physical Chemistry*, pages 55–109. World Scientific, Singapore, 1995.

[160] J. B. Foresman, M. Head-Gordon, J. A. Pople, and M. J. Frisch, J. Phys. Chem. **96**, 135 (1992).

[161] M. Head-Gordon, R. J. Rico, M. Oumi, and T. J. Lee, Chem. Phys. Lett. **219**, 21 (1994).

[162] J. F. Stanton, J. Gauss, N. Ishikawa, and M. Head-Gordon, J. Chem. Phys. **103**, 4160 (1995).

[163] D. Maurice and M. Head-Gordon, Int. J. Quantum Chem. Symp. **29**, 361 (1995).

[164] D. Maurice and M. Head-Gordon, J. Phys. Chem. **100**, 6131 (1996).

[165] J. Wasilewski, Int. J. Quantum Chem. **36**, 503 (1989).

[166] K. Dowd, *High Performance Computing*. O'Reilly, Sebastopol, CA, 1993.

[167] J. A. Pople, R. Seeger, and R. Krishnan, Int. J. Quantum Chem. Symp. **11**, 149 (1977).

[168] H.-J. Werner and E.-A. Reinsch, J. Chem. Phys. **76**, 3144 (1982).

[169] R. Ahlrichs, in *Proceedings of the 5th Seminar on Computational Methods in Quantum Chemistry, Groningen*, edited by P. T. van Duijen and W. C. Nieuwpoort. Max Planck Institut, Garching, Munchen, 1981.

[170] S. Wilson, Four-index transformations, in *Electron Correlation in Atoms and Molecules*, edited by S. Wilson, volume 1 of *Methods in Computational Chemistry*. Plenum, New York, 1987.

[171] M. Häser, J. Almlöf, and M. W. Feyereisen, Theor. Chim. Acta **79**, 115 (1991).

[172] M. Yoshimine, The use of direct access devices in problems requiring the reordering of long lists of data, Technical Report RJ-555, IBM Research Laboratory, San Jose, California, 1969.

[173] P.-Å. Malmqvist, Mathematical tools in quantum chemistry, in *Lecture Notes in Quantum Chemistry: European Summer School in Quantum Chemistry*, edited by B. O. Roos, volume 58 of *Lecture Notes in Chemistry*, pages 1–35. Springer-Verlag, New York, 1992.

[174] B. Liu, The simultaneous expansion method for the iterative solution of several of the lowest eigenvalues and corresponding eigenvectors of large real-symmetric matrices, Technical Report LBL-8158, Lawrence Berkeley Laboratory, University of California, Berkeley, 1978.

[175] C. W. Murray, S. C. Racine, and E. R. Davidson, J. Comput. Phys. **103**, 382 (1992).

[176] R. Shepard, J. Comput. Chem. **11**, 45 (1990).

[177] H. Dachsel and H. Lischka, Theor. Chim. Acta **92**, 339 (1995).

[178] J. H. van Lenthe and P. Pulay, J. Comput. Chem. **11**, 1164 (1990).

[179] Y. Saad, *Numerical Methods for Large Eigenvalue Problems*. Manchester University Press, Manchester, 1992.

[180] G. L. G. Sleijpen and H. A. van der Vorst, A generalized Jacobi-Davidson iteration method for linear eigenvalue problems, Technical Report Preprint 856, Dept. Math., Utrecht University, 1994.

[181] J. M. Bofill and J. M. Anglada, Chem. Phys. **183**, 19 (1994).

[182] H. J. J. van Dam, J. H. van Lenthe, G. L. G. Sleijpen, and H. A. van der Vorst, J. Comput. Chem. **17**, 267 (1996).

[183] A. O. Mitrushenkov, Chem. Phys. Lett. **217**, 559 (1994).

[184] C. Ribbing and C. Daniel, J. Chem. Phys. **100**, 6591 (1994).

[185] R. Pauncz, *Spin Eigenfunctions: Construction and Use.* Plenum, New York, 1979.

[186] R. Pauncz, *The Symmetric Group in Quantum Chemistry.* CRC Press, Boca Raton, 1995.

[187] W. Duch, Chem. Phys. Lett. **162**, 56 (1989).

[188] W. Duch and J. Meller, Int. J. Quantum Chem. **50**, 243 (1994).

[189] T. J. Martinez, A. Mehta, and E. A. Carter, J. Chem. Phys. **97**, 1876 (1992).

[190] T. J. Martinez, A. Mehta, and E. A. Carter, J. Chem. Phys. **99**, 4238(E) (1993).

[191] T. J. Martinez and E. A. Carter, J. Chem. Phys. **102**, 7564 (1995).

[192] G. Reynolds, T. J. Martinez, and E. A. Carter, J. Chem. Phys. **105**, 6455 (1996).

[193] B. Roos, Chem. Phys. Lett. **15**, 153 (1972).

[194] P. E. M. Siegbahn, J. Chem. Phys. **72**, 1647 (1980).

[195] P. E. M. Siegbahn, J. Chem. Phys. **70**, 5391 (1979).

[196] H. Lischka, R. Shepard, F. B. Brown, and I. Shavitt, Int. J. Quantum Chem. Symp. **15**, 91 (1981).

[197] M. Schüler, T. Kovar, H. Lischka, R. Shepard, and R. J. Harrison, Theor. Chim. Acta **84**, 489 (1993).

[198] H. Dachsel, H. Lischka, R. Shepard, J. Nieplocha, and R. J. Harrison, J. Comput. Chem. **18**, 430 (1997).

[199] W. Duch and J. Karwowski, Computer Phys. Rept. **2**, 93 (1985).

[200] W. Duch, Chem. Phys. Lett. **124**, 442 (1986).

[201] A. Guldberg, S. Rettrup, G. L. Bendazzoli, and P. Palmieri, Int. J. Quantum Chem. Symp. **21**, 513 (1987).

[202] W. Duch and J. Karwowski, Theor. Chim. Acta **71**, 187 (1987).

[203] W. Duch, Int. J. Quantum Chem. Symp. **234**, 683 (1990).

[204] N. Flocke, Int. J. Quantum Chem. **61**, 747 (1997).

[205] M. W. Lucht, Phys. Rev. A **54**, 266 (1996).

[206] R. D. Kent and M. Schlesinger, Phys. Rev. A **50**, 186 (1994).

[207] Z. Wen, Y. Wang, and H. Lin, Chem. Phys. Lett. **230**, 41 (1994).

[208] M. D. Gould and J. S. Battle, J. Chem. Phys. **99**, 5961 (1993).

[209] M. D. Gould and J. S. Battle, J. Chem. Phys. **99**, 5983 (1993).

[210] R. D. Kent, M. Schlesinger, and I. Shavitt, Int. J. Quantum Chem. **41**, 89 (1992).

[211] P. J. Burton and M. D. Gould, J. Chem. Phys. **96**, 5261 (1992).

[212] B. Jeziorski, J. Paldus, and P. Jankowski, Int. J. Quantum Chem. **56**, 129 (1995).

[213] P. Saxe, H. F. Schaefer, and N. C. Handy, Chem. Phys. Lett. **79**, 202 (1981).

[214] P. J. Knowles and N. C. Handy, Computer Phys. Commun. **54**, 75 (1989).

[215] A. Povill, J. Rubio, and F. Illas, Theor. Chim. Acta **82**, 229 (1992).

[216] A. O. Mitrushenkov and Y. Y. Dmitriev, Chem. Phys. Lett. **235**, 410 (1995).

[217] S. Zarrabian, C. R. Sarma, and J. Paldus, Chem. Phys. Lett. **155**, 183 (1989).

[218] P. J. Knowles and N. C. Handy, J. Chem. Phys. **91**, 2396 (1989).

[219] F. Illas, J. Rubio, J. M. Ricart, and P. S. Bagus, J. Chem. Phys. **95**, 1877 (1991).

[220] A. Povill and J. Rubio, Theor. Chim. Acta **92**, 305 (1995).

[221] R. Caballol and J. P. Malrieu, Chem. Phys. Lett. **188**, 543 (1992).

[222] S. Krebs and R. J. Buenker, J. Chem. Phys. **103**, 5613 (1995).

[223] R. J. Harrison, J. Chem. Phys. **94**, 5021 (1991).

[224] A. V. Luzanov, A. L. Wulfov, and V. O. Krouglov, Chem. Phys. Lett. **197**, 614 (1992).

[225] A. L. Wulfov, Chem. Phys. Lett. **255**, 300 (1996).

[226] A. O. Mitrushenkov, J. Chem. Phys. **105**, 10487 (1996).

[227] R. J. Cave, S. S. Xantheas, and D. Feller, Theor. Chim. Acta **83**, 31 (1992).

[228] A. L. Wulfov, Chem. Phys. Lett. **263**, 79 (1996).

[229] M. L. Leininger, C. D. Sherrill, W. D. Allen, and H. F. Schaefer, manuscript in preparation.

[230] W. Duch, *GRMS or Graphical Representation of Model Spaces*, volume 1. Springer-Verlag, Berlin, 1986.

[231] D. H. Lehmer, in *Applied Combinatorial Mathematics*, edited by E. F. Beckenbach. Wiley, New York, 1964.

[232] J. Olsen, Private communication, 1995.

[233] C. W. Bauschlicher, S. R. Langhoff, P. R. Taylor, and H. Partridge, Chem. Phys. Lett. **126**, 436 (1986).

[234] C. W. Bauschlicher, S. R. Langhoff, P. R. Taylor, N. C. Handy, and P. J. Knowles, J. Chem. Phys. **85**, 1469 (1986).

[235] C. W. Bauschlicher and P. R. Taylor, J. Chem. Phys. **85**, 2779 (1986).

[236] C. W. Bauschlicher and P. R. Taylor, J. Chem. Phys. **85**, 6510 (1986).

[237] C. W. Bauschlicher and P. R. Taylor, J. Chem. Phys. **86**, 858 (1987).

[238] C. W. Bauschlicher and P. R. Taylor, J. Chem. Phys. **86**, 1420 (1987).

[239] C. W. Bauschlicher and P. R. Taylor, J. Chem. Phys. **87**, 2844 (1987).

[240] C. W. Bauschlicher and S. R. Langhoff, J. Chem. Phys. **87**, 2919 (1987).

[241] C. W. Bauschlicher and S. R. Langhoff, J. Chem. Phys. **86**, 5595 (1987).

[242] C. W. Bauschlicher and P. R. Taylor, J. Chem. Phys. **86**, 5600 (1987).

[243] J. D. Watts, I. Cernusak, J. Noga, R. J. Bartlett, C. W. Bauschlicher, T. J. Lee, A. P. Rendell, and P. R. Taylor, J. Chem. Phys. **93**, 8875 (1990).

[244] C. W. Bauschlicher, J. Chem. Phys. **86**, 5591 (1987).

[245] P. R. Taylor, C. W. Bauschlicher, and S. R. Langhoff, J. Phys. B **21**, L333 (1988).

[246] C. W. Bauschlicher, J. Phys. Chem. **92**, 3020 (1988).

[247] F. Illas, J. M. Ricart, J. Rubio, and P. S. Bagus, J. Chem. Phys. **93**, 4982 (1990).

[248] J. Casanovas, J. Rubio, and F. Illas, Chem. Phys. Lett. **180**, 578 (1991).

[249] C. W. Bauschlicher, S. R. Langhoff, and P. R. Taylor, J. Chem. Phys. **88**, 2540 (1988).

[250] C. W. Bauschlicher, S. R. Langhoff, and P. R. Taylor, J. Chem. Phys. **93**, 502 (1990).

[251] O. Christiansen, J. Olsen, P. Jørgensen, H. Koch, and P.-Å. Malmqvist, Chem. Phys. Lett. **261**, 369 (1996).

[252] J. Olsen, A. M. Sánchez de Meras, H. J. Aa. Jensen, and P. Jørgensen, Chem. Phys. Lett. **154**, 380 (1989).

[253] C. W. Bauschlicher and P. R. Taylor, Theor. Chim. Acta **71**, 263 (1987).

[254] C. W. Bauschlicher and S. R. Langhoff, Chem. Phys. Lett. **135**, 67 (1987).

[255] C. W. Bauschlicher and S. R. Langhoff, Theor. Chim. Acta **73**, 43 (1988).

[256] C. W. Bauschlicher and S. R. Langhoff, Theor. Chim. Acta **79**, 93 (1991).

[257] H. Koch and R. J. Harrison, J. Chem. Phys. **95**, 7479 (1991).

[258] C. W. Bauschlicher, S. R. Langhoff, H. Partridge, and D. P. Chong, J. Chem. Phys. **89**, 2985 (1988).

[259] O. Vahtras, H. Ågren, P. Jørgensen, H. J. A. Jensen, T. Helgaker, and J. Olsen, J. Chem. Phys. **96**, 2118 (1992).

[260] M. M. Marino, W. C. Ermler, C. W. Kern, and V. E. Bondybey, J. Chem. Phys. **96**, 3756 (1992).

[261] P. R. Taylor, A. Komornicki, and D. A. Dixon, J. Am. Chem. Soc. **111**, 1259 (1988).

[262] J. M. Anglada and J. M. Bofill, Theor. Chim. Acta **92**, 369 (1995).

[263] Y. Yamaguchi, J. F. Gaw, R. B. Remington, and H. F. Schaefer, J. Chem. Phys. **86**, 5072 (1987).

[264] C. D. Sherrill, T. J. Van Huis, Y. Yamaguchi, and H. F. Schaefer, J. Mol. Struct. (Theochem) **400**, 139 (1997).

[265] T. J. Van Huis, M. L. Leininger, C. D. Sherrill, and H. F. Schaefer, manuscript in preparation.

[266] C. D. Sherrill, M. L. Leininger, T. J. Van Huis, and H. F. Schaefer, J. Chem. Phys., submitted.

[267] D. E. Woon, J. Chem. Phys. **100**, 2838 (1994).

[268] R. Moszynski, B. Jeziorski, A. Ratkiewicz, and S. Rybak, J. Chem. Phys. **99**, 8856 (1993).

[269] R. Moszynski, B. Jeziorski, and K. Szalewicz, J. Chem. Phys. **100**, 1312 (1994).

[270] I. Mayer, A. Vibok, and P. Valiron, Chem. Phys. Lett. **224**, 166 (1994).

[271] J. V. Burda, R. Zahradník, P. Hobza, and M. Urban, Mol. Phys. **89**, 425 (1996).

[272] M. R. A. Blomberg, P. E. M. Siegbahn, and B. O. Roos, Int. J. Quantum Chem. Symp. **14**, 229 (1980).

[273] R. A. Chiles and C. E. Dykstra, J. Chem. Phys. **74**, 4544 (1981).

[274] V. E. Bondybey, Chem. Phys. Lett. **109**, 436 (1984).

[275] H. Partridge, C. W. Bauschlicher, L. G. M. Pettersson, A. D. McLean, B. Liu, M. Yoshimine, and A. Komornicki, J. Chem. Phys. **92**, 5377 (1990).

[276] W. Koch, B. Liu, and G. Frenking, J. Chem. Phys. **92**, 2464 (1990).

[277] S. R. Langhoff, C. W. Bauschlicher, and P. R. Taylor, Chem. Phys. Lett. **135**, 543 (1987).

[278] J. Almlöf, B. J. DeLeeuw, P. R. Taylor, C. W. Bauschlicher, and P. Siegbahn, Int. J. Quantum Chem. Symp. **23**, 345 (1989).

[279] H. Partridge, S. R. Langhoff, C. W. Bauschlicher, and D. W. Schwenke, J. Chem. Phys. **88**, 3174 (1988).

[280] C. W. Bauschlicher, S. R. Langhoff, and L. G. M. Pettersson, J. Chem. Phys. **89**, 5747 (1988).

[281] K. Balasubramanian, J. Chem. Phys. **93**, 507 (1990).

[282] K. Balasubramanian, J. Phys. Chem. **94**, 7764 (1990).

[283] K. K. Das and K. Balasubramanian, J. Chem. Phys. **93**, 5883 (1990).

[284] Z. Ma and K. Balasubramanian, Chem. Phys. Lett. **181**, 467 (1991).

[285] K. Balasubramanian, Chem. Phys. Lett. **164**, 231 (1989).

[286] K. Balasubramanian and J. X. Tao, J. Chem. Phys. **94**, 3000 (1991).

[287] D.-W. Liao and K. Balasubramanian, Chem. Phys. Lett. **213**, 174 (1993).

[288] K. Balasubramanian, J. Chem. Phys. **93**, 8061 (1990).

[289] P. Saxe, H. F. Schaefer, and N. C. Handy, J. Phys. Chem. **85**, 745 (1981).

[290] C. W. Bauschlicher, S. R. Langhoff, and P. R. Taylor, J. Chem. Phys. **87**, 387 (1987).

[291] A. D. McLean, P. R. Bunker, R. M. Escribano, and P. Jensen, J. Chem. Phys. **87**, 2166 (1987).

[292] P. Jensen and P. R. Bunker, J. Chem. Phys. **89**, 1327 (1988).

[293] E. R. Davidson, D. Feller, and P. Phillips, Chem. Phys. Lett. **76**, 416 (1980).

[294] N. C. Handy, Y. Yamaguchi, and H. F. Schaefer, J. Chem. Phys. **84**, 4481 (1986).

[295] K. Balasubramanian, Chem. Phys. Lett. **127**, 585 (1986).

[296] K. K. Das and K. Balasubramanian, J. Chem. Phys. **91**, 2433 (1989).

[297] K. Balasubramanian, J. Chem. Phys. **91**, 2443 (1989).

[298] K. K. Das and K. Balasubramanian, J. Phys. Chem. **95**, 3979 (1991).

[299] K. Balasubramanian, Chem. Phys. Lett. **204**, 601 (1993).

[300] G. Parlant, J. Senekowitsch, S. V. ONeil, and D. R. Yarkony, J. Chem. Phys. **94**, 7208 (1991).

[301] M. R. Manaa and D. R. Yarkony, J. Chem. Phys. **95**, 6562 (1991).

[302] H. Hettema and D. R. Yarkony, J. Chem. Phys. **100**, 8991 (1994).

[303] D. L. Strout and G. E. Scuseria, J. Chem. Phys. **96**, 9025 (1992).

[304] H. J. Aa. Jensen, P. Jørgensen, T. Helgaker, and J. Olsen, Chem. Phys. Lett. **162**, 355 (1989).

[305] A. M. Sánchez de Meras, H. J. Aa. Jensen, P. Jørgensen, and J. Olsen, Chem. Phys. Lett. **186**, 379 (1991).

[306] D. Sundholm and J. Olsen, Chem. Phys. Lett. **198**, 526 (1992).

[307] D. Sundholm and J. Olsen, Chem. Phys. Lett. **217**, 451 (1994).

[308] T. J. Lee, R. B. Remington, Y. Yamaguchi, and H. F. Schaefer, J. Chem. Phys. **89**, 408 (1988).

[309] G. E. Scuseria, T. P. Hamilton, and H. F. Schaefer, J. Chem. Phys. **92**, 568 (1990).

[310] G. E. Scuseria and H. F. Schaefer, J. Chem. Phys. **88**, 7024 (1988).

[311] H. Tanaka and K. Nishimoto, J. Mol. Struct. (Theochem) **50**, 297 (1988).

[312] P. Du, D. A. Hrovat, and W. T. Borden, J. Am. Chem. Soc. **108**, 8086 (1986).

[313] R. A. King, C. D. Sherrill, and H. F. Schaefer, Spectrochim. Acta, Part A **53**, 1163 (1997).

[314] B. C. Hoffman, C. D. Sherrill, and H. F. Schaefer, Chem. Phys. Lett. , submitted.

[315] M. L. Leininger and H. F. Schaefer, J. Chem. Phys., in press.

A Critical Assessment of Multireference-Fock Space CCSD and Perturbative Third-Order Triples Approximations for Photoelectron Spectra and Quasidegenerate Potential Energy Surfaces

David E. Bernholdt* and Rodney J. Bartlett†

Quantum Theory Project
University of Florida
Gainesville, Florida 32611–8435

Abstract

Equations for the Fock space coupled cluster method, including all single, double, and triple excitations (FSCCSDT) for ionization potentials [(0,1) sector], are presented in both operator and spin orbital form. Two approximations to the full FSCCSDT equations are described, one being the simplest perturbative inclusion of triple excitation effects, FSCCSD+T(3), and a second that indirectly incorporates certain higher-order effects, FSCCSD+T*(3).

The performance of these approximations, along with FSCCSD, has been studied in comparison with single reference coupled cluster (CC) methods and with experiment for a variety of ionization potential (IP) and potential energy surface (PES) problems. (CH_2, CH_2NH, CH_2PH, O_2, H_2CO, N_2, ketene, and diazomethane for IPs and CO_2, NO_3, and C_3^+ for PES.) For ionization potentials, the FSCCD and FSCCSD+T*(3) methods are generally found to perform comparably to single reference CC with perturbative inclusion of triple excitations overall, while for the more demanding application to potential energy surfaces, FSCC methods with the current perturbative triple corrections do not appear to match the high-quality single reference CC results. But because of the speed and ease of use compared to single reference CC methods, FSCC methods, including triple excitation effects, are sufficiently accurate to be extremely useful tools when used with care. Unlike most single reference methods, Fock space CC methods are also particularly suited to "final state" studies of quasidegenerate

* Northeast Parallel Architectures Center, Syracuse University, Syracuse NY 13244–4100; *bernhold@npac.syr.edu*

† *bartlett@qtp.ufl.edu*

ADVANCES IN QUANTUM CHEMISTRY, VOLUME 34

0065-3276/99 $30.00

potential energy surfaces. Several examples of this type (CO_2, NO_3, and C_3^+) are analyzed.

Introduction

For nondegenerate systems, single reference coupled cluster (CC) methods have proven to be quite successful in their description of the electron correlation problem (1–3). This is primarily due to their (size) extensivity and ability to efficiently incorporate higher-order correlation effects—CC models including triple excitation effects are generally within 1–2 kcal mol^{-1} of full CI (3).

Multireference coupled cluster methods, which started development more recently, are generally divided into two types. Hilbert space CC methods use multiple reference functions to obtain a description of a few states, including the reference state (for a review see (4)). Fock space methods (for a review see (5)), on the other hand, provide direct state-to-state energy differences, relative to some common reference state. The Fock space approach is particularly well-suited to the calculation of ionization potentials (IPs), electron affinities (EAs), and excitation energies (EEs). For principal IPs and EAs, FSCC is equivalent (6, 7) to the EOM-IP and EOM-EA CC methods (1, 2, 7, 8). In this paper, we will focus primarily on the IP problem.

Calculations of IPs that have been performed using the FSCCD and FSCCSD methods (5, 6, 9–12) suggest that the results are numerically on par with other methods, and because it can provide results for many states at once, it can be significantly more efficient than single reference CC methods, which require separate calculations for each state. One of the fundamental differences between the Fock space and single reference approaches lies in the excitation operators. Equivalent truncations of the cluster operators do not result in an equivalent flexibility in the description of the correlated wavefunction. For example, certain double excitations in the single reference approach only appear as triple excitations in FSCC. Consequently, it is interesting to explore higher level FSCC treatments and compare them with the performance of simple Fock space methods such as FSCCSD, and with single reference calculations.

Haque and Kaldor (13), and Pal, Rittby, and Bartlett (14) have reported implementations of methods which incorporate the lowest order effects of triple excitations, here referred to as FSCCSD+T(3) and FSCCSD+T*(3), including a few demonstrative results. In this paper, we extend the previous work by presenting detailed equations in the spin orbital framework that allow for the use of both open- (15) and closed-shell reference functions. We then go on to examine the performance of these methods on a much wider range of systems than have been studied previously in order to assess their strengths and weaknesses.

Fock Space Coupled Cluster Theory

In the Fock space coupled cluster method, the Hartree-Fock solution for an N-electron state, $|0\rangle$, is used as the vacuum. The Fock space is divided into sectors, (m,n), according to how many electrons are added to and removed from $|0\rangle$. Thus, the vacuum is in the (0,0) sector, single ionizations are in the (0,1) sector, one-electron attached states are in (1,0), and (1,1) are single excitations relative to $|0\rangle$. The orbitals are also divided into *active*, which can change occupation, and *inactive*, for which the occupation is fixed. All possible occupations of the active orbitals in all possible sectors constitute the multireference *space* for the system.

The FSCC equations can be derived from the Schrödinger equation written in the form

$$H\Omega|\Psi_k\rangle = E_k\Omega|\Psi_k\rangle, \tag{1}$$

where the FSCC wavefunction,

$$|\Psi_{\mathrm{FSCC}}\rangle = \Omega|\Psi_k\rangle, \tag{2}$$

is expressed as a wave operator, Ω, operating on a linear combination of model space functions

$$|\Psi_k\rangle = \sum_i C_{ki}|\phi_i\rangle. \tag{3}$$

The wave operator is similar to that used in the single reference theory with the normal product imposed to eliminate contractions among the cluster operators themselves (which are not possible in the single reference case),

$$\Omega = \{e^S\}. \tag{4}$$

The cluster operator itself, however, has a somewhat different structure from the single reference case:

$$S = S^{(m,n)} = \sum_{\substack{k=0\ldots m \\ l=0\ldots n}} T^{(k,l)}, \tag{5}$$

where (m,n) is the highest sector relevant to the problem, and the $T^{(k,l)}$ for a given sector includes single, double, and higher excitation cluster operators for that sector:

$$T^{(k,l)} = T_1^{(k,l)} + T_2^{(k,l)} + T_3^{(k,l)} + \cdots. \tag{6}$$

Note that $T^{(0,0)}$ is simply the familiar (single reference) CC cluster operator.

This Schrödinger equation can be rewritten in terms of the model space functions by defining a matrix ϵ' having the E_k as eigenvalues and $\mathbf{C}$ as eigenvectors and using the model space projector, P, to effectively encompass the entire model space,

$$H\Omega P = \Omega\epsilon' P. \tag{7}$$

Using the fact that the (0,0) sector cluster operator commutes with the others (16), we can decouple the (0,0) sector calculation from the rest of the FSCC calculation. This requires redefining the wave operator,

$$\Omega = e^{T^{(0,0)}}\tilde{\Omega} = e^{T^{(0,0)}}\left\{e^{\tilde{S}^{(m,n)}}\right\}, \tag{8}$$

where

$$\tilde{S}^{(m,n)} = \sum_{\substack{k=0\ldots m, l=0\ldots n \\ k+l\neq 0}} T^{(k,l)}, \tag{9}$$

and shifting the eigenvalues, eliminating the energy of the (0,0) sector CC reference function, $E_{cc}|0\rangle$,

$$\epsilon = \epsilon' - E_{cc}|0\rangle. \tag{10}$$

The resulting equation,

$$\bar{H}_N\tilde{\Omega}P = \tilde{\Omega}\epsilon P, \tag{11}$$

requires the (0,0) sector CC wavefunction as a reference, but it is not changed by the FSCC calculation.

Projecting Eq. 11 on the left with $P\tilde{\Omega}^{-1}$, we can isolate ϵ as the FSCC *effective Hamiltonian,*

$$PH_{N,\text{eff}}P \equiv P\tilde{\Omega}^{-1}\bar{H}_N\tilde{\Omega}P = P\epsilon P, \tag{12}$$

which, upon diagonalization, gives the state-to-state energy differences we seek (relative to $E_{cc}|0\rangle$). Mukherjee and coworkers have shown that for complete and quasi-complete model spaces (the (0,1) sector is complete), $H_{N,\text{eff}}$ is connected, and the energies obtained by diagonalizing it are size extensive (17–20, 11, 21). To determine the cluster operators, we project Eq. 11 on the left with the complementary space determinants, giving

$$Q\bar{H}_N\tilde{\Omega}P - Q\tilde{\Omega}PH_{N,\text{eff}}P = 0, \tag{13}$$

which is often referred to as the Bloch equation.

As our objective is to determine the amplitudes in Eq. 9, we would need to find the $T^{(k,l)}$ for the various sectors to completely define the *valence universal* wave operator (16, 22). The first step is to obtain $T^{(0,1)}$, which, alone, is sufficient for principal IPs. This sector (and the (1,0) sector) can be solved with only the (0,0) results—they do not depend on any higher sectors. Using this fact, it is straightforward to expand the operators in Eq. 13 and obtain the specific equations for FSCCSDT in the (0,1) sector.

$$P^{(0,1)}\bar{H}_{N,\text{eff}}P^{(0,1)} = P^{(0,1)}\Big\{\bar{f}_N\Big(1 + T_1^{(0,1)} + T_2^{(0,1)}\Big) \Big\{+\bar{W}_N\Big(T_2^{(0,1)} + T_3^{(0,1)}\Big) + I\bar{I}I_N T_3^{(0,1)}\Big\}_c P^{(0,1)} \tag{14}$$

$$0 = Q_1^{(0,1)}\Big\{\bar{f}_N\Big(1 + T_1^{(0,1)} + T_2^{(0,1)}\Big) + \bar{W}_N\Big(T_2^{(0,1)} + T_3^{(0,1)}\Big) \Big\{+I\bar{I}I_N T_3^{(0,1)} - T_1^{(0,1)}\bar{H}_{N,\text{eff}}^{(0,1)}\Big\}_c P^{(0,1)} \tag{15}$$

$$0 = Q_2^{(0,1)}\Big\{\bar{f}_N\Big(T_2^{(0,1)} + T_3^{(0,1)}\Big) + \bar{W}_N\Big(1 + T_1^{(0,1)} + T_2^{(0,1)} + T_3^{(0,1)}\Big) \Big\{+I\bar{I}I_N\Big(T_2^{(0,1)} + T_3^{(0,1)}\Big) - T_2^{(0,1)}\bar{H}_{N,\text{eff}}^{(0,1)}\Big\}_c P^{(0,1)} \tag{16}$$

$$0 = Q_3^{(0,1)}\Big\{\bar{f}_N T_3^{(0,1)} + \bar{W}_N\Big(T_2^{(0,1)} + T_3^{(0,1)}\Big) + I\bar{I}I_N\Big(1 + T_1^{(0,1)} + T_2^{(0,1)} + T_3^{(0,1)}\Big) \Big\{-T_3^{(0,1)}\bar{H}_{N,\text{eff}}^{(0,1)}\Big\}_c P^{(0,1)} \tag{17}$$

Note that in these equations, we have $P^{(0,1)}$, which projects out model space determinants in the (0,1) sector, and its orthogonal complement, which is further decomposed into single, double, and triple excitations, $Q_1^{(0,1)}$, $Q_2^{(0,1)}$, and $Q_3^{(0,1)}$.

These operator equations can be transformed into spin-orbital form, essentially that necessary for a computer implementation, after spin integrations, via the usual CC methods. The resulting equations for the FSCCSDT method for ionization potentials are given in Eq. 18–21, below.

$$(H_{N,\mathrm{eff}})_{\bar{l}\bar{k}} = \bar{f}_{\bar{l}\bar{k}} - \bar{f}_{\dot{m}\bar{k}}\tau^{\bar{l}}_{\dot{m}} + \bar{f}_{me}\tau^{\bar{l}e}_{\bar{k}m} - \frac{1}{2}\left\langle mn\bar{\|}\ddot{k}e\right\rangle\tau^{\bar{l}e}_{mn} + \frac{1}{4}\langle mn\bar{\|}ef\rangle\tau^{\bar{l}ef}_{\bar{k}mn} \quad (18)$$

$$0 = \bar{f}_{\bar{l}\bar{k}} - \bar{f}_{\dot{m}\bar{k}}\tau^{\bar{l}}_{\dot{m}} + \bar{f}_{me}\tau^{\bar{l}e}_{\bar{k}m} - \frac{1}{2}\left\langle mn\bar{\|}\dot{k}e\right\rangle\tau^{\bar{l}e}_{mn} + \frac{1}{4}\langle mn\bar{\|}ef\rangle\tau^{\bar{l}ef}_{\bar{k}mn} + \tau^{\ddot{m}}_{\bar{k}}(H_{N,\mathrm{eff}})_{\bar{l}\ddot{m}} \quad (19)$$

$$\begin{aligned} 0 = {} & \left\langle \ddot{l}a\bar{\|}ki\right\rangle + \bar{f}_{ae}\tau^{\bar{l}a}_{ki} - (-1)^p P(ki)\bar{f}_{mi}\tau^{\bar{l}a}_{km} - \langle \dot{m}a\bar{\|}ki\rangle\tau^{\bar{l}}_{\dot{m}} \\ & + \frac{1}{2}(-1)^p P(ki)\langle mn\bar{\|}ki\rangle\tau^{\bar{l}a}_{mn} - \langle ma\bar{\|}ke\rangle\tau^{\bar{l}e}_{mi} - \frac{1}{2}\langle man\bar{\|}kie\rangle\tau^{\bar{l}e}_{mn} \\ & + \bar{f}_{me}\tau^{\bar{l}ae}_{kim} + \frac{1}{2}(-1)^p P(ki)\langle mn\bar{\|}ke\rangle\tau^{\bar{l}ea}_{mni} + \frac{1}{2}\langle ma\bar{\|}ef\rangle\tau^{\bar{l}ea}_{kmi} + \tau^{\ddot{m}a}_{ki}(H_{N,\mathrm{eff}})_{\bar{l}\ddot{m}} \end{aligned} \quad (20)$$

$$\begin{aligned} 0 = {} & \left\langle \ddot{l}ab\bar{\|}kij\right\rangle - (-)^p P(k/ij)\langle mb\bar{\|}ij\rangle\tau^{\bar{l}a}_{km} + (-)^p P(ki/j)\langle ab\bar{\|}ej\rangle\tau^{\bar{l}e}_{ki} \\ & + \frac{1}{2}(-)^p P(ab)\langle man\bar{\|}kij\rangle\tau^{\bar{l}b}_{mn} - (-)^p P(ki/j)\langle mib\bar{\|}kie\rangle\tau^{\bar{l}e}_{mj} - \langle \dot{m}ab\bar{\|}kij\rangle\tau^{\bar{l}}_{\dot{m}} \\ & + (-)^p P(ab)\bar{f}_{be}\tau^{\bar{l}ae}_{kij} - (-)^p P(ki/j)\bar{f}_{mj}\tau^{\bar{l}ab}_{kim} + (-)^p P(ki/j)\langle mn\bar{\|}ki\rangle\tau^{\bar{l}ab}_{mnj} \\ & - (-)^p P(k/ij,ab)\langle ma\bar{\|}ke\rangle\tau^{\bar{l}eb}_{mij} + \tau^{\ddot{m}ab}_{kij}(H_{N,\mathrm{eff}})_{\bar{l}\ddot{m}} \end{aligned} \quad (21)$$

Here, the Fock-space cluster amplitudes are called τ to avoid any possibility of confusion with the (0,0) sector amplitudes, t. The two- and three-body components of $\bar{H}_N$, $\bar{W}_N$ and $I\bar{I}I_N$ are written similarly to two- and three-electron integrals with the addition of a horizontal bar, $\langle pq\bar{\|}rs\rangle$ and $\langle pqr\bar{\|}stu\rangle$. A single dot on an orbital index, $\dot{m}$, indicates restriction to *inactive* orbitals, and a double dot, $\ddot{m}$, indicates restriction to *active* orbitals.

In the single reference CC world, the full CCSDT model (23–26) has seen modest use because it requires a substantial effort over CCSD to code, and because the resource requirements—CPU time, memory, disk—are significantly greater. As a result, a number of approximations to the full CCSDT method have been proposed and have proven quite effective at incorporating important effects of triple excitations while at the same time minimizing the above concerns (27–31). In the same spirit, we examine the FSCCSDT equations with an eye to approximating or ignoring the most expensive terms to evaluate. In this sense, the simplest possible approximation would be to evaluate the triple

excitation contribution perturbatively from converged FSCCSD amplitudes. The single reference analog to this approach is the CCSD+T(CCSD) (also known as CCSD[T]) method, in which the triple excitation contribution is correct through fourth order—the first order at which it appears.

For the FSCC perturbation expansion, we follow the choice of Pal, Rittby, and Bartlett (14) (which was also implicit in the work of Haque and Kaldor (13)), of counting orders in terms of H, the reference state Hamiltonian. Alternatives, such as using $\bar{H}$ would lead to inconsistencies between the (0,0) sector definitions and those of higher sectors. For example, $\bar{f}$ and $\bar{W}$ are first order in H, while the higher components, $I\bar{I}I, \ldots$ are at least second order. Counting orders in $\bar{H}$ would place all of these terms on the same level, making a perturbation expansion of Eq. 17 useless.

Although in both CC and FSCC the triple excitation amplitudes first appear in second order of perturbation theory, in the CC formalism, excitations beyond singles and doubles contribute only indirectly to the energy via their contributions to the singles and doubles amplitudes, and thus triples first appear in the energy in *fourth* order. In FSCC, all clusters contribute directly to $H_{N,\mathrm{eff}}$ and thus the energy, so the triples first manifest themselves in *third* order. Inclusion of the third order triples effects based on converged FSCCSD amplitudes was first proposed by Haque and Kaldor (13) and called CCSD+T. Later, Pal, Rittby, and Bartlett (14) discuss the third order model, MRCCSD+T(3), and propose several other approximations. The MRCCSD+T*(3) model attempts to include some higher-order terms by replacing the f and W required in T(3) with their counterparts from the effective Hamiltonian, $\bar{f}$ and $\bar{W}$. The nature of this method, which will be referred to as *FSCCSD+T(3)* in this work (32), can be seen from the spin orbital FSCCSDT equations given above. The terms that contribute to the $T_3^{(0,1)}$ amplitudes in second order are those on the first row of Eq. 21, with appropriate restrictions on the $\bar{H}_N$ elements: the $\bar{W}_N$ elements of the second and third terms are simply the bare two-electron integrals in first order, and only two terms of $\langle lab\bar{|}|kij\rangle$ appear at this level. The second-order triples amplitudes in turn contribute to $H_{N,\mathrm{eff}}$ (and thus the energy) in third order through the final term of $H_{N,\mathrm{eff}}$ in Eq. 18. More recently, another triples approximation in the IP-EOM-CC context has been suggested by Stanton and Gauss (33).

The FSCCSD+T(3) and T*(3) methods have been implemented for both RHF and UHF reference functions (15, 32) within the ACES II program system (34).

Effect of Changes in the Active Space on Approximations to FSCCSDT

It may be shown that for the (0,1) sector of Fock-space, the values of the roots obtained by diagonalizing $H_{N,\text{eff}}$ are independent of the active space used for the calculation. In other words, if two orbitals, a and b are taken as active, the resulting ionization potentials would be identical to those obtained from separate calculations with either a or b alone active. This is a very useful result because it means that we do not have to worry about choosing the "right" active space for a given calculation in order to get good results. However the proof of this invariance rests on the FSCC amplitudes and $H_{N,\text{eff}}$ satisfying the Fock-space Bloch equation 13. The approximate FSCCSDT methods described above do not satisfy Eq. 13, so the invariance is lost.

In order to assess the magnitude of this effect, calculations have been carried out on a number of molecules using different active spaces (32). The results suggest that a reasonable estimate of the error bars due to changes in the active space is ±2 mH (±0.05 eV or ±1.3 kcal mol^{-1}) for both the T(3) and T*(3) methods. Although some of the systems in the study displayed even larger variations for certain IPs, a great many were more than an order of magnitude better than this figure. Indeed, for molecules with symmetry, many of the IPs exhibit no variation because there is only one possible choice of active space in that symmetry. In addition, it is a fairly simple matter, and not computationally expensive, to obtain a feel for the variation of any molecule of interest. Only one (0,0) sector calculation is required to try out several FSCC active spaces, and the FSCC calculations themselves are very inexpensive compared to the (0,0) reference.

As a result, while the uncertainties associated with changing the active space in T(3) and T*(3) calculations for the general case might be considered large for some applications, much tighter limits may often be obtained with minimal effort. For the remainder of this paper, the active spaces used will correspond directly to those results which are reported. Uncertainties due to the active space will be introduced into discussions as appropriate.

Ionization Potentials

Although it can be used in many other ways, the "natural" result of a (0,1) sector FSCC calculation is the energy of the vertical ionization process—extracting an electron from a molecule without allowing the geometry to relax to that of the resulting ion. Calculation of ionization potentials is, thus far, the predominant application of the FSCCSD method and such calculations will provide the bulk of the data for characterization of the approximate triples

Table I. Vertical ionization potentials of $^1A_1$ and $^3B_1$ CH_2 (in eV) calculated with a DZP basis.

Method	$^1A_1 \rightarrow$			$^3B_1 \rightarrow$	
	1^2A_1	2^2A_1	$^2B_2$	$^2A_1$	$^2B_1$
FSCCSD	10.21	22.54	14.92	10.14	11.30
FSCCSD+T(3)	10.32	22.74	15.00	10.26	11.43
FSCCSD+T*(3)	10.28	22.68	14.96	10.23	11.39
Full CI	10.26	22.14	14.85	10.16	11.31
QRHF-CCSD	10.20	22.25	14.84	10.14	11.30
QRHF-CCSD[T]	10.25	22.28	14.85	10.16	11.31
QRHF-CCSDT-1	10.25	22.28	14.85		
QRHF-CCSDT	10.25	22.15	14.85		

Note: Geometry, basis set, and full CI results taken from Bauschlicher and Taylor (35). QRHF-CC results for $^1A_1$ ionizations from Watts and Bartlett (26). $^3B_1$ calculations used a UHF-CCSD reference function.

methods. These results will be compared with SRCC calculations, experimental results, and a benchmark full CI calculation for the methylene molecule (35).

Table I presents FSCC calculations on ionization potentials of methylene in comparison with both the full CI data and several QRHF-CC calculations (26). (Quasi-RHF in this case means taking the orbitals from neutral $^1A_1CH_2$ and occupying as required for the particular ionization.) At the FSCCSD level, four of the five calculated IPs are within 0.1 eV of the full CI number, while the $^1A_1 \rightarrow 2^2A_1$ result is 0.4 eV off. The effect of the T(3) correction to FSCCSD is to move all of the results away from full CI, but four of the roots are still within 0.1 eV, while the $^1A_1 \rightarrow 2^2A_1$ number has changed to 0.6 eV away from full CI. Introducing some higher-order effects via the T*(3) model shifts all of the results back toward full CI, but not as close as the FSCCSD result. These differences from full CI cannot result from uncertainties due to the choice of active space, which are about 0.001 eV (0.04 mH) for this particular molecule (32). By contrast, the single reference QRHF-CC calculations start out with all five ionizations within 0.11 eV of full CI, and the inclusion of triple excitations at various levels improves the results to match full CI within 0.01 eV. This behavior

suggests that the single reference CCSD provides a good approximation to the various states in question, and that triple excitations are relatively unimportant, which would seem to conflict with the FSCC results.

It is important to note, however, that there are fundamental differences between FSCC and SRCC with respect to the nature of their excitation operators. For a given truncation of the cluster operators beyond simple double excitations, the determinantal expansion space available in an FSCC calculation is smaller than those of SRCC calculations for the various model space determinants. A class of excitations called "spectator" triple excitations must be added to the FSCCSD method to achieve an expansion space that is in some sense equivalent to that of the SRCC. But even then, the FSCC amplitudes are restricted by the necessity to represent several ionized states simultaneously. Thus, we should not expect the FSCCSD to produce results identical to a single reference CCSD, nor should we expect triple excitation corrections to behave in the same way. The differences between FSCC and SRCC shown in Table I and others, below, should be interpreted as a manifestation of these differences.

These differences between single reference and Fock-space methods can also be seen in the other calculations presented here (Tables II–VII). The sign of the FSCC triples correction is frequently opposite that of the SRCC triples corrections, and their magnitudes do not appear to be related— a large SRCC triples contribution does not necessarily imply a large FSCC triples correction, and vice versa. The sizes of the SRCC and FSCC triples contributions are rather different as well. The largest SRCC effect is about 0.2 eV, while the FSCCSD+T(3) correction is as large as 0.8 eV, and 0.5 eV for T*(3). All this lends further support for the idea that the nature of the excitation operator hierarchy is different in single reference and Fock-space coupled cluster methods.

Table II. Vertical ionization potentials of CH_2NH (in eV) calculated at the experimental geometry with a DZP basis.

Basis/Method	Orbital			
	5a′	1a″	4a′	3a′
FSCCSD	10.34	12.29	15.08	17.19
FSCCSD+T(3)	10.71	12.35	15.30	17.46
FSCCSD+T*(3)	10.55	12.29	15.20	17.34
QRHF-CCSD	10.40	12.14	15.17	17.32
QRHF-CCSDT-1	10.43	12.28	15.11	17.14
Experiment (36)	10.52	12.43	15.13	17.04
Experiment (37)	10.70	12.48	15.11	17.07
Experiment (38)	10.56	12.44	15.00	17.00

Notes: Geometries, basis sets, and QRHF-CC results taken from (39).

Table III. Vertical ionization potentials of CH_2PH (in eV) calculated at the experimental geometry with a DZP basis.

Basis/Method	Orbital			
	1a″	5a′	4a′	3a′
FSCCSD	10.08	10.28	13.17	15.14
FSCCSD+T(3)	10.01	10.33	13.25	15.41
FSCCSD+T*(3)	9.98	10.28	13.25	15.27
QRHF-CCSD	9.90	10.22	13.15	15.15
QRHF-CCSDT-1	10.05	10.24	13.15	
Experiment (40)	10.30	10.70	13.20	15.00

Notes: Geometries, basis sets, and QRHF-CC results taken from (39).

Table IV. Vertical ionization potentials for $^3\Sigma_g^-$ O_2 (in eV) at the experimental geometry.

Method	Basis	O_2^+ Final State			
		$^2\Pi_g$	$^4\Sigma_g^-$	$^4\Pi_u$	$^4\Sigma_u^-$
FSCCSD	DZP	11.76	17.75	16.40	24.16
FSCCSD+T(3)	DZP	12.13	17.99	16.30	24.98
FSCCSD+T*(3)	DZP	12.08	17.87	16.29	24.66
UHF-CCSD	DZP	12.13	17.80	16.15	24.64
UHF-CCSD(T)	DZP	11.95	17.77	16.26	24.40
FSCCSD	PVQZ++	12.37	18.34	16.94	24.74
FSCCSD+T(3)	PVQZ++	12.82	18.48	16.74	25.43
FSCCSD+T*(3)	PVQZ++	12.57	18.34	16.71	25.11
UHF-CCSD(T)	PVQZ++	12.39	18.26	16.76	24.82
Expt. (Adiabatic)		12.07	18.17	16.11	24.58
Expt. (Vertical)		12.35	18.33	16.85	24.66

Notes: Geometry taken from Herzberg (41). Basis sets, SRCC, and experimental result taken from (15).

Examining the various tables, we see that the SRCC triples correction usually improves agreement with experiment, while the FSCC triples corrections appear to shift the calculated result away from the experimental one as often as towards it. It is also worth noting that the T*(3) correction is generally smaller than T(3) and gives better agreement with experimental results. Overall, FSCCSD and FSCCSD+T*(3) seem to do about the same in comparison with experiment, with an average absolute difference from the experimental results of roughly 0.2 eV. The single reference CCSD results have an average absolute difference of closer to 0.3 eV, which is improved to 0.2 eV by the addition of triple excitation effects. Thus, it would appear that FSCCSD and FSCCSD+T*(3) perform about as well as single reference CCSD(T) in comparison with experiment, but the single reference calculations (so far) have an edge in predictability.

In order to give proper weight to the performance of these methods relative to experiment, we must consider the potential problems inherent in experimental

Table V. Vertical ionization potentials of H_2CO (in eV) evaluated at the experimental geometry with a [5*s*3*p*1*d*/2*s*1*p*] basis.

Method	Orbital of ionized electron		
	$2b_2$	$1b_1$	$5a_1$
FSCCSD	10.51	14.36	15.75
FSCCSD+T(3)	10.96	14.49	16.30
FSCCSD+T*(3)	10.77	14.40	16.06
QRHF-CCSD	10.59	14.19	15.77
QRHF-CCSD[T]	10.63	14.37	15.83
QRHF-CCSDT-1b	10.63	14.39	15.83
QRHF-CCSDT-3	10.58	14.31	15.76
Experiment (42)	10.88	14.38	16.00

Notes: Geometry taken from Herzberg (41). The basis set consisted of Dunning's (9*s*5*p*)→[5*s*3*p*] set on C and O, and his (4*s*)→[2*s*] set with exponents scaled by 1.44 on H (43), with polarization functions exponents of 0.654 (C), 1.211 (O), and 0.7 (H) (44).

Table VI. Vertical ionization potentials of N_2 (in eV) at R=2.0693 au with a [5*s*4*p*1*d*] basis.

Method	Orbital of ionized electron		
	$3\sigma_g$	$1\pi_u$	$2\sigma_u$
FSCCSD	15.44	17.14	18.64
FSCCSD+T(3)	15.58	16.86	19.04
FSCCSD+T*(3)	15.44	16.88	18.81
QRHF-CCSD	15.39	16.69	18.71
QRHF-CCSDT-1	15.36	16.87	18.57
Experiment	15.60	16.98	18.78

Notes: Geometry, basis, and QRHF-CC and experimental results taken from Rittby and Bartlett (45).

Table VII. Vertical ionization potentials of ketene and diazomethane (in eV) calculated at experimental geometries calculated with a DZP basis.

Method	Ketene		Diazomethane	
	$2b_1$	$2b_2$	$2b_1$	$2b_2$
FSCCSD	9.40	14.25	8.60	13.79
FSCCSD+T(3)	9.39	14.49	8.52	13.85
FSCCSD+T*(3)	9.35	14.38	8.47	13.77
QRHF-CCSD	9.29	14.31	8.43	13.78
QRHF-CCSD(T)	9.38	14.24	8.54	13.73
Experiment	9.64 (a)	13.84 (a)	9.00 (a)	14.13 (v)

Notes: Geometries, basis sets, and experimental results taken from Rittby, Pal, and Bartlett (12). Experimental IPs are *adiabatic* or *vertical*, as indicated in the table.

data. The natural result of a FSCC calculation is a vertical ionization potential, while experiment may provide vertical, adiabatic, or both. Adiabatic IPs are not directly comparable with calculated vertical ionization potentials, since they depend on the change in geometry from the neutral to the ion. If the ion and neutral geometries are very similar, the vertical and adiabatic IPs will also be nearly the same, but in general, the adiabatic IP is only a lower bound for the vertical one. In cases where the experimental value is adiabatic or unspecified, a larger difference from the computed vertical IP must be expected.

A second problem with experimental results is that, as with theoretical methods, different experimental techniques can give somewhat different results. This is illustrated in Table II, which lists three sets of experimental data for methyleneamine, differing among themselves by as much as 0.2 eV.

A third complication of using experimental data is that details of the calculation other than the correlation method become important, particularly the basis set. Many of the calculations presented here use a DZP or slightly better quality basis set. While very useful for comparing one theoretical method to another, these basis sets may not be adequate, however, to obtain good results compared to experiment. Table IV shows the ionization potentials of O_2 as calculated using both DZP (32 functions) and an augmented PVQZ basis (126 functions) in order to demonstrate the effect of basis set on both the FSCC and SRCC IPs. It is clear that the PVQZ++ basis provides a much better

comparison with the experimental results than the DZP basis, for both FSCC and SRCC calculations. The change in FSCC results due to increasing the basis set is about 0.5–0.6 eV, and for the SRCC 0.4–0.5 eV. Although there is no experimental comparison, a similar basis set effect can also be seen in the HOF results in (32), where the change from a DZP to a PVQZ basis changes the IPs by 0.2–0.4 eV. It would seem, then, that correlated calculations with DZP-quality basis sets should not be expected to reproduce experimental results too well.

Given that the basis sets used here are modest, coupled with the other problems of the experimental data themselves, it would seem that an error of 0.2 eV for these calculations is not unreasonable and is not necessarily an indication of intrinsic problems with the method. Indeed, the fact that the SRCC results show a similar margin of error with respect to experiment is a good sign for FSCC. It would seem that the biggest difference in this regard between the single reference and Fock-space results is the relative lack of consistency of the FSCC triples corrections, which can probably be better understood with more experience in using the method.

Potential Energy Surfaces and Related Properties

Another use of FSCC methods is for the study of potential energy surfaces, especially with the ability to look at several surfaces in the same calculation. The basic result of the FSCC calculation is still an energy difference, but when added to the absolute energy of the (0,0) sector reference, it provides an absolute energy for the state of interest. In the (0,1) sector case, the state of interest has one electron removed relative to the reference (0,0) state. This "final state" objective has practical advantages in many cases. For calculations on molecules with low-lying electronic states or symmetry-breaking phenomena, direct calculation of the PES by traditional single reference methods frequently suffers from convergence and other problems due to the proximity of other states to the one of interest. On the other hand, the same molecule with another electron is often well-behaved at the same geometries. This is the same as the ionization process, but from the opposite point of view — in this case, we want to talk about the final state, while in IPs, it is traditional to look at it from the point of view of the initial state.

This application of FSCC methods is a recent development, but along with its IP-EOM-CC twin, there are few such applications in the literature (8, 33), and they frequently deal with symmetry-breaking problems. Comparisons are possible with single reference calculations, though as we shall see, the comparison of high-level SRCC calculations with Fock-space results does not always lead to an unambiguous determination of which approach is more reliable. Nevertheless, FSCC is very well suited to such applications and will undoubtedly

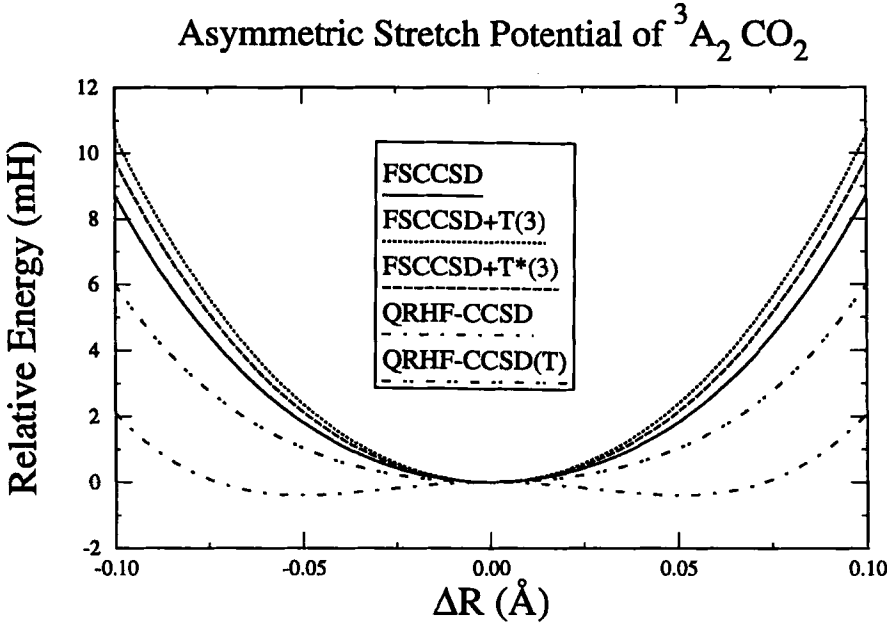

Figure 1. Potential curves for the asymmetric stretch mode ($\Delta R = \frac{1}{2}(R_1 - R_2)$) of $^3A_2$ CO_2 at various levels of theory. The C_{2v} structure is the DZP/FOCIB geometry of Engelbrecht and Liu (46).

see increasing use in the study of potential energy surfaces, so it is worth trying to get a feel for its performance.

Engelbrecht and Liu, in a 1983 paper (46), used multiconfiguration self-consistent field (MCSCF) plus CI calculations to characterize the $^3A_2$ state of CO_2. This state, which is bent (C_{2v} symmetry), has the SCF occupation

$$(\text{core})3a_1^2 2b_2^2 4a_1^2 3b_2^2 5a_1^2 1b_1^2 1a_2 4b_2^2 6a_1$$

and interacts strongly with the configuration

$$(\text{core})3a_1^2 2b_2^2 4a_1^2 3b_2^2 5a_1^2 1b_1 1a_2^2 4b_2^2 6a_1$$

because both the a_2 and b_1 orbitals transform as a'' in C_s symmetry. As a result, SCF calculations can obtain a lower energy by going to a C_s structure.

With suitable methods, such interactions can be treated properly, and reasonable potential energy surfaces obtained, but this requires the ability to describe inherently multireference states. Most such methods are not many-body in nature, and of course we prefer a size-extensive approach if possible.

It has been observed that QRHF-based coupled cluster methods are capable of handling many multireference problems when sufficient triple excitation effects are incorporated (3). In Figure 1, we see two QRHF-CC potential curves for the asymmetric stretch of CO_2, which were calculated from closed-shell CO_2^{2-} SCF orbitals. The QRHF-CCSD curve has a double minimum shape, while the QRHF-CCSD(T) method gives a stable C_{2v} structure. This is consistent with the MCSCF+CI calculations of Engelbrecht and Liu and their conclusion that the equilibrium structure of this state is C_{2v}.

The results of three sets of Fock-space coupled cluster calculations using $^2A_1$ CO_2^- as the (0,0) reference are also displayed in Figure 1. FSCCSD gets the proper shape of the PES even without triple excitation effects, and the inclusion of triples makes small adjustments to the shape of the surface. (Note that, as in the IP calculations, the FSCCSD+T*(3) results lie between FSCCSD and FSCCSD+T(3).) This behavior is what we might expect from a method that is designed in a multireference framework.

Another symmetry-breaking problem to which a number of single and multireference approaches have been applied is the nitrate radical, NO_3 (47). Different experiments have been interpreted in terms of either a totally symmetric D_{3h} equilibrium geometry, or a lower symmetry C_{2v} structure with one N-O bond length different from the other two. However, as Kawaguchi and coworkers (48) comment, no one has advanced a model which explains all of the available spectroscopic data.

In a recent theoretical examination of the problem, Stanton, Gauss, and Bartlett (47) located three stationary points on the NO_3 surface using the QRHF-CCSD method. The D_{3h} structure was determined to be a local minimum, and two C_{2v} structures were found. They are characterized by the relationship between the unique N-O bond distance and the other two: one long/two short (1L2S) or one two long/one short (2L1S). The 1L2S structure was also found to be a local minimum, and the 2L1S a transition state 192 cm^{-1} higher in energy than the 1L2S state; both C_{2v} structures being lower in energy than the totally symmetric structure. Their conclusion is that the molecule has a C_{2v} equilibrium geometry, but probably has an extremely low barrier to pseudorotation, which would give spectra characteristic of a D_{3h} system.

In a later paper focusing on different orbital choices for single reference treatments of symmetry breaking problems, Stanton *et al.* (49) calculated relative energies of the D_{3h} and C_{2v} minima using more sophisticated Brueckner orbital-based (B-CCD, B-CCD(T), and B-CCDT-3) methods than in their first paper. Their QRHF-CC results are shown in Table VIII along with FSCC results using the same basis sets and geometries. Using both DZP and PVTZ basis sets, QRHF-CCSD calculations favor the C_{2v} minimum by about 3 kcal mol^{-1}. As soon as triples corrections are introduced, either using the noniterative CCSD(T) approximation or the iterative CCSDT-3 model, the energies shift in favor of

Table VIII. Calculated relative energies (in kcal mol^{-1}) of C_{2v} and D_{3h} NO_3 structures.

Method	DZP basis		PVTZ basis	
	1L2S-D_{3h}	2L1S-D_{3h}	1L2S-D_{3h}	2L1S-D_{3h}
FSCCSD	2.50	1.05	2.94	1.05
FSCCSD+T(3)	3.03	1.64	3.72	1.73
FSCCSD+T*(3)	2.74	1.35	3.36	1.41
QRHF-CCSD	-2.59	-2.04	-2.96	
QRHF-CCSD(T)	0.34		0.57	
QRHF-CCSDT-3	0.21			

Notes: Geometries, optimized at the DZP/QRHF-CCSD level, taken from (47). The C_{2v} geometries are characterized by one of the NO bonds being longer (1L2S) or shorter (2L1S) than the other two. QRHF-CC relative energies taken from (49).

the totally symmetric structure, but by only 0.5 kcal mol^{-1}. FSCC, on the other hand, predicts the D_{3h} structure to be lower for all three methods shown, but by roughly 3 kcal mol^{-1}.

Given previous experience with QRHF-CC methods applied to problems of this sort, we should have greater confidence in the QRHF-CCSD(T) and T-3 results than in results without triple excitations, but with the available data, it is impossible to tell whether the single reference numbers including triple excitations or the FSCC results are more reliable. As Stanton *et al.* (49) observe, "An extremely sophisticated (and expensive) calculation would be required to firmly establish the nature of the D_{3h} stationary point."

C_3^+ is another molecule for which both experimental and theoretical studies have produced differing opinions on the nature of the ground state. Coulomb explosion data can be interpreted in terms of either a floppy linear molecule or a bent structure, depending on the vibrational temperature of the sample (50, 51). On the theoretical side, the consensus is that the ground state is a bent $^2B_2$ with the linear $^2\Sigma_u^+$ higher in energy (52). The energy difference between these two states is still not a settled issue. This is important because if the barrier is small enough, the molecule may be quasilinear—although the true ground state

Table IX. Optimized geometries and vibrational frequencies of $^2B_2$ C_3^+, using a DZP basis.

Method	R (Å)	θ (°)	ω_1 (a_1) (cm^{-1})	ω_2 (a_1) (cm^{-1})	ω_3 (b_2) (cm^{-1})
FSCCSD	1.328	71.6	1685	583	1269
FSCCSD+T(3)	1.336	70.2	1643	614	1221
FSCCSD+T*(3)	1.335	70.5	1651	603	1225
CCSD	1.337	68.3	1668	687	1215
CCSD(T)	1.350	68.3	1601	515	1074
CCSDT-1	1.350	69.0	1558	569	1078
CCSDT-2	1.347	69.0	1612	595	1213
CCSDT	1.350	68.0	1601	638	1021

Notes: Basis set and SRCC results taken from Watts *et al.* (52).

is bent, a large amplitude bending motion could bring the molecule through the linear structure.

Tables IX and X present the results of FSCC optimizations, vibrational frequency calculations, and relative energies in comparison with single reference CC results from Watts *et al.* (52) which include full CCSDT calculations. All three Fock-space methods give essentially the same geometry for both structures, comparing most closely with the single reference CCSD results. For the vibrational frequencies of the $^2B_2$ state, the FSCC results are also basically the same, and correspond most closely with the CCSDT-2 approximate iterative triples model among the single reference calculations. On the basis of several calculations with a larger basis set, Watts and coworkers suggest that the true harmonic frequencies should lie in the ranges 1590–1629, 592–638, and 1094–1173 cm^{-1}, and compared to these, the FSCC ω_1 and ω_3 are slightly high.

The asymmetric stretching frequency (σ_u) of the $^2\Sigma_u^+$ state (Table X) is a more complex problem. An imaginary frequency in this mode indicates that the $D_{\infty h}$ structure is a transition state, and a lower energy can be obtained by changing the bond lengths asymmetrically. For both single reference and Fock-space methods, the calculated frequency varies widely. Also, the bending mode (π_u) changes dramatically with the choice of FSCC method. Such large changes due to different correlation methods are usually an indication that important aspects of the problem are not being taken into account, and a more detailed

Table X. Optimized geometries, and vibrational frequencies of $^2\Sigma_u^+$ C_3^+, and energy relative to $^2B_2$ C_3^+, using a DZP basis.

Method	R (Å)	$\omega(\pi_u)$ (cm^{-1})	$\omega(\sigma_g)$ (cm^{-1})	$\omega(\sigma_u)$ (cm^{-1})	E($^2\Sigma_u^+$ - $^2B_2$) (kcal mol^{-1})
FSCCSD	1.312	88	1227	492*i*	7.1
FSCCSD+T(3)	1.315	71*i*	1203	1911	10.9
FSCCSD+T*(3)	1.316	532	1205	1462	8.6
CCSD	1.314			2500*i*	13.2
CCSD(T)	1.327			1431*i*	2.9
CCSDT-1	1.339			1135	-1.7
CCSDT-2	1.329			1595	2.2
CCSDT	1.327			451*i*	4.9

Notes: Basis set and SRCC results taken from Watts *et al.* (52).

examination, using both single reference and Fock-space methods would be in order.

Table X also presents the energy differences between the linear and bent structures. Note that the single reference CCSDT-1 method places the linear structure lower in energy than the bent one. Watts *et al.* attributed this to an apparent tendency for the iterative nature of the CCSDT-1 method to overemphasize potential problems in the closely related CCSD(T) model in difficult cases, thus producing poorer results than the perturbative CCSD(T) method.

Their CCSDT ΔE of 4.9 kcal mol^{-1} is in reasonable accord with CISDTQ calculations of Grev, Alberts, and Schaefer (53, 54) indicating a 4.1 kcal mol^{-1} difference. Taylor *et al.* (55) used multireference CI methods to obtain a separation of 1.68 kcal mol^{-1} with a DZP basis set, and claim that this should be very close to the full CI limit. These authors also show that multireference effects are important for both the bent and linear structures. Despite the multireference character of the FSCC approach, all three methods presented here give a significantly larger energy gap than Taylor's calculations. The problem with the relative energies of the two states may be due, at least in part, to the apparent problems in properly describing the $^2\Sigma_u^+$ state. It would seem, on this minimal evidence, that where single reference methods including triple

excitations have problems, Fock-space methods do as well. Analytical gradients for the related IP-EOM-CCSD form of FSCCSD have been presented (8), making "final state" applications of the methodology widely possible.

Acknowledgments

We are grateful to Martin Vala, William Weltner, John Stanton, and John Watts for many helpful discussions during the course of this work. This work was supported by the Office of Naval Research, under grant number N00014–92–J-1100.

References

[1] R. J. Bartlett and J. F. Stanton, Applications of post-hartree-fock methods: A tutorial, in *Reviews in Computational Chemistry, Volume 5*, edited by D. Boyd and K. Lipkowitz, page 65, VCH Publishers, New York, 1994.

[2] R. J. Bartlett, Coupled-cluster theory: An overview of recent developments, in *Modern Electronic Structure Theory*, edited by D. R. Yarkony, pages 1047–1131, World Scientific Publishing Co., Singapore, 1995.

[3] R. J. Bartlett, J. Phys. Chem. **93**, 1697 (1989).

[4] J. Paldus, Coupled-cluster theory, in *Methods in Computational Molecular Physics NATO, Volume 293*, edited by S. Wilson and G. H. F. Diercksen, pages 99–194, Plenum, New York, 1992.

[5] D. Mukherjee and S. Pal, Adv. Quantum Chem. **20**, 292 (1989).

[6] D. Sinha, S. K. Mukhopadhyay, R. Chaudhuri, and D. Mukherjee, Chem. Phys. Lett.. **154**, 544 (1989).

[7] M. Nooijen and R. J. Bartlett, J. Chem. Phys. **102**, 3629 (1995).

[8] J. Stanton and J. Gauss, J. Chem. Phys. **101**, 8938 (1994).

[9] S. Pal, M. Rittby, R. J. Bartlett, D. Sinha, and D. Mukherjee, Chem. Phys. Lett. **137**, 273 (1987).

[10] U. Kaldor, J. Computat. Chem. **8**, 448 (1987).

[11] S. Pal, M. Rittby, R. J. Bartlett, D. Sinha, and D. Mukherjee, J. Chem. Phys. **88**, 4357 (1988).

[12] M. Rittby, S. Pal, and R. J. Bartlett, J. Chem. Phys. **90**, 3214 (1989).

[13] A. Haque and U. Kaldor, Chem. Phys. Lett. **120**, 261 (1985).

[14] S. Pal, M. Rittby, and R. J. Bartlett, Chem. Phys. Lett. **160**, 212 (1989).

[15] J. F. Stanton, R. J. Bartlett, and C. M. L. Rittby, J. Chem. Phys. **97**, 5560 (1992).

[16] D. Mukherjee, Pramāna **12**, 203 (1979).

[17] D. Mukherjee, Chem. Phys. Lett. **125**, 207 (1986).

[18] D. Sinha, S. K. Mukhopadhyay, M. D. Prasad, and D. Mukherjee, Chem. Phys. Lett. **125**, 213 (1986).

[19] D. Sinha, S. Mukhopadhyay, and D. Mukherjee, Chem. Phys. Lett. **129**, 369 (1986).

[20] I. Lindgren and D. Mukherjee, Physics Reports **151**, 93 (1987).

[21] R. Chaudhuri, D. Sinha, and D. Mukherjee, Chem. Phys. Lett. **163**, 165 (1989).

[22] M. A. Haque and D. Mukherjee, J. Chem. Phys. **80**, 5058 (1984).

[23] J. Noga and R. J. Bartlett, J. Chem. Phys. **86**, 7041 (1987).

[24] J. Noga and R. J. Bartlett, J. Chem. Phys. **89**, 3401 (1988).

[25] G. E. Scuseria and H. F. S. III, Chem. Phys. Lett. **152**, 382 (1988).

[26] J. D. Watts and R. J. Bartlett, J. Chem. Phys. **93**, 6104 (1990).

[27] Y. S. Lee, S. A. Kucharski, and R. J. Bartlett, J. Chem. Phys. **81**, 5906 (1984).

[28] Y. S. Lee, S. A. Kucharski, and R. J. Bartlett, J. Chem. Phys. **82**, 5761 (1985).

[29] M. Urban, J. Noga, S. J. Cole, and R. J. Bartlett, J. Chem. Phys. **83**, 4041 (1985).

[30] S. J. Cole and R. J. Bartlett, J. Chem. Phys. **86**, 873 (1987).

[31] J. Noga, R. J. Bartlett, and M. Urban, Chem. Phys. Lett. **134**, 126 (1987).

[32] D. E. Bernholdt, *Triple Excitation Effects in the Fock-Space Coupled Cluster Method*, PhD thesis, University of Florida, Department of Chemistry, Gainesville, FL 32611, 1993.

[33] J. Stanton and J. Gauss, Theoret. Chimica Acta **98**, 303 (1996).

[34] J. F. Stanton, J. Gauss, J. D. Watts, and R. J. Bartlett, ACES II, an *ab initio* program system.

[35] C. W. Bauschlicher, Jr. and P. R. Taylor, J. Chem. Phys. **86**, 2844 (1987).

[36] J. B. Peel and G. D. Willett, J. Chem. Soc., Faraday Trans. 2 **71**, 1799 (1975).

[37] H. Bock, R. Dammel, and L. Horner, Chem. Ber. **114**, 220 (1981).

[38] R. Schulz and A. Schweig, J. Electron Spectrosc. Relat. Phenom. **28**, 33 (1982).

[39] J. D. Watts, M. Rittby, and R. J. Bartlett, J. Am. Chem. Soc. **111**, 4155 (1989).

[40] S. Lacombe et al., J. Am. Chem. Soc. **110**, 6964 (1988).

[41] G. Herzberg, *Electronic Spectra and Electronic Structure of Polyatomic Molecules*, volume III of *Molecular Spectra and Molecular Structure*, D. Van Nostrand, Princeton, New Jersey, 1966.

[42] C. Baker and D. W. Turner, J. Chem. Soc. D: Chem. Comm. , 480 (1969).

[43] T. H. Dunning, Jr., J. Chem. Phys. **53**, 2823 (1970).

[44] L. T. Redmon, G. D. Purvis III, and R. J. Bartlett, J. Am. Chem. Soc. **101**, 2856 (1979).

[45] M. Rittby and R. J. Bartlett, J. Phys. Chem. **92**, 3033 (1988).

[46] L. Engelbrecht and B. Liu, J. Chem. Phys. **78**, 3097 (1983).

[47] J. F. Stanton, J. Gauss, and R. J. Bartlett, J. Chem. Phys. **94**, 4084 (1991).

[48] K. Kawaguchi, E. Hirota, T. Ishiwata, and I. Tanaka, J. Chem. Phys. **93**, 951 (1990).

[49] J. F. Stanton, J. Gauss, and R. J. Bartlett, J. Chem. Phys. **97**, 5554 (1992).

[50] A. Faibis, E. P. Kanter, L. M. Tack, E. Bakke, and B. J. Zabransky, J. Phys. Chem. **91**, 6445 (1987).

[51] Z. Vager and E. P. Kanter, J. Phys. Chem. **93**, 7745 (1989).

[52] J. D. Watts, J. F. Stanton, J. Gauss, and R. J. Bartlett, J. Chem. Phys. **94**, 4320 (1991).

[53] R. S. Grev, I. L. Alberts, and H. F. Schaefer III, J. Phys. Chem. **94**, 3379 (1990).

[54] R. S. Grev, I. L. Alberts, and H. F. Schaefer III, J. Phys. Chem. **94**, 8744 (1990).

[55] P. R. Taylor, J. M. L. Martin, J. P. François, and R. Gijbels, J. Phys. Chem. **95**, 6530 (1991).

EOMXCC: A NEW COUPLED-CLUSTER METHOD FOR ELECTRONIC EXCITED STATES

Piotr Piecuch[a] and Rodney J. Bartlett

Quantum Theory Project, University of Florida, Gainesville, FL 32611

TABLE OF CONTENTS

[a] Permanent address: Department of Chemistry, Michigan State University, East Lansing, MI 48824-1322, U.S.A.

ADVANCES IN QUANTUM CHEMISTRY, VOLUME 34

0065-3276/99 $30.00

Abstract

A new coupled-cluster (CC) theory for electronically excited, electron-attached, and ionized states of molecular systems, which takes advantages of the similarity transformation of the Hamiltonian, the equation of motion (EOM) CC method, and the expectation value CC (XCC) approach, is proposed and analyzed. The new method, which we refer to as the EOMXCC theory, is based on diagonalization of the doubly transformed Hamiltonian $\bar{\bar{H}} = e^{T^\dagger} \bar{H} e^{-T^\dagger}$, where T represents the cluster operator and $\bar{H} = e^{-T} H e^{T}$ is the EOMCC Hamiltonian. In order to preserve the simple, EOMCC-like, structure of the final equations, the T cluster operators describing the ground-state problem are determined by solving the XCC equations. The new method, which is formally a single-reference approach, offers a number of advantages, which are discussed in detail. One of the important features of the EOMXCC formalism is that it seems to be capable of describing contributions from the connected triexcited clusters, which normally enter the doubles-singles block of the EOMCCSDT (EOMCC singles, doubles, and triples) eigenvalue problem, at the EOMXCCSD (EOMXCC singles and doubles) level of approximation. This finding may eventually lead to a new hierarchy of approximations, which should be capable of improving the results for the low-lying excited states dominated by double excitations from the reference, where inclusion of triples in the EOMCC scheme is essential, without using the expensive steps of the EOMCCSDT theory. The

EOMXCC method is general and applies to all types of references, including RHF, UHF, and ROHF determinants. It also applies to all sectors of the Fock space. A few approximate EOMXCC schemes are considered in detail. The final equations of the EOMXCCSD theory are presented in a factorized form using recursively generated intermediates. It is demonstrated that the EOMXCC method can be viewed as a Hermitized EOMCC theory, which is capable of describing the corrections from important high-order clusters at a lower level of approximation. Along with the EOMXCC method, we discuss the possibility of generalization of the extended CC (ECC) approach to excited states. The proposed EOMECC theory uses the doubly transformed Hamiltonian $\bar{\bar{H}}^{\Sigma} = e^{\Sigma}\bar{H}e^{-\Sigma}$, where the operators T and Σ satisfy the ECC stationary conditions. The use of two independent operators T and Σ makes the EOMECC formalism even more flexible than EOMXCC, leads to a more symmetric treatment of the left- and right-hand eigenvalue problems, and to a completely exponential treatment of the left ground-state problem.

1. Introduction

The success of single-reference (SR) coupled-cluster (CC) theory [1–9] in describing the non-degenerate ground states of molecular systems has stimulated a considerable activity aimed at the formulation and implementation of new classes of CC methods that would be capable of describing quasi-degenerate, open-shell, and excited electronic states. As a result, the recent twenty years have witnessed remarkable developments in multi-reference (MR) CC methodology (cf., e.g., Refs. 8, 10–12 for representative reviews). Several practical schemes based on the so-called genuine MRCC theories [8, 13] of valence-universal (VU) or Fock-space type [10–18] and state-universal or Hilbert-space type [19–25] (see, also, Refs. 5, 26) have been proposed and investigated. These advances have been paralleled by the development and coding of various MRCC and OSCC methods of the state-specific or state-selective (SS) type [27–30], by the introduction of a new category of SRCC-like methods, which are based on selecting higher-order cluster components in ordinary SRCC theory using MRCC arguments [31], and by the formulation and implementation of the equation of motion (EOM) CC method [32–34] (cf., also, Refs. 35–37) that allows one to describe electronically excited states [32–36], electron-attached states [38] (cf., also, Ref. 39), and ionized states [9, 38] of closed- and open-shell molecular systems (for more information about the EOM method itself, see, e.g., Ref. 40). The corresponding three types of EOMCC methods are usually referred to as the EE-EOMCC, EA-EOMCC, and IP-EOMCC

schemes, respectively.

The EOMCC theory can be regarded as an essentially SR theory, in which the electronically excited, electron-attached, and ionized states are generated by applying an elementary excitation operator to the ground-state wave function resulting from the SRCC calculation. The excitation operator of the EE-EOMCC theory has exactly the same form as the usual excitation operators used in the configuration-interaction (CI) method. The EOMCC theory is potentially an exact formalism if we choose to use the full CI (FCI) expansion to represent the excitation operator and the full CC expansion to represent the ground-state wave function. The final equations of the EOMCC theory can be cast in the form of equations for energy differences representing vertical excitation energies (VEEs), vertical electron affinities (VEAs), and vertical ionization potentials (VIPs). Thus, the EOMCC theory falls into the same category of methods as Green's function and propagator [41] and general EOM [40] techniques, which are based on a balanced treatment of ground and excited states and aim at energy differences rather than energies themselves. The EOMCC method is formally related to time-dependent CC and linear-response CC theories [35–37, 42]. It has also a lot in common with the early SSCC approach of Paldus et al. [29] and with the symmetry-adapted cluster CI (SAC-CI) method of Nakatsuji et al. [30].

The EOMCC method offers a number of advantages compared to genuine MRCC methods. First of all, the concept of a multi-dimensional active space (cf., e.g., Refs. 8, 10–12, 19, 43) is completely eliminated from the formalism. Thus, the EOMCC theory is a step towards having a "black box" procedure for excited states, where no *a priori* knowledge of multi-configurational nature of a given electronic state is required. In fact, the EOMCC calculations are no more difficult than the standard SRCI or SRCC calculations. More importantly, the EOMCC methods are free from the intruder state problem which often plagues the genuine MRCC methods based on the Bloch wave operator formalism (see, e.g., Refs. 17, 18, 23). Just like all VUCC methods, the EOMCC theory is applicable to any sector of Fock space. In the EOMCC theory, this is achieved by choosing a suitable form of the excitation operator acting on the SRCC ground state [9, 38]. In fact, there is an intimate relationship between the VUCC and EOMCC methods [44, 45], even though in EOMCC theory we do not face problems that complicate VUCC calculations, such as the existence of multiple and singular solutions [17, 18].

The major difference between the Fock-space CC methods and the EOMCC theory lies in the fact that in VUCC approaches different sectors of the Fock space are considered simultaneously (cf. the valence universality condition that VUCC theories must obey [8, 12, 13]), whereas the EOMCC theory treats different sectors of the Fock space as separate prob-

lems. The only element that is common to EOMCC calculations of excited, ionized, and electron-attached states is the similarity transformed Hamiltonian $\bar{H} = e^{-T}He^{T}$, which defines the corresponding eigenvalue problems (T is the cluster operator representing the ground-state SRCC wave function). The fact that the electronically excited, ionized, and electron-attached states are calculated in EOMCC theory separately is an advantage. The valence-universality condition, on which the VUCC theories are based, requires that the multi-dimensional active space be large enough to describe a whole family of electronic states corresponding to a given system and all its ions up to and including the one in which all active electrons are removed [8, 12, 13]. It is often difficult to come up with an active space which is so universal. Thus, the EOMCC formalism is a much simpler approach to essentially the same problem. By focusing on a single sector of the Fock space at a time, in EOMCC calculations we do not have to worry about the problem of compromising accuracy as a consequence of using an active space which does not provide a balanced description of a given system and its ions (cf. Refs. 17, 18). Also, inclusion of higher-than-doubly excited clusters in the EOMCC theory is generally much simpler compared to genuine MRCC methods (cf., e.g., Refs. 18, 20), even though some many-body components of the similarity-transformed Hamiltonian $\bar{H}$ used in the EOMCC approach that begin to appear once we include the triexcited components of the cluster operator in the calculations (as is done in the EOMCCSDT or EOMCC singles, doubles, and triples method [46]) are quite difficult to handle. Fortunately, most of the many-body components of $\bar{H}$ do not enter the corresponding EOMCC eigenvalue problem or can be neglected without compromising the accuracy [46].

The spin-adaptation of the EOMCC theory is simpler than the spin-adaptation of genuine MRCC methods (particularly, the SUCC theories [20, 21]), even though the orthogonally spin-adapted [20, 21, 47–49] EOMCC equations have yet to be presented [50] (cf., however, Ref. 36). The spin-adaptation of the EOMCC method is essentially no more difficult than the spin-adaptation of the standard SRCI theory (cf. Ref. 47). In case of open-shell systems, one can always use the ground-state wave function of the related closed-shell ion as a reference and employ the EA-EOMCC or IP-EOMCC equations to define the spin-adapted states of a given many-electron system [38]. One can also propose EOMCC schemes, which are approximately spin adapted [39]. All this is very important from the point of view of applications, since spin-adaptation allows us to treat states of different multiplicity as separate problems. For comparison, spin-adaptation of the SUCC theory has only been accomplished for a special case of active space consisting of two closed-shell reference configurations [20, 21]. Finally, the EOMCC method is applicable to any type of molecular orbitals. This gives us an option of calculating excited-states of open-shell systems by gen-

erating molecular orbitals in the restricted open-shell Hartree-Fock (ROHF) or unrestricted Hartree-Fock (UHF) calculations as well as the possibility of using the idea of quasirestricted Hartree-Fock (QRHF) orbitals [51].

There is of course a price that we have to pay for having all these advantages in EOMCC. First of all, an eigenvalue problem characterizing EOMCC equations is based on a similarity transformed Hamiltonian operator $\bar{H}$, which is not Hermitian. In consequence, treatment of properties other than the energy (e.g., transition dipole moments between various electronic states and the corresponding oscillator strengths) requires, at least in principle, the knowledge of both the left-hand and the right-hand eigenstates of $\bar{H}$ [34]. These eigenstates would also be needed if one wanted to calculate molecular (hyper)polarizabilities and other second- and higher-order properties, such as nuclear spin-spin coupling constants, using sum-over-state expressions (cf. Refs. 4, 52). It can be shown, however, [52–55] that sum-over-states expressions for static and dynamic (hyper)polarizabilities and NMR spin-spin coupling constants can be given a compact form which is related to standard Λ operator of the analytic gradient SRCC theory [56] (or to analogous vector quantities that have been introduced in early papers on SRCC gradients [57] and in more recent papers on linear-response CC method [58]). This eliminates the need for the left- and right-hand eigenvectors of $\bar{H}$ representing EOMCC excited states in property calculations using the EOMCC approach. As it has been demonstrated in Refs. 52–55, the only left-hand eigenstate of $\bar{H}$ that we have to know in this case is the left-hand ground state, which equals [4, 33, 34, 53] $\langle\Phi|(1+\Lambda)$, where $|\Phi\rangle$ is the reference configuration and, at the same time, the right-hand eigenstate of $\bar{H}$ corresponding to ground-state SRCC wave function $e^T|\Phi\rangle$.

The second problem that we must deal with, when we use truncated EOMCC schemes, such as the EOMCCSD approach (EOMCC singles and doubles method), is the presence of unlinked terms in the EOMCC energy and property expressions [44, 45] (cf., also, Refs. 52, 54). This is a consequence of a CI-like description of excited states in the EOMCC theory. As a result, the excited states resulting from truncated EOMCC calculations may not correlate with the right eigenstates of ionized and electron-attached subsystems when separation of a given molecular system into ionic fragments is considered. It can be shown, however, that this problem of EOMCC can be eliminated by conveniently modifying ("dressing") the matrix elements of $\bar{H}$ [45]. On the other hand, the EOMCC excited states correlate with the right eigenstates of subsystems if subsystems are neutral. Occasionally, the non-Hermiticity of $\bar{H}$ might lead to complex excitation energies, although this has only been observed to happen in complicated quasidegenerate situations, where the SRCC theory itself does not provide an adequate representation of the ground-state wave function [36].

The EOMCC theory in its basic, least expensive, EOMCCSD approximation has been very successful in describing the electronically excited states dominated by single excitations from the independent particle model (IPM) configuration chosen as a reference [32–34, 38, 39, 59–62] (see, also, Refs. 46, 63, 64). The same is true for the electron-attached and ionized states as long as they can be reasonably well described by the corresponding primary spaces, i.e. the $1p$ and $1h$ sectors of the Fock-space, respectively [38, 62, 65]. The relatively low cost of EOMCCSD calculations can be further significantly reduced by transforming the EOMCC Hamiltonian $\bar{H}$ one more time as is done in the recently proposed STEOMCCSD method [66]. The role of the second transformation is to reduce the coupling between the block of $\bar{H}$, which corresponds to singles, and other blocks of $\bar{H}$ that correspond to doubles and selected triples and quadruples, and to bring most of the information about this coupling into the singles block, which makes the final diagonalization step as cheap as the CIS (CI singles) calculation. The STEOMCCSD results for a number of molecular systems, including molecules as big as free base porphin, are most encouraging [66, 67]. Problems arise when we want to use EOMCC or STEOMCC methods to describe excited states dominated by double excitations from the reference (low-lying electronic states are often of this type). In this case, one has to go beyond the standard CCSD approximation and include connected triexcited clusters in the calculation (use the EOMCCSDT scheme or one of its approximate variants), since errors in the EOMCCSD excitation energies for states dominated by double excitations may become as large as 0.5 – 1.0 eV [46] (cf., also, Refs. 61, 63, 64). The EOMCCSDT method provides an excellent description of excited states dominated by single as well as double excitations and a systematic improvement over the EOMCCSD results [46] (for comparison, inclusion of triexcited clusters in VUCC theories may worsen the results [18]). However, the EOMCCSDT method is very expensive (it is an n^8 procedure, where n is the number of molecular orbitals employed) and thus has practical limitations. A possible remedy is to use one of the approximate EOMCCSDT schemes, such as the n^7 EOMCCSDT-1 approach or its non-iterative EOMCCSD(T) analog [63], in which the effect of triexcited clusters is estimated using MBPT (many-body perturbation theory) arguments. One might also use the EOMCCSDT-3 method and its non-iterative approximations, EOMCCSD($\tilde{\mathrm{T}}$) and EOMCCSD(T′) [64], which are respectively slightly more expensive than the EOMCCSDT-1 and EOMCCSD(T) procedures, but still less expensive than the complete EOMCCSDT method [for examples of applications of the EOMCCSD($\tilde{\mathrm{T}}$) method, see Refs. 61, 62]. An alternative solution to all these approaches is to use the method proposed in this paper.

The purpose of the present work is to propose a new EOMCC theory, which very likely incorporates, in a natural way, the effect of high-order connected clusters at a low-level of approximation (e.g., triples at the CCSD level, quadruples at the CCSDT level, etc.), so that we might, for example, suggest inexpensive CCSD-like EOMCCSDT schemes that are potentially accurate and that scale as n^6. Our aim is to perform the second transformation of the EOMCC Hamiltonian $\bar{H}$ in such a way that the effects due to ground-state higher-order clusters, such as the connected triexcited cluster components T_3, enter the excited state description while the ground-state CC (for example, CCSD) solution remains practically unchanged (it should be mentioned that the standard EOMCCSDT scheme and its approximate variants improve description of both the ground state and the excited states). We believe that the primary reason for the failure of the EOMCCSD method is an unbalanced description of the ground and excited states. The CCSD ground state is usually good but we cannot say the same about excited states. Inclusion of higher-than-doubly excited cluster components in $\bar{H}$ is in our view an important step towards improving the balance between ground and excited states within EOMCC description. For example, some perturbative EOMCCSDT-like approaches, such as EOMCCSD($\tilde{\mathrm{T}}$), have a tendency to overestimate the triples corrections and often produce excitation energies that are lower than the exact (FCI) or experimental ones (cf., e.g., Refs. 61, 64). Thus, we need new approaches which will provide us with a more balanced description of various kinds of higher-order effects and which will be at the same time inexpensive.

We would like the new formalism to satisfy a number of criteria. We would like to have an EOMCC-like theory, which brings at least some effects related to triexcited and higher-order clusters into one- and two-body terms of the similarity transformed Hamiltonian. We also want the new theory to be exact in the limit where all excitations are included. We want the new theory to be applicable to any type of molecular orbitals, including the restricted Hartree-Fock (RHF), ROHF, QRHF, and UHF ones, so that we will have various ways of treating open-shell states. We would like the new theory to be applicable to any sector of the Fock space, so that the electron-attached and ionized states could be studied with it along with the electronically excited states. We also require that the new theory allows for a straightforward adaptation to spin symmetry of the Hamiltonian. Finally, we would like the new theory to be formulated in terms of a more Hermitian similarity transformed Hamiltonian (the EOMCC Hamiltonian $\bar{H}$ is not Hermitian), so that strictly Hermitian EOMCC-like schemes (obtained, most simply, by Hermitizing the Hamiltonian $\bar{H}$ of the standard EOMCC theory) could be treated in a rigorous manner (this would eliminate the problem of having left- and right-hand eigenstates present in the standard EOMCC and STEOMCC methods). This is more or less the same

as requiring that the new theory uses both excitation and deexcitation operators in some way and it is well known from the traditional EOM [40] and random-phase-approximation (RPA) [40, 68] studies that the presence of deexcitation operators in EOM-like formalisms (RPA can be formulated using EOM concepts [40]) leads to a more balanced description of ground and excited states.

The fact that certain higher-order effects can be brought into consideration by combining excitation and deexcitation operators together was one of the factors that led to a formulation and implementation of the expectation value CC (XCC) [69, 70] and unitary CC (UCC) [15, 16, 28, 70–73] approaches. In these CC methods, which allow for an accurate description of molecular ground states, products involving cluster operators and their Hermitian adjoints are used to mimic the effect of connected quadruples [69–71]. Interestingly enough, there is an intimate relationship between the new theory proposed in this paper and the XCC theory of the ground state studied earlier [69, 70]. For this reason, the formalism described in this paper is referred to as the EOMXCC approach. There is also a connection between the EOMXCC approach discussed in this paper and a strictly Hermitian approach of Paldus et al. [29].

It should be mentioned that the XCC formalism belongs to a broad category of alternative CC theories, which are obtained if we study the stationary conditions of the CC energy functional [74, 75]. Other examples of alternative CC ansätze include the aforementioned unitary CC (UCC) approach [15, 16, 28, 70–73] (Refs. 15, 16, 28 discuss the MRCC variants of the UCC method), the symmetric expectation value CC (SXCC) method [70, 74, 75], the strongly-connected XCC (SC-XCC) theory and its UCC (SC-UCC) analog [75], and the extended CC (ECC) approach [76, 77]. A possibility to extend the EOMCC theory to the ECC case via the new EOMECC formalism is considered in this study as well.

The paper is organized as follows. In Section 2, we give a short synopsis of the standard EOMCC theory and introduce basic notation. In Section 3, we describe the fundamental equations of the EOMXCC method, while the general equations characterizing the EOMCCSD scheme are presented in Section 4. A few approximate variants of the EOMXCCSD approach are discussed in Section 5, and in Section 6 we present arguments that suggest that triexcited cluster components can be brought into the EOMXCC scheme at the CCSD level of approximation. Other alternative EOMCC schemes, among them the extension of the EOMCC theory to the ECC case via the EOMECC formalism, are discussed in Section 7. In view of formal similarities with the EOMXCC approach, our discussion of the EOMECC theory is restricted to basic equations. The last Section 8 summarizes the results and discusses future projects. The detailed equations of the EOMX-

CCSD approximation are given in Appendices A and B.

2. Basic definitions and synopsis of the EOMCC theory

Consider an electronic Schrödinger equation for the ground and excited states $|\Psi_K\rangle$ and the corresponding energies E_K of an N-electron system,

$$H_N |\Psi_K\rangle = \Delta E_K |\Psi_K\rangle. \tag{1}$$

Here H_N is the Hamiltonian in the normal product form,

$$H_N = H - \langle\Phi|H|\Phi\rangle = F_N + V_N, \tag{2}$$

where $|\Phi\rangle$ is a single-determinantal reference state (e.g., the Hartree-Fock wave function), which we choose as Fermi vacuum, and

$$\Delta E_K = E_K - \langle\Phi|H|\Phi\rangle. \tag{3}$$

The one- and two-electron parts of the Hamiltonian, F_N and V_N, respectively, are defined in a standard way, i.e.

$$F_N = f_p^q N\{X^p X_q\}, \tag{4}$$

$$V_N = \tfrac{1}{4} v_{pq}^{rs} N\{X^p X^q X_s X_r\}, \tag{5}$$

where

$$f_p^q = z_p^q + v_{pi}^{qi}, \tag{6}$$

and $z_p^q \equiv \langle p|z|q\rangle$ and $v_{pq}^{rs} \equiv \langle pq|v|rs\rangle - \langle pq|v|sr\rangle$ are the usual one-electron and antisymmetrized two-electron molecular integrals. We use X_p (X^p) to designate the annihilation (creation) operators (clearly, $X^p = X_p^\dagger$) and $N\{\cdots\}$ stands for the normal product relative to the Fermi vacuum $|\Phi\rangle$. We use letters i, j, k, l, m, n, o to designate the spin-orbitals which are occupied in the reference $|\Phi\rangle$ and a, b, c, d, e, f, g designate the unoccupied orbitals. Indices p, q, r, s are generic indices that run over all (occupied and unoccupied) spin-orbitals. We also use the Einstein summation convention to indicate the summation over repeated upper and lower indices [cf., e.g., Eqs. (4)-(6)].

In the standard EOMCC theory [32–34], we represent the excited states $|\Psi_K\rangle$ of an N-electron system as

$$|\Psi_K\rangle = R_K |\Psi_0\rangle, \tag{7}$$

and use the single-reference CC ansatz to describe the ground state $|\Psi_0\rangle$, so that

$$|\Psi_0\rangle = e^T|\Phi\rangle. \tag{8}$$

Here,

$$T = \sum_{n=1}^{N} T_n \tag{9}$$

is the cluster operator whose various many-body components T_n ($n = 1, 2, \ldots, N$) are defined in terms of the excitation operators

$$G^{a_1\ldots a_n}_{i_1\ldots i_n} = \prod_{\kappa=1}^{n} X^{a_\kappa} X_{i_\kappa} \tag{10}$$

and cluster amplitudes $t^{i_1\ldots i_n}_{a_1\ldots a_n}$ as follows,

$$T_n = \left(\frac{1}{n!}\right)^2 t^{i_1\ldots i_n}_{a_1\ldots a_n} G^{a_1\ldots a_n}_{i_1\ldots i_n}. \tag{11}$$

In particular,

$$T_1 = t^i_a G^a_i, \tag{12}$$

$$T_2 = \tfrac{1}{4} t^{ij}_{ab} G^{ab}_{ij}, \tag{13}$$

for the singly- and doubly-excited components of T. As in any other CC method, in approximate variants of the EOMCC theory, we terminate the summation (9) at a suitably chosen (preferably low) excitation level $n = M_T$, where $M_T < N$. In the EOMXCC formalism discussed in this paper, we also need the operator $T^\dagger$, whose many-body components $T^\dagger_n$ have the form

$$T^\dagger_n = \left(\frac{1}{n!}\right)^2 t^{a_1\ldots a_n}_{i_1\ldots i_n} G^{i_1\ldots i_n}_{a_1\ldots a_n}, \tag{14}$$

where

$$t^{a_1\ldots a_n}_{i_1\ldots i_n} = (t^{i_1\ldots i_n}_{a_1\ldots a_n})^* \tag{15}$$

and

$$G^{i_1\ldots i_n}_{a_1\ldots a_n} = (G^{a_1\ldots a_n}_{i_1\ldots i_n})^\dagger. \tag{16}$$

Moreover, in order to obtain the compact form of equations characterizing the EOMXCCSD theory, it is convenient to introduce the two-index antisymmetrizers

$$\mathcal{A}^{pq} = \mathcal{A}_{pq} = 1 - (pq), \tag{17}$$

where (pq) designates a transposition of spin-orbital indices p and q.

We assume that R_K can be expressed in terms of the operators Ω_λ which are strings of quasi-particle operators Y^p, where, by definition, $Y^a = X^a$

and $Y^i = X_i$, so that R_K commutes with T (but does not commute with $T^\dagger$). We allow a situation where R_K changes the number of particles, so that different sectors of the Fock space are made accessible [9, 38]. In particular, we describe the $(N-1)$-particle eigenstates $|\Psi_K\rangle$ by using

$$\Omega_\lambda^{\rm IP} = X_i,\ X^b X_j X_i,\ \ldots = G_i,\ G_{ij}^{\ b},\ \ldots, \tag{18}$$

the N-particle states $|\Psi_K\rangle$ by using

$$\Omega_\lambda^{\rm EE} = 1, X^a X_i,\ X^a X^b X_j X_i,\ \ldots = 1,\ G_a^i,\ G_{ab}^{ij},\ \ldots, \tag{19}$$

and the $(N+1)$-particle states $|\Psi_K\rangle$ by using

$$\Omega_\lambda^{\rm EA} = X^a,\ X^a X^b X_j,\ \ldots = G^a,\ G_j^{ab},\ \ldots\ . \tag{20}$$

Here, we define

$$G_{ii_1\ldots i_n}^{\ \ a_1\ldots a_n} = X_i\, G_{i_1\ldots i_n}^{\ \ a_1\ldots a_n}, \tag{21}$$

$$G_{i_1\ldots i_n}^{a a_1\ldots a_n} = X^a\, G_{i_1\ldots i_n}^{\ \ a_1\ldots a_n}, \tag{22}$$

for $n \geq 1$ and

$$G_i = X_i \tag{23}$$

$$G^a = X^a. \tag{24}$$

For these three important cases, the corresponding many-body expansions

$$R_K = \sum_\lambda r_{K,\lambda}\, \Omega_\lambda \tag{25}$$

assume the following forms,

$$R_K^{\rm IP} = \sum_{n=0}^{M_R} R_{K,(n+1)h-np}, \tag{26}$$

with

$$R_{K,(n+1)h-np} = \frac{1}{n!(n+1)!}\, r^{ii_1\ldots i_n}_{\ \ a_1\ldots a_n}(K)\, G_{ii_1\ldots i_n}^{\ \ a_1\ldots a_n} \quad (n \geq 1),$$

$$R_{K,1h-0p} \equiv R_{K,h} = r^i(K)\, G_i, \tag{27}$$

$$R_K^{\rm EE} = \sum_{n=0}^{M_R} R_{K,n}, \tag{28}$$

with

$$R_{K,n} = \left(\frac{1}{n!}\right)^2 r^{i_1\ldots i_n}_{\ \ a_1\ldots a_n}(K)\, G_{i_1\ldots i_n}^{\ \ a_1\ldots a_n} \quad (n \geq 1), \qquad R_{K,0} = r_0(K), \tag{29}$$

and

$$R_K^{\mathrm{EA}} = \sum_{n=0}^{M_R} R_{K,(n+1)p-nh}, \tag{30}$$

with

$$\begin{aligned} R_{K,(n+1)p-nh} &= \frac{1}{n!(n+1)!}\, r_{aa_1\ldots a_n}^{i_1\ldots i_n}(K)\, G^{aa_1\ldots a_n}_{i_1\ldots i_n} \quad (n \geq 1), \\ & R_{K,1p-0h} \equiv R_{K,p} = r_a(K)\, G^a, \end{aligned} \tag{31}$$

where $M_R = N$ in the exact case and $M_R < N$ in approximate EOMCC schemes. We can easily extend the formalism to other sectors of the Fock-space by making suitable choices for Ω_λ and R_K. The EE-EOMCC, EA-EOMCC, and IP-EOMCC methods are obtained when the operator R_K equals R_K^{EE}, R_K^{EA}, and R_K^{IP}, respectively [38]. In order to generalize Eq. (7), so that it applies to ground ($K = 0$) as well as excited ($K \geq 1$) states, we define

$$R_0 = 1. \tag{32}$$

In order to obtain the basic equations defining the EOMCC approach, we substitute Eqs. (7) and (8) into Eq. (1) and multiply both sides of the resulting equation on the left by e^{-T}. Since R_K and T commute, we obtain,

$$\bar{H}_N\, R_K|\Phi\rangle = \Delta E_K\, R_K|\Phi\rangle, \tag{33}$$

where

$$\bar{H}_N = e^{-T} H_N e^T = (H_N e^T)_C \tag{34}$$

is the similarity transformed Hamiltonian used in the EOMCC theory. The subscript C in Eq. (34) designates the connected part of the corresponding operator product. We further assume that the cluster amplitudes defining the operator T are obtained by solving the ordinary SRCC equations,

$$\langle\Phi|G^{i_1\ldots i_n}_{a_1\ldots a_n}\bar{H}_N|\Phi\rangle = \langle\Phi|G^{i_1\ldots i_n}_{a_1\ldots a_n}\bar{H}_{N,\mathrm{open}}|\Phi\rangle = 0, \quad (n = 1,\ldots) \tag{35}$$

where $G^{i_1\ldots i_n}_{a_1\ldots a_n}$ is defined by Eq. (16) and

$$\bar{H}_{N,\mathrm{open}} = (H_N e^T)_{C,\mathrm{open}}. \tag{36}$$

Here and elsewhere in the present paper, we use a notation in which the subscript *open* indicates that the only diagrams that have to be considered are those having external lines. Once the system (35) is solved and T clusters are determined, we calculate the ground-state CC energy using the well-known formula

$$\begin{aligned} \Delta E_0^{\mathrm{CC}} &= \langle\Phi|\bar{H}_N|\Phi\rangle = \bar{H}_{N,\mathrm{close}} = (H_N e^T)_{C,\mathrm{close}} \\ &= f_i^a\, t_a^i + \tfrac{1}{4} v_{ij}^{ab}(t_{ab}^{ij} + 2\, t_a^i\, t_b^j), \end{aligned} \tag{37}$$

where the subscript *close* indicates that only vacuum diagrams are considered (i.e. diagrams having no external lines).

With T satisfying Eq. (35) and ground-state energy defined by Eq. (37), the EOMCC eigenvalue problem (33) becomes

$$(\bar{H}_{N,\mathrm{open}} R_{K,\mathrm{open}})_C|\Phi\rangle = \omega_K R_K|\Phi\rangle, \tag{38}$$

or

$$[\bar{H}_{N,\mathrm{open}}, R_{K,\mathrm{open}}]|\Phi\rangle = \omega_K R_K|\Phi\rangle, \tag{39}$$

in which we directly calculate energy differences

$$\omega_K = \Delta E_K - \Delta E_0 = E_K - E_0. \tag{40}$$

An operator $R_{K,\mathrm{open}}$ equals R_K for the IP and EA cases and $R_K - R_{K,0}$ for the EE case. Clearly, the eigenvalues ω_K can be interpreted as VEEs when R_K is defined in terms of the operators $\Omega_\lambda^{\mathrm{EE}}$, Eq. (19). The energy differences ω_K, Eq. (40), represent VEAs and VIPs when R_K is defined in terms of the operators $\Omega_\lambda^{\mathrm{EA}}$ and $\Omega_\lambda^{\mathrm{IP}}$, Eqs. (20) and (18), respectively. The presence of the commutator $[\bar{H}_{N,\mathrm{open}}, R_{K,\mathrm{open}}]$ in Eq. (39) reflects the EOM nature of the EOMCC method. The presence of only connected components of the operator product $\bar{H}_{N,\mathrm{open}} R_{K,\mathrm{open}}$ in Eq. (38) is an immediate consequence of the fact that the disconnected part of $\bar{H}_{N,\mathrm{open}} R_{K,\mathrm{open}}|\Phi\rangle$, i.e. $R_{K,\mathrm{open}} \bar{H}_{N,\mathrm{open}}|\Phi\rangle$ vanishes if T satisfies Eq. (35).

It can be shown that Eq. (38) remains valid when many-body expansions of T and R_K are truncated. Indeed, let us consider an approximation in which

$$T = \sum_{n=1}^{M_T} T_n, \quad (M_T < N) \tag{41}$$

and let us use M_R to designate the truncated many-body expansions of R_K^{IP}, R_K^{EE}, and R_K^{EA} [cf. Eqs. (26)-(31)]. Let us also introduce projection operators P corresponding to excitations included in the many-body expansions of $R_{K,\mathrm{open}}$. In case of truncated IP, EE, and EA EOMCC schemes, the corresponding operators P assume the following form,

$$P^{\mathrm{IP}} = \sum_{n=0}^{M_R} \sum_{\substack{i<i_1<\cdots<i_n \\ a_1<\cdots<a_n}} G_{ii_1\ldots i_n}^{a_1\ldots a_n}|\Phi\rangle\langle\Phi|G_{a_1\ldots a_n}^{ii_1\ldots i_n}, \tag{42}$$

$$P^{\mathrm{EE}} = \sum_{n=1}^{M_R} \sum_{\substack{i_1<\cdots<i_n \\ a_1<\cdots<a_n}} G_{i_1\ldots i_n}^{a_1\ldots a_n}|\Phi\rangle\langle\Phi|G_{a_1\ldots a_n}^{i_1\ldots i_n}, \tag{43}$$

$$P^{\mathrm{EA}} = \sum_{n=0}^{M_R} \sum_{\substack{i_1<\cdots<i_n \\ a<a_1<\cdots<a_n}} G^{aa_1\ldots a_n}_{i_1\ldots i_n}|\Phi\rangle\langle\Phi|G^{i_1\ldots i_n}_{aa_1\ldots a_n}, \tag{44}$$

where, obviously,

$$G^{ii_1\ldots i_n}_{a_1\ldots a_n} = (G^{a_1\ldots a_n}_{ii_1\ldots i_n})^\dagger, \tag{45}$$

and

$$G^{i_1\ldots i_n}_{aa_1\ldots a_n} = (G^{aa_1\ldots a_n}_{i_1\ldots i_n})^\dagger. \tag{46}$$

When M_R satisfies the condition $M_R \leq M_T$, the truncated EOMCC problem assumes the form which is reminiscent of the exact equation (38), namely (cf. also, Ref. 38),

$$P(\bar{H}_{N,\mathrm{open}}\, R_{K,\mathrm{open}})_C|\Phi\rangle = \omega_K\, R_{K,\mathrm{open}}|\Phi\rangle, \tag{47}$$

where, obviously, $R_{K,\mathrm{open}} = P\, R_{K,\mathrm{open}} = P\, R_K$. We can also show that

$$\bar{H}^P_{N,\mathrm{open}}\, R_{K,\mathrm{open}}|\Phi\rangle = \omega_K\, R_{K,\mathrm{open}}|\Phi\rangle, \tag{48}$$

where, in general,

$$X^P = PXP, \tag{49}$$

for any operator X. This means that we can solve the truncated EOMCC problem in the space spanned by the excited configurations only and directly obtain the energy differences ω_K. The same becomes obvious if we look at the structure of matrix $\bar{\mathbf{H}}$ representing $\bar{H}_{N,\mathrm{open}}$. For example, in the EE-EOMCC theory we have

$$\bar{\mathbf{H}} = \begin{pmatrix} 0 & \bar{\mathbf{H}}_{\mathbf{0S}} & \bar{\mathbf{H}}_{\mathbf{0D}} & \cdots \\ \mathbf{0} & \bar{\mathbf{H}}_{\mathbf{SS}} & \bar{\mathbf{H}}_{\mathbf{SD}} & \cdots \\ \mathbf{0} & \bar{\mathbf{H}}_{\mathbf{DS}} & \bar{\mathbf{H}}_{\mathbf{DD}} & \cdots \\ \mathbf{0} & \cdots & \cdots & \cdots \end{pmatrix}, \tag{50}$$

where the subscript 0 refers to reference determinant $|\Phi\rangle$ and 0S, 0D, SS, SD, DS, DD, etc. designate the reference-singles, reference-doubles, singles-singles, singles-doubles, doubles-singles, doubles-doubles, etc. blocks of $\bar{\mathbf{H}}$. The first column of $\bar{\mathbf{H}}$ consists of zeros, since cluster operator T satisfies the SRCC equations, Eq. (35).

A few words should be mentioned about the EOMCC left eigenvalue problem. The EOMCC Hamiltonian $\bar{H}_N$, being non-Hermitian, has the left-hand (bra) eigenstates $\langle\Phi|L_K$, which are different from the right-hand (ket) eigenstates $R_K|\Phi\rangle$, although both sets of eigenstates correspond to the same set of eigenvalues ΔE_K (see, for example, Ref. 78). The left eigenvalue

problem, which corresponds to the right eigenvalue problem (38), has the form [33, 34, 38],

$$\langle\Phi|L_K\bar{H}_{N,\mathrm{open}} = \omega_K\langle\Phi|L_K. \tag{51}$$

Notice that unlike in the right eigenvalue problem, Eq. (38), where only connected part of $\bar{H}_{N,\mathrm{open}}R_{K,\mathrm{open}}$ is needed, both connected and disconnected components of the operator product $L_K\bar{H}_{N,\mathrm{open}}$ enter Eq. (51). This is a consequence of the fact that the SRCC cluster operator T, which satisfies Eq. (35), cannot simultaneously satisfy a system of equations $\langle\Phi|\bar{H}_{N,\mathrm{open}}G^{a_1\ldots a_n}_{i_1\ldots i_n}|\Phi\rangle = 0$. As a result, the disconnected part of $\langle\Phi|L_K\bar{H}_{N,\mathrm{open}}$, i.e. $\langle\Phi|\bar{H}_{N,\mathrm{open}}L_K$, does not vanish (cf., e.g., Refs. 59, 60, 64).

The left- and right-hand eigenstates, $\langle\Phi|L_K$ and $R_K|\Phi\rangle$, respectively, form a biorthogonal set, which can be chosen to be biorthonormal [34] (cf., also, Ref. 53), so that

$$\langle\Phi|L_K\,R_{K'}|\Phi\rangle = \delta_{K,K'}. \tag{52}$$

Formally, each operator L_K is a deexcitation operator, whose many-body expansion is

$$L_K = \sum_\lambda l_{K,\lambda}\,\Omega^\dagger_\lambda. \tag{53}$$

The left-hand eigenstates $\langle\Phi|L_K$ can be used to construct the EOMCC bra states $\langle\tilde{\Psi}_K|$, which equal [34, 53]

$$\langle\tilde{\Psi}_K| = \langle\Phi|L_Ke^{-T}. \tag{54}$$

In particular, the bra state $\langle\tilde{\Psi}_0|$, which corresponds to CC ground state $|\Psi_0\rangle$, Eq. (8), is defined as [34, 53] (see, also, Ref. 59)

$$\langle\tilde{\Psi}_0| = \langle\Phi|(1+\Lambda)e^{-T}, \tag{55}$$

where Λ is the well-known "lambda" deexcitation operator of the analytic gradient CC theory [56]. Recall that the operator Λ satisfies the left-hand analog of the connected Schrödinger equation

$$\bar{H}_N|\Phi\rangle = \Delta E_0|\Phi\rangle \tag{56}$$

i.e. the equation

$$\langle\Phi|(1+\Lambda)\,\bar{H}_N = \Delta E_0\langle\Phi|(1+\Lambda). \tag{57}$$

Equations (54) and (55) show that operators L_K cannot be regarded as ordinary deexcitation operators. Indeed, we cannot use L_K in the same way as we use R_K to define the excited ket states [see Eq. (7)]. The excited

bra states of the EOMCC theory, Eq. (54), are not identical to what one might regard as "true" excited bra states [59] $\langle\tilde{\Psi}_0|L'_K = \langle\Phi|(1+\Lambda)e^{-T}L'_K$ (L'_K designates the relevant deexcitation operator).

As mentioned in the Introduction, we do not have know the left-hand eigenstates of $\bar{H}_N$ if we are not interested in properties other than the energy. However, we cannot avoid left-hand eigenstates in various property calculations. For example, the EOMCC transition moments involving the operator Θ (Θ is, for example, the dipole moment operator) are defined as [34]

$$\langle\tilde{\Psi}_K|\Theta|\Psi_{K'}\rangle = \langle\Phi|L_K\bar{\Theta}R_{K'}|\Phi\rangle, \tag{58}$$

where

$$\bar{\Theta} = e^{-T}\Theta\, e^{T} = (\Theta\, e^{T})_C \tag{59}$$

is the similarity transformed operator Θ. The EOMCC ground-state properties, such as multipole moments and (hyper)polarizabilities [53–55] and nuclear spin-spin coupling constants [52], have to be defined in terms of the operator Λ, since [4, 33, 34, 53]

$$L_0 = 1 + \Lambda. \tag{60}$$

Examples of truncated EOMCC schemes are the IP-EOMCCSD [9] (cf., also, Ref. 38), EE-EOMCCSD [32–34], and EA-EOMCCSD [38] methods, where

$$T = T_1 + T_2, \tag{61}$$

so that $M_T = 2$, and $M_R \leq 2$. In the most complete variant of the IP-EOMCCSD method, in which M_R assumes the maximum possible value of $M_R = M_T = 2$, we have

$$R_K^{\mathrm{IP}} = R_{K,h} + R_{K,2h-p} + R_{K,3h-2p}, \tag{62}$$

in the most complete variant of the EE-EOMCCSD method, we have

$$R_K^{\mathrm{EE}} = R_{K,0} + R_{K,1} + R_{K,2}, \tag{63}$$

and in the most complete variant of the EA-EOMCCSD scheme, we have

$$R_K^{\mathrm{EA}} = R_{K,p} + R_{K,2p-h} + R_{K,3p-2h}. \tag{64}$$

The standard formulation of the EE-EOMCCSD theory is based on Eqs. (61) and (63) (in general, the standard truncation scheme for the EE-EOMCCSD method is characterized by the condition $M_R = M_T$). However, in the truncated IP-EOMCC and EA-EOMCC approaches, it is customary to assume that $M_R = M_T - 1$. Therefore, the standard EA-EOMCCSD method is in fact equivalent to what we would call here the

EA-EOMCCSD/$2p-h$ approach corresponding to $M_T = 2$ and $M_R = 1$ (certainly, the EA-EOMCCSD method presented in Ref. 38 belongs to this category since it neglects the $3p-2h$ terms in R_K^{EA}). In this case

$$R_K^{\mathrm{EA}} = R_{K,p} + R_{K,2p-h}. \tag{65}$$

Approximations of this type are useful, since it is much easier to solve the EA-EOMCCSD eigenvalue problem if the only unknown coefficients are $r_a(K)$ and $r_{ab}^{\ j}(K)$. The more complete EA-EOMCCSD problem using Eq. (64) instead of Eq. (65) would require an explicit consideration of $r_{abc}^{\ jk}(K)$ coefficients, in addition to all $r_a(K)$ and $r_{ab}^{\ j}(K)$ coefficients of the incomplete EA-EOMCCSD scheme. The number of $r_{abc}^{\ jk}(K)$ coefficients, which describe the $R_{K,3p-2h}$ operator, is of the same order of magnitude as the number of all triexcited configurations, which is usually quite large (this was, in fact, one of the reasons for neglecting the $R_{K,3p-2h}$ term in Ref. 38).

Review of the EOMCC formalism would not be complete if we did not say a word about the many-body expansion of $\bar{H}_{N,\mathrm{open}}$, which we write as

$$\bar{H}_{N,\mathrm{open}} = \sum_{n\geq 1} \bar{H}_n, \tag{66}$$

where

$$\bar{H}_n = (H_N e^T)_{C,n} \tag{67}$$

represents all n-body components of the connected operator product $(H_N e^T)_C$. For example, when $T = T_1 + T_2$,

$$\bar{H}_{N,\mathrm{open}} = \sum_{n=1}^{6} \bar{H}_n. \tag{68}$$

Although length of the many-body expansion of $\bar{H}_{N,\mathrm{open}}$ is enormous, very few terms enter a particular approximate scheme. For example, the EOMCCSD method needs one- and two-body components of $\bar{H}$ and certain types of the three-body $\bar{H}_3$ terms [33, 34] (for further comments, see Ref. 60; cf., also, Sections 4 and 5). The situation gets complicated if we want to go beyond the EOMCCSD approximation and represent T as a sum of, for example, T_1, T_2, and T_3 components. For this reason, the only higher-than-two-body terms included in the current implementation of the EOMCCSDT scheme are the three-body terms of the EOMCCSD method [46]. This approximation seems to work very well, even though the EOMCCSDT procedure defined in this way remains an n^8 method.

3. The EOMXCC theory: Basic formalism

The purpose of this section is to introduce the basic equations of the new EOMXCC theory of electronically excited, ionized, and electron-attached states of molecular systems. As mentioned in the Introduction, the EOMXCC method is strongly linked to the so-called XCC theory, which applies to the ground-state problem. The specific variants of the EOMXCC formalism that apply to electron-attached states, ionized states, and electronically excited states are referred to as the EA-EOMXCC, IP-EOMXCC, and EE-EOMXCC methods, respectively.

As in the ordinary EOMCC theory, in the EOMXCC method we solve the electronic Schrödinger equation (1) assuming that the excited states $|\Psi_K\rangle$ are represented by Eq. (7). We use the exponential representation of the ground-state wave function $|\Psi_0\rangle$, Eq. (8), but no longer assume that the cluster components T_n result from standard SRCC calculations (see below). The many-body expansions of the excitation operator R_K have the same form as in the ordinary EOMCC formalism. In particular, the three different forms of R_K discussed in the previous section [R_K^{EE}, R_K^{EA}, and R_K^{IP}, Eqs. (28), (30), and (26), respectively] are used to define the EE-EOMXCC, EA-EOMXCC, and IP-EOMXCC methods. As in the standard EOMCC method, by making suitable choices for the operators Ω_λ, which define R_K, we can always extend the EOMXCC theory to other sectors of the Fock space.

As mentioned in the Introduction, one of our purposes is reduction of the non-Hermitian character of the ordinary EOMCC formalism (or, in some variants of the new theory, its complete elimination). Unlike the original Hamiltonian H_N, the transformed Hamiltonian $\bar{H}$ used in the EOMCC method is no longer Hermitian and the non-Hermiticity of $\bar{H}$ measured by a difference $\bar{H} - (\bar{H})^\dagger$ shows up already in the first-order of MBPT, i.e.

$$\bar{H} - (\bar{H})^\dagger = O(\mathcal{V}), \tag{69}$$

where, in general, $O(\mathcal{V}^k)$ designates terms which are of at least k-th order in the usual MBPT sense. One of the consequences of the non-Hermiticity of $\bar{H}$ is the fact that the left- and right-hand eigenvectors of $\bar{H}$ are not identical and, as a result, one has to know both types of eigenvectors in the calculations that require the explicit knowledge of the wave functions (e.g. transition moments and oscillator strengths). Moreover, we would like to enrich the structure of the transformed Hamiltonian with the deexcitation operators that would bring higher-order effects into the new theory at a small cost. One way of accomplishing this goal that we explore in this paper is a second transformation of the electronic Schrödinger equation with another non-singular operator, such as $e^{T^\dagger}$. The $T^\dagger$ operator

generates deexcitations [cf. Eq. (14)] and it is known that the operator products involving low-order components of T and $T^\dagger$ (e.g. T_2 and $T_2^\dagger$) can be used to describe the effect of higher-order cluster components, such as T_4 [69–71]. This has been verified in various studies of the ground-state problem (cf., e.g., the XCC(5) [69, 70, 79], CCSDT+Q(CCSDT) [80], CCSD+TQ*(CCSD) [81], and various CC5SD[TQ] and CC5SD(TQ) [82] methods). Our purpose is to extend these types of theories to electronically excited states, where the role of higher-order cluster components is likely to be larger compared to the ground state, as the recent EOMCCSDT studies of excited states clearly demonstrate [46] (cf., also, Refs. 61, 63, 64).

We thus transform Eq. (33) with an operator $e^{T^\dagger}$. We multiply both sides of Eq. (33) on the left by $e^{T^\dagger}$, insert $e^{-T^\dagger}e^{T^\dagger} = 1$ into the operator product $\bar{H}_N R_K$ and replace $|\Phi\rangle$ by $e^{-T^\dagger}|\Phi\rangle$ (this is possible since $T^\dagger$ and its positive powers annihilate $|\Phi\rangle$). As a result, we obtain a new eigenvalue problem to deal with, namely,

$$\bar{\bar{H}}_N \bar{R}_K|\Phi\rangle = \Delta E_K \bar{R}_K|\Phi\rangle, \tag{70}$$

where

$$\bar{\bar{H}}_N = e^{T^\dagger}\bar{H}_N e^{-T^\dagger} = (e^{T^\dagger}\bar{H}_N)_C = [e^{T^\dagger}(H_N e^T)_C]_C \tag{71}$$

and

$$\bar{R}_K = e^{T^\dagger}R_K e^{-T^\dagger} = (e^{T^\dagger}R_K)_C. \tag{72}$$

In particular, the ground-state ($K = 0$) problem now becomes

$$\bar{\bar{H}}_N|\Phi\rangle = \Delta E_0|\Phi\rangle. \tag{73}$$

Clearly, the doubly transformed Hamiltonian $\bar{\bar{H}}$, Eq. (71), is more Hermitian than $\bar{H}$, i.e.,

$$\bar{\bar{H}} - (\bar{\bar{H}})^\dagger = O(\mathcal{V}^2), \tag{74}$$

and strictly Hermitian variants of $\bar{\bar{H}}$ can be designed (see Section 5). As a result, the difference between left- and right-hand eigenvectors of $\bar{\bar{H}}$ should be smaller than the difference between left- and right-hand eigenvectors of $\bar{H}$ resulting from ordinary EOMCC calculations (this difference is zero in the strictly Hermitian variants of the EOMXCC theory). Moreover, the algebraic structure of $\bar{\bar{H}}$ is richer, when compared to $\bar{H}$. Various operator products involving both T and $T^\dagger$ are present in $\bar{\bar{H}}$, allowing us to describe the effect of higher-order excitations using low-order components of T, as we are going to demonstrate later (see Section 6). Clearly, the transformed Hamiltonian $\bar{\bar{H}}$, when written as a power series in T and $T^\dagger$, is manifestly finite, independently of the level of approximation applied to T. This is

similar to the well-known property of the operator $\bar{H}$, which does not contain any terms that involve products of more than four cluster operators. We can expect, however, that the many-body expansion of $\bar{\bar{H}}$ is significantly more complicated than that of $\bar{H}$. In general, this might be a problem, but it can be shown that only few terms of the many-body expansion of $\bar{\bar{H}}$ are needed when we truncate T (and, consequently, R_K or $\bar{R}_K$) at a low level of approximation (such as CCSD; see below). The finiteness of the operator $\bar{\bar{H}}$ is a consequence of the *internally connected* character of the expression $[e^{T^\dagger}(H_N e^T)_C]_C$ defining $\bar{\bar{H}}$ [70].

An important new element of Eq. (70) is the operator $\bar{R}_K$, which is obtained by transforming R_K with $e^{T^\dagger}$. Its algebraic structure may not look entirely obvious, but it is easy to verify that the transformed operator $\bar{R}_K$, when acting on $|\Phi\rangle$, has the same general form as the parent operator R_K used to define it. Indeed, we can replace the operator $\bar{R}_K$ in Eq. (70) by an operator

$$C_K = (e^{T^\dagger} R_K)_{FC}, \tag{75}$$

where FC indicates that all lines of vertices representing $T^\dagger$ are connected to R_K, so that the only external lines of diagrams representing C_K are those originating from R_K. Replacement of $\bar{R}_K$ by C_K, Eq. (75), in Eq. (70) is possible since all lines of $T^\dagger$ represent operators Y_p ($Y_a = X_a$ and $Y_i = X^i$) and these operators annihilate $|\Phi\rangle$ if they are left uncontracted. On the other hand, since all external lines of the diagrams representing C_K, Eq. (75), must originate from the vertices representing R_K, all external lines of C_K correspond to quasi-particle operators Y^p. As a result, we can use operators Ω_λ, Eqs. (18)-(20), to define the many-body expansion of C_K in the same way as we use these operators to define R_K [cf. Eqs. (26)-(31)]. We obtain,

$$\bar{\bar{H}}_N C_K|\Phi\rangle = \Delta E_K C_K|\Phi\rangle, \tag{76}$$

where

$$C_K = \sum_\lambda c_{K,\lambda}\, \Omega_\lambda. \tag{77}$$

The explicit relationship between the expansion coefficients $c_{K,\lambda}$ and analogous coefficients $r_{K,\lambda}$ defining expansion of R_K in terms of Ω_λ is discussed at the end of this section.

Equations (70) or (76) and (73) are the basic equations of the new EOMXCC theory. In order to solve an eigenvalue problem (70) we must decide about the source of information about the cluster operator T that defines $\bar{\bar{H}}$. We find the cluster amplitudes defining T by projecting Eq. (73) against the excited configurations included in the many-body expansion of

T. Thus, we first solve the system of energy-independent equations

$$\langle\Phi|G^{i_1\ldots i_n}_{a_1\ldots a_n}\bar{\bar{H}}_N|\Phi\rangle = \langle\Phi|G^{i_1\ldots i_n}_{a_1\ldots a_n}\bar{\bar{H}}_{N,\mathrm{open}}|\Phi\rangle = 0, \quad (n = 1,\ldots) \tag{78}$$

which looks similar to standard SRCC system (35) but is different, since we now use the doubly transformed Hamiltonian

$$\bar{\bar{H}}_{N,\mathrm{open}} = (e^{T^\dagger}\bar{H}_{N,\mathrm{open}})_{C,\mathrm{open}}, \tag{79}$$

instead of $\bar{H}_{N,\mathrm{open}}$. We then use the converged cluster amplitudes satisfying Eq. (78) to calculate the ground-state energy using a formula

$$\Delta E_0 = \langle\Phi|\bar{\bar{H}}_N|\Phi\rangle = \bar{\bar{H}}_{N,\mathrm{close}}, \tag{80}$$

where

$$\bar{\bar{H}}_{N,\mathrm{close}} = (e^{T^\dagger}\bar{H}_N)_{C,\mathrm{close}}. \tag{81}$$

It is easy to see that

$$\begin{aligned}\Delta E_0 &= \Delta E_0^{\mathrm{CC}} + (e^{T^\dagger}\bar{H}_{N,\mathrm{open}})_{C,\mathrm{close}} \\ &= \Delta E_0^{\mathrm{CC}} + [(e^{T^\dagger} - 1)\bar{H}_{N,\mathrm{open}}]_{C,\mathrm{close}},\end{aligned} \tag{82}$$

where ΔE_0^{CC} is the energy expression of the standard SRCC theory [see Eq. (37)]. As it was demonstrated earlier [69, 75], the energy expression

$$\Delta E_0 = \langle\Phi|\bar{\bar{H}}_N|\Phi\rangle = \langle\Phi|[e^{T^\dagger}(H_N e^T)_C]_C|\Phi\rangle, \tag{83}$$

which we use in this paper, is equivalent to a formula

$$\Delta E_0 = \langle\Phi|(e^{T^\dagger}H_N e^T)_C|\Phi\rangle \tag{84}$$

defining the energy functional used in the original XCC papers [69, 70]. The amplitude equations obtained in these papers [defining the hierarchy of XCC(n) schemes] are essentially identical to our Eq. (78), provided that we truncate Eq. (78) using arguments similar to those presented in Refs. 69, 70. Clearly, there must be a relationship between the theory discussed here and early XCC work, although we have not arrived at Eqs. (78) and (80) by analyzing the conditions that make the energy functional (84) stationary. Let us discuss this relationship for a moment.

As explained in Ref. 75, in the ideal XCC theory one is interested in making the energy functional (84) stationary with respect to T and $T^\dagger$. This leads (after some manipulations) to amplitude equations, which are equivalent to Eq. (78), but we cannot use Eq. (83) as an energy functional [we must use Eq. (84) instead]. If we insist on using Eq. (83) as an energy functional, we can only make it stationary with respect to $T^\dagger$. The

resulting amplitude equations are then identical to Eq. (78) and Eqs. (80) or (83) become legitimate energy expressions [74, 75]. Although early XCC studies [69, 70] used Eq. (84) as an energy functional, the actual amplitude equations were derived by considering the energy expressions, which are reminiscent of truncated Eq. (83). Indeed, each XCC(n) scheme discussed in Refs. 69, 70 was obtained by truncating the exact energy functional, Eq. (84), at a given MBPT order (n) and by rewriting the resulting truncated energy functional in the internally connected form, similar to Eq. (83), using lower-order amplitude equations to eliminate the internally disconnected terms. Once the internally connected form of the truncated energy functional was obtained, variation with respect to $T^\dagger$ was performed to obtain the final amplitude equations. If the internally disconnected terms were not eliminated early on, variation of truncated functionals resulting from Eq. (84) with respect to $T^\dagger$ would introduce disconnected terms into the XCC(n) equations (cf. Ref. 70). Variation with respect to T was not considered at all in Refs. 69, 70. From this description, it immediately follows that all XCC(n) equations presented in Refs. 69, 70 could be directly obtained by considering the truncated forms of Eq. (83) from the very beginning. The amplitude equations that would result from making the truncated Eq. (83) stationary with respect to $T^\dagger$ would be essentially the same as truncated Eq. (78). This means that the XCC(n) equations proposed earlier [69, 70] represent various approximations to our amplitude and energy equations (78) and (80), even though we do not focus on stationary conditions in derivations described in the present paper. This simple relationship between the original XCC(n) approximations and our Eqs. (83) or (80) and (78) is precisely the reason why we call the new theory the EOMXCC approach.

With T satisfying Eq. (78) and ground-state energy defined by Eq. (80), we can replace Eq. (70) by an eigenvalue problem

$$\bar{\bar{H}}_{N,\mathrm{open}} C_K|\Phi\rangle = \omega_K C_K|\Phi\rangle, \tag{85}$$

or

$$\bar{\bar{H}}_{N,\mathrm{open}} C_{K,\mathrm{open}}|\Phi\rangle = \omega_K C_K|\Phi\rangle, \tag{86}$$

where ω_K is defined by Eq. (40). An operator

$$C_{K,\mathrm{open}} = (e^{T^\dagger} R_K)_{FC,\mathrm{open}} \tag{87}$$

can be regarded as an EOMXCC analog of $R_{K,\mathrm{open}}$. It equals C_K for the IP and EA cases and $C_K - C_{K,0}$, where $C_{K,0} = (e^{T^\dagger} R_K)_{FC,\mathrm{close}}$ is the zero-body part of C_K, for the EE case (of course it may happen that $C_{K,0} = 0$ for symmetry reasons; in this case $C_K = C_{K,\mathrm{open}}$ in the EE case as well).

An eigenvalue problem characterizing the EOMXCC theory, Eq. (86), is similar to an eigenvalue problem characterizing the EOMCC formalism [cf. Eq. (33)]. The only essential difference is the type of the similarity transformed Hamiltonian used in both theories ($\bar{H}$ in EOMCC and $\bar{\bar{H}}$ in EOMXCC). Similarity between the EOMCC and EOMXCC theories becomes even more transparent when we realize that we can replace the operator product $\bar{\bar{H}}_{N,\mathrm{open}} C_{K,\mathrm{open}}$ in Eq. (86), by the explicitly connected expression $(\bar{\bar{H}}_{N,\mathrm{open}} C_{K,\mathrm{open}})_C$, i.e.

$$(\bar{\bar{H}}_{N,\mathrm{open}} C_{K,\mathrm{open}})_C|\Phi\rangle = \omega_K C_K|\Phi\rangle. \tag{88}$$

Equivalence of Eqs. (86) and (88) is an immediate consequence of the fact that the cluster operator T satisfies Eq. (78), so that the disconnected part of $\bar{\bar{H}}_{N,\mathrm{open}} C_{K,\mathrm{open}}|\Phi\rangle$, i.e. $C_{K,\mathrm{open}} \bar{\bar{H}}_{N,\mathrm{open}}|\Phi\rangle$, vanishes. We can also arrive at Eq. (88) multiplying both sides of Eq. (73) on the left by C_K and subtracting the resulting equation from Eq. (76). This gives,

$$[\bar{\bar{H}}_N, C_K]|\Phi\rangle = \omega_K C_K|\Phi\rangle, \tag{89}$$

which reduces to Eq. (88) if we realize that

$$[\bar{\bar{H}}_N, C_K] = [\bar{\bar{H}}_{N,\mathrm{open}}, C_{K,\mathrm{open}}] = (\bar{\bar{H}}_{N,\mathrm{open}} C_{K,\mathrm{open}})_C. \tag{90}$$

As in the standard EOMCC method, Eq. (88) is applicable to truncated EOMXCC schemes. Let us consider an approximation, in which the cluster operator T is truncated at the M_T-body term T_{M_T} [cf. Eq. (41)]. If M_R defines the length of the truncated many-body expansions of R_K^{IP}, R_K^{EE}, and R_K^{EA} [cf. Eqs. (26), (28), and (30)], we can also write

$$C_K^{\mathrm{IP}} = C_{K,\mathrm{open}}^{\mathrm{IP}} = \sum_{n=0}^{M_R} C_{K,(n+1)h-np}, \tag{91}$$

with

$$\begin{aligned} C_{K,(n+1)h-np} &= \frac{1}{n!(n+1)!}\, c^{ii_1\ldots i_n}_{a_1\ldots a_n}(K)\, G_{ii_1\ldots i_n}^{a_1\ldots a_n} \quad (n \geq 1), \\ C_{K,1h-0p} &\equiv C_{K,h} = c^i(K)\, G_i, \end{aligned} \tag{92}$$

$$C_K^{\mathrm{EE}} = C_{K,0} + C_{K,\mathrm{open}}^{\mathrm{EE}} = \sum_{n=0}^{M_R} C_{K,n}, \tag{93}$$

with

$$\begin{aligned} C_{K,n} &= \left(\frac{1}{n!}\right)^2 c^{i_1\ldots i_n}_{a_1\ldots a_n}(K)\, G_{i_1\ldots i_n}^{a_1\ldots a_n} \quad (n \geq 1), \\ C_{K,0} &= c_0(K), \end{aligned} \tag{94}$$

and

$$C_K^{\mathrm{EA}} = C_{K,\mathrm{open}}^{\mathrm{EA}} = \sum_{n=0}^{M_R} C_{K,(n+1)p-nh}, \tag{95}$$

with

$$\begin{aligned} C_{K,(n+1)p-nh} &= \frac{1}{n!(n+1)!}\, c_{aa_1\ldots a_n}^{i_1\ldots i_n}(K)\, G_{i_1\ldots i_n}^{aa_1\ldots a_n} \quad (n \geq 1), \\ & C_{K,1p-0h} \equiv C_{K,p} = c_a(K)\, G^a. \end{aligned} \tag{96}$$

Clearly, for $n = M_R$, we have $C_{K,(n+1)h-np} = R_{K,(n+1)h-np}$, $C_{K,n} = R_{K,n}$, and $C_{K,(n+1)p-nh} = R_{K,(n+1)p-nh}$. As in the EOMCC theory, we further assume that $M_R \leq M_T$. Since $P\,C_K = P\,C_{K,\mathrm{open}} = C_{K,\mathrm{open}}$, independently of the type of the EOMXCC theory considered (IP, EE, or EA), and since $C_K^X = C_{K,\mathrm{open}}^X$ ($X = \mathrm{IP}, \mathrm{EA}$) and $P^{\mathrm{EE}}\bar{\bar{H}}_{N,\mathrm{open}}|\Phi\rangle = 0$ for $M_R \leq M_T$, the eigenvalue problem (85) written for the truncated EOMXCC scheme becomes,

$$P\,\bar{\bar{H}}_{N,\mathrm{open}}\,C_K|\Phi\rangle = P\,\bar{\bar{H}}_{N,\mathrm{open}}\,C_{K,\mathrm{open}}|\Phi\rangle = \omega_K\,C_{K,\mathrm{open}}|\Phi\rangle, \tag{97}$$

or

$$\bar{\bar{H}}_{N,\mathrm{open}}^P\,C_{K,\mathrm{open}}|\Phi\rangle = \omega_K\,C_{K,\mathrm{open}}|\Phi\rangle, \tag{98}$$

where, according to Eq. (49), $\bar{\bar{H}}_{N,\mathrm{open}}^P = P\bar{\bar{H}}_{N,\mathrm{open}}P$. When M_R satisfies the condition $M_R \leq M_T$, Eqs. (97) and (98) are equivalent to

$$P(\bar{\bar{H}}_{N,\mathrm{open}}\,C_{K,\mathrm{open}})_C|\Phi\rangle = \omega_K\,C_{K,\mathrm{open}}|\Phi\rangle. \tag{99}$$

Indeed, when $M_R \leq M_T$, the disconnected component of the left-hand side of Eq. (97), i.e. the expression $P\,C_{K,\mathrm{open}}\,\bar{\bar{H}}_{N,\mathrm{open}}|\Phi\rangle$, vanishes, since cluster amplitudes defining T, Eq. (41), satisfy equations (78) with $n = 1, \ldots, M_T$. Equation (99) represents a generalization of the exact Eq. (88) to truncated EOMXCC schemes. Again, the only significant difference between the EOMXCC equations (98) and (99) and their EOMCC analogs (48) and (47), respectively, is the similarity transformed Hamiltonian used by both theories. As in the EOMCC theory, Eqs. (98) and (99) have the same general form (in particular, they rely on the same similarity transformed Hamiltonian) for all the sectors of Fock space.

Since the cluster operator T used in the EOMXCC scheme is obtained by solving the XCC system of equations (78), matrix $\bar{\bar{\mathbf{H}}}$ representing the similarity transformed Hamiltonian $\bar{\bar{H}}_{N,\mathrm{open}}$ of the EOMXCC formalism, has a structure which is very similar to a structure of matrix representing

$\bar{H}_{N,\mathrm{open}}$ [cf. Eq. (50)]. Indeed, in the EE-EOMXCC theory, the matrix representing $\bar{\bar{H}}_{N,\mathrm{open}}$ has the form

$$\bar{\bar{\mathbf{H}}} = \begin{pmatrix} 0 & \bar{\bar{\mathbf{H}}}_{\mathbf{0S}} & \bar{\bar{\mathbf{H}}}_{\mathbf{0D}} & \cdots \\ \mathbf{0} & \bar{\bar{\mathbf{H}}}_{\mathbf{SS}} & \bar{\bar{\mathbf{H}}}_{\mathbf{SD}} & \cdots \\ \mathbf{0} & \bar{\bar{\mathbf{H}}}_{\mathbf{DS}} & \bar{\bar{\mathbf{H}}}_{\mathbf{DD}} & \cdots \\ \mathbf{0} & \cdots & \cdots & \cdots \end{pmatrix}. \tag{100}$$

Zeros in the first column of $\bar{\bar{\mathbf{H}}}$ are a consequence of the fact that the cluster operator T satisfies the XCC system of equations, Eq. (78). Their presence allows us to solve the EOMXCC eigenvalue problem in the space spanned by excited configurations only and obtain energy differences ω_K directly.

The EOMXCC Hamiltonian $\bar{\bar{H}}_N$ is in general non-Hermitian, so that its left-hand eigenstates $\langle\Phi|\tilde{C}_K$, are different from the right-hand eigenstates $C_K|\Phi\rangle$, although, as in the EOMCC case, both sets of eigenstates correspond to the same set of eigenvalues ΔE_K. The left eigenvalue problem corresponding to the right eigenvalue problem (88), can be given the form,

$$\langle\Phi|\tilde{C}_K\bar{\bar{H}}_{N,\mathrm{open}} = \omega_K\langle\Phi|\tilde{C}_K, \tag{101}$$

where

$$\tilde{C}_K \equiv \bar{L}_K = L_K e^{-T^\dagger} \tag{102}$$

is a deexcitation operator, which can be viewed as the EOMXCC analog of L_K. In particular [cf. Eq. (60)],

$$\tilde{C}_0 = L_0 e^{-T^\dagger} = (1+\Lambda)e^{-T^\dagger}, \tag{103}$$

so that we can also write,

$$\tilde{C}_0 = 1 + \Lambda^{\mathrm{XCC}}, \tag{104}$$

where Λ^{XCC} is the "lambda" operator of the XCC theory, which is defined through the equation,

$$(1+\Lambda^{\mathrm{XCC}})e^{T^\dagger} = 1 + \Lambda, \tag{105}$$

in complete agreement with the considerations presented in Ref. 75. Notice that all left-hand operators $\tilde{C}_K$, Eq. (102), the ground-state left-hand operator $\tilde{C}_0$ in particular, are more exponential than their standard EOMCC counterparts L_K. The possibility to have a completely exponential ansatz for the left-hand operator $\tilde{C}_0$ is discussed at the end of this paper, when we introduce the basic equations of the EOMECC method (cf. Section 7).

As in the EOMCC case, both connected and disconnected components of the operator product $\tilde{C}_K \bar{\bar{H}}_{N,\mathrm{open}}$ enter Eq. (101), although only the connected part of $\bar{\bar{H}}_{N,\mathrm{open}} C_{K,\mathrm{open}}$ enters Eq. (88). Indeed, since the XCC cluster operator T is obtained by solving Eq. (78), it cannot simultaneously satisfy a system of equations $\langle\Phi|\bar{\bar{H}}_{N,\mathrm{open}} G^{a_1\ldots a_n}_{i_1\ldots i_n}|\Phi\rangle = 0$ [this is more or less the same as saying that the XCC energy functional (83) cannot be made stationary with respect to both T and $T^\dagger$]. In consequence, the disconnected part of $\langle\Phi|\tilde{C}_K \bar{\bar{H}}_{N,\mathrm{open}}$, i.e. $\langle\Phi|\bar{\bar{H}}_{N,\mathrm{open}}\tilde{C}_K$, is a nonzero quantity. As in the EOMCC case, the left- and right-hand eigenstates of the EOMXCC theory, $\langle\Phi|\tilde{C}_K$ and $C_K|\Phi\rangle$, respectively, form a biorthogonal set, which can be made biorthonormal, since

$$\langle\Phi|\tilde{C}_K\, C_{K'}|\Phi\rangle = \langle\Phi|L_K\, R_{K'}|\Phi\rangle = \delta_{K,K'}. \tag{106}$$

We do not have to determine the left-hand eigenstates of $\bar{\bar{H}}_N$ if we are only interested in excitation energies. However, properties other than the energy need both left- and right-hand eigenstates of $\bar{\bar{H}}_N$. For example, the EOMXCC definition of transition moments involving the operator Θ, which is compatible with expression (58), looks as follows,

$$\langle\tilde{\Psi}_K|\Theta|\Psi_{K'}\rangle = \langle\Phi|\tilde{C}_K\bar{\bar{\Theta}}C_{K'}|\Phi\rangle, \tag{107}$$

where

$$\bar{\bar{\Theta}} = e^{T^\dagger}\bar{\Theta}\,e^{-T^\dagger} = (\bar{\Theta}\,e^{T^\dagger})_C \tag{108}$$

is the doubly transformed operator Θ.

Examples of truncated EOMXCC schemes are the IP-EOMXCCSD, EE-EOMXCCSD, and EA-EOMXCCSD methods, in which $M_T = 2$ and $M_R \leq 2$. In the most complete ($M_R = 2$) variant of the IP-EOMXCCSD method, where R^{IP}_K is given by Eq. (62), the formula for the corresponding operator C^{IP}_K becomes

$$C^{\mathrm{IP}}_K = C^{\mathrm{IP}}_{K,\mathrm{open}} = C_{K,h} + C_{K,2h-p} + C_{K,3h-2p}, \tag{109}$$

with

$$\begin{aligned} C_{K,h} \;=\; & R_{K,h} + (T_1^\dagger R_{K,2h-p})_{FC} + (T_2^\dagger R_{K,3h-2p})_{FC} \\ & + [\tfrac{1}{2}(T_1^\dagger)^2 R_{K,3h-2p}]_{FC}, \end{aligned} \tag{110}$$

$$C_{K,2h-p} = R_{K,2h-p} + (T_1^\dagger R_{K,3h-2p})_{FC}, \tag{111}$$

$$C_{K,3h-2p} = R_{K,3h-2p}. \tag{112}$$

In the most complete variant of the EE-EOMXCCSD method, where $R_K^{\rm EE}$ is given by Eq. (63), the operator $C_K^{\rm EE}$ assumes the form

$$C_K^{\rm EE} = C_{K,0} + C_{K,\rm open}^{\rm EE} = C_{K,0} + C_{K,1} + C_{K,2}, \tag{113}$$

with

$$C_{K,0} = R_{K,0} + (T_1^\dagger R_{K,1})_{FC} + (T_2^\dagger R_{K,2})_{FC} + [\tfrac{1}{2}(T_1^\dagger)^2 R_{K,2}]_{FC}, \tag{114}$$

$$C_{K,1} = R_{K,1} + (T_1^\dagger R_{K,2})_{FC}, \tag{115}$$

$$C_{K,2} = R_{K,2}. \tag{116}$$

Finally, in the most complete variant of the EA-EOMXCCSD scheme, where $R_K^{\rm EA}$ is defined by Eq. (64), the corresponding operator $C_K^{\rm EA}$ becomes

$$C_K^{\rm EA} = C_{K,\rm open}^{\rm EA} = C_{K,p} + C_{K,2p-h} + C_{K,3p-2h}, \tag{117}$$

with

$$\begin{aligned} C_{K,p} &= R_{K,p} + (T_1^\dagger R_{K,2p-h})_{FC} + (T_2^\dagger R_{K,3p-2h})_{FC} \\ &\quad + [\tfrac{1}{2}(T_1^\dagger)^2 R_{K,3p-2h}]_{FC}, \end{aligned} \tag{118}$$

$$C_{K,2p-h} = R_{K,2p-h} + (T_1^\dagger R_{K,3p-2h})_{FC}, \tag{119}$$

$$C_{K,3p-2h} = R_{K,3p-2h}. \tag{120}$$

It should be emphasized that once the coefficients $c_{K,\lambda}$ defining C_K are found, we can always retrieve the coefficients $r_{K,\lambda}$ defining the parent operator R_K. The relationship between these two types of coefficients is always straightforward. In case of the EE-EOMXCCSD scheme, this relationship is [cf. Eqs. (114)-(116)]

$$c_0(K) = r_0(K) + t_m^e\, r_e^m(K) + \tfrac{1}{4}(t_{mn}^{ef} + 2\, t_m^e\, t_n^f) r_{ef}^{mn}(K), \tag{121}$$

$$c_a^i(K) = r_a^i(K) + t_m^e\, r_{ea}^{mi}(K), \tag{122}$$

$$c_{ab}^{ij}(K) = r_{ab}^{ij}(K), \tag{123}$$

where $c_0(K)$, $c_a^i(K)$, and $c_{ab}^{ij}(K)$ are the coefficients defining $C_{K,0}$, $C_{K,1}$, and $C_{K,2}$ [cf. Eq. (94)] and $r_0(K)$, $r_a^i(K)$, and $r_{ab}^{ij}(K)$ are the coefficients defining $R_{K,0}$, $R_{K,1}$, and $R_{K,2}$ [cf. Eq. (29)]. Similar equations can be written for the IP and EA cases. In complete analogy to standard truncation schemes used in the IP-EOMCC and EA-EOMCC methods, it is worthwhile to consider the approaches with $M_R = M_T - 1$ (cf. the previous section). An example of such an approach would be the EA-EOMXCCSD/$2p-h$

method corresponding to $M_T = 2$ and $M_R = 1$. In this case, we would have [cf. Eq. (65)]

$$C_K^{\mathrm{EA}} = C_{K,\mathrm{open}}^{\mathrm{EA}} = C_{K,p} + C_{K,2p-h}, \tag{124}$$

with

$$C_{K,p} = R_{K,p} + (T_1^\dagger R_{K,2p-h})_{FC}, \tag{125}$$

$$C_{K,2p-h} = R_{K,2p-h}. \tag{126}$$

Before proceeding to the next section, we should emphasize that although the many-body expansion of $\bar{\bar{H}}_{N,\mathrm{open}}$, which we write as

$$\bar{\bar{H}}_{N,\mathrm{open}} = \sum_{n\geq 1} \bar{\bar{H}}_n, \tag{127}$$

where

$$\bar{\bar{H}}_n = (e^{T^\dagger} \bar{H}_{N,\mathrm{open}})_{C,n} \tag{128}$$

represents all n-body connected components of the operator product $e^{T^\dagger} \bar{H}_{N,\mathrm{open}}$, is far more complicated than in the EOMCC case (for $T = T_1 + T_2$, $\bar{\bar{H}}_{N,\mathrm{open}} = \sum_{n=1}^{18} \bar{\bar{H}}_n$, whereas $\bar{H}_{N,\mathrm{open}}$ contains at most six-body terms), very few terms enter truncated EOMXCC schemes. For example, the EOMXCCSD theory does not require higher-than-four-body components $\bar{\bar{H}}_n$. In fact, only selected types of three- and four-body terms enter the EOMXCCSD problem and we can always think of dropping some of them anyway. From this point of view, the EOMXCC theory is not much more complicated than the EOMCC method. At the same time, the EOMXCCSD equations seem to contain the T_3 contributions of the EOMCCSDT method (interestingly enough, many of them are described by one- and two-body components of $\bar{\bar{H}}_{N,\mathrm{open}}$; see Section 6). Thus, it is likely that the EOMXCCSD method allows us to incorporate at least some effects due to the ground-state T_3 components without using the expensive n^8 steps of the EOMCCSDT approach. As we demonstrate below, the EOMXCCSD formalism is an n^6 procedure.

A comparison of the most basic elements of the EOMCC and EOMXCC theories is given in Table 1. This table also shows basic equations of the CI approach indicating the fact that the EOMCC and EOMXCC methods can be regarded as methods which are built on top of CI (by replacing the Hamiltonian by its similarity transformed analogs).

Table 1. A comparison of basic elements of CI, EOMCC, and EOMXCC theories.

Method	**CI**	**EOMCC**	**EOMXCC**
Wave function ansatz	$\|\Psi_K\rangle = R_K\|\Phi\rangle$	$\|\Psi_K\rangle = R_K e^T\|\Phi\rangle$	$\|\Psi_K\rangle = R_K e^T\|\Phi\rangle$
Hamiltonian	$H_N = F_N + V_N$	$\bar{H}_N = (H_N e^T)_C$	$\bar{\bar{H}}_N = [e^{T^\dagger}(H_N e^T)_C]_C$
Eigenvalue problem	$H_N\, R_K\|\Phi\rangle = \Delta E_K\, R_K\|\Phi\rangle$	$\bar{H}_N\, R_K\|\Phi\rangle = \Delta E_K\, R_K\|\Phi\rangle$	$\bar{\bar{H}}_N\, \bar{R}_K\|\Phi\rangle = \Delta E_K\, \bar{R}_K\|\Phi\rangle$
Ground-state equation	$H_N\, R_0\|\Phi\rangle = \Delta E_0\, R_0\|\Phi\rangle$	$\bar{H}_N\|\Phi\rangle = \Delta E_0\|\Phi\rangle$	$\bar{\bar{H}}_N\|\Phi\rangle = \Delta E_0\|\Phi\rangle$
Hermiticity of Hamiltonian	$H - H^\dagger = 0$	$\bar{H} - (\bar{H})^\dagger = O(\mathcal{V})$	$\bar{\bar{H}} - (\bar{\bar{H}})^\dagger = O(\mathcal{V}^2)$

4. The EOMXCCSD method

In this and in the following sections we focus on the EE-EOMXCCSD formalism, which from now on we abbreviate as EOMXCCSD. We are primarily interested in the complete ($M_T = M_R = 2$) scheme and focus on the right eigenvalue problem (99).

According to general considerations presented in the previous section, we first solve the ground-state XCCSD equations,

$$\langle\Phi|G_a^i \bar{\bar{H}}_{N,\mathrm{open}}|\Phi\rangle = 0, \tag{129}$$

$$\langle\Phi|G_{ab}^{ij} \bar{\bar{H}}_{N,\mathrm{open}}|\Phi\rangle = 0, \tag{130}$$

where

$$G_a^i = (G_i^a)^\dagger, \tag{131}$$

$$G_{ab}^{ij} = (G_{ij}^{ab})^\dagger, \tag{132}$$

and $T = T_1 + T_2$. Once these equations are solved, so that the singly- and doubly-excited cluster amplitudes t_a^i and t_{ab}^{ij} are known, we calculate the ground-state energy using formula (82), construct the relevant components of the doubly transformed Hamiltonian $\bar{\bar{H}}_{N,\mathrm{open}}$, and solve the eigenvalue problem (99), where

$$C_{K,\mathrm{open}} = C_{K,1} + C_{K,2} \tag{133}$$

and

$$P = \sum_{i,a} |\Phi_i^a\rangle\langle\Phi_i^a| + \sum_{i>j,a>b} |\Phi_{ij}^{ab}\rangle\langle\Phi_{ij}^{ab}|, \tag{134}$$

with

$$|\Phi_i^a\rangle = G_i^a|\Phi\rangle, \tag{135}$$

and

$$|\Phi_{ij}^{ab}\rangle = G_{ij}^{ab}|\Phi\rangle. \tag{136}$$

In terms of many-body components of $\bar{\bar{H}}_{N,\mathrm{open}}$, the eigenvalue problem (99) becomes,

$$\langle\Phi|G_a^i \left[(\bar{\bar{H}}_1 + \bar{\bar{H}}_2)(C_{K,1} + C_{K,2}) + \bar{\bar{H}}_3 C_{K,2}\right]|\Phi\rangle = \omega_K C_a^i, \tag{137}$$

$$\begin{aligned}\langle\Phi|G_{ab}^{ij} \Big[&\bar{\bar{H}}_1 C_{K,2} + \bar{\bar{H}}_2(C_{K,1} + C_{K,2}) + \bar{\bar{H}}_3(C_{K,1} + C_{K,2}) \\ &+ \bar{\bar{H}}_4 C_{K,2}\Big]|\Phi\rangle = \omega_K C_{ab}^{ij},\end{aligned} \tag{138}$$

where $C_a^i \equiv c_a^i(K)$ and $C_{ab}^{ij} \equiv c_{ab}^{ij}(K)$ are the coefficients defining $C_{K,1}$ and $C_{K,2}$, respectively, i.e.,

$$C_{K,1} = C_a^i G_i^a, \tag{139}$$

$$C_{K,2} = \tfrac{1}{4} C_{ab}^{ij} G_{ij}^{ab}. \tag{140}$$

The XCCSD equations needed to determine t_a^i and t_{ab}^{ij} reduce to

$$\bar{\bar{h}}_a^i = \langle \Phi | G_a^i \bar{\bar{H}}_1 | \Phi \rangle = 0, \tag{141}$$

$$\bar{\bar{h}}_{ab}^{ij} = \langle \Phi | G_{ab}^{ij} \bar{\bar{H}}_2 | \Phi \rangle = 0, \tag{142}$$

where, in general, $\bar{\bar{h}}_p^q$ and $\bar{\bar{h}}_{pq}^{rs}$ represent matrix elements defining $\bar{\bar{H}}_1$ and $\bar{\bar{H}}_2$, i.e.

$$\bar{\bar{H}}_1 = \bar{\bar{h}}_p^q N\{X^p X_q\}, \tag{143}$$

$$\bar{\bar{H}}_2 = \tfrac{1}{4} \bar{\bar{h}}_{pq}^{rs} N\{X^p X_r X^q X_s\}. \tag{144}$$

We can see that higher-than-four-body components of $\bar{\bar{H}}_{N,\mathrm{open}}$ do not enter the EOMXCCSD problem. We should also note that we could drop the subscript C indicating the connected components of the operator product $\bar{\bar{H}}_{N,\mathrm{open}} C_{K,\mathrm{open}}$ in Eqs. (137) and (138) (no disconnected terms can be generated in this case). It is interesting to observe how the $\langle \Phi | G_{ab}^{ij} \bar{\bar{H}}_1 C_{K,1} | \Phi \rangle$ term, which contributes to a DS part (doubles-singles block) of the EOMXCCSD eigenvalue problem, disappears from Eq. (138). This term is apparently disconnected (it equals $\mathcal{A}_{ab} \mathcal{A}^{ij} \bar{\bar{h}}_a^i c_b^j$, where $\bar{\bar{h}}_a^i = \langle \Phi | G_a^i \bar{\bar{H}}_1 | \Phi \rangle$) and vanishes, since $\bar{\bar{h}}_a^i = 0$ for the converged XCCSD amplitudes [cf. Eq. (141)].

In order to proceed further, let us introduce the following notation,

$${}^{1,2}\Lambda_a^i = \langle \Phi | G_a^i (\bar{\bar{H}}_1 + \bar{\bar{H}}_2)(C_{K,1} + C_{K,2}) | \Phi \rangle, \tag{145}$$

$${}^{1,2}\Lambda_{ab}^{ij} = \langle \Phi | G_{ab}^{ij} \left[\bar{\bar{H}}_1 C_{K,2} + \bar{\bar{H}}_2 (C_{K,1} + C_{K,2}) \right] | \Phi \rangle, \tag{146}$$

$${}^{3}\Lambda_a^i = \langle \Phi | G_a^i \bar{\bar{H}}_3 C_{K,2} | \Phi \rangle, \tag{147}$$

$${}^{3}\Lambda_{ab}^{ij} = \langle \Phi | G_{ab}^{ij} \bar{\bar{H}}_3 (C_{K,1} + C_{K,2}) | \Phi \rangle, \tag{148}$$

$${}^{4}\Lambda_{ab}^{ij} = \langle \Phi | G_{ab}^{ij} \bar{\bar{H}}_4 C_{K,2} | \Phi \rangle. \tag{149}$$

The EOMXCCSD equations now become,

$${}^{1,2}\Lambda_a^i + {}^{3}\Lambda_a^i = \omega_K C_a^i, \tag{150}$$

$${}^{1,2}\Lambda_{ab}^{ij} + {}^{3}\Lambda_{ab}^{ij} + {}^{4}\Lambda_{ab}^{ij} = \omega_K C_{ab}^{ij}. \tag{151}$$

We can now use the diagrammatic methods of MBPT to derive explicit expressions for the quantities Λ. For the one- and two-body contributions, ${}^{1,2}\Lambda_a^i$ and ${}^{1,2}\Lambda_{ab}^{ij}$, we obtain,

$$\begin{aligned} {}^{1,2}\Lambda_a^i &= \bar{\bar{h}}_a^e C_e^i - \bar{\bar{h}}_m^i C_a^m + \bar{\bar{h}}_{am}^{ie} C_e^m + \bar{\bar{h}}_m^e C_{ae}^{im} + \tfrac{1}{2} \bar{\bar{h}}_{am}^{ef} C_{ef}^{im} \\ &\quad - \tfrac{1}{2} \bar{\bar{h}}_{mn}^{ie} C_{ae}^{mn}, \end{aligned} \tag{152}$$

$$\begin{aligned} {}^{1,2}\Lambda_{ab}^{ij} &= \mathcal{A}_{ab} \bar{\bar{h}}_{ma}^{ij} C_b^m - \mathcal{A}^{ij} \bar{\bar{h}}_{ab}^{ei} C_e^j + \mathcal{A}_{ab} \bar{\bar{h}}_a^e C_{eb}^{ij} - \mathcal{A}^{ij} \bar{\bar{h}}_m^i C_{ab}^{mj} \\ &\quad + \tfrac{1}{2} \bar{\bar{h}}_{mn}^{ij} C_{ab}^{mn} + \tfrac{1}{2} \bar{\bar{h}}_{ab}^{ef} C_{ef}^{ij} + \mathcal{A}_{ab} \mathcal{A}^{ij} \bar{\bar{h}}_{am}^{ie} C_{eb}^{mj}. \end{aligned} \tag{153}$$

Since the number of $\bar{\bar{h}}_p^q$ and $\bar{\bar{h}}_{pq}^{rs}$ matrix elements is more or less the same as the number of one- and two-electron integrals z_p^q and v_{pq}^{rs}, their storage is not a major problem (we can actually think of overwriting the corresponding integral files once they are no longer needed). Thus, we calculate ${}^{1,2}\Lambda_a^i$ and ${}^{1,2}\Lambda_{ab}^{ij}$ from the precomputed one- and two-body matrix elements $\bar{\bar{h}}_p^q$ and $\bar{\bar{h}}_{pq}^{rs}$ using Eqs. (152) and (153). The required expressions for $\bar{\bar{h}}_p^q$ and $\bar{\bar{h}}_{pq}^{rs}$ in terms of one- and two-electron molecular integrals and cluster amplitudes t_a^i and t_{ab}^{ij} can easily be obtained by using the diagrammatic methods of MBPT. We discuss these expressions in subsequent sections and, in considerable detail, in Appendix A.

Since we want to avoid storing three- and four-body quantities, we do not calculate the three- and four-body matrix elements $\bar{\bar{h}}_{pqr}^{stu}$ and $\bar{\bar{h}}_{pqrs}^{stuv}$ defining $\bar{\bar{H}}_3$ and $\bar{\bar{H}}_4$. Instead, in complete analogy to direct CI procedures, we recalculate the three- and four-body terms ${}^3\Lambda_a^i$, ${}^3\Lambda_{ab}^{ij}$, and ${}^4\Lambda_{ab}^{ij}$ every time we need them using Eqs. (147)-(149) and current values of CI-like coefficients C_a^i and C_{ab}^{ij}. It should be emphasized that only very specific types of three- and four-body terms of $\bar{\bar{H}}_{N,\mathrm{open}}$ enter ${}^3\Lambda_a^i$, ${}^3\Lambda_{ab}^{ij}$, and ${}^4\Lambda_{ab}^{ij}$. This means that recalculation of ${}^3\Lambda_a^i$, ${}^3\Lambda_{ab}^{ij}$, and ${}^4\Lambda_{ab}^{ij}$ in every iteration of the procedure used to solve the EOMXCCSD eigenvalue problem does not make the method significantly more expensive. This will become clear once we present the final, fully vectorizable, expressions for ${}^3\Lambda_a^i$, ${}^3\Lambda_{ab}^{ij}$, and ${}^4\Lambda_{ab}^{ij}$ in terms of recursively generated intermediates (see the next section and Appendix B).

The explicit expressions for $\bar{\bar{h}}_p^q$ and $\bar{\bar{h}}_{pq}^{rs}$, and ${}^3\Lambda_a^i$, ${}^3\Lambda_{ab}^{ij}$ and ${}^4\Lambda_{ab}^{ij}$ depend, of course, on the specific form of the Hamiltonian $\bar{\bar{H}}_{N,\mathrm{open}}$. A few approximate variants of the EOMXCCSD scheme, which are based on different forms of $\bar{\bar{H}}_{N,\mathrm{open}}$, are discussed next.

5. Approximate EOMXCCSD schemes

Since each many-body component $\bar{\bar{H}}_n$ entering the EOMXCCSD problem contains a number of high-order terms involving high powers of T_1, T_2, $T_1^\dagger$, and $T_2^\dagger$ and since it is likely that many of these high-order terms can be ignored, in this initial study of the EOMXCCSD formalism we investigate the role of each contribution to $\bar{\bar{H}}_n$ using arguments originating from MBPT and focus on the dominant, low-order terms. In the main approximation that we propose below [referred to as the EOMXCCSD(PE3) method; cf. Section 5.1], we keep all terms contributing to $\bar{\bar{H}}_n$ that appear in the first three orders of MBPT. In this way, as we demonstrate in Section 6, we may be able to introduce the lowest-order contributions of the EOMCCSDT theory within the EOMXCCSD framework and obtain an n^6 EOMCC procedure which has the T_3 clusters built in. In some approximations that we propose in this section, we also keep selected higher-order terms; in some others we ignore them. Some contributions to $\bar{\bar{H}}_n$ have a lot in common with the standard EOMCCSD expressions. For this reason, we keep these contributions in unexpanded form, so that we can utilize the existing EOMCCSD codes [34]. No assumption is made, however, as to what molecular orbitals are employed. We want to have a formalism that applies to both the Hartree-Fock and non-Hartree-Fock orbitals.

5.1 Primary approximation: A partially expanded formula for $\bar{\bar{H}}_{N,\mathrm{open}}$. The EOMXCCSD(PE3) method

We begin our considerations by splitting each many-body component of $\bar{\bar{H}}_{N,\mathrm{open}}$ into contributions that originate from various many-body components of $\bar{H}_{N,\mathrm{open}}$. Thus, we write

$$\bar{\bar{H}}_n = \sum_k \bar{\bar{H}}_n(k), \tag{154}$$

where

$$\bar{\bar{H}}_n(k) = (e^{T^\dagger} \bar{H}_k)_{C,n} \tag{155}$$

is the n-body component of $\bar{\bar{H}}_{N,\mathrm{open}}$ that originates from the k-body component of $\bar{H}_{N,\mathrm{open}}$.

The explicit expressions for one- and two-body components of $\bar{H}_{N,\mathrm{open}}$ and three-body contributions entering the EOMCCSD problem can be found elsewhere [34] (cf., also, Appendices A and B; a few expressions presented in Table 1 of Ref. 34, and thus in Ref. 60, are incorrect; for

the complete list of errors in expressions for one- and two-body matrix elements of $\bar{H}_{N,\mathrm{open}}$, see Ref. 83; for additional comments on the three-body contributions, see footnote 2 in Ref. 60). For example, the one- and two-body components of $\bar{H}_{N,\mathrm{open}}$ are defined in terms of the corresponding matrix elements $\bar{h}_p^q$ and $\bar{h}_{pq}^{rs}$ (designated previously as $\mathcal{F}_{pq}$ and $\mathcal{W}_{pqrs}$, respectively [34]) as follows,

$$\bar{H}_1 = \bar{h}_p^q \, N\{X^p X_q\}, \tag{156}$$

$$\bar{H}_2 = \tfrac{1}{4} \bar{h}_{pq}^{rs} \, N\{X^p X_r X^q X_s\}. \tag{157}$$

The explicit expressions for $\bar{h}_p^q$ and $\bar{h}_{pq}^{rs}$ relate these quantities to one- and two-electron molecular integrals f_p^q and v_{pq}^{rs} and, in case of the CCSD approximation, to cluster amplitudes t_a^i and t_{ab}^{ij} [34] (cf., however, Ref. 83; see, also Appendix A). We use these expressions in this paper as well, since some many-body components of $\bar{\bar{H}}_N$ can easily be related to $\bar{h}_p^q$ and $\bar{h}_{pq}^{rs}$ (provided that we use the XCCSD rather than CCSD amplitudes t_a^i and t_{ab}^{ij}, which means that $\bar{h}_a^i$ and $\bar{h}_{ab}^{ij}$ are no longer zero; see Appendix A). The number of $\bar{h}_p^q$ and $\bar{h}_{pq}^{rs}$ matrix elements is practically the same as the number of one- and two-electron molecular integrals f_p^q and v_{pq}^{rs}, so that they can be precalculated and stored for future use. In principle, one could consider similar expressions for matrix elements $\bar{h}_{pqr}^{stu}$ defining the three-body component $\bar{H}_3$, which, as we demonstrate below, is also needed in the EOMXCCSD theory, but this would not be very practical because of the large storage requirements for $\bar{h}_{pqr}^{stu}$. It is much better to recalculate the relevant contributions $P(\bar{H}_3 \, C_{K,n})_C|\Phi\rangle$ every time we need them. This was a strategy utilized in earlier papers on the EOMCCSD method (cf. Ref. 34), and this is what we do in the EOMXCCSD context. Again, we can use the explicit expressions for $P(\bar{H}_3 \, C_{K,n})_C|\Phi\rangle$ presented elsewhere [34, 60] (cf., however, footnote 2 in Ref. 60).

As pointed out earlier, k in Eq. (154) cannot exceed 6 if T is approximated by its mono- and doubly excited components. Furthermore, we do not have to consider higher-than-four-body components of $\bar{\bar{H}}_{N,\mathrm{open}}$ at the CCSD level of the EOMXCC formalism. In fact, the only three- and four-body terms that we need in the EE-EOMXCCSD scheme are $\bar{\bar{H}}_3^P$ and $\bar{\bar{H}}_4^P$, where P is defined by Eq. (134). These observations simplify our analysis, since very few three- and four-body contributions enter the projected Hamiltonian components $\bar{\bar{H}}_3^P$ and $\bar{\bar{H}}_4^P$. In addition, many terms that enter $\bar{\bar{H}}_3^P$ and $\bar{\bar{H}}_4^P$ appear in higher orders of MBPT and can be neglected.

Careful mathematical analysis exploiting diagrammatic methods of MBPT leads to the following results: For the one-body components of

$\bar{\bar{H}}$, we can write

$$\bar{\bar{H}}_1 = \sum_{k=1}^{6} \bar{\bar{H}}_1(k), \tag{158}$$

where $\bar{\bar{H}}_1(k)$, $k = 1, 2$, are kept in unexpanded form and

$$\bar{\bar{H}}_1(3) = \bar{\bar{H}}_1(T_2^\dagger, T_2) + O(\mathcal{V}^4), \tag{159}$$

$$\bar{\bar{H}}_1(k) = O(\mathcal{V}^5). \quad (k = 4 - 6) \tag{160}$$

For the two-body components of $\bar{\bar{H}}$, we can write

$$\bar{\bar{H}}_2 = \sum_{k=1}^{6} \bar{\bar{H}}_2(k), \tag{161}$$

where $\bar{\bar{H}}_2(k)$, $k = 1, 2$, are kept in unexpanded form and

$$\bar{\bar{H}}_2(3) = \bar{\bar{H}}_2(T_2^\dagger, T_2) + \bar{\bar{H}}_2(T_1^\dagger, T_2) + O(\mathcal{V}^4), \tag{162}$$

$$\bar{\bar{H}}_2(k) = O(\mathcal{V}^4). \quad (k = 4 - 6) \tag{163}$$

For the three-body components of $\bar{\bar{H}}$ that enter the EOMXCCSD problem, we can write

$$\bar{\bar{H}}_3^P = \sum_{k=2}^{6} \bar{\bar{H}}_3^P(k), \tag{164}$$

where $\bar{\bar{H}}_3^P(2)$ is kept unexpanded and

$$\bar{\bar{H}}_3^P(3) = \bar{H}_3^P + \bar{\bar{H}}_3^P(T_2^\dagger, T_2) + \bar{\bar{H}}_3^P(T_1^\dagger, T_2), \tag{165}$$

$$\bar{\bar{H}}_3^P(k) = O(\mathcal{V}^4), \quad (k = 4 - 6) \tag{166}$$

and, finally, for the four-body components of $\bar{\bar{H}}$ that enter the EOMXCCSD problem, we obtain

$$\bar{\bar{H}}_4^P = \sum_{k=3}^{6} \bar{\bar{H}}_4^P(k), \tag{167}$$

where

$$\bar{\bar{H}}_4^P(3) = \bar{\bar{H}}_4^P(T_2^\dagger, T_2), \tag{168}$$

$$\bar{\bar{H}}_4^P(k) = O(\mathcal{V}^4). \quad (k = 4 - 6) \tag{169}$$

We use the notation in which

$$\bar{\bar{H}}_n(T_2^\dagger, T_2) = [T_2^\dagger (V_N T_2)_{C,3}]_{C,n} + \tfrac{1}{2} [T_2^\dagger (F_N T_2^2)_{C,3}]_{C,n}, \quad (n = 1 - 3) \tag{170}$$

$$\bar{\bar{H}}_4(T_2^\dagger, T_2) = [T_2^\dagger (V_N T_2)_{C,3}]_{C,4}, \tag{171}$$

$$\bar{\bar{H}}_n(T_1^\dagger, T_2) = [T_1^\dagger (V_N T_2)_{C,3}]_{C,n} + \tfrac{1}{2}\,\delta_{n,2}\,[T_1^\dagger (F_N T_2^2)_{C,3}]_{C,n}. \quad (n = 2,3) \tag{172}$$

As before, $O(\mathcal{V}^k)$ designates terms that we do not wish to specify and whose MBPT order is at least k [this does not necessarily imply that $O(\mathcal{V}^k)$ represents all terms of k-th and higher orders].

We keep the components $\bar{\bar{H}}_n(k)$, $k, n = 1, 2$, in unexpanded form, since this allows us to utilize the existing expressions for $\bar{h}_p^q$ and $\bar{h}_{pq}^{rs}$ in terms of f_p^q, v_{pq}^{rs}, t_a^i, and t_{ab}^{ij} [34, 83] (cf., also, Appendix A). In order to see this, let us introduce the following definitions,

$$\sum_{k=1}^{2} \bar{\bar{H}}_1(k) = \bar{\bar{h}}_p^q(1,2)\, N\{X^p X_q\}, \tag{173}$$

and

$$\sum_{k=1}^{2} \bar{\bar{H}}_2(k) = \tfrac{1}{4}\,\bar{\bar{h}}_{pq}^{rs}(1,2)\, N\{X^p X_r X^q X_s\}. \tag{174}$$

Since [cf. Eq. (155)]

$$\sum_{k=1}^{2} \bar{\bar{H}}_n(k) = [(\bar{H}_1 + \bar{H}_2)^\dagger e^T]_{C,n}^\dagger, \tag{175}$$

we can always obtain the explicit expressions for matrix elements $\bar{\bar{h}}_p^q(1,2)$ and $\bar{\bar{h}}_{pq}^{rs}(1,2)$ in terms of $\bar{h}_p^q$ and $\bar{h}_{pq}^{rs}$ and cluster amplitudes t_i^a and t_{ij}^{ab} defining $T_1^\dagger$ and $T_2^\dagger$ by performing the following substitutions in $\bar{h}_q^p$ and $\bar{h}_{rs}^{pq}$: $f_p^q \to \bar{h}_q^p$, $v_{pq}^{rs} \to \bar{h}_{rs}^{pq}$, $t_a^i \to t_i^a$, $t_{ab}^{ij} \to t_{ij}^{ab}$ (note that each of these substitutions is accompanied by a flip of the corresponding spin-orbital indices which, according to our notation, is equivalent to calculation of a complex conjugate expression). This operation corresponds to a replacement of an operator $\bar{H}_n = [(F_N + V_N)e^T]_{C,n}$ by its EOMXCCSD analog $[(\bar{H}_1 + \bar{H}_2)^\dagger e^T]_{C,n}$ and taking the Hermitian conjugate of the latter operator as Eq. (175) requires.

A similar substitution procedure works for the three-body term $\bar{\bar{H}}_3^P(2)$, which we also leave unexpanded, since

$$\bar{\bar{H}}_3^P(2) = [(\bar{H}_2^\dagger e^T)_{C,3}^P]^\dagger. \tag{176}$$

We can thus utilize the known expressions for

$$\bar{H}_3^P = (H_N e^{T_1+T_2})_{C,3}^P = (V_N e^{T_1+T_2})_{C,3}^P, \tag{177}$$

in terms of $\bar{h}^{rs}_{pq}$, v^{rs}_{pq}, and t^{ij}_{ab} [34, 60] (cf. footnote 2 in Ref. 60; see, also, Appendix B) and evaluate $\bar{\bar{H}}^P_3(2)$ by performing the following substitutions: $\bar{h}^{rs}_{pq} \rightarrow \bar{\bar{h}}^{pq}_{rs}(1,2)$, $v^{rs}_{pq} \rightarrow \bar{h}^{pq}_{rs}$, $t^{ij}_{ab} \rightarrow t^{ab}_{ij}$, followed by taking a Hermitian conjugate of the resulting Hamiltonian matrix. This is not, however, a very good method of deriving the explicit expressions for $\bar{\bar{H}}^P_3(2)$, since we are rather interested in the expression $P[\bar{\bar{H}}_3(2)\, C_{K,n}]_C|\Phi\rangle$, $n = 1, 2$, which enters the EOMXCCSD equations, whereas the above substitution procedure is efficient only if one applies it to individual matrix elements from the SS, SD, DS, and DD blocks of the matrix representing $\bar{\bar{H}}^P_3(2)$. Thus, we used the substitution method only to check the correctness of the final equations for $P[\bar{\bar{H}}_3(2)\, C_{K,n}]_C|\Phi\rangle$. In fact, even the final expressions for the matrix elements $\bar{\bar{h}}^q_p(1,2)$ and $\bar{\bar{h}}^{rs}_{pq}(1,2)$ defining $\bar{\bar{H}}_n(k)$, $k, n = 1, 2$, which we present in this paper and which are easier to handle, were obtained using diagrammatic methods of MBPT rather than by performing substitutions in $\bar{h}^p_q$ and $\bar{h}^{pq}_{rs}$ described above. The substitution procedure was used, however, to make sure that the final results for $\bar{\bar{h}}^q_p(1,2)$ for $\bar{\bar{h}}^{rs}_{pq}(1,2)$ given in this paper are correct. We find these correspondences between the EOMXCCSD and EOMCCSD approaches very interesting and worth exploring.

Equations (158)-(169) allow us to propose an approximation which we call the partially expanded EOMXCCSD scheme correct through third-order [EOMXCCSD(PE3) or PE3, for short]. In this variant of the EOMXCCSD approach, the required one-, two-, three-, and four-body components of $\bar{\bar{H}}_{N,\mathrm{open}}$ assume the following form,

$$\bar{\bar{H}}_n = \sum_{k=1}^{2} \bar{\bar{H}}_n(k) + \bar{\bar{H}}_n(T_2^\dagger, T_2) + \delta_{n,2}\bar{\bar{H}}_n(T_1^\dagger, T_2) + O(\mathcal{V}^4), \quad (n = 1, 2) \tag{178}$$

$$\bar{\bar{H}}^P_3 = \bar{H}^P_3 + \bar{\bar{H}}^P_3(2) + \bar{\bar{H}}^P_3(T_2^\dagger, T_2) + \bar{\bar{H}}^P_3(T_1^\dagger, T_2) + O(\mathcal{V}^4), \tag{179}$$

and

$$\bar{\bar{H}}^P_4 = \bar{\bar{H}}^P_4(T_2^\dagger, T_2) + O(\mathcal{V}^4). \tag{180}$$

The unspecified higher-than-third-order terms $O(\mathcal{V}^4)$ are ignored.

In the EOMXCCSD(PE3) or PE3 scheme, the approximate form of the transformed Hamiltonian $\bar{\bar{H}}_N$ given by Eqs. (178)-(180) is first used to construct the ground-state XCCSD equations, Eqs. (141) and (142). These do not require other than one- and two-body components of $\bar{\bar{H}}_{N,\mathrm{open}}$ and we can construct them using the $\bar{\bar{h}}^i_a$ and $\bar{\bar{h}}^{ij}_{ab}$ matrix elements corresponding to Eq. (178). The EOMXCCSD eigenvalue problem, Eqs. (150) and (151), requires, however, that we calculate the three- and four-body contributions

${}^3\Lambda_a^i$, ${}^3\Lambda_{ab}^{ij}$, and ${}^4\Lambda_{ab}^{ij}$, Eqs. (147)-(149), along with almost all one- and two-body terms $\bar{\bar{h}}_p^q$ and $\bar{\bar{h}}_{pq}^{rs}$ [cf. Eqs. (152) and (153)]. From Eqs. (179) and (180), it follows that

$$\begin{aligned} {}^3\Lambda_a^i &= [\bar{\bar{\mathbf{H}}}_{\mathbf{3}}(\mathbf{2})_{\mathbf{SD}} \cdot \mathbf{C}]_a^i + [\bar{\bar{\mathbf{H}}}_{\mathbf{3}}(\mathbf{T}_{\mathbf{2}}^\dagger, \mathbf{T_2})_{\mathbf{SD}} \cdot \mathbf{C}]_a^i \\ &\quad + [\bar{\bar{\mathbf{H}}}_{\mathbf{3}}(\mathbf{T}_{\mathbf{1}}^\dagger, \mathbf{T_2})_{\mathbf{SD}} \cdot \mathbf{C}]_a^i, \end{aligned} \tag{181}$$

$$ {}^3\Lambda_{ab}^{ij} = {}^3\Lambda_{ab}^{ij}(\mathrm{DS}) + {}^3\Lambda_{ab}^{ij}(\mathrm{DD}), \tag{182}$$

where

$$\begin{aligned} {}^3\Lambda_{ab}^{ij}(\mathrm{DS}) &= [\bar{\mathbf{H}}_{\mathbf{3,DS}} \cdot \mathbf{C}]_{ab}^{ij} + [\bar{\bar{\mathbf{H}}}_{\mathbf{3}}(\mathbf{T}_{\mathbf{2}}^\dagger, \mathbf{T_2})_{\mathbf{DS}} \cdot \mathbf{C}]_{ab}^{ij} \\ &\quad + [\bar{\bar{\mathbf{H}}}_{\mathbf{3}}(\mathbf{T}_{\mathbf{1}}^\dagger, \mathbf{T_2})_{\mathbf{DS}} \cdot \mathbf{C}]_{ab}^{ij}, \end{aligned} \tag{183}$$

and

$$\begin{aligned} {}^3\Lambda_{ab}^{ij}(\mathrm{DD}) &= [\bar{\mathbf{H}}_{\mathbf{3,DD}} \cdot \mathbf{C}]_{ab}^{ij} + [\bar{\bar{\mathbf{H}}}_{\mathbf{3}}(\mathbf{2})_{\mathbf{DD}} \cdot \mathbf{C}]_{ab}^{ij} + [\bar{\bar{\mathbf{H}}}_{\mathbf{3}}(\mathbf{T}_{\mathbf{2}}^\dagger, \mathbf{T_2})_{\mathbf{DD}} \cdot \mathbf{C}]_{ab}^{ij} \\ &\quad + [\bar{\bar{\mathbf{H}}}_{\mathbf{3}}(\mathbf{T}_{\mathbf{1}}^\dagger, \mathbf{T_2})_{\mathbf{DD}} \cdot \mathbf{C}]_{ab}^{ij}, \end{aligned} \tag{184}$$

and

$$ {}^4\Lambda_{ab}^{ij} = [\bar{\bar{\mathbf{H}}}_{\mathbf{4}}(\mathbf{T}_{\mathbf{2}}^\dagger, \mathbf{T_2})_{\mathbf{DD}} \cdot \mathbf{C}]_{ab}^{ij}. \tag{185}$$

As in the earlier sections, bold quantities indicate matrices or vectors representing the corresponding operators and subscripts SS, SD, DS, and DD designate the singles-singles, singles-doubles, doubles-singles, and doubles-doubles blocks of the transformed Hamiltonian matrix.

All three- and four-body contributions listed above are evaluated directly without storing the corresponding three- and four-body matrix elements. The final expressions are given in Appendix B. The only precomputed (and, possibly, stored) matrix elements are those which define one- and two-body components of $\bar{\bar{H}}_{N,\mathrm{open}}$ defined by Eq. (178). As it is demonstrated in Appendix A, we can express the corresponding one- and two-body matrix elements $\bar{\bar{h}}_p^q$ and $\bar{\bar{h}}_{pq}^{rs}$ in terms of $\bar{\bar{h}}_p^q(1,2)$ and $\bar{\bar{h}}_{pq}^{rs}(1,2)$, Eqs. (173) and (174), respectively, and $\bar{\bar{h}}_p^q(3)$, $\bar{\bar{h}}_{pq}^{rs}(3)$, and $\bar{\bar{h}}_{pq}^{rs}(3')$, where we define

$$\bar{\bar{H}}_1(T_2^\dagger, T_2) = \bar{\bar{h}}_p^q(3)\, N\{X^p X_q\}, \tag{186}$$

$$\bar{\bar{H}}_2(T_2^\dagger, T_2) = \tfrac{1}{4}\, \bar{\bar{h}}_{pq}^{rs}(3)\, N\{X^p X_r X^q X_s\}, \tag{187}$$

and

$$\bar{\bar{H}}_2(T_1^\dagger, T_2) = \tfrac{1}{4}\, \bar{\bar{h}}_{pq}^{rs}(3')\, N\{X^p X_r X^q X_s\}. \tag{188}$$

The complete list of expressions for $\bar{\bar{h}}_p^q$ and $\bar{\bar{h}}_{pq}^{rs}$ is given in Appendix A.

It can be easily demonstrated [using Eq. (82) and diagrammatic methods of MBPT] that the energy expression consistent with the PE3 scheme can be given the following form,

$$\Delta E_0 = \Delta E_0^{\rm CC} + \bar{h}_a^i\, t_i^a + \tfrac{1}{4}\, \bar{h}_{ab}^{ij}(t_{ij}^{ab} + 2\, t_i^a\, t_j^b) + O(\mathcal{V}^4). \tag{189}$$

If the amplitudes t_a^i and t_{ab}^{ij} were obtained by solving the standard SRCCSD equations, we could simplify Eq. (189) by dropping all terms but $\Delta E_0^{\rm CC}$, since

$$\bar{h}_a^i = \langle \Phi | G_a^i \bar{H}_{N,\rm open} | \Phi \rangle \tag{190}$$

and

$$\bar{h}_{ab}^{ij} = \langle \Phi | G_{ab}^{ij} \bar{H}_{N,\rm open} | \Phi \rangle \tag{191}$$

represent the left-hand-sides of the SRCCSD equations, which vanish for the converged SRCCSD amplitudes. Although we cannot do this here, we can show that for the converged XCCSD amplitudes based on the PE3 approximation for $\bar{\bar{H}}$,

$$\bar{h}_{ab}^{ij} = -\bar{\bar{h}}_{ab}^{ij}(3') = O(\mathcal{V}^3), \tag{192}$$

[see Eqs. (247) and (295) in Appendix A and Eqs. (172) and (188); we use the fact that singly and doubly excited cluster amplitudes are at least the first-order quantities in the MBPT sense]. We can also show that

$$\bar{\bar{h}}_a^i(1,2) + \bar{\bar{h}}_a^i(3) = \bar{h}_a^i + \bar{h}_{ae}^{im}\, t_m^e + \bar{\bar{h}}_a^i(3) = 0, \tag{193}$$

for the converged XCCSD(PE3) amplitudes [see Eqs. (246) and (250) in Appendix A], so that

$$\bar{h}_a^i = -\bar{h}_{ae}^{im}\, t_m^e - \bar{\bar{h}}_a^i(3) = O(\mathcal{V}^3), \tag{194}$$

since $\bar{h}_{ae}^{im}$ and $\bar{\bar{h}}_a^i(3)$ are the quantities of at least third-order of MBPT [see Eq. (192) above and Eq. (282) in Appendix A; cf., also, Eqs. (170) and (186)]. In consequence,

$$\bar{h}_a^i\, t_i^a + \tfrac{1}{4}\, \bar{h}_{ab}^{ij}(t_{ij}^{ab} + 2\, t_i^a\, t_j^b) = O(\mathcal{V}^4), \tag{195}$$

and Eq. (189) can be replaced by

$$\Delta E_0 = \Delta E_0^{\rm CC} + O(\mathcal{V}^4), \tag{196}$$

which shows that we can use the standard SRCC formula for the ground-state energy in the XCCSD(PE3) scheme. On the other hand, it might be useful sometimes to keep some higher-order terms in the ground-state energy expression and use Eq. (189) instead.

We should emphasize that we make no particular assumption as to what orbitals are employed. Some of the contributions to $\bar{\bar{H}}$ discussed here show up in higher orders of MBPT if the Hartree-Fock reference is used. For example, we can drop all $\bar{\bar{H}}_n(T_1^\dagger, T_2)$ contributions from Eqs. (178) and (179), since they become fourth- and higher-order terms when the Hartree-Fock orbitals are employed (there is no first-order contribution to T_1 in this case). We can also eliminate the $\frac{1}{2}\,[T_2^\dagger (F_N T_2^2)_{C,3}]_{C,n}$ contribution from Eq. (170) defining $\bar{\bar{H}}_n(T_2^\dagger, T_2)$, $n = 1-3$, since $\frac{1}{2}(F_N T_2^2)_{C,3}$ is zero in the Hartree-Fock case. We may decide, however, to keep all these terms even if the Hartree-Fock orbitals are employed (which is the most common choice for molecular orbitals), since some contributions involving T_1 may lead to a more balanced description of excitation energies [cf. the CCSD+T(CCSD) = CCSD[T] = CC4SD[T] [49, 82, 84, 85] and CCSD(T) [86] or CC4SD(T) [82] methods, which are used in the ground-state calculations; the CCSD(T) = CC4SD(T) method offers a slightly better balance of various effects, when compared to CCSD[T] = CC4SD[T], since it contains certain higher-order terms involving T_1 which are neglected at the CCSD[T] = CC4SD[T] level]. This should not increase the computational complexity of the PE3 scheme, since $\bar{\bar{H}}_n(T_1^\dagger, T_2)$ terms are significantly less expensive compared to $\bar{\bar{H}}_n(T_2^\dagger, T_2)$ contributions, which we have to consider anyway if we want to have the T_3 terms of EOMCCSDT in EOMXCCSD (see Section 6). Terms involving $\frac{1}{2}(F_N T_2^2)_{C,3}$, which vanish in the Hartree-Fock case, can easily be incorporated in terms containing $(V_N T_2)_{C,3}$ by using effective two-electron vertices w defined in Appendix A, so that their explicit elimination from the calculations using Hartree-Fock orbitals does not offer any saving of computer time and is not worth pursuing.

A quick look at the similarity transformed Hamiltonian characterizing the PE3 approximation, Eqs. (178)-(180), shows that the PE3 approximation is to a large extent equivalent to a Hermitized EOMCCSD scheme. This can also be seen diagrammatically by comparing, for example, diagrams representing three-body terms $\bar{H}_3^P$ and $\bar{\bar{H}}_3^P(2)$ (see Figure 1). If we restrict ourselves to the leading terms in $\bar{\bar{H}}_3^P(2)$ and replace vertices representing $\bar{H}_2$ in $\bar{\bar{H}}_3^P(2)$ by vertices representing V_N, we can see that both sets of diagrams representing $\bar{H}_3^P$ and $\bar{\bar{H}}_3^P(2)$ become mirror images and that $\bar{\bar{H}}_3^P(2)$ terms symmetrize the EOMCCSD three-body terms $\bar{H}_3^P$ [in particular, the SD block of $\bar{\bar{\mathbf{H}}}$ gets filled with terms which are Hermitian conjugates to an $\bar{H}_3^P$ contribution to DS block of $\bar{\bar{\mathbf{H}}}$; cf. Eqs. (328) and (331) in Appendix B]. This interesting feature of the EOMXCC approach becomes even more transparent when we analyze other EOMXCCSD approximations that result from the PE3 scheme by dropping various higher-

order terms. An example of such approximation is the PE3′ method, which we discuss next.

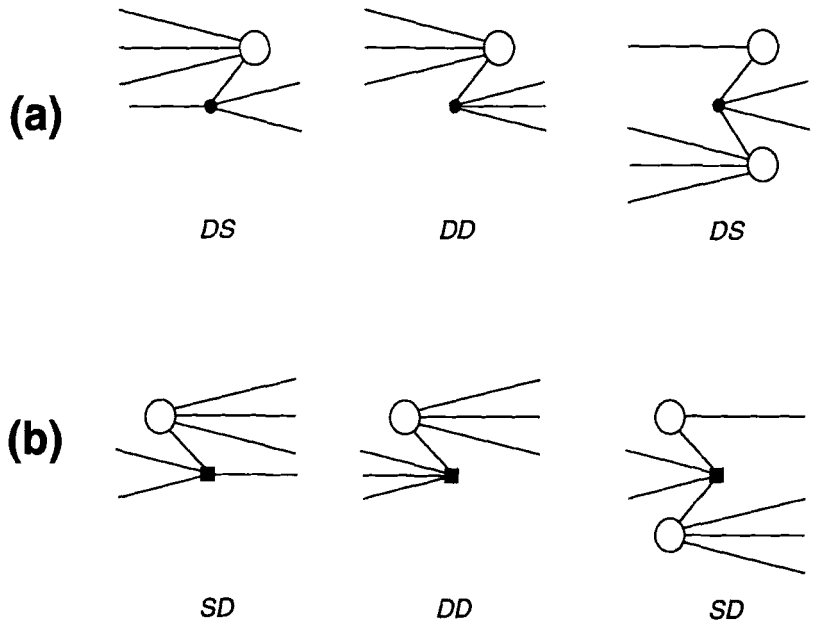

FIG. 1. Non-oriented Hugenholtz skeletons representing the three-body terms $\bar{H}_3^P$ (a) and $\bar{\bar{H}}_3^P(2)$ (b) of the EOMXCCSD(PE3) Hamiltonian. Solid circles represent the two-electron interaction vertices (V_N operators), solid squares represent the two-body part of $\bar{H}_N$ (i.e. the $\bar{H}_2$ component), open circles with lines pointing to the left represent T_1 and T_2 (the T_1 vertex has two lines attached to it and the T_2 vertex has four lines attached), and open circles with lines pointing to the right represent $T_1^\dagger$ and $T_2^\dagger$ (again, we distinguish between $T_1^\dagger$ and $T_2^\dagger$ by using different numbers of lines that are attached to open circles).

5.2. *Modified EOMXCCSD(PE3) scheme: The EOMXCCSD(PE3′) method*

An alternative approximation to a complete EOMXCCSD method can be proposed if we replace the $\bar{H}_3^P$ and $\bar{\bar{H}}_3^P(2)$ terms contributing to $\bar{\bar{H}}_3^P$, Eq. (179), by their low-order counterparts obtained by using the formulas (cf. Figure 1),

$$\bar{H}_3^P = (V_N\, T_2)_{C,3}^P + (V_N\, T_1\, T_2)_{C,3}^P, \tag{197}$$

$$\bar{\bar{H}}_3^P(2) = (T_2^\dagger\, \bar{H}_2)_{C,3}^P + (T_1^\dagger\, T_2^\dagger\, \bar{H}_2)_{C,3}^P, \tag{198}$$

with

$$\bar{H}_2 = V_N + (H_N\, T_2)_{C,2} + (V_N\, T_1)_{C,2} + (F_N\, T_1\, T_2)_{C,2} + O(\mathcal{V}^3). \tag{199}$$

The resulting modified EOMXCCSD(PE3) method, referred to as the EOMXCCSD(PE3′) or PE3′ approach, is defined by Eqs. (178) and (180) and the formula

$$\begin{aligned}
\bar{\bar{H}}_3^P \;=\; & (V_N\, T_2)_{C,3}^P + (V_N\, T_1\, T_2)_{C,3}^P + (T_2^\dagger\, V_N)_{C,3}^P + (T_1^\dagger\, T_2^\dagger\, V_N)_{C,3}^P \\
& + \bar{\bar{H}}_3^P(T_2^\dagger, T_2) + \bar{\bar{H}}_3^P(T_1^\dagger, T_2) + [T_2^\dagger (H_N T_2)_{C,2}]_{C,3}^P \\
& + [T_2^\dagger (V_N T_1)_{C,2}]_{C,3}^P + [T_2^\dagger (F_N T_1 T_2)_{C,2}]_{C,3}^P \\
& + [T_1^\dagger T_2^\dagger (F_N T_2)_{C,2}]_{C,3}^P + O(\mathcal{V}^4)
\end{aligned} \tag{200}$$

for the three-body components of $\bar{\bar{H}}_{N,\mathrm{open}}^P$. The PE3′ approach, just like its parent PE3 approximation, Eqs. (178)-(180), uses the similarity transformed Hamiltonian which is correct through third order of MBPT.

An interesting feature of the PE3′ approximation, apart from its potential usefulness in the calculations (the T_3-like terms analogous to T_3 contributions to EOMCCSDT that enter the PE3 and PE3′ approximations are the same; see Section 6), is its clear relationship to the following decomposition of the similarity transformed Hamiltonian $\bar{\bar{H}}_{N,\mathrm{open}}^P$,

$$\begin{aligned}
\bar{\bar{H}}_{N,\mathrm{open}}^P \;=\; & \bar{H}_{N,\mathrm{open}}^P + (\bar{H}_{N,\mathrm{open}}^\dagger)^P - H_N \\
& + \{(e^{T^\dagger} - 1)[H_N(e^T - 1)]_{C,\mathrm{open}}\}_{C,\mathrm{open}}^P,
\end{aligned} \tag{201}$$

where, obviously,

$$\bar{H}_{N,\mathrm{open}}^P = \bar{H}_1^P + \bar{H}_2^P + \bar{H}_3^P, \tag{202}$$

and

$$\{(e^{T^\dagger} - 1)[H_N(e^T - 1)]_{C,\mathrm{open}}\}_{C,\mathrm{open}}^P = \sum_{n=1}^{4} \sum_{k=1}^{6} \{(e^{T^\dagger} - 1)[H_N(e^T - 1)]_{C,k}\}_{C,n}^P, \tag{203}$$

in the EOMXCCSD case. As before [cf. Eqs. (67), (128), and (155)], the subscripts C,k and C,n designate all k- and n-body connected components of a given operator product. Let us discuss this relationship for a moment.

First of all, it should be emphasized that Eq. (201) has an interesting mathematical structure. It explicitly shows that the leading terms of the similarity transformed Hamiltonian of the EOMXCC theory are obtained by symmetrizing (Hermitizing) the $\bar{H}$ Hamiltonian of the standard EOMCC formalism. In particular, Eq. (202) represents the similarity transformed Hamiltonian of the EOMCCSD method, when projected on a manifold of singly and doubly excited configurations. In this case, the first three terms in Eq. (201) correspond to Hermitized EOMCCSD method. The departure from Hermiticity of $\bar{\bar{H}}$ is described by Eq. (203), which contains second- and higher-order components of $\bar{\bar{H}}$.

Careful, order-by-order, analysis of Eqs. (201)-(203) leads to the following results,

$$\bar{H}_1^P + \bar{H}_2^P + (\bar{H}_1^\dagger)^P + (\bar{H}_2^\dagger)^P - H_N + \sum_{n=1}^{2}\sum_{k=1}^{2}\{(e^{T^\dagger}-1)[H_N(e^T-1)]_{C,k}\}_{C,n}^P = \sum_{n=1}^{2}\sum_{k=1}^{2}\bar{\bar{H}}_n^P(k), \quad (204)$$

$\bar{H}_3^P$ is given by Eq. (197), so that

$$(\bar{H}_3^\dagger)^P = (T_2^\dagger V_N)_{C,3}^P + (T_1^\dagger T_2^\dagger V_N)_{C,3}^P, \quad (205)$$

$$\sum_{n=3}^{4}\sum_{k=1}^{2}\{(e^{T^\dagger}-1)[H_N(e^T-1)]_{C,k}\}_{C,n}^P = [T_2^\dagger(H_N T_2)_{C,2}]_{C,3}^P + [T_2^\dagger(V_N T_1)_{C,2}]_{C,3}^P + [T_2^\dagger(F_N T_1 T_2)_{C,2}]_{C,3}^P + [T_1^\dagger T_2^\dagger(F_N T_2)_{C,2}]_{C,3}^P + O(\mathcal{V}^4), \quad (206)$$

and, finally,

$$\sum_{n=1}^{4}\sum_{k=3}^{6}\{(e^{T^\dagger}-1)[H_N(e^T-1)]_{C,k}\}_{C,n}^P = \sum_{n=1}^{4}\bar{\bar{H}}_n^P(T_2^\dagger,T_2) + \sum_{n=2}^{3}\bar{\bar{H}}_n^P(T_1^\dagger,T_2) + O(\mathcal{V}^4). \quad (207)$$

It is immediately obvious that we obtain the similarity transformed Hamiltonian of the PE3′ method, Eqs. (178), (180), and (200), when we add Eqs. (197) and (204)-(207) together.

The above relationship between the PE3′ approximation and Eq. (201) allows us to better understand the general structure of the EOMXCCSD equations. We can clearly see, for example, which terms are responsible for the non-Hermitian nature of the EOMXCCSD approach and what is the effect of Hermitizing the standard EOMCCSD approach in terms of various contributions to equations characterizing the EOMXCCSD(PE3′) scheme. As we are going to demonstrate in Section 6, the most important non-Hermitian terms of the EOMXCCSD(PE3) and EOMXCCSD(PE3′) approaches are the $\bar{\bar{H}}_n^P(T_2^\dagger, T_2)$ components, since it is quite likely that these components allow us to calculate some T_3 contributions of the EOMCCSDT scheme via the n^6 computational procedure.

Further simplifications in the PE3′ Hamiltonian lead to two more approximate EOMXCCSD schemes, referred to as the PE2 and PE1 methods. They should not be as accurate as the higher-order PE3 or PE3′ schemes, but they are worth mentioning here.

5.3. Simplified EOMXCCSD schemes: The EOMXCCSD(PE2) and EOMXCCSD(PE1) approximations and EOMXCCSD(PE-12) and EOMXCCSD(PE-123) schemes

The EOMXCCSD(PE2) approximation (or PE2, for short) is obtained if we ignore third and higher-order terms in Eqs. (178), (180), and (200) defining the PE3′ approximation and keep one- and two-body contributions to $\bar{\bar{H}}$ resulting from one- and two-body components of $\bar{H}$ in unexpanded form (all three- and four-body components of $\bar{\bar{H}}$ that enter the EOMXCCSD scheme are expanded in MBPT series and terms that show up in third and higher orders are dropped). It is easy to show that

$$\bar{\bar{H}}_n = \sum_{k=1}^{2} \bar{\bar{H}}_n(k) + O(\mathcal{V}^3), \quad (n = 1, 2) \tag{208}$$

$$\bar{\bar{H}}_3^P = (V_N T_2)_{C,3}^P + (T_2^\dagger V_N)_{C,3}^P + [T_2^\dagger (F_N T_2)_{C,2}]_{C,3}^P + O(\mathcal{V}^3), \tag{209}$$

and

$$\bar{\bar{H}}_4^P = O(\mathcal{V}^3). \tag{210}$$

We can thus ignore the four-body contributions $\bar{\bar{H}}_4^P$ and use a very simple form of the similarity transformed Hamiltonian $\bar{\bar{H}}$, which is based on Eqs. (208) and (209) and is correct through second order. This, almost Hermitian, form of the EOMXCCSD approach is referred to as the PE2 scheme.

Finally, we can also show that [cf. Eq. (209)]

$$\bar{\bar{H}}_3^P = O(\mathcal{V}^2), \tag{211}$$

and that [see Eq. (204)]

$$\bar{\bar{H}}_n = \bar{H}_n + \bar{H}_n^\dagger - H_n + O(\mathcal{V}^2), \quad (n = 1,2;\ H_1 = F_N,\ H_2 = V_N) \tag{212}$$

so that one can contemplate the approach [called here the EOMXCCSD(PE1) or PE1, for short] which, as suggested by Eq. (212), uses only one- and two-body components of the EOMCCSD Hamiltonian $\bar{H}$ and their Hermitian conjugates. An approximate form of the similarity transformed Hamiltonian used in the PE1 approach is correct through first order. Experience with the EOMCCSD approach indicates, however, that the three-body terms entering the EOMCCSD method are important, so that it is probably safer to use an approach based on Eq. (212) for one- and two-body components of $\bar{\bar{H}}$ and the formula [cf. Eq. (209)]

$$\bar{\bar{H}}_3^P = (V_N\, T_2)_{C,3}^P + (T_2^\dagger\, V_N)_{C,3}^P + O(\mathcal{V}^2) \tag{213}$$

for the three-body components. The resulting modified PE1 scheme would be practically equivalent to a Hermitized EOMCCSD method [obtained by adding the EOMCCSD Hamiltonian (202) to its Hermitian adjoint].

An alternative EOMXCCSD approach that we might suggest, referred to as the EOMXCCSD(PE-12) or PE-12 (for short) method, is obtained if we only use one- and two-body terms of the PE3 Hamiltonian, Eq. (178). An approximation of this type makes a lot of sense since quite a few T_3-like contributions that are reminiscent of T_3 terms of EOMCCSDT are buried in one- and two-body terms $\bar{\bar{H}}_n(T_2^\dagger, T_2)$, Eq. (170) (cf. the next section). We can also contemplate the EOMXCCSD(PE-123) or PE-123 approximation, which is based on one-, two-, and three-body terms of the PE3 Hamiltonian, Eqs. (178) and (179), and in which the four-body contributions $\bar{\bar{H}}_4(T_2^\dagger, T_2)$, Eq. (171), are ignored. Although the similarity transformed Hamiltonian of the PE-123 theory is no longer correct through third order [see Eq. (210)], it contains the same information about T_3 terms of the EOMCCSDT formalism as the more complete PE3 scheme. The four-body terms $\bar{\bar{H}}_4(T_2^\dagger, T_2)$ do not bring any information about connected triples (see Section 6). This shows that we have two different ways of truncating the EOMXCC equations (on top of truncating the many-body expansions of T and R_K). We may drop terms in $\bar{\bar{H}}$ according to perturbation theory order, as we did in case of the PE3 or PE3′ schemes. We may also drop terms in $\bar{\bar{H}}$ according to the rank of many-body components $\bar{\bar{H}}_n$ and still be able to propose schemes, such as PE-12 or PE-123, which are based on one- and

two-body or one-, two-, and (all or only some) three-body components of $\bar{\bar{H}}$. It is possible that the low-rank (in the sense of many-body expansion of $\bar{\bar{H}}$) PE-12 or PE-123 approximations will be more accurate than the low-order PE1 or PE2 schemes, since only the former two approximations contain terms that resemble the T_3 contributions of the EOMCCSDT formalism. A comparison of the EOMXCCSD methods with the EOMCCSDT scheme is discussed next.

6. EOMXCCSD vs EOMCCSDT

We have reasons to believe that the EOMXCCSD scheme allows us to include the T_3 contributions of the EOMCCSDT scheme, which show up in the

$$\begin{pmatrix} \bar{\mathbf{H}}_{\mathbf{SS}} & \bar{\mathbf{H}}_{\mathbf{SD}} \\ \bar{\mathbf{H}}_{\mathbf{DS}} & \bar{\mathbf{H}}_{\mathbf{DD}} \end{pmatrix} \tag{214}$$

block of the EOMCCSDT Hamiltonian $\bar{H}$, using inexpensive n^6 steps. If this is indeed the case, the electronically excited states (also, electron-attached and ionized states) resulting from EOMXCCSD calculations should have their energies corrected for the effect of T_3 components. We do not expect that this effect is large in itself. Also, we cannot expect that the entire information about the T_3 contribution to EOMCC excited states can be included at the simple EOMXCCSD level. However, inclusion of even some T_3 components may help to counterbalance the lowering of the excited-state energies due to the inclusion of the $R_{K,3}$ term in R_K. We must realize that the lowering of excited-state energies due to a combined effect of R_3 and T_3 can be as large as 0.5–1.0 eV for states having significant contribution from doubly excited determinants relative to Hartree-Fock reference [46] (cf., also, Refs. 61, 63, 64), and it is not always easy to achieve the right balance of various higher-order effects in EOMCC calculations, as the EOMCCSD($\tilde{\mathrm{T}}$) results indicate [61, 64]. At the same time, as we demonstrate below, almost no information about the T_3 contributions to the ground-state CC equations is included in the XCCSD calculations (cf. Ref. 69). Thus, the XCCSD and CCSD ground states should have similar energies [no significant energy lowering should be observed in this case, cf. Ref. 72; cf., also, Eq. (196) for the XCCSD(PE3) energy].

A quick analysis of the EOMCCSDT problem shows that the only T_3 contribution to $\bar{H}^P_{N,\mathrm{open}}$, where P is given by Eq. (134), is the $(V_N T_3)^P_C$ term. This term enters a DS block of the projected $\bar{\mathbf{H}}$ matrix (214) (see Ref. 46). Three non-oriented Hugenholtz skeletons that correspond to $(V_N T_3)^P_C$

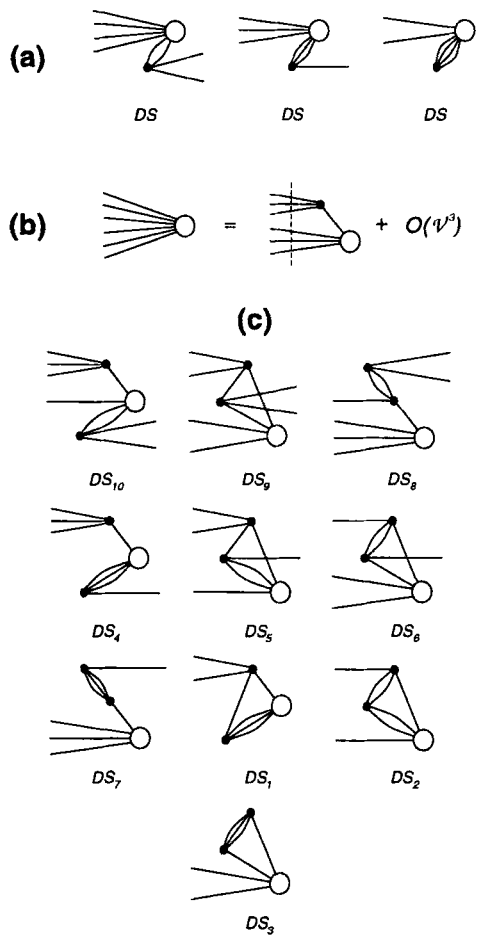

FIG. 2. (a) Non-oriented Hugenholtz skeletons representing $(V_N T_3)_C^P$, where P is given by Eq. (134). (b) Diagrammatic interpretation of Eq. (215). (c) Non-oriented Hugenholtz skeletons that are obtained from diagrams representing $(V_N T_3)_C^P$, with P defined by Eq. (134) [cf. Figure 2 (a)], by substituting all T_3 vertices in (a) according to relationship (215) [illustrated diagrammatically in (b)]. As in Figure 1, solid circles represent V_N and open circles with lines pointing to the left represent various many-body components of T. The vertical dashed line in (b) indicates the presence of the denominator associated with the resolvent operator $R_0^{(3)}$ [cf. Eq. (215)]. Each diagram in (a) and (c) is labeled by the name of the block of $\bar{\mathbf{H}}$, to which it contributes. An extra subscript κ, $\kappa = 1 - 10$, at each symbol DS in (c) is used to facilitate the identification of the EOMXCCSD terms $[T_2^\dagger (V_N T_2)_{C,3}]_{C,n}^P$ (shown in Figure 3) with diagrams of this figure representing the EOMCCSDT contribution $(V_N T_3)_C^P$.

are shown in Figure 2 (a). In the following, we focus on the leading contributions to $(V_N T_3)_C^P$, which we obtain by replacing T_3 using the formula [see, also, Figure 2 (b)],

$$T_3 = R_0^{(3)}(V_N T_2)_{C,3} + O(\mathcal{V}^3), \tag{215}$$

on which the CCSDT-1 [49,87], ACCSDT-1 ~ ACPTQ [49], CCSD+T(CCSD) [49,82,84,85], CCSDQ'+T(CCSDQ') [88], ACCSD+T(ACCSD) [88] (cf., also, Refs. 85, 89), and CCSD(T) [82,86] perturbative schemes are based. Here,

$$R_0^{(n)} = \sum_{\substack{i_1<\cdots<i_n \\ a_1<\cdots<a_n}} G^{a_1\ldots a_n}_{i_1\ldots i_n}|\Phi\rangle\langle\Phi|G^{i_1\ldots i_n}_{a_1\ldots a_n}/(\epsilon_{i_1}-\epsilon_{a_1}+\cdots+\epsilon_{i_n}-\epsilon_{a_n}), \tag{216}$$

is the n-body component of the reduced resolvent R_0 [$n = 3$ in Eq. (215)] and ϵ_p are orbital energies. Ten non-oriented Hugenholtz skeletons that are obtained from diagrams representing $(V_N T_3)_C^P$ [cf. Figure 2 (a)] by performing the substitution $T_3 \to R_0^{(3)}(V_N T_2)_{C,3}$ are shown in Figure 2 (c).

Let us now look at diagrams representing the $[T_2^\dagger(V_N T_2)_{C,3}]_{C,n}$ contributions to $\bar{\bar{H}}_n(T_2^\dagger, T_2)$, where $n = 1-3$, Eq. (170). These contributions are present in the similarity transformed Hamiltonians defining the PE3, PE3', and PE-123 schemes (the PE-12 Hamiltonian has also some of them, namely those with $n = 1, 2$). We focus on one-, two-, and three-body terms $[T_2^\dagger(V_N T_2)_{C,3}]_{C,n}$ that enter the EOMXCCSD problem, i.e. on the projected expressions $[T_2^\dagger(V_N T_2)_{C,3}]_{C,n}^P$, $n = 1-3$, where P is given by Eq. (134). Six non-oriented Hugenholtz skeletons that correspond to the one-body term $[T_2^\dagger(V_N T_2)_{C,3}]_{C,1}^P$ are shown in Figure 3 (a). Note that in this case three skeletons contribute to a DS block of matrix $\bar{\bar{\mathbf{H}}}$. Nine skeletons that represent the two-body term $[T_2^\dagger(V_N T_2)_{C,3}]_{C,2}^P$ are displayed in Figure 3 (b). Four of them contribute to a DS block of $\bar{\bar{\mathbf{H}}}$. Finally, all eight skeletons that can be drawn for the three-body term $[T_2^\dagger(V_N T_2)_{C,3}]_{C,3}^P$ are shown in Figure 3 (c). In this case, only three skeletons contribute to a DS block of $\bar{\bar{\mathbf{H}}}$.

Each diagram presented in Figure 3 (a)–(c) [as well as each diagram shown in Figure 2 (a) and (c)] is labeled by the name of the block (SS, DD, DS, or SD) of the similarity transformed Hamiltonian to which it contributes [in case of Figure 2 (a) and (c), the EOMCC Hamiltonian $\bar{\mathbf{H}}$, and in case of Figure 3 (a)–(c), the EOMXCC Hamiltonian $\bar{\bar{\mathbf{H}}}$]. In addition, we use an extra subscript κ, $\kappa = 1-10$, at each symbol DS to identify these EOMXCCSD diagrams corresponding to $[T_2^\dagger(V_N T_2)_{C,3}]_{C,n}^P$

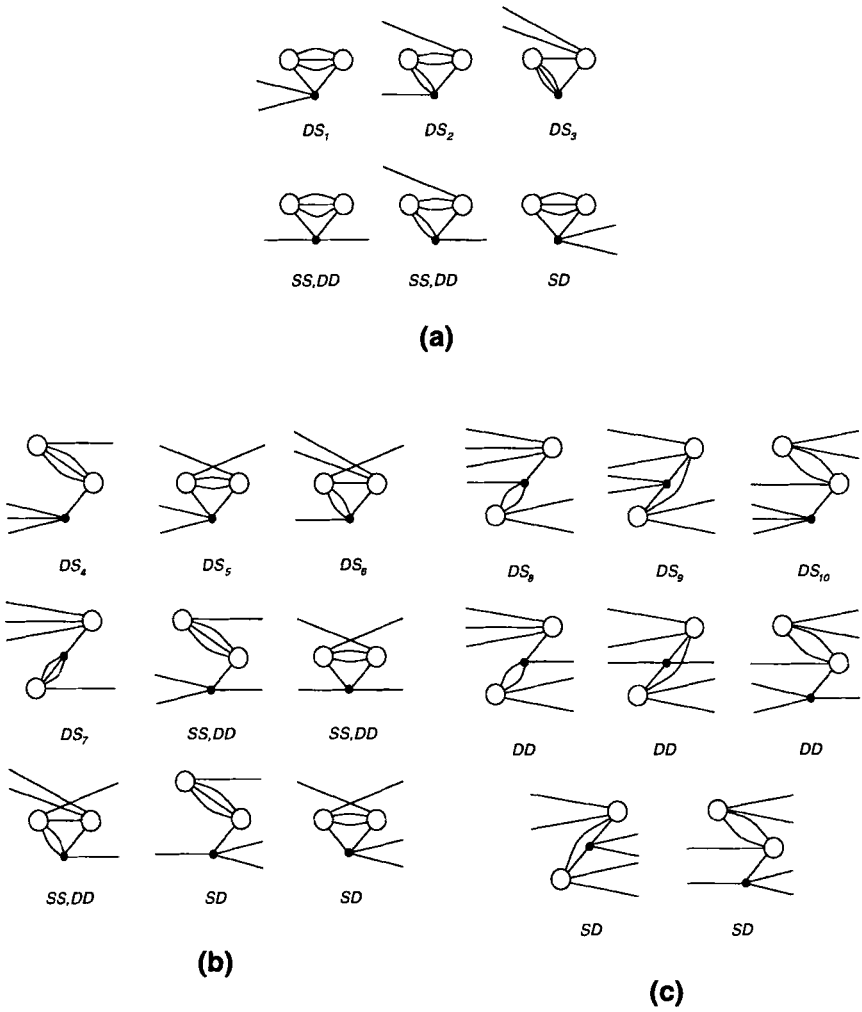

FIG. 3. Non-oriented Hugenholtz skeletons representing (a) $[T_2^\dagger(V_N T_2)_{C,3}]^P_{C,1}$, (b) $[T_2^\dagger(V_N T_2)_{C,3}]^P_{C,2}$, and (c) $[T_2^\dagger(V_N T_2)_{C,3}]^P_{C,3}$. As before, P is defined by Eq. (134) and solid circles represent V_N. Open circles with lines pointing to the left represent T_2 and open circles with lines pointing to the right represent $T_2^\dagger$. As in Figure 2, each diagram in (a)–(c) is labeled by the name of the block of $\bar{\bar{\mathbf{H}}}$, to which it contributes. An extra subscript κ, $\kappa = 1 - 10$, at each symbol DS is used to identify diagrams, which represent the EOMXCCSD terms $[T_2^\dagger(V_N T_2)_{C,3}]^P_{C,n}$, $n = 1 - 3$, with diagrams which represent the T_3 contributions to a DS block of $\bar{\mathbf{H}}$ [shown in Figure 2 (c); see the text for details].

($n = 1 - 3$) terms, which seem to be equivalent [up to $O(\mathcal{V}^4)$ terms] to dominant T_3 contributions to a DS block of $\bar{\mathbf{H}}$ [displayed diagrammatically in Figure 2 (c)]. The fact that each diagram DS_κ of Figure 2 (c) can be regarded as identical [up to $O(\mathcal{V}^4)$ terms] to a similar diagram DS_κ shown in Figure 3 (a)–(c) is an immediate consequence of the well-known relationship

$$T_2 = (R_0^{(2)} V_N)_{C,2} + O(\mathcal{V}^2). \tag{217}$$

This relationship or, better, its conjugate form,

$$T_2^\dagger = (V_N R_0^{(2)})_{C,2} + O(\mathcal{V}^2), \tag{218}$$

allows us to replace the left-most vertex representing $T_2^\dagger$ in each diagram DS_κ shown in Figure 3 (a)–(c) by the vertex representing V_N.

The above reasoning, although somewhat heuristic, suggests that diagrams representing $(V_N T_3)_C^P$ form a subset of diagrams representing $[T_2^\dagger (V_N T_2)_{C,3}]_{C,n}^P$ or $\bar{\bar{H}}_n^P(T_2^\dagger, T_2)$ with $n = 1 - 3$ [if we ignore, of course, some $O(\mathcal{V}^4)$ terms]. We can express this fact symbolically by writing,

$$\sum_{n=1}^{3} \bar{\bar{H}}_n^P(T_2^\dagger, T_2) = (V_N T_3)_C^P + \cdots . \tag{219}$$

If Eq. (219) is true (and it seems that it is), the excited states obtained in the PE3, PE3′, and PE-123 calculations should be corrected for the effect of EOMCCSDT triples as described by the $(V_N T_3)_C^P$ contribution. The small $O(\mathcal{V}^4)$ difference between the $(V_N T_3)_C^P$ terms and the corresponding terms in $\sum_{n=1}^{3} \bar{\bar{H}}_n^P(T_2^\dagger, T_2)$ is precisely the reason why we proposed the PE3 approximation. As explained in Section 5, the PE3 approximation is based on the similarity transformed Hamiltonian, which is correct through third-order.

Interestingly enough, seven out of ten skeletons that correspond to the $(V_N T_3)_C^P$ contributions are included in one- and two-body terms $\bar{\bar{H}}_n^P(T_2^\dagger, T_2)$. Thus, at least statistically, a significant portion of the $(V_N T_3)_C^P$ triples effect may already be described by the PE-12 method, which uses only one- and two-body components of $\bar{\bar{H}}$. We do not need the four-body term $\bar{\bar{H}}_4^P(T_2^\dagger, T_2)$, Eq. (171), in the EOMXCCSD Hamiltonian to describe these T_3 contributions of the EOMCCSDT theory. We can thus ignore this term altogether. On the other hand, the most expensive term in $\bar{\bar{H}}_4^P(T_2^\dagger, T_2)$ scales as $n_o^2 n_u^4$ (n_o is the number of occupied orbitals and n_u is the number of unoccupied orbitals), so that inclusion of $\bar{\bar{H}}_4^P(T_2^\dagger, T_2)$ is no more expensive than the standard CCSD calculation (see Appendix B for the details).

As mentioned earlier, the EOMXCCSD(PE3) theory is an n^6 procedure. This, in particular, applies to all $\bar{\bar{H}}^P_n(T_2^\dagger, T_2)$ contributions that correspond to $(V_N T_3)^P_C$. As explained in Appendices A and B, the most expensive terms of the EOMXCCSD(PE3) scheme scale as n_u^6. Although these terms represent contributions to $\bar{\bar{H}}^P_2(T_2^\dagger, T_2)$ and $\bar{\bar{H}}^P_3(T_2^\dagger, T_2)$ that go into a DD block of $\bar{\bar{\mathbf{H}}}$, we may try to ignore them, since they do not represent any of the triples contribution of the EOMCC theory. Most contributions to $\bar{\bar{H}}^P_n(T_2^\dagger, T_2)$ that mimic the effect of $(V_N T_3)^P_C$ can be obtained in inexpensive n^6 steps, such as $n_o^3 n_u^3$ and $n_o^4 n_u^2$ (see Appendices A and B). The most expensive contribution to $\bar{\bar{H}}^P_n(T_2^\dagger, T_2)$ that mimics a triples effect of the EOMCC approach scales as $n_o n_u^5$ (see Appendix A). This is less than the $n_o^3 n_u^4$ scaling of the EOMCCSDT-1 or EOMCCSD(T) methods [63], provided that $n_u < n_o^2$ (this condition is often satisfied in electronic structure studies, particularly when n_o becomes large) and certainly less than the $n_o^3 n_u^5$ scaling of the EOMCCSDT procedure [46]. On the other hand, we do not consider the $R_{K,3}$ term of R_K (included in the EOMCCSDT procedure) in the simple EOMXCCSD approach discussed here. If we restrict to only one- and two-body terms $\bar{\bar{H}}^P_n(T_2^\dagger, T_2)$, $n = 1, 2$, which seem to contain an information about some T_3 effects in EOMCC, the scaling of the corresponding EOMXCCSD scheme remains the same as the scaling of the complete EOMXCCSD(PE3) approach, but we drop quite a few $n_o^2 n_u^4$ terms, which should lower the cost quite significantly (cf. Appendices A and B). Needless to say, none of the intermediates used to formulate the EOMXCCSD approach is a three-body quantity (see Appendices A and B). The EOMCCSDT scheme has a problem of storing three-body quantities, such as the T_3 cluster amplitudes [46] (not used in the EOMXCCSD approximation).

Let us now see if the XCCSD approach (in its PE3 approximation) gives us information about T_3 contributions to ground-state CC equations. Terms that involve T_3 components and that enter the SRCC equations projected on singly and doubly excited configurations (clearly, we cannot analyze the T_3 contributions to SRCC equations projected on triples if the XCCSD approximation is invoked) are: $\langle \Phi | G^i_a (V_N T_3)_C | \Phi \rangle$, $\langle \Phi | G^{ij}_{ab} (F_N T_3)_C | \Phi \rangle$, $\langle \Phi | G^{ij}_{ab} (V_N T_3)_C | \Phi \rangle$, and $\langle \Phi | G^{ij}_{ab} (V_N T_1 T_3)_C | \Phi \rangle$. The corresponding Hugenholtz skeletons are shown in Figure 4 (a)–(d).

We can use Eqs. (215) and (218) to show that $\langle \Phi | G^i_a [T_2^\dagger (V_N T_2)_{C,3}]_{C,1} | \Phi \rangle$ terms of XCCSD produce the $\langle \Phi | G^i_a (V_N T_3)_C | \Phi \rangle$ term. Indeed, let us use Eq. (215) to replace the T_3 vertex in diagram 4 (a) by two vertices representing $(V_N T_2)_{C,3}$. The resulting three Hugenholtz skeletons become identical [up to neglected $O(\mathcal{V}^4)$ terms] to the three skeletons presented in Figure 3 (a) and labeled as DS_1, DS_2, and DS_3, provided that we use Eq. (218)

to replace the leftmost $T_2^\dagger$ vertex in each diagram DS_κ, $\kappa = 1 - 3$, by a two-body vertex representing V_N [which we can do, of course, if we ignore $O(\mathcal{V}^4)$ terms].

Similar arguments allow us to show that $\langle\Phi|G_{ab}^{ij}[T_1^\dagger(V_N T_2)_{C,3}]_{C,2}|\Phi\rangle$ terms of XCCSD produce the $\langle\Phi|G_{ab}^{ij}(F_N\, T_3)_C|\Phi\rangle$ contribution of SRCC. In this case, we must use Eq. (215) [to replace vertices representing T_3 in skeletons shown in Figure 4 (b) by $(V_N T_2)_{C,3}$] and the formula

$$T_1^\dagger = \sum_{i,a} f_i^a\, G_a^i/(\epsilon_i - \epsilon_a) + O(\mathcal{V}^2), \tag{220}$$

which allows us to identify (ignoring again higher-order terms) the leftmost F_N vertex of $\langle\Phi|G_{ab}^{ij}(F_N\, T_3)_C|\Phi\rangle$ with the first-order contribution to $T_1^\dagger$. It is interesting to note that the $\langle\Phi|G_{ab}^{ij}(F_N\, T_3)_C|\Phi\rangle$ term vanishes in the Hartree-Fock case. This is reflected in the behavior of the $\langle\Phi|G_{ab}^{ij}[T_1^\dagger(V_N T_2)_{C,3}]_{C,2}|\Phi\rangle$ term: The corresponding operator $[T_1^\dagger(V_N T_2)_{C,3}]_{C,2}$ becomes a fourth-order quantity and as such can be ignored in the XCCSD(PE3) calculations.

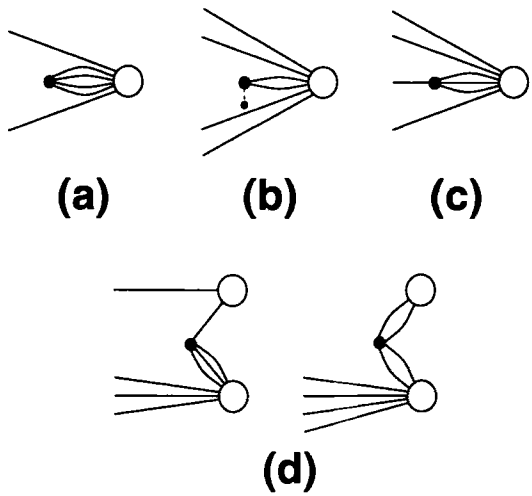

FIG. 4. Nonoriented Hugenholtz skeletons representing (a) $\langle\Phi|G_a^i(V_N\, T_3)_C|\Phi\rangle$, (b) $\langle\Phi|G_{ab}^{ij}(F_N\, T_3)_C|\Phi\rangle$, (c) $\langle\Phi|G_{ab}^{ij}(V_N T_3)_C|\Phi\rangle$, and (d) $\langle\Phi|G_{ab}^{ij}(V_N\, T_1\, T_3)_C|\Phi\rangle$. The meaning of solid and open circles is the same as in Figures 1–3. The only new element is the one-body vertex in (b) with a dotted line attached to it, which represents F_N.

Interestingly enough, none of the XCCSD(PE3) terms gives the dominant T_3 contribution to the SRCC equations, which is represented by the $\langle\Phi|G^{ij}_{ab}(V_N T_3)_C|\Phi\rangle$ term. A similar argument applies to $\langle\Phi|G^{ij}_{ab}(V_N T_1 T_3)_C|\Phi\rangle$. As a result, the XCCSD(PE3) equations look very similar to SRCCSD equations. The only essential difference between both types of equations is the presence of $\bar{\bar{h}}^i_a(3)$ terms, which represent $\bar{\bar{H}}_1(T_2^\dagger, T_2)$ or $[T_2^\dagger(V_N T_2)_{C,3}]_{C,1}$ [cf. Eq. (186)] and thus (as we showed above) $\langle\Phi|G^i_a(V_N T_3)_C|\Phi\rangle$, in the XCCSD equations projected on singly excited configurations, and the presence of $\bar{\bar{h}}^{ij}_{ab}(3')$ terms, which represent $\bar{\bar{H}}_2(T_1^\dagger, T_2)$ or $[T_1^\dagger(V_N T_2)_{C,3}]_{C,2}$ [see Eq. (188)] and thus $\langle\Phi|G^{ij}_{ab}(F_N T_3)_C|\Phi\rangle$, in the XCCSD equations projected on doubly excited configurations [see Eqs. (246) and (247) in Appendix A]. Lack of T_3-like contributions in the ground-state XCCSD(PE3) equations parallels an observation made in the original XCC paper [69] that the XCCSD method is incapable of mimicing T_3 effects unless they are explicitly included in XCC equations (as is done in the XCC(4) method [69, 70], which is almost the same as the well-known CCSDT-1 model [49, 87]; cf. Refs. 69, 70 for further details). Numerical consequences of this statement were observed in Ref. 72, where it was clearly demonstrated that the XCCSD(4) method [69], in which T_3 clusters are ignored, gives virtually the same results as the standard SRCCSD approach.

The above analysis shows that the similarity transformation of the EOMCC Hamiltonian $\bar{H}$, as defined by an operator $e^{T^\dagger}$, may have a very interesting effect on the calculated energy spectrum. When we use the full CC expansion for T, the full CI expansion for R_K, and the exact representation of the doubly transformed Hamiltonian $\bar{\bar{H}}$, the spectra of three Hamiltonians, H_N, $\bar{H}_N$, and $\bar{\bar{H}}_N$, are identical. In this case of course, EOMCC=EOMXCC=FCI. The situation changes, however, when many-body expansions of T and R_K are truncated. When T and R_K are truncated at the doubly excited level, some higher-order excitations are folded into the EOMCC Hamiltonian $\bar{H}$ and, as a result, the excitation energies obtained in EOMCCSD calculations become significantly better compared to those obtained in SRCISD calculations, even though higher-order effects associated with T_3 components of T do not enter the EOMCCSD scheme. If we want to insist on using a singly transformed Hamiltonian, as is done in the standard EOMCC theory, we can only include these high-order terms via the EOMCCSDT scheme or one of its approximate variants. However, a less expensive solution might be offered by transforming the EOMCC Hamiltonian $\bar{H}$ with $e^{T^\dagger}$. In this case, when T and R_K are truncated at the doubly excited level (the EOMXCCSD approximation), the T_3 contributions of the EOMCCSDT method that enter a DS block of $\bar{H}$ seem to be

"rotated" into a DS block of matrix $\bar{\bar{\mathbf{H}}}$ representing a doubly transformed Hamiltonian $\bar{\bar{H}}$. *This can only change the excited part of the spectrum of* $\bar{H}$ *without affecting the ground-state results.* This interesting property of the EOMXCC approach may lead to formulation of a new category of methods which, once the $R_{K,3}$ component is properly incorporated, should be characterized by a better balance between ground and excited states (giving accurate VEE values). We should also observe an improvement in the calculated VEAs and VIPs, once methods of this type are implemented. A similar behavior should be found in EOMECC calculations, which we discuss next.

7. The EOMECC theory

Before summarizing the results, we would like to comment on the possibility of generalizing other alternative CC schemes, such as UCC, SXCC, SC-XCC, SC-UCC, and ECC mentioned in the Introduction (cf. Refs. 69–72, 74–77), to electronically excited, electron-attached, and ionized states, using the EOM formalism. This generalization should be particularly straightforward (and interesting) in case of the ECC theory of Arponen, Bishop, and their coworkers [76, 77] (see, also, Refs. 74, 75), which is based on finding the stationary conditions for the energy functional

$$\Delta E(\Sigma, T) = \langle \Phi | [e^{\Sigma}(H_N e^T)_C]_C | \Phi \rangle = \langle \Phi | \bar{\bar{H}}_N^{\Sigma} | \Phi \rangle = \bar{\bar{H}}_{N,\mathrm{close}}^{\Sigma}, \tag{221}$$

where Σ is a connected deexcitation operator and we define

$$\bar{\bar{H}}_N^{\Sigma} = e^{\Sigma} \bar{H}_N e^{-\Sigma} = (e^{\Sigma} \bar{H}_N)_C = [e^{\Sigma}(H_N e^T)_C]_C. \tag{222}$$

Notice that the similarity transformed Hamiltonian $\bar{\bar{H}}_N^{\Sigma}$, Eq. (222), has the same formal structure as the EOMXCC Hamiltonian $\bar{\bar{H}}_N$. We may thus contemplate an approach (referred to as the EOMECC method), in which we transform the EOMCC eigenvalue problem, Eq. (33), using the operator e^{Σ} to obtain (cf. Ref. 77)

$$\bar{\bar{H}}_N^{\Sigma} C_K^{\Sigma} | \Phi \rangle = \Delta E_K C_K^{\Sigma} | \Phi \rangle, \tag{223}$$

where, in complete analogy to Eqs. (75) and (77),

$$C_K^{\Sigma} = (e^{\Sigma} R_K)_{FC} = \sum_{\lambda} c_{K,\lambda}^{\Sigma} \, \Omega_{\lambda} \tag{224}$$

(FC now indicates that all lines of vertices representing Σ are connected to R_K). The corresponding ground-state problem (right eigenvalue problem),

$$\bar{\bar{H}}_N^{\Sigma}|\Phi\rangle = \Delta E_0|\Phi\rangle, \tag{225}$$

or, equivalently,

$$\langle\Phi|G_{a_1\ldots a_n}^{i_1\ldots i_n}\bar{\bar{H}}_N^{\Sigma}|\Phi\rangle = 0, \tag{226}$$

with ΔE_0 given by Eq. (221), looks similar to the XCC system of equations, Eqs. (78) and (80), except for the fact that now we have to determine two operators, T and Σ. Clearly, Eq. (226) alone is not sufficient to determine both operators. We need another set of equations to accompany Eq. (226), if we want to determine T and Σ, and thus $\bar{\bar{H}}_N^{\Sigma}$. These can be obtained if we analyze the stationary conditions for the energy functional $\Delta E(\Sigma, T)$, Eq. (221) [75–77].

It can be easily verified that the stationarity of $\Delta E(\Sigma, T)$ with respect to Σ yields Eq. (226). In the exact (full CC) limit, the system of equations defined by Eq. (226) becomes equivalent to standard CC equations for T, Eq. (35), and $\Delta E(\Sigma, T)$ becomes identical to ΔE_0^{CC} [75]. It can be further demonstrated that the stationarity of $\Delta E(\Sigma, T)$ with respect to T yields (again, in the full CC limit) the "lambda" equation of the analytic gradient SRCC theory,

$$\langle\Phi|(1+\Lambda)\bar{H}_N G_{i_1\ldots i_n}^{a_1\ldots a_n}|\Phi\rangle = \Delta E_0\langle\Phi|(1+\Lambda)G_{i_1\ldots i_n}^{a_1\ldots a_n}|\Phi\rangle \tag{227}$$

[see, also, Eq. (57)], provided that we identify e^{Σ} with $1+\Lambda$ (this identification is possible only in the exact, full CI = full CC, limit). This simple relationship between T and Λ of the SRCC theory and T and Σ of the ECC formalism allows us to suggest several ways of calculating T and Σ.

We may, for example, try simple solutions, such as determination of T and Σ by solving first the standard SRCC equations, Eq. (35) for T, then using this T to define $\bar{H}_N$, solving Eq. (227) for Λ, and finally calculating Σ through the relationship

$$\Sigma = \ln(1+\Lambda). \tag{228}$$

This would allow us to use the existing analytic gradient CC codes. The operators Σ and T defined in this way would no longer make the functional $\Delta E(\Sigma, T)$ stationary, but we might benefit from the fact that we already use two different operators T and Σ to define $\bar{\bar{H}}_N^{\Sigma}$. We might also contemplate a slightly better (even though still *ad hoc* and simple) alternative of using Eq. (228) to replace the left eigenvalue problem (57) by its explicitly connected analog

$$\langle\Phi|\bar{\bar{H}}_N^{\Sigma} = \Delta E_0\langle\Phi|, \tag{229}$$

so that Σ is calculated by solving

$$\langle\Phi|\bar{\bar{H}}_N^{\Sigma} G_{i_1\ldots i_n}^{a_1\ldots a_n}|\Phi\rangle = 0, \tag{230}$$

with T obtained by solving the standard SRCC equations.

A much better alternative (and, certainly, a much more rigorous procedure) is to solve a coupled system of equations for T and Σ defined by Eqs. (226) and (230) (cf. Ref. 74). The resulting operators T and Σ make the functional $\Delta E(\Sigma, T)$ stationary with respect to Σ and approximately stationary with respect to T [75] (we are now assuming that many-body expansions for T and Σ are truncated). More importantly, with T and Σ obtained by solving Eqs. (226) and (230), we can replace Eq. (223) by

$$(\bar{\bar{H}}_{N,\mathrm{open}}^{\Sigma} C_{K,\mathrm{open}}^{\Sigma})_C|\Phi\rangle = \omega_K C_K^{\Sigma}|\Phi\rangle, \tag{231}$$

where, in complete analogy to Eqs. (38) and (88), the only components of the operator product $\bar{\bar{H}}_{N,\mathrm{open}}^{\Sigma} C_{K,\mathrm{open}}^{\Sigma}$ that enter the eigenvalue problem are the connected components $(\bar{\bar{H}}_{N,\mathrm{open}}^{\Sigma} C_{K,\mathrm{open}}^{\Sigma})_C$ (cf., also, Ref. 77). With this choice of T and Σ, the ground-state energy is still given by Eq. (221).

One of the most interesting features of the EOMECC method is the form of the left eigenvalue problem. When T and Σ are obtained by solving Eqs. (226) and (230), the left eigenvalue problem corresponding to Eq. (223), i.e.

$$\langle\Phi|\tilde{C}_K^{\Sigma} \bar{\bar{H}}_N^{\Sigma} = \Delta E_K \langle\Phi|\tilde{C}_K^{\Sigma}, \tag{232}$$

assumes the following form,

$$\langle\Phi|(\tilde{C}_K^{\Sigma} \bar{\bar{H}}_{N,\mathrm{open}}^{\Sigma})_C = \omega_K \langle\Phi|\tilde{C}_K^{\Sigma}. \tag{233}$$

Contrary to EOMCC and EOMXCC methods, no disconnected components of $\tilde{C}_K^{\Sigma} \bar{\bar{H}}_{N,\mathrm{open}}^{\Sigma}$ enter Eq. (233) [the disconnected part of $\langle\Phi|\tilde{C}_K^{\Sigma} \bar{\bar{H}}_{N,\mathrm{open}}^{\Sigma}$, i.e. $\langle\Phi|\bar{\bar{H}}_{N,\mathrm{open}}^{\Sigma} \tilde{C}_K^{\Sigma}$, vanishes if Eq. (230) is satisfied]. In consequence, the left and right eigenvalue problems of the EOMECC approach have formally the same connected structure as long as T and Σ are obtained by solving Eqs. (226) and (230).

The left-hand deexcitation operator $\tilde{C}_K^{\Sigma}$ is defined in a similar way as the left-hand operator $\tilde{C}_K$ of the EOMXCC theory [cf. Eq. (102)],

$$\tilde{C}_K^{\Sigma} = L_K e^{-\Sigma}. \tag{234}$$

As in the EOMXCC theory, the left-hand operators $\tilde{C}_K^{\Sigma}$, Eq. (234), are more exponential than the EOMCC operators L_K. Together with the right-hand eigenstates $C_K^{\Sigma}|\Phi\rangle$, the left-hand states $\langle\Phi|\tilde{C}_K^{\Sigma}$ form a biorthogonal set, which can be made biorthonormal,

$$\langle\Phi|\tilde{C}_K^{\Sigma} C_{K'}^{\Sigma}|\Phi\rangle = \delta_{K,K'}. \tag{235}$$

Interestingly enough, for the left-hand ground-state $\langle\Phi|\tilde{C}_0^{\Sigma}$, we obtain

$$\langle\Phi|\tilde{C}_0^{\Sigma} = \langle\Phi|L_0 e^{-\Sigma} = \langle\Phi|(1+\Lambda)e^{-\Sigma} = \langle\Phi|, \tag{236}$$

so that the reference configuration Φ is both the right-hand and the left-hand eigenfunction of $\bar{\bar{H}}^{\Sigma}_{N,\mathrm{open}}$, in complete agreement with Eqs. (225) and (229) and original ECC papers [76, 77]. In order to obtain Eq. (236), we used Eqs. (60) and (228). If we combine these equations with Eq. (55), we also obtain (cf. Refs. 76, 77)

$$\langle\tilde{\Psi}_0| = \langle\Phi|e^{\Sigma}e^{-T}, \tag{237}$$

so that the EOMECC bra state $\langle\tilde{\Psi}_0|$ has a completely exponential (and thus size-extensive) form. This feature of the EOMECC theory should help to eliminate unlinked terms from the EOMCC expressions for various ground-state properties (in the current formulation of the EOMCC theory, we need to eliminate unlinked terms from expressions for second- and higher-order properties if we insist on using the "CI-like" approximation; the resulting "linear linked" approximation is clearly an *ad hoc* procedure; cf. Refs. 52, 54, 55).

A completely symmetric treatment of the left- and right-hand ground states of $\bar{\bar{H}}^{\Sigma}_{N,\mathrm{open}}$ and an almost symmetric treatment of the left and right eigenvalue problems for excited states [cf. Eqs. (233) and (231)], along with a fully exponential treatment of the left-hand and right-hand ground-state problems, make the EOMECC formalism very special and probably worth pursuing. Another special feature of the formalism based on solving Eqs. (226), (230), (231), and (233) is the structure of matrix representing $\bar{\bar{H}}^{\Sigma}_{N,\mathrm{open}}$. Unlike in EOMCC and EOMXCC, matrix representing $\bar{\bar{H}}^{\Sigma}_{N,\mathrm{open}}$ in the EE-EOMECC case has zeros both in the first row and in the first column,

$$\bar{\bar{\mathbf{H}}}^{\mathbf{\Sigma}} = \begin{pmatrix} 0 & \mathbf{0} & \mathbf{0} & \cdots \\ \mathbf{0} & \bar{\bar{\mathbf{H}}}^{\mathbf{\Sigma}}_{\mathbf{SS}} & \bar{\bar{\mathbf{H}}}^{\mathbf{\Sigma}}_{\mathbf{SD}} & \cdots \\ \mathbf{0} & \bar{\bar{\mathbf{H}}}^{\mathbf{\Sigma}}_{\mathbf{DS}} & \bar{\bar{\mathbf{H}}}^{\mathbf{\Sigma}}_{\mathbf{DD}} & \cdots \\ \mathbf{0} & \cdots & \cdots & \cdots \end{pmatrix}, \tag{238}$$

which is an immediate consequence of the fact that T and Σ satisfy Eqs. (226) and (230). Thanks to the presence of zeros in the first row and column of $\bar{\bar{\mathbf{H}}}^{\mathbf{\Sigma}}$, the left- and right-hand eigenstates of $\bar{\bar{\mathbf{H}}}^{\mathbf{\Sigma}}$, which correspond to the ground-state problem, are identical and equal to Φ. The left- and right-hand excited states are not identical since the submatrix of $\bar{\bar{\mathbf{H}}}^{\mathbf{\Sigma}}$ corresponding

to excited configurations, i.e.,

$$\bar{\bar{\mathbf{H}}}^{\Sigma,P} = \begin{pmatrix} \bar{\bar{\mathbf{H}}}^{\Sigma}_{\mathbf{SS}} & \bar{\bar{\mathbf{H}}}^{\Sigma}_{\mathbf{SD}} & \cdots \\ \bar{\bar{\mathbf{H}}}^{\Sigma}_{\mathbf{DS}} & \bar{\bar{\mathbf{H}}}^{\Sigma}_{\mathbf{DD}} & \cdots \\ \cdots & \cdots & \cdots \end{pmatrix}, \tag{239}$$

is in general non-Hermitian. The fact that the left-hand eigenvectors of $\bar{\bar{\mathbf{H}}}^{\Sigma,P}$ are more exponential than the EOMCC left-hand eigenstates may help us to restore the additive separability of the state energies going to ionized and electron-attached states resulting from EOMCC calculations [similar, in fact, should apply to EOMXCC theory, since restoration of additive separability of excited-state energies is more or less equivalent to inclusion of higher excitations in EOMCCSD equations; it is possible that some higher excitations are already included in the EOMXCCSD(PE3) approximation; cf. Ref. 45 for further details]. Clearly, a more detailed analysis would be required to be more conclusive.

The explicit equations of the EOMECC theory proposed above are almost identical to equations presented in Appendices A and B [provided, of course, that we use the CCSD approximation, $T = T_1 + T_2$, $\Sigma = \Sigma_1 + \Sigma_2$, and that we approximate $\bar{\bar{H}}^{\Sigma}_{N,\mathrm{open}}$ by Eqs. (178)-(180), in which $T^\dagger$ is replaced by Σ]. The only change that we have to make in these equations is $t_i^a \to s_i^a$, $t_{ij}^{ab} \to s_{ij}^{ab}$, where s_i^a and s_{ij}^{ab} are the amplitudes defining Σ_1 and Σ_2, respectively. For example, the system of coupled equations for T and Σ [cf. Eqs. (226) and (230)] characterizing the EOMECCSD(PE3) approach takes the following simple form,

$$\bar{\bar{h}}_a^i = 0, \tag{240}$$

$$\bar{\bar{h}}_{ab}^{ij} = 0, \tag{241}$$

$$\bar{\bar{h}}_i^a = 0, \tag{242}$$

$$\bar{\bar{h}}_{ij}^{ab} = 0, \tag{243}$$

where the explicit expressions for $\bar{\bar{h}}_a^i$, $\bar{\bar{h}}_{ab}^{ij}$, $\bar{\bar{h}}_i^a$, and $\bar{\bar{h}}_{ij}^{ab}$ are identical to those in Appendix A, except that we replace t_i^a and t_{ij}^{ab} by s_i^a and s_{ij}^{ab}, respectively. We can thus use the results of this paper to encode two approaches, the EOMXCCSD(PE3) method and its simplified variants considered in Section 5, and the EOMECCSD(PE3) approach, in spite of the fact that the similarity of EOMXCC and EOMECC approaches [cf. Eqs. (88) and (231)] is only formal. As explained in Ref. 75, operator Σ of the ECC (and thus EOMECC) theory, which makes the functional $\Delta E(\Sigma, T)$ stationary, is essentially different from $T^\dagger$. This is related to the well-known

property of the XCC formalism (mentioned in Section 3), which states that the XCC energy functional, Eq. (83), cannot be made stationary with respect to T and $T^\dagger$ [75] (we can only make it stationary with respect to $T^\dagger$, in which case we obtain the XCC scheme used in this paper). It is thus somewhat surprising that the results of this paper are more general than they appear to be. On the other hand, the MBPT analysis shows that the lowest-order estimates of Σ (or Λ) and $T^\dagger$ are identical (see Ref. 56; cf., also, Refs. 82, 90), so that the EOMXCC and EOMECC equations must be related (since $\Sigma \approx T^\dagger$ in the low MBPT orders, we can regard the EOMXCC method as an approximation to EOMECC theory). In particular, the EOMECC(PE3) method should include some T_3 contributions of the EOMCCSDT formalism [essentially, the same terms that enter the EOMXCCSD(PE3) equations; diagrammatic arguments presented in Section 6 should apply to both formalisms]. It is, therefore, likely that the EOMECCSD(PE3) method will change the results for excited states in a similar way as the EOMXCCSD(PE3) approach.

8. Summary and concluding remarks

A new CC method for electronically excited, electron-attached, and ionized states of many-electron systems, referred to as the EOMXCC theory, has been formulated. The EOMXCC method is based on diagonalization of the doubly transformed Hamiltonian $\bar{\bar{H}} = e^{T^\dagger} \bar{H} e^{-T^\dagger}$, where $\bar{H} = e^{-T} H e^{T}$ is the EOMCC Hamiltonian, and on solving the corresponding XCC equations for the ground-state cluster amplitudes. The new method is potentially exact (in its full CI and full CC limits) and general, so that it applies to all sectors of Fock space and all types of single-determinantal reference configurations, including RHF, UHF, ROHF, and QRHF determinants. As in the standard EOMCC theory, the concept of active space is completely eliminated from the formalism, which is one more step towards having an accurate and fast "black-box" method for excited states. The EOMXCC theory is operationally a single-reference method, though it has within it the ability to describe all kinds of excited states. For example, we should be able to use the EOMXCC method to propose approximations that are capable of describing excited states which have a significant contribution from double excitations.

It has been demonstrated that the $\bar{\bar{H}}$ Hamiltonian is more Hermitian than the EOMCC Hamiltonian $\bar{H}$. As a result, the difference between left- and right-hand eigenstates of $\bar{\bar{H}}$ is shifted to higher MBPT orders and strictly Hermitian EOMXCC schemes, in which left- and right-hand eigenstates of $\bar{\bar{H}}$ are indistinguishable, can be proposed. This may lead to some

improvements in the EOMCC results and facilitate various property (e.g. transition moment) calculations, which require the knowledge of wave functions (in the EOMCC language, left- and right-hand eigenfunctions of $\bar{H}$). It has been demonstrated that non-Hermitian Hamiltonians of EOMCC-like schemes may occasionally lead to complex excitation energies [36], so that a nearly Hermitian character of the EOMXCC approach is a desirable feature.

A completely Hermitian and variational CC scheme for excited and ionized states has been considered as early as in 1978 [29]. In fact, many terms that enter our EOMXCC expressions are similar to terms considered by these authors. For example, our $\bar{\bar{H}}_n^P(T_2^\dagger, T_2)$ terms can be regarded as analogs of the $T_2^\dagger W_k^\dagger H W_l T_2$, $k,l = 1,2$, terms of the theory presented in Ref. 29 (W is an analog of our CI-like C_K operator). The most important difference between our EOMXCC scheme and the method described in Ref. 29 is the fact that we built a very rich cluster structure associated with e^T and $e^{T^\dagger}$ directly into the doubly transformed Hamiltonian $\bar{\bar{H}}$, Eq. (71), whereas the authors of Ref. 29 analyze individual products $T^k W^\dagger H W T^l$, where k and l are nonnegative integers, according to their MBPT order. We thus have a systematic and relatively easy way of adding various high-order terms that result from using the exponential operators e^T and $e^{T^\dagger}$. In fact, by defining matrix elements of $\bar{H}$ and $\bar{\bar{H}}$ as basic quantities, which we can always precompute, we can keep at least some terms, such as $\sum_{k=1}^2 \bar{\bar{H}}_n(k)$ and $\bar{\bar{H}}_3^P(2)$, Eqs. (178) and (179), in unexpanded form. None of this is really possible within the formalism of Ref. 29. Moreover, by using a doubly transformed Hamiltonian $\bar{\bar{H}}$, which has an internaly connected form [in order to define $\bar{\bar{H}}$, we first form a connected expression from H and e^T; cf. Eq. (71)], we do not have to deal with a problem of non-terminating series in T and $T^\dagger$ components that results from using the $(e^{T^\dagger} W^\dagger H W e^T)_C$ and $(e^{T^\dagger} W^\dagger W e^T)_C$ expressions of the theory presented in Ref. 29. Many-body expansions representing our $\bar{H}$ and $\bar{\bar{H}}$ Hamiltonians terminate in a natural way [cf. Eq. (68) and a discussion below Eq. (128)]. Also, we do not have to worry about complicated renormalization terms of the $(e^{T^\dagger} W^\dagger W e^T)_C$ type, which generate many diagrams by themselves, since the exponential operators e^T and $e^{T^\dagger}$ are buried in a transformed Hamiltonian $\bar{\bar{H}}$ and our eigenvalue problem, Eq. (88), becomes at the end a simple CI-like problem (the only essential difference with CI is that our EOMXCC eigenvalue problem is a biorthogonal problem due to non-Hermiticity of $\bar{\bar{H}}$). As pointed out in Ref. 36, a large number of diagrams associated with renormalization terms of the $(e^{T^\dagger} W^\dagger W e^T)_C$ type makes the variational approach of Ref. 29 unmanageable. It would certainly be difficult to see if there is a clear

connection between the EOMCCSDT theory and the approach of Ref. 29. This connection becomes clear if we use the EOMXCC method instead. A difficulty in handling numerous terms that appear in the approach of Ref. 29, even when we truncate T and W at the basic biexcited level, forced the authors of Ref. 29 to consider relatively poor (using present day standards) approximations. We do not have to do any of that. The EOMXCC method allows us to incorporate various contributions coming from high MBPT orders at the low level of approximation, such as EOMXCCSD, and we can do it without generating too many diagrams. The use of "effective interaction" vertices representing the transformed operator $\bar{H}$ and the use of recursively generated intermediates significantly reduces the number of diagrams that show up in the EOMXCC theory. We can thus develop approximate EOMXCC procedures that are potentially very accurate.

A few approximate EOMXCCSD schemes, such as the PE3 method for electronically excited states discussed in Sections 5 and 6, have been considered in detail. The final equations of the PE3 scheme have been presented in a fully factorized form using recursively generated intermediates. In this way, we should be able to achieve the optimum performance, once the PE3 method is implemented, since each intermediate can be represented as a product of two arrays, which can be very efficiently evaluated using fast matrix multiplication routines. All EOMXCCSD approximations are n^6 procedures, even though we may encounter terms which scale as $n_o n_u^5$ or n_u^6. The most expensive n_u^6 terms (there are only two terms which scale as n_u^6) can likely be discarded since they have no relationship with the T_3 contributions of the standard EOMCC formalism.

The EOMCCSD method uses up to three-body terms of $\bar{H}$. The EOMXCCSD approach needs certain types of three- and four-body components of $\bar{H}$ as well as all one- and two-body terms. Although the presence of four-body terms in the EOMXCCSD approach makes this approach slightly more complicated compared to EOMCCSD, the four-body terms of $\bar{H}$ that enter the EOMXCCSD eigenvalue problem are inexpensive (they scale as $n_o^2 n_u^4$ or less) and we may also think of eliminating them altogether, since they do not bring any information about T_3 components of EOMCC.

An important finding of the present work is the fact that the EOMXCCSD method contains terms that look very similar to contributions from the connected triexcited (T_3) clusters entering the EOMCCSDT scheme. This fact can be utilized in several ways, for example, by proposing in the future a family of new approximations, which will be characterized by a better balance between various higher-order effects than that provided by some existing non-iterative EOMCCSDT-like procedures. This in turn may lead to improvement in the results for the low-lying excited states dominated by double excitations from the reference, where inclusion of triples in

the EOMCC scheme becomes essential. The EOMXCCSD method is an n^6 procedure which requires the storage of at most two-body quantities. The EOMCCSDT scheme is an n^8 method, which is characterized by the $n_o^3 n_u^3$ storage requirements for the three-body cluster amplitudes and three-body CI-like coefficients of the excitation operator R_K, and the existing perturbative EOMCCSDT-like schemes are n^7 procedures. Interestingly enough, the similarity transformation of $\bar{H}$ using $e^{T^\dagger}$ brings T_3-like effects only to the excited state problem without affecting the CCSD ground state. This may lead to additional improvements in the balance between ground and excited states within the EOMCC description.

As stated above, the EOMXCC method can be partly viewed as a Hermitized EOMCC theory, which in addition incorporates the effect of high-order clusters at the low level of approximation. As a result, the strictly Hermitian variants of the standard EOMCC methods, such as the Hermitized EOMCCSD scheme, obtained by Hermitizing $\bar{H}$ according to Eqs. (212) and (213), can be treated rigorously. More importantly, the EOMXCC scheme provides us with alternative expressions for the T_3 contributions to a regular EOMCC formalism in terms of T_2 and $T_2^\dagger$ [see Eq. (219)]. We can thus propose a new variant of approximate EOMCCSDT method, in which the $\bar{\bar{H}}_n(T_2^\dagger, T_2)$, $n = 1 - 3$, components of $\bar{\bar{H}}$ (which contribute to a DS block of $\bar{\bar{\mathbf{H}}}$) are simply added to a DS block of $\bar{\mathbf{H}}$. This would give us an alternative to the existing EOMCCSD(T) and EOMCCSDT-1 approximations [63], which are n^7 procedures (with most expensive steps scaling as $n_o^3 n_u^4$), and the possibility to calculate at least some T_3 corrections of EOMCC in n^6 ($n_o n_u^5$ at worst) steps. A strategy of this type would be a reasonable alternative to the EOMXCCSD approach discussed in previous sections, since the ground-state cluster amplitudes of the standard SRCC approach, on which the EOMCCSD(T) and EOMCCSDT-1 methods are based, and the T_1 and T_2 amplitudes of XCC, which are used in EOMXCCSD calculations, are expected to be similar (cf. Section 6). An approximate EOMCCSDT method, which uses $\bar{\bar{H}}_n(T_2^\dagger, T_2)$ to describe the effect of T_3 could be regarded as an excited-state analog of factorized CCSDTQ-like schemes used in ground-state calculations, in which the effects due to T_4 are approximated using T_2, T_3, and $T_2^\dagger$ cluster components [80–82, 90]. We may in fact contemplate various extensions of the EOMXCCSD approach in which we would approximate the effect of both T_3 and T_4 using low-order components of T and $T^\dagger$. This might lead to a hierarchy of approximate EOMCCSDTQ schemes, which are no more expensive than the ground-state CCSDT theory and, judging by the accuracy of CCSDTQ-like approaches in ground-state calculations, almost equivalent to full (exact) EOMCC scheme.

It should be mentioned that at least for closed-shell references $|\Phi\rangle$, the orthogonal spin-adaptation [47–49] of the EOMXCCSD scheme should be almost as straightforward as the spin-adaptation of the CISD method [47], even though we have not discussed any details in this paper. The doubly transformed Hamiltonian $\bar{\bar{H}}$ is not very much different than the electronic Hamiltonian H as far as its spin-properties are concerned if T is obtained in closed-shell calculations (i.e. $\bar{\bar{H}}$ commutes with S^2 and S_z spin operators). The only difference between $\bar{\bar{H}}$ (or $\bar{H}$) and H is the presence of three- and higher-rank many-body terms in $\bar{\bar{H}}$ and $\bar{H}$. Orthogonal spin-adaptation of many-body terms of $\bar{\bar{H}}$ that enter the EOMXCCSD problem can be handled rather easily by using the diagrammatic methods of spin algebras (cf. Ref. 91) and we plan to demonstrate this in the future (the same applies to orthogonal spin-adaptation of the EOMCCSD method [50]). The orthogonal spin-adaptation of the EOMCCSD and EOMXCCSD methods would certainly be useful as it would allow us to study excited states of different multiplicity as well-defined separate problems. The aforementioned restriction to closed-shell references should eventually be eliminated, but already with closed-shell references we can study excited states of open-shell systems via the IP or EA versions of the EOMXCC or EOMCC theories (cf. Ref. 38).

We will study the performance of the EOMXCCSD method in actual calculations as soon as the method is implemented. We still have to derive the detailed equations for the IP and EA versions of the EOMXCCSD theory, even though the explicit expressions for the one- and two-body components of $\bar{\bar{H}}$ that are presented in this work can already be used in calculations of VIPs and VEAs. It might be interesting to see if various higher-order terms which are present in one- and two-body components of $\bar{\bar{H}}$ improve the EOMCCSD results for VIPs and VEAs.

Finally, we will continue to explore the possibility of generalizing other alternative CC schemes, such as UCC, SXCC, SC-XCC, SC-UCC, and ECC (cf. Refs. 69–72, 74–77), to electronically excited, electron-attached, and ionized states, via the EOM formalism. As demonstrated in Section 7, this generalization is particularly straightforward in case of the ECC theory [76, 77] (see, also, Refs. 74, 75). The resulting EOMECC method, which is based on Eqs. (221), (226), (230), (231), and (233), allows for a completely symmetric treatment of the left-hand and right-hand ground-state problems (the EOMECC bra and ket ground states have both the exponential form) and a nearly symmetric treatment of the left-hand and right-hand eigenvalue problems for excited states. The working equations characterizing the EOMECCSD approximation are formally identical to equations characterizing the EOMXCCSD scheme (once $T^\dagger$ is identified with Σ). This should facilitate the implementation of the EOMECCSD

approach and its variants.

The EOMXCC and EOMECC methods described in this work are only the examples of how the alternative CC theories can be generalized to electronically excited, electron-attached, and ionized states. These and other ways of extending the standard EOMCC formalism will be considered by us in the future. In particular, we will look into another possibility of enriching the algebraic structure of EOMCC equations by introducing deexcitation operators directly in the elementary excitation operator R_K, as is routinely done in the traditional EOM and RPA techniques [40, 68]. Although this will complicate the algebra (deexcitation part of the new R_K operator will no longer commute with T), we may eventually benefit from having deexcitations in R_K, as numerous EOM and RPA calculations clearly demonstrate. An elegant extension of the ECC theory to excited states, which for single excitations reduces to RPA, has been considered in Ref. 77, but further work is required to see if this and similar approaches are useful in applications to electronically excited states of molecules.

Acknowledgments

We wish to thank the Editors, particularly Professor John Sabin, for inviting us to write an article in *Advances in Quantum Chemistry.* This work has been supported by the United States Air Force Office of Scientific Research under grant number AFOSR-F49620-95-1-0130. We would like to thank Professor Marcel Nooijen and Dr. Leszek Meissner for carefully reading this paper and commenting on its contents. We would also like to thank Dr. John Watts for providing us with some details on the role of triexcited configurations in EOMCC calculations and for his interest in this study. Finally, we appreciate useful discussions with Professors Josef Paldus and Stanisław Kucharski, and Dr. Steven Gwaltney.

Appendix A: One- and two-body components of $\bar{\bar{H}}$ in the PE3 approximation

The easiest way to derive the explicit equations of the EOMXCC method is by using the diagrammatic methods of MBPT. In this and in the next Appendix B, we focus on equations describing the EE-EOMXCCSD(PE3) scheme, which uses the Hamiltonian defined by Eqs. (178)-(180). We begin with the expressions for one-and two-body components $\bar{\bar{H}}_1$ and $\bar{\bar{H}}_2$.

By using diagrammatic approach, we can show that one- and two-body matrix elements $\bar{\bar{h}}_p^q$ and $\bar{\bar{h}}_{pq}^{rs}$, which define $\bar{\bar{H}}_1$ and $\bar{\bar{H}}_2$ [cf. Eqs. (143) and (144)] and which enter Eqs. (152) and (153) for ${}^{1,2}\Lambda_a^i$ and ${}^{1,2}\Lambda_{ab}^{ij}$, take the form:

$$\bar{\bar{h}}_p^q = \bar{\bar{h}}_p^q(1,2) + \bar{\bar{h}}_p^q(3), \tag{244}$$

and

$$\bar{\bar{h}}_{pq}^{rs} = \bar{\bar{h}}_{pq}^{rs}(1,2) + \bar{\bar{h}}_{pq}^{rs}(3) + \bar{\bar{h}}_{pq}^{rs}(3'), \tag{245}$$

where $\bar{\bar{h}}_p^q(1,2)$ and $\bar{\bar{h}}_{pq}^{rs}(1,2)$ define $\bar{\bar{H}}_n(k)$, $k,n = 1,2$ [cf. Eqs. (173) and (174)], and $\bar{\bar{h}}_p^q(3)$, $\bar{\bar{h}}_{pq}^{rs}(3)$, and $\bar{\bar{h}}_{pq}^{rs}(3')$ are the matrix elements defining $\bar{\bar{H}}_1(T_2^\dagger, T_2)$, $\bar{\bar{H}}_2(T_2^\dagger, T_2)$, and $\bar{\bar{H}}_2(T_1^\dagger, T_2)$, respectively [cf. Eqs. (186)-(188)]. In particular, the XCCSD equations (141) and (142) reduce to (assuming the PE3 approximation)

$$\bar{\bar{h}}_a^i = \bar{\bar{h}}_a^i(1,2) + \bar{\bar{h}}_a^i(3) = \bar{h}_a^i + \bar{h}_{ae}^{im} t_m^e + \bar{\bar{h}}_a^i(3) = 0, \tag{246}$$

$$\bar{\bar{h}}_{ab}^{ij} = \bar{\bar{h}}_{ab}^{ij}(1,2) + \bar{\bar{h}}_{ab}^{ij}(3') = \bar{h}_{ab}^{ij} + \bar{\bar{h}}_{ab}^{ij}(3') = 0, \tag{247}$$

where we already used the explicit expressions for $\bar{\bar{h}}_a^i(1,2)$ and $\bar{\bar{h}}_{ab}^{ij}(1,2)$ and the fact that $\bar{\bar{h}}_{ab}^{ij}(3)$ vanishes (see equations below). As explained in Section 6, the $\bar{\bar{h}}_a^i(3)$ term present in Eq. (246) (strictly speaking, its $\langle\Phi|G_a^i[T_2^\dagger(V_N T_2)_{C,3}]_{C,1}|\Phi\rangle$ component) can be identified with the $\langle\Phi|G_a^i(V_N T_3)_C|\Phi\rangle$ term of standard SRCC theory. The latter term shows up in higher orders than dominant terms of the SRCC equations projected on monoexcited configurations, such as $\langle\Phi|G_a^i(V_N T_2)_C|\Phi\rangle$, and as such it plays a relatively small role. A similar argument should apply to the $\bar{h}_{ae}^{im} t_m^e$ contribution, which, at least in the Hartree-Fock case, is a small fifth-order term, when the converged XCCSD(PE3) amplitudes are used [see Eq. (192)]. In fact, if the SRCC amplitudes were employed, this term would vanish. We can also show (see Section 6) that $\bar{\bar{h}}_{ab}^{ij}(3')$ corresponds to the $\langle\Phi|G_{ab}^{ij}(F_N T_3)_C|\Phi\rangle$ contribution of the standard SRCC theory, which is again small and which in the Hartree-Fock case equals zero. In consequence, the XCCSD(PE3) equations (246) and (247) are nearly identical to the ordinary SRCCSD equations

$$\bar{h}_a^i = 0, \tag{248}$$

$$\bar{h}_{ab}^{ij} = 0. \tag{249}$$

The explicit expressions for $\bar{\bar{h}}_p^q(1,2)$ and $\bar{\bar{h}}_{pq}^{rs}(1,2)$ are given in part A.1 below. Expressions for $\bar{\bar{h}}_p^q(3)$, $\bar{\bar{h}}_{pq}^{rs}(3)$, and $\bar{\bar{h}}_{pq}^{rs}(3')$ are listed in part A.2.

A.1. Expressions for matrix elements defining $\bar{\bar{H}}_n(k)$, $k,n = 1,2$

The following expressions can be derived using diagrammatic methods of MBPT,

$$\bar{\bar{h}}^{\,i}_{a}(1,2) = \bar{h}^{i}_{a} + \bar{h}^{im}_{ae}\, t^{e}_{m}, \tag{250}$$

$$\bar{\bar{h}}^{\,j}_{i}(1,2) = \chi^{j}_{i} + \bar{\bar{h}}^{\,j}_{e}(1,2)\, t^{e}_{i}, \tag{251}$$

$$\bar{\bar{h}}^{\,b}_{a}(1,2) = \bar{h}^{b}_{a} + \bar{h}^{bm}_{ae}\, t^{e}_{m} + \tfrac{1}{2}\, \bar{h}^{mn}_{ae}\, t^{eb}_{mn} - \bar{\bar{h}}^{\,m}_{a}(1,2)\, t^{b}_{m}, \tag{252}$$

$$\begin{aligned}\bar{\bar{h}}^{\,a}_{i}(1,2) = {} & \bar{h}^{a}_{i} + \bar{\bar{h}}^{\,a}_{e}(1,2)\, t^{e}_{i} - \chi^{m}_{i}\, t^{a}_{m} + \bar{\bar{h}}^{\,m}_{e}(1,2)\, t^{ae}_{im} + \bar{h}^{ma}_{ei}\, t^{e}_{m} \\ & + \tfrac{1}{2}\, \bar{h}^{am}_{ef}\, t^{ef}_{im} + \tfrac{1}{2}\, \bar{h}^{mn}_{ie}\, t^{ea}_{mn},\end{aligned} \tag{253}$$

$$\bar{\bar{h}}^{\,ij}_{ab}(1,2) = \bar{h}^{ij}_{ab}, \tag{254}$$

$$\bar{\bar{h}}^{\,ci}_{ab}(1,2) = \bar{h}^{ci}_{ab} - \bar{h}^{mi}_{ab}\, t^{c}_{m} = \pi^{ci}_{ab} - \tfrac{1}{2}\, \bar{h}^{mi}_{ab}\, t^{c}_{m}, \tag{255}$$

$$\bar{\bar{h}}^{\,ij}_{ka}(1,2) = \bar{h}^{ij}_{ka} + \bar{h}^{ij}_{ea}\, t^{e}_{k} = \bar{\pi}^{ij}_{ka} + \tfrac{1}{2}\, \bar{h}^{ij}_{ea}\, t^{e}_{k}, \tag{256}$$

$$\bar{\bar{h}}^{\,ij}_{kl}(1,2) = \bar{h}^{ij}_{kl} + \mathcal{A}_{kl}\, \bar{\pi}^{ij}_{ke}\, t^{e}_{l} + \tfrac{1}{2}\, \bar{h}^{ij}_{ef}\, t^{ef}_{kl}, \tag{257}$$

$$\bar{\bar{h}}^{\,cd}_{ab}(1,2) = \omega^{cd}_{ab} + \tfrac{1}{2}\, \bar{h}^{mn}_{ab}\, t^{cd}_{mn}, \tag{258}$$

$$\begin{aligned}\bar{\bar{h}}^{\,ab}_{ci}(1,2) = {} & \bar{h}^{ab}_{ci} + \bar{h}^{ab}_{ce}\, t^{e}_{i} - \bar{\bar{h}}^{\,m}_{c}(1,2)\, t^{ab}_{mi} - \tfrac{1}{2}\, \bar{\bar{h}}^{\,mn}_{ic}(1,2)\, t^{ab}_{mn} \\ & + \mathcal{A}^{ab}\left[\bar{\bar{h}}^{\,bm}_{ce}(1,2)\, t^{ae}_{mi} + \theta^{ma}_{ci}\, t^{b}_{m}\right],\end{aligned} \tag{259}$$

$$\begin{aligned}\bar{\bar{h}}^{\,ka}_{ij}(1,2) = {} & \bar{h}^{ka}_{ij} - \bar{h}^{km}_{ij}\, t^{a}_{m} + \bar{\bar{h}}^{\,k}_{e}(1,2)\, t^{ea}_{ij} - \tfrac{1}{2}\, \bar{\bar{h}}^{\,ak}_{ef}(1,2)\, t^{ef}_{ij} \\ & + \mathcal{A}_{ij}\left[\bar{\bar{h}}^{\,km}_{je}(1,2)\, t^{ea}_{im} - \tilde{\theta}^{ka}_{ei}\, t^{e}_{j}\right],\end{aligned} \tag{260}$$

$$\bar{\bar{h}}^{\,ib}_{aj}(1,2) = \phi^{ib}_{aj} + \tfrac{1}{2}\, \bar{h}^{im}_{ae}\, t^{be}_{jm}, \tag{261}$$

$$\begin{aligned}\bar{\bar{h}}^{\,ab}_{ij}(1,2) = {} & \bar{h}^{ab}_{ij} + \mathcal{A}^{ab}\, \bar{\bar{h}}^{\,b}_{e}(1,2)\, t^{ae}_{ij} - \mathcal{A}_{ij}\, \bar{\bar{h}}^{\,m}_{j}(1,2)\, t^{ab}_{im} + \tfrac{1}{2}\, \omega^{ab}_{ef}\, t^{ef}_{ij} \\ & + \tfrac{1}{2}\, \bar{\bar{h}}^{\,mn}_{ij}(1,2)\, t^{ab}_{mn} + \mathcal{A}_{ij}\mathcal{A}^{ab}\, \phi^{mb}_{ej}\, t^{ae}_{im} \\ & + \mathcal{A}_{ij}\, \psi^{ab}_{ej}\, t^{e}_{i} + \mathcal{A}^{ab}\, \tilde{\psi}^{ma}_{ij}\, t^{b}_{m}.\end{aligned} \tag{262}$$

The explicit formulas for $\bar{h}^{q}_{p}$ and $\bar{h}^{rs}_{pq}$, which represent one- and two-body matrix elements of $\bar{H}$, can be found in Ref. 34 (for the list of misprints in expressions presented in Table 1 of Ref. 34, see Ref. 83). The only expressions that cannot be found in Ref. 34 are those for $\bar{h}^{i}_{a}$ and $\bar{h}^{ij}_{ab}$, since they vanish in the EOMCCSD case (they no longer vanish when the EOMXCCSD method using XCCSD amplitudes is employed). The explicit expressions for $\bar{h}^{i}_{a}$ and $\bar{h}^{ij}_{ab}$ (which are, of course, the left-hand sides of the SRCCSD equations, provided that we use XCCSD amplitudes) are

$$\bar{h}^{i}_{a} = f^{i}_{a} + \bar{h}^{e}_{a}\, t^{i}_{e} - X^{i}_{m}\, t^{m}_{a} + \bar{h}^{e}_{m}\, t^{im}_{ae} + v^{ei}_{ma}\, t^{m}_{e} + \tfrac{1}{2}\, v^{ef}_{am}\, t^{im}_{ef}$$

$$+\tfrac{1}{2}\,v_{mn}^{ie}\,t_{ea}^{mn}, \tag{263}$$

$$\bar{h}_{ab}^{ij} = v_{ab}^{ij} + \mathcal{A}_{ab}\,\bar{h}_{b}^{e}\,t_{ae}^{ij} - \mathcal{A}^{ij}\,\bar{h}_{m}^{j}\,t_{ab}^{im} + \tfrac{1}{2}\,\Omega_{ab}^{ef}\,t_{ef}^{ij} + \tfrac{1}{2}\,\bar{h}_{mn}^{ij}\,t_{ab}^{mn} + \mathcal{A}_{ab}\mathcal{A}^{ij}\,\Phi_{mb}^{ej}\,t_{ae}^{im} + \mathcal{A}^{ij}\,\Psi_{ab}^{ej}\,t_{e}^{i} + \mathcal{A}_{ab}\,\tilde{\Psi}_{ma}^{ij}\,t_{b}^{m}. \tag{264}$$

The above expressions for $\bar{\bar{h}}_{p}^{q}(1,2)$ and $\bar{\bar{h}}_{pq}^{rs}(1,2)$ are defined in terms of recursively generated intermediates [92], which we list below,

$$\chi_{i}^{j} = \bar{h}_{i}^{j} + \bar{h}_{ie}^{jm}\,t_{m}^{e} + \tfrac{1}{2}\,\bar{h}_{ef}^{jm}\,t_{im}^{ef}, \tag{265}$$

$$X_{j}^{i} = f_{j}^{i} + v_{jm}^{ie}\,t_{e}^{m} + \tfrac{1}{2}\,v_{jm}^{ef}\,t_{ef}^{im}, \tag{266}$$

$$\pi_{ab}^{ci} = \bar{h}_{ab}^{ci} + \tfrac{1}{2}\,\bar{h}_{ab}^{im}\,t_{m}^{c}, \tag{267}$$

$$\tilde{\pi}_{ka}^{ij} = \bar{h}_{ka}^{ij} - \tfrac{1}{2}\,\bar{h}_{ae}^{ij}\,t_{k}^{e}, \tag{268}$$

$$\phi_{aj}^{ib} = \bar{h}_{aj}^{ib} + \bar{h}_{ja}^{im}\,t_{m}^{b} + \tfrac{1}{2}\,\bar{h}_{ae}^{im}\,t_{jm}^{be} - \bar{\bar{h}}_{ae}^{bi}(1,2)\,t_{j}^{e}, \tag{269}$$

$$\omega_{ab}^{cd} = \bar{h}_{ab}^{cd} - \mathcal{A}^{cd}\,\pi_{ab}^{cm}\,t_{m}^{d}, \tag{270}$$

$$\eta_{aj}^{ib} = \bar{h}_{aj}^{ib} + \tfrac{1}{2}\,\bar{h}_{ja}^{im}\,t_{m}^{b} - \tfrac{1}{2}\,\pi_{ae}^{bi}\,t_{j}^{e}, \tag{271}$$

$$\psi_{ci}^{ab} = \bar{h}_{ci}^{ab} + \tfrac{1}{2}\,\bar{h}_{ce}^{ab}\,t_{i}^{e} + \mathcal{A}^{ab}\,\eta_{ci}^{ma}\,t_{m}^{b}, \tag{272}$$

$$\tilde{\psi}_{ij}^{ka} = \bar{h}_{ij}^{ka} - \tfrac{1}{2}\,\bar{h}_{ij}^{km}\,t_{m}^{a}, \tag{273}$$

$$\theta_{aj}^{ib} = \eta_{aj}^{ib} - \tfrac{1}{2}\,\pi_{ae}^{bi}\,t_{j}^{e}, \tag{274}$$

$$\tilde{\theta}_{aj}^{ib} = \bar{h}_{aj}^{ib} - \tfrac{1}{2}\,\bar{h}_{ae}^{bi}\,t_{j}^{e} + \tilde{\pi}_{ja}^{im}\,t_{m}^{b}, \tag{275}$$

$$\Pi_{ci}^{ab} = v_{ci}^{ab} + \tfrac{1}{2}\,v_{im}^{ab}\,t_{c}^{m}, \tag{276}$$

$$\Phi_{ib}^{aj} = v_{ib}^{aj} + v_{im}^{ja}\,t_{b}^{m} + \tfrac{1}{2}\,v_{im}^{ae}\,t_{be}^{jm} - \bar{h}_{bi}^{ae}\,t_{e}^{j}, \tag{277}$$

$$\Omega_{cd}^{ab} = v_{cd}^{ab} - \mathcal{A}_{cd}\,\Pi_{cm}^{ab}\,t_{d}^{m}, \tag{278}$$

$$\mathrm{H}_{ib}^{aj} = v_{ib}^{aj} + \tfrac{1}{2}\,v_{im}^{ja}\,t_{b}^{m} - \tfrac{1}{2}\,\Pi_{bi}^{ae}\,t_{e}^{j}, \tag{279}$$

$$\Psi_{ab}^{ci} = v_{ab}^{ci} + \tfrac{1}{2}\,v_{ab}^{ce}\,t_{e}^{i} + \mathcal{A}_{ab}\,\mathrm{H}_{ma}^{ci}\,t_{b}^{m}, \tag{280}$$

$$\tilde{\Psi}_{ka}^{ij} = v_{ka}^{ij} - \tfrac{1}{2}\,v_{km}^{ij}\,t_{a}^{m}. \tag{281}$$

Note that all expressions for matrix elements of $\bar{\bar{H}}$ that are shown in this paper have the same general form. Each matrix element of $\bar{\bar{H}}$ is a product of at most two matrices (typically, a product of the previously generated intermediate and a cluster amplitude). This is to make sure that the resulting equations have a fully vectorizable form (matrix products can always be evaluated using efficient matrix multiplication routines; cf., e.g., Ref. 92). It can be easily verified that none of the matrix elements $\bar{\bar{h}}_{p}^{q}(1,2)$ and $\bar{\bar{h}}_{pq}^{rs}(1,2)$ listed above requires steps that are more expensive than $n_o^2 n_u^4$ and that most of the operations needed to form $\bar{\bar{h}}_{p}^{q}(1,2)$ and $\bar{\bar{h}}_{pq}^{rs}(1,2)$ are significantly cheaper than $n_o^2 n_u^4$ steps of the standard SRCCSD calculation.

A.2. Expressions for matrix elements defining $\bar{\bar{H}}_n(T_2^\dagger, T_2)$, $n = 1, 2$, *and* $\bar{\bar{H}}_2(T_1^\dagger, T_2)$

The following is a complete list of expressions for $\bar{\bar{h}}_p^q(3)$, $\bar{\bar{h}}_{pq}^{rs}(3)$, and $\bar{\bar{h}}_{pq}^{rs}(3')$,

$$\bar{\bar{h}}_a^i(3) = -\tfrac{1}{2} w_{na}^{im} \tau_m^n + \tfrac{1}{2} w_{ae}^{fi} \tau_f^e + (\nu_{mn}^{ie} - \tfrac{1}{4} \tilde{\nu}_{mn}^{ie}) t_{ea}^{mn} + v_{ae}^{fm} \tau_{fm}^{ie} - \tfrac{1}{4} v_{ao}^{mn} \tau_{mn}^{oi} - \tfrac{1}{2} (\nu_m^e - \tilde{\nu}_m^e) t_{ea}^{mi}, \quad (282)$$

$$\bar{\bar{h}}_i^j(3) = \tfrac{1}{2} v_{in}^{jm} \tau_m^n - \tfrac{1}{2} v_{ie}^{jf} \tau_f^e + \tfrac{1}{4} v_{io}^{mn} \tau_{mn}^{jo} + v_{ie}^{fm} \tau_{fm}^{je}, \quad (283)$$

$$\bar{\bar{h}}_a^b(3) = \tfrac{1}{2} v_{an}^{bm} \tau_m^n - \tfrac{1}{2} v_{ae}^{bf} \tau_f^e - v_{ne}^{bm} \tau_{am}^{ne} + \tfrac{1}{4} \bar{\bar{\nu}}_{mn}^{be} t_{ea}^{mn}, \quad (284)$$

$$\bar{\bar{h}}_i^a(3) = \tfrac{1}{2} v_{in}^{am} \tau_m^n - \tfrac{1}{2} v_{ie}^{af} \tau_f^e, \quad (285)$$

$$\bar{\bar{h}}_{ab}^{ij}(3) = 0, \quad (286)$$

$$\bar{\bar{h}}_{kl}^{ij}(3) = \tfrac{1}{2} \mathcal{A}_{kl} v_{km}^{ij} \tau_l^m - \tfrac{1}{2} \mathcal{A}^{ij} \mathcal{A}_{kl} v_{kn}^{im} \tau_{ml}^{nj} + \mathcal{A}^{ij} \mathcal{A}_{kl} v_{ke}^{if} \tau_{fl}^{je} + \mathcal{A}_{kl} \bar{\nu}_{kl}^{ef} t_{ef}^{ij}, \quad (287)$$

$$\bar{\bar{h}}_{ab}^{cd}(3) = \tfrac{1}{2} \mathcal{A}^{cd} v_{ab}^{ce} \tau_e^d - \tfrac{1}{2} \mathcal{A}_{ab} \mathcal{A}^{cd} v_{ae}^{cf} \tau_{fb}^{ed} + \mathcal{A}_{ab} \mathcal{A}^{cd} v_{an}^{cm} \tau_{bm}^{nd} + \mathcal{A}^{cd} \bar{\nu}_{mn}^{cd} t_{ab}^{mn}, \quad (288)$$

$$\bar{\bar{h}}_{ci}^{ab}(3) = \tfrac{1}{2} \mathcal{A}^{ab} v_{ci}^{ae} \tau_e^b + \tfrac{1}{2} v_{cm}^{ab} \tau_i^m - v_{me}^{ab} \tau_{ci}^{me} - \mathcal{A}^{ab} v_{im}^{an} \tau_{cn}^{mb} + \tfrac{1}{2} \mathcal{A}^{ab} v_{ie}^{af} \tau_{fc}^{eb}, \quad (289)$$

$$\bar{\bar{h}}_{ij}^{ka}(3) = \tfrac{1}{2} \mathcal{A}_{ij} v_{im}^{ka} \tau_j^m + \tfrac{1}{2} v_{ij}^{ke} \tau_e^a - v_{ij}^{em} \tau_{em}^{ka} - \mathcal{A}_{ij} v_{if}^{ae} \tau_{ej}^{kf} + \tfrac{1}{2} \mathcal{A}_{ij} v_{in}^{am} \tau_{mj}^{nk}, \quad (290)$$

$$\bar{\bar{h}}_{aj}^{ib}(3) = \tfrac{1}{2} v_{aj}^{ie} \tau_e^b + \tfrac{1}{2} v_{am}^{ib} \tau_j^m - v_{me}^{ib} \tau_{aj}^{me} - v_{aj}^{em} \tau_{em}^{ib} - v_{jn}^{im} \tau_{am}^{nb} - v_{ae}^{bf} \tau_{fj}^{ie} + \tfrac{1}{2} v_{je}^{if} \tau_{fa}^{eb} + \tfrac{1}{2} v_{an}^{bm} \tau_{mj}^{ni} - (\bar{\nu}_{jm}^{eb} + \bar{\nu}_{mj}^{be} - \tfrac{1}{2} \bar{\bar{\nu}}_{jm}^{be} - \tfrac{1}{2} \bar{\bar{\nu}}_{jm}^{be}) t_{ea}^{mi}, \quad (291)$$

$$\bar{\bar{h}}_{ab}^{ci}(3) = \tfrac{1}{2} w_{ab}^{ei} \tau_e^c + w_{ab}^{em} \tau_{em}^{ic} - \mathcal{A}_{ab} w_{na}^{mi} \tau_{bm}^{nc} + \tfrac{1}{2} \mathcal{A}_{ab} w_{fa}^{ei} \tau_{eb}^{fc} - \bar{\nu}_{mn}^{ic} t_{ab}^{mn} - \mathcal{A}_{ab} (\bar{\nu}_{am}^{ec} - \tfrac{1}{2} \bar{\bar{\nu}}_{am}^{ce}) t_{eb}^{mi} - \tfrac{1}{2} \tilde{\nu}_m^c t_{ab}^{mi}, \quad (292)$$

$$\bar{\bar{h}}_{ka}^{ij}(3) = \tfrac{1}{2} w_{ma}^{ij} \tau_k^m + w_{me}^{ij} \tau_{ak}^{me} - \mathcal{A}^{ij} w_{ea}^{fi} \tau_{fk}^{je} + \tfrac{1}{2} \mathcal{A}^{ij} w_{ma}^{ni} \tau_{nk}^{mj} - \bar{\nu}_{ak}^{ef} t_{ef}^{ij} - \mathcal{A}^{ij} (\bar{\nu}_{mk}^{ie} - \tfrac{1}{2} \bar{\bar{\nu}}_{km}^{ie}) t_{ea}^{mj} - \tfrac{1}{2} \nu_k^e t_{ea}^{ij}, \quad (293)$$

$$\bar{\bar{h}}_{ij}^{ab}(3) = \tfrac{1}{2} \mathcal{A}^{ab} v_{ij}^{ae} \tau_e^b + \tfrac{1}{2} \mathcal{A}_{ij} v_{im}^{ab} \tau_j^m, \quad (294)$$

$$\begin{aligned}
\bar{\bar{h}}^{ij}_{ab}(3') &= -\mathcal{A}_{ab}\, v^{ij}_{am}\, \sigma^m_b + \mathcal{A}^{ij}\, v^{ie}_{ab}\, \sigma^j_e + \mu^{ij}_{mn}\, t^{mn}_{ab} - v^{me}_{ab}\, \sigma^{ij}_{me} \\
&\quad -\mathcal{A}_{ab}\mathcal{A}^{ij}\, \mu^{ie}_{am}\, t^{mj}_{eb} - \mathcal{A}_{ab}\mathcal{A}^{ij}\, v^{im}_{an}\, \sigma^{nj}_{mb} \\
&\quad +\mathcal{A}_{ab}\, \mu^e_a\, t^{ij}_{eb} - \mathcal{A}^{ij}\, \mu^i_m\, t^{mj}_{ab}, \qquad (295) \\
\bar{\bar{h}}^{ij}_{kl}(3') &= \mathcal{A}^{ij}\, v^{ie}_{kl}\, \sigma^j_e - v^{me}_{kl}\, \sigma^{ij}_{me}, \qquad (296) \\
\bar{\bar{h}}^{cd}_{ab}(3') &= -\mathcal{A}_{ab}\, v^{cd}_{am}\, \sigma^m_b + \mu^{cd}_{mn}\, t^{mn}_{ab}, \qquad (297) \\
\bar{\bar{h}}^{ab}_{ci}(3') &= v^{ab}_{im}\, \sigma^m_c, \qquad (298) \\
\bar{\bar{h}}^{ka}_{ij}(3') &= -v^{ae}_{ij}\, \sigma^k_e, \qquad (299) \\
\bar{\bar{h}}^{ib}_{aj}(3') &= v^{ib}_{jm}\, \sigma^m_a - v^{be}_{aj}\, \sigma^i_e + \mu^{be}_{jm}\, t^{mi}_{ea} - v^{bm}_{jn}\, \sigma^{ni}_{ma}, \qquad (300) \\
\bar{\bar{h}}^{ci}_{ab}(3') &= v^{ce}_{ab}\, \sigma^i_e - \mathcal{A}_{ab}\, v^{ci}_{am}\, \sigma^m_b - \mu^{ic}_{mn}\, t^{mn}_{ab} - \mu^c_m\, t^{mi}_{ab} \\
&\quad -\mathcal{A}_{ab}\, v^{cm}_{an}\, \sigma^{ni}_{mb} + \mathcal{A}_{ab}\, \mu^{ce}_{am}\, t^{mi}_{eb}, \qquad (301) \\
\bar{\bar{h}}^{ij}_{ka}(3') &= -v^{ij}_{km}\, \sigma^m_a + \mathcal{A}^{ij}\, v^{ie}_{ka}\, \sigma^j_e - v^{me}_{ka}\, \sigma^{ij}_{me} + \mu^e_k\, t^{ij}_{ea} \\
&\quad -\mathcal{A}^{ij}\, v^{im}_{kn}\, \sigma^{nj}_{ma} + \mathcal{A}^{ij}\, \mu^{ie}_{km}\, t^{mj}_{ea}, \qquad (302) \\
\bar{\bar{h}}^{ab}_{ij}(3') &= 0. \qquad (303)
\end{aligned}$$

The corresponding intermediates are

$$\begin{aligned}
\nu^a_i &= v^{am}_{ef}\, t^{ef}_{mi}, \qquad (304) \\
\tilde{\nu}^a_i &= v^{mn}_{ie}\, t^{ea}_{mn}, \qquad (305) \\
\nu^{ka}_{ij} &= w^{km}_{ie}\, t^{ea}_{mj}, \qquad (306) \\
\tilde{\nu}^{ka}_{ij} &= w^{ak}_{ef}\, t^{ef}_{ij}, \qquad (307) \\
\bar{\nu}^{qa}_{pi} &= v^{qm}_{pe}\, t^{ea}_{mi}, \qquad (p,q) = (j,b),\ (c,b),\ (j,k), \qquad (308) \\
\bar{\bar{\nu}}^{ab}_{pq} &= v^{mn}_{pq}\, t^{ab}_{mn}, \qquad (p,q) = (i,j),\ (c,i), \qquad (309) \\
\bar{\bar{\nu}}^{pq}_{ij} &= v^{pq}_{ef}\, t^{ef}_{ij}, \qquad (p,q) = (a,b),\ (k,a), \qquad (310) \\
\mu^j_i &= w^{jm}_{ie}\, t^e_m = \mu^{jm}_{im}, \qquad (311) \\
\mu^b_a &= w^{bm}_{ae}\, t^e_m = \mu^{mb}_{am}, \qquad (312) \\
\mu^a_i &= v^{am}_{ie}\, t^e_m = -\mu^{ma}_{im}, \qquad (313) \\
\mu^{ij}_{kl} &= w^{ij}_{ke}\, t^e_l, \qquad (314) \\
\mu^{ab}_{ci} &= v^{ab}_{ce}\, t^e_i, \qquad (315) \\
\mu^{ka}_{ij} &= v^{ka}_{ie}\, t^e_j, \qquad (316) \\
\mu^{ib}_{aj} &= w^{bi}_{ae}\, t^e_j, \qquad (317) \\
\mu^{ab}_{ij} &= v^{ab}_{ie}\, t^e_j, \qquad (318)
\end{aligned}$$

where

$$w^{ij}_{ka} = v^{ij}_{ka} + f^e_k\, t^{ij}_{ea}, \qquad (319)$$

$$w_{ab}^{ci} = v_{ab}^{ci} - f_m^c \, t_{ab}^{mi}, \tag{320}$$

and

$$\tau_i^j = t_{im}^{ef} \, t_{ef}^{mj}, \tag{321}$$
$$\tau_b^a = t_{mn}^{ae} \, t_{eb}^{mn}, \tag{322}$$
$$\tau_{ij}^{kl} = t_{ij}^{ef} \, t_{ef}^{kl}, \tag{323}$$
$$\tau_{cd}^{ab} = t_{mn}^{ab} \, t_{cd}^{mn}, \tag{324}$$
$$\tau_{aj}^{ib} = t_{ae}^{im} \, t_{mj}^{eb}, \tag{325}$$
$$\sigma_a^i = t_m^e \, t_{ea}^{mi}, \tag{326}$$
$$\sigma_{ka}^{ij} = t_k^e \, t_{ea}^{ij}. \tag{327}$$

Note that the $\frac{1}{2}\,[T_2^\dagger (F_N T_2^2)_{C,3}]_{C,n}$ and $\frac{1}{2}\,\delta_{n,2}\,[T_1^\dagger (F_N T_2^2)_{C,3}]_{C,n}$ contributions to $\bar{\bar{H}}_n(T_2^\dagger, T_2)$ and $\bar{\bar{H}}_n(T_1^\dagger, T_2)$, respectively, where $n = 1, 2$, can be combined with the corresponding $[T_2^\dagger (V_N T_2)_{C,3}]_{C,n}$ and $[T_1^\dagger (V_N T_2)_{C,3}]_{C,n}$ terms by introducing the effective interaction w, Eqs. (319) and (320). This interaction reduces to ordinary v if the Hartree-Fock orbitals are employed.

The most expensive one- and two-body terms among those defining $\bar{\bar{H}}_n(T_2^\dagger, T_2)$, $n = 1, 2$, and $\bar{\bar{H}}_2(T_1^\dagger, T_2)$ are the second term in Eq. (288) for $\bar{\bar{h}}_{ab}^{cd}(3)$, the last term in Eq. (289) for $\bar{\bar{h}}_{ci}^{ab}(3)$, and the fourth term in Eq. (292) for $\bar{\bar{h}}_{ab}^{ci}(3)$. Their calculation requires the n_u^6, $n_o n_u^5$, and $n_o n_u^5$ steps, respectively. The remaining terms scale as $n_o^2 n_u^4$ or better. In fact, most steps required to compute $\bar{\bar{H}}_n(T_2^\dagger, T_2)$, $n = 1, 2$, and $\bar{\bar{H}}_2(T_1^\dagger, T_2)$ are inexpensive n^6 steps and there are many steps which scale as n^5 and even n^4.

The n_u^6 contribution to $\bar{\bar{h}}_{ab}^{cd}(3)$ is not related to any of the T_3 terms of the EOMCCSDT formalism discussed in Section 6 [none of the $\bar{\bar{h}}_{ab}^{cd}$ terms contributes to a DS block of $\bar{\bar{\mathbf{H}}}$ as T_3 contributions would do; the $\bar{\bar{h}}_{ab}^{cd}$ terms contribute to a DD block of $\bar{\bar{\mathbf{H}}}$; cf. Eq. (153)]. In fact, none of the diagrams representing $\bar{\bar{h}}_{ab}^{cd}(3)$ has any relationship to EOMCCSDT. We can thus consider an option of eliminating the $\bar{\bar{h}}_{ab}^{cd}(3)$ contribution to $\bar{\bar{h}}_{ab}^{cd}$ altogether. An obvious alternative is to keep $\bar{\bar{h}}_{ab}^{cd}(3)$ terms in the formalism, but then we must realize that they might become more expensive than the most expensive $n_o^3 n_u^4$ steps of approximate EOMCCSDT theories, such as EOMCCSDT-1 or EOMCCSD(T), when $n_u > n_o^{3/2}$.

The $n_o n_u^5$ term in $\bar{\bar{h}}_{ci}^{ab}(3)$ is not related to any of the T_3 terms of EOMCCSDT either [$\bar{\bar{h}}_{ci}^{ab}(3)$ contributes to an SD block of $\bar{\bar{\mathbf{H}}}$; cf. Eq. (152)]. Thus, we may think of dropping $\bar{\bar{h}}_{ci}^{ab}(3)$ altogether. However, the $n_o n_u^5$ term

in $\bar{\bar{h}}^{ci}_{ab}(3)$ is related to a T_3 contribution of EOMCCSDT labeled as DS_5 [see Figures 2 (c) and 3(b)]. This term is less expensive than $n_o^3 n_u^4$ steps of EOMCCSDT-1 and EOMCCSD(T) provided that $n_u < n_o^2$ (this condition is usually satisfied in actual calculations). We could choose an alternative representation of the $\frac{1}{2}\mathcal{A}_{ab}\, w^{ei}_{fa}\, \tau^{fc}_{eb}$ contribution to $\bar{\bar{h}}^{ci}_{ab}(3)$, which in its present form scales as $n_o n_u^5$, by writing it as $\frac{1}{2}\mathcal{A}_{ab}\,(w^{ei}_{fb}\, t^{mn}_{ae})\, t^{fc}_{mn}$, which would lead to $n_o^3 n_u^4$ scaling for this term. We have not done this since the $n_o^3 n_u^4$ scaling is usually not as good as the $n_o n_u^5$ scaling. Moreover, by choosing the new form we would also have to deal with three-body intermediates corresponding to a product $(w^{ei}_{fb}\, t^{mn}_{ae})$, which would contradict our strategy of formulating the EOMXCCSD theory via one- and two-body intermediates.

The fact that certain terms of the EOMCCSD approach can be given different forms, which are characterized by different scalings, is an interesting feature of this approach. Clearly, this feature of the EOMXCC theory allows us to choose the scaling which is most favorable and which leads to the smallest storage requirements for the quantities involved. The fact that we have this flexibility in the EOMXCC method is related to the presence of the $T^\dagger$ operators in EOMXCC expressions. Thanks to their presence, in addition to the usual intermediates involving V_N (or F_N) and T and their analogs involving previously formed intermediates and T, we can also form intermediates involving $T^\dagger$ and V_N or $T^\dagger$ and T, depending on what is more convenient. We do not have the same flexibility in the ordinary EOMCC method, where we can only form intermediates involving V_N (or F_N) and T or their higher-rank analogs involving previously calculated intermediates and T. This is the main reason, why we can replace various n^7 steps, which are similar to n^7 steps of the approximate EOMCCSDT methods, such as EOMCCSDT-1 or EOMCCSD(T), by n^6 steps when the EOMXCCSD approximation is invoked, and still obtain a theory which potentially includes some T_3 effects. As we demonstrate in Appendix B, similar flexibility exists when we study three- and four-body terms of $\bar{\bar{H}}$ entering the EOMXCCSD equations.

Appendix B: Three- and four-body components of $\bar{\bar{H}}^P$ in the PE3 approximation

As explained in Section 4 (cf., also, Section 5), the three- and four-body components of the operator $\bar{\bar{H}}^P$ entering the EOMXCCSD equations (recall that P is a projector on the subspace spanned by singly and doubly excited configurations) are computed directly by forming the quantities ${}^3\Lambda^i_a$, ${}^3\Lambda^{ij}_{ab}$,

and ${}^4\Lambda^{ij}_{ab}$ defined by Eqs. (147)-(149) [cf., also, Eqs. (150) and (151)]. In other words, we use a direct CI procedure, in which we recalculate the products of the relevant three- and four-body components of matrix $\bar{\bar{\mathbf{H}}}^P$ and a CI-like vector $\mathbf{C} = \{\ldots, C^i_a, \ldots, C^{ij}_{ab}, \ldots\}$ every time we need them. In case of the PE3 approximation, the quantities ${}^3\Lambda^i_a$, ${}^3\Lambda^{ij}_{ab}$, and ${}^4\Lambda^{ij}_{ab}$ are defined by Eqs. (181)-(185). By forming these quantities, we eliminate large storage requirements associated with a huge number of $\bar{\bar{h}}^{stu}_{pqr}$ and $\bar{\bar{h}}^{stuv}_{pqrs}$ matrix elements defining $\bar{\bar{H}}_3$ and $\bar{\bar{H}}_4$.

We begin our presentation with the final expressions for ${}^3\Lambda^i_a$, ${}^3\Lambda^{ij}_{ab}$, and ${}^4\Lambda^{ij}_{ab}$, which we group according to blocks of $\bar{\bar{\mathbf{H}}}$ to which they contribute (part B.1). The corresponding intermediates are listed in part B.2 of this Appendix.

B.1. Explicit expressions for the three- and four-body components of $\bar{\bar{H}}^P$

Application of diagrammatic methods of MBPT to general expressions defining ${}^3\Lambda^i_a$, ${}^3\Lambda^{ij}_{ab}$, and ${}^4\Lambda^{ij}_{ab}$ in the PE3 approximation, Eqs. (181)-(185), gives the following results:

SD block

$$[\bar{\bar{\mathbf{H}}}_3(\mathbf{2})_{\mathbf{SD}} \cdot \mathbf{C}]^i_a = -\tfrac{1}{2}\left(\bar{\bar{h}}^{ik}_{la}(1,2)\,\tilde{\delta}^l_k - \bar{\bar{h}}^{di}_{ac}(1,2)\,\tilde{\delta}^c_d\right), \quad (328)$$

$$[\bar{\bar{\mathbf{H}}}_3(\mathbf{T}^\dagger_2, \mathbf{T}_2)_{\mathbf{SD}} \cdot \mathbf{C}]^i_a = \Gamma^c_k\, t^{ki}_{ca} + \Gamma^{ic}_{kl}\, t^{kl}_{ca} + v^{cd}_{ak}\,\Gamma^{ik}_{cd} + \tfrac{1}{8}\,\bar{\bar{\gamma}}^{kl}_{ma}\,\tau^{mi}_{kl}, \quad (329)$$

$$[\bar{\bar{\mathbf{H}}}_3(\mathbf{T}^\dagger_1, \mathbf{T}_2)_{\mathbf{SD}} \cdot \mathbf{C}]^i_a = \tfrac{1}{2}\left(\gamma^k_l\,\sigma^{li}_{ka} + E^c_k\, t^{ki}_{ca}\right), \quad (330)$$

DS block

$$[\bar{\bar{\mathbf{H}}}_{3,\mathbf{DS}} \cdot \mathbf{C}]^{ij}_{ab} = \mathcal{A}_{ab}\,\bar{\gamma}^c_a\, t^{ij}_{cb} - \mathcal{A}^{ij}\,\bar{\gamma}^i_k\, t^{kj}_{ab}, \quad (331)$$

$$[\bar{\bar{\mathbf{H}}}_3(\mathbf{T}^\dagger_2, \mathbf{T}_2)_{\mathbf{DS}} \cdot \mathbf{C}]^{ij}_{ab} = -\mathcal{A}^{ij}\,\Gamma^i_k\, t^{kj}_{ab} + \mathcal{A}_{ab}\,\Gamma^c_a\, t^{ij}_{cb} - \mathcal{A}_{ab}\mathcal{A}^{ij}\,\Gamma^{ic}_{ak}\, t^{kj}_{cb} + \mathcal{A}_{ab}\mathcal{A}^{ij}\, v^{ik}_{al}\,\Gamma^{lj}_{kb} + \Gamma^{ij}_{kl}\, t^{kl}_{ab} - v^{ck}_{ab}\,\Gamma^{ij}_{kc} - \mathcal{A}^{ij}\, w^{ci}_{ab}\,\Gamma^j_c + \mathcal{A}_{ab}\, w^{ij}_{ka}\,\Gamma^k_b, \quad (332)$$

$$[\bar{\bar{\mathbf{H}}}_3(\mathbf{T}^\dagger_1, \mathbf{T}_2)_{\mathbf{DS}} \cdot \mathbf{C}]^{ij}_{ab} = -v^{cd}_{ab}\, E^{ij}_{cd} - E^{ij}_{kl}\, t^{kl}_{ab} - \mathcal{A}_{ab}\mathcal{A}^{ij}\, v^{ic}_{ak}\, E^{jk}_{bc} - \mathcal{A}_{ab}\mathcal{A}^{ij}\, E^{ic}_{ak}\, t^{jk}_{bc} + \mathcal{A}_{ab}\, E^c_a\, t^{ij}_{cb} + \mathcal{A}^{ij}\, E^i_k\, t^{kj}_{ab}, \quad (333)$$

DD block

$$[\bar{\mathbf{H}}_{\mathbf{3,DD}} \cdot \mathbf{C}]^{ij}_{ab} = \tfrac{1}{2}\left(\mathcal{A}_{ab}\,\bar{\bar{\gamma}}^{c}_{a}\,t^{ij}_{cb} + \mathcal{A}^{ij}\,\bar{\bar{\gamma}}^{i}_{k}\,t^{kj}_{ab}\right), \tag{334}$$

$$[\bar{\bar{\mathbf{H}}}_{\mathbf{3}}(\mathbf{2})_{\mathbf{DD}} \cdot \mathbf{C}]^{ij}_{ab} = \tfrac{1}{2}\left(\mathcal{A}_{ab}\,\bar{h}^{ij}_{ac}\,\tilde{\delta}^{c}_{b} + \mathcal{A}^{ij}\,\bar{h}^{ik}_{ab}\,\tilde{\delta}^{j}_{k}\right), \tag{335}$$

$$\begin{aligned}[\bar{\bar{\mathbf{H}}}_{\mathbf{3}}(\mathbf{T}^{\dagger}_{\mathbf{2}},\mathbf{T}_{\mathbf{2}})_{\mathbf{DD}} \cdot \mathbf{C}]^{ij}_{ab} = {} & \mathcal{A}_{ab}\,\Delta^{c}_{a}\,t^{ij}_{cb} + \mathcal{A}^{ij}\,\Delta^{i}_{k}\,t^{kj}_{ab} - \mathcal{A}_{ab}\,\Delta^{cd}_{ab}\,t^{ij}_{cd} \\ & -\mathcal{A}^{ij}\,\Delta^{ij}_{kl}\,t^{kl}_{ab} + \mathcal{A}_{ab}\mathcal{A}^{ij}\,\Delta^{ic}_{ak}\,t^{kj}_{cb} \\ & +\mathcal{A}_{ab}\mathcal{A}^{ij}\,v^{ic}_{ak}\,\Delta^{kj}_{cb} + \mathcal{A}^{ij}\,v^{cd}_{ab}\,\Gamma^{ij}_{cd} \\ & +\mathcal{A}_{ab}\,v^{ij}_{kl}\,\Gamma^{kl}_{ab},\end{aligned} \tag{336}$$

$$\begin{aligned}[\bar{\bar{\mathbf{H}}}_{\mathbf{3}}(\mathbf{T}^{\dagger}_{\mathbf{1}},\mathbf{T}_{\mathbf{2}})_{\mathbf{DD}} \cdot \mathbf{C}]^{ij}_{ab} = {} & \mathcal{A}_{ab}\,\bar{\gamma}^{ck}_{ab}\,\sigma^{ij}_{kc} + \mathcal{A}^{ij}\,\Xi^{ij}_{kl}\,t^{kl}_{ab} \\ & +\mathcal{A}_{ab}\mathcal{A}^{ij}\left(\bar{\gamma}^{ik}_{la} + \tfrac{1}{2}\,\bar{\bar{\gamma}}^{ik}_{la}\right)\sigma^{lj}_{kb} \\ & +\mathcal{A}_{ab}\mathcal{A}^{ij}\,\Xi^{ic}_{ak}\,t^{kj}_{cb} + \mathcal{A}_{ab}\,\Xi^{c}_{a}\,t^{ij}_{cb} \\ & -\mathcal{A}^{ij}\,\Xi^{i}_{k}\,t^{kj}_{ab},\end{aligned} \tag{337}$$

$$\begin{aligned}[\bar{\bar{\mathbf{H}}}_{\mathbf{4}}(\mathbf{T}^{\dagger}_{\mathbf{2}},\mathbf{T}_{\mathbf{2}})_{\mathbf{DD}} \cdot \mathbf{C}]^{ij}_{ab} = {} & \tfrac{1}{2}\Big(\mathcal{A}_{ab}\,\tilde{E}^{c}_{a}\,t^{ij}_{cb} + \mathcal{A}^{ij}\,\tilde{E}^{i}_{k}\,t^{kj}_{ab} + v^{cd}_{ab}\,\tilde{E}^{ij}_{cd} \\ & +\tilde{E}^{ij}_{kl}\,t^{kl}_{ab} + \mathcal{A}_{ab}\mathcal{A}^{ij}\,\tilde{E}^{ic}_{ak}\,t^{kj}_{cb}\Big).\end{aligned} \tag{338}$$

Before presenting the formulas for the recursively generated intermediates which appear in the above expressions, let us mention that most terms contributing to ${}^{3}\Lambda^{i}_{a}$, ${}^{3}\Lambda^{ij}_{ab}$, and ${}^{4}\Lambda^{ij}_{ab}$ scale as $n_o^3 n_u^3$ or $n_o^4 n_u^2$. There are relatively few contributions which scale as $n_o^2 n_u^4$ and quite a few contributions which are obtained in inexpensive n^5, n^4, or even n^3 steps. Interestingly enough, only one of the four-body terms in $[\bar{\bar{\mathbf{H}}}_{\mathbf{4}}(\mathbf{T}^{\dagger}_{\mathbf{2}},\mathbf{T}_{\mathbf{2}})_{\mathbf{DD}} \cdot \mathbf{C}]^{ij}_{ab}$ scales as $n_o^2 n_u^4$. The remaining four-body contributions scale as $n_o^3 n_u^3$, $n_o^2 n_u^3$, or better. Although four-body terms have nothing to do with the T_3 terms of EOMCCSDT, they are rather inexpensive and it might be useful to keep them.

The most expensive step in the calculation of ${}^{3}\Lambda^{i}_{a}$, ${}^{3}\Lambda^{ij}_{ab}$, and ${}^{4}\Lambda^{ij}_{ab}$ is the n_u^6 step associated with formation of Δ^{cd}_{ab} in the third term of $[\bar{\bar{\mathbf{H}}}_{\mathbf{3}}(\mathbf{T}^{\dagger}_{\mathbf{2}},\mathbf{T}_{\mathbf{2}})_{\mathbf{DD}} \cdot \mathbf{C}]^{ij}_{ab}$ [see Eq. (336); for definition of Δ^{cd}_{ab}, see part B.2, Eq. (372)]. None of the other terms in ${}^{3}\Lambda^{i}_{a}$, ${}^{3}\Lambda^{ij}_{ab}$, and ${}^{4}\Lambda^{ij}_{ab}$ scales like that. In fact, none of the terms in ${}^{3}\Lambda^{i}_{a}$, ${}^{3}\Lambda^{ij}_{ab}$, and ${}^{4}\Lambda^{ij}_{ab}$ scales as $n_o n_u^5$. Since none of the contributions to a DD block of $\bar{\bar{\mathbf{H}}}$ can be related to T_3 terms of EOMCCSDT, we can think of dropping all $[\bar{\bar{\mathbf{H}}}_{\mathbf{3}}(\mathbf{T}^{\dagger}_{\mathbf{2}},\mathbf{T}_{\mathbf{2}})_{\mathbf{DD}} \cdot \mathbf{C}]^{ij}_{ab}$, $[\bar{\bar{\mathbf{H}}}_{\mathbf{4}}(\mathbf{T}^{\dagger}_{\mathbf{2}},\mathbf{T}_{\mathbf{2}})_{\mathbf{DD}} \cdot \mathbf{C}]^{ij}_{ab}$, and $[\bar{\bar{\mathbf{H}}}_{\mathbf{3}}(\mathbf{T}^{\dagger}_{\mathbf{1}},\mathbf{T}_{\mathbf{2}})_{\mathbf{DD}} \cdot \mathbf{C}]^{ij}_{ab}$ terms altogether, which would eliminate the n_u^6 step mentioned above. This would also lead to a

simplified formula for ${}^3\Lambda^{ij}_{ab}(\mathrm{DD})$, Eq. (184), namely,

$$ {}^3\Lambda^{ij}_{ab}(\mathrm{DD}) = [\bar{\mathbf{H}}_{\mathbf{3,DD}} \cdot \mathbf{C}]^{ij}_{ab} + [\bar{\bar{\mathbf{H}}}_{\mathbf{3}}(\mathbf{2})_{\mathbf{DD}} \cdot \mathbf{C}]^{ij}_{ab} \tag{339} $$

and

$$ {}^4\Lambda^{ij}_{ab} = 0, \tag{340} $$

without sacrificing terms that might be related to triexcited cluster contributions of the EOMCCSDT approach.

B.2. Intermediates for $\bar{\bar{H}}^P_n$, $n = 3, 4$

In this part of Appendix B, we present the explicit expressions for the intermediates entering Eqs. (328)-(338). We first introduce the set of auxiliary quantities (part B.2.1). The final intermediates, which enter Eqs. (328)-(338), are discussed in part B.2.2.

B.2.1. Auxiliary quantities

The complete list of auxiliary intermediates looks as follows:

$$ \gamma^j_i = v^{ef}_{im} C^{mj}_{ef}, \tag{341} $$
$$ \gamma^a_b = v^{ae}_{mn} C^{mn}_{eb}, \tag{342} $$
$$ \bar{\gamma}^j_i = \bar{h}^{je}_{im} C^m_e, \tag{343} $$
$$ \bar{\gamma}^a_b = \bar{h}^{ae}_{bm} C^m_e, \tag{344} $$
$$ \bar{\bar{\gamma}}^j_i = \bar{h}^{ef}_{im} C^{mj}_{ef}, \tag{345} $$
$$ \bar{\bar{\gamma}}^a_b = \bar{h}^{ae}_{mn} C^{mn}_{eb}, \tag{346} $$
$$ \bar{\gamma}^{ij}_{ka} = v^{ie}_{km} C^{mj}_{ea}, \tag{347} $$
$$ \bar{\gamma}^{ci}_{ab} = v^{ce}_{am} C^{mi}_{eb}, \tag{348} $$
$$ \bar{\bar{\gamma}}^{ij}_{ka} = v^{ef}_{ka} C^{ij}_{ef}, \tag{349} $$
$$ \delta^a_i = t^{ae}_{im} C^m_e, \tag{350} $$
$$ \delta^j_i = t^e_i C^j_e, \tag{351} $$
$$ \delta^a_b = t^a_m C^m_b, \tag{352} $$
$$ \delta^{kl}_{ij} = t^{ef}_{ij} C^{kl}_{ef}, \tag{353} $$
$$ \delta^{ib}_{aj} = t^{be}_{jm} C^{mi}_{ea}, \tag{354} $$
$$ \delta^{ab}_{cd} = t^{ab}_{mn} C^{mn}_{cd}, \tag{355} $$
$$ \delta^{ij}_{ka} = t^e_k C^{ij}_{ea}, \tag{356} $$
$$ \tilde{\delta}^j_i = t^{ef}_{im} C^{mj}_{ef} = \delta^{mj}_{im}, \tag{357} $$
$$ \tilde{\delta}^a_b = t^{ae}_{mn} C^{mn}_{eb} = \delta^{ae}_{eb}. \tag{358} $$

These and some of the previously defined quantities allow us to define the primary quantities which enter Eqs. (328)-(338). Before presenting these primary intermediates (cf. part B.2.2), we would like to point out that as before, we fully exploit the presence of $T^\dagger$ in EOMXCC expressions. This operator allows us to form the auxiliary intermediates involving $T^\dagger$ and C, in addition to intermediates involving V_N and C (or $\bar{H}_2$ and C). For comparison, the ordinary EOMCC formalism would only allow us to form intermediates involving V_N (or $\bar{H}_2$) and C. Thanks to this flexibility, which we have in the EOMXCC theory, we can reduce the scaling of various T_3-like terms that appear in the EOMXCCSD equations from n^7 to n^6. Application of direct CI approach to three- and four-body contributions to $\bar{\bar{\mathbf{H}}}^{\boldsymbol{P}}$ is also important as it enables us to form the intermediates which involve C instead of T. The possibility to form the intermediates involving the CI-like vertices C, and the possibility to form the intermediates involving $T^\dagger$, are the two main reasons why the calculation of three- and four-body terms of the EOMXCCSD theory is so inexpensive. If we did not apply a direct CI approach to three- and four-body contributions to $\bar{\bar{\mathbf{H}}}^{\boldsymbol{P}}$ and attempted to compute the $\bar{\bar{h}}^{stu}_{pqr}$ and $\bar{\bar{h}}^{stuv}_{pqrs}$ matrix elements defining $\bar{\bar{H}}_3$ and $\bar{\bar{H}}_4$ instead of ${}^3\Lambda^i_a$, ${}^3\Lambda^{ij}_{ab}$, and ${}^4\Lambda^{ij}_{ab}$, we would end up with a much more complicated and very expensive procedure.

B.2.2. Primary quantities

The auxiliary intermediates introduced in part B.2.1 allow us to define the set of primary intermediates which can be found in Eqs. (328)-(338). They are defined as follows:

$$\Gamma^i_a = t^{im}_{ae}\,\delta^e_m = \Gamma^{im}_{ma}, \tag{359}$$

$$\Gamma^j_i = v^{jm}_{ie}\,\delta^e_m, \tag{360}$$

$$\Gamma^a_b = v^{am}_{be}\,\delta^e_m, \tag{361}$$

$$\Gamma^a_i = \tfrac{1}{4}\left(\bar{\bar{\gamma}}^{mn}_{ie} + 4\,\bar{\gamma}^{mn}_{ie}\right) t^{ea}_{mn} - \tfrac{1}{4}\,v^{ao}_{mn}\,\delta^{mn}_{oi} - v^{af}_{me}\,\delta^{me}_{fi}, \tag{362}$$

$$\Gamma^{ij}_{ab} = \tau^{ie}_{am}\,C^{mj}_{eb}, \tag{363}$$

$$\Gamma^{ij}_{ka} = t^{ij}_{ae}\,\delta^e_k, \tag{364}$$

$$\Gamma^{ij}_{kl} = w^{ij}_{ke}\,\delta^e_l, \tag{365}$$

$$\Gamma^{ka}_{ij} = \tfrac{1}{8}\,v^{ka}_{mn}\,\delta^{mn}_{ij} + \bar{\gamma}^{km}_{ie}\,t^{ea}_{mj}, \tag{366}$$

$$\Gamma^{ib}_{aj} = w^{bi}_{ae}\,\delta^e_j, \tag{367}$$

$$\Delta^j_i = \tfrac{1}{4}\,v^{mn}_{io}\,\delta^{oj}_{mn} + \bar{\nu}^{ef}_{im}\,C^{mj}_{ef}, \tag{368}$$

$$\Delta^a_b = \tfrac{1}{4}\left(\bar{\bar{\nu}}^{ae}_{mn} + 4\,\bar{\nu}^{ae}_{mn}\right) C^{mn}_{eb}, \tag{369}$$

$$\Delta_{ab}^{ij} = \tfrac{1}{4}\left(\tau_{mn}^{ij}\, C_{ab}^{mn} + t_{ab}^{mn}\, \delta_{mn}^{ij}\right) - \Gamma_{ab}^{ji} - \Gamma_{ba}^{ij}, \tag{370}$$

$$\Delta_{kl}^{ij} = \tfrac{1}{2}\, v_{kn}^{im}\, \delta_{ml}^{nj} - v_{ke}^{if}\, \delta_{fl}^{je}, \tag{371}$$

$$\Delta_{cd}^{ab} = \tfrac{1}{2}\, v_{ce}^{af}\, \delta_{fd}^{eb} - v_{cn}^{am}\, \delta_{dm}^{nb}, \tag{372}$$

$$\Delta_{aj}^{ib} = \tfrac{1}{2}\left(v_{je}^{if}\, \delta_{fa}^{eb} + v_{an}^{bm}\, \delta_{mj}^{ni}\right) - v_{ae}^{bf}\, \delta_{fj}^{ie} - v_{jn}^{im}\, \delta_{am}^{nb} + v_{em}^{ib}\, \delta_{aj}^{me} + v_{aj}^{me}\, \delta_{em}^{ib}, \tag{373}$$

$$E_i^j = v_{im}^{jn}\, \delta_n^m - v_{ie}^{jf}\, \delta_f^e, \tag{374}$$

$$E_b^a = v_{bf}^{ae}\, \delta_e^f - v_{bn}^{am}\, \delta_m^n, \tag{375}$$

$$E_i^a = \gamma_e^a\, t_i^e, \tag{376}$$

$$E_{ab}^{ij} = t_{ae}^{ij}\, \delta_b^e, \tag{377}$$

$$E_{kl}^{ij} = v_{km}^{ij}\, \delta_l^m, \tag{378}$$

$$E_{aj}^{ib} = v_{am}^{ib}\, \delta_j^m, \tag{379}$$

$$\tilde{E}_i^j = v_{ie}^{jf}\, \tilde{\delta}_f^e - v_{im}^{jn}\, \tilde{\delta}_n^m, \tag{380}$$

$$\tilde{E}_b^a = v_{bn}^{am}\, \tilde{\delta}_m^n - v_{bf}^{ae}\, \tilde{\delta}_e^f, \tag{381}$$

$$\tilde{E}_{ab}^{ij} = t_{ae}^{ij}\, \tilde{\delta}_b^e, \tag{382}$$

$$\tilde{E}_{kl}^{ij} = v_{km}^{ij}\, \tilde{\delta}_l^m, \tag{383}$$

$$\tilde{E}_{aj}^{ib} = v_{aj}^{ie}\, \tilde{\delta}_e^b + v_{am}^{ib}\, \tilde{\delta}_j^m, \tag{384}$$

$$\Xi_i^j = v_{in}^{me}\, \delta_{me}^{nj} + \tfrac{1}{2}\, \overline{\overline{\gamma}}_{ie}^{jm}\, t_m^e, \tag{385}$$

$$\Xi_b^a = \mu_{mn}^{ae}\, C_{eb}^{mn} - \tfrac{1}{2}\, v_{mn}^{ao}\, \delta_{ob}^{mn}, \tag{386}$$

$$\Xi_{kl}^{ij} = \bar{\gamma}_{ke}^{ij}\, t_l^e, \tag{387}$$

$$\Xi_{aj}^{ib} = v_{am}^{be}\, \delta_{je}^{mi} - \tfrac{1}{2}\, v_{mn}^{ib}\, \delta_{ja}^{mn}. \tag{388}$$

As in the case of one- and two-body terms $\bar{\bar{H}}_n(T_2^\dagger, T_2)$, the $\frac{1}{2}\,[T_2^\dagger (F_N T_2^2)_{C,3}]_{C,3}$ contribution to a three-body term $\bar{\bar{H}}_3(T_2^\dagger, T_2)$ is combined with the corresponding $[T_2^\dagger (V_N T_2)_{C,3}]_{C,3}$ term by introducing the effective interaction w, Eqs. (319) and (320), and the intermediates Γ_{kl}^{ij} and Γ_{aj}^{ib}, Eqs. (365) and (367), respectively [see the $-\mathcal{A}_{ab}\mathcal{A}^{ij}\, \Gamma_{ak}^{ic}\, t_{cb}^{kj}$, $\Gamma_{kl}^{ij}\, t_{ab}^{kl}$, $-\mathcal{A}^{ij}\, w_{ab}^{ci}\, \Gamma_c^j$, and $\mathcal{A}_{ab}\, w_{ka}^{ij}\, \Gamma_b^k$ terms in Eq. (332)].

References

1. F. Coester, Nucl. Phys. **7**, 421 (1958); F. Coester and H. Kümmel, *ibid.* **17**, 477 (1960).

2. J. Čížek, J. Chem. Phys. **45**, 4256 (1966); Adv. Chem. Phys. **14**, 35 (1969); J. Čížek and J. Paldus, Int. J. Quantum Chem. **5**, 359 (1971); J. Paldus, J. Čížek, and I. Shavitt, Phys. Rev. A **5**, 50 (1972).

3. R.J. Bartlett, Ann. Rev. Phys. Chem. **32**, 359 (1981); J. Phys. Chem. **93**, 1697 (1989).

4. R.J. Bartlett, in *Modern Electronic Structure Theory*, Part I, edited by D.R. Yarkony (World Scientific, Singapore, 1995), pp. 1047-1131.

5. J. Paldus, in *New Horizons of Quantum Chemistry*, edited by P.-O. Löwdin and B. Pullman (Reidel, Dordrecht, 1983), pp. 31-60.

6. R.J. Bartlett, C.E. Dykstra, and J. Paldus, in *Advanced Theories and Computational Approaches to the Electronic Structure of Molecules*, edited by C.E. Dykstra (Reidel, Dordrecht, 1984), pp. 127-159.

7. Theoret. Chim. Acta **80** (1991), Nos. 2-6.

8. J. Paldus, in *Methods in Computational Molecular Physics*, Vol. 293 of *NATO Advanced Study Institute, Series B: Physics*, edited by S. Wilson and G.H.F. Diercksen (Plenum, New York, 1992), pp. 99-194.

9. R.J. Bartlett and J.F. Stanton, in *Reviews in Computational Chemistry*, Vol. 5, edited by K.B. Lipkowitz and D.B. Boyd (VCH Publishers, New York, 1994), pp. 65-169.

10. I. Lindgren and J. Morrison, *Atomic Many-Body Theory* (Springer, Berlin, 1982).

11. I. Lindgren and D. Mukherjee, Phys. Rep. **151**, 93 (1987).

12. D. Mukherjee and S. Pal, Adv. Quantum Chem. **20**, 291 (1989).

13. B. Jeziorski and J. Paldus, J. Chem. Phys. **90**, 2714 (1989).

14. F. Coester, in *Lectures in Theoretical Physics*, Vol. 11B, edited by K.T. Mahanthappa and W.E. Brittin (Gordon and Breach, New York, 1969), pp. 157-186; D. Mukherjee, R.K. Moitra, and A. Mukhopadhyay, Mol. Phys. **30**, 1861 (1975); R. Offerman, W. Ey, and H. Kümmel, Nucl. Phys. A **273**, 349 (1976); R. Offerman, *ibid.* **273**, 368 (1976); D. Mukherjee, R.K. Moitra, and A. Mukhopadhyay, Mol. Phys. **33**, 955 (1977); W. Ey, Nucl. Phys. A **296**, 189 (1978); I. Lindgren, Int. J. Quantum Chem. Symp. **12**, 33 (1978); A. Mukhopadhyay, R.K. Moitra, and D. Mukherjee, J. Phys. B **12**, 1 (1979); A. Haque and D. Mukherjee, J. Chem. Phys. **80**, 5058 (1984); L. Stolarczyk and H.J. Monkhorst, Phys. Rev. A **32**, 725, 743 (1985);

A. Haque and U. Kaldor, Chem. Phys. Lett. **117**, 347 (1985); **120**, 261 (1985); I. Lindgren, Phys. Scr. **32**, 291, 611 (1985); D. Sinha, S.K. Mukhopadhyay, M.D. Prasad, and D. Mukherjee, Chem. Phys. Lett. **125**, 213 (1986); D. Sinha, S. Mukhopadhyay, and D. Mukherjee, *ibid.* **129**, 369 (1986); A. Haque and U. Kaldor, Int. J. Quantum Chem. **29**, 425 (1986); D. Mukherjee, Chem. Phys. Lett. **125**, 207 (1986); W. Kutzelnigg, D. Mukherjee, and S. Koch, J. Chem. Phys. **87**, 5902 (1987); D. Mukherjee, W. Kutzelnigg, and S. Koch, *ibid.* **87**, 5911 (1987); U. Kaldor, J. Chem. Phys. **87**, 467 (1987); S. Pal, M. Rittby, R.J. Bartlett, D. Sinha, and D. Mukherjee, Chem. Phys. Lett. **137**, 273 (1987); S. Koch and D. Mukherjee, Chem. Phys. Lett. **145**, 321 (1988); K. B. Ghose and S. Pal, J. Chem. Phys. **97**, 3863 (1988); L. Stolarczyk and H.J. Monkhorst, Phys. Rev. A **37**, 1908, 1926 (1988); S. Pal, M. Rittby, R.J. Bartlett, D. Sinha, and D. Mukherjee, J. Chem. Phys. **88**, 4357 (1988); R. Chaudhuri, D. Sinha, and D. Mukherjee, Chem. Phys. Lett. **163**, 165 (1989); U. Kaldor, S. Roszak, P.C. Hariharan, and J.J. Kaufman, J. Chem. Phys. **90**, 6395 (1989); M. Rittby, S. Pal, and R.J. Bartlett, *ibid.* **90**, 3214 (1989); S. Pal, M. Rittby, and R.J. Bartlett, Chem. Phys. Lett. **160**, 212 (1989); J.D. Watts, M. Rittby, and R.J. Bartlett, J. Am. Chem. Soc. **111**, 4155 (1989); R. Mattie, M. Rittby, R.J. Bartlett, and S. Pal, in *Aspects of Many-Body Effects in Molecules and Extended Systems*, edited by D. Mukherjee, Lecture Notes in Chemistry, Vol. 50 (Springer, Berlin, 1989), pp. 143-153. I. Lindgren, J. Phys. B **24**, 1143 (1991); U. Kaldor, Chem. Phys. Lett. **166**, 599 (1990); **170**, 17 (1990); Theor. Chim. Acta **80**, 427 (1991); K. Jankowski, J. Paldus, and J. Wasilewski, J. Chem. Phys. **95**, 3549 (1991); M. Barysz, H. Monkhorst, and L.Z. Stolarczyk, Theor. Chim. Acta **80**, 483 (1991); C.M.L. Rittby and R.J. Bartlett, *ibid.* **80**, 469 (1991); J.F. Stanton, C.M.L. Rittby, R.J. Bartlett, and D.W. Toohey, J. Phys. Chem. **95**, 2107 (1991); J.F. Stanton, R.J. Bartlett, and C.M.L. Rittby, J. Chem. Phys. **97**, 5560 (1992); M. Barysz, M. Rittby and R.J. Bartlett, Chem. Phys. Lett. **193**, 373 (1992); S.R. Hughes and U. Kaldor, *ibid.* **194**, 99 (1992); **204**, 339 (1993); Phys. Rev. A **47**, 4705 (1993); N. Vaval, K.B. Ghose, S. Pal, and D. Mukherjee, Chem. Phys. Lett. **209**, 292 (1993).

15. W. Kutzelnigg, J. Chem. Phys. **77**, 3081 (1982); W. Kutzelnigg and S. Koch, *ibid.* **79**, 4315 (1983); W. Kutzelnigg, *ibid.* **80**, 822 (1984).

16. S. Pal, M.D. Prasad, and D. Mukherjee, Theor. Chim. Acta **62**, 523 (1983); **66**, 311 (1984).

17. K. Jankowski, J. Paldus, I. Grabowski, and K. Kowalski, J. Chem. Phys. **97**, 7600 (1992); **101**, 1759 (1994) [Erratum].

18. K. Jankowski, J. Paldus, I. Grabowski, and K. Kowalski, J. Chem. Phys. **101**, 3085 (1994).

19. B. Jeziorski and H.J. Monkhorst, Phys. Rev. A **24**, 1668 (1981).

20. B. Jeziorski and J. Paldus, J. Chem. Phys. **88**, 5673 (1988).

21. J. Paldus, L. Pylypow, and B. Jeziorski, in *Many-Body Methods in Quantum Chemistry*, edited by U. Kaldor, Lecture Notes in Chemistry, Vol. 52 (Springer, Berlin, 1989), pp. 151-170; P. Piecuch and J. Paldus, Theor. Chim. Acta **83**, 69 (1992); P. Piecuch and J. Paldus, J. Chem. Phys. **101**, 5875 (1994).

22. J. Paldus, P. Piecuch, B. Jeziorski, and L. Pylypow, in *Recent Progress in Many-Body Theories*, Vol. 3, edited by T.L. Ainsworth, C.E. Campbell, B.E. Clements and E. Krotschek (Plenum, New York, 1992) pp. 287-303; X. Li, P. Piecuch, and J. Paldus, Chem. Phys. Lett. **224**, 267 (1994); P. Piecuch, X. Li, and J. Paldus, *ibid.* **230**, 377 (1994); P. Piecuch and J. Paldus, J. Phys. Chem. **99**, 15354 (1995).

23. J. Paldus, P. Piecuch, L. Pylypow, and B. Jeziorski, Phys. Rev. A **47**, 2738 (1993); P. Piecuch, R. Toboła and J. Paldus, Chem. Phys. Lett. **210**, 243 (1993); P. Piecuch and J. Paldus, Phys. Rev. A **49**, 3479 (1994).

24. L. Meissner, K. Jankowski, and J. Wasilewski, Int. J. Quantum Chem. **34**, 535 (1988); L. Meissner, S.A. Kucharski, and R.J. Bartlett, J. Chem. Phys. **91**, 6187 (1989); L. Meissner and R.J. Bartlett, *ibid.* **92**, 561 (1990); S.A. Kucharski and R.J. Bartlett, *ibid.* **95**, 8227 (1991); A. Balková, S.A. Kucharski, L. Meissner, and R.J. Bartlett, Theor. Chim. Acta **80**, 335 (1991); S.A. Kucharski and R.J. Bartlett, Int. J. Quantum Chem. Symp. **26**, 107 (1992); S.A. Kucharski, A. Balková, P.G. Szalay, and R.J. Bartlett, J. Chem. Phys. **97**, 4289 (1992); A. Balková, S.A. Kucharski, and R.J. Bartlett, Chem. Phys. Lett. **182**, 511 (1991); A. Balková, S.A. Kucharski, L. Meissner, and R.J. Bartlett, J. Chem. Phys. **95**, 4311 (1991); A. Balková and R.J. Bartlett, Chem. Phys. Lett. **193**, 364 (1992); J. Chem. Phys. **99**, 7907 (1993); P.G. Szalay and R.J. Bartlett, *ibid.* **101**, 4936 (1994); A. Balková and R.J. Bartlett, *ibid.* **101**, 8972 (1994); **102**, 7116 (1995).

25. S. Berkovic and U. Kaldor, Chem. Phys. Lett. **199**, 42 (1992); J. Chem. Phys. **98**, 3090 (1993).

26. W.D. Laidig and R.J. Bartlett, Chem. Phys. Lett. **104**, 424 (1984); W.D. Laidig, P. Saxe, and R.J. Bartlett, J. Chem. Phys. **86**, 887 (1987).

27. F.E. Harris, Int. J. Quantum Chem. Symp. **11**, 403 (1977); A. Banerjee and J. Simons, Int. J. Quantum Chem. **19**, 207 (1981); J. Chem. Phys. **76**, 4548 (1982); H. Baker and M.A. Robb, Mol. Phys. **50**, 20 (1983); C.L. Janssen and H.F. Schaefer III, Theor. Chim. Acta **79**, 1 (1991); J. Paldus and X. Li, in *Symmetries in science VI*, edited by B. Gruber (Plenum, New York, 1993), pp. 573-591; X. Li and J. Paldus, Int. J. Quantum Chem. Symp. **27**, 269 (1993); J. Chem. Phys. **101**, 8812 (1994).

28. R. Tanaka and H. Terashima, Chem. Phys. Lett. **106**, 558 (1984); M.R. Hoffman and J. Simons, J. Chem. Phys. **88**, 993 (1988); Chem. Phys. Lett. **142**, 451 (1987).

29. J. Paldus, J. Čížek, M. Saute, and A. Laforgue, Phys. Rev. A **17**, 805 (1978); M. Saute, J. Paldus, and J. Čížek, Int. J. Quantum Chem. **15**, 463 (1979).

30. H. Nakatsuji and K. Hirao, Chem. Phys. Lett. **47**, 569 (1977); J. Chem. Phys. **68**, 2053, 4279 (1978); H. Nakatsuji, Chem. Phys. Lett. **59**, 362 (1978); **67**, 329, 334 (1979); K. Hirao and H. Nakatsuji, J. Chem. Phys. **69**, 4535, 4548 (1978); K. Ohta, H. Nakatsuji, K. Hirao, and T. Yonezawa, *ibid.* **73**, 1770 (1980); H. Nakatsuji and K. Hirao, Int. J. Quantum Chem. **20**, 1301 (1981); H. Nakatsuji, K. Ohta, and K. Hirao, J. Chem. Phys. **75**, 2952 (1981); H. Nakatsuji, Int. J. Quantum Chem. Symp. **17**, 241 (1983); J. Chem. Phys. **83**, 713 (1985); H. Nakatsuji, O. Kitao, and M. Komori, in *Aspects of Many-Body Effects in Molecules and Extended Systems*, edited by D. Mukherjee, Lecture Notes in Chemistry, Vol. 50 (Springer, Berlin, 1989), pp. 101-122; H. Nakatsuji, J. Chem. Phys. **95**, 4296 (1991); Acta Chim. Hung. **129**, 719 (1992); in *Computational Chemistry: Reviews of Current Trends*, edited by J. Leszczyński (World Scientific, Singapore, 1997), Vol. 2, p. 62.

31. N. Oliphant and L. Adamowicz, J. Chem. Phys. **94**, 1229 (1991); **96**, 3739 (1992); Int. Rev. Phys. Chem. **12**, 339 (1993); P. Piecuch, N. Oliphant, and L. Adamowicz, *ibid.* **99**, 1875 (1993); P. Piecuch and L. Adamowicz, *ibid.* **100**, 5792 (1994); Chem. Phys. Lett. **221**, 121 (1994); J. Chem. Phys. **102**, 898 (1995); V. Alexandrov, P. Piecuch

and L. Adamowicz, *ibid.* **102**, 3301 (1995); K. B. Ghose and L. Adamowicz, *ibid.* **103**, 9324 (1995); K.B. Ghose, P. Piecuch, and L. Adamowicz, *ibid.* **103**, 9331 (1995); K.B. Ghose, P. Piecuch, S. Pal, and L. Adamowicz, *ibid.* **104**, 6582 (1996); L. Adamowicz, P. Piecuch, and K.B. Ghose, Mol. Phys. **94**, 225 (1998); P. Piecuch, S.A. Kucharski, and R.J. Bartlett, unpublished.

32. H. Sekino and R.J. Bartlett, Int. J. Quantum Chem. Symp. **18**, 255 (1984); J. Geertsen, M. Rittby, and R.J. Bartlett, Chem. Phys. Lett. **164**, 57 (1989).

33. D.C. Comeau and R.J. Bartlett, Chem. Phys. Lett. **207**, 414 (1993).

34. J.F. Stanton and R.J. Bartlett, J. Chem. Phys. **98**, 7029 (1993).

35. K. Emrich, Nucl. Phys. A **351**, 376 (1981); D. Mukherjee and P.K. Mukherjee, Chem. Phys. **39**, 325 (1979); S. Ghosh, D. Mukherjee, and S.N. Bhattacharya, Chem. Phys. **72**, 161 (1982); Mol. Phys. **43**, 173 (1981); S.S.Z. Adman, S. Bhattacharya, and D. Mukherjee, Chem. Phys. Lett. **85**, 204 (1982); S. Ghosh and D. Mukherjee, Proc. Ind. Acad. Sci. **93**, 947 (1984); D. Sinha, S.K. Mukhopadhyay, M.D. Prasad, and D. Mukherjee, Chem. Phys. Lett. **125**, 213 (1986).

36. M. Takahashi and J. Paldus, J. Chem. Phys. **85**, 1486 (1986).

37. H. Monkhorst, Int. J. Quantum Chem. Symp. **11**, 421 (1977); E. Daalgard and H. Monkhorst, Phys. Rev. A **28**, 1217 (1983).

38. M. Nooijen and R.J. Bartlett, J. Chem. Phys. **102**, 3629 (1995).

39. M. Nooijen and R.J. Bartlett, J. Chem. Phys. **102**, 6735 (1995).

40. D.J. Rowe, Rev. Mod. Phys. **40**, 153 (1968); C.W. McCurdy, Jr., T.N. Rescigno, D.L. Yeager, and V. McKoy, in *Modern Theoretical Chemistry*, edited by H.F. Schaefer III (Plenum, New York, 1977), Vol. 3, pp. 339-386, and references therein.

41. J. Linderberg and Y. Öhrn, *Propagators in Quantum Chemistry* (Academic, New York, 1973); P. Jørgensen, Annu. Rev. Phys. Chem. **26**, 359 (1975); Y. Öhrn, in *The World of Quantum Chemistry*, edited by B. Pullman and R. Parr (Reidel, Boston, 1976), p. 57; L.S. Cederbaum and W. Domcke, Adv. Chem. Phys. **36**, 205 (1977); J. Oddershede, Adv. Quantum Chem. **11**, 275 (1978); Y. Öhrn and G. Born, *ibid.* **13**, 1 (1981); W. von Niessen, J. Schirmer, and L.S. Cederbaum, Comp. Phys. Rep. **1**, 57 (1984); J. Oddershede, P. Jørgensen, and D.L. Yeager, *ibid.* **2**, 33 (1984); J. Oddershede, Adv. Chem. Phys.

59, 201 (1987); J.V. Ortiz, in *Computational Chemistry: Reviews of Current Trends*, edited by J. Leszczyński (World Scientific, Singapore, 1997), Vol. 2, pp. 1-61; J.V. Ortiz, V.G. Zakrzewski, and O. Dolgounitcheva, in *Conceptual Perspectives in Quantum Chemistry*, edited by J.-L. Calais and E. Kryachko (Kluwer, Dordrecht, 1997), pp. 465-517.

42. H. Koch and P. Jørgensen, J. Chem. Phys. **93**, 3333 (1990); H. Koch, H.J.Aa. Jensen, P. Jørgensen, and T. Helgaker, *ibid.* **93**, 3345 (1990).

43. B.H. Brandow, Rev. Mod. Phys. **39**, 771 (1967).

44. L. Meissner and R.J. Bartlett, J. Chem. Phys. **94**, 6670 (1991); D. Mukhopadhyay, S. Mukhopadhyay, R. Chaudhuri, and D. Mukherjee, Theor. Chim. Acta **80**, 441 (1991).

45. L. Meissner and R.J. Bartlett, J. Chem. Phys. **102**, 7490 (1995).

46. J.D. Watts and R.J. Bartlett, J. Chem. Phys. **101**, 3073 (1994).

47. J. Paldus, B. Adams, and J. Čížek, Int. J. Quantum Chem. **11**, 813 (1977).

48. J. Paldus, J. Chem. Phys. **67**, 303 (1977); B.G. Adams and J. Paldus, Phys. Rev. A **20**, 1 (1979); P. Piecuch and J. Paldus, Int. J. Quantum Chem. **36**, 429 (1989).

49. P. Piecuch and J. Paldus, Theor. Chim. Acta **78**, 65 (1990).

50. P. Piecuch and R.J. Bartlett, unpublished.

51. M. Rittby and R.J. Bartlett, J. Phys. Chem. **92**, 3033 (1988).

52. H. Sekino and R.J. Bartlett, Chem. Phys. Lett. **225**, 486 (1994); S.A. Perera, M. Nooijen, and R.J. Bartlett, J. Chem. Phys. **104**, 3290 (1996).

53. J.F. Stanton and R.J. Bartlett, J. Chem. Phys. **99**, 5178 (1993).

54. P.B. Różyczko, S.A. Perera, M. Nooijen, and R.J. Bartlett, J. Chem. Phys. **107**, 6736 (1997).

55. P.B. Różyczko and R.J. Bartlett, J. Chem. Phys. **107**, 10823 (1997).

56. E.A. Salter, G.W. Trucks, and R.J. Bartlett, J. Chem. Phys. **90**, 1752 (1989); E.A. Salter and R.J. Bartlett, *ibid.* **90**, 1767 (1989).

57. L.A. Adamowicz, W.D. Laidig, and R.J. Bartlett, Int. J. Quantum Chem. Symp. **18**, 245 (1984); R.J. Bartlett, in *Geometrical Derivatives of Energy Surfaces and Molecular Properties*, NATO Advanced Study Institute, Series C: Mathematical and Physical Sciences, edited by P. Jørgensen and J. Simons (Reidel, Dordrecht, 1986), Vol. 166, pp. 35-61; G. Fitzgerald, R.J. Harrison, and R.J. Bartlett, J. Chem. Phys. **85**, 5143 (1986); A.C. Scheiner, G.E. Scuseria, J.E. Rice, T.J. Lee, and H.F. Schaefer III, J. Chem. Phys. **87**, 5361 (1987).

58. H. Koch, H.J.Aa. Jensen, P. Jørgensen, T. Helgaker, G.E. Scuseria, and H.F. Schaefer III, J. Chem. Phys. **92**, 4924 (1990); R. Kobayashi, H. Koch, and P. Jørgensen, *ibid.* **101**, 4956 (1994); A.E. Kondo, P. Piecuch, and J. Paldus, *ibid.* **102**, 6511 (1995).

59. S.R. Gwaltney and R.J. Bartlett, Chem. Phys. Lett. **241**, 26 (1995).

60. S.R. Gwaltney, M. Nooijen, and R.J. Bartlett, Chem. Phys. Lett. **248**, 189 (1996).

61. J.D. Watts, S.R. Gwaltney, and R.J. Bartlett, J. Chem. Phys. **105**, 6979 (1996); J.E. Del Bene, J.D. Watts, and R.J. Bartlett, *ibid.* **106**, 6051 (1997).

62. R.J. Bartlett, J.E. Del Bene, S.A. Perera, and R.P. Mattie, J. Mol. Struct. (THEOCHEM) **400**, 157 (1997).

63. J.D. Watts and R.J. Bartlett, Chem. Phys. Lett. **233**, 81 (1995).

64. J.D. Watts and R.J. Bartlett, Chem. Phys. Lett. **258**, 581 (1996).

65. G.L. Gutsev, M. Nooijen, and R.J. Bartlett, Phys. Rev. A **57**, 1646 (1998).

66. M. Nooijen and R.J. Bartlett, J. Chem. Phys. **106**, 6441 (1997); **107**, 6812 (1997).

67. M. Nooijen and R.J. Bartlett, J. Chem. Phys. **106**, 6449 (1997).

68. D.J. Thouless, *Quantum Mechanics of Many-Body Systems* (Academic, New York, 1961).

69. R.J. Bartlett and J. Noga, Chem. Phys. Lett. **150**, 29 (1988).

70. R.J. Bartlett, S.A. Kucharski, J. Noga, J.D. Watts, and G.W. Trucks, in *Many-Body Methods in Quantum Chemistry*, edited by U. Kaldor, Lecture Notes in Chemistry, Vol. 52 (Springer, Berlin, 1989), pp. 124-150.

71. R.J. Bartlett, S.A. Kucharski, and J. Noga, Chem. Phys. Lett. **155**, 133 (1989).

72. J.D. Watts, G.W. Trucks, and R.J. Bartlett, Chem. Phys. Lett. **157**, 359 (1989).

73. W. Kutzelnigg, in *Modern Theoretical Chemistry*, edited by H.F. Schaefer III (Plenum, New York, 1977), Vol. 3, p. 129; S. Koch and W. Kutzelnigg, Theor. Chim. Acta **59**, 387 (1981); S. Pal, *ibid.* **66**, 207 (1984).

74. P.G. Szalay and R.J. Bartlett, Int. J. Quantum Chem. Symp. **26**, 85 (1992).

75. P.G. Szalay, M. Nooijen, and R.J. Bartlett, J. Chem. Phys. **103**, 281 (1995).

76. J.S. Arponen, Ann Phys. **151**, 311 (1983); J.S. Arponen, R.F. Bishop, and E. Pajanne, Phys. Rev. A **36**, 2519 (1987); Condensed Matter Theor. **2**, 357 (1987); R.F. Bishop, J.S. Arponen, and E. Pajanne, in *Aspects of Many-Body Effects in Molecules and Extended Systems*, edited by D. Mukherjee, Lecture Notes in Chemistry, Vol. 50 (Springer, Berlin, 1989), p. 79; R.F. Bishop and J.S. Arponen, Int. J. Quantum Chem. Symp. **24**, 197 (1990); J.S. Arponen and R.F. Bishop, Ann. Phys. **207**, 171 (1991); R.F. Bishop, N.I. Robinson, and J. Arponen, Condensed Matter Theor. **5**, 37 (1990); R.F. Bishop, Theor. Chim. Acta **80**, 95 (1991); J. Arponen, Phys. Rev. A **55**, 2686 (1997).

77. J.S. Arponen, R.F. Bishop, and E. Pajanne, Phys. Rev. A **36**, 2539 (1987).

78. P.-O. Löwdin, J. Math. Phys. **24**, 70 (1983).

79. J. Noga, S.A. Kucharski, and R.J. Bartlett, J. Chem. Phys. **90**, 3399 (1989).

80. S.A. Kucharski and R.J. Bartlett, Chem. Phys. Lett. **158**, 550 (1989).

81. R.J. Bartlett, J.D. Watts, S.A. Kucharski, and J. Noga, Chem. Phys. Lett. **165**, 513 (1990).

82. S.A. Kucharski and R.J. Bartlett, J. Chem. Phys. **108**, 5243 (1998).

83. The explicit expressions for $\bar{h}_{ij}^{ka}$ and $\bar{h}_{ia}^{jk}$ in Table 1 of Ref. 34 (designated in Ref. 34 as $\mathcal{W}_{ijka}$ and $\mathcal{W}_{iajk}$, respectively) are incorrect. If we use the notation of Ref. 34, the correct expression for $\mathcal{W}_{iajk} \equiv \bar{h}_{ia}^{jk}$

should read: $\mathcal{W}_{iajk} = \langle ia||jk\rangle + \mathcal{P}(kj)\, t^{ae}_{km}\, \langle im||je\rangle + \frac{1}{2}\, \tau^{ef}_{jk}\, \langle ia||ef\rangle - t^{ae}_{jk}\, \mathcal{F}_{ie} - t^{a}_{m}\, \mathcal{W}_{imjk} + \mathcal{P}(kj)\, t^{e}_{j}[\langle ia||ek\rangle - t^{af}_{mk}\, \langle im||ef\rangle]$. The formula for $\mathcal{W}_{ijka}$ presented in Ref. 34, i.e. $\langle jk||ia\rangle + t^{e}_{i}\, \langle jk||ea\rangle$, should really be regarded as a formula for $\mathcal{W}_{jkia} \equiv \bar{h}^{ia}_{jk}$. Finally, a small change has to be made in expression for $\mathcal{W}_{abci} \equiv \bar{h}^{ci}_{ab}$. The antisymmetrized two-electron integral $\langle ci||mn\rangle$ in the third term of expression for $\mathcal{W}_{abci}$ has to be replaced by $\langle mn||ci\rangle$ (which is only important if the molecular orbitals are not real). The correct expressions have been used in all calculations [32–34, 38, 39, 46, 59–65].

84. M. Urban, J. Noga, S.J. Cole, and R.J. Bartlett, J. Chem. Phys. **83**, 4041 (1985); S.J. Cole and R.J. Bartlett, *ibid.* **86**, 873 (1987).

85. P. Piecuch, R. Toboła, and J. Paldus, Int. J. Quantum Chem. **55**, 133 (1995).

86. K. Raghavachari, G.W. Trucks, J.A. Pople, and M. Head-Gordon, Chem. Phys. Lett. **157**, 479 (1989).

87. Y.S. Lee and R.J. Bartlett, J. Chem. Phys. **80**, 4371 (1984); Y.S. Lee, S.A. Kucharski, and R.J. Bartlett, *ibid.* **81**, 5906 (1984); **82**, 5761 (1985) (Erratum).

88. P. Piecuch, R. Toboła, and J. Paldus, Phys. Rev. A **54**, 1210 (1996).

89. J. Paldus and P. Piecuch, Int. J. Quantum Chem. **42**, 135 (1992).

90. S.A. Kucharski and R.J. Bartlett, J. Chem. Phys. **108**, 5255 (1998).

91. A. Jucys, J. Levinsonas, and V. Vanagas, *Mathematical Apparatus of the Theory of Angular Momentum* (Institute of Physics and Mathematics of the Academy of Sciences of the Lithuanian S.S.R., Vilnius, 1960) [in Russian]; English Translations: Israel Program for Scientific Translations, Jerusalem, 1962; Gordon and Breach, New York, 1964; A. Jucys and A. Bandzaitis, *The Theory of Angular Momentum in Quantum Mechanics*, 2nd ed. (Mokslas, Vilnius, 1977) [in Russian]; D.M. Brink and G.R. Satchler, *Angular Momentum*, 2nd ed. (Clarendon, Oxford, 1968); E. El Baz and B. Castel, *Graphical Methods of Spin Algebras in Atomic, Nuclear and Particle Physics* (Marcel Dekker, New York, 1972); for a brief review of these methods, see, e.g., Ref. 10; see, also, Appendices of Ref. 47 and P. Piecuch, in *Molecules in Physics, Chemistry and Biology*, Vol. 2, *Physical Aspects of Molecular Systems*, edited by J. Maruani (Kluwer, Dordrecht, 1988), pp. 417-505.

92. S.A. Kucharski and R.J. Bartlett, Theor. Chim. Acta **80**, 387 (1991).

Subject Index

D

E

F

G

H

I

J

K

L

M

N

O

P

R

S

T

V

W

X